# Computational and Experimental Investigations on Biodiesel Combustion Process

Ayedh Alajmi

Department of Engineering

De Montfort University

A thesis submitted for the degree of

*Doctor of Philosophy*

June 2014

*To my family,*

# Abstract

The combustion process of liquid conventional and biofuels depend on factors ranging from the thermophysicochemical properties associated with such fuels to the combustion infrastructure used to burn them. A third class of fuels commonly referred to as surrogate fuels can be obtained by mixing conventional and biofuels. It is thought that the existence of oxygen atoms in biofuels play a crucial role in the way they burn in a stream of air, influencing not only the efficiency of the combustion process of such class of fuels but also the emissions. The mechanisms through which the existing oxygen atoms influence the combustion process of biofuels (and its surrogates) are still debatable and unestablished.

This thesis sheds light on the points mentioned in the paragraph above. Extensive computational and experimental work was done to elucidate the combustion process of conventional, surrogate and biofuels. Some of the reaction mechanisms used in modelling the current reactive flow simulation are already tested while others were developed during the course of this work.

The computational results have shown good agreement with the available experimental data. One of the most important observations and findings reported in this work was that when comprehensive reaction models were used, the injected fuels burned at a slower rate compared to the situation when reduced models were employed. While such comprehensive models predicted better flame structure and far better by-products compared to the existing experimental results, it has also led to differences in some parameters, especially the temperature field. The computational prediction has also shown that biodiesel

produces a marginally higher rate of $CO_x$ compared to diesel which was also observed experimentally using a Compression Ignition Engine (CIE). Having said so, the experimental work also showed that surrogate fuels perform far better than pure diesel and biodiesel in CIE) in terms of emissions. The experimental work further addressed some phyisical and spectral analysis of diesel, biodiesel and nine blends as well as assessing the performance of a combination of these fuels in a compression ignition engine. The results are in line with what has reported in the literature but also sheds light on important features related to surrogate fuels and explain better the expected structure of such blends which may influence the way they burn under different environments.

With regards to the harmfull emissions of the combustion of liquid fuels, biodiesel was found to produce harmful emissions in a lower quantity compared to conventional diesel which is in line with the findings of many experimental data. The computational findings have also predicted less energy content and temperature range for biofuels of order 10-15% which is also in agreement with many experimental findings cited in the literature.

# Declaration

I declare that the material presented in this thesis consists of original work undertaken solely by myself. Information derived from the published and unpublished work of others has been properly referenced. The material has not been submitted in substantially the same form for the award of a higher degree elsewhere.

**Ayedh Alajmi**

June 2014

# Acknowledgements

I would like to thank my first supervisor Dr. Ibrahim Abdalla as well as extending my thankfulness to Dr. Kalok Lee and Dr Yong Sun for the support and encouragement which they gave me during my work. Their guidance, constructive criticism, advice and discussions significantly helped me to accomplish this work.

I am also thankful to Mr. Paul Dean, the chief Technician at Demontfort University for his great support during the experimental phase both in the engine test cell and at the chemistry laboratory at De Montfort University.

Next, I would like to express my gratitude to Dr. Masoud Almariy of Kuwait Institute for Scientific Research (KISR) for his technical support.

Special thanks is also due to my friend Dr. Abdullah Alajmi who has been with me through thick and thin.

Last, but not the least, I would like to thank my parents, my wife and my children for their patience and support during the long and difficult journey of my PhD. Without their constant support and understanding this thesis would not have been possible.

Ayedh Alajmi
De Montfort University
June 2014

# Contents

**Contents** vi

**List of Figures** xi

**List of Tables** xx

**List of Abbreviations** xxiv

**List of Notations** xxvi

**1 Introduction** 1

1.1 Thesis Objectives . . . . . 5

1.2 Thesis Outline . . . . . 6

**2 Literature Review** 7

2.1 History of Biodiesels and their Potential Applications . . . . . 7

2.1.1 Techniques . . . . . 8

2.1.2 Biodiesel Resources . . . . . 10

2.1.3 Potential and Limitations of Biodiesel . . . . . 12

2.1.4 Diesel Blend Specifications . . . . . 12

2.1.5 Cetane Number of Biodiesels . . . . . 14

2.2 Recent Works on Spray Combustion . . . . . 15

2.3 Emissions in Biofuels . . . . . 17

2.4 Summary of the Literature Review . . . . . 21

**3 Research Methodology** **23**
3.1 Introduction . . . 23
3.2 Steady RANS Combustion Modelling . . . 24
3.2.1 Species ($\widetilde{u_i'' Y_k''}$) and Enthalpy ($\widetilde{u_i'' h_s''}$) Turbulent Fluxes . . 26
3.2.2 Laminar Diffusive Fluxes for Species or Enthalpy . . . 27
3.2.3 Pressure-Velocity Correlation $\overline{u_i'' \partial p / \partial x_i}$ . . . 27
3.3 Turbulence Model . . . 27
3.4 Combustion of Liquid Fuels (Spray Combustion) . . . 29
3.4.1 Reaction Mechanisms and Parameters that Influence their Consideration . . . 31
3.4.2 Governing Equations for $NO_x$ Transport . . . 35
3.4.3 Combustion Model - The Laminar Flamelt Model (LFM) . 35
3.4.4 Atomiser Model: The Air-Blast/Air-Assist Atomizer Model 38
3.4.5 The Pressure-Swirl Atomizer Model Theory . . . 39
3.4.5.1 Film Formation . . . 40
3.4.5.2 Sheet Breakup and Atomization . . . 41
3.4.6 Chemical Mechanisms . . . 44
3.5 Radiation Model . . . 44
3.6 Benchmark and Computational Model . . . 45

**4 Results and Discussion: EXGAS Reaction Model (EGRM) Validation Using Methanol** **52**
4.1 Validation of the CFD Results Using Temperature . . . 53
4.2 SDRM - Profiles of Other Relevant Parameters . . . 58
4.2.1 Profiles of Relevant Turbulence Parameters . . . 58
4.2.2 Profiles of Carbon Oxides ($CO$ and $CO_2$) at the Exit and within the Flame Region . . . 63
4.2.3 Profiles of Fuel ($CH_3OH$) within the Flame Region . . . 69
4.2.4 Profiles of Nitrogen Oxides within the Flame Region . . . 69
4.2.5 Profiles of Water Vapour within the Flame Region . . . 72
4.2.5.1 Profiles of Mean Mixture Fraction at the Exit and within the Flame Region . . . 75

4.3 Combustion Modelling of Methanol using EXGAS-generated and Modified Advanced Reaction Mechanism . . . . . 81
4.4 Temperature Field . . . . . 83
4.4.1 Turbulent Parameters . . . . . 90
4.5 Emissions . . . . . 94
4.6 Nitrogen Oxide . . . . . 99
4.7 Water Vapour . . . . . 100
4.8 PDF Variables . . . . . 102
4.8.1 Mixture Fraction . . . . . 102
4.8.2 Mixture Fraction Variance and Dissipation Rate . . . . . 103

**5 Combustion Modelling of Conventional fuels and Biofuels based on Advanced Reaction Mechanism 108**
5.1 Results and Discussion . . . . . 109
5.1.1 Temperature Field . . . . . 109
5.1.2 Turbulence Parameters . . . . . 114
5.1.2.1 Turbulence Reynolds Number . . . . . 114
5.1.2.2 Turbulence Intensity . . . . . 115
5.1.3 Emissions . . . . . 117
5.1.3.1 Carbon Dioxide ($CO_2$) . . . . . 117
5.1.3.2 Nitrogen Oxides ($NO$ and $NO_x$) . . . . . 119
5.1.3.3 Water Vapour ($H_2O$) . . . . . 120
5.1.3.4 Diesel $C_{12}H_{26}$ Concentration: . . . . . 123
5.1.3.5 PDF Variables: Mixture Fraction . . . . . 125
5.1.3.6 Mixture Fraction Variance and Dissipation Rate . 127
5.1.3.7 Other Relevant By-products . . . . . 128
5.2 Biodiesel Case Study . . . . . 131
5.2.1 Temperature Field . . . . . 133
5.2.2 Turbulence Parameters . . . . . 135
5.2.3 Emissions from Biodiesel Combustion Modelling . . . . . 139
5.2.3.1 Carbon Dioxide ($CO_2$) . . . . . 139
5.2.3.2 Water Vapour ($H_2O$) . . . . . 140
5.2.3.3 Nitrogen Oxides ($NO$ and $NO_x$) . . . . . 142

5.2.3.4 Concentration of Soot . . . 145
5.2.3.5 Fuel $C_{11}H_{22}O_2$ and PDF Variables . . . 145
5.2.3.6 Mixture Fraction Variance and Dissipation Rate . 149
5.3 Summary . . . 152

**6 Study of the Effect of Radiative Heat Transfer on the Outcome of the Combustion 155**
6.1 Temperature Field . . . 156
6.2 Turbulence Parameters . . . 158
6.3 Effect of Radiation Model on Emissions . . . 158
6.4 PDF Variables . . . 160
6.5 Summary . . . 164

**7 Biodiesel Analysis 167**
7.1 Physicochemical Properties of Biodiesel Fuels . . . 167
7.1.1 Density . . . 168
7.1.2 Viscosity . . . 170
7.1.2.1 Density - Viscosity Correlation . . . 172
7.1.3 Cetane Number . . . 175
7.1.4 Flash Point . . . 178
7.1.5 Low-Temperature Properties . . . 179
7.1.5.1 Cloud Point . . . 179
7.1.5.2 Pour Point Temperature . . . 181
7.1.6 Sulfer Content . . . 183
7.1.7 Water Content . . . 186
7.1.8 Acid Number . . . 188
7.1.9 Nitrogen Contents . . . 189
7.1.10 Boiling Point . . . 190
7.1.11 Oxygen Behavior and Stability . . . 193
7.2 Diesel Engine Anlysis . . . 197
7.2.1 Thermal Performance Analysis . . . 205
7.2.2 Emission Analysis . . . 208

**8 Conclusions and Recommendations for Further Work** **214**
8.1 Recommendation for further work . . . . . 217

**References** **219**

**Appendix A: San Diego Mechanism - Methanol** **239**

**Appendix B: EXGAS Mechanism - Methanol** **245**

**Appendix C: EXGAS Mechanism - Decane (Diesel)** **260**

# List of Figures


1.1 World marketed energy use, in quadrillion Btu, by fuel type, 1990–2035 (International Energy Outlook, 2010 [2]). . . . . 1
1.2 World oil production (World Energy Outlook, 2010 [3]). . . . . 2
1.3 WEO oil prices projection for 2010–2035 (World Energy Outlook, 2010 [3].) . . . . . 3

2.1 Illustration of the transesterification process [6]. The idea is to transform a triglyceride into a fatty acid methyl ester. The triglyceride is a glyceride (oil/fat) with three fatty acids. Here, R1, R2, and R3 represent the fatty acids. . . . . 9
2.2 Break-down of different feedstocks for biodiesel. The results are displayed in ascending order of saturated fatty acid content [42]. . 11
2.3 Chemical structure for (a) methyl decanoate and (b) decane. . . . 19

3.1 Energy conversion cycle . . . . . 30
3.2 Closures of the chemical source term in terms of its relationship to the joint composition Probability Density Function (PDF). . . . . 33
3.3 General description of the EXGAS system . . . . . 34
3.4 Atomiser (Fluent) . . . . . 39
3.5 Burner CAD model . . . . . 47
3.6 Meshed 3D model . . . . . 47
3.7 Inner view of the meshed burner model . . . . . 48
3.8 A central slice of the meshed model . . . . . 48
3.9 Vertical lines locations . . . . . 50
3.10 Horizontal lines locations . . . . . 51

4.1 Vertical temperature location . . . . . 54
4.2 Comparison between the computational results using San Diego Mechanism and the experimental data. . . . . 55
4.3 Temperature profiles corresponding to the (a) horizontal lines shown in Fig. 3.10 and (b) vertical lines shown in Fig. 3.9. (c) Cross-sectional temperature profiles close to the injector. (d) Temperature contours for a central slice. . . . . 56
4.4 Turbulent Reynolds number profiles corresponding to the (a) vertical lines shown in Fig. 3.9 and (b) horizontal lines shown in Fig. 3.10. Velocity profiles corresponding to the (c) horizontal lines shown in Fig. 3.10 and (d) vertical lines shown in Fig. 3.9. . 60
4.5 Turbulent Reynolds number (a) profiles close to the injector, and (b) for a central (x,y)-plane. Turbulent intensity (c) profiles close to the injector, and (d) number for a central (x,y)-plane. . . . . 62
4.6 Experimental and Computational Fluid Dynamics (CFD) (San Diego Reaction Mechanism (SDRM) model) results for $CO_2$ . . . 64
4.7 $CO_2$ profiles corresponding to the (a) horizontal lines shown in Fig. 3.10 and (b) vertical lines shown in Fig. 3.9. (c) Cross-sectional profiles of $CO_2$ close to the injector. (d) Mole fraction of $CO_2$ for a central (x,y)-plane ($z = 0$) . . . . . 65
4.8 Experimental and CFD (SDRM model) results for $CO$ . . . . . 66
4.9 $CO$ profiles corresponding to the (a) horizontal lines of Fig. 3.10, and (b) vertical lines of Fig. 3.9.(c) Cross-sectional profiles of $CO$ close to the injector. (d) Mole fraction of $CO$ for a central (x,y)-plane ($z = 0$) . . . . . 68
4.10 Fuel ($CH_3OH$) profiles close to the injector - SDRM model . . . . 69
4.11 $NO_x$ ($N_2O$) profiles corresponding to the (a) vertical lines shown in Fig. 3.9 and (b) horizontal lines shown in Fig. 3.10. . . . . 71
4.12 Horizontal line all - soot mole fraction . . . . . 73
4.13 Water vapour profiles corresponding to the (a) vertical lines shown in Fig. 3.9 and (b) horizontal lines shown in Fig. 3.10. Water vapour (c) cross-sectional profiles close to the injector and (d) profiles corresponding to a central (x,y)-plane. . . . . 74

4.14 Mean mixture fraction profiles corresponding to the (a) horizontal lines shown in Fig. 3.10 and (b) vertical lines shown in Fig. 3.9. Mean mixture fraction for a central ($z = 0$) (c) cross sectional profile starting at $y = 0.2m$ and (d) (x,y)-plane. . . . . 77
4.15 Mixture fraction variance for a (a) vertical profile at the exit region, (b) span-wise cross-sectional profile starting at $y = 0.2m$, and (c) central slice SDRM. . . . . 79
4.16 Scalar dissipation for (a) vertical profile at exit region, (b) span-wise cross-sectional profiles starting at $y = 0.2m$, and (c) central slice SDRM . . . . . 80
4.17 Temperature profiles corresponding to the (a) horizontal lines shown in Fig. 3.10, (b) vertical lines shown in Fig. 3.9, and (c) cross-sectional profile close to the injector. (d) Temperature contours for a central slice. . . . . 89
4.18 Turbulent Reynolds number profiles corresponding to the (a) vertical lines shown in Fig. 3.9, (b) horizontal lines shown in Fig. 3.10, (c) central (x,y)-plane using EXGAS Reaction Model (EGRM), and (d) close to the injector using EGRM. . . . . 91
4.19 Velocity profiles close to the injector using (a) SDRM and (b) EGRM. EGRM based (c) turbulent intensity profiles close to the injector and (d) turbulent intensity number for a central (x,y)-plane. 92
4.20 $CO_2$ comparison between the experimental, SDRM and EGRM simulations . . . . . 95
4.21 $CO_2$ profiles corresponding to the (a) vertical lines shown in Fig. 3.9 and (b) horizontal lines shown in Fig. 3.10. (c) Cross-sectional profiles of $CO_2$ close to the injector. (d) Mole fraction of $CO_2$ for a central (x,y)-plane ($z = 0$). . . . . 96
4.22 Cross-sectional profiles of $CH_3OH$ close to and above the injector for (a) EGRM and (b) SDRM. EGRM based $NO_x$ ($N_2O$) profiles corresponding to the (c) vertical lines shown in Fig. 3.9 and (d) horizontal lines shown in Fig. 3.10. . . . . 98

4.23 Water vapour profiles corresponding to the (a) vertical lines shown in Fig. 3.9 and (b) horizontal lines shown in Fig. 3.10. (c) Water vapour cross-sectional profiles close to the injector. (d) Water vapour profiles corresponding to a central (x,y)-plane. . . . . 101
4.24 Mean mixture fraction profiles corresponding to the (a) horizontal lines shown in Fig. 3.10 and (b) vertical lines shown in Fig. 3.9. Mean mixture fraction for a central ($z = 0$) (c) cross-sectional profile starting at $y = 0.2m$ and (d) (x,y)-plane. . . . . 104
4.25 Mixture fraction variance (a) for a vertical profile at the exit region, (b) for a span-wise cross-sectional profile starting at $y = 0.2m$, and (c) contours for a central slice. . . . . 106
4.26 Scalar dissipation (a) for a vertical profile at the exit region, (b) for a span-wise cross-sectional profile starting at $y = 0.2m$, and (c) contours for a central slice. . . . . 107

5.1 Diesel CFD simulations using EGRM-diesel: Temperature profiles corresponding to (a) vertical lines shown in Fig. 3.9, (b) horizontal lines shown in Fig. 3.10, and (c) cross-sectional profiles starting at $0.2m$ from the burner bottom wall at $0.05m$ increment along the vertical axis, and (d) Temperature contours for a central slice. . . 113
5.2 Diesel CFD simulations using EGRM-diesel: Turbulence Reynolds number profiles corresponding to (a) vertical lines shown in Fig. 3.9, (b) horizontal lines shown in Fig. 3.10, and (c) cross-sectional profile starting at $0.2m$ from the burner bottom wall at $0.05m$ increment along the vertical axis, and (d) Turbulence Reynolds number contours for a central slice. . . . . 116
5.3 Diesel CFD simulations using EGRM-diesel: Turbulence intensity profiles corresponding to the (a) vertical lines at the burner exit (Fig. 3.9), (b) cross-sectional profiles starting at $0.2m$ from the burner bottom wall at $0.05m$ increment along the vertical axis, and (c) contours for a central slice. . . . . 118
5.4 $CO_2$ comparison between the experimental, SDRM and EGRM simulations for methanol and diesel. . . . . 120

5.5 Diesel CFD simulation using EGRM-diesel: $CO_2$ mole fraction profiles corresponding to (a) vertical lines shown in Fig. 3.9, (b) horizontal lines shown in Fig. 3.10, (c) cross-sectional profiles starting at $0.2m$ from the burner bottom wall at $0.05m$ increment along the vertical axis, and (d) contours for a central slice. . . . . 121
5.6 Diesel CFD simulations using EGRM-diesel: Nitrogen oxide ($NO$) mole fraction profiles corresponding to the (a) vertical lines shown in Fig. 3.9, (b) horizontal lines shown in Fig. 3.10, and (c) central (x,y)-plane showing contours. . . . . 122
5.7 Diesel CFD simulation using EGRM-diesel: Water vapour ($H_2O$) mole fraction profiles corresponding to (a) vertical lines shown in Fig. 3.9, (b) horizontal lines shown in Fig. 3.10, (c) cross-sectional profiles starting at $0.2m$ from the burner bottom wall at $0.05m$ increment along the vertical axis, and (d) contours for a central slice. 124
5.8 Diesel CFD simulation using EGRM-diesel: Fuel ($C_{12}H_{26}$) mole fraction profile corresponding to the (a) vertical lines shown in Fig. 3.9, (b) cross-sectional profiles starting at $0.2m$ from the burner bottom wall at $0.05m$ increment along the vertical axis, and (c) contours for a central slice. . . . . 126
5.9 Diesel CFD simulation using EGRM-diesel: Mean mixture fraction profiles corresponding to the (a) vertical lines in Fig. 3.9, (b) horizontal lines shown in Fig. 3.10, (c) cross-sectional profiles starting at $0.2m$ from the burner bottom wall at $0.05m$ increment along the vertical axis, and (d) contours for a central slice. . . . . 129
5.10 Diesel CFD simulation using EGRM-diesel: Mean mixture fraction variance profiles corresponding to the (a) vertical lines of Fig. 3.9, (b) horizontal lines of Fig. 3.10, (c) cross-sectional profiles starting at $0.2m$ from the burner bottom wall at $0.05m$ increment along the vertical axis, and (d) contours for a central slice. . . . . 130

5.11 Diesel CFD simulation using EGRM-diesel: Scalar dissipation profiles corresponding to the (a) vertical lines of Fig. 3.9, (b) horizontal lines of Fig. 3.10, (c) cross-sectional profiles starting at $0.2m$ from the burner bottom wall at $0.05m$ increment along the vertical axis, and (d) contours for a central slice. . . . . 131
5.12 Contours for mole fraction of (a) hydrogen at a central (x,y) slice, (b) R1H radical at a central (x,y) slice, (c) R2OH radical at a central (x,y) slice, and (d) RC3H radical at a central (x,y) slice. . 132
5.13 Biodiesel CFD simulation using EGRM: Temperature profiles corresponding to the (a) vertical lines shown in Fig. 3.9, (b) horizontal lines shown in Fig. 3.10, (c) cross-sectional profiles starting at $0.2m$ from the burner bottom wall at $0.05m$ increment along the vertical axis, and (d) contours for a central slice. . . . . 136
5.14 Biodiesel CFD simulation using EGRM: Turbulence e Reynolds number profiles corresponding to the (a) vertical lines shown in Fig. 3.9, (b) horizontal lines shown in Fig. 3.10, (c) cross-sectional profiles starting at $0.2m$ from the burner bottom wall at $0.05m$ increment along the vertical axis, and (d) contours for a central slice. 137
5.15 Biodiesel CFD simulation using EGRM: Turbulence intensity profiles corresponding to the (a) vertical lines in Fig. 3.9, (b) horizontal lines shown in Fig. 3.10, (c) cross-sectional profiles starting at $0.2m$ from the burner bottom wall at $0.05m$ increment along the vertical axis, and (d) contours for a central slice. . . . . 138
5.16 $CO_2$ comparison between the experimental, SDRM and EGRAM simulations for methanol, diesel and biodiesel . . . . . 140
5.17 Biodiesel CFD simulation using EGRM: $CO_2$ profiles corresponding to the (a) vertical lines of Fig. 3.9, (b) horizontal lines shown in Fig. 3.10, (c) cross-sectional profiles starting at $0.2m$ from the burner bottom wall at $0.05m$ increment along the vertical axis, and (d) contours for a central slice. . . . . 141

5.18 Biodiesel CFD simulation using EGRM: Water vapour ($H_2O$) profiles corresponding to the (a) vertical lines shown in Fig. 3.9, (b) horizontal lines shown in Fig. 3.10, (c) cross-sectional profiles starting at $y = 0.2m$ from the burner bottom wall at $0.05m$ increment along the vertical axis, and (d) contours for a central slice. . . . . 143
5.19 Biodiesel CFD simulation using EGRM-biodiesel: Nitrogen oxide ($NO$) mole fraction profiles corresponding to the (a) vertical lines shown in Fig. 3.9, (b) horizontal lines shown in Fig. 3.10, and (c) contours for a central (x,y)-plane. . . . . 144
5.20 Biodiesel CFD simulation using EGRM-biodiesel: Soot mole fraction profiles corresponding to the (a) vertical lines shown in Fig. 3.9, (b) horizontal lines shown in Fig. 3.10, and (c) contours for a central (x,y)-plane. . . . . 146
5.21 Biodiesel CFD simulation using EGRM-biodiesel: Mole fraction of biodiesel ($C_{11}H_{22}O_2$ profiles corresponding to the (a) vertical lines shown in Fig. 3.9, (b) horizontal lines shown in Fig. 3.10, (c) cross-sectional profiles starting at $0.2m$ from the burner bottom wall at $0.05m$ increment along the vertical axis., (d) contours for a central slice. . . . . 148
5.22 Biodiesel CFD simulation using EGRM-biodiesel: Mean mixture fraction profiles corresponding to the (a) vertical lines shown in Fig. 3.9, (b) horizontal lines shown in Fig. 3.10, (c) cross-sectional profiles starting at $0.2m$ from the burner bottom wall of $0.05m$ increment along the vertical axis, and (d) contours for a central slice. 150
5.23 Biodiesel CFD simulation using EGRM-biodiesel: Dissipation rate corresponding to the (a) vertical lines shown in Fig. 3.9, (b) horizontal lines shown in Fig. 3.10, (c) cross-sectional profiles starting at $0.2m$ from the burner bottom wall of $0.05m$ increment along the vertical axis, and (d) contours for a central slice. . . . . 151

5.24 Biodiesel CFD simulation using EGRM-biodiesel: Mean mixture fraction variance profiles corresponding to the (a) vertical lines shown in Fig. 3.9, (b) horizontal lines shown in Fig. 3.10, (c) cross-sectional profiles starting at $0.2m$ from the burner bottom wall at $0.05m$ increment along the vertical axis, and (d) contours for a central slice. . . . . 153

6.1 Temperature profiles corresponding to the (a) vertical lines shown in Fig. 3.9, (b) horizontal lines shown in Fig. 3.10, and (c) cross-sectional profiles close to the injector (starting at $y = 0.2m$), and (d) contours for a central (x,y)-plane. . . . . 157
6.2 Turbulence Reynolds number profiles corresponding to the (a) vertical lines shown in Fig. 3.9, (b) horizontal lines shown in Fig. 3.10, (c) cross-sectional profiles close to the injector (starting at $y = 0.2m$), and (d) contours for a central (x,y)-plane. . . . . 159
6.3 Carbon Dioxide ($CO_2$) profiles corresponding to the (a) vertical lines shown in Fig. 3.9, (b) horizontal lines shown in Fig. 3.10, (c) cross-sectional profiles close to the injector (starting at $y = 0.2m$), and (d) contours for a central (x,y)-plane. . . . . 161
6.4 Water vapour ($H_2O$) profiles corresponding to the (a) vertical lines shown in Fig. 3.9, (b) horizontal lines shown in Fig. 3.10, (c) cross-sectional profiles close to the injector (starting at $y = 0.2m$), and (d) contours for a central (x,y)-plane. . . . . 162
6.5 Mean mixture fraction profiles corresponding to the (a) horizontal lines shown in Fig. 3.10, (b) cross-sectional profiles close to the injector (starting at $y = 0.2m$), and (c) contours for a central (x,y)-plane. . . . . 164
6.6 Mixture fraction variance profiles corresponding to the (a) vertical lines shown in Fig. 3.9, (b) horizontal lines shown in Fig. 3.10, (c) cross-sectional profile close to the injector (starting at $y = 0.2m$), and (d) contours for a central (x,y)-plane. . . . . 165

7.1 Viscosity variation . . . . . 173
7.2 (a) Density relation. (b) Viscosity relation. . . . . 174

7.3 Relationship between density and viscosity of diesel-biodiesel mixture. . . . 175
7.4 Cetane index variation . . . 177
7.5 (a) Flash Point (FP) variation. (b) Cloud Point (CP) variation . . 182
7.6 Pour Point (PP) variation . . . 183
7.7 Transesterification process and biodiesel production . . . 185
7.8 (a) Sulfur content variation, (b) Water content variation, (c) Acid number, and (d) Nitrogen content . . . 191
7.9 Boiling point . . . 192
7.10 Transmittance wave number spectra for diesel, biodiesel, B10 and B20. . . . 198
7.11 Transmittance wave number spectra for B30 and B40, B50 and B60. 199
7.12 Transmittance wave number spectra for B70 and B80, B90 and (diesel fuel (DF), biodiesel (BD), B20, B40, B60 and B80) in one graph. . . . 200
7.13 Transmittance wave number spectra for B10 and B20, B30 and B40 before and after ten days storage period. . . . 201
7.14 Transmittance wave number spectra for B50 and B60, B70 and B80 before and after ten days storage period. . . . 202
7.15 (top-left) Ford Transit 4-Stroke DI Diesel Engine & Dynamometer, (top-right) Fuel mixing tank and , (bottom-left) Fuel Meter, (bottom-right) Total Unburned Hydrocarbon (THC) and $NO_x$ Emission Analyser . . . 204
7.16 Schematic Diagram of Experimental Setup . . . 205
7.17 (a) Indicated power, (b) Air/Fuel (A/F) ratio, (c) Specific fuel consumption, and (d) Brake thermal efficiency . . . 207
7.18 (a) Carbon monoxide ($CO$) and (b) Nitrogen oxide ($NO$). . . . 210
7.19 (a) Carbon dioxide ($CO_2$) and (b) Nitrogen oxide ($NO_x$) . . . 211
7.20 (a) Bosch opacity, (b) Bosch smoke number, and (c) Total unburned hydrocarbon. . . . 213

# List of Tables


1.1 EU emission standards for diesel and petrol passenger cars . . . . 3

2.1 American Society for Testing and Materials (ASTM) D7467 Specification for diesel blends B6 to B20 [42]. . . . . 13

2.2 Statistics of effects of pure biodiesel on engine performances and emissions ([79]) . . . . . 18

3.1 Operating conditions for the baseline experiment of Widmann and Presser [1] . . . . . 50

4.1 Temperature data at the exit: experimental data and CFD results 54

5.1 Fuel properties of ordinary diesel and common vegetable based biodiesel (Arbab *et al.* [133] and Sadeghinezhad *et al.* [134]) . . . 110

7.1 Density of diesel fuel (DF), biodiesel (BD) and nine surrogate fuels. 168

7.2 Viscosity, density and FP measurements of eight vegetable oil methyl esters [136] . . . . . 169

7.3 Viscosity, density and FP measurements of ten vegetable oils [37] 169

7.4 Viscosity of diesel fuel (DF), biodiesel (BD) and nine surrogate fuels (B10–B90) . . . . . 172

7.5 Viscosity, density and FP measurements of oil methyl esters (Sridharan and Mathai [136]) . . . . . 173

7.6 Cetane Number (CN) of diesel fuel (DF), biodiesel (BD) and nine surrogate fuels (B10–B90) . . . . . 176

7.7 Measured and calculated CP (in degrees Kelvin) of biodiesel fuel from various oils/fats feedstocks with their fatty acid composition [147] . . . . . 180
7.8 CP for diesel (DF), biodiesel (BD) and surrogate fuels (B10–B90) 181
7.9 PP for biodiesel B2 and biodiesel fuels blends (four replicates) [148] 181
7.10 Physicochemical properties of biodiesel fuels Hideki et al. [143] . . 184
7.11 Sulfur content for diesel fuel (DF), biodiesel (BD) and surrogate fuels (mg/kg) . . . . . 186
7.12 Water content of diesel fuel (DF), biodiesel (BD) and surrogate fuels (B10–B90)(mg/kg) . . . . . 187
7.13 Water content for diesel fuel (DF), biodiesel (BD) and surrogate fuels (mg/kg) . . . . . 189
7.14 Nitrogen content for diesel fuel (DF), biodiesel (BD) and surrogate fuels (B10–B90)(mg/kg) . . . . . 189
7.15 Characteristic infrared absorption wavenumbers of some functional groups . . . . . 195
7.16 Substitution patterns of the banzene ring . . . . . 196
7.17 Diesel engine specifications . . . . . 205

# List of Abbreviations

| | |
|---|---|
| ASTM | American Society for Testing and Materials. xix, 8, 13–15, 110, 166, 168, 174–176, 179, 181–183, 186, 190, 191, 213 |
| BMEP | Brake Mean Effective Pressure. 202, 204 |
| BP | Boiling Point. 13, 188, 190 |
| BTE | Beef Tallow Ester. 10 |
| CFD | Computational Fluid Dynamics. ii, xi, xiii–xvii, xix, 22, 23, 49, 53–55, 58, 59, 63, 64, 66, 67, 69, 78, 81, 87, 100, 109, 114, 116, 118, 121, 122, 124, 126, 129–131, 136, 137, 139, 141, 143, 144, 146, 148, 150, 151, 153, 154, 204, 205, 207, 212, 215, 216 |
| CIE | Compression Ignition Engine. iii, 6, 13, 14, 16–18, 21, 40, 138, 142, 165, 169, 170, 173, 174, 177, 201, 204, 207, 209, 212, 215, 216 |
| CME | Canola Methyl Ester. 10 |
| CN | Cetane Number. xix, 9, 13–15, 110, 166, 173–176, 182, 191, 214 |
| CP | Cloud Point. xviii, xx, 9, 14, 166, 177–180, 182, 214 |
| CVCA | Constant Volume Combustion Apparatus. 191 |

| | |
|---|---|
| DNS | Direct Numerical Simulation. 103, 149 |
| EDC | Eddy Dissipation Concept. 22, 63 |
| EGRM | EXGAS Reaction Model. xii–xvii, 52, 83–85, 87, 88, 90–95, 97–100, 102–105, 109, 110, 112–122, 124, 126, 127, 129–131, 133, 134, 136–141, 143, 144, 146–151, 153, 210 |
| FP | Flash Point. xviii, xix, 14, 110, 166, 167, 171, 176, 177, 180, 182 |
| FTIR | Fourier Transform Infrared Spectroscopy. 63, 192, 214 |
| HCCI | Homogeneous Charge Compression Ignition. 4 |
| HHV | Higher Heating Value. 166 |
| ICE | Internal Combustion Engine. 16, 19, 21, 82, 195 |
| IEO2010 | International Energy Outlook 2010. 1 |
| LES | Large Eddy Simulation. ii, 78, 103, 149, 215 |
| LFM | Laminar Flamelet Model. 24, 35, 36 |
| LISA | Linearized Instability Sheet Atomization. 40 |
| LME | Linseed Methyl Ester. 10 |
| NFPA | National Fire Protection Association. 177 |
| NREL | National Renewable Energy Lab. 214 |
| OSI | Oil Stability Index. 191 |
| PDF | Probability Density Function. x, 34, 36, 37 |
| PP | Pour Point. xviii, xx, 166, 177, 179, 181, 214 |

| | |
|---|---|
| RANS | Reynolds-Averaged Navier-Stokes. 23–25, 45 |
| RME | Rapeseed Methyl Ester. 10 |
| SDRM | San Diego Reaction Mechanism. xi–xv, 52–54, 56, 57, 61, 63, 64, 66, 67, 69, 72, 76, 79–81, 83–85, 87, 88, 90–95, 97–100, 102, 103, 105, 112, 113, 115, 117–120, 123, 125, 127, 138, 140 |
| SFC | Specific Fuel Consumption. 205 |
| SLFM | Steady Laminar Flamelet Model. 22, 24 |
| SME | Sunflower Methyl Ester. 10 |
| SST | Shear Stress Transport. ii, 24, 27, 28 |
| ULFM | Unsteady Laminar Flamelet Model. 24 |
| WEO2010 | World Energy Outlook 2010. 2 |

# List of Notations

| | |
|---|---|
| $C$ | Linear Anisotropic Phase Function Coefficient. 44, 45 |
| $G$ | Incident Radiation. 44 |
| $I$ | Radiation Intensity. 44 |
| $N$ | Total Number of Species. 26 |
| $P_k$ | Turbulence Energy. 29 |
| $S$ | Strain Rate Tensor. 26, 28 |
| $Sc_{kt}$ | Turbulent Schmidt Number for Species k. 27 |
| $U$ | Velocity. 41 |
| $Z_i$ | Elemental Mass Fraction for Element $i$. 75 |
| $\Delta H$ | Enthalpy of Reaction. 32 |
| $\Delta\phi$ | Difference Between the Azimuthal Stop and Start Angles. 40 |
| $\Omega$ | Maximum Growth Rate. 42 |
| $\alpha$ | Absorption Coefficient. 44 |
| $\dot{m}_{eff}$ | Effective Mass Flow Rate. 40 |
| $f$ | Mixture Fraction. 23 |
| $\eta_0$ | Initial Wave Amplitude. 41 |
| $\mu$ | Laminar Dynamic Viscosity. 26 |
| $\mu_t$ | Turbulent Viscosity. 27 |
| $\nu$ | Kinematic Viscosity. 29 |
| $\omega$ | Magnitude of the Vorticity Vector. 29 |
| $\overline{D}$ | Mean Species Molecular Diffusion Coefficient. 27 |
| $\overline{\lambda}$ | Mean Thermal Diffusivity. 27 |

| | |
|---|---|
| $\sigma$ | Stefan-Boltzmann Constant. 45 |
| $\sigma_s$ | Scattering Coefficient. 44 |
| $\tau_{i,j}$ | Viscous Stress Tensor. 25 |
| $\theta$ | Spray Angle. 41 |
| $d_{inj}$ | Injector Exit Diameter. 40 |
| $e_w$ | Wall Emissivity. 45 |
| $k_v$ | Velocity Coefficient. 41 |
| $q_{r,w}$ | Flux of the Radiation at Walls. 45 |
| $q_r$ | Radiation Flux. 44 |
| $t$ | Thickness of a film. 40 |
| $u$ | Axial Component of Velocity at the Injector Exit. 40 |
| $y$ | Normal Distance to the Nearest Wall. 29 |

# Chapter 1

# Introduction

Energy is a vital component for the existence of human, marine, plant, and all other forms of biological life on planet earth. In addition, energy is the main driving momentum for all technological advances that have been achieved so far and based on which nations and societies can be classified as developed, developing or under-developed. Every economy needs energy not only to power it and sustain its growth but also to make life possible and comfortable in harsh climates.

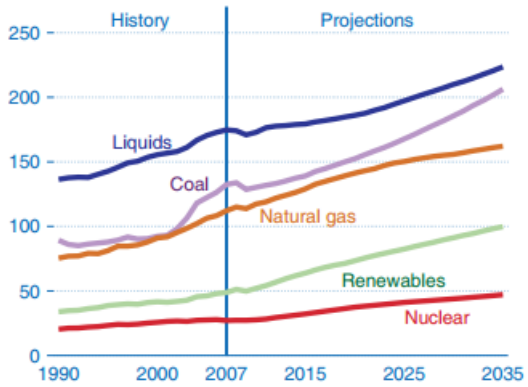


Figure 1.1: World marketed energy use, in quadrillion Btu, by fuel type, 1990–2035 (International Energy Outlook, 2010 [2]).

Global energy demand is probably growing on daily basis and huge energy resources may be required to sustain the needs of different nations in the future. An estimate of global energy need and its projection in the near future can be seen in Fig. 1.1 [2]. The International Energy Outlook 2010 (IEO2010) projection

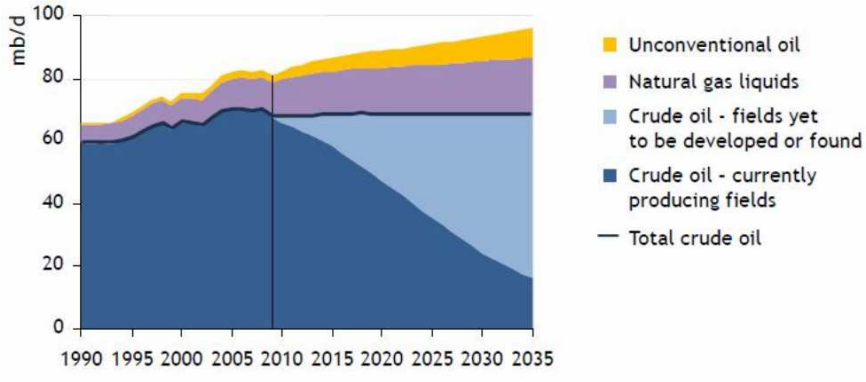


Figure 1.2: World oil production (World Energy Outlook, 2010 [3]).

indicates that the total world consumption of marketed energy is expected to increase by 49% from 2007 to 2035 as seen from Fig. 1.1. Fossil fuels will remain the primary sources of energy and oil will remain the single largest fuel in the structure of the world energy. However, the projection of the world oil production shown in Fig. 1.2 does not convey enough optimism that the expected outcome (yet to be discovered oil) would satisfy the needs from crude oil. Not only that, with reference to the World Energy Outlook 2010 (WEO2010) report [3], the projection of prices of crude petroleum indicates that the barrel may cost over $200 in 2028 and continue to rise up to the year 2035 (Fig. 1.3). Not only there is a concern about the future availability and cost of conventional fuels, the need to reduce the emission of gases which are harmful for the health and the atmosphere are all creating the need for putting pressure on the consumption of petroleum-based conventional fuels. For example, the new emission standards set for European vehicles is shown in Table 1.1.

Table 1.1 shows, Euro 4 emissions standards implemented in 2005 mandate maximum Particulate Matter (PM) emissions be less than 0.025 g/km (0.04 g/mile), and $NO_x$ emissions be less than 0.25 g/km (0.40 g/mile) (EPC, 98/69/EC [4]). Euro 5 legislation that came into effect for new cars in 2009 and existing models in 2011, reduces these limits considerably, to 0.005 g/km (0.008 g/mile) for PM emissions and 0.18 g/km (0.29 g/mile) for $NO_x$ emissions (EPC, 715/2007 [5]). Euro 6 regulations further reduces these limits for diesel passenger cars starting in 2014 for new platforms and 2015 for existing vehicles. The Euro 6 emissions

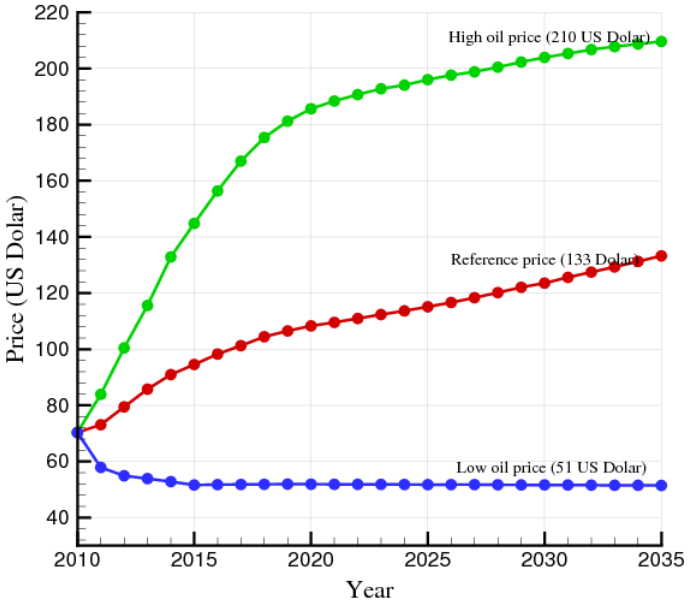


Figure 1.3: WEO oil prices projection for 2010–2035 (World Energy Outlook, 2010 [3].)

Table 1.1: EU emission standards for diesel and petrol passenger cars

| Compression Ignition (Diesel) | | | | | | | |
|---|---|---|---|---|---|---|---|
| Standard | Date | $CO$ | $HC$ | $HC+NO_x$ | $NO_x$ | $PM$ | $PN$ |
| | g/km | | | | | | #km |
| Euro 4 | 2005 | 0.50 | - | 0.3 | 0.25 | 0.025 | - |
| Euro 5a | 2009 | 0.50 | - | 0.23 | 0.18 | 0.005 | - |
| Euro 5b | 2011 | 0.50 | - | 0.23 | 0.18 | 0.005 | $6.0\times10^{11}$ |
| Euro 6 | 2014 | 0.50 | - | 0.17 | 0.08 | 0.005 | $6.0\times10^{11}$ |
| Spark ignition (Gasoline) | | | | | | | |
| Euro 4 | 2005 | 1.0 | 0.1 | - | 0.08 | - | - |
| Euro 5 | 2009 | 1.0 | 0.1 | - | 0.06 | 0.005 | - |
| Euro 6 | 2014 | 1.0 | 0.1 | - | 0.06 | 0.005 | - |

limits are 0.080 g/km (0.13 g/mile) of $NO_x$, and 0.003 g/km (0.005 g/mile) of particulates, with a new limit on the number of particles added as well (EPC, 715/2007 [5]).

Fossil fuels (from crude petroleum) take millions of years to form and are non-renewable resources, the reserves of which are being depleted faster than they are being regenerated. Thus, such sources are limited, and are expected to exhaust in the near future. Add to this, the production and transport of fossil fuels is currently surrounded by many security issues which might be one of the reasons for their high prices. All these factors combined raised the interest in various types of renewable energies. Therefore, it is important to explore alternative sources of renewable energy. These include: solar, wind, hydro, geothermal, biomass, hydrogen and nuclear etc.

Biofuels are an important class of renewable liquid fuels that have recently gained popularity. Such biofuels consist of large methyl and ethyl esters which are derived from vegetable and other oils [6]. For over two decades, research on these types of biofuels has operated well in diesel and Homogeneous Charge Compression Ignition (HCCI) engines. An interesting feature of the biodiesel is that the oxygen atoms embedded inside the biodiesel fuel molecule help to reduce the production of soot in diesel engines ([7] and [8]). Not only that, some experts believe that these types of fuels are more environment-friendly i.e., they reduce air pollution, slow-down the global warming, and address other sustainability issues etc. [9].

As mentioned above that fossil fuels will remain the primary sources of energy and oil will remain the single largest fuel in the structure of the world energy and the bulk of its increase will come mainly from the demand in the transport sector. All hydrocarbons (liquid and solid fuels) provide energy through the process of combustion. Combustion processes are very important in our day-to-day lives and in industries. They fulfil approximately 90% of our energy needs. For example, they are used in electrical power generation, heating, chemical industry, etc.). In spite of this importance, the basic working of combustion and the interactions of different combustion processes with each other are not fully recognized.

Biofuels are gaining grounds as an important source of energy especially in the transport sector. However, the chemical composition of these fuels differ from conventional fuels extracted from petroleum crude. An important difference was the existence of the oxygen element in them which may play some role in the combustion process. Indeed all combustion processes occur with oxygen but the

fact that oxygen is embedded in the composition of the fuel may influence the chemical reaction in a different way compared to the situation where oxygen in pumped to mix with the flow field before or during combustion. However, the current availability status of such fuels does not indicate that they will replace conventional fuels in the near future. Rather, the current trend is to mix biofuels (with certain percentages) with diesel to produce new surrogate fuels. The thermo-chemical and physical properties of such surrogate fuels are far from being established.

Referring to the difficulties in obtaining conventional fuels in the long run, there exists a need to run combustion processes more economically. Additionally, there exists the need to optimize either the operating or the geometrical parameters of the process in order to minimize environmental risks, e.g., the emission of unburned hydrocarbons.

Taking all the above facts into account, there are two main aims of this thesis. The first is to address the thermo-physicochemical properties of biofuels and surrogate fuels that are of interest to their combustion. The second aim is to perform computational and experimental work to study the combustion processes of biofuels and their surrogates in different platforms using reduced and advanced reaction mechanisms and to study the thermal and emission characteristics of such fuels.

## 1.1 Thesis Objectives

The thesis has the following objectives:

- Provide a comprehensive and critical review of the manufacturing processes of biofuels and shed some light on the nature of the produced biodiesel
- Establishment of thermochemical properties of biofuels: As a specific biodiesel will be used for experimentation in a CIE, two sub-objectives are:
  - Carry out some fundamental analysis and establish some properties of the biodiesel which would be later used in experimental work using CIE.

  - Produce a range of surrogate fuels (mixture between diesel and biodiesel) and establish the characteristics and thermo-physicochemical properties of such new fuels.

- Modelling of combustion process: Most of the combustion modelling whether on simple geometries or complex ones is based on simple and reduced reaction mechanism. Hence, the sub-objectives for this part are:

  - Develop an advanced and comprehensive reaction mechanism suitable for modelling both conventional and biofuels.
  - Model combustion process on simple burners using both reduced reaction mechanisms and advanced reaction mechanisms developed for this purpose and perform critical analysis of the results.

- CIE experiment: Perform experimental work using CIE using diesel, biodiesel and surrogate fuels and study the emission rates and thermal performance of the engine and optimises the surrogate fuels to give the best thermal performance and emission rates from CIE.

## 1.2 Thesis Outline

The rest of the thesis is organized in the following fashion:

Relevant literature is reviewed in Chapter 2. Chapter 3 briefly highlights the methods used and the benchmarks adopted in this study. Chapter 4 focuses on validating the computational results with the developed reaction mechanism while Chapter 5 discusses the results of modelling the combustion of dodecane (considered for representing petroleum diesel) and methyl ester (considered as a representation for biodiesel). Chapter 6 presents a study of the effect of radiative heat transfer on the outcome of the combustion process while Chapter 7 presents a study of the Physicochemical properties of biodiesel fuels and a study of the diesel engine. Conclusions and suggestions for further work are presented in Chapter 8.

# Chapter 2

# Literature Review

The scope, aims and objective of this thesis were mentioned in Chapter 1, Section 1.1. In order to build a strong background on the topics that cover the aims and objectives, a brief critical review is presented in this chapter to justify the work of this thesis. Moreover, information about biofuels including the manufacturing processes, expected properties as well as the recent history of using such fuels in different combustion structures and the output of such work will be discussed in this chapter.

## 2.1 History of Biodiesels and their Potential Applications

Biodiesel is quite old. In fact, when Rudolph Diesel first introduced his ideas for a new engine in 1893, he was of the opinion that he had designed something which could be fuelled easily by the farmers using the peanut oil. In 1990, he demonstrated his idea by using groundnut (peanut) oil as a fuel for his engine [10].

As is the case with conventional petroleum-based fuels, many different feedstocks and processes are allowed by ASTM to be used in the making of biodiesel. The ASTM has specified some requirements for making sure that B100 can be safely used in diesel engines. These sets of requirements are mainly independent of the type of feedstock and are based on performance. Different oils and fats can be used to make commerical biodiesel. These include:

- Animal fats: edible, inedible, and all other variations of tallow, lard, choice white grease, yellow grease, poultry fats, and fish oils
- Plant oils: soy, corn, canola, sunflower, rapeseed [11], cottonseed
- Recycled greases: used cooking oils and restaurant frying oils.

Other fats and conventional and recycled oils can be used in the making of biodiesel. For example mustard [12, 13], palm [14, 15, 16], coconut [17], peanut [18], olive, sesame [19], coriander seeds [20], safflower oils [21, 22], trap greases [23], and also oils made from algae [24, 25], fungi [26], bacteria, molds, and yeast [27]. The type of feedstock used, is of great importance. It determines many of the characteristics of finished biodiesel including its CN, CP, and stability.

### 2.1.1 Techniques

Many techniques have been developed for the making of biodiesel from different sources including vegetable oils, animal fats and other biological resources. Commonly, it is prepared with the help of esterification of the feedstock from fat or oil with methyl alcohol under alkaline conditions. The methyl esters produced as a result of this process are cleaned of their co-product, glycerol, and is isolated as biodiesel. The transesterification reaction takes place, regardless of whether a catalyst is present or not. It uses monohydric aliphatic alcohols (primary or secondary) having eighteen carbon atoms according to the relation:

$$Triglycerides + Monohydric\ alcohol \rightleftharpoons Glycerin + Monoalkyl\ esters \quad (2.1)$$

In the transesterification process, the free fatty acids of a triglyceride or a complex fatty acid are neutralized, glycerine is removed, and an alcohol ester is created. This reaction can be seen in Eq. 2.1 and Fig. 2.1. Transesterification reaction, theoretically, is in equilibrium. However, in this reaction, additional quantity of methanol was added to shift the equilibrium of the reaction to the right hand side of the equation and, as a result, produces more methyl esters. The rate

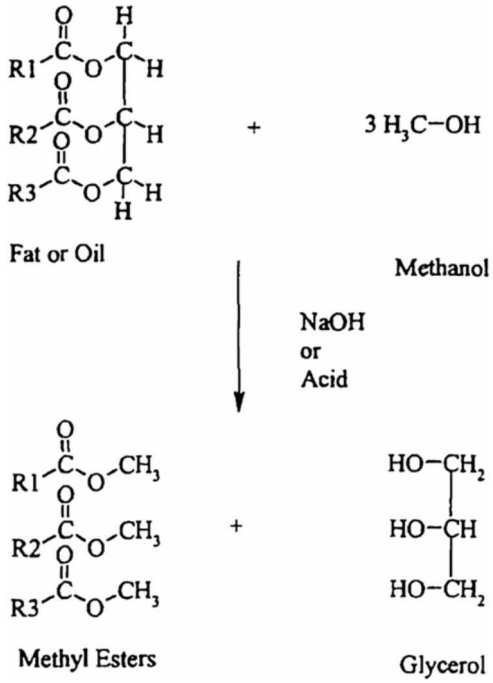


Figure 2.1: Illustration of the transesterification process [6]. The idea is to transform a triglyceride into a fatty acid methyl ester. The triglyceride is a glyceride (oil/fat) with three fatty acids. Here, R1, R2, and R3 represent the fatty acids.

of reaction and the yield can generally be improved with the use of a catalyst. The paragraphs below shed some light on this process adopted by different researchers. There are many recent and old review papers in biodiesel production including the manuscripts by Dixit et al. [28] and Garcia-Perez et al. [29]. Other review papers combined the capacity of biodiesel production worldwide and impact of societal policies that may impact the rate of production of biodiesel ([30]).

Many techniques have been used in biodiesel production. Few examples to mention include the work of Ahn et al. [31] who employed a two-stage reaction to make biodiesel by converting methyl esters from different sources (including Canola Methyl Ester (CME), Rapeseed Methyl Ester (RME), Linseed Methyl Ester (LME), Beef Tallow Ester (BTE) and Sunflower Methyl Ester (SME)) into biodiesel in a synthesized batch reactor. The catalysts used during the process include sodium hydroxide, potassium hydroxide and sodium methoxide. In contrast, Cvengro and Povaz's approach [11] to biodiesel production involves a two-step low-temperature transesterification of cold pressed rapeseed oil with

methanol at temperatures range. Crabbe et al.'s study [32] focused on the effect of molar ratio of methanol and oil, the quantity of catalyst and the reaction temperature on the yield of acid-catalysed production of methyl ester (biodiesel) from crude palm oil. According to Zhang et al. [33], the acid-catalysed process using waste cooking oil is technically feasible and is less complex compared to the alkali-catalysed process using waste cooking oil. The effects of reaction time and reaction temperature on the quality and the quantity of ester were studied by Gerpen in [34]. It was concluded in this study that the reaction completeness was one of the most important parameter to evaluate the quality of a fuel. It provides a middle-ground between reaction time and the reaction temperature. Karmee and Chadha [35] adopted a different approach. They produced biodiesel from Pongamia pinnata with the help of transesterification and using potassium hydroxide as a catalyst. For more on this topic, the reader is advised to refer to the manuscript by Ranganathan and Sampath [36].

### 2.1.2 Biodiesel Resources

Chemically, diesel fuel is made up of many different compounds. On the other hand, the chemical compositions of different fats and oils commonly used in biodiesel are very similar i.e., a single molecule of such a fat or oil consists of a glycerine structure of three carbon atoms, on each of which is connected a long-chained fatty acid. The reaction of this fatty acid with methanol produces methyl ester, or biodiesel. The glycerine structure is converted into glycerine and is stocked as a by-product of biodiesel. The fats and oils are composed of ten regular kinds of fatty acids that have twelve to twenty two carbons. More commonly i.e., over 90% of them have sixteen to eighteen carbons. These chains are found in three forms: saturated, monounsaturated, amd polyunsaturated. Within the range specified in the specification, the difference in the levels of saturation can affect some properties of biodiesel fuel. Each feedstock can be differentiated from the others as it comprises of different percentages of saturated, monounsaturated, and polyunsaturated fatty acids as seen in Fig. 2.2.

According to [37, 38, 39], oil is produced from over three hundred and fifty different types of crops. But only a certain types of oils can be used potentially

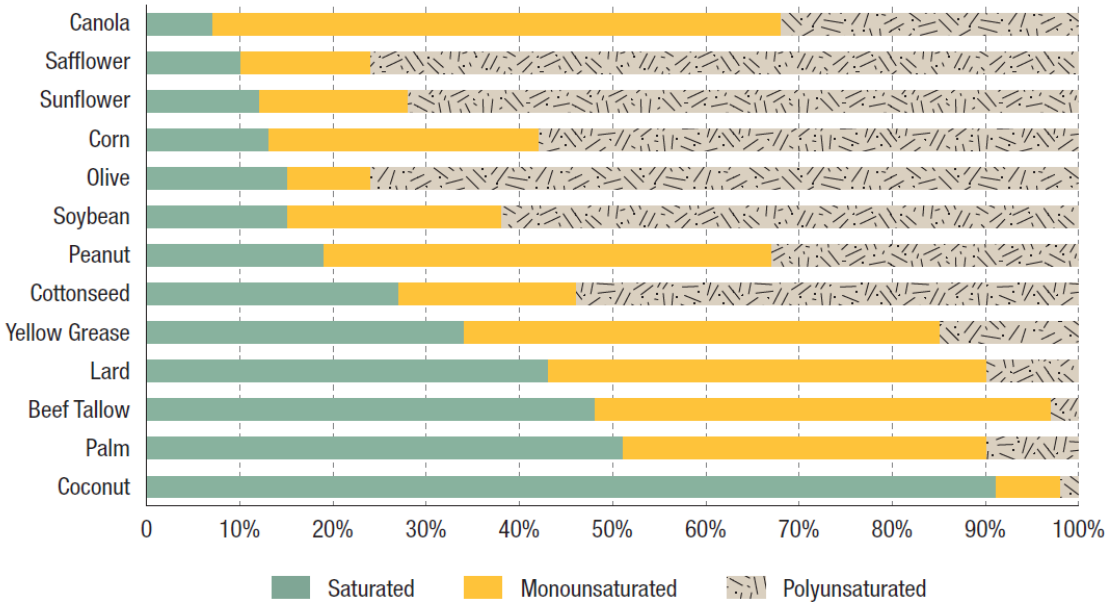


Figure 2.2: Break-down of different feedstocks for biodiesel. The results are displayed in ascending order of saturated fatty acid content [42].

as fuels in diesel engines. These are: sunflower oil, safflower oil, soybean oil, cottonseed oil, rapeseed oil and peanut oil. An important problem with using vegetable oils as fuels in diesel engines is the high fuel viscosity in compression ignition [40]. Nearly three decades ago, the idea of using vegetable oil as fuel as an alternative to petroleum, gained popularity. From macroscopic point of view, the advantages of vegetable oils as diesel fuel, as listed in [41], are:

1. Liquid nature-portability
2. Ready availability
3. Renewability
4. Higher heat content (about 88% of no. 2 diesel fuel)
5. Lower sulfur content
6. Lower aromatic content

7. Biodegradability

The disadvantages of vegetable oils as diesel fuel are:

1. Higher viscosity
2. Lower volatility
3. The reactivity of unsaturated hydrocarbon chains

### 2.1.3 Potential and Limitations of Biodiesel

The following discussion focuses on the properties of biodiesel and mainly oriented to shed light on these properties with respect to the application in this proposed work - that is combustion of biodiesel and surrogate fuels in CIE and simple burners. Table 2.1 summarises the main data for biodiesel obtained from the Biodiesel Handling and User Guide 2009 [42] based on ASTM specification. This table will be used as an indicator to the biodiesel used in this work in order to track it is origin and whether it meets the standard specification for biodiesel.

### 2.1.4 Diesel Blend Specifications

Diesel fuel properties are rather loosely regulated: the primary diesel fuel properties currently controlled by legislation are maximum sulfur content, maximum aromatic content, and minimum cetane number or index. Diesel fuels in the US and Europe are largely free of sulfur (US limit of 15 ppm, EU limit of 50 ppm but mandate complete availability of sulfur-free diesel fuel) (CFR, 80.520; EPC, 98/70; EPC, 2003/17). Diesel fuels in the United States must have a cetane index of at least 40 or a maximum aromatics concentration of 35%, while European fuels must have a CN of 51 or greater (CFR, 80.29; EPC, 98/70). The range of CN, however, is substantial. In the United States, the CN of diesel fuels sold at filling-stations can range between 38–mid-50s. Its average value is approximately 46 [43, 44]. A 15-point variation in CN indicates a big variation in the ignition behavior of a fuel.

The fact that diesel fuels with a wide range of CN are there in the market, makes it important to understand how the newly developed advanced diesel

Table 2.1: ASTM D7467 Specification for diesel blends B6 to B20 [42].

| Property | Test Method | Grade | | |
|---|---|---|---|---|
| | | B6 to B20 S15 | B6 to B20 S500 | B6 to B20 S5000 |
| Acid Number, mg KOH/g, max. | D664 | 0.3 | 0.3 | 0.3 |
| Viscosity, mm2/s at 40 °C | D445 | 1.9–4.1 | 1.9–4.1 | 1.9–4.1 |
| FP, °C, min | D93 | 52 | 52 | 52 |
| CP, °C, max | D2500 | - | - | - |
| Sulfur Content ($\mu$g/g)d<br>mass %, max.<br>mass %, max. | D5453<br>D2622<br>D129 | 15<br>-<br>- | -<br>0.05<br>- | -<br>-<br>0.50 |
| Distillation Temperature,°C, 90% evaporated, max. | D86 | 343 | 343 | 343 |
| Ramsbottom carbon residue on 10% bottoms, mass %, max. | D524 | 0.35 | 0.35 | 0.35 |
| CN, min. | D613 | 40 | 40 | 40 |
| One of the following must be met: | | | | |
| (1) Cetane index, min. | D976–80 | 40 | 40 | 40 |
| (2) Aromaticity, vol. %, max. | D1319–88 | 35 | 35 | - |
| Ash Content, mass %, max. | D482 | 0.01 | 0.01 | 0.01 |
| Water and Sediment, vol %, max. | D2709 | 0.05 | 0.05 | 0.05 |
| Copper Corrosion, 3 h @ 50°C, max. | D130 | No. 3 | No. 3 | No. 3 |
| Biodiesel Content, % (V/V) | DXXXX | 6–20 | 6–20 | 6–20 |
| Oxidation Stability, hours, min. | EN14112 | 6 | 6 | 6 |
| Lubricity, HFRR @ 60°C, micron, max. | D6079 | 520 | 520 | 520 |

combustion strategies react to differences in CN. This is critical for the implementation of production. Moreover, optimizing an engine for one fuel specification likely will not give optimum performance

### 2.1.5 Cetane Number of Biodiesels

The CNs and the Boiling Points (BPs) of esters correlated well with each other. It was confirmed after performing quantitative correlations and comparisons with various physical properties of fatty esters, that indeed the BP provides a very good approximation of CN [35]. One difference between gasoline and diesel fuel is that the former is ignited by a spark, while the latter is ignited by the heat generated as a result of compression in the engine. For this reason, the diesel engine is also known as a CIE. As there are many differences in the ignition processes, each process requires fuel with different physical and chemical properties.

Similar to gasoline, the diesel fuel is normally obtained by the cracking of petroleum. It starts boiling at an initial distillation temperature of 160$^o$C. It is also called a middle distillate due to the fact that its boiling range is in the mid-range of cracking products.

The quality of ignition of diesel fuel is conventionally measured using the specification ASTM D613 and is inferred from the CN of a fuel. The ignition characteristics are determined from the ignition delay time of the fuel in the engine. The smaller this time is, the bigger its CN will be. Cetane scale is a scale that can be used to position different compounds based on their CN. For this purpose, hexadecane ($C16H34$), is assigned a CN of 100. This is because its ignition delay is very low. On the other extreme, 2, 2, 4, 4, 6, 8, 8-heptamethylnonane, which has a very long ignition delay, is given a CN of 15. It is important to note that the cetane scale is arbitrary and that compounds with CN $>$ 100 or those with CN $<$ 15 have been identified. According to ASTM D975, a minimum of CN 40 is needed for conventional diesel fuel.

The cetane scale helps to clarify a key aspect of the composition/structure of the compounds used in diesel fuel. The ignition quality of long-chained, unbranched, saturated hydrocarbons (alkanes) is very good since they have high CNs. On the other hand, the ignition quality of branched hydrocarbons is very poor since they have low CNs. Extremely low and extremely high CNs are undesirable since they can cause problems. For example, in the case of extremely high CNs, combustion can happen prematurely, i.e., even before the fuel and air have well mixed. This can result in incomplete combustion and smoke. On the other

hand, in the instance of extremely low CNs, some of the problems that can occur are: the engine can get rough, it can misfire, the temperature of the air can rise, the warming up of the engine can get slow, and the combustion can be rendered incomplete. Therefore, many engine manufacturers assign a range of CN that is required to be used their engines. A common range in this case is: 40–50.

The ASTM D975 classifies different grades for diesel fuel. That is, DF1, DF2, DF3, and DF4 representing diesel fuel no. 1, no. 2, no 3, and no. 4 respectively. DF1 consist of volatile fuel oils from kerosene to intermediate distillates. These are particularly useful in high-speed engines where engine speed and load vary widely and frequently. They are required to be used in extremely low temperatures. The volatility of DF2 is lower compared to DF1. They consist of distillate gas oils. This fuel grade is appropriate for use in high-speed engines under comparatively inflated loads and uniform speeds. DF2 is also useful in engines which do not require highly volatile fuels or the other properties specified for DF1. DF2 is mainly used in transportation vehicles. Biodiesel is generally compared to this fuel grade. Lastly, DF4 is a heavy distillate fuel or a blend of distillate and residual oil. It is generally used only in low/medium speed engines which work under perpetual load at relatively constant speeds.

## 2.2 Recent Works on Spray Combustion

Having shed light on fuels and their production methods and how this affects their chemical, physical and thermal properties, this section will look at the latest developments in experimental work and modelling done so far for the combustion of such fuels in burners and Internal Combustion Engines (ICEs). Focus will be on the latest work rather than reviewing the historical part done in this regard.

Experimental work in the field of spray combustion either in burners of ICEs is available although not on a large scale. One would mention the work of Vaitilingom [45] who cited the fact that using pure vegetable oils in standard domestic burners has led to burning colder parts of the burner (in particular the air deflector) and draining of unburned fuel. This problem is associated with the high viscosity and low volatility of bio-oils leading to ignition problems as well burning of the colder parts of the combustor as a result of thermal decomposition and

polymerization when subjected to a varying range of temperature and heating. It is worth to mention that similar problems were cited by other researchers in the field of CIE including Korus [46], Srivastava [47], Kalam [48], and Ramadhas [49]. As a result, most of the experimental work where biodiesel is used in burners, a pre-heating of the fuels is used as a precaution to ensure that the above cited problems will not reoccur [[50] - [56]] and the recent work of Daho et al [57].

In terms of modelling spray combustion in burners, there are a few attempts to model the combustion of liquid conventional fuels but there are scarce attempt to simulate biofuels. Not only that, most of the work we centred on low hydrocarbons (C1-C4) and using very basic reaction mechanisms if the work of Herbinet [58], Warth [59] and his group is excluded. Indeed, the work of Herbinet [58], Warth [59] and his group do not take the turbulent environment into account and centrally focused on proving the kinetic and chemistry of combustion in ideal environments. Therefore, a new aspect of this thesis is addressing the combustion of both low and large-hydrocarbon.

Experimental work using compression ignition engine can be looked at in two aspects. Experiments which focus on evaluating the thermal and emission performance of CIEs, and there is an abundance of this work in the literature. To mention the most recent work in this area, one would cite the work of Wei et al. [60] which is focused on investigating the influence of the effects of blended diesel on ignition delay. In a recent review paper, Sanjid et al. [61] shed light on the use of palm oil and its derivatives as a replacement for diesel in CIE and noted the effect of this type of biodiesel in reducing $NO_x$. Most of the literature state that common types of biodiesl increase the rates of $NO_x$ production as stated in the recent review by Hoekman and Robbins [62]. Few studies to mention in this regard include the work of Song et al. [63] who also examined the $NO_x$ and soot emission in a biodiesel-fuelled diesel engine. In this regard, one also mentions the work of Dong et al [64] in which they assessed the emission of carbon oxides and unburned hydrocarbon in a CIE operated with blended fuels (mixture of diesel and biodiesel) where $CO$ emission was found to be influenced by equivalence ratio ($\Phi$). All these focus on evaluating the thermal and emission performance of a diesel engine that operate with biodiesel or a blended diesel. However, one point missing was a deeper understanding of the nature of the fuel and its

chemical structure especially after mixing diesel with biodiesel. The proposed work examines this point prior to testing a diesel engine as will be discussed in the closing chapters of this thesis.

The main benchmark adopted in this work the work of Widman and Presser [1] which is focused on spray combustion in a vertical burner. Widman and Presser [1] reported a good data from the spray combustion of methanol ($CH_3OH$) in a burner and their data was so far was used in only one simulation (Collazo et al [65]). Having said so, combustion in burners has been a focus of many studies as it is central to many applications including industrial and domestic ones as cited in the paragraph above. The work will also examine the nature and the structure of the biofuel used and its surrogates before been tested in an a CIE.

## 2.3 Emissions in Biofuels

Narrowing down the topic of renewable energy sources to liquid fuels, it is a fact that demand of using biofuels and specifically biodiesel in the transport sector in the UK, US, European Union and worldwide is rising due to many reasons including cost, security and environmental issues associated with conventional fuels. Despite the fact that biofuels have the potential to replace conventional fuels, their current and future availability status indicates that they can only be partially used to blend conventional fuels rather than completely replace them. Not only that, for an optimal use by the existing combustion infrastructure (combustion chambers in ICEs or other burners), an effective combustion process is essential to ensure that maximum energy is extracted from biofuels (or surrogate fuels) with a minimum impact on air quality by keeping the emissions of harmful pollutant at lower rates as well as minimising the corrosive effects on engine (or burner) components. It is a well-established fact that the by-products of combustion of liquid fuels (from crude petroleum or vegetable sources) include harmful gases that results from the combustion process. Carbon oxides ($CO_x$) and nitrogen oxides ($NO_x$) are the main by-products from the combustion of liquid diesel, petrol and other types of liquid fuels originating from crude petroleum.

The rate of emission of such gases is a function of many parameters, some of them can be described as macro-scale parameters (such as the equivalence ratio,

$\Phi$) while others are associated with a much smaller feature set of the combustion process such as the chemical reactions and how they proceed under different temperature range and pressures. The two types of parameters are not independent and they impact each other in a quite complex fashion. While it is easy to change and understand the effect of macroscopic parameters on the combustion, the microscopic parameters such as the reaction mechanism necessary to model the burning of liquid or gaseous hydrocarbons under a specific environment has been and still poses a challenge.

There is some evidence that biofuels produce less emission of such harmful gases compared to conventional fuels when burned under specific controlled environment although this fact is debatable. It was stated in many research papers for the case when biofuels replace conventional petroleum fuels in ICEs e.g., Enweremadu and Rutto [73], Gumus [74], Lapuerta et al. [75], Agarwal [76]) or other types of burners (Jaichandar and Annamalai [77], Ranzi et al. [78] are few to mention). Having said so, and based on a recent review paper by Xue et al. [79], one would surmise the literature statistics on whether pure biodiesel decreases or increases emissions when used in internal combustion engines in accordance with Table 2.2.

Table 2.2: Statistics of effects of pure biodiesel on engine performances and emissions ([79])

| Variable | Total no. of References | Increase | Similar | Decrease |
|---|---|---|---|---|
| Power performance | 27 | 2 | 6 | 19 |
| Economy performance | 62 | 54 | 2 | 6 |
| $PM$ emissions | 73 | 7 | 2 | 64 |
| $NO_x$ emissions | 69 | 45 | 4 | 20 |
| $CO$ emissions | 66 | 7 | 2 | 57 |
| $HC$ emissions | 57 | 3 | 3 | 51 |
| $CO_2$ emissions | 13 | 6 | 2 | 5 |
| Aromatic compounds | 13 | - | 2 | 11 |
| Carbonyl compounds | 10 | 8 | - | 2 |

Relying on the statistics shown in Table 2.2, one would be inclined to believe that biofuels do produce lower emission of $CO_x$ and $NO_x$ and the experimental

evidence does support this. Having said so, the mechanisms behind this important fact and how to capitalise on it in order to reduce emissions from burning biofuels of surrogate fuels in different platforms is far from been established and a subject of an ongoing debate between engineers and chemistry specialists. It is a fact that combustion was defined as a fast exothermic reaction between a hydrocarbon and an oxidant (usually oxygen). However, how the reactions takes place is a quite complex process and are shaped by many factors including the chemical structure of the hydrocarbon fuel and down to the types of bonds that connect the hydrogen (and oxygen in biofuels) to the carbon atoms.

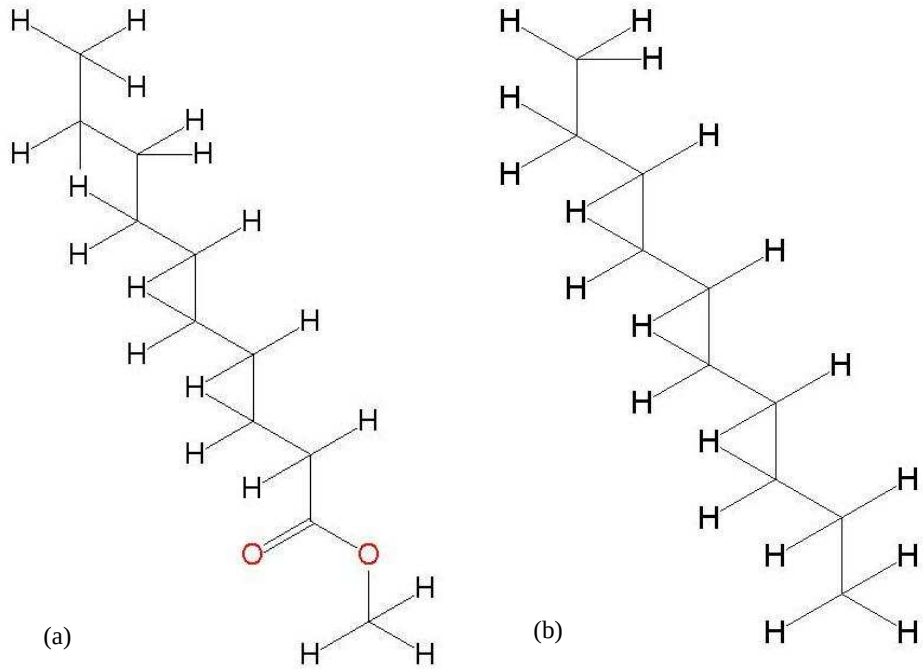


Figure 2.3: Chemical structure for (a) methyl decanoate and (b) decane.

A typical example of two hydrocarbons is shown in Fig. 2.3 where Fig. 2.3 (a) is methyl decanoate ($C_{11}H_{22}O_2$), a biofuel whose closest conventional hydrocarbon is decane ($C_{10}H_{22}$), shown in Fig. 2.3 (b). It is apparent that there is a difference between the two hydrocarbons not only in the number of carbon and hydrogen atoms, but also in the type of bonds. On top of this, the biofuel (methyl-decanoate) descending from methyl esters has two oxygen atoms in its composition. These two oxygen atoms are bonded in a different fashion to the

carbon and hydrogen atoms (both double and single bonds are clearly distinct). The existence of such oxygen atom has influenced the whole structure of the biofuels compared to its conventional counterpart even in the way the hydrogen atoms are connected to the carbon atoms. Therefore, one would expect that the way these hydrocarbons react and burn in a stream of air will differ. The reaction mechanism influences not only the heat liberated from the combustion but also the by-products of the combustion of such hydrocarbons (both conventional and biodiesel). Therefore, in order to adequately predict both the heat liberated and the rate of generation of the emission of carbon oxides ($CO_x$) and nitrogen oxides ($NO_x$) and other intermediate by-products, it is essential to use the representative reaction mechanism to model most, if not all, of the expected reactions in a combustion process. Having said so, these reactions in themselves are not easy to design and much validation under a varying range of temperatures is essential.

Most of the research done so far (ICEs or burners) mainly focuses on the effects of biodiesel blends on engine performance including fuel and thermal efficiencies as well as emission characteristics including $CO_x$, $NO_x$ soot and total unburned hydrocarbons in the exhaust. The reports are varying as can be read from Table 2.2 for CIE experimental work. The in-depth reason why biofuels produce less emission compared to conventional ones is not fully explained so far. There are some broad statements in the literature that attribute the decrease in emission from biofuel combustion compared to conventional ones to the existence of oxygen atom(s) in the chemical structure of biofuels. Presumably this is the reason, one would straight away conclude that it is down to the way this oxygen atom influence the reactions - or - the reaction mechanism.

Based on these arguments and the discussion presented in the paragraphs above, the main goal of this thesis is to present computational results for the spray combustion of different hydrocarbons (both conventional and biofuels) using advanced reaction mechanism to satisfy different objectives. The objectives behind the study can be summarised in two parts. The first is to study the differences and test and validate a specific reaction mechanism for the combustion of methanol used in the experimental studies of Widman et al. [1] and hence develop more mechanisms to model the combustion of other hydrocarbons that represent conventional and biofuels. The second objective is perform comprehensive analy-

sis for the computational results and comment on the amount of energy liberated and emission produced from the combustion of conventional and biofuels from the CFD predictions based on such advanced reactions mechanisms.

It is worth mentioning the fact that the exact work of Widman et al. [1] has been modelled only once by Collazo et al. [65] who used basic combustion model in the form of Eddy Dissipation Concept (EDC) model. The best combustion model cited in the literature that is not only more accurate but can accommodate advanced reaction mechanism is either Steady Laminar Flamelet Model (SLFM) or its unsteady version. For more discussion on this topic the reader is advised to refer to many text books including the recently published book by Cant and Mastorrakos [80] and Fox [81]. More details on the turbulence and combustion models used in this work will follow in Chapter 3.

## 2.4 Summary of the Literature Review

The literature review presented earlier in this chapter has shown many shortcomings. These shortcomings are not only related to the outcomes of the studies performed in the field of combustion but also in their applications. Most of the cited work focused on the experimental work related to ICE environment that examined the macro-scale performance parameters and ignored the micro-scale parameters associated with the combustion process. The computational work cited earlier in this chapter was based on simple combustion models, and most of it considered the chemical kinetics only in the absence of turbulence. The reaction mechanisms used in most, if not all, of the cited work are simple and contain few reaction steps and species. This is because such studies are aiming to reduce the uncertainty related to a large number of species and reaction steps.

The author believes that in order to obtain a complete picture of the combustion process, all reactions and associated species should be considered as they influence both the combustion process and the energy release. Therefore, developing and testing comprehensive reaction mechanisms for both conventional and biofuels is the main motivation of this work. Exploring the outcome from modelling the combustion of conventional and biofuels and shedding light on the micro-structure aspects of such fuels, especially the oxygenated nature of biofuels,

is the driving momentum behind this work.

# Chapter 3

# Research Methodology

## 3.1 Introduction

The computations performed in this thesis are based on steady CFD techniques using Reynolds-Averaged Navier-Stokes (RANS) equation. The experimental database and benchmark adopted for validation of the reaction mechanisms used to model the spray combustion of conventional and biofuels is that of Widman et al. [1]. The CFD code used to perform the current steady state calculations for the reactive flow described in this thesis is Fluent 12 [82].

In the literature, a typical non-premixed combustion case in a standard burner geometry is commonly referred to as turbulent diffusive combustion or combustion in diffusion flames because diffusion is the rate controlling process in such situations. Based on specific assumption, the thermochemistry of combustion can be reduced to one important parameter i.e., the mixture fraction (commonly referred to as $f$. The mixture fraction is the mass fraction of the fuel stream, or, the local mass fraction of burnt and unburnt fuel stream elements (including $C$, $H$, etc.) in all the by-products ($CO_2$, $H_2O$, $O_2$, etc.). The beauty of the mixture fraction approach is based on the fact that the atomic elements are preserved in chemical reactions which means that the mixture fraction is a preserved scalar quantity. Hence, the transport equation governing it, lacks a source term. This supports the fact that combustion can be viewed as a mixing problem, and the difficulties and uncertainties related to closing non-linear mean reaction rates

no more exist. Once the mixture status is achieved, the combustion and chemistry can be modelled as being in three distinct approaches based on three main assumptions:

1. Assuming the mixture is in chemical equilibrium: the Equilibrium model can be used.

2. Assuming the mixture is in near chemical equilibrium: the SLFM is adequate.

3. Assuming the mixture is significantly deviating from chemical equilibrium: more adequate to use the Unsteady Laminar Flamelet Model (ULFM)

In spray combustion, the flamelet concept has proved to be the most successful in modelling the combustion phenomena. Many argue that the unsteady flamelet is more efficient compared to the steady one. The reader is advised to refer to a recent book produced by Cant and Mastorakos [80] for a comprehensive review on this topic and comparisons between different combustion models. In the work of this thesis, and assuming a near chemical equilibrium, the Laminar Flamelet Model (LFM) is used. It is worth to mention that Laminar Flamelet Model is either based on mixture fraction [83], or on G-equation [84]. In the current work, the LFM uses the concept of mixture fraction and hence the thermochemical structure of the flame is a function of mixture fraction and its dissipation rate. The Shear Stress Transport (SST) k-$\omega$ [85] was used as a turbulence model necessary to close the RANS equation. The following sections summarise both the turbulence and combustion model used as per their implementation in Fluent 12.1 [82]

## 3.2 Steady RANS Combustion Modelling

The direct approach of handling combustion is to use an appropriate chemical kinetic mechanism for the particular fuel that is being investigated and to follow this with a solution to the transport equations for all the species in the mechanism and, lastly, to model the mean chemical source term. However, a realistic

chemical mechanism may contain a large number of species and an even larger number of elementary reactions even for a simple hydrocarbon fuel like methane is considered.

It is difficult (and may be irrelevant to the work of this thesis) to present all details of the models used in spray combustion, however, a summary of the models used in turbulence and reaction will be highlighted in this section. Detailed mathematical formulation can be found in Poinsot and Veynante [86], Champion and Libby [87], Williams [88], Borghi and Champion [89] and in many textbooks too. The equations governing flows with chemical reactions are the continuity, the species conservation equations and the energy. A solution to these equations provides, theoretically, all the particulars sought from a reacting flow. The equations for the mean quantities in the RANS approach are obtained by averaging the instantaneous governing equations using mass-weighted averages (Favre averages).

In Favre averaging, all the instantaneous values of velocity and scalars ($\phi$) except for pressure and density are decomposed into a steady and fluctuating part as:

$$u_i = \frac{\overline{\rho u_i}}{\bar{\rho}} + u_i'' = \widetilde{u_i} + u_i'' \quad and \quad \phi_i = \widetilde{\phi_i} + \phi_i'' \tag{3.1}$$

Favre mean is denoted by a tilde while the fluctuation about the Favre mean is given by double prime

It is worth mentioning again that the equations presented in this section are taken in consultation with Fluent 12.1 [82]. The averaged governing equations can be written as follows:

- Conservation of Mass

$$\frac{\partial \overline{\rho}}{\partial t} + \frac{\partial}{\partial x_i}(\overline{\rho}\widetilde{u_i}) = 0 \tag{3.2}$$

- Conservation of Momentum

$$\frac{\partial \overline{\rho}\widetilde{u_i}}{\partial t} + \frac{\partial}{\partial x_i}(\overline{\rho}\widetilde{u_i}\widetilde{u_j}) + \frac{\partial \overline{p}}{\partial x_j} = \frac{\partial}{\partial x_i}(\overline{\tau}_{i,j} - \widetilde{\overline{\rho}u_i''u_j''}) \tag{3.3}$$

Where the viscous stress tensor $\tau_{i,j}$ for a Newtonian fluid and incompressible

flow is given by

$$\tau_{i,j} = 2\frac{\mu}{\rho}S_{ij} \tag{3.4}$$

where $\mu$ is the laminar dynamic viscosity, and $S$ is the strain rate tensor defined as:

$$S_{ij} = \frac{1}{2}\left(\frac{\partial \widetilde{u_i}}{\partial x_j} + \frac{\partial \widetilde{u_j}}{\partial x_i}\right) \tag{3.5}$$

- Conservation of chemical species

$$\frac{\partial(\overline{\rho}\widetilde{Y_k})}{\partial t} + \frac{\partial}{\partial x_i}(\overline{\rho}\widetilde{u_i}\widetilde{Y_k}) = -\frac{\partial}{\partial x_i}(\overline{V_{k,i}Y_k} + \overline{\rho}\widetilde{u_i''Y_k''}) + \overline{\dot{\omega}}_k \tag{3.6}$$

where $k$=1,2,... $N$ species

- Conservation of energy

$$\frac{\partial \overline{\rho}\widetilde{h_s}}{\partial t} + \frac{\partial}{\partial x_i}(\overline{\rho}\widetilde{u_i}\widetilde{h_s}) = \overline{\dot{\omega}}_T + \frac{\overline{Dp}}{Dt} + \frac{\partial}{\partial x_i}(\lambda\overline{\frac{\partial T}{\partial x_i}} - \overline{\rho u_i'' h_s''}) + \overline{\tau_{i,j}\frac{\partial u_i}{\partial x_j}} - \frac{\partial}{\partial x_i}(\overline{\rho\sum_{k=1}^{N} h_{s,k}Y_k V_{k,i}}) \tag{3.7}$$

where

$$\overline{\frac{DP}{Dt}} = \frac{\partial \overline{p}}{\partial t} + \overline{u_i\frac{\partial p}{\partial x_i}} = \frac{\partial \overline{p}}{\partial t} + \widetilde{u}_i\frac{\partial \overline{p}}{\partial t} + \overline{u''\frac{\partial p}{\partial x_i}} \tag{3.8}$$

- Any conserved scalar (such as mixture fraction):

$$\frac{\partial}{\partial t}\left(\overline{\rho}\widetilde{Z}\right) + \frac{\partial}{\partial x_i}\left(\overline{\rho}\widetilde{u}_k\widetilde{Z}\right) = \frac{\partial}{\partial x_i}\left(\widetilde{D}^z\right) - \frac{\partial}{\partial x_i}\left(\widetilde{\rho u_k'' Z''}\right) \tag{3.9}$$

This averaging procedure introduces unclosed quantities that have to be modelled.

### 3.2.1 Species ($\widetilde{u_i''Y_k''}$) and Enthalpy ($\widetilde{u_i''h_s''}$) Turbulent Fluxes

.

These fluxes are normally closed using a classical gradient supposition:

$$\widetilde{\rho u_i'' Y_k''} = -\frac{\mu_t}{Sc_{kt}} \frac{\partial \widetilde{Y}_k}{\partial x_i} \tag{3.10}$$

where $\mu_t$ represents the turbulent viscosity, approximated using the turbulence model, and $Sc_{kt}$ represents turbulent Schmidt number for species $k$.

### 3.2.2 Laminar Diffusive Fluxes for Species or Enthalpy

These molecular terms are generally neglected against turbulent transport, assuming a sufficiently large turbulence level (large Reynolds number limit). They may also be retained by adding a laminar diffusivity to the turbulent viscosity $\mu_t$ in Eq. 3.10.

$$\overline{V_{k,i} Y_k} = -\overline{\rho D_k \frac{\partial Y_k}{\partial x_i}} \approx -\overline{\rho}\,\overline{D}_k \frac{\partial \widetilde{Y}_k}{\partial x_i} \tag{3.11}$$

where $\overline{D}$ is mean species molecular diffusion coefficient. The laminar heat diffusion flux in the enthalpy equation is generally rewritten as:

$$\overline{\lambda \frac{\partial T}{\partial x_i}} = \overline{\lambda} \frac{\partial \widetilde{T}}{\partial x_i} \tag{3.12}$$

where $\overline{\lambda}$ is the mean thermal diffusivity.

### 3.2.3 Pressure-Velocity Correlation $\overline{u_i'' \partial p / \partial x_i}$

This term is used to compute the mean quantities. Mean quantities can be very different from instantaneous quantities. In this study this term is neglected.

## 3.3 Turbulence Model

The Reynolds stresses term ($u_i'' u_j''$) is approximated by a turbulence model. In this study the SST turbulence is employed which has a similar form to the Wilcox

$k-\omega$ model. The SST model unites the benefits of two models: (i) Wilcox $k-\omega$ model and (ii) the $k-\varepsilon$ model. The former is used in the inner region of the boundary layer and a high Reynolds number version of the former is used in the outer region of the boundary layer. Although the current problem is a reactive mixture problem rather than a boundary layer problem, the author believes that still the SST model is the best choice. The model has the form:

$$\frac{\partial}{\partial t}(\overline{\rho}k) + \frac{\partial}{\partial x_i}(\overline{\rho}\widetilde{u}_i k) = \frac{\partial}{\partial x_i}[(\mu + \frac{\mu_t}{\sigma_k})\frac{\partial k}{\partial x_i}] + P_k - \beta'\overline{\rho}k\omega \tag{3.13}$$

$$\frac{\partial}{\partial t}(\overline{\rho}\omega)+\frac{\partial}{\partial x_i}(\overline{\rho}\widetilde{u}_i\omega) = \frac{\partial}{\partial x_i}[(\mu+\frac{\mu_t}{\sigma_\omega})\frac{\partial \omega}{\partial x_i}]+(1-F_1)2\overline{\rho}\frac{1}{\sigma_{\omega 2}\omega}\frac{\partial k}{\partial x_i}\frac{\partial w}{\partial x_i}+\alpha_2\frac{\omega}{k}P_k-\beta_2\overline{\rho}\omega^2 \tag{3.14}$$

The constants used in the model constants are:
$\beta' = 0.09$, $\sigma_k = 1.176$ $\sigma_\omega = 2$, $\alpha_2 = 0.44$, $\beta_2 = 0.0828$, $\sigma_{\omega 2} = 1/0.856$

The equation of $\omega$ is multiplied by blending function $(1 - F_1)$. This is done to make sure that the equations of the model act well in both the near-wall and far-field zones. The modified turbulent viscosity will be calculated by:

$$\mu_t = \frac{a_1 k\overline{\rho}}{max(a_1 w, SF_2)} \tag{3.15}$$

where $F_2$ is blending function just like $F_1$, which limits the limiter to the wall boundary layer. $S$ is the strain rate tensor and $a_1 = 0.31$

The success of the method depends on the blending functions. The formulation of these functions depend on two aspects: (i) the distance to the nearest surface and (ii) the flow variables.

$$F_1 = \tanh(\arg_1^4) \tag{3.16}$$

with

$$\arg_1 = min(max(\frac{\sqrt{k}}{\beta'\omega y} \ , \ \frac{500\nu}{y^2\omega}) \ , \ \frac{4\overline{\rho}k}{CD_{k\omega}\sigma_{\omega 2}y^2}) \tag{3.17}$$

where $y$ represents the normal distance to the nearest wall, $\nu$ represents the kinematic viscosity and $CD_{k\omega}$ represents the positive portion of the cross-diffusion term written as:

$$CD_{k,\omega} = max\left(2\overline{\rho}\sigma_{\omega 2}\frac{1}{\omega}\frac{\partial k}{\partial x_i}\frac{\partial \omega}{\partial x_i}\ ,\ 1.0\times 10^{-10}\right) \tag{3.18}$$

The eddy viscosity($\nu_t = \frac{\mu}{\overline{\rho}}$) is calculated from

$$\nu_t = \frac{a_1\, k}{max(a_1\,\omega, \Omega\, F_2)} \tag{3.19}$$

where $F_2$ is given by

$$F_2 = tanh(\arg_2^2) \tag{3.20}$$

with

$$\arg_2 = max(\frac{2\sqrt{k}}{\beta'\omega y}\ ,\ \frac{500\nu}{y^2\omega}) \tag{3.21}$$

Here $\omega$ is the magnitude of the vorticity vector.

One drawback of standard turbulence models is that they generate extravagant turbulence energy, $P_k$, near the stagnation points. The model is comparatively insensitive to the free stream value of $\omega$. For the sake of avoiding the accumulation of turbulent kinetic energy in stagnation regions, a formulation of limiters for the production term in the turbulence equations is introduced by Menter [85].

$$P_k = \mu_t\frac{\partial \widetilde{u}_i}{\partial x_j}(\frac{\partial \widetilde{u}_i}{\partial x_j} + \frac{\partial \widetilde{u}_j}{\partial x_i}) \quad \rightarrow \quad \widetilde{P_k} = (P_k, 10\rho\beta k\omega) \tag{3.22}$$

## 3.4 Combustion of Liquid Fuels (Spray Combustion)

It is a common process that in non-premixed combustion of liquid fuels, atomizers are used to injected fuels into combustion chambers. The function of atomizers is to disintegrate the liquid into a spray of droplets. When the vaporised fuel surrounding the droplets ignites, it leads to an elevated rate of evaporation, thus forming reaction zones enclosing the respective droplet or in an area where fuel-

to-air ratios are within limits of inflammability. Having said so, the combustion process is very complicated phenomena in most practical systems and proceeds through a set of physical and chemical processes, the gross features of which are best described by the scheme shown in Fig. 3.1. Therefore, to understand the steps involved in spray combustion, it is essential to know:

- the mechanism of combustion of the individual droplets,
- any interaction between the droplets, and
- the statistics related to the size and the spatial distribution of the droplets

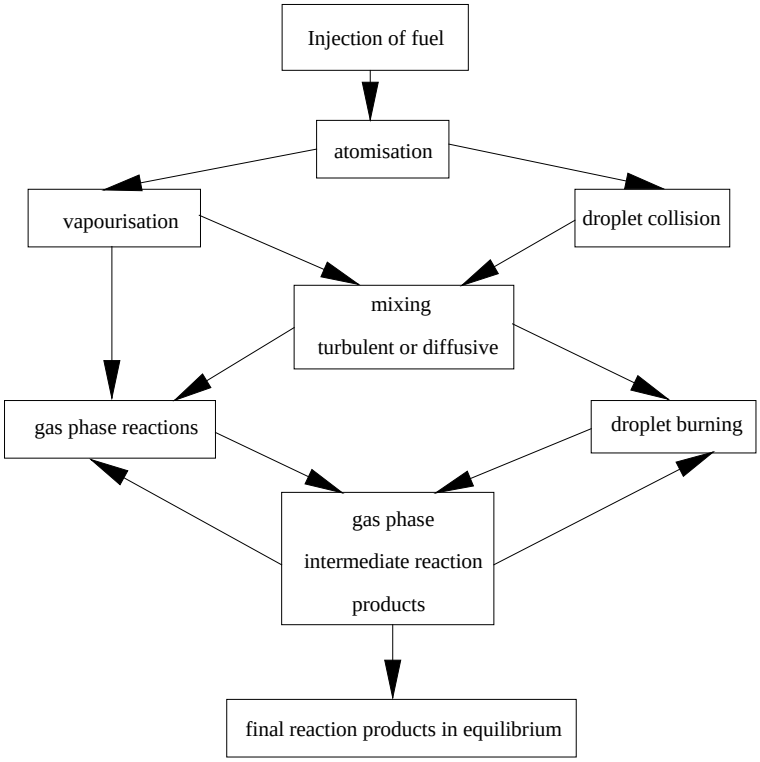


Figure 3.1: Energy conversion cycle

Whilst it is feasible to model the last two points, both classical and modern experimental studies have proved that it is hard to collect detailed information on the reaction mechanism or the burning rate of spray combustion (Nomura et al. [90]). Having said so, it is worth to mention that with the evolution of

experimental equipment together with the development of novel experimental techniques, a good insight of the combustion process of spray combustion has been achieved. However, one of the fronts that is making good progress in understanding and unfolding the reaction mechanism of the combustion of different fuels is based on pure theoretical approaches and methodologies. Developing a reaction mechanism based on specific parameters has been made possible through few studies. As one of the subjects of this chapter is to develop and test a reaction mechanism based on a specific approach, it is worth shedding some light on the most important parameters that influence the development of such reaction mechanisms.

### 3.4.1 Reaction Mechanisms and Parameters that Influence their Consideration

In general, the combustion of hydrocarbon fuels is conceptually simple. Provided that complete combustion occurs, any hydrocarbon react with oxygen and the by-products are carbon dioxide ($CO_2$) and water ($H_2O$). During chemical reactions, bonds are broken in the reactants and new ones are made in the products. Considering the fact that the breaking of a bond is an is an endothermic process while the making of a bond is an exothermic process, the combustion process is followed by a release of heat energy which is estimated by the enthalpy of reaction $\Delta H$. $\Delta H$ is the difference of all the energy absorbed in the breaking of bonds and all the energy released in making of bonds, or

$$\Delta H = \sum_{P} n_j h_j - \sum_{R} n_i h_i$$

where the subscript $p$ stands for products and $R$ for reactants.

In reality, the details of how conversion of a hydrocarbon to carbon dioxide and water, accompanied by natural release of energy occurs are enormously complex. The complexity of the combustion of any hydrocarbon is influenced by many factors, some of which are associated with the microstructure of the hydrocarbon itself (elements involved and how they are bonded), while other factors are associated with the environment of combustion (temperature, pressure,

mixture fraction etc.). On top of this, it depends whether the hydrocarbon is in the gaseous or the liquid state.

Examining the structure of the two hydrocarbons shown in Fig. 2.3, it becomes apparent that neither the amount of liberated heat (which depends on the bonds breaking/formation) nor the combustion process (which is influenced by the elements involved and how they are bonded), would be the same. One of the distinct features of biodiesel is the existence of two oxygen atoms within the compound structure. The questions on how such atoms influence the combustion of biofuels in comparison to its counterparts remain fairly answered on macroscales but there is a scarce of studies that exist so far to elaborate on the influence of the existence of oxygen atoms on hydrocarbons when they burn. Based on these simple facts, the combustion of even a relatively simple hydrocarbon may involve thousands of elementary to secondary steps. In order to optimise the combustion of such hydrocarbons thus extracting the maximum amount of energy with minimum release of pollution (by-products), it is essential to obtain detailed knowledge of the energetics and reaction mechanism of each of these steps.

The author is also inclined to the fact that if one is interested in accurate prediction of pollutants ($CO_x$ and $NO_x$), accounting for all the possible reaction pathways becomes a necessity and the overall mechanism should be a comprehensive one. In order to satisfy this criteria (involving the maximum possible species and related reactions), not all the combustion models developed and used so far allow detailed reaction mechanism. The chemical source term appearing in Eq. 3.6 is modelled using different approaches as shown in Fig. 3.2 (Fox [91]).

The flamelet concept does permit the use of advanced reaction mechanism to model the combustion process of hydrocarbon. Having agreed that the flamelet is the way forward, one needs to think about developing a comprehensive reaction mechanism that is capable of representing the actual reactions and species associated with the fuel under hand. This study uses existing detailed reaction mechanisms in order to validate the simulation results and then develop, modify and validate an advanced reaction to model the combustion of a selected conventional hydrocarbon fuel and a biofuel.

In this work, an aid software (EXGAS) was used to generate the necessary

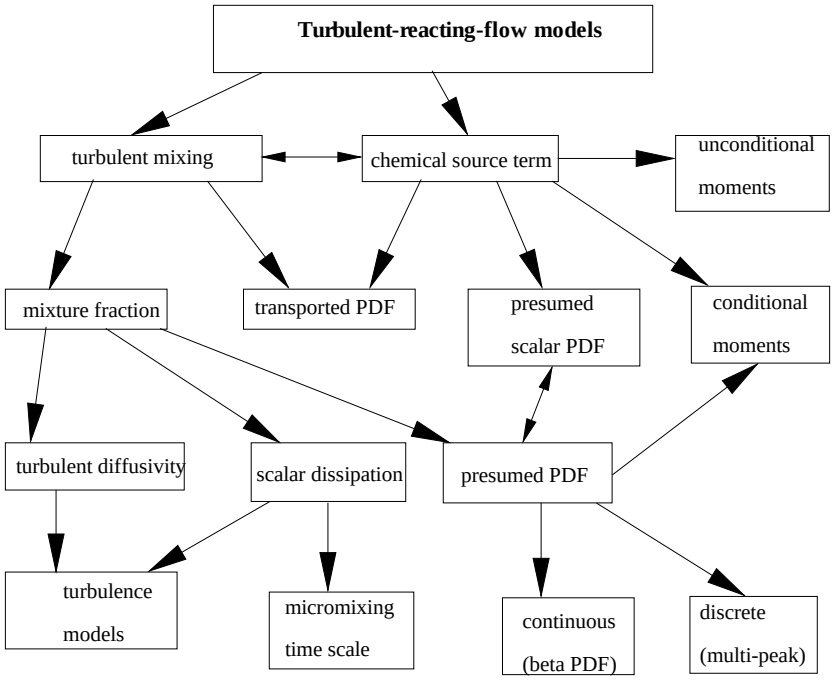


Figure 3.2: Closures of the chemical source term in terms of its relationship to the joint composition PDF.

reaction mechanism. The software includes three main components: (i) EXGAS, which automatically generates the reaction mechanisms, (ii) THERGAS, which calculates the thermochemical data, and (iii) KINGAS, which calculates the kinetic data. For more description on how the reaction mechanism is produced (types of reactions and justifications), the reader is advised to refer to a couple of publications including the work of Herbinet et al. [58] and others [92]–[99]. However, other data was taken from relevant websites (specifically the thermal data from Burcat [100]). EXGAS produces two files compatible with CHEMKIN-CFD currently offered free with Fluent (the software used in performing the current simulations). The detailed reaction mechanism (including the species involved and the relevant reaction pathways) is imported into Fluent to generate a flamelet and a PDF table for performing flamelet modelling of the combustion.

The software connects the three components in the fashion shown in Fig. 3.3

and produces reaction mechanisms compatible with CHEMKIN-CFD for ANSYS FLUENT. This enables the flamelet model described above to be used.

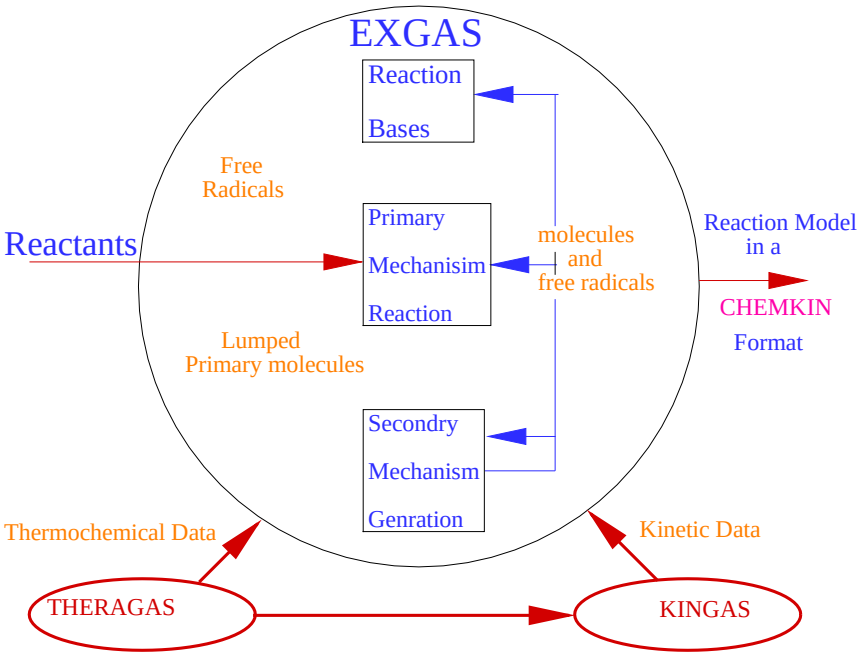


Figure 3.3: General description of the EXGAS system

In addition to the reaction mechanism developed with the aid of EXGAS, the well-known "San Diego Mechanism" [101] was also used. The model was mainly useful for modelling flames, high temperature ignition and detonations. In comparison to the developed reaction mechanism in this study, the San Diego Mechanism is considered as reduced one. This is because in San Diego Mechanism the number of species and reactions are kept to the minimum required to describe the systems and phenomena addressed, thereby minimizing the uncertainties in the underlying rate parameters as much as possible. In one way this is good as the results obtained using this mechanism have less certainties, however, if completeness of the combustion process is sought, the model may fall short of achieving this goal - which is the point the authors of this manuscript are after. Having said so, in an attempt to involve all the possibly related elementary stages

in the developed mechanism, significant investigation and scrutiny to the reaction mechanism was made to ensure the obtained results are of good quality and reduced uncertainties. For more documentation of the San Diego Mechanism, the reader is advised to refer to [101] in which comprehensive description and documentation of this mechanism has been provided. San Diego Mechanism is taken as a secondary reference after the experimental results which will be used to validate the data here.

### 3.4.2 Governing Equations for $NO_x$ Transport

Zeldovich mechanism consists of a set of chemical reactions that are highly sensitive to temperature. This mechanism plays a significant role in the formation of thermal $NO_x$. Following are the main reactions involved in the formation of thermal $NO_x$ from molecular nitrogen:

$$\mathrm{O} + \mathrm{N_2} \rightleftharpoons \mathrm{N} + \mathrm{NO}$$

$$\mathrm{N} + \mathrm{O_2} \rightleftharpoons \mathrm{O} + \mathrm{NO}$$

It has been shown that a third reaction can help in the formation of thermal $NO_x$, specifically in near-stoichiometric conditions and in mixtures that are rich in fuel:

$$\mathrm{N} + \mathrm{OH} \rightleftharpoons \mathrm{H} + \mathrm{NO}$$

### 3.4.3 Combustion Model - The Laminar Flamelt Model (LFM)

The chemical reaction source term in Eq. 3.6 will be calculated using LFM [84] and the turbulent flame is considered to contain an ensemble of small laminar flamelet. Although turbulence can influence the internal structure of the flamelet through flame straining and curvature, a laminar structure is maintained. Therefore, if the attributes of the laminar flamelet are known, a solution to the turbulent flame can be found.

The theory of existence of laminar flamelet in turbulent flows was first proposed by Williams [102] who assumed that a turbulent diffusion flame consists of an ensemble of 'flamelet' that stretches in a turbulent reacting flow. Assuming a fixed level of stretching, all the thermo-chemical properties of a flamelet can be expressed as a function of conserved scalar, the mixture fraction which quantifies the extent of mixing of the reactants. Therefore, in the flamelet model concepts, the thermo-chemical structure of a turbulent non-premixed flame is dependent only on mixture fraction and scalar dissipation rate which are statistically distributed in a turbulent flow. To adequately model and predict the non-equilibrium effects in turbulent non-premixed flames, flamelets are introduced into turbulent flow by considering their joint probability density function. Although the derivation of the governing equations for reactive flows is available in many texts books (including Peters [84], Poinsot and Veynante [86], Turns [103], Champion and Libby [87], Williams [88], Borghi and Champion [89] and Cant et al. [80], a brief summary of these equations and the way they are implemented into Fluent 12 is explained below.

LFM provides a cost effective, step-by-step analysis of thermo-chemical and hydrodynamic phenomena. Laminar flames, that represent an instantaneous structure of the turbulent flame front, subjected to a certain state of disturbances by the turbulent motion, are calculated a priori. The data collected from these calculations is stored in a database for the succeeding computation of the multi-dimensional turbulent flame. The flamelet data is differentiated with the help of a few important scalar parameters, the statistics of which are calculated in the turbulent flame computation. The incorporation of detailed chemistry is allowed, since the chemistry is applied within confines of a laminar system. The extreme closure difficulties related to bringing in full chemistry within a turbulent calculation do therefore not occur and the chemical mechanism used within the laminar flame does not lead to increased computational requirements within the turbulent flame computation.

PDFs can be used to describe the effect of turbulent fluctuations on the chemical system. The mean value of a quantity $\Phi$ tabulated in the flamelet library

(database) is obtained using the following formula:

$$\overline{\Phi}(x,r) = \int_0^\infty \int_0^1 \Phi(\xi,\chi_{st}) pdf(\xi,\chi_{st};x,r) d\xi d\chi_{st}. \tag{3.23}$$

For the supposition of statistical independence $pdf(\xi,\chi_{st};x,r)$ can be represented as:

$$pdf(\xi,\chi) = pdf(\xi).pdf(\chi). \tag{3.24}$$

A $\beta-$function has been considered for the PDF of the mixture fraction:

$$pdf(\xi) = \frac{\xi^{\alpha-1}(1-\xi)^{\beta-1}}{\int_0^1 \xi^{\alpha-1}(1-\xi)^{\beta-1}d\xi} = \frac{\Gamma(\alpha+\beta)}{\Gamma(a)\Gamma(b)}\xi^{\alpha-1}(1-\xi)^{\beta-1}. \tag{3.25}$$

where $\Gamma(x)$is :

$$\Gamma(x) = \int_0^\infty e^{-t}t^{x-1}dt \tag{3.26}$$

The parameter $\alpha$ is a function of the mean value of the mixture fraction while $\beta$ is a function of the variance of the mixture fraction

$$\alpha = \frac{\tilde{\xi}^2(1-\tilde{\xi})}{\widetilde{\xi''}} - \tilde{\xi}, \qquad \beta = \alpha(\frac{1-\tilde{\xi}}{\tilde{\xi}}) \tag{3.27}$$

The PDF of the scalar dissipation rate $pdf(\chi_{st})$ considers log-normal distribution:

$$pdf(\chi_{st}) = \frac{loge}{\chi_{st}\sigma_{log}\sqrt{2\pi}} Exp(-\frac{(log\chi_{st}-\mu_{log})^2}{2\sigma_{log}^2}). \tag{3.28}$$

The parameter $\mu_{log}$ represents the mean value of the transformed property $f_x = log\chi_{st}$ while $\sigma_{log}$ represents its variance. They use the mean and variance of the scalar dissipation rate and can be derived as follows:

$$\chi_{st} = Exp(\mu_{log} + \frac{\sigma_{log}^2}{2}), \tag{3.29}$$

$$\chi_{st}''^2 = Exp(\sigma_{log}^2 - 1)\ Exp(2\mu_{log} + \sigma_{log}^2). \tag{3.30}$$

The equation of the mean value of the scalar dissipation rate $\chi_{st}$ is modelled as:

$$\chi_{st} = C_\chi \xi''^2 \frac{\tilde{\varepsilon}}{\tilde{k}} \quad with \quad C_\chi = 2. \tag{3.31}$$

$\mu_{log}$ can be calculated from the above equations and $\sigma_{log}$ is supposed to have a value of $\sigma_{log} = \sqrt{2}$. The work of Liew et al. (1984) shows only little influence of the precise value of $\sigma_{log}$ on the results obtained from flamelet computations.

It is apparent from the math argument mentioned here that all the thermochemical properties of any single flamelet are functions of conserved scalar mixture fraction and scalar dissipation rate. It is also clear that the variable that influences the stretch in the flamelets is scalar dissipation rate. In this order, the flamelet model represents the turbulent flame structure as a thermochemical flame or fire with statistical distribution of mixture fraction and scalar dissipation rate. As mentioned previously, the advantage of using flamelet model is that realistic chemical kinetics effects can be included into turbulent flames.

### 3.4.4 Atomiser Model: The Air-Blast/Air-Assist Atomizer Model

A common approach for breaking up of liquid sheets and atomising liquid fuels (in different combustion infrastructure) is through the introduction of a supplementary air stream aimed through the atomizer. This method is commonly referred to as air-assisted or air-blast atomization and it is a function of two main variables: (i) the quantity of air and (ii) the velocity of air. The air used in this technique not only helps in the atomisation process but also contributes positively for the dispersion of the droplets and the prevention of collisions between them, thus enhancing the burning process. Air-assisted atomization methodology bears many similarities for pressure-swirl atomization which is often used when fine atomization is required. Fluent's air-blast atomization model is in fact a version of the pressure-swirl model with few differences, including:

- the sheet thickness: has to be set by the user in the air-blast atomizer model used in Fluent.

- user has to specify the maximum relative velocity responsible for producing the sheet and air.
- air-blast atomizer model supposes that the sheet breakup occurs as a result of short waves due to the fact that the typically the sheet found in air-blast atomizers is thicker.

Similar features of Fluent's air-blast atomization model to the pressure-swirl model that the user should input are the mass flow rate and spray angle. More details on the description of Fluent's air-blast atomization can be found in Fluent manual [82].

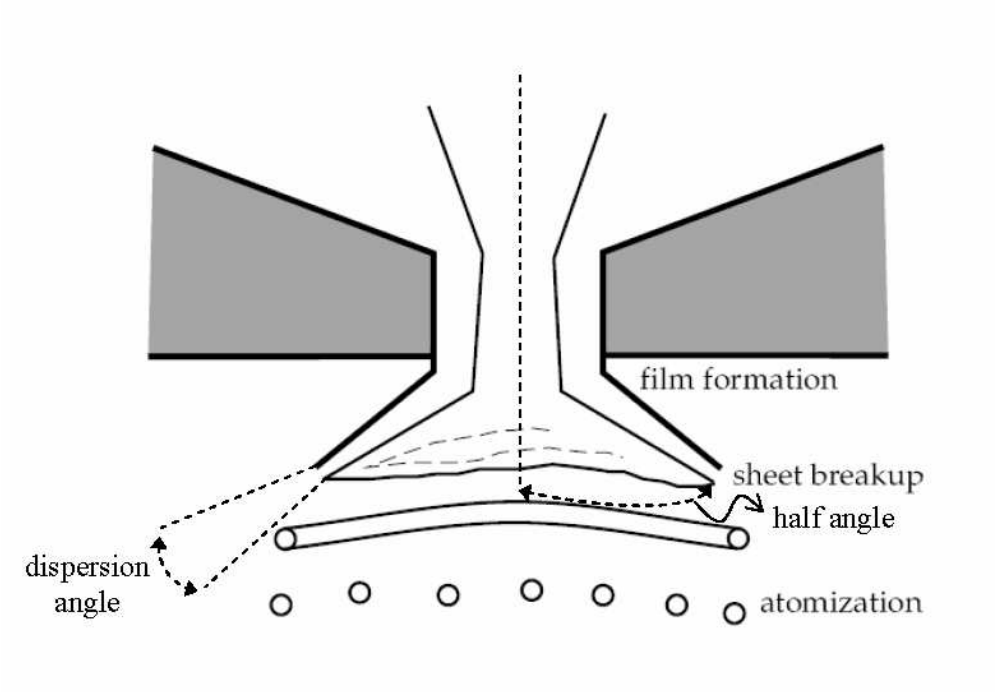


Figure 3.4: Atomiser (Fluent)

### 3.4.5 The Pressure-Swirl Atomizer Model Theory

The pressure-swirl atomizer operates by accelerating the liquid through nozzles and into a central swirl chamber. The swirling liquid fuel pushes against the walls of the swirl chamber and creates a hollow air core that exits the orifice in

the form of a thin unstable sheet that eventually breaks up into ligaments and droplets. The pressure-swirl atomizer is commonly employed in gas turbines, oil furnaces, and CIEs. The overall process can be split into three main stages:

1. Film formation
2. Sheet breakup
3. Atomization

Schematic sketch of these three stages is shown in Fig. 3.4 and the mathematical description is presented in Sections 3.4.5.1 and 3.4.5.2 below with reference to Fluent manual [82]. This model is commonly known as the Linearized Instability Sheet Atomization (LISA) model of Schmidt et al. [104].

#### 3.4.5.1 Film Formation

It is assumed that the centrifugal motion of the liquid within the injector creates an air core surrounded by a liquid film where the thickness of this film, $t$ , is related to the mass flow rate by

$$\dot{m}_{eff} = \pi \, \rho \, u \, t \, (d_{inj} - t) \tag{3.32}$$

where $d_{inj}$ represents the exit diameter of the injector, while $\dot{m}_{eff}$ represents the effective mass flow rate. It can be described using Eq. 3.33 .

$$\dot{m}_{eff} = \frac{2\pi \, \dot{m}}{\Delta \, \phi} \tag{3.33}$$

Where $\Delta\phi$ denotes the difference of the azimuthal stop and start angles, for the user to input. The other unknown in Eq. 3.33 is $u$ which represents the axial part of velocity at the exit of injector. $u$ is a function that represents the internal characteristics of the injector. It is extremely difficult to estimate. However, following the technique of Han et al. [105], the relation between the total velocity and the injector pressure can be given as:

$$U = k_v \sqrt{\frac{2 \, \Delta \, p}{\rho_l}} \tag{3.34}$$

Here $k_v$ is the velocity coefficient expressed as:

$$k_v = max\left[0.7, \frac{4\,m_{eff}}{d_0^2\,\rho_l\,cos\theta}\sqrt{\frac{\rho_l}{2\,\Delta\,p}}\right] \tag{3.35}$$

As $\Delta\,p$ is already known, first, $U$ can be found using Eq.3.34, after which $u$ can be computed as:

$$u = U\,cos\theta \tag{3.36}$$

Here $\theta$ represents the spray angle and is supposed to be known.

#### 3.4.5.2 Sheet Breakup and Atomization

The key suppositions used to develop the model are: (i) the liquid sheet is two-dimensional, (ii) it is viscous, (iii) it is incompressible of thickness $2h$, and (iv) its velocity is $U$ and it moves through a passive, non-viscous and incompressible gas medium. Denoting the density of the liquid by $\rho_l$, the density of the gas by $\rho_g$, the viscosity of the liquid by $\mu_l$ and considering a coordinate system that moves along the sheet, and a spectrum of infinitesimal wavy disturbances of the following description:

$$\eta = \eta_0\,e^{ikx+\omega\,t} \tag{3.37}$$

is forced on the initially steady motion. Such disturbances lead to fluctuating velocities and pressures of both the liquid and the gas.

In Eq.3.37, $\eta_0$ represents the initial wave amplitude, $k = \frac{2\pi}{\lambda}$ represents the wave number, while $\omega = \omega_r + \omega_i$ represents the complex growth rate.

The largest value of $\omega_r$, represented here by $\Omega$, is assigned to the most unstable disturbance. The sheet breakup is supposed to be due to this disturbance. Therefore, it is essential to evaluate a dispersion relation $\omega = \omega(k)$ from which $\Omega$ can be computed as a function of the wave number. Two solutions, or modes, exist that can be used to solve the governing equations s.t. the boundary conditions at the upper and lower interfaces [106, 107, 108].

In the first solution, also known as the sinuous mode, the waves at the upper and lower interfaces are in phase. In the second solution, also known as the

varicose mode, the waves at the upper and lower interfaces are out of phase. Senecal et al. [109] found that the sinuous mode dominates the growth of varicose waves at low velocities and small gas-to-liquid density ratios. Therefore, the atomization model in Fluent is based upon the growth of sinuous waves on the liquid sheet described by the relations:

$$\omega^2 \left[tanh(kh) + Q\right] + \left[4\nu_l k^2 tanh(kh) + 2ikQU\right] +$$

$$4\nu_l k^4 tanh(kh) - 4\nu_l^2 k^3 l tanh(lh) - QU^2k^2 + \nu_l^2 k^3 l tanh(lh) - QU^2k^2 + \frac{\sigma\, k^3}{\rho_l} \quad (3.38)$$

where $Q = \rho_g/\rho_g$ and $l^2 = k^2 + \frac{\omega}{\nu_l}$.

The fastest-growing waves are classified as either long or short in comparison with the sheet thickness, based on Weber number. For short waves, the second order terms of viscosity can be ignored and thus the equation can be reduced to:

$$\omega_r = \frac{1}{tanh(kh) + Q} 2\nu_l k^2 tanh(kh)$$

$$\sqrt{2\nu_l k^4 tanh^2(kh) - Q^2U^2Qk2 - [tanh(kh) - Q]\left[-QU^2k2 + \frac{\sigma\, k^3}{\rho_l}\right]} \quad (3.39)$$

For long waves, Dombrowski and Johns [110] technique for the disintegration of sheet is adopted. In this model, long waves, ligaments are supposed to be made as a result of the sheet breakup process once the unstable waves reach a critical height. When the surface disturbance reaches a value of $\lambda_b$ at breakup, a breakup time, $\tau$ , can be found using:

$$\lambda_b = \lambda_0\, e^{\Omega\, t} \Rightarrow \frac{1}{\Omega} ln\left(\frac{\lambda_b}{\lambda_0}\right) \quad (3.40)$$

Here, the maximum growth rate, denoted by $\Omega$ can be computed by numerically maximising Eq. 3.40 as a function of $k$. The sheet breaks up and ligaments

are made at a length $L_b$:

$$L_b = U\,\tau\; = \frac{U}{\Omega} ln\left(\frac{\lambda_b}{\lambda_0}\right) \tag{3.41}$$

Here $ln\left(\frac{\lambda_b}{\lambda_0}\right)$ represents an empirical sheet. This is specified by the user. For liquid jets, Weber [111] theoretically found a default value of 12. This value is used in the current work with other different values with no difference in results. It was shown in [110] that the value of 12 agrees favourably with experimental lengths over a wide range of Weber numbers i.e., between 2 to 200.

The diameter of the ligaments made at the breakup point is computed from a mass balance based on the relation:

$$d_L\; = \sqrt{\frac{8h}{k_s}} \tag{3.42}$$

Here $k_s$ denotes the wave number associated with $\Omega$. The diameter of the ligament is based on the thickness of the sheet. In turn, the thickness of the sheet is a function of the breakup length. The thickness of the film is computed using the breakup length and the radial distance from the center line to the mid-line of the sheet at the atomizer exit, $r_0$ as:

$$h_{end} = \frac{r_0\, h_0}{r_0\; + L_b\, sin\left(\frac{\theta}{2}\right)} \tag{3.43}$$

For short waves, the diameter of the ligament is supposed to be linearly proportional to the wavelength that breaks up the sheet according to the relation:

$$d_L = \frac{2\pi\, C_L}{K_s} \tag{3.44}$$

Here $C_L = 0.5$ by default.

In both the cases, the breakup from ligaments to droplets is supposed to behave as stated in Weber's [111] analysis for capillary instability.

$$d_0 = 1.88 d_L\,(1 + 3OH)^{\frac{1}{6}} \tag{3.45}$$

Here, $OH$ denotes the Ohnesorge number. It is a combination of the Reynolds

number and the Weber number and is defined as:

$$OH = \frac{\sqrt{We}}{Re} \tag{3.46}$$

Once $d_0$ has been determined from Eq. 3.45, it is supposed that this diameter of the droplet is most likely the droplet size of a Rosin-Rammler distribution with a spread parameter of 3.5 and a default dispersion angle of $6^o$ . It can be changed in the software. When using this model, the user must specify the spray cone angle.

### 3.4.6 Chemical Mechanisms

The chemical models used in this study are mainly the San Diego mechanism where its documentation is available at the dedicated website [101] and another mechanism generated (for both diesel and biodiesel) using EXGAS mechanism which is illustrated in Fig. 3.3. EXGAS software has been used for generating mechanisms for the alkanes (Warth et al. [59], Buda et al. [112], Biet et al. [113], Glaude et al. [92] and Touchard et al. [114]. A summary of the mechanisms used in modelling methanol ($CH3OH$) is given in Appendix B.

## 3.5 Radiation Model

The accuracy of the model can be improved if radiation model is included in it. On the other hand, it can result in extinguishing flamelets at low strain rates. Hence, it is important to treat the radiation source term with care [84]. The radiation model used in this study is the P-1 model. It is the most basic version of the more general P-N model. The P-N model involves the expansion of the radiation intensity $I$ into an orthogonal series of spherical harmonics [115]. The radiation flux $q_r$ can be obtained using the following:

$$q_r = -\frac{1}{3(\alpha + \sigma_s) - C\sigma_s}\nabla G \tag{3.47}$$

Here $\alpha$ and $\sigma_s$ are the absorption and scattering coefficients respectively, while $G$ is the incident radiation and $C$ is the linear anisotropic phase function coeffi-

cient. It denotes the amount of radiation scattered in the forward direction and has values between $-1$ and $+1$. A positive value of $C$ indicates that more radiant energy is scattered in the forward than in the backward with $C = 1$ standing for fully backward scattering. A zero value of $C$ denotes isotropic scattering. This estimation is implemented in these simulations.

The transport equation for $G$ is:

$$\nabla(\frac{1}{3(\alpha+\sigma_s)-C\sigma_s}\nabla G) - \alpha G + 4\alpha\sigma T^4 = 0 \tag{3.48}$$

where $\sigma$ represents the Stefan-Boltzmann constant. Eq. 3.47 and Eq. 3.48 can be combined:

$$-\nabla q_r = \alpha G + 4\alpha\sigma T^4 = 0 \tag{3.49}$$

The flux of the radiation at walls, $q_{r,w}$, can then be calculated as:

$$q_{r,w} = -\frac{e_w}{2(2-e_w)}(4\sigma T_w^4 - G_w) \tag{3.50}$$

where $e_w$ is wall emissivity.

## 3.6 Benchmark and Computational Model

The benchmark adopted as a validation case is that of Widmann and Presser [1]. The 3-dimensional CAD model for the burner used in this study is shown in Fig. 3.5 and a meshed one is shown in Fig. 3.6. To show the mesh quality and the inner components of the burner, and open-sided meshed model is shown in Fig. 3.7. The inner view shows both the injector position as well as the air inflow boundary. A central plane showing the quality of the mesh is displayed in Fig. 3.8, and it is apparent that the mesh was made quite fine near the walls and the injector and inflow boundary. The reason behind this is to help solve the most important regions where the physics of fluid is important and complex as well. Despite the fact that the RANS approach has been used here, it is still important to resolve the flow structures close to the wall boundaries and the flame region. Some initial trials have been conducted with different meshes

of order 750 thousand and 1.5 million mesh size, however, the mesh shown in Fig. 3.7 and Fig. 3.8 consist of more than two million finite elements and it is the mesh adopted in the current simulation. It is worth to mention that results of the temperature and velocity profiles from initial trials of the last two meshes (1.5 million and 2 million) show no difference, indicating that increasing the mesh density further may not bring any substantial benefits in terms of results. Rather, refining the mesh further can lead to other inherited errors (errors associated with both the solution of Navier-Stokes equation in unstructured mesh and the different schemes employed in linearising them) and may lead to unrealistic and corrupted results.

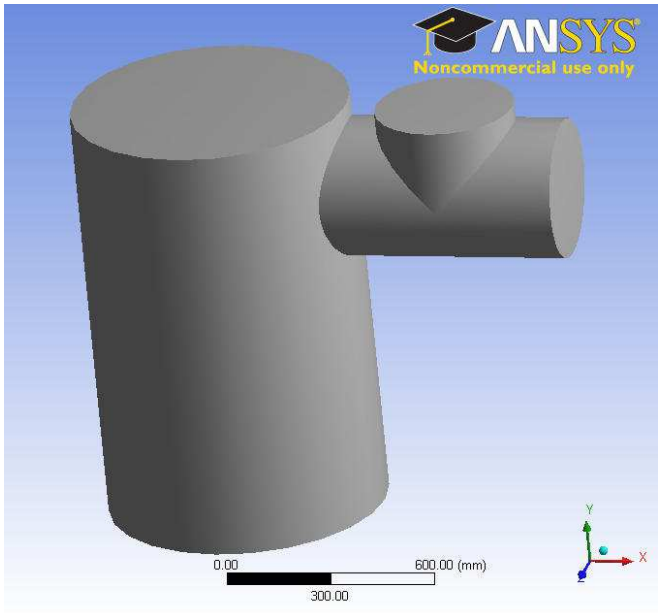


Figure 3.5: Burner CAD model

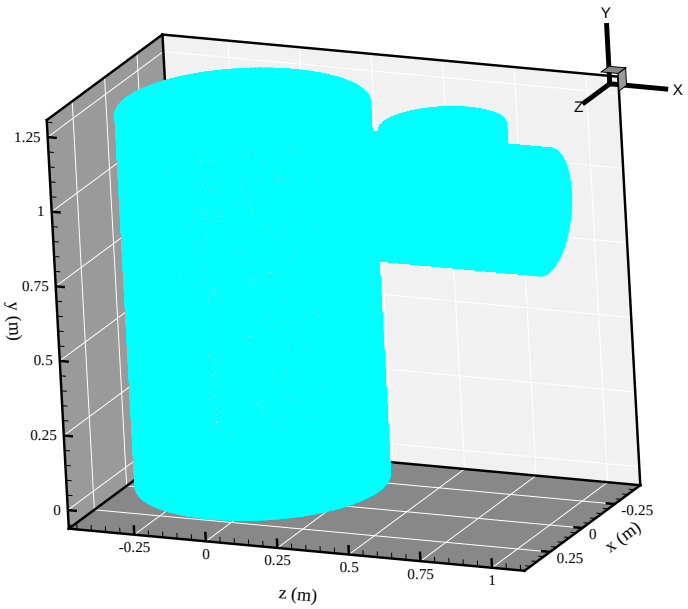


Figure 3.6: Meshed 3D model

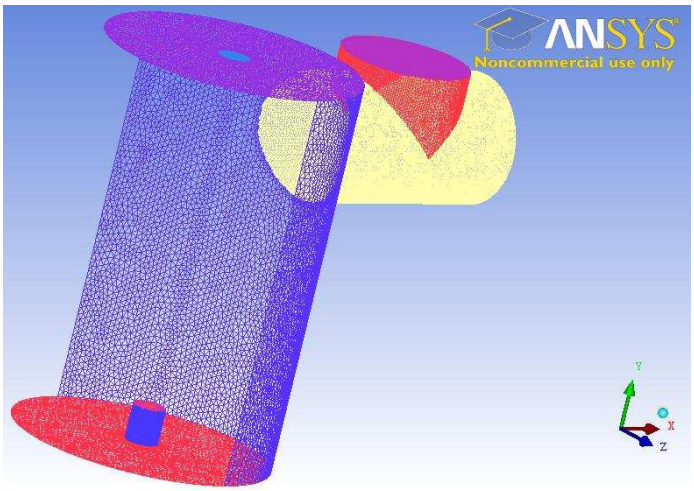


Figure 3.7: Inner view of the meshed burner model

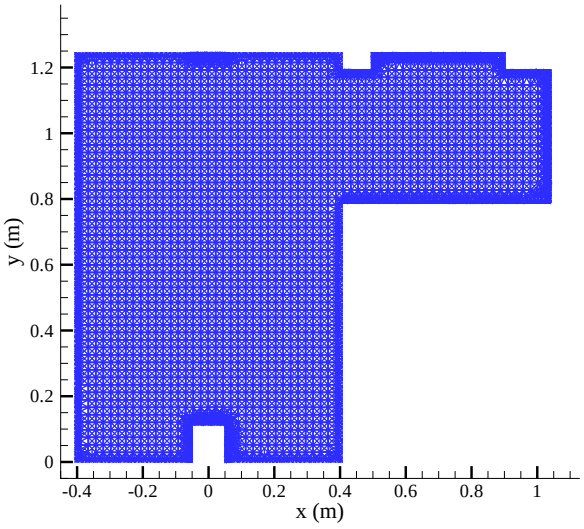


Figure 3.8: A central slice of the meshed model

Widmann and Presser [1] used liquid methanol ($CH_3O_3$) and an atomisation process to spray and burn the liquid methanol within the burner geometry described above and under specific operating boundary conditions detailed in Table 3.1. They obtained a range of data including temperature and velocity fields and emission data for carbon oxides ($CO$ and $CO_2$) using some thermocouples and some gas analysers. For the temperature, they focused on obtaining result via a specific thermocouple located at the exit region of the computational domain. In the current CFD model for the base case of Widmann and Presser [1], quite a few profiles at the exact location of the experimental work and the surrounding region are obtained and diagrammatically shown in Fig. 3.9 and Fig. 3.10. In most of their readings, they estimated a percentage error for most of the data obtained (for example the sonic nozzle used to spray liquid methanol has a manufacturer uncertainty of order 3% and hence one would expect a difference in results between the CFD results for this case and the experimental data. In this study, several horizontal and vertical profiles matching the position of Widman thermocouples and close proximity were obtained for almost every piece of data the simulation offer. These profiles are used to validate the current computational work with the experimental data and build more confidence in the model developed by the author of this thesis to study more complex models. Further results in terms of contours to the different parameters involved is also presented to give further insight on the spray combustion of liquid methanol ($CH_3OH$) using the models presented in this study. The CFD simulations were done with lots of caution and initially ignoring radiation effect in order to assess using a detailed reaction mechanism in obtaining relevant results. Therefore Section 4.1 discusses the results of the most simple case ignoring radiation and shed light on degree of agreement between the CFD and the experimental results. The case also used more trusted advanced but reduced reaction mechanism, that of San Diego.

Table 3.1: Operating conditions for the baseline experiment of Widmann and Presser [1]

| | |
|---|---|
| Fuel type | Methanol |
| Fuel flow rate | 3.0 kg/h |
| Fuel temperature | Ambient |
| Equivalence ratio | 0.3 |
| Air flow rate | 56.7 $m_3/h$ |
| Air temperature | Ambient |
| Vane angle | $50^o$ |
| Swirl number | 0.58 |
| Flame standoff distance | 5 mm |
| Chamber pressure | Ambient |

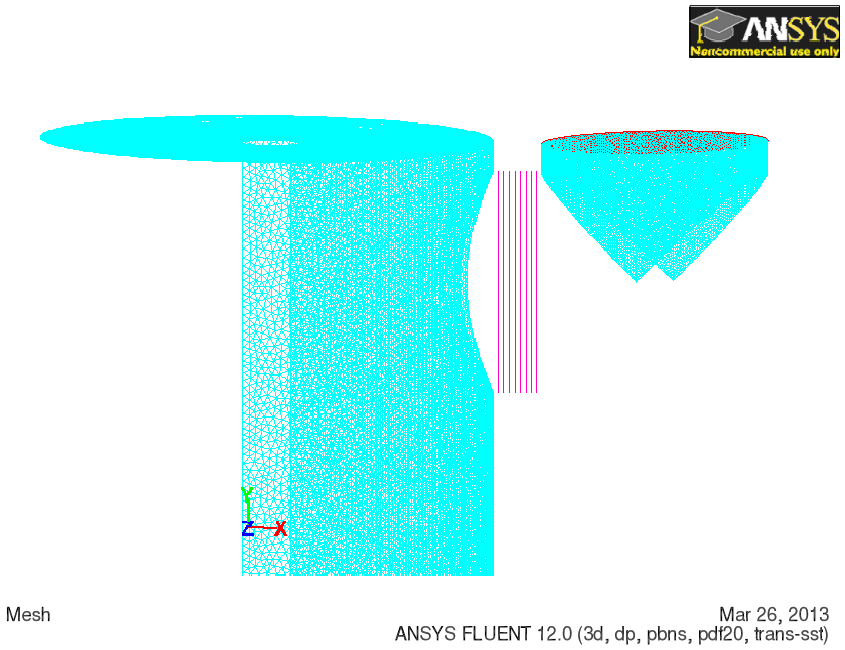


Figure 3.9: Vertical lines locations

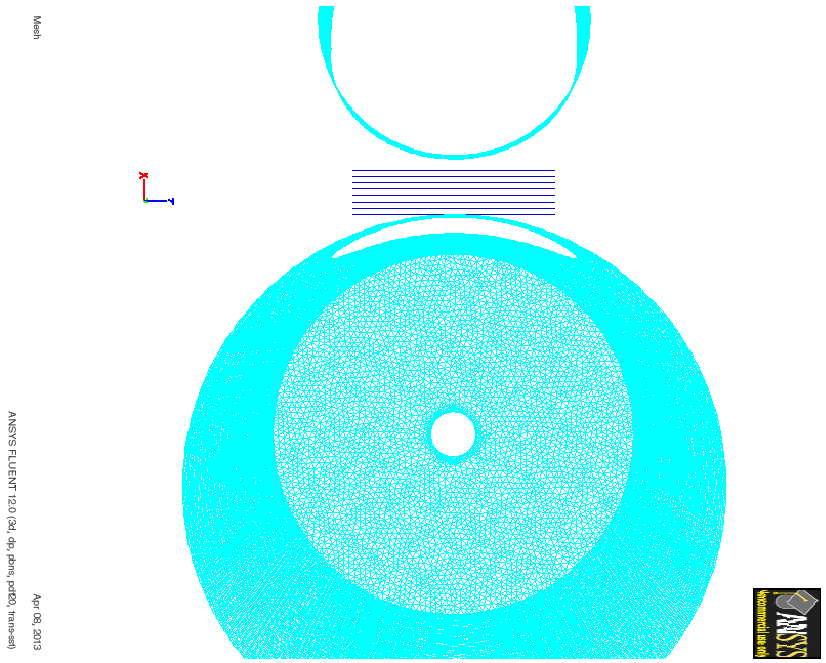


Figure 3.10: Horizontal lines locations

# Chapter 4

# Results and Discussion: EXGAS Reaction Model (EGRM) Validation Using Methanol

One of the objectives of this work is to develop and test a comprehensive reaction mechanism and study the effect of including more reaction steps and species in the combustion of conventional and biofuels. However, it is thought that it is a wise step to model the combustion process of methanol based on existing and well tested advanced but reduced mechanisms. The author of this thesis selected the mechanism developed by the combustion group at University of California, San Diego, well known as "*The San Diego Mechanism*" [116], which is abbreviated and referred to here as SDRM. In the SDRM, the number of species and reaction steps are kept to the minimum and only those necessary to describe the reaction systems and phenomena are taken into consideration - that is the philosophy behind developing the SDRM reaction mechanism. Of course this is very good in scaling down the uncertainties in the results obtained, however, on the other hand, the complete combustion process will not be modelled in the opinion of the author of this thesis. The author strongly believes that all species that are generated while the combustion process is advancing in time and the relevant reactions between all these species with the base hydrocarbon fuel used should be taken into consideration in order to obtain a complete combustion process. Having said

so, and from the literature review of related work, the author is aware of the deficiencies that occur as a result of employing comprehensive reaction mechanism, especially for modelling large hydrocarbons. As the philosophy of this thesis is to seek completeness of modelling the combustion process of small and large hydrocarbon, models developed will attempt to include all potentially relevant elementary reaction steps and species. However, it is thought that the SDRM should be used first to model the methanol and the outcome should be compared with the experimental results and then adopt this as a ground for assessing the performances of the developed model. More importantly, the SDRM mechanism is not suitable for modelling large hydrocarbon, and hence, a developed model is a must to advance the proposed work of this thesis.

## 4.1 Validation of the CFD Results Using Temperature

One of the most adequate data offered by the experiment of Widmann and Presser [1] is the exit gas temperatures on a disc at the exit are according to the thirteen points shown in Fig. 4.1. Using the SDRM reaction mechanism, the CFD results obtained from the simulation at the exact location of Widmann and Presser [1] are listed in Table 4.1 and plotted in Fig. 4.2. The figure clearly shows that the predicted results are in very good agreement with the experimental data. Overall, the results shown in Fig. 4.2 offer one good point, the validity of the setup used in the computational model. It is clear that the way the problem was set in Fluent is correct and the predicted results are representative and one can confidently rely on the model set up to model the rest of the required benchmarks in this first part of the proposed CFD work associated with the first benchmark - the burner of Widmann and Presser [1]. The results indeed provide a solid background and help in commenting on the rest of the computational work for the different types of fuels that are part of the aims and objectives of this thesis.

On top of considering the exact locations of the exit temperature of Widmann and Presser [1] shown in Fig. 4.2, temperature profiles within the proximity of

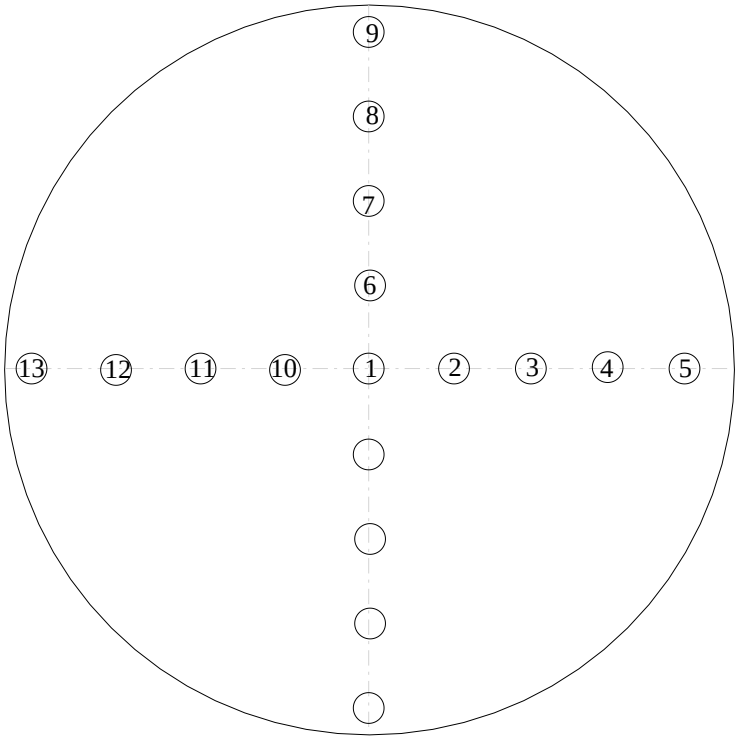


Figure 4.1: Vertical temperature location

Table 4.1: Temperature data at the exit: experimental data and CFD results

| Location | Radial Coordinate | Angle | EXP ($^oC$) | EXP (K) | CFD (K) |
|---|---|---|---|---|---|
| 1 | 0 | 1 | 244 | 517 | 509 |
| 2 | 44.5 | 0 | 265 | 538 | 524 |
| 3 | 88.9 | 0 | 282 | 555 | 541 |
| 4 | 133.4 | 0 | 288 | 561 | 567 |
| 5 | 177.8 | 0 | 266 | 539 | 540 |
| 6 | 44.5 | 90 | 251 | 524 | 510 |
| 7 | 88.9 | 90 | 258 | 531 | 533 |
| 8 | 133.4 | 90 | 271 | 544 | 545 |
| 9 | 177.8 | 90 | 277 | 550 | 552 |
| 10 | 44.5 | 180 | 221 | 494 | 505 |
| 11 | 88.9 | 180 | 207 | 480 | 502 |
| 12 | 133.4 | 180 | 182 | 455 | 505 |
| 13 | 177.8 | 180 | 160 | 433 | 501 |

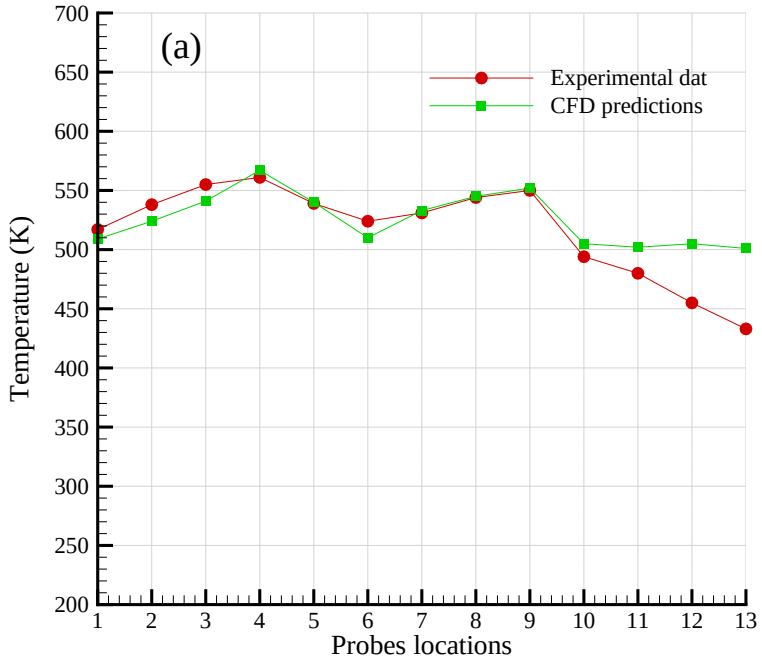


Figure 4.2: Comparison between the computational results using San Diego Mechanism and the experimental data.

the exit (corresponding to the vertical and horizontal lines shown in Figs. 3.9 and 3.10) were obtained from the same simulation that uses the SDRM. The results were presented in Fig. 4.3(a) and Fig. 4.3(b) for the horizontal and vertical profiles respectively. Examining the temperature ranges and comparing them with that of Fig. 4.2, they reveal the same range and do agree with the measured values of the experimental data very well. this consolidate the confidence in the CFD setup for this simulation and provide further evidence for validating the CFD results.

Having examined the temperature at some relevant locations associated with the experimental work, it is worth examining the temperature range within the flame region and close to the injector location. The values at these locations not only offer an indication of the amount of energy released, but also provide an insight to the flame structure.

Shown in Fig. 4.3(c) are the temperature profiles for cross-sectional lines start-

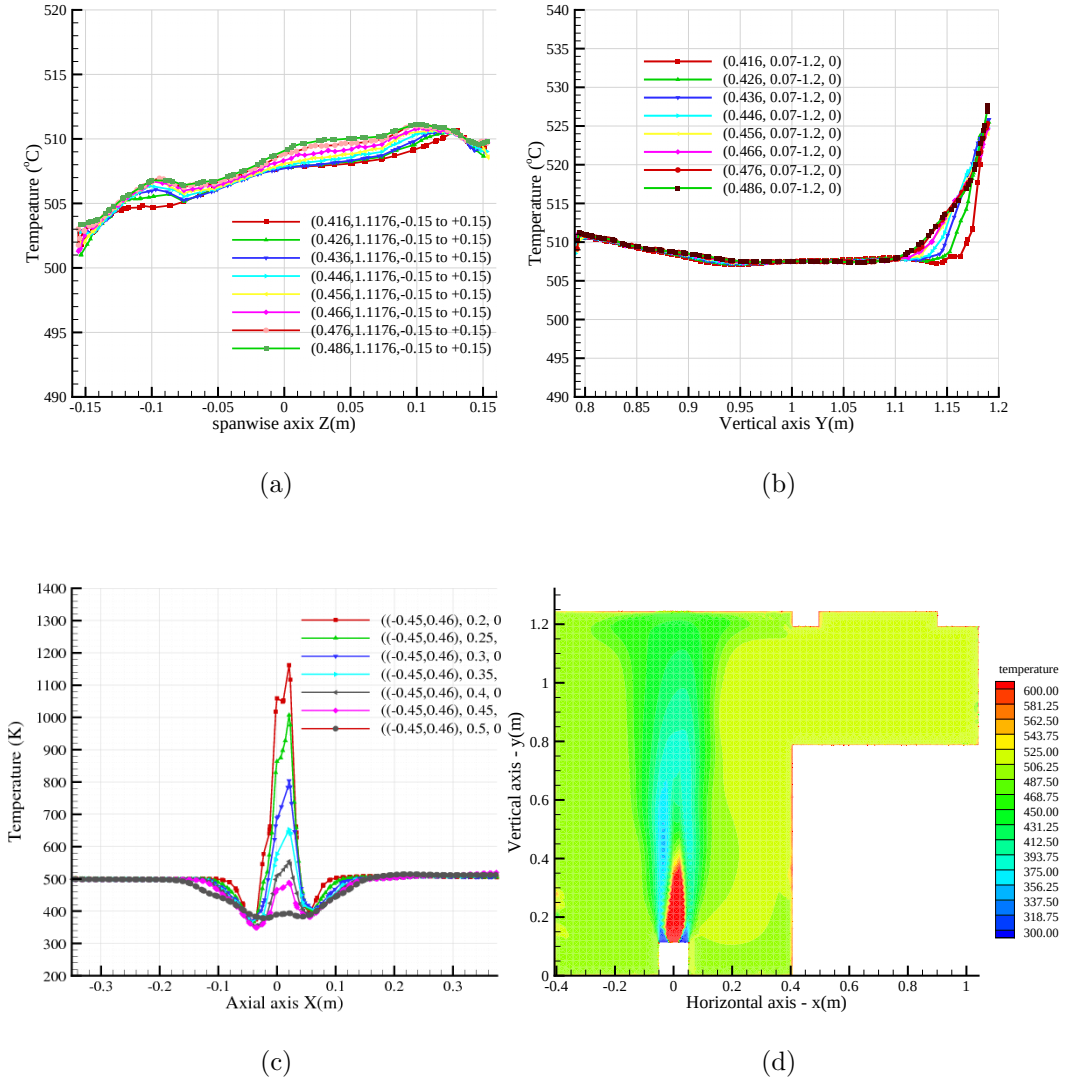


Figure 4.3: Temperature profiles corresponding to the (a) horizontal lines shown in Fig. 3.10 and (b) vertical lines shown in Fig. 3.9. (c) Cross-sectional temperature profiles close to the injector. (d) Temperature contours for a central slice.

ing 0.2m from the base of the burner (Fig. 3.5 and Fig. 3.6) and increasing by 0.05m increment along the vertical coordinate and spanning the whole spanwise dimension. It is clear that the temperature at close proximity to the injector ($y = 0.2m$) is quite high (of order $1200K$) decreasing gradually upon moving

along the normal axis to a vale of order 500K, which is the average temperature of the whole burner - in agreement with the experimental work of Widmann and Presser [1]. This behaviour elucidates the structure and the length of the flame. Fig. 4.3(c) clearly indicates that the flame length is of order 0.4m and considering the length of the injector height from the base of the burner, the estimated flame length is of order 0.35m. The figure also shows that the maximum width of the flame is of order 0.1m. To support these information, temperature contours for a central x-y plane ($z = 0$) is shown in Fig. 4.3(d). The contours provide a clear two-dimensional image (view) of the flame structure and the distribution of temperature in the burner in general. The image displays a short, but a well-established flame. The predicted temperature distribution is in agreement with the experiment of Widmann and Presser [1] (the benchmark adopted for validation), where the temperature range is 500–600$K$ on other parts of the burner. The figure also show that the liberated heat provide a plume-like structure surrounding the flame. The hot gases impinge on the upper wall and because the opening is on one side only, this has influenced the movement of hot (less dense) gases towards the exit. It is worth mentioning that the geometry is not an easy one to model for validation as it seems complex not only in shape but the inclusion of multi-pipes with the main exit pipe closed at the end and another pipe sitting on top of it providing the outflow boundary.

These general features are from a reduced but advanced reaction mechanism, the SDRM. Based on the fact that the results obtained showed good agreement with the experiential benchmark adopted in this study (Widmann and Presser [1]), they would provide a platform to compare the rest of the simulations based on other types of developed comprehensive reaction mechanisms and different fuels (both conventional and biofuels). However, before moving on from this simulation using the SDRM, it is essential to examine other important parameters associated with this reactive flow, this is done in the sections below.

## 4.2 SDRM - Profiles of Other Relevant Parameters

The above discussion focused on temperature as the main parameter used for validating the CFD results. The computational results offer much more parameters and this section will look at some of them that may shed more light on the nature of the turbulent reactive flow under consideration.

### 4.2.1 Profiles of Relevant Turbulence Parameters

The value of Reynolds number is always of interest in fluid mechanics and used as the non-dimensional parameters that shows whether the flow is laminar, transitional or turbulent. Shown in Fig. 4.4(a) is the profile for the Turbulent Reynolds number for the vertical lines of Fig. 3.9 while those for the horizontal lines (Fig. 3.10) are shown in Fig. 4.4(b). These are the locations at the exit where most of the experimental data was obtained.

Turbulent Reynolds number, $Re_y$ is defined according to the relation:

$$Re_y = \frac{\rho\, y\, \sqrt{k}}{\mu} \tag{4.1}$$

In the code used in the current work (Fluent 12.1 [82]) uses a couple of approaches to model the new-wall region. The first is near-wall model in which the viscosity-affected near-wall region is completely resolved all the way to the viscous sub-layer. The second method is the two-layer approach, which is an integral part of the enhanced wall treatment in the SST model employed here. This approach specifies both $\epsilon$ and the turbulent viscosity in the near-wall cells. In the two-layer approach, the whole computational domain is subdivided into a viscosity-affected region and a fully-turbulent region where the boundary of the two regions is determined by a wall-distance-based, turbulent Reynolds number, $\mathrm{Re}_y$, defined above. In Eq. 4.1, the $y$ is the normal distance from the wall at the cell centers. Fluent interprets $y$ as the distance to the nearest wall, and in this fashion, $y$ is independent of the mesh topology used, and is definable even on unstructured meshes. It is apparent that the definition of $y$ in this fashion

makes it independent of the mesh topology used, and is definable even on unstructured meshes. As a common approach, the fully turbulent region is defined for $Re_y > 200$) where the flow is modelled by the well known $k$- $\epsilon$ models. In the near-wall region ($Re_y < 200$) where viscosity effects influence the flow field, the one-equation model of Wolfstein [117] is employed as discussed in Section 3.2.

Although there is no available experimental data to compare this parameter with, the CFD results are examined both at the exit and at cross-sectional profiles just above the injection point along the normal axis. Shown in Fig. 4.4(a) and Fig. 4.4(b) are respectively the profiles for $\mathrm{Re}_y$ corresponding to the vertical and horizontal lines shown in Fig. 3.9 and Fig. 3.10. The first observation was that $\mathrm{Re}_y$ based on the normal direction parameters has higher range compared to that based on the horizontal or spanwise parameters. This is expected as most of the parameters (velocity, turbulent kinetic energy etc.) are smaller along the span wise compared to those along the normal (vertical axis). An evidence is displayed in Fig. 4.4(c) and Fig. 4.4(d) where the velocity magnitude, defined as $\sqrt{\bar{u}^2 + \bar{v}^2 + \bar{w}^2}$) is shown for the horizontal and vertical lines of Fig. 3.9 and Fig. 3.10. Although the difference in velocity is not that much, it makes a difference in connection with related values of the density $\rho$ and $k$. Focusing on the figures themselves, one would read that there is a small wall region that has $\mathrm{Re}_y$ of order 200 or less, which corresponds to the viscous sub-layer. Beyond this region, the flow displays a fully turbulent (unsteady) nature. Taking into consideration the reactive nature of the flow and the high rate of generation of temperature around the flame region, and the geometrical complexity, all add to the degree of complexity of such flows. On top of this, the flow strongly includes an element of buoyancy as cold flow is drawn from beneath the injector, although the oxygen is consumed in burning the flow, the nature of the cold flow holds and this generates a high rate of bouncy productions. This element will be highlighted upon discussion of the Prandtl number downstream of this discussion. The buoyancy, in particular, was not cared for in the model used and hence could be one of the weak links that contribute as a major source of error in these simulations.

Close to the injector location, a cross-sectional profile at the centre of the plane ($z = 0$) for the Turbulent Reynolds number are shown in Fig. 4.5(a), while the contours for this variable on a central (x,y)-plane appear in Fig. 4.5(b). The

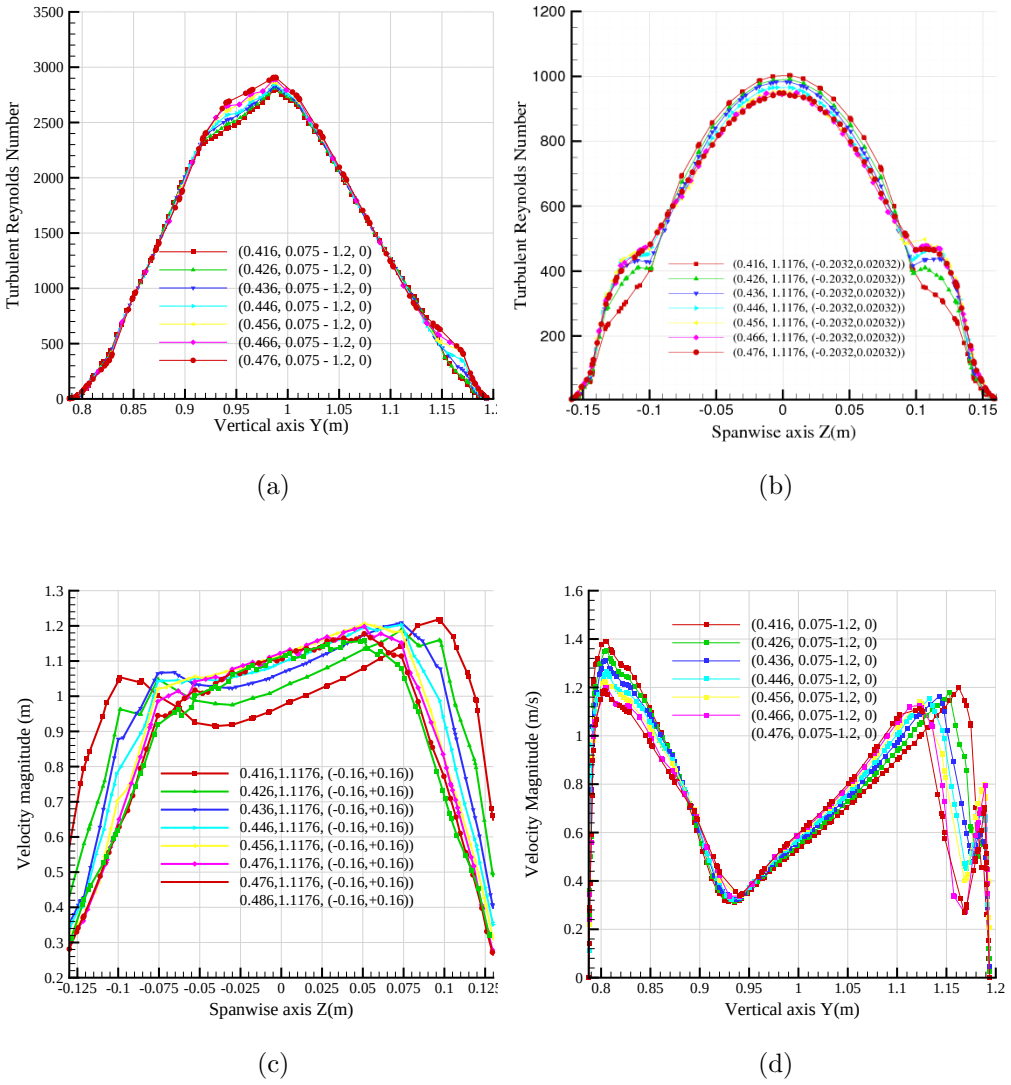


Figure 4.4: Turbulent Reynolds number profiles corresponding to the (a) vertical lines shown in Fig. 3.9 and (b) horizontal lines shown in Fig. 3.10. Velocity profiles corresponding to the (c) horizontal lines shown in Fig. 3.10 and (d) vertical lines shown in Fig. 3.9.

profiles of Turbulent Reynolds number (Fig. 4.5(a)) clearly shows that around the region surrounding the flame, the flow is fully turbulent with $\mathrm{Re}_y$ magnitude of order 9000. The profiles also indicate that the unsteady nature of the flow - values of $\mathrm{Re}_y$ do not exhibit a smooth curve with a maximum value. The contours

of $\mathrm{Re}_y$ (Fig. 4.5(b)) on the other hand, show a clear qualitative distribution of this variable within the computational domain. The figure highlights the regions of turbulent flow which include the exit region of the computational domain.

The other relevant parameter that has been looked at to shed more light on the flow field is the turbulence intensity $I$, defined as:

$$I = rms(\frac{u^{'}}{u_{avg}}) \tag{4.2}$$

that is, it is the ratio of the root-mean-square of the velocity fluctuations, $u^{'}$, to the mean flow velocity, $u_{avg}$. As a general rule, a turbulence intensity of 1% or less is considered low and turbulence intensities greater than 10% are considered high. To examine this parameter in this SDRM simulation, the turbulence intensity profiles for horizontal cross-sectional lines above the heat source are shown in Fig. 4.5(c) while the contours for a central (x,y)-plane are displayed in Fig. 4.5(d). The profiles show that the maximum turbulence intensity (within the flame region) is of order 40% with lower values far from the central region. This is an indication to the fully turbulent nature of this reactive flow. The contours of turbulence intensity, on the other hand, show the unsteady nature of the flow and the non-uniformity of this parameter distribution within the computational domain.

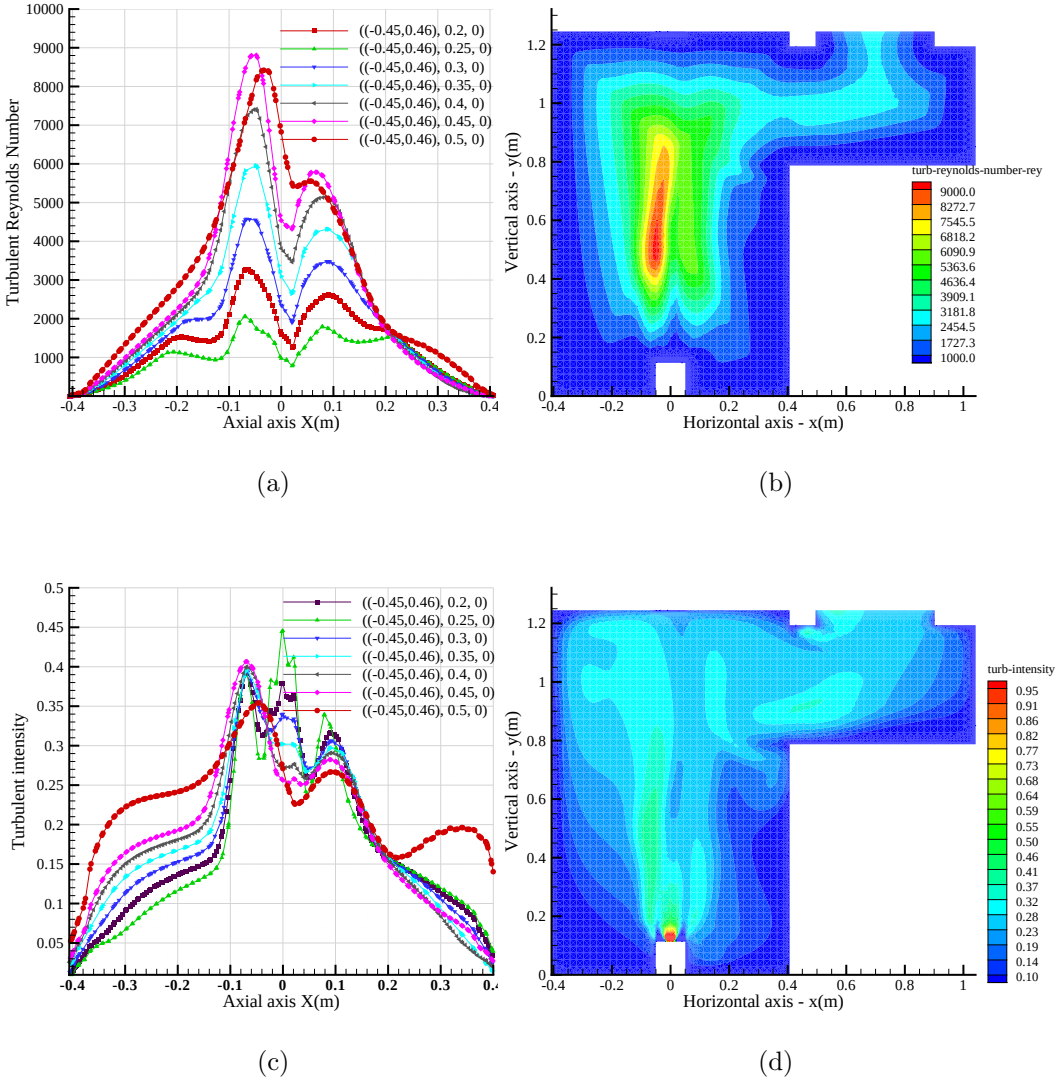


Figure 4.5: Turbulent Reynolds number (a) profiles close to the injector, and (b) for a central (x,y)-plane. Turbulent intensity (c) profiles close to the injector, and (d) number for a central (x,y)-plane.

### 4.2.2 Profiles of Carbon Oxides ($CO$ and $CO_2$) at the Exit and within the Flame Region

Having commented on the nature of the temperature and flow field in Section 4.1 and Section 4.2 above, the next important variables to consider relevant to this reactive flow simulation using the SDRM is the emissions (carbon oxides ($CO$ and $CO_2$) and nitrogen oxide ($NO_x$)).

A comparison between the CFD predictions with the experiment at specific locations at the burner exit is shown in Fig. 4.6. The CFD results (based on the SDRM) shows acceptable agreement with the experimental data, slightly under predicted the experimental values (recording lower values) but by a small marginal difference. The difference can be explained as due to many issues including the uncertainty surrounding the experimental data. This is another validation of results for the CFD predictions which supports the fact that the current simulation results are representative of the physical combustion phenomena that occurs in this burner geometry. It also provides an additional support for the adequate set-up of the simulation complex parameters involved in the simulation and provides strong platform for the rest of the simulations intended to follow this validation case.

It is worth mentioning that in a previous study by Collazo et al. [65] where primitive combustion model was used, the predictions has shown better agreement with the experiment. They used the EDC model proposed by Magnussen [118] with three reactions only. However, considering the fact that even Widmann and Presser [1] mentioned that there is a marginal uncertainty in their results and also considering the fact that these experimental works used slightly old Fourier Transform Infrared Spectroscopy (FTIR) spectroscopy to determine the $CO_2$ and $CO$, the fact that the SDRM involves quite a few species with a set of reactions connecting these species, in the author's opinion, that any CFD results that exactly match the experimental results may be representative but have an element of being unrealistic. On top of this, the author of this work strongly believes that using advanced reaction mechanism which includes many intermediate species and reaction steps would definitely lead to a difference in results, but to the positive side rather than on the erroneous side. Based on these

arguments, the predictions shown in this work so far are realistic and probably more accurate from the author's point of view.

Carbon dioxide ($CO_2$) profile on the vertical and horizontal lines (Fig. 3.10 and Fig. 3.9) matching and close to the measuring station of Widmann and Presser [1] are obtained from the simulation and plotted in Fig. 4.7(a) and Fig. 4.7(b) respectively. Generally, the concentration (mole fraction) range is of order 0.01 to 0.0149 with lower values close to the walls. Again this is slightly under predicted compared to the experimental values which are of order 0.017 - 0.02, however, as argued above that the experimental values are subjected to some marginal uncertainty while the CFD results are produced using more advanced reaction mechanism (the SDRM) that might have led to these marginal differences. Above all one can conclude that the prediction of this variable ($CO_2$) is good compared to the experimental data.

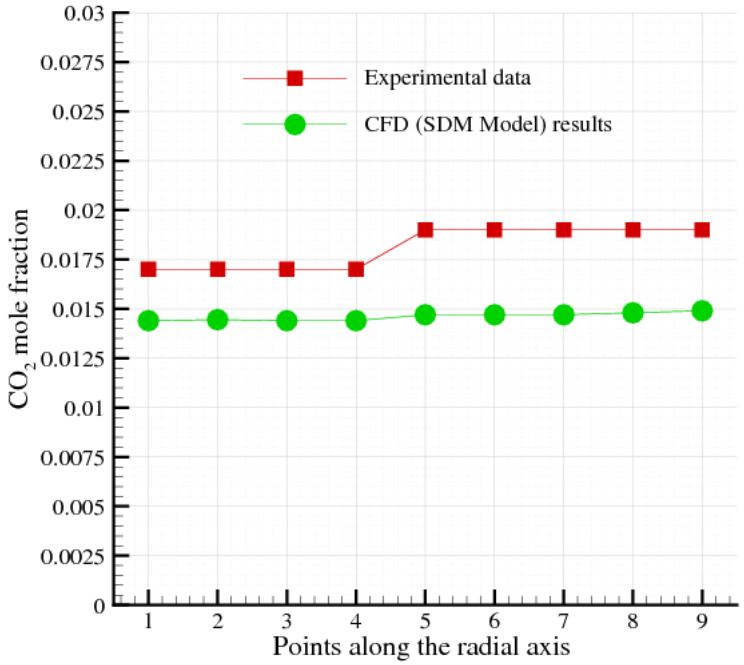


Figure 4.6: Experimental and CFD (SDRM model) results for $CO_2$

Profile of $CO_2$ corresponding to cross-sectional lines close to the injector (start

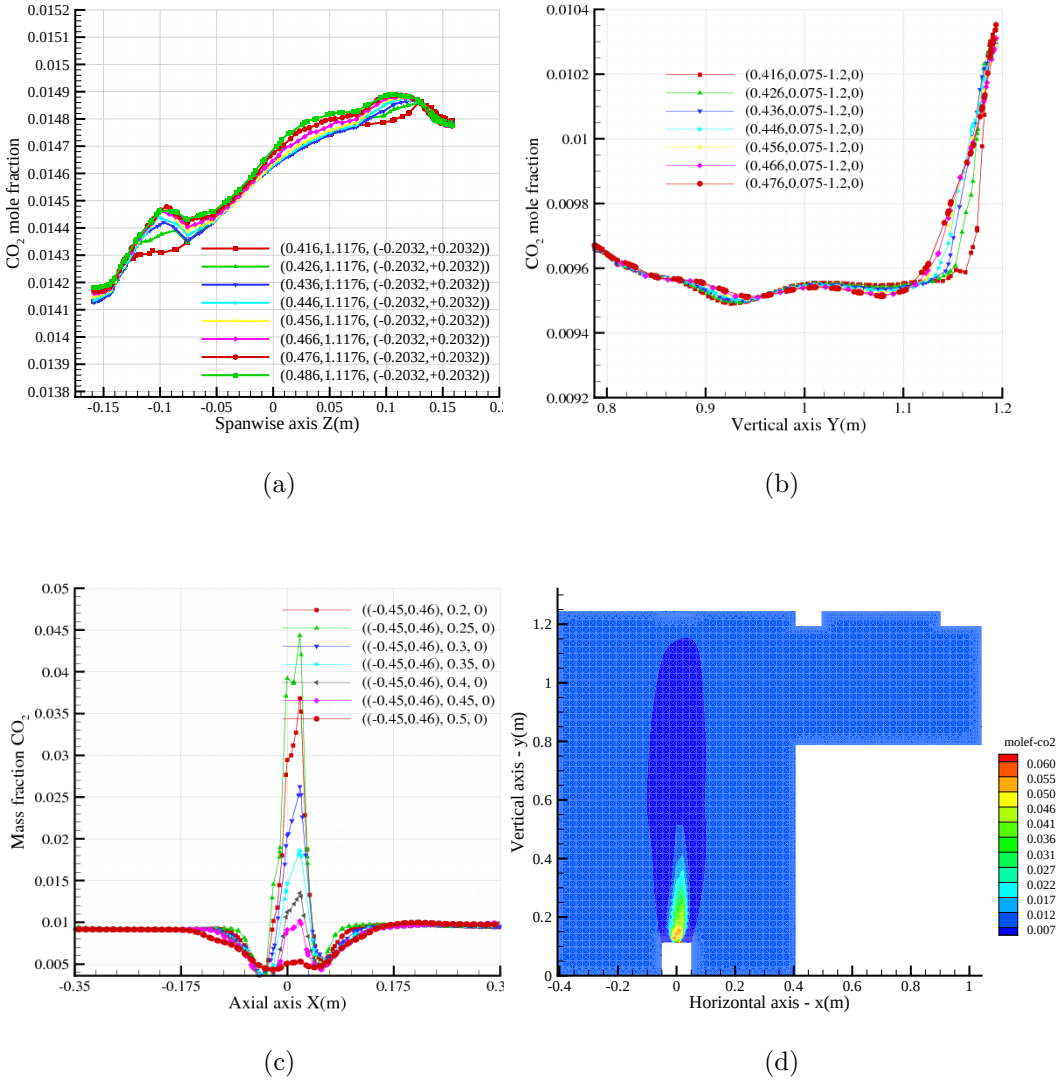


Figure 4.7: $CO_2$ profiles corresponding to the (a) horizontal lines shown in Fig. 3.10 and (b) vertical lines shown in Fig. 3.9. (c) Cross-sectional profiles of $CO_2$ close to the injector. (d) Mole fraction of $CO_2$ for a central (x,y)-plane ($z = 0$)

at $y = 0.2m$ from the burner bottom surface increasing with 0.05m along the normal axis) are shown in Fig. 4.7(c) and contours for a central (x,y)-plane are displayed in Fig. 4.7(d). The profiles show a symmetry around the flame region with a maximum mole fraction of order 0.045 decreasing gradually upon moving

upwards along the normal axis from the injector. The normal value on the larger part of the burner is of order 0.01. Both the cross-sectional profiles and the central indicate very low traces of $CO_2$.

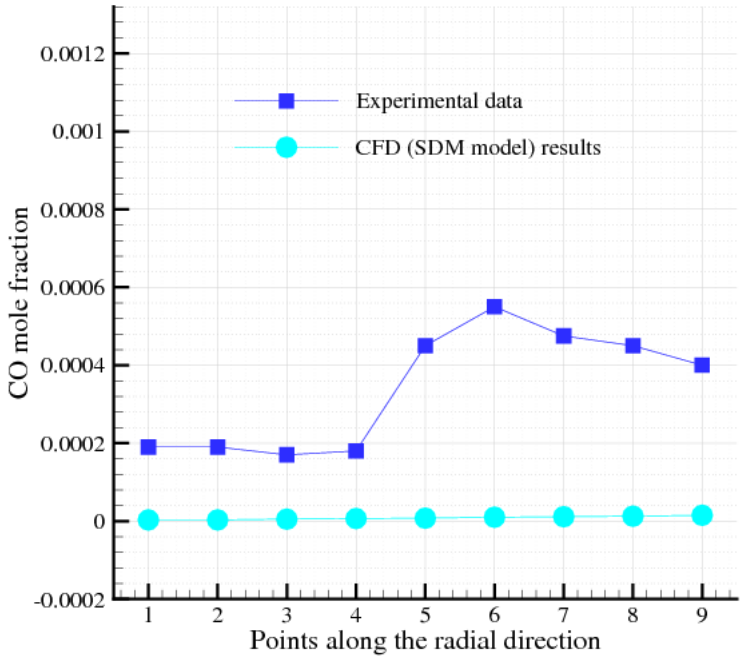


Figure 4.8: Experimental and CFD (SDRM model) results for $CO$

On the other hand, the rate of production of $CO$ is very low for both the measured experimental values and the CFD results. The measured values are of order $2 \times 10^{-4}$ increasing to $5.75 \times 10^{-4}$ while the predicted results reach a maximum of $1.5 \times 10^{-5}$ declining to zero value near the wall. It is apparent that these are quite small values to accurately predict, however, there is still agreement in the trend of $CO$ distribution along the radial direction although the CFD using the SDRM has under predicted the experimental data by a margin. However, consider the very small concentration of this variable ($CO$), one would still mention that the predictions are in line with the CFD results.

The best way to look at $CO$ distribution is through Fig. 4.9(a) and Fig. 4.9(b) which shows the $CO$ concentration on the horizontal and vertical lines at the exit

of the burner (Fig. 3.10 and Fig. 3.9) in close proximity of the measuring stations of Widmann and Presser [1]. It is worth mentioning that Widmann and Presser [1] pointed out that the concentration of $CO_2$ is approximately 50 times greater than that of $CO$, an indication to the fact that the rate of methanol conversion to $CO_2$ and $H_2O$ is occurring at a rate approximately 50 times faster than the conversion to $CO$ and $H_2O$. However, simulation indicates that this rate is even much higher than what the experiment revealed. This is most likely to be due to the inclusion of many species as well as many reaction steps thus affecting the rate of generation not only of $CO$ but all the by-products of combustion. The rate of conversion of species is one of the complex phenomena of combustion in general and becomes more complex when trying to model most (if not all) the species involved and the associated reactions. All this strongly suggest the difficulty on predicting this by-product ($CO$) and other emission data in an accurate rate. Having said this, examining Fig. 4.9(a) and Fig. 4.9(b), it is apparent that the CFD results show a similar trend to the results although there is a difference in the range of the values especially at central locations - the agreement is good for locations below the central points.

Examining the cross-sectional profiles for $CO$ at the central region close to the injector location and moving upward (by $0.05m$ interval), the concentration of this variable is shown in Fig. 4.9(c) while Fig. 4.9(d) displays the contours for a central (x,y)-plane. It is clear that highest rate of $CO$ predicted by the CFD SDRM model is of order 0.025, compared to 0.045 for $CO_2$. The contours of Fig. 4.9(d) suggest that $CO$ is concentrated in a small region around and on top of the flame region.

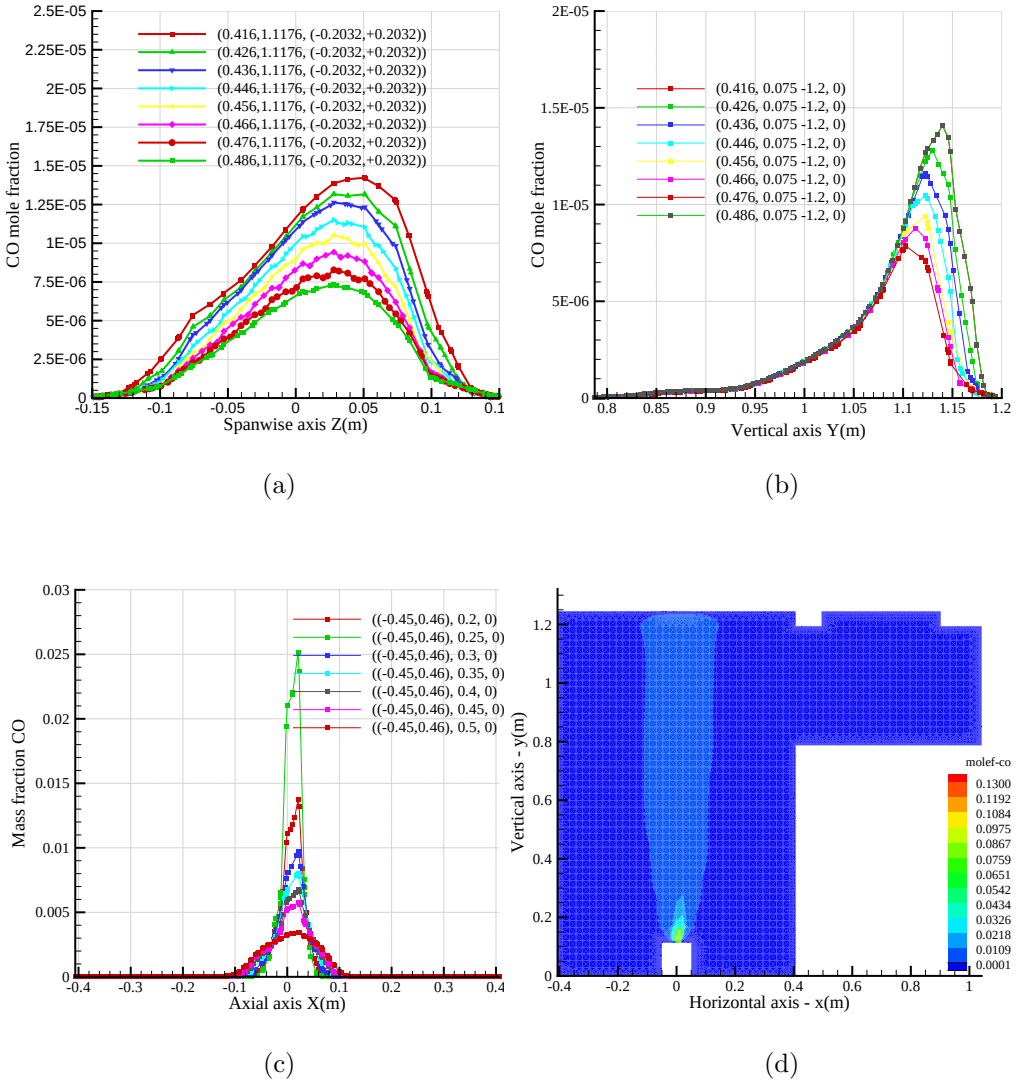


Figure 4.9: *CO* profiles corresponding to the (a) horizontal lines of Fig. 3.10, and (b) vertical lines of Fig. 3.9.(c) Cross-sectional profiles of *CO* close to the injector. (d) Mole fraction of *CO* for a central (x,y)-plane ($z = 0$)

### 4.2.3 Profiles of Fuel ($CH_3OH$) within the Flame Region

The last parameter that was discussed by Widmann and Presser [1] is the unburned fuel ($CH_3OH$). The CFD prediction at the exit shows very low values for $CH_3OH$, however, a central profile close to the injection point shows that the concentration (mole fraction) at a height of 0.2m from the burner base is of order 0.0035 as seen from Fig. 4.10. The close to zero values at the exit indicates that a high percentage or almost all of the fuel was burned. Referring to the fact that the CFD predictions showed slightly lower values than other by-products ($CO$ and $CO_2$) strongly suggest that the inclusion of more species and their associated reactions contribute to effective combustion of the fuel and probably reveals a realistic picture.

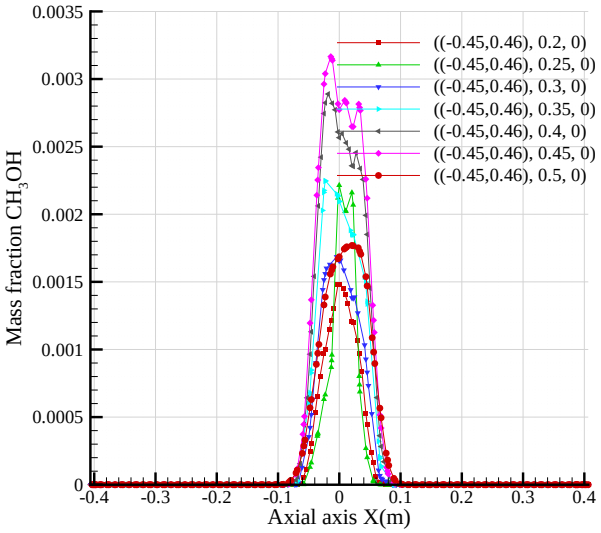


Figure 4.10: Fuel ($CH_3OH$) profiles close to the injector - SDRM model

### 4.2.4 Profiles of Nitrogen Oxides within the Flame Region

One of the emission variables that was not measured by Widmann and Presser [1] or looked at by Collazo et al. [65] is the nitrogen oxides ($NO_x$). Profiles of $NO$ and $N_2O$ at exit locations (normal and span-wise lines shown in Fig. 3.9 and Fig. 3.10)

are respectively shown in Fig. 4.11(a) and Fig. 4.11(b). The profiles show that the concentration (mole fraction) of these $NO_x$ components are small (of order $1 \times 10^4$ - $1.4 \times 10^4$). This is similar to the other emission components ($CO_x$). The question that pops up here is that, weather the lower-than experimentally predicted value for these parameters is due to the use of comprehensive reaction mechanisms or is it a deficiency of the computational models. Based on the fact that including most (if not all) of the species and the reaction steps possible in modelling a reactive flow offer the most accurate results, the author believes that the under predicted values of by-product are on the accurate side rather than on the erroneous side. Having said so, more studies using other reaction mechanisms and better quality meshes are essential to comment on such predictions.

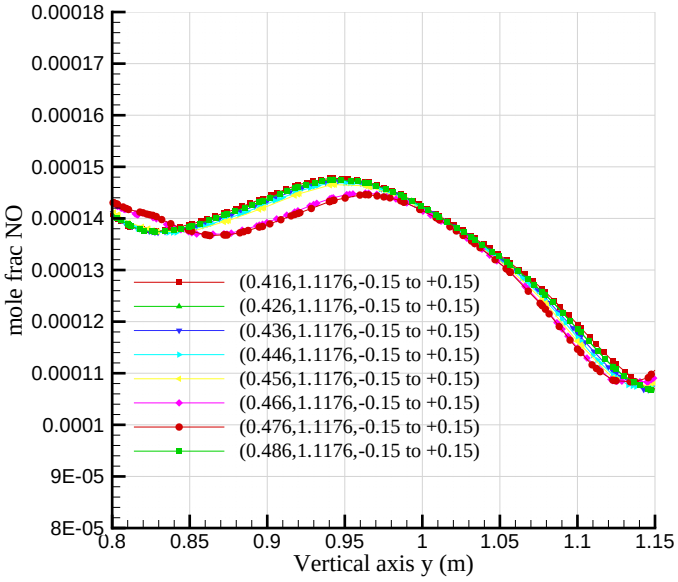


(a)

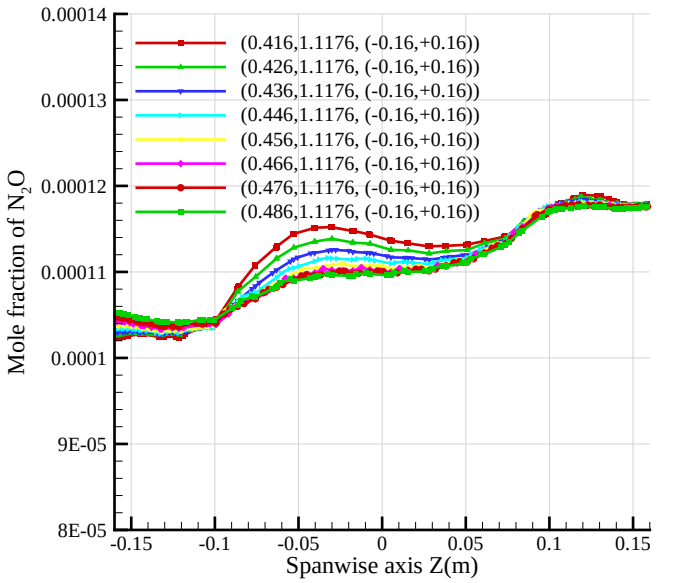


(b)

Figure 4.11: $NO_x$ ($N_2O$) profiles corresponding to the (a) vertical lines shown in Fig. 3.9 and (b) horizontal lines shown in Fig. 3.10.

### 4.2.5 Profiles of Water Vapour within the Flame Region

For the water vapour, Widmann and Presser [1] did not report any experimental data, however, and based on the experimental rates of production of $CO$ and $CO_2$, they estimated the rate of production on the exit part of the burner as equivalent to 0.045. This estimation is based on two simple reactions:

$$2CH_3OH + 3O_2 \xrightarrow{r_1} 2CO_2 + 4H_2O$$

$$CH_3OH + O_2 \xrightarrow{r_2} 2CO + 2H_2O$$

where

$$\frac{r_1}{r_2} = 50$$

Shown in Fig. 4.13(a) and Fig. 4.13(b) are profiles of water vapour for the vertical and horizontal lines of Fig. 3.9 and Fig. 3.10 respectively, at the exit region of the burner. The predicted results from the SDRM simulation show that water vapour concentration is of order 0.02, under predicting the experimental data. However, taking into consideration that these are theoretical results obtained on two rates of reactions obtained from the experimental data, one would still expect some marginal difference in these estimations. Taking all these arguments into consideration and the nature of the small quantities of these by-products, one would still acknowledge that the predictions are in line with the experimental data.

Water vapour profiles corresponding to cross-sectional lines starting at $y = 0.2$, increasing by 0.05 increment along the verticals are shown in Fig. 4.13(c). A central slice for $H_2O$ appears in Fig. 4.13(d). The figures shows that

It is worth to mention at this point that other parameters of by-product including soot formation have been looked at at the exit of the burner (Fig. 4.12), however, the rate of soot is almost negligible.

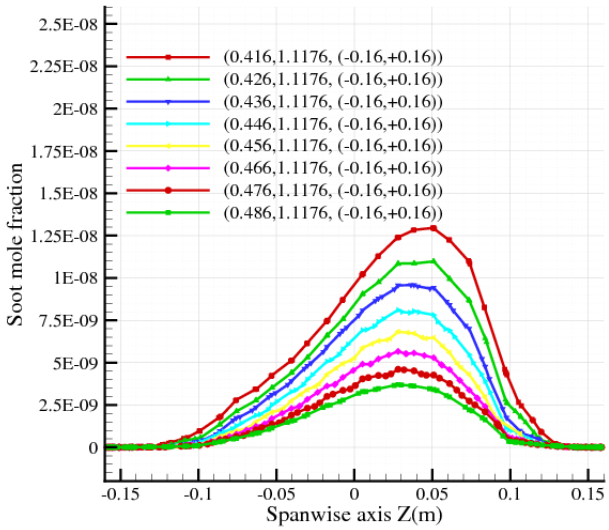


Figure 4.12: Horizontal line all - soot mole fraction

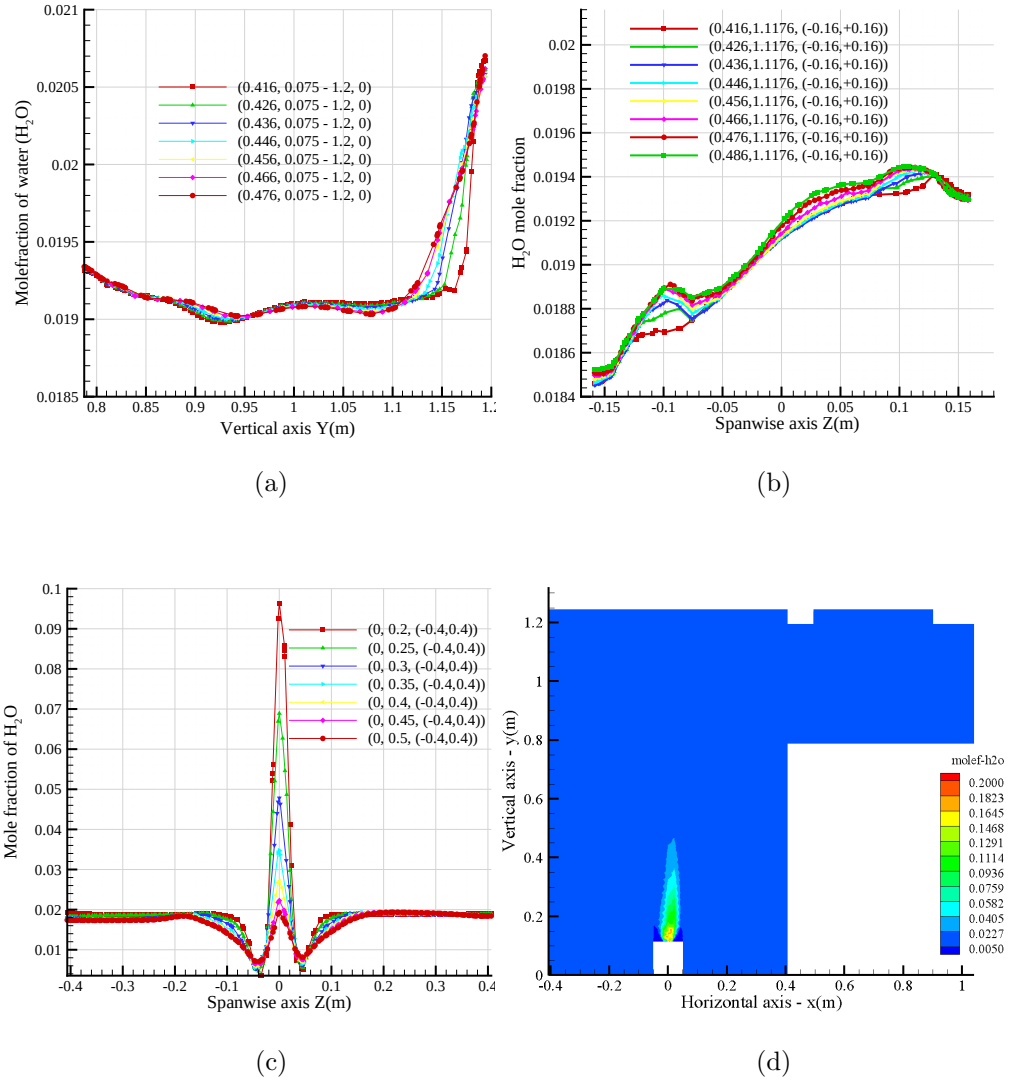


Figure 4.13: Water vapour profiles corresponding to the (a) vertical lines shown in Fig. 3.9 and (b) horizontal lines shown in Fig. 3.10. Water vapour (c) cross-sectional profiles close to the injector and (d) profiles corresponding to a central (x,y)-plane.

#### 4.2.5.1 Profiles of Mean Mixture Fraction at the Exit and within the Flame Region

The mixture fraction concept and the PDF method was thoroughly discussed in Chapter 3 where the mixture fraction is defined as:

$$\frac{Z_i - Z_{i,ox-}}{Z_{i,fuel} - Z_{i,ox-}} \tag{4.3}$$

In Eq. 4.3, $Z_i$ stands for the elemental mass fraction for element $i$, while the subscript *ox* refers to the oxidizer stream inlet and the subscript *fuel* denotes the value at the fuel stream inlet. In case the diffusion coefficients for all species are equal, Eq. 4.3 is identical for all elements, and the mixture fraction definition becomes unique. It refers mainly to the elemental mass fraction that originated from the fuel stream.

In case a secondary stream (an additional fuel or oxidant, or another non-reacting stream) is involved, the fuel and secondary mixture fractions become the elemental mass fractions of the fuel and secondary streams, respectively. It is apparent that the summation of all three mixture fractions in the system (fuel, secondary stream, and oxidizer) should add to unity, i.e.

$$f_{fuel} + f_{sec} + f_{ox} = 1 \tag{4.4}$$

Based on these simple definitions and conceptual facts about the mean mixture fraction, it is apparent that it indicates the rate of burning of the fuel. Considering the fact that only the fuel and the oxidant (oxygen in atmospheric air) are involved in this non-premixed problem, relations above should not include any secondary additional fuel or oxidant. This fact offers another simple way to understand the mean mixture fraction by relating it to the equivalence ration $\phi$ as:

$$f = \frac{\phi}{\phi + R} \tag{4.5}$$

where $R$ is the air/fuel ratio. Equivalence ratio represents the actual ratio of the actual available fuel mass to the available oxygen (or air) mass, the stoichio-

metric mass fuel to oxygen (or air) ratio.

$$\phi = \frac{(\text{fuel/air})_{\text{actual}}}{(\text{fuel/air})_{\text{stoichiometric}}} \tag{4.6}$$

In the Fluent code, the mixture fraction *f*, is the mass fraction that originated from the fuel stream. In other words, it is the local mass fraction of burnt and unburnt fuel stream elements ($C$, $H$, etc.) in all the species ($CO_2$, $H_2O$, $O_2$, etc.). Based on this perception, the magnitude is an indicator of remains from the fuel stream. The mixture fraction variance is a strong indicator and a parameter commonly looked at as an estimate of the fluctuations in the mixing field. As mentioned previously, the scalar dissipation determines the stretch in the flamelets.

From the above arguments, the study of the mean mixture fraction and its variance and the scalar dissipation rate is important in elucidating both the magnitude of the chemical reaction and the flame structure. In the SDRM simulation, the mean mixture fractions at the exit of the burner corresponding to the vertical lines and horizontal lines of Fig. 3.9 and Fig. 3.10 are respectively shown in Fig. 4.14(b) and Fig. 4.14(a). Both of the figures indicate that the mixture fraction is of order 0.0107 at the exit. Close to the injector (the flame region), Fig. 4.14(c) shows the profiles for seven cross-sectional profiles starting at $y = 0.2m$ from the burner base (lower wall), increasing with $0.05m$ increment along the vertical y-coordinate. The cross-sectional profiles clearly elucidate the flame region, its structure (width variation with length) and the height where extinction occurs. Close to the injection point ($y = 0.2m$), the mixture fraction peak value is of order 0.1 decreasing gradually to 0.02 at $y = 0.5m$ along the vertical coordinate. The mean mixture fraction contours for a central (x,y)-slice is shown in Fig. 4.14(d) which clearly indicates that the flame is extinct at a height of order $0.7m$ measured from the burner base wall.

The mixture fraction variance at the exit of the burner (profiles corresponding to the vertical lines of Fig. 3.9) are shown in Fig. 4.15(a), similar range was reported for profiles corresponding for the horizontal lines of Fig. 3.10. It is clear that the values of mixture fraction variance are significantly small as expected as this region is not associated with the flame location.

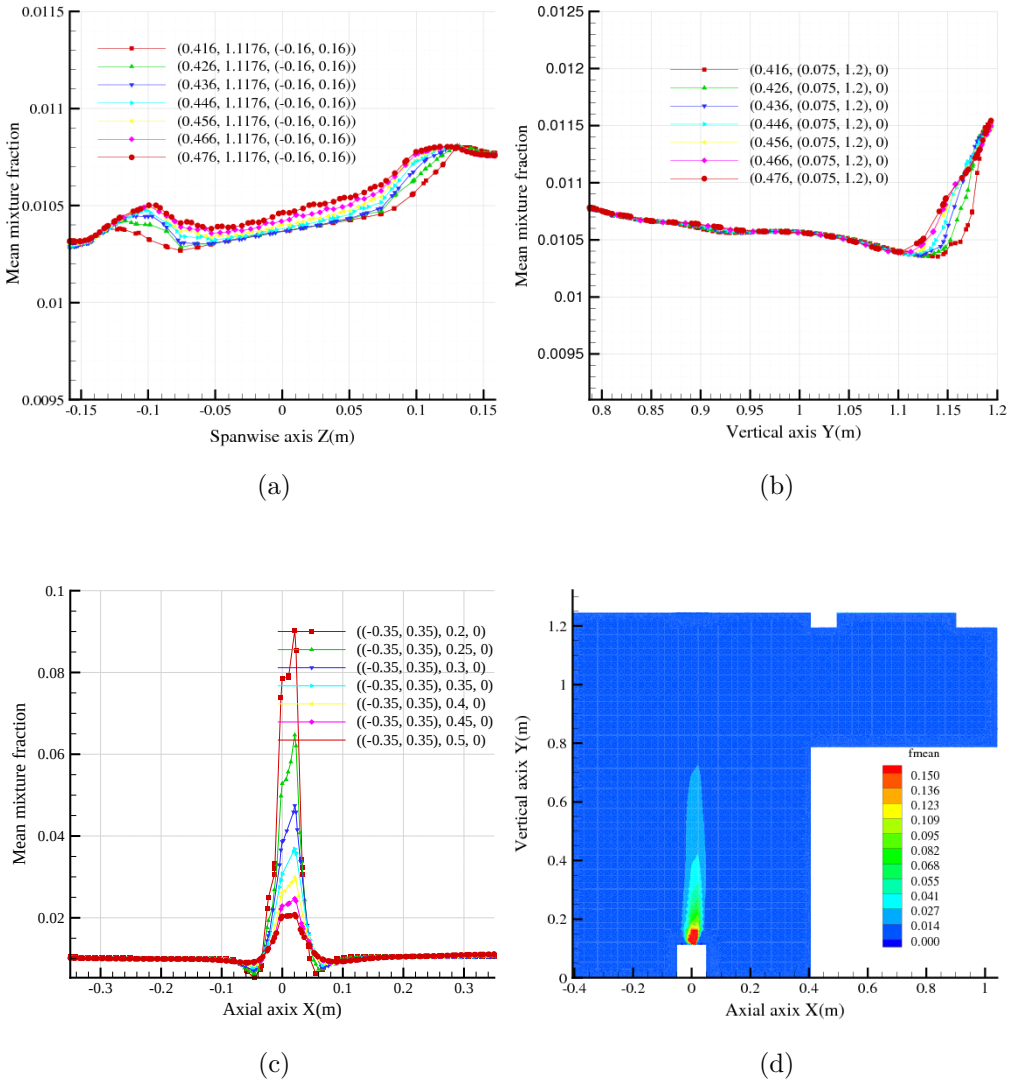


Figure 4.14: Mean mixture fraction profiles corresponding to the (a) horizontal lines shown in Fig. 3.10 and (b) vertical lines shown in Fig. 3.9. Mean mixture fraction for a central ($z = 0$) (c) cross sectional profile starting at $y = 0.2m$ and (d) (x,y)-plane.

In the flame region (just above the injector point), the profiles for mixture fraction variance starting at $y = 0.2m$ above the burner bottom wall and increasing with a $0.05m$ increment are shown in Fig. 4.15(b) while a central (x,y) slice showing the contours for this parameter is displayed in Fig. 4.15(c). The values

range from 0.006 for almost all of the profiles at all heights considered. This is also apparent from the contours of Fig. 4.15(c) which is an interesting observation. Although there are no experimental data, however, looking at the literature, similar behaviour was observed in many studies including the Large Eddy Simulation (LES) work of Sadasivuni et al. [119]. The distribution of mixture fraction variance supports the fact that the flame is characterised by continuous unsteadiness and hence it is best to be modelled using unsteady CFD methodologies such as LES.

From the mathematical expressions for the scalar dissipation rate, a function of the mixture fraction can be looked at as inverse of the characteristic diffusion time. The literature indicates that the relation between the scalar dissipation rate and the variance of mixture fraction is the same as the dissipation rate for the turbulent kinetic energy in turbulence [86]. Other studies relate the scalar dissipation rate to flamelet stretch [120]. Because of its relation to mixture fraction variance, a similar presentation of figures will be considered for the sake of connecting it to the variable.

Shown in Fig. 4.16(a) is the scalar dissipation rate for the vertical profiles at the burner exit which displays similar distribution to the mixture fraction of Fig. 4.15(a) an indication to the relation of these two variables and to the accurate setup of this CFD simulation. However, and as mentioned, these variables are more relevant to the flame region rather than at locations far away such as the burner exit in this simulation.

Cross-sectional profiles of the scalar dissipation rate (starting at $y = 0.2m$ and moving upward with $0.05m$ increment) within the flame region, Fig. 4.16(b) and Fig. 4.16(c) correspond to these profiles. The profiles exhibit a symmetrical order around the injection point similar to that of the mixture fraction and the mixture fraction variance. Also the dissipation rate decreases gradually with increasing height above the injector similar to the trend of the mean mixture fraction. This symmetrical behaviour and range is also displayed in Figs. 4.16(c) which shows the contours of the scalar dissipation rate on a central (x,y)-slice. Although there are experimental data from the work of Widman and Presser [1], the results shown in terms of the mean mixture fraction, mixture fraction variance and scalar dissipation rate (Fig. 4.14 - Fig. 4.16) reveal expected results. The results are also

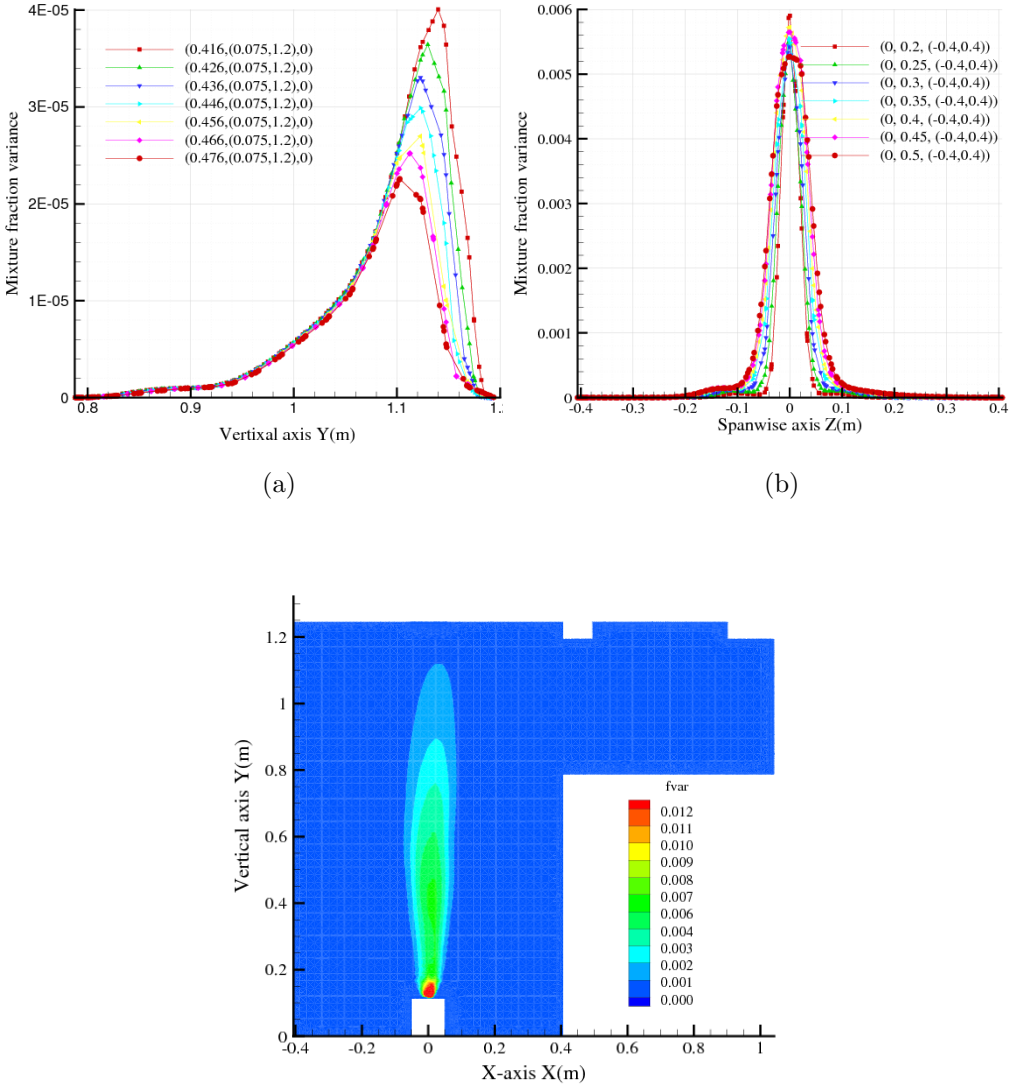


(a) (b)

(c)

Figure 4.15: Mixture fraction variance for a (a) vertical profile at the exit region, (b) span-wise cross-sectional profile starting at $y = 0.2m$, and (c) central slice SDRM.

in line with other fields discussed in the previous chapter (temperature and other flow fields). The only observation the author can note here was the fact that the variation of the mixture fraction variance within the flame region (Fig. 4.25(b))

shows a slow decrease with height while those of the mean mixture fraction and the scalar dissipation rate (Fig. 4.15(b) and Fig. 4.16(b)) show a gradual decrease with height.

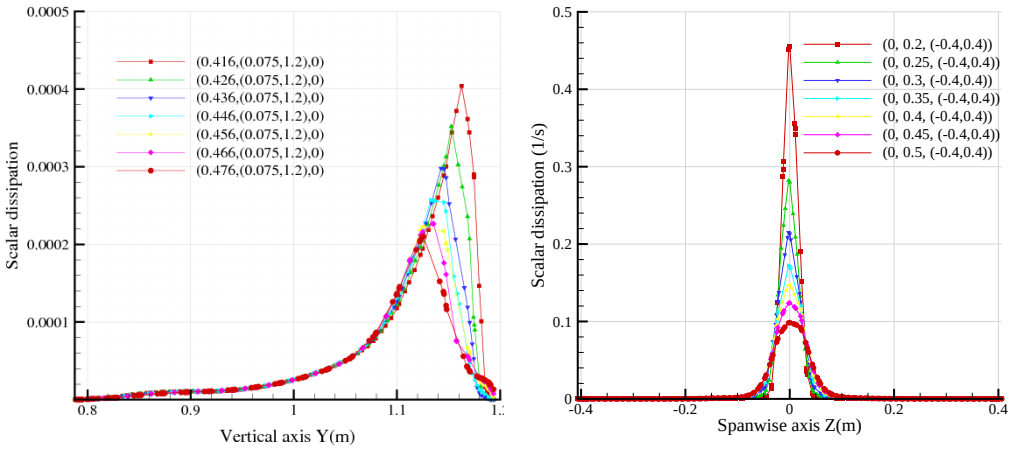


(a) (b)

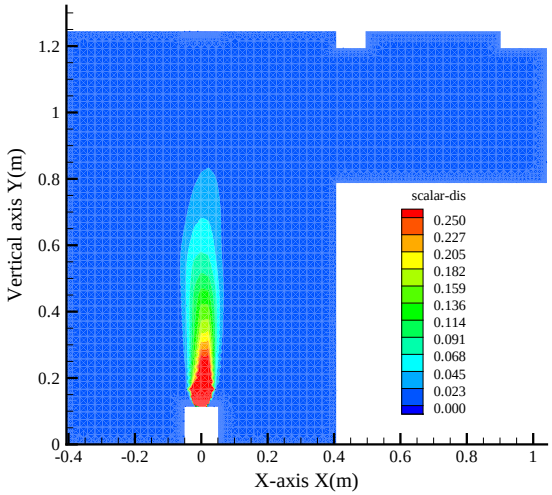


(c)

Figure 4.16: Scalar dissipation for (a) vertical profile at exit region, (b) span-wise cross-sectional profiles starting at $y = 0.2m$, and (c) central slice SDRM

## 4.3 Combustion Modelling of Methanol using EXGAS-generated and Modified Advanced Reaction Mechanism

Having validated the results of the CFD setup and simulation of the basic case of Widmann and Presser [1] using the reduced but well tested SDRM, a comprehensive mechanism that includes two hundred and twenty species, and a few more than this figure in terms of reaction steps, was developed and used in modelling the spray combustion of methanol in the burner geometry described in Chapter 3. Before indulging in the business of elaborating and describing deeper details and aspects of this mechanism, the author would like to stress on the fact that the main objective of this thesis is to study the combustion of different types of fuels and focus more on the physics of fluids of the combustion phenomena. The chemistry side and the chemical kinetics is of secondary importance. However, without passing through it, the work would seem to have an open loop and a missing link. Hence, a brief review to the method adopted in generating this new reaction mechanism will be highlighted in the coming paragraphs. The main precautions exercised here and during the generation of the new reaction mechanism are summarised in the following paragraphs:

The option of high temperature was considered for generating the reaction mechanisms. This is justified by the fact that the expected temperature from burning either of the fuels considered in this work (methanol - $CH_3OH$; diesel, represented as decane ($C_{10}H_{22}$ and biodiesel, represented as methyl decanoate ($C_{11}H_{22}O_2$) all generate high temperatures and therefore opting to high temperature option is more realistic than the low temperature option. It is worth to mention that the temperature influences the expected species and their reaction steps, especially free radicals which have been a big challenge to deal with in this study. Defined as a species (an atom, molecule, or ion) that has unpaired electrons or an open electron shell [121], free radicals are seen as having one or more dangling covalent bonds. The production of radicals begins with homolysis of a relatively weak bond, initiated by addition of energy which is in the form of heat in the field of combustion. For more information on the influence of rad-

icals on the combustion processes (especially in ICEs), the reader is advised to consult with an informative manuscript by Wallington et al. [121]. Both primary and secondary reaction mechanisms were considered in generating the reaction mechanism for methanol ($CH_3OH$). Therefore radicals from scission, isomerisation, decomposition of O-rings, metatheses and other secondary reactions are all considered in the developed reaction mechanism. Only radicals obtained by unimolecular and bimolecular initiation for high temperature reactions are taken into consideration. For more information on this the reader may refer to the many work cited here in developing the EXGAS software. Important reactions considered during the generation of this reaction mechanism include (but are not limited to):

- Alkanes reactions
- Orings decomposition
- Alkenes reaction
- Alkohol reactions
- Formation of Allylic free radicals (by metethesis)
- readctions of allylic free radicals on alkenes
- Aldehde reactions
- Ketone reactions
- Diels Adler reactions
- Terminations

All these reactions were taken into considerations upon generating the reaction mechanism. The resultant mechanism includes the order hundred species and four hundred and forty eight reaction steps. The author relies on the fact that modelling each reaction step and associated species is essential to provide insight into the combustion process and help in obtaining accurate results for both energy released and emissions produced. In comparison, the SDRM model contains

about thirty five species and hundred reaction steps. It is worth to mention that the generated mechanism was modified using some data from Burkhast [100] as well as consulting with other data sources from Daresburry Laboratory [122].

The reaction model was used to model the burning of methanol ($CH_3OH$) in the same burner geometrical configuration employed in the case study of the SDRM model. The results obtained are discussed below. Similar parameters were investigated for comparison purposes.

## 4.4 Temperature Field

In a similar fashion to the trend of discussion presented above for the case of SDRM, the temperature field was looked at first here. As the same geometry has been used in this simulation, some references to previous figures will be used. Shown in Fig. 4.17(a) and Fig. 4.17(b) are the temperature profiles corresponding to horizontal and vertical line locations displayed in Fig. 4.17(a) and Fig. 3.9 respectively. These two figures also correspond to Fig.4.3(a) and Fig. 4.3(b) where the SDRM has been used. Fig. 4.17(a) shows the temperature range corresponding to the measuring locations of Widmann and Presser [1]. Consulting with Table 3.1, it is apparent that the experimental measurements indicate a temperature range of $433 - 567K$. The SDRM simulation predicted a range of temperature of $510 - 528K$ which is in the range of the experimental data, slightly under predicting the maximum value. However, there was quite good agreement when the exact locations of the measuring stations of Widmann and Presser [1] are considered. In comparison with the mechanism developed using the EGRM, one would observe that the temperature range predicted by the EGRM is higher than that predicted by the SDRM. Talking in terms of figures, the EGRM temperature predicted range is $620 - 700K$. This range is slightly higher than the experimental values. In other words, one would say that the EGRM model over predicted the experimental measured temperature while reporting higher temperature range compared to the SDRM as well. Two questions arise here: the first is why the simulation based on the EGRM model predicted higher temperature range than the experimental value, and the second is why the EGRM simulation predicted higher temperature than the SDRM.

The best way to explain the points raised in the previous paragraph is to focus on the difference in species involved and the reaction steps considered when the EGRM model was developed. Examining the two mechanisms it is apparent that there is a large difference both in the number of species used and in the number of reaction steps. Noticeably the mechanism used here includes many classes of species including as described above.

By a careful examination of the two mechanisms, one would state that the species used in SDRM mechanism are mainly the primary species considered by the EGRM mechanism. Neither secondary molecules (species) nor the five types of radicals considered in the EGRM are included in the SDRM. The Kinetic data and the thermal data for the EGRM and SDRM are shown in Appendix A and Appendix B respectively. Examining the reactions used, one would judge that on top of the difference on the number of species used by the EGRM, the number of reactions included in this mechanism is twice the number used in SDRM. Whilst the author would not like to look into further details of the reactions used and their minor details, it is worth to mention that huge difficulties were faced in running the simulation with the EGRM and many reactions that deemed unimportant were not considered. The EGRM shown in Appendix A is considered an optimised one rather than the comprehensive one originally generated by the EXGAS software [123, 124]. Some reaction rates were carefully examined and compared with other available websites like Burkast data and free software was also used to generate such data to ensure accuracy of the data involved.

The Radicals have been the subject of scrutiny. Their importance and whether to involve them in the EGRM has been a subject of a debate with some experts in the field from the chemistry departments at De Montfort University. It is apparent that any detailed reaction mechanism associated with the combustion of any hydrocarbon becomes more complicated as a result of the diversity of molecules and radicals involved. Not only that, the complexity is enhanced by the transient (time dependent) nature of the evolution of the combustion process with the chain mechanism (chain branching) of radicals playing crucial role making the process self-accelerated. The behaviour of the resultant intermediate products (elements) depends mainly on temperature leading to different evolution of the combustion process at different temperatures.

The literature indicates that developing a comprehensive reaction mechanism becomes more complex when considering larger hydrocarbons. As a result of the complexity of the combustion, the findings for many studies produced a varying range of success. Most of these studies are mainly seeking to study the kinetics of the combustion of such hydrocarbons in stable systems. Turbulence is well-known to enhance the mixing process and it is very relevant to non-premixed combustion systems such as the case of the current burner case under consideration. When turbulence is taken into consideration, it will add another dimension to the complexity of the evolution of the combustion process and hence it is most unlikely that experimental and numerical simulation match each other. The reason for the differences may be attributed to the number of species and intermediate products expected during the combustion process as well as to uncertainty underlying the science of generating such comprehensive mechanism and using them in environments different than that for which they are mainly developed.

As mentioned at the beginning of this section that the computational results using the EGRM over-predicted the experimental values and also reported slightly higher temperatures than the range predicted using the SDRM. Hence there are two questions to answer here: the first is: why the EGRM over-predicted the experimental values for temperature, and the second is: why has it produced higher range of temperature than the SDRM?

One reason could be attributed to the nature for the EGRM having many species and a huge number of reaction mechanisms. However, looking back to the literature, this fact was reported by others including the software developers although they stated that it predicts better flame structure.

Another aspect is the nature of the spray combustion used. All these reaction mechanisms were developed for the gas-phase oxidation and combustion of specific type of hydrocarbons. Therefore, if they are applied for the combustion of a hydrocarbon on a gaseous phase they may perform very well as the reaction steps come closer to the assumption made when these mechanisms were developed. As an example, the software used in this study (EXGAS) was validated for the gas-phase oxidation of quite a few fuels including several alkanes. As an example, the study of Wrath et al. has considered many alkanes including n-butane [59], n-heptane [125], iso-octane [126, 125], n-octane [59], n-decane [127, 128], and

mixtures of n-heptane and iso-octane [129]. The autoignition of iso-butane and iso-pentane in a shock tube from 1100 to 2000$K$ were studied by Oehlschaeger et al. [130]. However, there are many differences between the current case study and the studies mentioned. First, in the current work, spray combustion is involved where the initially liquid-phase fuel has been sprayed in the form of drops with varying diameters. It would have been more informative if some information about the size of such droplets was available. However the versions of the software used do not provide this information. Although small in diameter, the combustion of such droplets is not instantaneous and takes a fraction of a second to burn leading to what is commonly known as delay period. The evaporation of such droplets takes place around the peripheries while leaving the fuel surrounding the centre to be in liquid phase. This process continues while the droplets travel randomly and interact with other droplets in many ways that affect the dynamics of combustion. While travelling in such turbulent flow, droplets eventually vaporise and burn completely although the word completely is not 100% correct as some of the by-products of any combustion is unburned hydrocarbon which sometimes includes element of the fluid itself in addition to other intermediate by-products. Therefore, the mechanism is not used to model the combustion of a gaseous hydrocarbon, rather a more complicated system is used.

Another difference was that the studies cited above, where the mechanism was validated, are done on slight controlled steady environment of shock tubes. The shock tube environment is different from the combustion phenomena in a turbulent flow in a complex geometry like the burner used in this case study. All these reasons most likely explain the difference in results observed above. The option of choosing higher temperature rather than lower temperature to generate the reaction mechanism may also explain part of the difference. If the assumption of lower temperature was chosen, the scenario may have been different. Having said so, most of the literature indicates that such reaction mechanisms are used to model the combustion process of some hydrocarbons at temperatures above about 1000$K$ and, within these arrangements, limited attention was paid to reactions and species that are most likely to happen at lower temperature [131]. In spray combustion, the core of the droplet is much colder than the surrounding air and latent heat of vaporisation is absorbed from the surrounding hot gases to help in

the vaporisation (gasification) process to enable burning of the fluid. Hence, lower temperature reactions might be of importance to model spray combustion. Having said so, the literature indicates that it is not simple to design a reaction model that takes care of chemical kinetics at low temperatures, mainly as a result of the very large number of possible reactions, intermediate products and reactions involved. All these explain the fundamental difficulties in developing a reaction mechanism that accurately models both low-, medium-, and high-temperature expected regions in a domain where the combustion process is taking place. Assembling such a reaction model manually could be very difficult, and will need a lot of testing and is much prone to errors than using the current infrastructure (codes) to develop one. The author followed this approach (manually assembling a reaction mechanism) with inconclusive outcome and it was decided that it was much more adequate to use the EXGAS software to generate the mechanism and modify it as necessary. Although assuming high temperatures to generate and do the simulation for this case, the author strongly believes that low-temperature reactions and intermediate products are necessary to provide a complete picture of the spray combustion of liquid fuels considered here. One would only raise this point as a recommendation for further investigation.

Having discussed the possible sources that might have contributed to the over-prediction of the experimental results, the author would like to mention that the difference is not that big and one can still state that taking all the circumstances of the current simulation into considerations, the obtained CFD results reflect good agreements and are quite encouraging for future research in this area.

However, after all this critical analysis of the temperature profiles predicted by the EGRM, the model has produced one good result regarding the shape of the flame. Fig. 4.17(c) displays the temperature profiles for cross-sectional lines starting at a vertical distance of $0.2m$ from the bottom of the computational domain with an increment of $0.05m$ along the vertical axis. The figure shows adequate symmetrical profiles along the centre with a maximum temperature (close to the injector location) of order $1600K$. Comparing this figure with its correspondence from the SDRM simulation (Fig. 4.3(c)), it is clear that the EGRM model predicted slightly higher temperatures compared to the ones obtained using the SDRM. However, it is more interesting when looking at Fig. 4.17(d) which shows

the temperature contours for a central slice similar to that shown in Fig. 4.3(d). Both Fig.4.3(d) and Fig. 4.17(d) indicate that the flame structure of the EGRM is much more realistic and displays similar features of the flame although slightly longer. It is however noticeable that the flame of EGRM simulation extends for a considerable distance along the vertical axis. This fact holds the key to explaining the high temperatures especially at the measuring stations (Fig. 4.17(a) and Fig. 4.17(b)) observed for the case of the EGRM simulation. Whilst the SDRM simulation shows a flame that extends up to $y = 0.4$, the EGRM prediction shows that the flame extends to a distance of order $y = 0.7m$ along the normal. Having a hot region with temperature equivalent to the burning temperature of methanol up to almost half of the computation has contributed to the generally higher temperature range in the computational domain of the burner.

Based on the discussion above, one would conclude that the EGRM produced a better structured flame than the SDRM, posing another question on the effect of including comprehensive number of species and reaction steps in producing better and accurate results than using a reduced model. The author of this thesis would think about one important parameter that comes here, that is the equivalence ratio $\phi$. Because both of the simulations (SDRM and EGRM) are based on the same specification shown in Table 3.1, the most obvious reason was that, for the same amount of air, the EGRM produced a better shaped flame with deeper penetration along the vertical dimension of the domain. This feature is mainly explained by the combustion process for the two cases. It is a strong indication that including all possible species and reaction steps leads to more realistic and efficient combustion of the sprayed fuel. Considering the fact that Widmann and Presser [1] has mentioned some significant uncertainty in their measurement, it can be concluded, overall, that the EGRM has produced very good results.

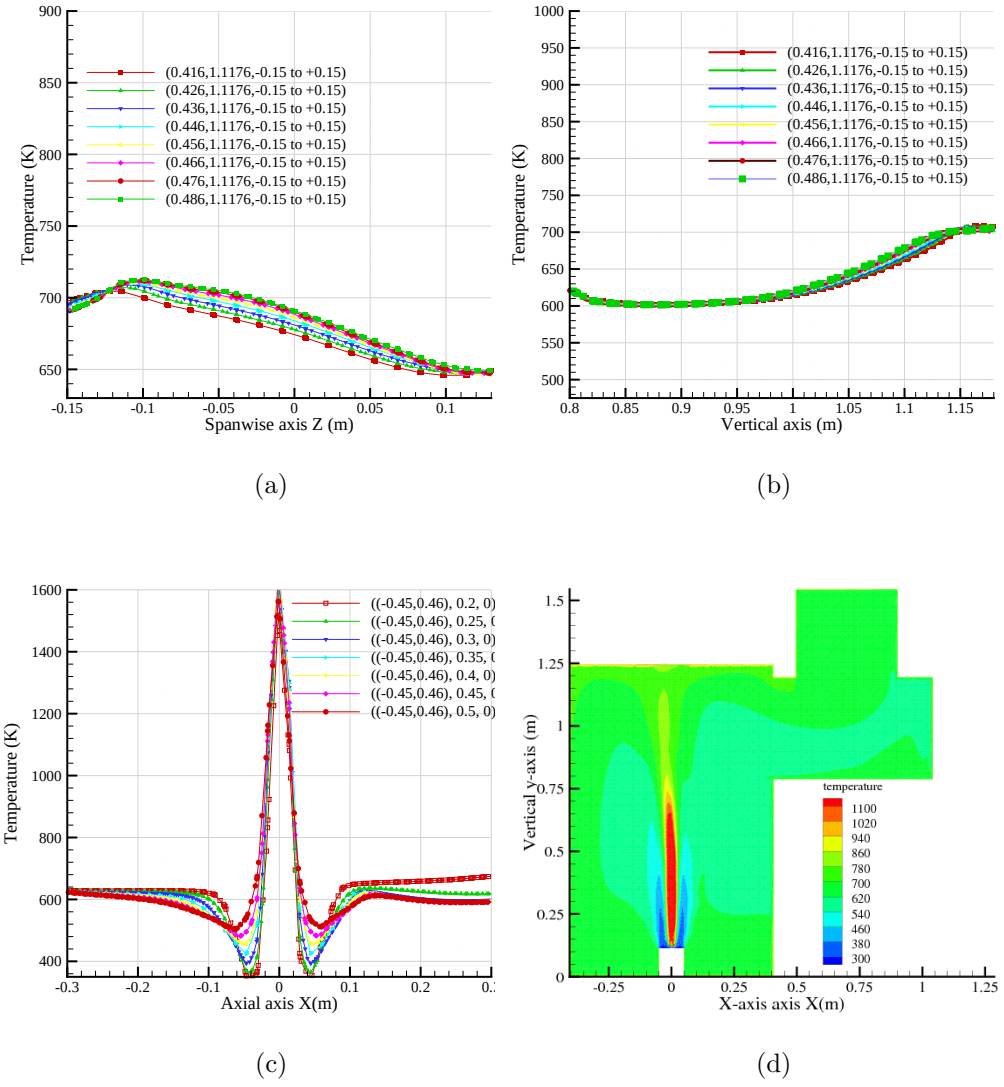


Figure 4.17: Temperature profiles corresponding to the (a) horizontal lines shown in Fig. 3.10, (b) vertical lines shown in Fig. 3.9, and (c) cross-sectional profile close to the injector. (d) Temperature contours for a central slice.

### 4.4.1 Turbulent Parameters

One of the differences predicted by the EGRM simulation compared to the SDRM model is the shape and the depth of penetration of the flame into the computational domain. To investigate whether this feature made a difference in the flow field, similar variables investigated in the case of the SDRM are looked at here in the EGRM simulation.

Shown in Fig. 4.18(a) and Fig. 4.18(b) are the Turbulent Reynolds number for the horizontal and vertical lines corresponding to those of Fig. 3.10 and Fig. 3.9) respectively. These two figures correspond to Fig. 4.4(a) and Fig. 4.4(b) for the SDRM simulation. A general comparison between the SDRM and EGRM in terms of $Re_y$ shows no difference in terms of the magnitude where both the ranges were equally predicted ($Re_y = 3000$ for the vertical lines while $Re_y = 1000$ for the horizontal lines). However, the difference appears in the shape of the distribution of $Re_y$ especially along the vertical dimension. It is apparent that $Re_y$ for the SDRM case has larger width while moving from the base along the vertical direction compared to the predicted results from the EGRM. This is mainly attributed to the larger width of the flame for the SDRM simulation.

Examining Fig. 4.18(d) and Fig. 4.18(c) in comparison with their respective correspondence from the SDRM simulations, Fig.4.4(d) and Fig. 4.4(c), one would also observe some differences especially in the cross-sectional profiles taken at close proximity of the injector and moving forward. The maximum range for the EGRM simulation is of order $Re_y = 14000$ while for the SDRM, the peak of $Re_y$ is of order 9000, lower than the EGRM. Examining the velocity range for the SDRM and EGRM in these locations (Fig. 4.19(a) and Fig. 4.19(b) respectively), one would observe a difference in magnitude with the EGRM simulation reporting higher velocities compared to the SDRM simulation. Although in the setup, the air velocity of the EGRM simulation is slightly higher than that for the SDRM, this observed difference cannot be solely due to this factor. One of the explanations was that the difference observed is attributed to the longer depth of penetration shown by the EGRM along the vertical dimension of the computational domain thus energising the flow and creating higher velocities. The contours for a central slice for $Re_y$ is shown in Fig. 4.18(d) corresponding

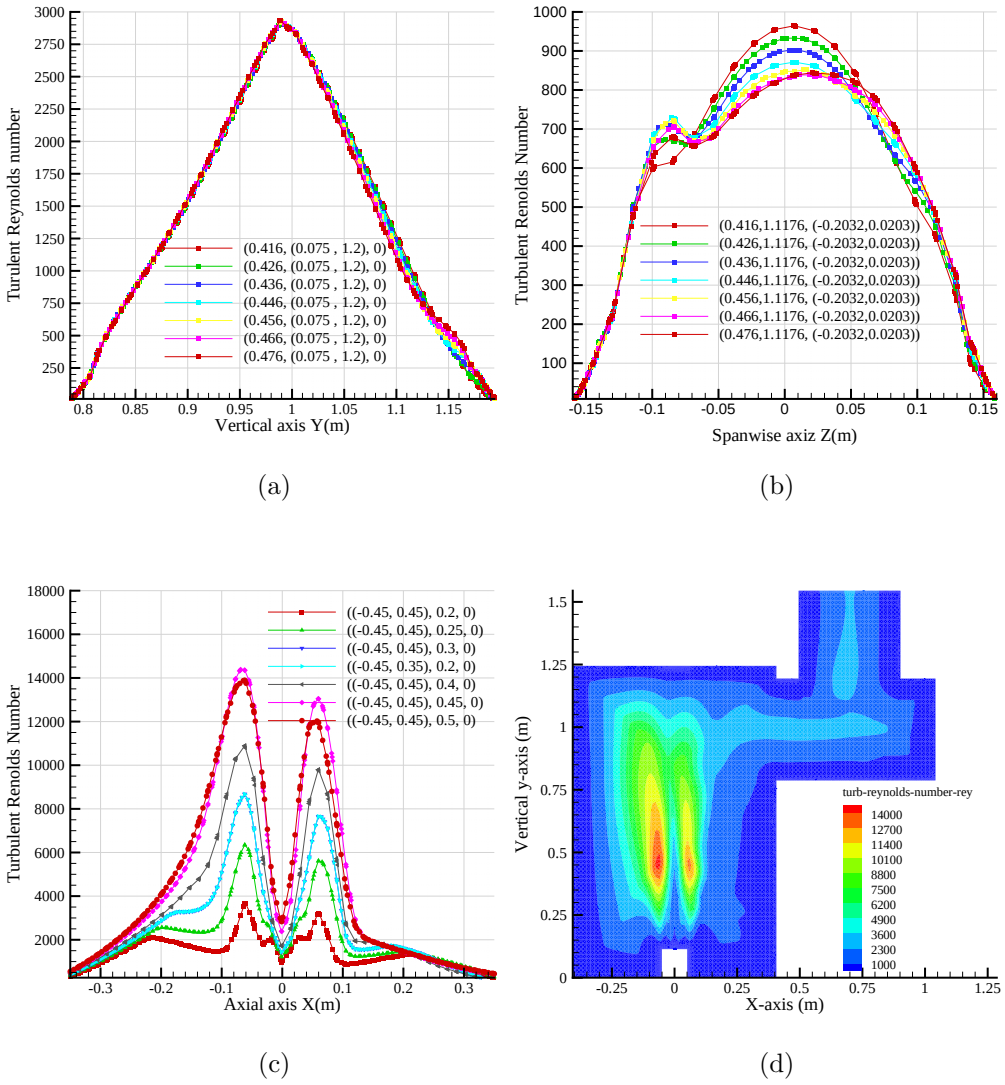


Figure 4.18: Turbulent Reynolds number profiles corresponding to the (a) vertical lines shown in Fig. 3.9, (b) horizontal lines shown in Fig. 3.10, (c) central (x,y)-plane using EGRM, and (d) close to the injector using EGRM.

to Fig. 4.5(b) in the SDRM simulations. The distribution of $Re_y$ shows a similar trend apart from the difference in magnitude which is explained in the above few lines.

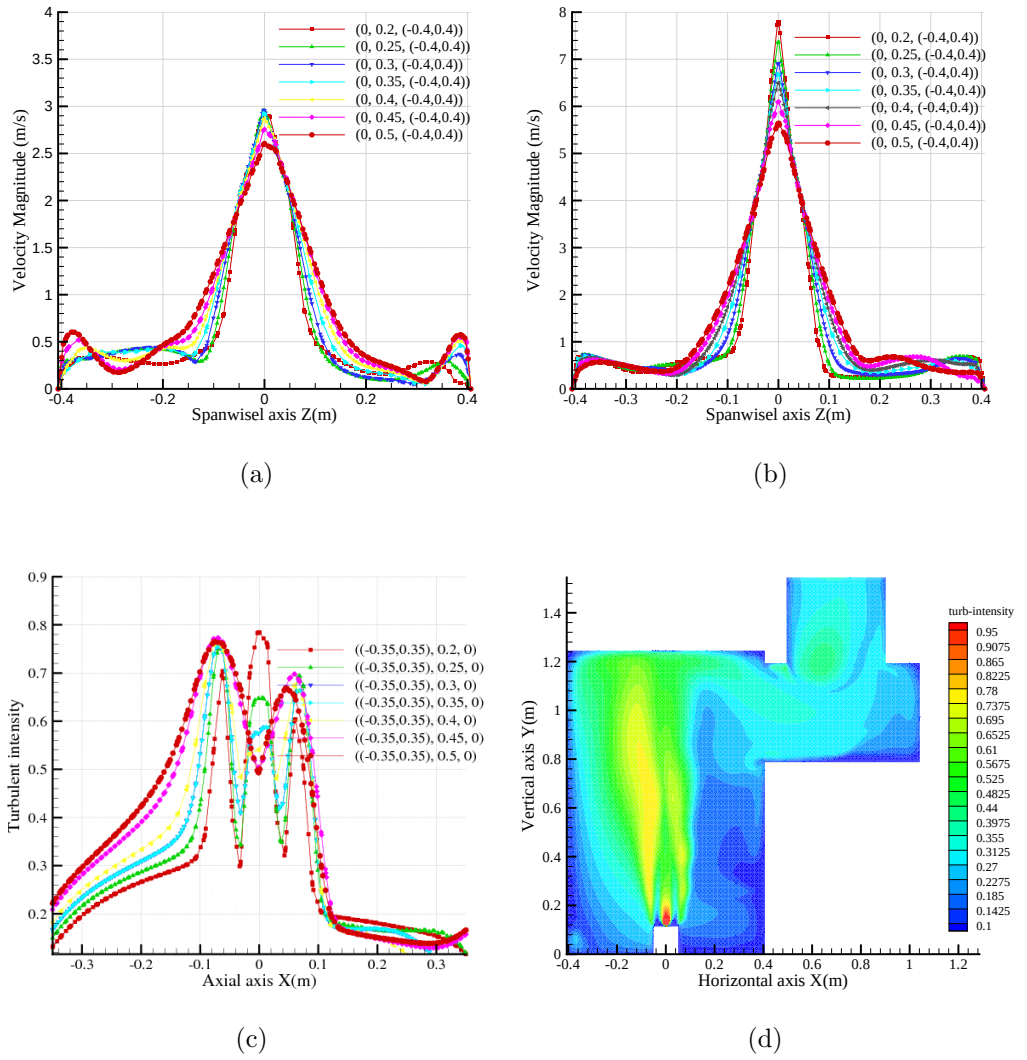


Figure 4.19: Velocity profiles close to the injector using (a) SDRM and (b) EGRM. EGRM based (c) turbulent intensity profiles close to the injector and (d) turbulent intensity number for a central (x,y)-plane.

To further investigate the turbulent field parameters, profile of turbulent intensity and a central slice from the EGRM simulation are shown in Fig.4.19(c) and Fig. 4.19(d) respectively. The equivalent to these figures from the SDRM simulations are Fig.4.5(c) and Fig. 4.5(d). Comparing the turbulence intensity profiles, it is noticeable that the turbulence intensity level is higher in the EGRM simulation compared to the SDRM one although the distribution is more or less the same. The contour for the central slice for the EGRM simulations (Fig. 4.19(d)) also displays higher range compared to the SDRM simulation (Fig. 4.5(d)) although it is apparent that the whole computational domain is enhanced by a turbulent flow. Therefore, it is evident from the discussion above that the shape and depth of penetration of the flame definitely have some effect on the flow field which in turn influences the heat transfer and thus the temperature distribution. The fact that similar mechanisms based on the principles of EGRM model predict better flame structures are mentioned in the literature (Sarathy et al. [131]) although the environment may be slightly different. This further validates this study.

It is worth to mention that Widman and Presser [1] did not present any experimental data for turbulence parameters including turbulence intensity and Reynolds numbers. However, Particle Image Velocimetry (PIV) measurements of the tangential, radial and axial velocities were performed and the velocities were presented. From the obtained experiment data for the velocities, the profiles are similar to those shown in Fig. 4.19(a) for the three components with slightly flatter pattern although the peak value was observed. The axial velocity recorded a value of a flat peak value of order 2.5 and the radial of order 2.25. These values were reported by Widman and Presser [1] at a few downstream radial positions. The velocity presented in Fig. 4.19(a) is the velocity magnitude which is defined as:

$$v = \sqrt{u^2 + v^2 + w^2}$$

and it shows a peak of order 3 m/s decreasing to a value of 0.25 within the interior of the domain. Using this formula to obtain a velocity magnitude from the experimental values, one obtains:

$$v = \sqrt{2.5^2 + 0.2^2 + 2.25^2} = 3.369$$

Comparing this with the peak value of Fig. 4.19(a), it is apparent that there is an excellent agreement between the SDRM simulation and the experimental values. This is because the setup of the SDRM matches the experimental input exactly. For other simulations (especially the heavy fuels using EGRM), more air was needed to ensure the burning and hence higher velocities were observed compared to the experimental data. This is shown in Fig. 4.19(b)

## 4.5 Emissions

As mentioned in the early chapters of this thesis, involving a detailed reaction mechanism is very important in accurately predicting both the energy and emissions from burning a hydrocarbon under a specific environment. In a similar fashion to the SDRM simulation, emission profiles and contours for different by-products are examined in the EGRM simulation.

Shown in Fig. 4.21(a) are the profiles of $CO_2$ that corresponds to the location of the horizontal lines shown in Fig. 3.10 which matches the regions of the measurements in Widmann and Presser's [1] experimental studies. The profiles shows that $CO_2$ mole fraction increase from 0.013 to 0.018. $CO_2$ profiles corresponding to the vertical profiles of Fig. 3.9 are shown in Fig. 4.21(b). Again the profiles indicate that in the exit area the mole fraction of $CO_2$ is of order 0.015 to 0.018, within the range revealed by the horizontal profiles. Comparing these values with the result from SDRM simulation (Fig. 4.7(a) and Fig. 4.7(b)), which predict a range of values for $CO_2$ between 0.01 to 0.015, it is clear that the EGRM simulation predicted slightly higher range for $CO_2$ in comparison to the SDRM. Referring to the experimental values, it is apparent that the EGRM simulation predicted almost a matching data. The experimental data measuring 9 station reported a range between 0.017–0.019 more fraction for $CO_2$. The exact location of the measuring station based on the EGRM is extracted and plotted against the experimental values in Fig. 4.20 together with the SDRM predictions. The figure clearly shows that the EGRM predicted this variable ($CO_2$) to a very accurate

level. This is a strong indication that the comprehensive reaction mechanism used is indeed necessary for predicting emission. Despite the fact that the range of the date is associated with very small values, yet the comprehensive mechanism predicted much closer values to the experimental data than the reduced San Diego mechanism. This is strong evidence that including all necessary reactions and intermediate products are essential and are the way forward in modelling the combustion phenomena in different platforms.

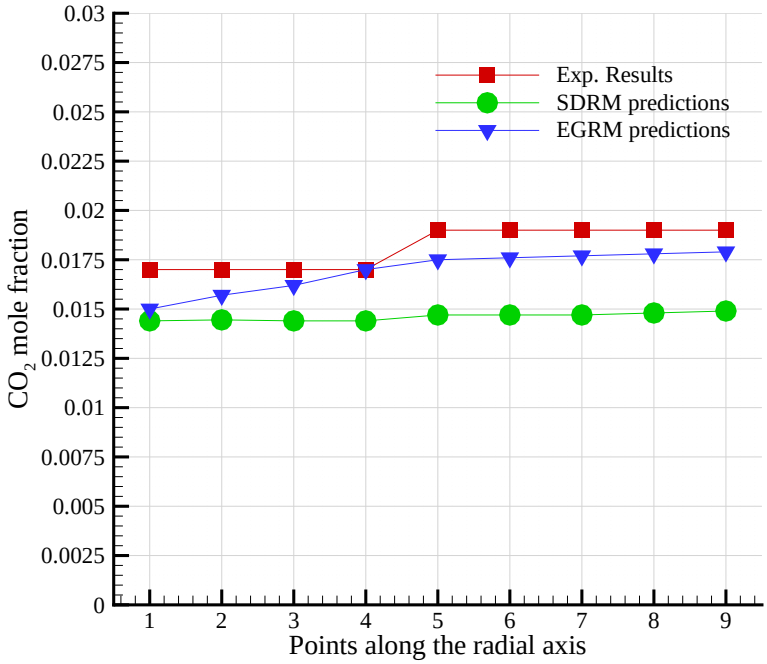


Figure 4.20: $CO_2$ comparison between the experimental, SDRM and EGRM simulations

Examining the values of $CO_2$ closer to the injector location, Fig. 4.21(c) displays seven profiles starting from $0.2m$ above the bottom of the burner geometry with $0.05m$ increment. The profiles show symmetrical distribution of $CO_2$ around the injector with the peak value of order 0.0725. This is supported by the contours of $CO_2$ for this EGRM simulation shown in Fig. 4.21(d).

Comparing the profiles of $CO_2$ from the EGRM simulation (4.21(c)) with the

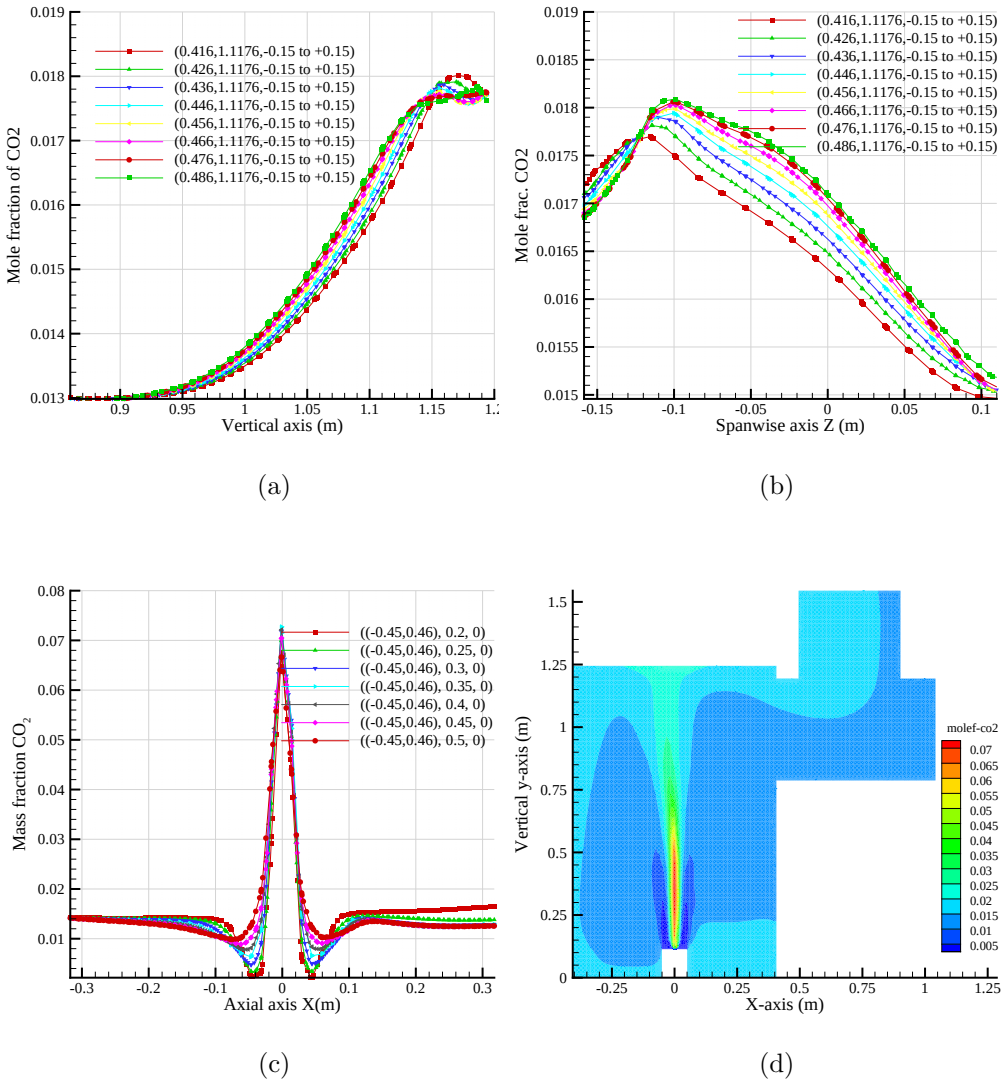


Figure 4.21: $CO_2$ profiles corresponding to the (a) vertical lines shown in Fig. 3.9 and (b) horizontal lines shown in Fig. 3.10. (c) Cross-sectional profiles of $CO_2$ close to the injector. (d) Mole fraction of $CO_2$ for a central (x,y)-plane ($z = 0$).

corresponding values from SDRM simulation (Fig. 4.7(c)), it is noticeable that the EGRM simulation has predicted higher level compared to the SDRM. However, as the EGRM predictions have shown very good agreement with the experimental values, one can conclude that although reduced mechanisms are able to predict

emissions to comparable levels with the experiment, most likely they may slightly under-predict the exact values. Involving more species and intermediate products and the relevant reaction steps may be the ultimate way to accurately predict the combustion process and its by-products.

Shown in Fig. 4.22(a) and Fig. 4.22(b) are the mole fraction for cross-sectional profiles of the fuels for the EGRM and SDRM respectively. These profiles provide information on the rate of burning of the fuels and hence how much distance along the vertical axis fuel droplets can travel before they are totally burned. This decides both the shape and length of the flame. Obviously, this feature is mainly a function of the combustion process and definitely a function of the number of species and reaction steps involved provided that the boundary condition is the same.

In both of the simulations, the sprayed amount of liquid methanol is kept the same as per Table 3.1. Examining these two figures, it is apparent that the SDRM (Fig. 4.22(b)) produced a much higher burning rate for the injected amount of fuels as the rates of fuel existence at the same height above the burner injector location indicate much lower rate than those predicted by the EGRM simulation (Fig. 4.22(a)). In the literature, there is a reference to the fact that advanced reaction mechanism produced via the EXGAS reaction generator produces a better flame shape, however, not enough information is given to explain why this happens and what are the main mechanisms behind it. From this section, it is apparent to the author that involving many reaction steps, species and intermediate products more or less leads to a higher delay in burning compared to the situation when a reduced mechanism is used instead. This allows more chances for the droplet to travel further distance along the vertical axis while burning, hence producing a better flame shape as well as well-predicted combustion by-products.

Data for $CO_2$ from Widman and Presser [1] experiment was only provided at the exit of the burner and that was used to validate the CFD prediction in Fig. 4.20. Their experiment did not provide data for emissions parameters within the burner interior and hence there is no data to compare with for the CFD predictions shown in Fig. 4.21(c). However, taking in consideration the good agreement between the CFD results and the experimental data at the exit, one can conclude that these results are representative and reflect the distribution of

$CO_2$ within the burner geometry.

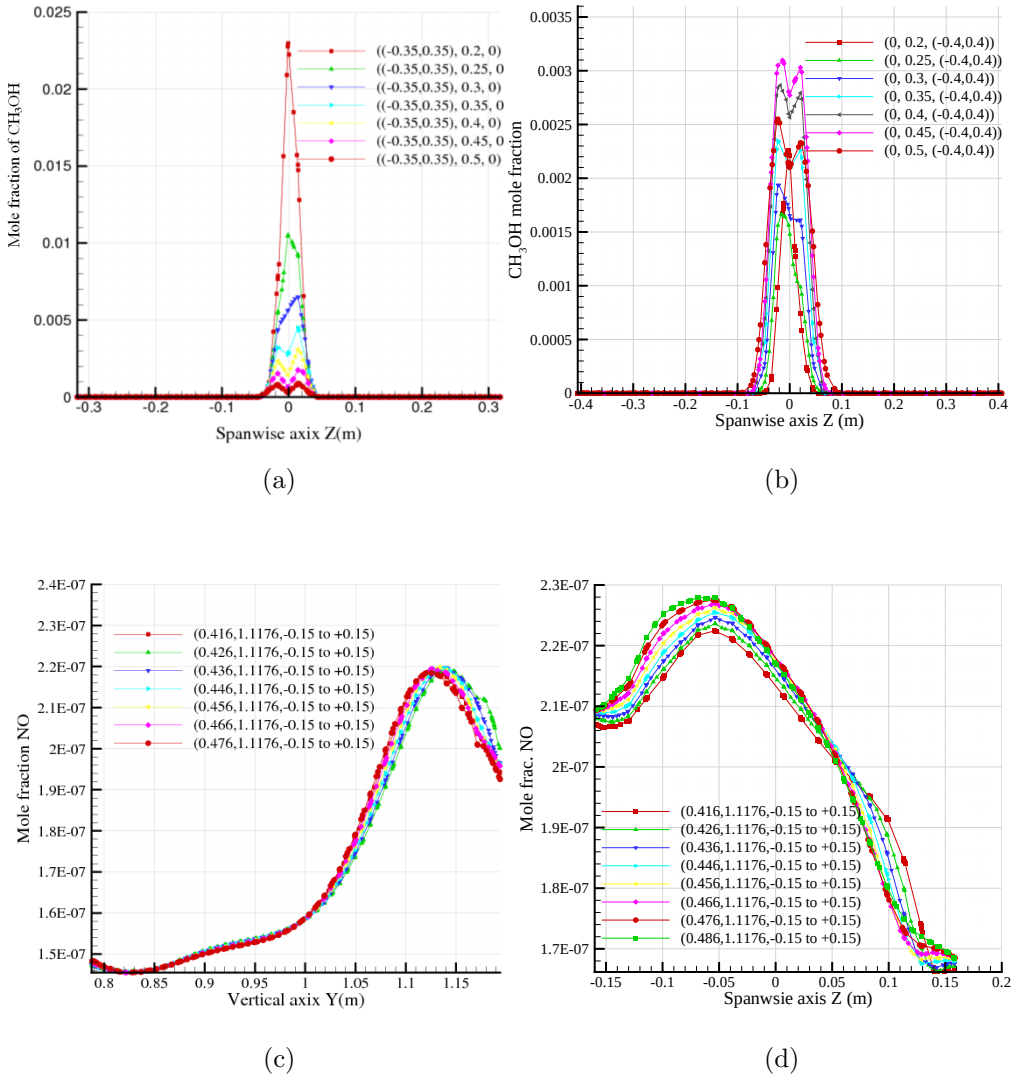


Figure 4.22: Cross-sectional profiles of $CH_3OH$ close to and above the injector for (a) EGRM and (b) SDRM. EGRM based $NO_x$ ($N_2O$) profiles corresponding to the (c) vertical lines shown in Fig. 3.9 and (d) horizontal lines shown in Fig. 3.10.

## 4.6 Nitrogen Oxide

Moving from carbon oxide to nitrogen oxides, Fig. 4.22(c) and Fig. 4.22(d) respectively display the mole fraction for $NO$ for the vertical and horizontal lines at the exit (corresponding to Fig. 3.9 and Fig. 3.10 respectively). This is within the measuring locations of the experiment of Widmann and Presser [1]. Although the range of this variable is too small to comment on, comparing $NO$ values of Fig. 4.22(c) and Fig. 4.22(d) with the corresponding figures from the SDRM (Fig. 4.11(a) and Fig. 4.11(b)), it is apparent that the EGRM predicted lower values. As there are no experimental values to compare with, one would only argue about the validity of the two simulations. Nitrogen oxides ($NO$ and $NO_2$) came from two main sources when a fuel (a hydrocarbon) is considered. The first source has been the oxidation of the fuel-bound nitrogen, and the second source is due to high temperature oxidation of nitrogen in the air. Recognising the fact that nitrogen is present in the fuel, this was not considered in this study because the chemical equation (based on which the reaction mechanism was generated) does not include nitrogen. Thus, all of $NO_x$ emissions come from oxidation of atmospheric nitrogen initiated via reaction with oxygen atoms. The mechanism of formation of $NO_x$ in this study is discussed in Section 3.4.2 where both thermal, prompt, and fuel $NO_x$ formation were considered.

It is well established that $NO_x$ are promoted by higher temperature and excess oxygen. There is an abundance of literature that supports this fact in different combustion platforms. With reference to the temperature field for the two simulations (using the SDRM and EGRM), the EGRM simulation has predicted a slightly higher range of temperature compared to the SDRM simulation. Based on this, one would expect that the EGRM should predict higher range in $NO_x$ as well as both the temperatures are higher, and as mentioned previously, there is slightly more air in this simulation. Yet the results shows that the EGRM predicted lower $NO_x$ than the SDRM simulation.

Examining the predictions for the two simulations, the EGRM simulation has shown far better agreement in terms of predicting pollutants ($CO_x$). The author is very much inclined towards believing in the predictions of the EGRM based on this circumstantial evidence.

For nitrogen oxides, Widman and Presser [1] experimental work did not provide any data. The only study that attempted to simulate the work of Widman and Presser [1] was that of Collazo et al [65], which also did not include any data related to nitrogen oxides. Therefore, the accuracy of the presented results rely on the validated results which was done using temperature, $CO_2$ and water vapour as will come later.

## 4.7 Water Vapour

Looking at other products of combustion, water vapour profiles at the exit locations for the vertical and horizontal lines of Fig. 3.9 and Fig. 3.10 are respectively displayed in Fig. 4.23(b) and Fig.4.23(a). It is apparent that the range of values of mole fraction of water vapour varies between 0.026–0.036. This is compared to 0.06 range estimation of Widmann and Presser [1] based on their calculations as discussed in Section 4.2.5. The SDRM prediction is of order 0.02 (Fig. 3.9 and Fig. 3.10), hence it is apparent that the EGRM simulation prediction is much closer to the experimental values than the SDRM which under-predict the water vapour content at the exit. Again this result strongly supports the fact that the comprehensive EGRM performs far better than the reduced SDRM when it comes to predicting the by-products of a combustion system. It is also obvious from these simulations that an advanced reaction mechanism is the way forward to studying the combustion processes and for accurate predictions of the outcome of such processes.

Looking at the water vapour content within the body of the burner, Fig. 4.23(c) displays water vapour contents along a cross-sectional profiles along the vertical axis starting from $y = 0.2m$ measured from the bottom of the burner with an increment of $0.25m$, while a central slice showing the contours of water vapour appear in Fig. 4.23(d). The profiles predict high water contents of order 0.25 at $y = 0.2m$ compared to 0.1 at the same location in SDRM simulation as shown in Fig. 4.13(c). The contours of Fig. 4.23(d) also show that depth of penetration along the vertical axis in the case of the EGRM simulation reaches a higher height compared to that of the SDRM simulation shown in Fig. 4.13(d). It is apparent that the shape of the flame influences the water vapour distribution along the

vertical axis leading to far better agreement between the CFD predictions and the experimental results.

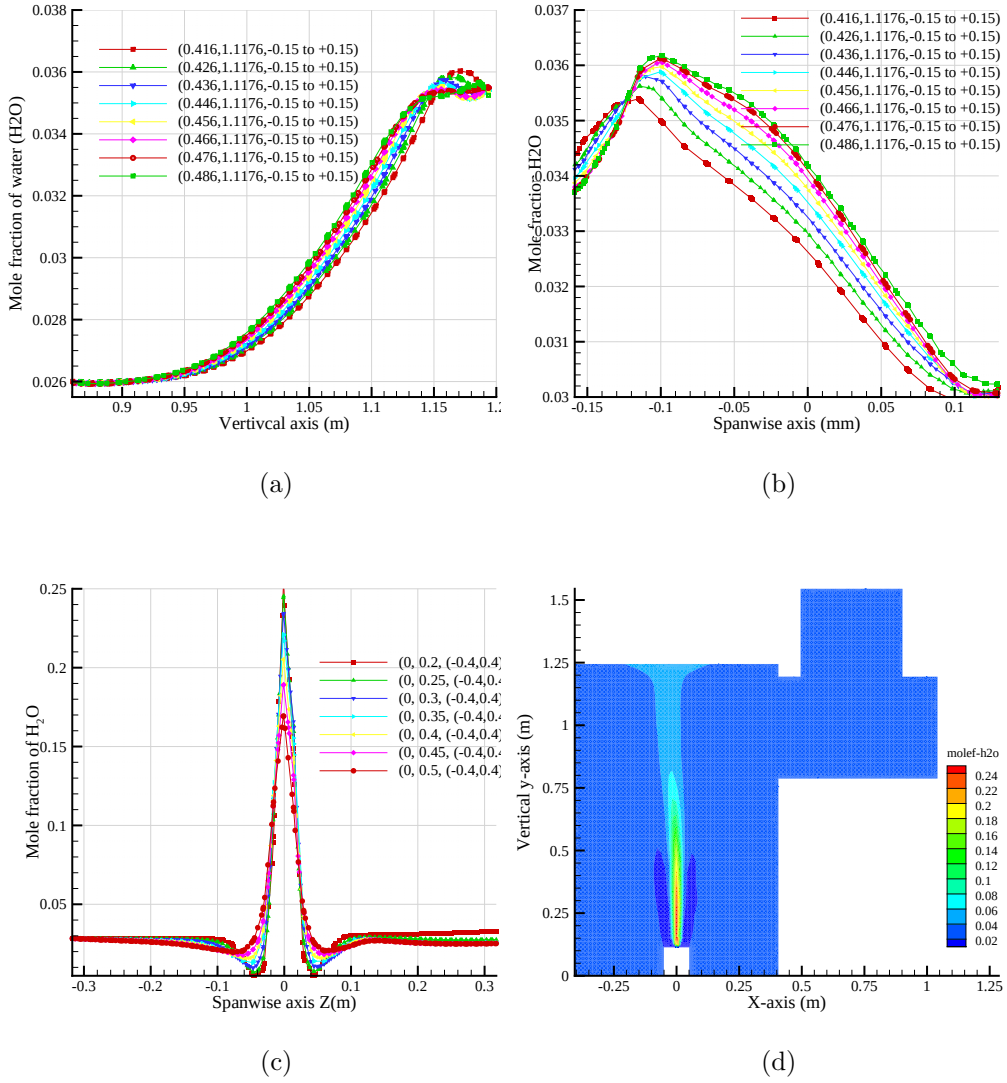


Figure 4.23: Water vapour profiles corresponding to the (a) vertical lines shown in Fig. 3.9 and (b) horizontal lines shown in Fig. 3.10. (c) Water vapour cross-sectional profiles close to the injector. (d) Water vapour profiles corresponding to a central (x,y)-plane.

Data for water vapour $H_2O$ from Widman and Presser [1] experiment was only calculated (not measured) at the exit of the burner. The obtained CFD

results were compared against Widman and Presser [1] in the beginning of this section and good agreement was found between the experimental and CFD predictions. Fig. 4.23(b) and Fig. 4.23(a) represent more data at the exit, however, for Fig. 4.23(c), which shows the water vapour distribution within the burner, there are no data to compare with. Having said so, the fact that there is agreement between the CFD results and the experimental data at the exit location of the burner strongly supports the accuracy of the CFD prediction.

## 4.8 PDF Variables

### 4.8.1 Mixture Fraction

The mean mixture fraction, mixture fraction variance and dissipation rate are important parameters that determine the flame structure and the rate of burning as discussed in previous sections. It is essential to understand the effect of more species and reaction steps (comprehensive reaction mechanism) in these parameters and hence elucidate whether the rates of emission are also influenced by these parameters.

With reference to Fig. 4.24(a) and Fig. 4.24(b), the mixture fraction of the horizontal and vertical lines at the burner exit (corresponding to the respective horizontal and vertical lines of Fig. 3.10 and Fig. 3.9) are displayed.

At the exit location, the mixture fraction magnitude is low (of order 0.017 – 0.02) compared to a maximum value of order 0.275 at close proximity of the injector location (Fig. 4.24(c)). It is apparent that most, if not all, burning species are burnt within the flame region as shown in Fig. 4.24(d) and Fig. 4.14(d). However, as one of the main subjects of this work is to examine the effect of comprehensive reaction mechanisms in all aspects of combustion of different fuels, it is worth to compare these values with the outcomes of the SDRM mechanism. As discussed in Section 4.2.5.1, the obtained values for the mean mixture fraction for these exit locations (Fig. 4.14(a) and Fig. 4.14(b)) are of order 0.01025 to 0.011, which is much lower that the values obtained using the EGRM in modelling the combustion under the same boundary conditions. This strongly indicates that the combustion process occurs in a much slower fashion when a comprehensive

mechanism is used instead of a reduced one. This also indicates that it is possible that more unburnt species or more intermediate species will come in the form of by-products in the case of EGRM prediction in comparison to SDRM simulation.

Focusing on the mean mixture fraction within the flame region, Fig. 4.24(c) displays the mixture fraction profiles for cross-sectional locations starting $0.2m$ from the burner bottom wall and moving with $0.05m$ increment along the normal (y) axis. A central (x,y)-slice for this parameter is also shown in Fig. 4.24(d). At $y = 0.2m$, the mixture fraction peak value is of order 0.28 compared to 0.09 from the SDRM prediction (Section. 4.2.5.1). This is a high difference and confirms the slow burning process predicted by the simulation when a comprehensive number of species and associated reactions are considered (as in the case of the EGRM) than using a reduced reaction mechanism (as in the case of the SDRM). At a height $y = 0.5$ above the burner bottom wall, the peak value of the mean mixture fraction predicted by the EGRM simulation is of order 0.12 compared to 0.02 for the SDRM simulation, again, strongly indicating that the burning process is very slow in the EGRM compared to the SDRM simulation. Again this can be due to the fact that including more species and reaction steps in the reaction mechanism used leads to a delay in the way the combustion process in general proceeds in time. The best way to investigate this further is through a transient simulation (using LES or Direct Numerical Simulation (DNS)). The contours for the central slices clearly indicate that traces of the mean mixture fraction can be detected within the flame region until close to the top wall of the burner. This strongly indicates a longer flame where unburned fractions of the injected fuel are able to travel some distance along the vertical direction with the mixture fraction fade some close distance to the top wall of the burner.

### 4.8.2 Mixture Fraction Variance and Dissipation Rate

Other important parameters relevant to PDF are the mixture fraction variance and the scalar dissipation. Both of these parameters were discussed previously in the SDRM simulation and their mathematical association with the mixture fraction and the PDF function based on which the steady flamelet model employed here is built. The mixture fraction variance has been employed in the closure

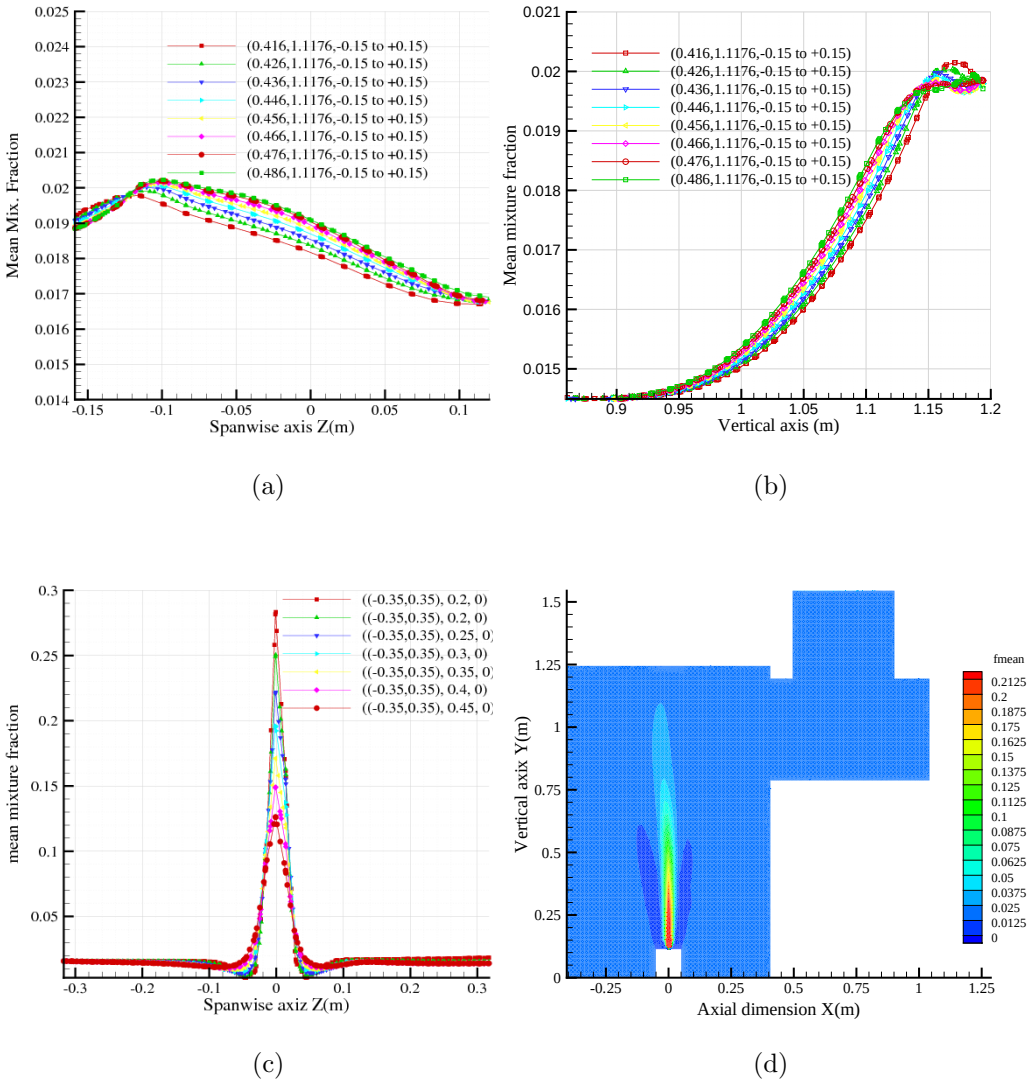


Figure 4.24: Mean mixture fraction profiles corresponding to the (a) horizontal lines shown in Fig. 3.10 and (b) vertical lines shown in Fig. 3.9. Mean mixture fraction for a central ($z = 0$) (c) cross-sectional profile starting at $y = 0.2m$ and (d) (x,y)-plane.

model describing turbulence-chemistry interactions as discussed in Section 4.2.5.1. The mixture fraction variance is the parameter which determines the fluctuations in the mixing field and hence can be used as an indicator to the degree of mixing within the flow field while dissipation rate performs the role of dissipating the

mixture fraction variance. Hence, it is worth to shed light on the variation of these two parameters in the closing section of this chapter.

For the EGRM simulation, the predicted mixture fraction variance distribution for cross-sectional profiles along the vertical lines of Fig. 3.9 (at the exit of the burner) are shown in Fig. 4.25(a) and the predicted values for the dissipation rate in the same location appear in Fig. 4.26(a). The values for the horizontal lines (Fig. 3.10) show similar values and hence not presented here. It is apparent that the two variables display a similar trend with extremely low values, an indication that the profiles fall in a region far from the flame.

For span-wise cross-sectional profiles starting at $y = 0.2m$ from the bottom of the burner geometry along the vertical direction (increasing with an increment of $0.05m$) are shown in Fig. 4.25(c). The corresponding profiles for the dissipation rate are shown in Fig. 4.26(b). Within the flame region, the profiles for the two parameters display similar trends showing a symmetrical profile around the flame region with a maximum peak value for the dissipation rate much higher than that for the mixture fraction variance. Similar behaviour was observed for the predictions by the SDRM simulation, however, the predicted values for both of the parameters are having much higher range in the case of EGRM. This is again a sign for the slow chemistry predicted by the EGRM as a result of including much more species and reaction steps in the form of a comprehensive reaction mechanism developed in this work. Central (x,y) slices for the two parameters respectively are shown in Fig. 4.25(c) and Fig. 4.26(c)

It is worth to mention that with regards to the PDF variables discussed above (the mixture fraction, variance and dissipation scale), the Widman and Presser [1] experimental work did not provide any data for them. This is because they are characteristics of the combustion model used in the CFD simulation rather than a parameter that can be measured experimentally. One would rely on the validation of the CFD result to comment on these variables that the distribution shown is reasonably correct. To strengthen this, it is worth to mention that the pattern seen for these variables agrees well with what was observed in the Large-eddy simulation of Sadasivuni [132] which adds strength to the setup of the problem as mentioned earlier.

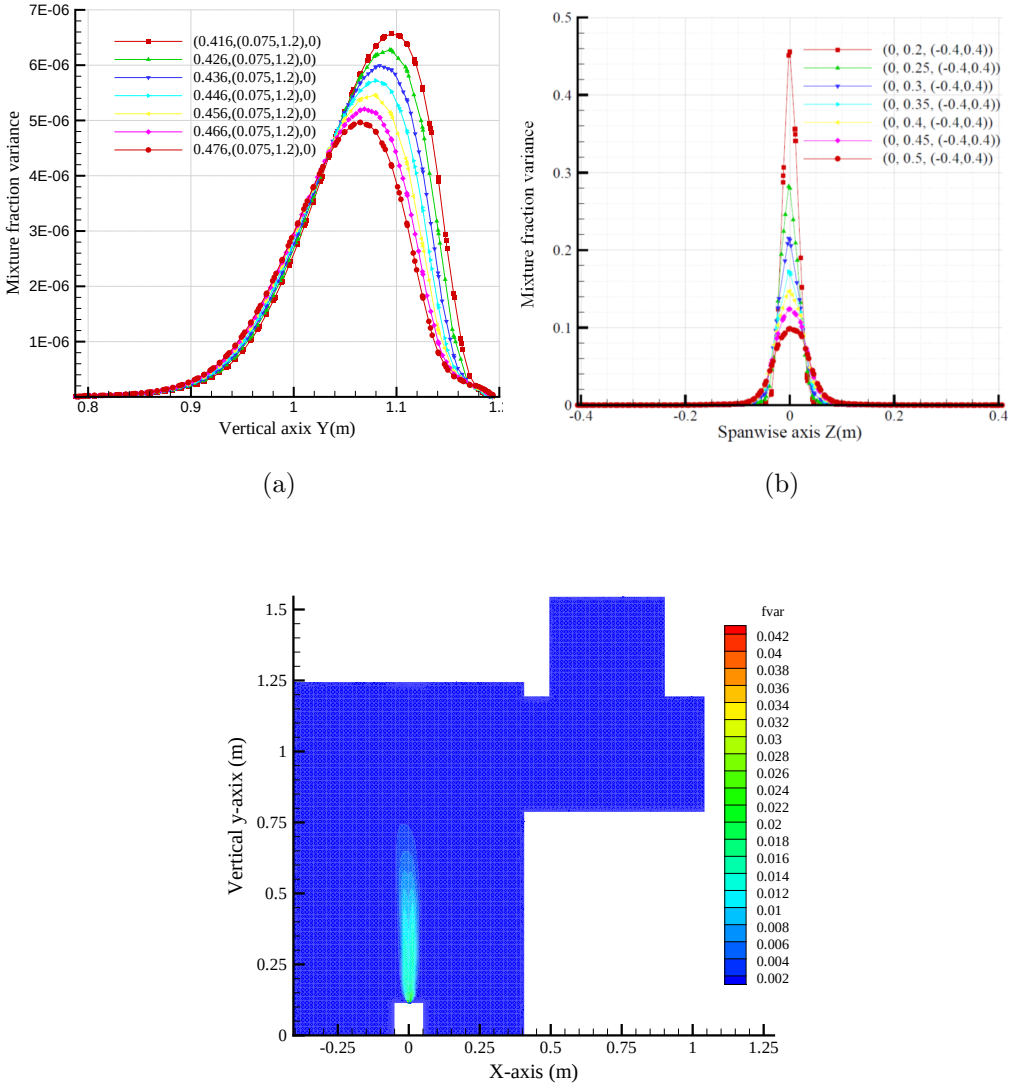


(a) (b)

(c)

Figure 4.25: Mixture fraction variance (a) for a vertical profile at the exit region, (b) for a span-wise cross-sectional profile starting at $y = 0.2m$, and (c) contours for a central slice.

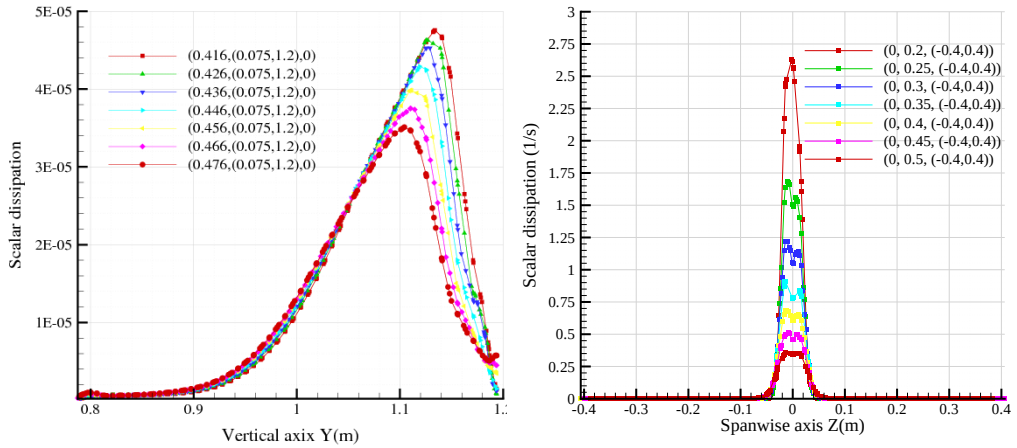


(a) (b)

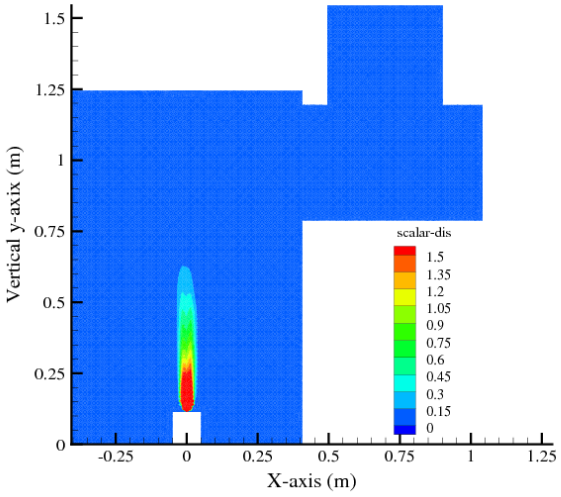


(c)

Figure 4.26: Scalar dissipation (a) for a vertical profile at the exit region, (b) for a span-wise cross-sectional profile starting at $y = 0.2m$, and (c) contours for a central slice.

# Chapter 5

# Combustion Modelling of Conventional fuels and Biofuels based on Advanced Reaction Mechanism

Having gained confidence in the methodology adopted here, where two detailed reaction mechanisms (the reduced San Diego mechanism and the comprehensive EXGAS one) are used to model the spray combustion of methanol ($CH_3OH$), a low hydrocarbon, it is part of the objective of this thesis to shed light on the spray combustion of heavy hydrocarbons in the form of both conventional fuels and biofuels. From the conventional fuels, decane ($C_{10}H_{22}$) was considered and from biofuels family, methyl decanoate ($C_{11}H_{22}O_2$) is taken as representatives. The selection of these two candidates is based on the fact that they are the closest in structure and composition as shown in Fig. 2.3

Many documented researches have shown that energy content of conventional diesel is between 10-15% higher than bio-diesel. For example, Table 5.1, taken from recent reviews, shows the calorific value (among other properties) of biodiesel from vegetarian sources compared to conventional diesel. On the other hand, lower hydrocarbons (such as methanol), do contain lower energy than high hydrocarbon fuel. The average calorific value for methanol is of order $20MJ/kg$.

Compared to diesel and biodiesel, this is almost half (or slightly lower than) the calorific value for diesel and biodiesel.

With reference to this discussion, one would expect that combustion of diesel would produce slightly higher energy than biodiesel and that both biodiesel and diesel will beyond doubt produce higher energy than methanol. In this thesis, the flame temperature produced is used as an indicator to energy release. The following sections discuss the CFD results from the burning of both diesel and biodiesel in the same burner geometry used to study the spray combustion of methanol discussed in the previous chapters.

It is important to note that the SDRM mechanism used to model the combustion of methanol is not qualified to study the combustion of higher hydrocarbons unless a major modification is carried out manually to incorporate as many as possible reactions associated with the different intermediate products and radicals expected as a result of the combustion of such class of hydrocarbons. As mentioned in Section 3.4, such process will lead to a high degree of uncertainty and shadow the results obtained. To avoid this uncertainty the EXGAS software was adopted to generate the reaction mechanisms, for both the diesels ($C_{12}H_{26}$) (referred to as EGRM-diesel), and biodiesel ($C_{12}H_{26}O_2$) (referred to as EGRM-biodiesel).

## 5.1 Results and Discussion

In order to facilitate adequate comparison between the results of diesel and biodiesel, together with methanol, a similar approach to the analysis of methanol case is adopted. Similar variables will be looked at in the same context in order to elucidate any difference between the two fuels.

### 5.1.1 Temperature Field

The temperature profiles for the vertical and horizontal lines (Fig. 3.9 and Fig. 3.10) which matche the probe locations of the experimental work of Widmann and Presser [1] are respectively shown in Fig. 5.1(a) and Fig. 5.1(b). It is clear that the EGRM simulation of diesel produced an exit temperature of order

Table 5.1: Fuel properties of ordinary diesel and common vegetable based biodiesel (Arbab *et al.* [133] and Sadeghinezhad *et al.* [134])

| Properties | Kinetic viscosity 40 $^o$C (cSt) | Density (kg/m3) | CN | Calorific value (MJ/kg) | FP ($^o$C) |
|---|---|---|---|---|---|
| ASTM limit | 1.9 - 6 | - | 47 minimum | - | 130 $^o$C minimum |
| Diesel | 2.5 - 5.7 | 816 - 840 | 45 - 55 | 42 - 45.950 | 50 - 98 |
| Jatropha | 3.7 - 5.8 | 864 - 880 | 46 - 55 | 38.5 - 42 | 163 - 238 |
| Palm | 2.95 - 4.92 | 843 - 890 | 49 - 65 | 38.73 - 40.39 | 135 - 259 |
| Coconut | 2.61 - 4.1 | 844 - 930 | 51 - 60 | 35 - 38.1 | 112 - 241.5 |
| Cottonseed | 4 - 4.9 | 874 - 885 | 51.2 - 55 | 40.32 - 42.73 | 70 - 110 |
| Sunflower | 4.5 - 5.9 | 877 - 882 | 49 - 52 | 39.7 - 40.56 | 85 - 178 |
| Soybean | 4.08 - 4.97 | 884 - 896 | 40 - 53 | 38.31 - 39.76 | 69 - 144 |
| Canola or rapeseed | 4.2 - 4.5 | 837 - 886 | 49 - 52.9 | 36.55 - 40.5 | 94 - 183 |

$665K$. In comparison with the results obtained for methanol simulation using the SDRM (Fig. 4.3(b) and Fig. 4.3(a)) where the predicted values are in the range $505 - 515K$, it is apparent that the combustion of diesel led to a higher temperature range. Although there is no experimental data to reference here, one would say that these results are realistic. A quick check reveals the percentage increase in temperature range for diesel is of order:

$$\frac{665 - 510}{510} = 30\%$$

With reference to the fact that diesel has almost twice the calorific value of methanol, the obtained results with 30% higher temperature range in the case of diesel is quite acceptable. One would not expect exactly twice the range of temperature as the temperature is not an exact measure to the energy released, rather an indicator of the amount of energy that may be released although the

enthalpies may be a better indicator. It is for consistency reason that the author shows the temperature field. It would have been an adequate approach to evaluate the energy release from all fuels considered in this thesis, but that can only be put as a recommendation for future work.

To elucidate the temperature field of the combustion of diesel, Fig. 5.1(c) shows the profiles of temperature for cross-sectional lines starting from $y = 0.2m$ with a $0.05m$ increment along the vertical axis, while Fig. 5.1(d) shows the temperature contours for a central (x,y)-slice. These figures correspond to Fig. 4.3(c) and Fig. 4.3(d) for the simulation of methanol. From the cross-sectional temperature profiles there are two distinct observations. In the case of diesel, the results show that the inner temperature for the diesel simulation is of order $650K$ while that for the methanol is of order $500K$. The second observation is related to the maximum temperature attained in the case of diesel and methanol where at $y = 0.2m$, the methanol reports slightly higher temperature, $1190K$ compared to $1000K$ in the case of diesel. The later might appear as a discrepancy, however, the author attributes this to the differences in the simulation. While the low-carbon methanol is easy to predict with many advanced reaction mechanisms having been developed and validated, large hydrocarbons such as diesel and biodiesel are still in progress. The result from the methanol experiments have shown very good agreement with the available experimental results and there is no reason to criticise it. At this point, the author needs to mention the fact that many radicals and their associated reactions have been omitted from the developed reaction mechanism. Although this was done on the recommendation of chemistry experts, the author believes that their contribution should have been involved. Their omission come as a result of unavailable kinetic data for them and it is possible that their inclusion based on data from website may increase the uncertainty of the results. Although the exit temperature for the diesel simulation shows reasonable increase at the exit location which is supported by the interior temperature within the burner ($650K$), the maximum temperature within the flame region is lower than that for methanol. The fact that the temperature within the burner interior is higher in diesel simulation compared to methanol can be attributed to the nature of the flame structure displayed in Fig. 5.1(d) for diesel and in Fig. 4.3(d) for methanol. It is apparent that the longer and well-structured flame in the case of

the diesel simulation has led to the difference in temperature within the burner. As mentioned previously, the literature has shown that EGRM model predicts a good flame structure.

It is worth looking at the simulations of methanol using EGRM (Fig. 4.17) and compare them with the results for diesel. In summary, the temperature profiles at the exit of the burner for methanol using EGRM predict slightly lower range than the case of diesel which still supports the validity of the diesel simulation using an EGRM. While this still supports the obtained results for diesel using EGRM-Diesel, it is a point worth further investigation. As discussed in Section 4.4, EGRM has produced a long flame in the case of methanol, however, the cross-sectional profile has shown a much higher range of temperature (of order $1600K$ peak value compared to $1000K$ for diesel). This clearly indicates that using EXGAS software for different classes of hydrocarbons (low and high) may lead to different results, overall indicating the difficulty of ruling out uncertainties. However, it is noticeable that the reaction mechanism developed using EXGAS led to a higher temperature range compared to reduced and well documented reaction mechanisms such as SDRM. It could be due to the fact that the EGRM mechanism developed for diesel was modified via the removal of a few radicals. These radicals are associated with low temperature oxidation reactions of the fuel, and hence, it becomes essential that only higher temperature reactions alone should not be considered for developing reaction mechanisms for heavy hydrocarbons. It is well established that at high temperatures (in the range of 1500–$2500K$) more reaction channels become kinetically active and the decomposition processes increase and become of particular importance to the combustion process. Decomposition via $C$-$C$ beta-scission (which is involved in developing the mechanism) is a major loss mechanism for alkyl radicals during high temperature combustion and the author would like to note this point for any further research to consider all radicals and both low- and high-temperature range reactions and associated steps, hopefully will improve the outcome.

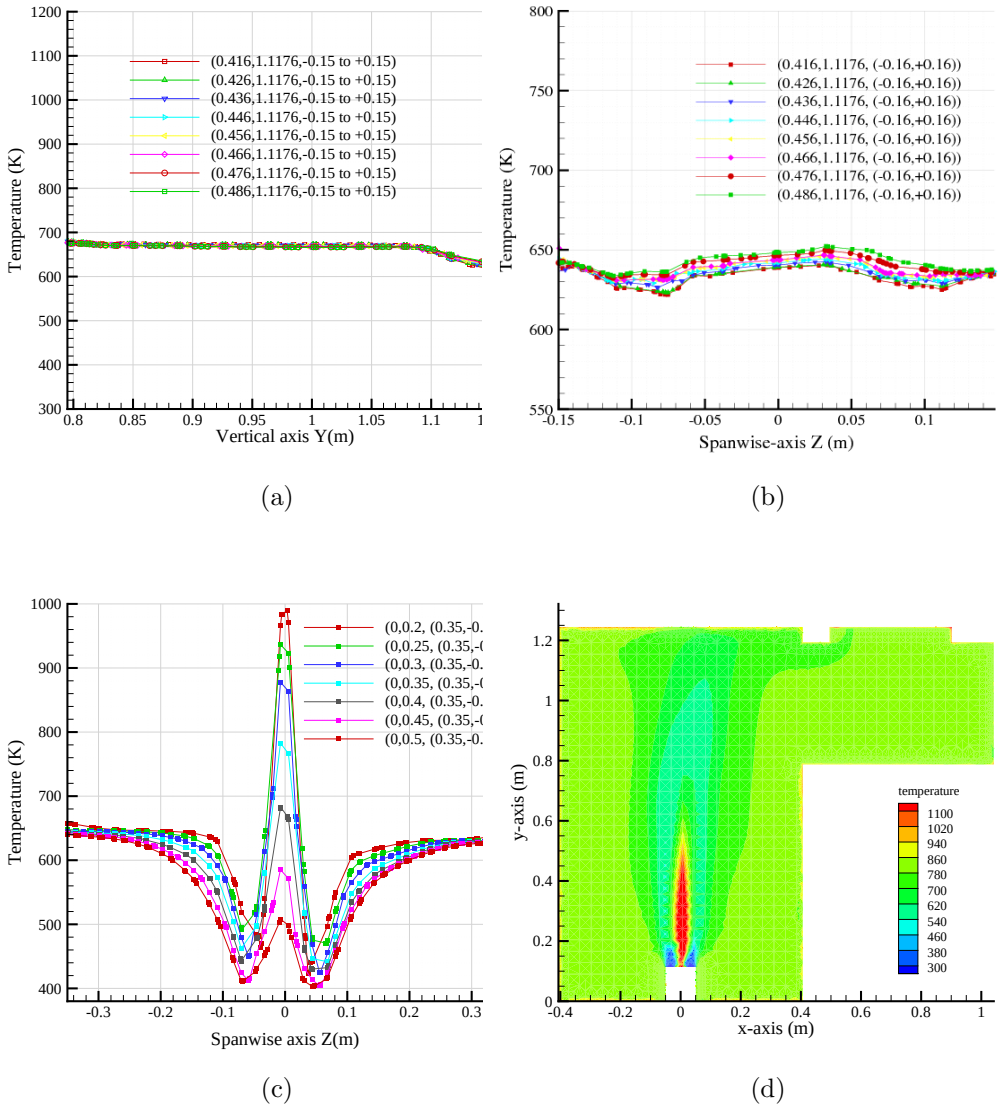


Figure 5.1: Diesel CFD simulations using EGRM-diesel: Temperature profiles corresponding to (a) vertical lines shown in Fig. 3.9, (b) horizontal lines shown in Fig. 3.10, and (c) cross-sectional profiles starting at $0.2m$ from the burner bottom wall at $0.05m$ increment along the vertical axis, and (d) Temperature contours for a central slice.

### 5.1.2 Turbulence Parameters

#### 5.1.2.1 Turbulence Reynolds Number

The first turbulence parameter that has been observed in the case of diesel simulation include turbulence Reynolds number ($\mathrm{Re}_y$) described in Section 4.2.1. Fig. 5.2(a) and Fig. 5.2(b) show the profiles for vertical and horizontal lines of Fig. 3.9 and Fig. 3.10 at the exit of the burner and in the region where Widmann and Presser [1] collected their data. The figures show symmetrical profiles which is an indication to a developed flow. The values are less than those predicted for methanol using both the SDRM (Fig. 4.4(a) and Fig. 4.4(b)) and the EGRM (Fig. 4.18(a) and Fig. 4.18(b)). Although slightly higher air velocity is used in the latter simulation (for methanol), that may not be the only reason behind the lower $\mathrm{Re}_y$ predicted for diesel. Based on stoichiometric simple combustion, the relations below indicate that the stoichiometric air/fuel ratio (on molar basis) for diesel and methanol are:

$$C_{12}H_{26} + \frac{37}{2}\left(O_2 + \frac{79}{21}N_2\right) 12CO_2 + 13H_2O + \frac{79}{21}\frac{37}{2}N_2$$

$$\left(\frac{A}{F}\right)_{st} = \frac{22.26}{1}$$

for methanol

$$CH_3OH + 2\left(O_2 + \frac{79}{21}N_2\right) CO_2 + 2H_2O + 2\frac{79}{21}N_2$$

$$\left(\frac{A}{F}\right)_{st} = \frac{9.52}{1}$$

The above is explained in the following: one kilomole of diesel fuel needs 22.6 kilomole of air to burn completely compared to 9.52 for methanol. It is apparent that the stoichiometric air/fuel ratio $\left(\frac{A}{F}\right)$ is much larger than for the large hydrocarbon (diesel) than hydrocarbon fuels with one, two or three carbon atoms in their structure. Aware of this fact, the author of this thesis varied slightly the amount of air in the case of diesel and biodiesel not only to ensure that stoichiometric conditions are met but also due to difficulties met while performing

the simulation for the two large hydrocarbons (diesel and biodiesel). These two hydrocarbons failed to burn under similar air inflow conditions of methanol and burning proved difficult to start. Hence, the difference in Turbulence Reynolds number ($\mathrm{Re}_y$) may be attributed to different factors as discussed here.

Close to the flame injector region, however, the profiles of $\mathrm{Re}_y$ show close values those for methanol simulation using EGRM. Shown in Fig. 5.2(c) are $\mathrm{Re}_y$ profiles for cross-sectional profiles starting at $y = 0.2m$ and with increment of $0.05m$ along the vertical axis, while Fig. 5.2(d) shows the contours for Turbulence Reynolds number at a central (x,y)-plane. These two figures correspond to Fig. 4.5(a) and Fig. 4.5(b) respectively from the EGRM simulation of methanol and the range of $\mathrm{Re}_y$ is comparable. This mainly reflects the close speed of air used in the two cases. It is worth mentioning that it is higher in the case of diesel. The shape displayed by the $\mathrm{Re}_y$ cross-sectional profile does reflect the turbulent feature of the flow starting from very close distance from the injector position. The M-shape of $\mathrm{Re}_y$ profile agrees with many simulations in the field and the irregular shape indicates the turbulent nature of this reactive flow.

In comparison with EGRM simulation of methanol (Fig. 4.18), the diesel simulation using EGRM-Diesel shows similar features with differences as discussed in the paragraph above.

#### 5.1.2.2 Turbulence Intensity

The second turbulence parameter observed in the case of diesel simulation is the turbulence intensity shown in Fig. 5.3(a) for the vertical profiles at the exit region of the burner (corresponding to the vertical lines of Fig. 3.9), horizontal profiles at the exit showed similar range. Fig. 5.3(b) and Fig. 5.3(c) display the turbulence intensity for the lower cross-sectional profiles along the vertical axis (starting at $y = 0.2m$ and moving vertically with an increment of $0.05m$), while Fig. 5.3(c) shows the contours for a central (x,y)-slice respectively. At the exit of the burner, turbulence intensity is low but significant (of order 0.05–0.2).

Close to the injector location and within the flame region, the cross-sectional profiles show turbulence intensity of order 0.25–0.4 at the flame region decreasing to a zero value when approaching the wall. In comparison with the methanol

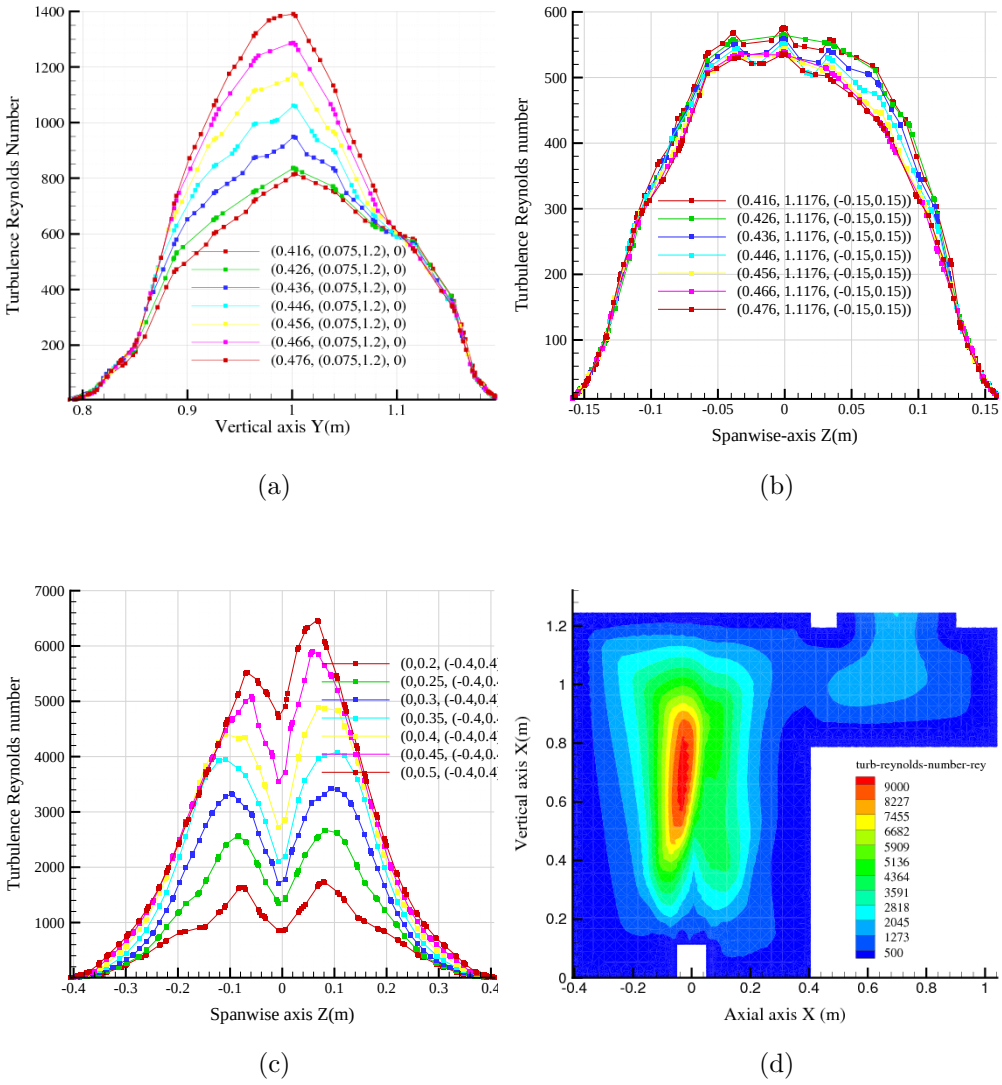


Figure 5.2: Diesel CFD simulations using EGRM-diesel: Turbulence Reynolds number profiles corresponding to (a) vertical lines shown in Fig. 3.9, (b) horizontal lines shown in Fig. 3.10, and (c) cross-sectional profile starting at $0.2m$ from the burner bottom wall at $0.05m$ increment along the vertical axis, and (d) Turbulence Reynolds number contours for a central slice.

SDRM simulation, the range of turbulence intensity is the same, reflecting a turbulent environment of the reactive flow in the two situations. Comparing the prediction for this parameter for the diesel simulation with the methanol

simulation (Fig. 4.19(c)), it is apparent that the levels of turbulence intensity is high (0.785), almost double the predicted values for the diesel simulation and the EGRM simulation for methanol. As previously mentioned, this is partly explained by the long nature of the flame predicted by the EGRM simulation of methanol. It is a matter of fact that the environment within the interior region of the burner will be extremely buoyant, a feature that will be enhanced by a longer flame. The deeper the flame moves along the vertical axis, the more buoyant is the flow that it creates and that enhances turbulence intensity. This is clearly displayed by the turbulence intensity contours from the central plane shown in Fig. 5.3(c), where most parts of the domain show some level of turbulence intensity and no symmetry - a sign of the non-steady nature of the flow.

### 5.1.3 Emissions

Emission from burning low hydrocarbons in the form of methanol are discussed in Chapters 4 using both the reduced SDRM and the comprehensive EGRM. In the coming few sections, emission of diesel will be discussed.

#### 5.1.3.1 Carbon Dioxide ($CO_2$)

The rates of carbon dioxides $CO_2$ from burning diesel in the burner geometry has been observed at the exit, and found matching the experimental measuring stations of Widmann and Presser [1]. The profiles of $CO_2$ for the vertical lines (Fig. 3.9) and horizontal lines (Fig. 3.10) at the exit of the burner (covering all measuring stations of the experiment of Widmann and Presser [1]) are respectively shown in Fig. 5.5(b) and Fig. 5.5(a). It is apparent from the two figures that the EGRM model predicted a mole fraction for $CO_2$ of order 0.017–0.0185. Fig. 5.4 compares the prediction of $CO_2$ for the methanol simulations with the SDRM and EGRM and the EGRM-diesel simulation with the experimental data of Widmann and Presser [1]. Two trends are observed from the figure. The first is that the rates of the emission of $CO_2$ from diesel are higher in comparison with methanol. That is expected as heavier fuels can indeed produce higher carbon oxides due to the existence of large amount of carbon (carbon atoms) in their structure, although the rates are a function of many other parameters

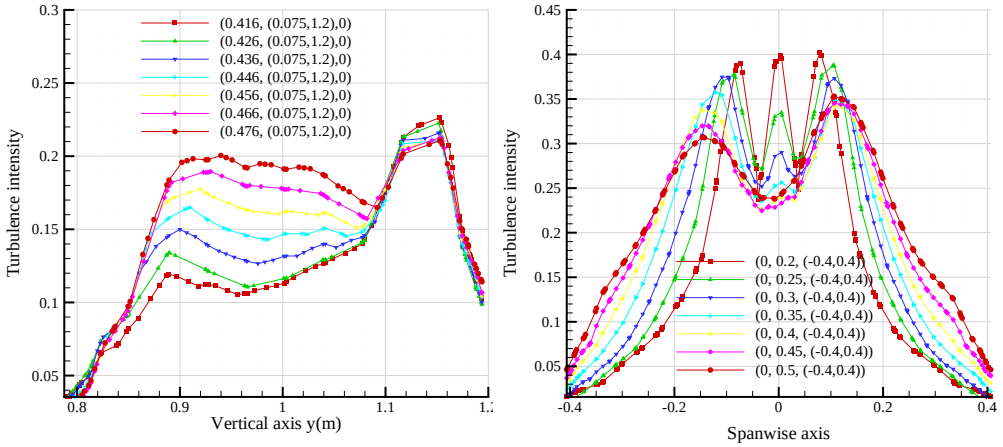


(a) (b)

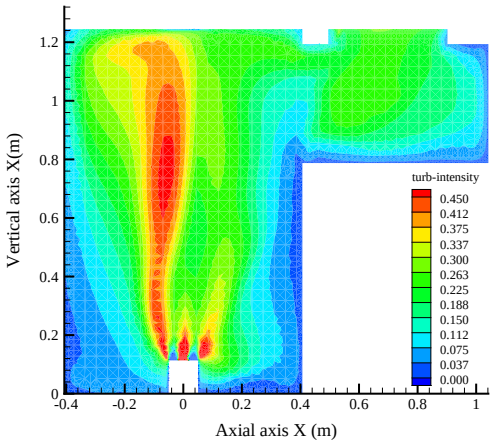


(c)

Figure 5.3: Diesel CFD simulations using EGRM-diesel: Turbulence intensity profiles corresponding to the (a) vertical lines at the burner exit (Fig. 3.9), (b) cross-sectional profiles starting at $0.2m$ from the burner bottom wall at $0.05m$ increment along the vertical axis, and (c) contours for a central slice.

including the boundary condition of the combustion. Having said so, and considering the similar environment under which combustion of the fuels occur, it is in good order that the rate of predictions of $CO_2$ for diesel is slightly higher than that for methanol. The second is that the predicted rates of $CO_2$ exceed

that of the experimental values at specific measuring stations but lag a slightly below the experimental values at some other measuring stations. Having said so, the difference (positive or negative) is very small. Overall, one would say that EGRM-diesel has produced very good results for $CO_2$ and predicted this variable well.

$CO_2$ profiles for cross-sectional lines starting at $0.2m$ from the bottom of the burner with $0.05m$ increment along the vertical axis are shown in Fig. 5.5(c). Contours of $CO_2$ for a central (x,y)-plane are shown in Fig. 5.5(d). The profiles show that the highest level of $CO_2$ is of order 0.045 decreasing with height and most of the computational domain has a level of 0.0175 $CO_2$ mole fraction. Comparing these ranges with the SDRM and EGRM simulations of methanol (Fig. 4.7(c)), it is clear that methanol produces $CO_2$ of order 0.09 for the SDRM simulation and 0.015 for the EGRM simulation. Hence, it is apparent that diesel produces almost double the rates of methanol SDRM and slightly higher than the EGRM simulation within the interior region of the burner. This is a consistent result and indicates good execution of the diesel simulations and the other methanol simulations as well.

#### 5.1.3.2 Nitrogen Oxides (*NO* and $NO_x$)

Nitrogen oxides (NO) for modelling the combustion of diesel are examined at the exit of the burner. Profiles corresponding to the vertical and horizontal lines (Fig. 3.9 and Fig. 3.10) are respectively shown in Fig. 5.6(a) and Fig. 5.6(b). The figures indicate that small amount of this type of nitrogen oxide exists. The mole fraction for those exit locations is within the range 0.0015 to 0.00325. In comparison to the values obtained from the simulation of methanol (Fig. 4.11(a) and Fig. 4.11(b)), the rates produced from the methanol is of order 0.0001 to 0.00014. This renders the rates of $NO$ production from burning diesel to be much higher (of order 10 folds). It is apparent from these results that on theoretical basis, heavy hydrocarbon produces higher rates of $NO_x$ than lighter hydrocarbons. It is well established that diesel engine produces high rates of $NO_x$ as it operates on lean fuel mixtures. In this regard, the results obtained for $NO_x$ from the simulation of diesel on the burner geometry is not that different and the higher

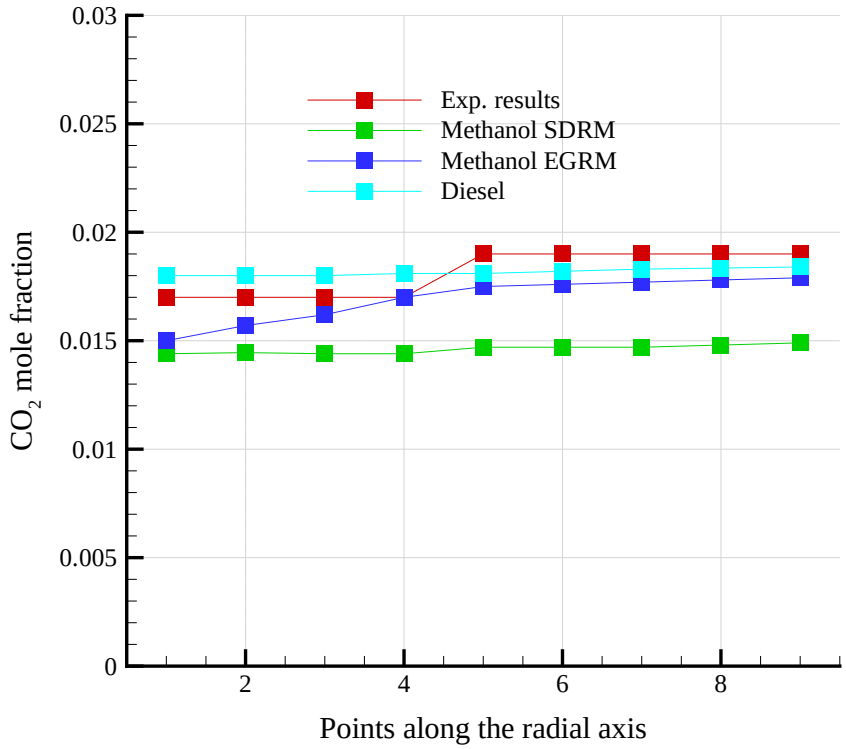


Figure 5.4: $CO_2$ comparison between the experimental, SDRM and EGRM simulations for methanol and diesel.

rates of $NO_x$ are relevant. The contours of this variable for a central (x,y)-slice is shown in Fig. 5.6(c). It is apparent that the rates are almost zero within the flame region as expected, with unsteady distribution on other parts of the burner interior.

#### 5.1.3.3 Water Vapour ($H_2O$)

Water vapour from burning diesel is examined quantitatively both at the exit of the burner as well as close to the injector location. Profiles of $H_2O$ at the exit of the burner (corresponding to Fig. 3.9 and Fig. 3.10) are respectively shown in Fig. 5.7(a) and Fig. 5.7(b)). The figures show that the water vapour mole fraction at the exit ranges between 0.018–0.2. These are very close values to those obtained

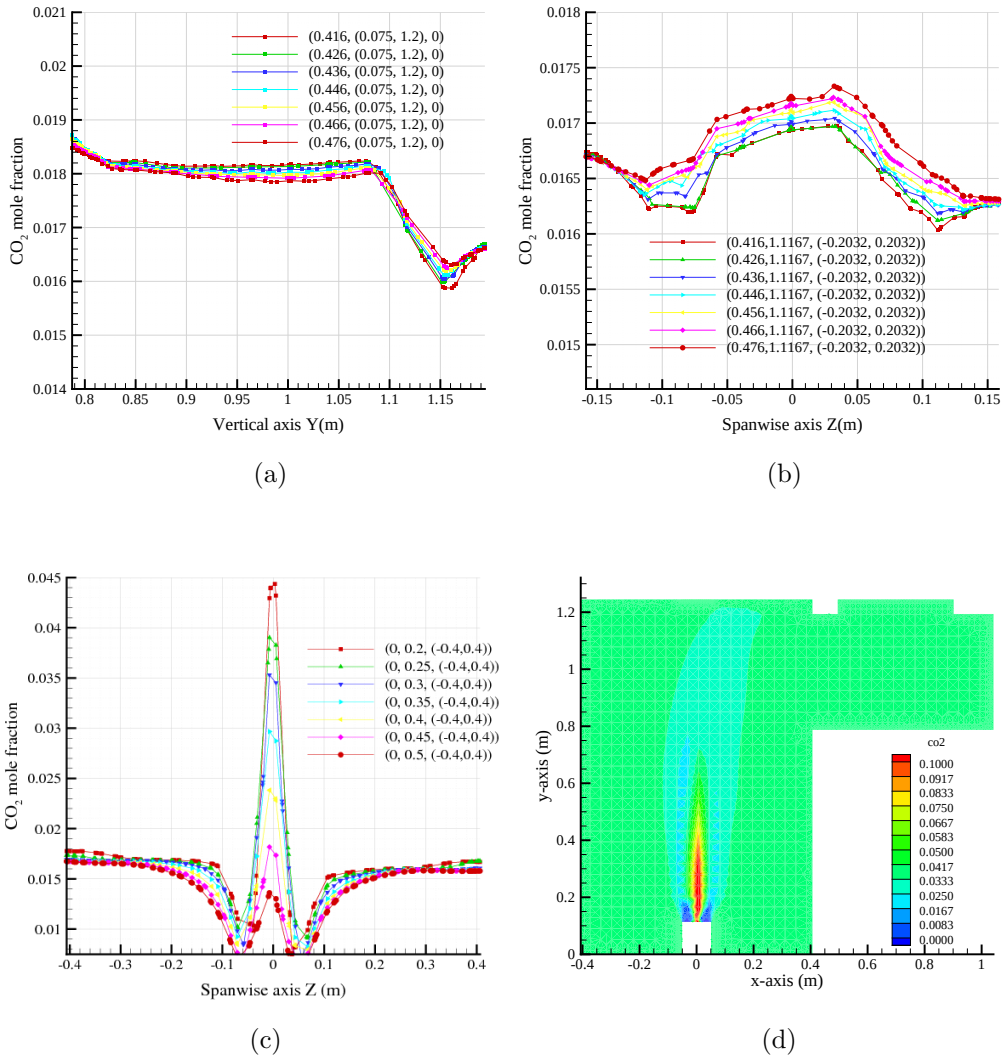


Figure 5.5: Diesel CFD simulation using EGRM-diesel: $CO_2$ mole fraction profiles corresponding to (a) vertical lines shown in Fig. 3.9, (b) horizontal lines shown in Fig. 3.10, (c) cross-sectional profiles starting at $0.2m$ from the burner bottom wall at $0.05m$ increment along the vertical axis, and (d) contours for a central slice.

from modelling methanol using the SDRM (Fig. 4.13(a) and Fig. 4.13(b)). Close to the injector point and at locations above the injector along the vertical axis (flame region), cross-sectional profile of water vapour is shown in Fig. 5.7(c) while the contours for a central (x,y)-plane is displayed in Fig. 5.7(d). The

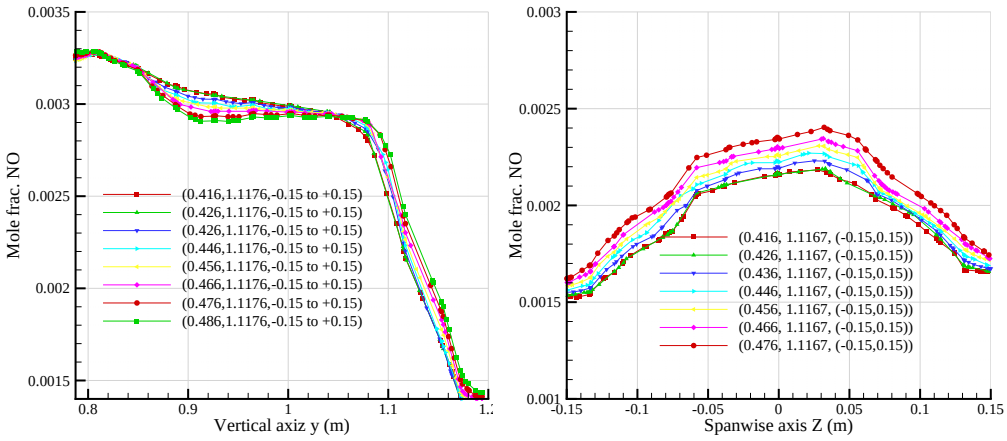


(a) (b)

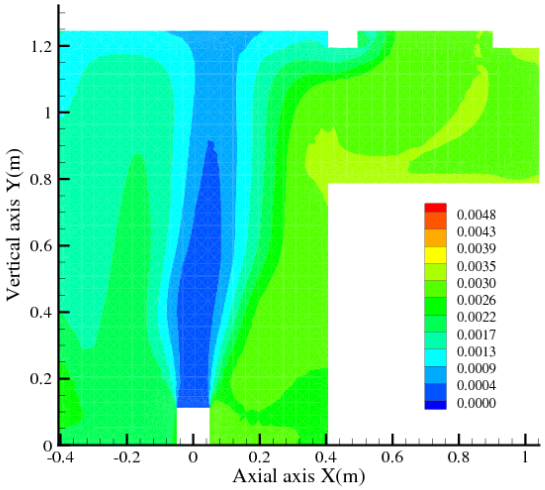


(c)

Figure 5.6: Diesel CFD simulations using EGRM-diesel: Nitrogen oxide ($NO$) mole fraction profiles corresponding to the (a) vertical lines shown in Fig. 3.9, (b) horizontal lines shown in Fig. 3.10, and (c) central (x,y)-plane showing contours.

maximum amount of water vapour mole fraction close to the injector ($y = 0.2$) is of order 0.05 with a level just below the value of 0.02 maintained for the interior region of the boiler. In comparison to the SDRM simulation of methanol

(Fig. 4.13(c)), close to the injector location ($y = 0.2$), water vapour mole fraction is of order 0.1 (almost double that for diesel) with a level just above the value of 0.02 (similar to diesel) maintained for the interior region. Since the amount of such combustion products are conserved, it is apparent that the distribution of water vapour within the burner body in the case of diesel simulation does explain the situation. However, it is noticeable that hydrocarbons with oxygen content tend to produce more water vapour than those which do not have any oxygen atoms embedded in their microstructures. The predicted results for biodiesel also have higher rates of water vapour compared to diesel as will come later in the course of this chapter.

#### 5.1.3.4 Diesel $C_{12}H_{26}$ Concentration:

Unburned hydrocarbons, whether in the form of the fuel itself or other intermediate products are very important species in combustion. In real experimental work, unburned hydrocarbon can be measured as will come in Chapter 7. Many forms of unburned hydrocarbon can be detected including ketones, aldehydes and organic acids and other forms of intermediate products. Unburned hydrocarbons are indicators of the efficiency of combustion as well as of the environment under which combustion occurs. Of interest to this work is the fuel itself i.e., how the fuel burns under the setup of this computational combustion problem?

The concentration (mole fraction) of diesel at the exit of the burner (corresponding the vertical lines displayed in Fig. 3.9) is shown in Fig. 5.8(a). It is apparent that there are negligible traces of the fuel (of order $10^{-9}$), a sign of the fact that complete burning of the fuel occurred within the flame region.

To examine the burning of the injected liquid diesel in close proximity of the injection point, cross-sectional profiles along the vertical axis (starting at $y = 0.2m$ above the burner base, $0.05m$ spaced) and a central (x,y)-plane showing the contours of the fuel (dodecane - $C_{12}H_{26}$) are respectively shown in Fig. 5.8(b) and Fig. 5.8(c) respectively. The profiles indicate that mole fraction of the fuels fall to a level of 0.001 at a height $0.035m$ mainly at the central part of the flame. Very small traces are able to reach a depth of $0.8m$ as shown by the contours of Fig. 5.8(c). In comparison to the methanol simulation with SDRM (Fig. 4.10), it

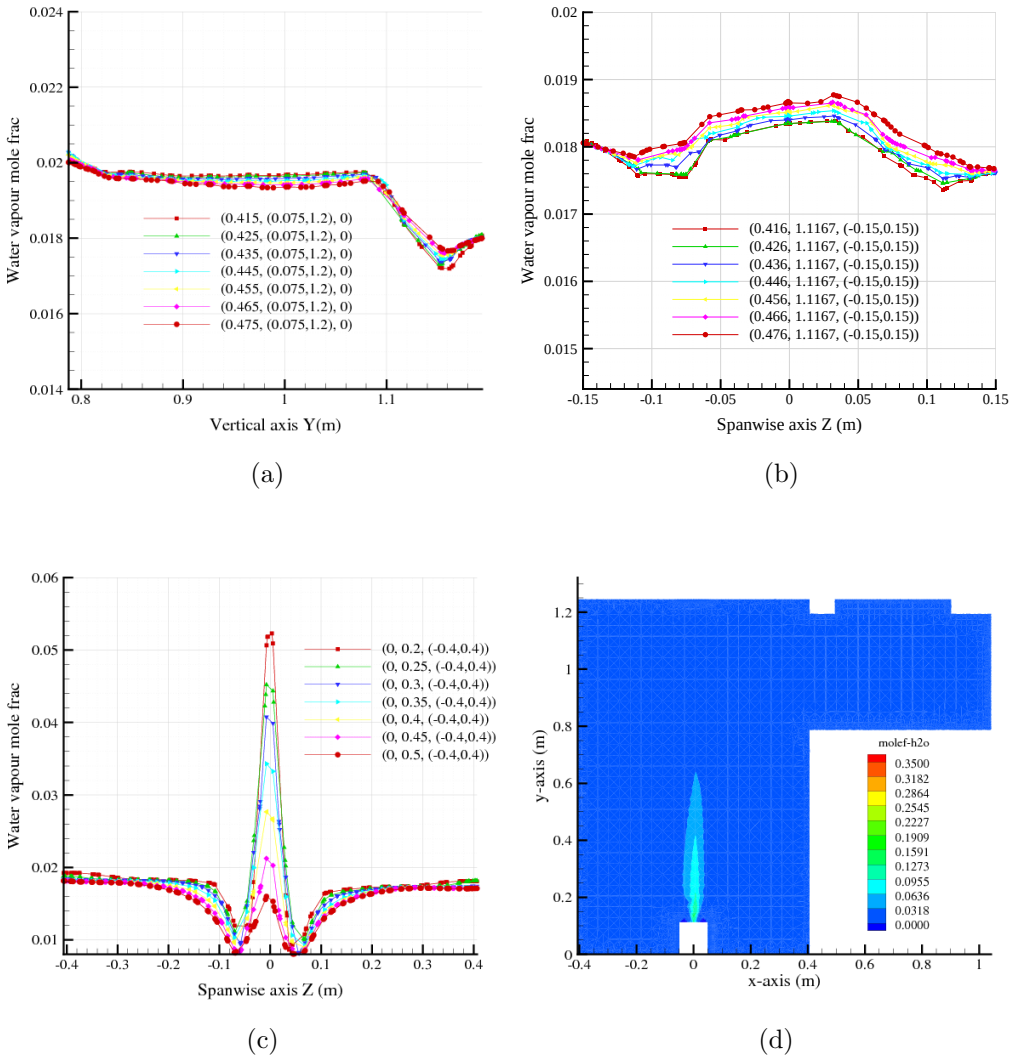


Figure 5.7: Diesel CFD simulation using EGRM-diesel: Water vapour ($H_2O$) mole fraction profiles corresponding to (a) vertical lines shown in Fig. 3.9, (b) horizontal lines shown in Fig. 3.10, (c) cross-sectional profiles starting at $0.2m$ from the burner bottom wall at $0.05m$ increment along the vertical axis, and (d) contours for a central slice.

is clear that methanol burnt at a rate higher than diesel with only mole fractions of order 0.03 measured closed to the injector at $0.2m$ above the burner base. This may be explained in two ways, the first is associated with burning heavy hydrocarbon such as diesel in comparison to light ones such as methanol. This is

related to the reaction mechanism used in modelling the combustion process of the two fuels. The best way to further this discussion and come out of concrete evidence is the to investigate all individual intermediate products from the combustion of the two fuels, a topic that needs further simulations under different environments and can only be suggested for further research in this field. Some light will be shed on further combustion products other than what is considered as conventional pollutants later in the thesis.

#### 5.1.3.5 PDF Variables: Mixture Fraction

The mixture fraction is thoroughly discussed in Chapter 3 and as mentioned previously, it is used as an indicator of the combustion of the fuel. As mentioned earlier, for the pdf of the mixture fraction, a $\beta-$function has been assumed where other parameters ($\alpha$ and $\beta$) are functions of the mean value and the variance of the mixture fraction. The pdf of the scalar dissipation rate $pdf(\chi_{st})$ is assumed to have the shape of a logarithmic normal distribution described by Eq. 3.28 with other parameters ($\mu_{log}$ and $\sigma_{log}$) representing the mean value and the variance of the transformed property $f_x = log\chi_{st}$. For further explanation on how these parameters are linked, the reader is advised to refer to Chapter 3

Based on the above definition, the mean mixture fraction, mixture fraction variance and scalar dissipation will be examined for diesel simulation. These three parameters give an indication of the photochemistry of combustion and flame development and extinction.

Shown in Fig. 5.9(b) and Fig. 5.9(a) are the mixture fractions for the vertical and horizontal lines (of Fig. 3.9 and Fig. 3.10) at the exit of the burner. Lower cross-section profile for the mixture fraction close to the injector and moving along the vertical axis are shown in Fig. 5.9(c) and a central (x,y)-plane showing the contours for the mixture fraction is displayed in Fig. 5.9(d). It can be observed from these figures that the rate of the mixture fraction is very low at the exit of the burner (of order 0.008–0.009), an indication of almost complete combustion of the fuel.

In comparison to the methanol SDRM predictions (Fig. 4.14(a) and Fig. 4.14(b)) where the rates of the mean mixture fraction is reported as of order 0.01 and

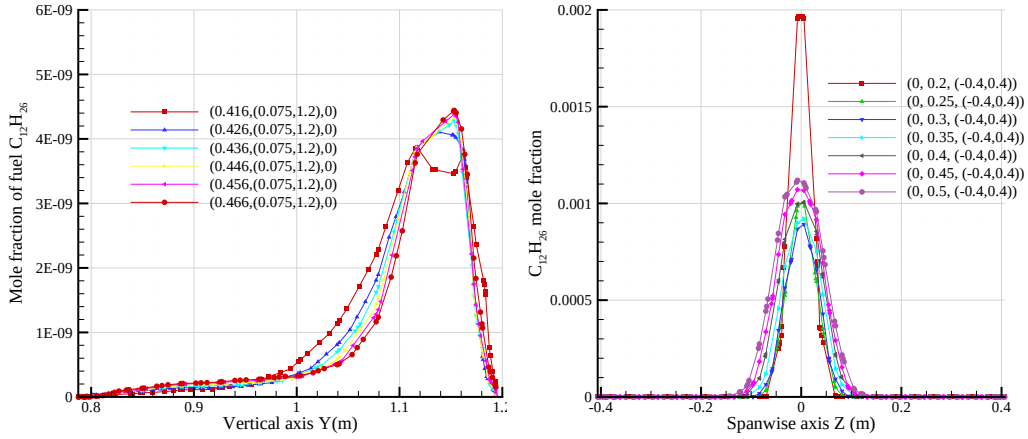


(a) (b)

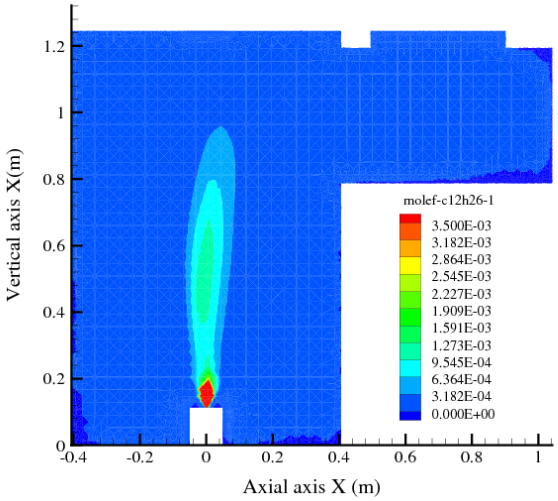


(c)

Figure 5.8: Diesel CFD simulation using EGRM-diesel: Fuel ($C_{12}H_{26}$) mole fraction profile corresponding to the (a) vertical lines shown in Fig. 3.9, (b) cross-sectional profiles starting at $0.2m$ from the burner bottom wall at $0.05m$ increment along the vertical axis, and (c) contours for a central slice.

EGRM prediction (Fig. 4.24(a) and Fig. 4.24(b)) where the rates are reported as of order 0.02, it is clear that mean mixture fraction of diesel using EGRM

matches that of methanol based on SDRM. As discussed previously in Chapter 4 that EGRM simulations indeed slow the chemistry leading to a longer flame. Why this is not happening with diesel is a question mark. It is apparent that the EXGAS software used to develop the mechanism used here needs a closer scrutiny when developing reaction mechanisms for different fuels, particularly when the fuel has oxygen atom(s) embedded in its microstructure.

Close to the injector (flame region), the mixture fraction shows a maximum value of order 0.04 (at $y = 0.2m$ above the burner bottom wall) reducing to 0.015 further along the vertical axis (at $y = 0.5m$ above the burner bottom wall). The contour also shows that the mixture fraction is mainly relevant within the flame region and maintains a value of zero at a height of $0.7m$. All this indicates the stoichiometric combustion of the injected fuel.

In comparison to the methanol SDRM predictions (Fig. 4.14(c) and Fig. 4.14(d)), the rates of the mean mixture fraction are reported as of order 0.09–0.02 at $y = 0.2m$ and $y = 0.5m$ respectively. For the EGRM prediction (Fig. 4.24(c) and Fig. 4.24(d)) the rates of the mean mixture fraction are reported as of order 0.3–0.125 at $y = 0.2m$ and $y = 0.5m$ respectively. It is clear that the mean mixture fraction of diesel using EGRM matches closer to that of methanol based on SDRM and the difference is expandable as heavy hydrocarbon is expected to burn at a lower rate than light ones. However, a similar question associated with the simulation of methanol using EGRM arises as the predicted rate is too high to pass un-noticed. Again the author will point to the reaction mechanism when oxygenated fuels are dealt with.

#### 5.1.3.6 Mixture Fraction Variance and Dissipation Rate

Related to the mean mixture fraction is the mixture fraction variance and its dissipation rate. As mentioned previously, the mixture fraction variance is a parameter that is considered as an estimate of the fluctuations in the mixing field while the dissipation rate performs a similar role as that of the energy dissipation ($\epsilon$) to the Kinetic Energy $K$ in turbulent models. Looking from these perspectives, the mixture fraction variance for the vertical and horizontal location at the burner exit are shown in Fig. 5.10(a) and Fig. 5.10(b), while low-cross-sectional

profiles along the vertical axis and a central (x,y)-plane for the mixture fraction variance are respectively shown in Fig. 5.10(c) and Fig. 5.10(d). In a similar trend, the scalar dissipation for the vertical and horizontal location at the burner exit are shown in Fig. 5.11(a) and Fig. 5.11(b), while low cross-sectional profiles along the vertical axis and a central (x,y)-plane for the mixture fraction variance are respectively shown in Fig. 5.11(c) and Fig. 5.11(d). With the exception of the scalar dissipation close to the injector location and within the flame region (displayed in Fig. 5.11(c) and Fig. 5.11(d)), the rest of the figures reveal very low values for both the mixture fraction variance and the scalar dissipation. The very low values of the mixture variance and the scalar dissipation indicate complete burning or these locations do not fall within the flame region where these parameters are supposed to be significant. However, within the flame region both the variance and the dissipation parameters show a range of values with the variance showing a low range (0.003–0.002). The low values of the mixture fraction variance most likely indicate the laminar nature of the flame and stoichiometric conditions and complete burning as well as extinction of the flame well below the top wall of the burner. The considerable values of the scalar dissipation close to the injector were expected as the fuel at this low height above the injector is still burning and this is the main region of the flame which is subjected to straining and dissipation up to extinction.

#### 5.1.3.7 Other Relevant By-products

Other by-products that emerged from the simulation of diesel using EGRM are hydrogen (Fig. 5.12(a)) and radicals including $r1h$, $r2OH$ and $rc3h5$ shown respectively in Fig. 5.12(b), Fig. 5.12(c) and Fig. 5.12(d). The figures clearly show that including more comprehensive reaction mechanisms can predict the emission of other products that are normally ignored in simple mechanisms. This shows the usefulness of using detailed reaction mechanisms.

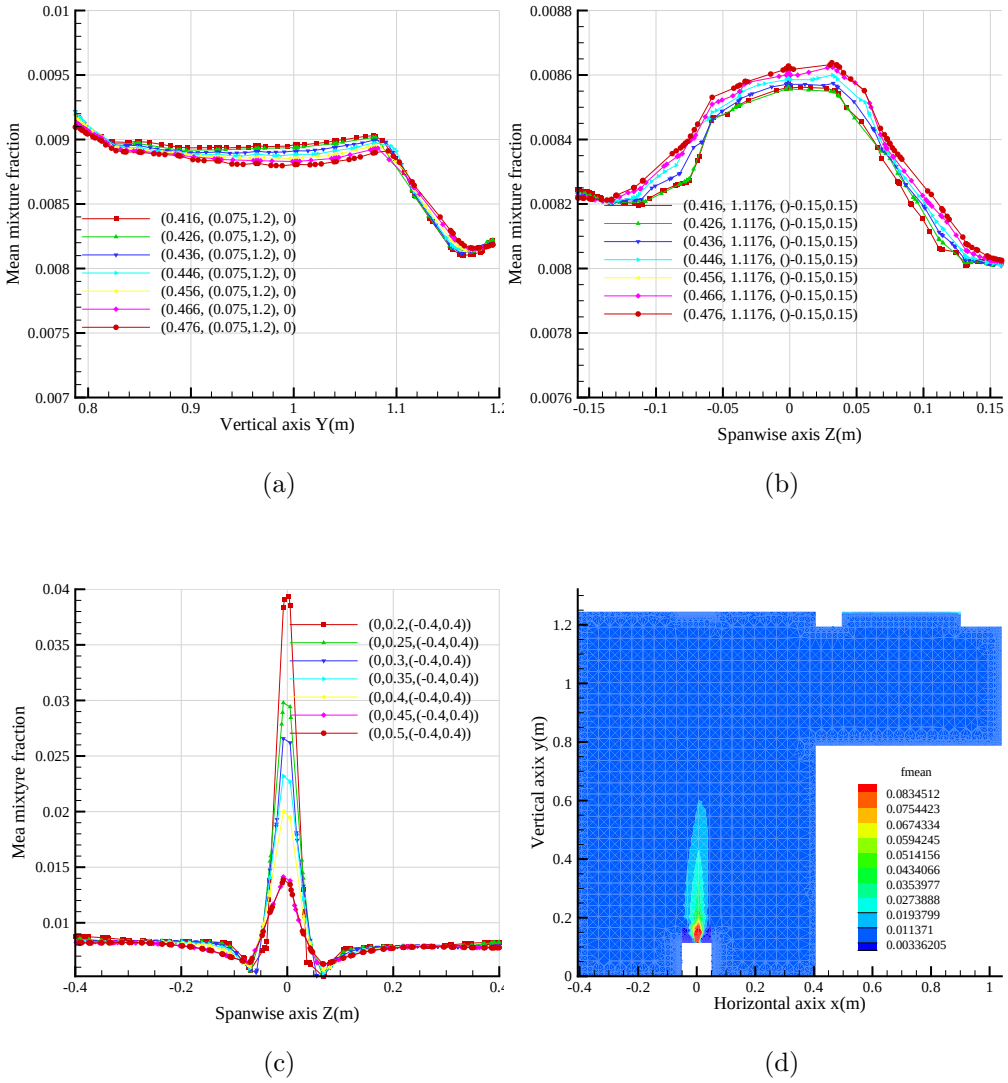


Figure 5.9: Diesel CFD simulation using EGRM-diesel: Mean mixture fraction profiles corresponding to the (a) vertical lines in Fig. 3.9, (b) horizontal lines shown in Fig. 3.10, (c) cross-sectional profiles starting at $0.2m$ from the burner bottom wall at $0.05m$ increment along the vertical axis, and (d) contours for a central slice.

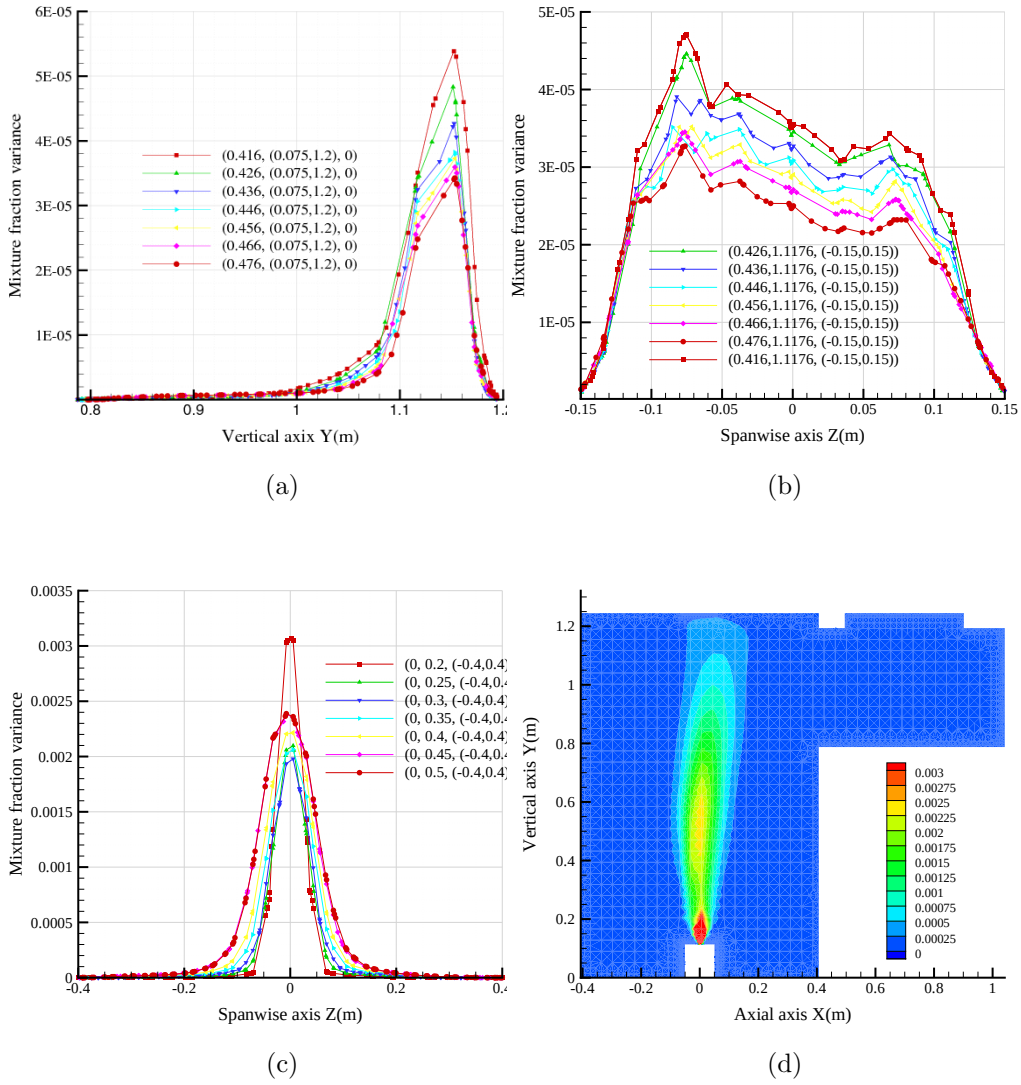


Figure 5.10: Diesel CFD simulation using EGRM-diesel: Mean mixture fraction variance profiles corresponding to the (a) vertical lines of Fig. 3.9, (b) horizontal lines of Fig. 3.10, (c) cross-sectional profiles starting at $0.2m$ from the burner bottom wall at $0.05m$ increment along the vertical axis, and (d) contours for a central slice.

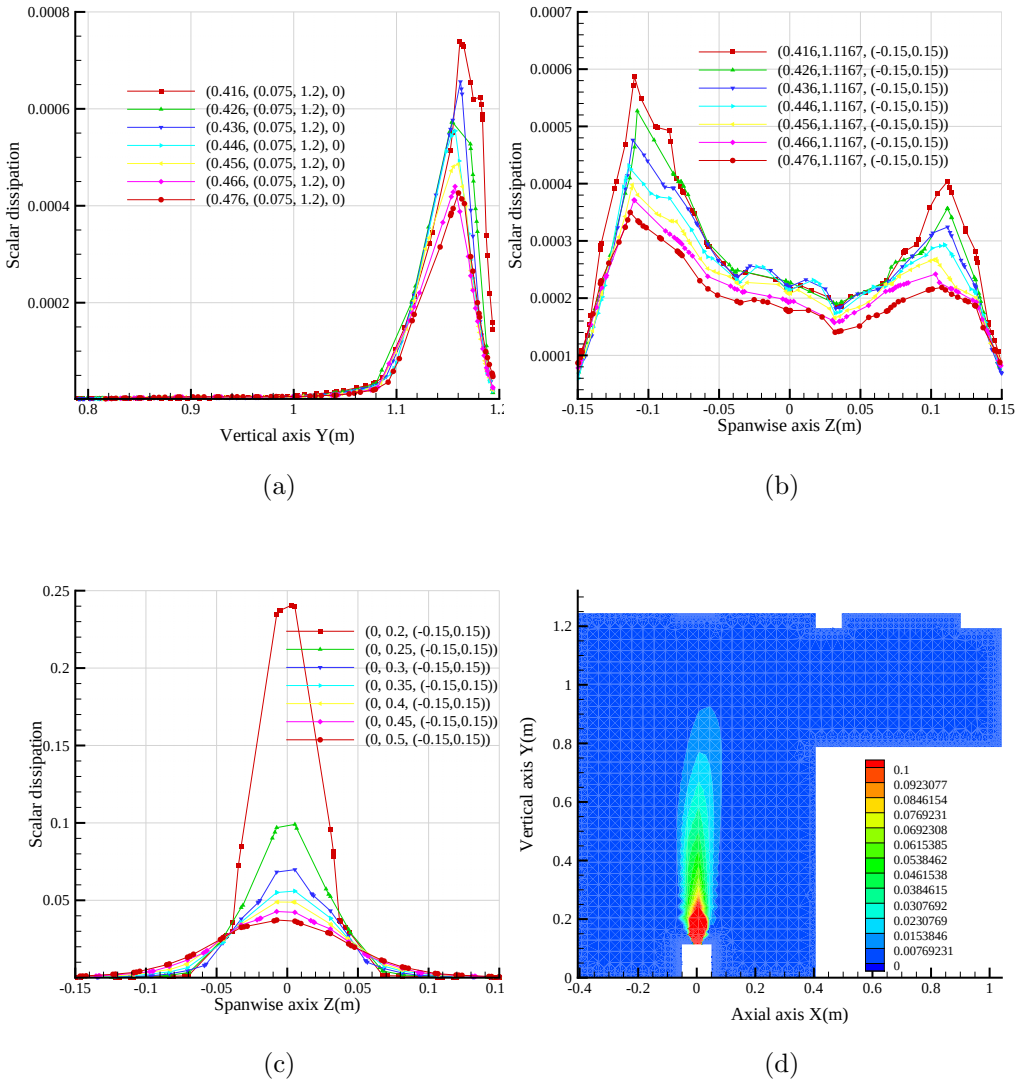


Figure 5.11: Diesel CFD simulation using EGRM-diesel: Scalar dissipation profiles corresponding to the (a) vertical lines of Fig. 3.9, (b) horizontal lines of Fig. 3.10, (c) cross-sectional profiles starting at $0.2m$ from the burner bottom wall at $0.05m$ increment along the vertical axis, and (d) contours for a central slice.

## 5.2 Biodiesel Case Study

Having studied the spray combustion results for methanol and diesel, this section is dedicated to the discussion of the simulation of the spray combustion of a can-

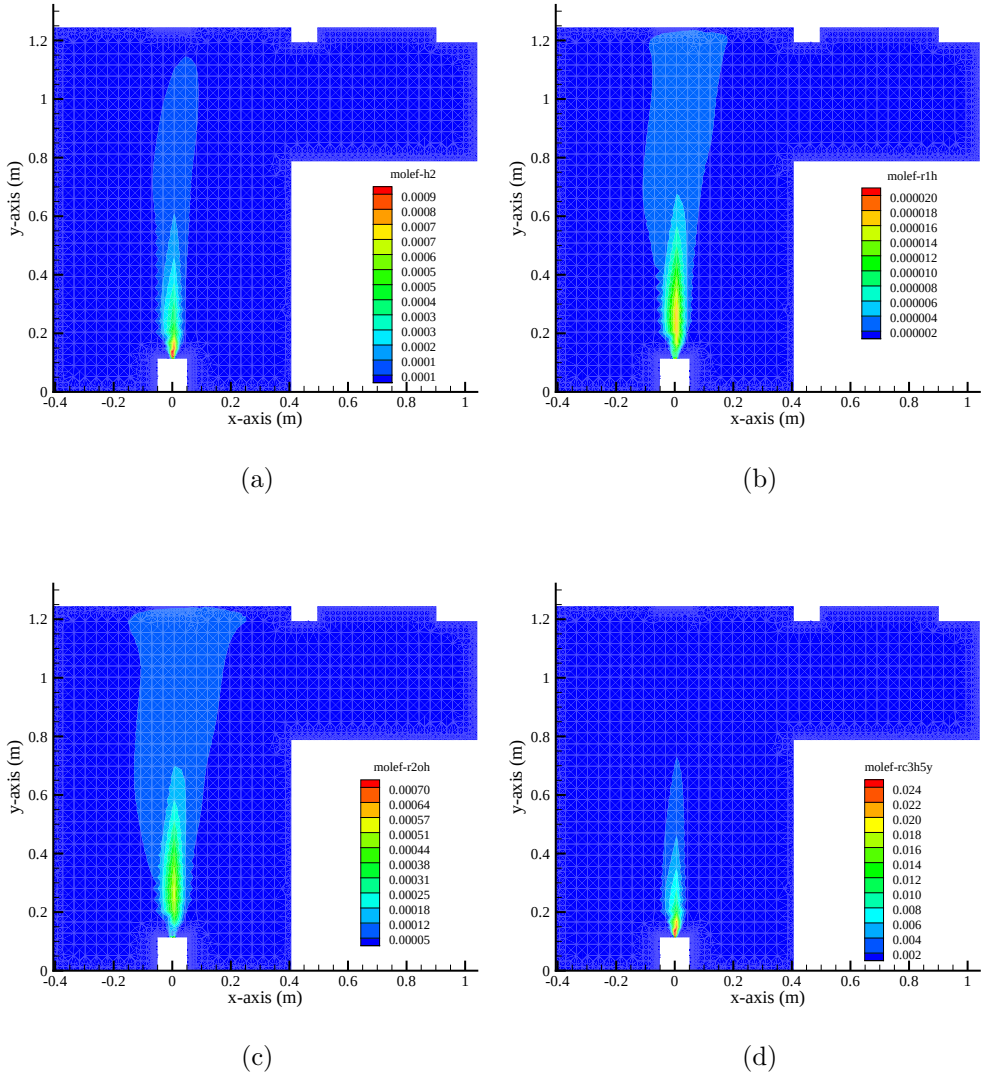


Figure 5.12: Contours for mole fraction of (a) hydrogen at a central (x,y) slice, (b) R1H radical at a central (x,y) slice, (c) R2OH radical at a central (x,y) slice, and (d) RC3H radical at a central (x,y) slice.

didate of biofuels, the closest to conventional diesel. Methyl decanoate $C_{11}H_{22}O_2$ was selected as a suitable candidate that is expected to yield results close to those of dodecane which is considered as equivalent to diesel. The EXGAS software was used to generate an advanced reaction mechanism to model the combustion

of methyl decanoate in the burner (Fig. 3.6). The same parameters (including high temperature option) selected for diesel fuels was considered for biodiesel in the form of methyl decanoate. Of interest to this simulation of course is the study of the effect of oxygen atoms in the structure of biodiesel and how the software EXGAS will react to such fuels and how the developed reaction mechanism succeeds in modelling and producing reasonably accepted results. To answer these questions, a similar approach for analysing the result of diesel and methanol is adopted for biodiesel. To start with, the most important parameter, temperature, is presented first.

### 5.2.1 Temperature Field

The temperature profiles at the exit of the burner (corresponding to the vertical and horizontal lines of Fig. 3.9 and Fig. 3.10) for the biodiesel EGRM predictions are shown in Fig. 5.13(a) and Fig. 5.13(b). As discussed in the beginning of this chapter, biodiesels are expected to yield lower value of energy (by the order of 10-15%) based on the measured calorific value which is documented in many researches and other related works. Based on this fact, one would expect that the temperature (used here as an indicator rather than a measure to energy released) from the combustion would be slightly lower than that of diesel. However, the temperature at the exit of the burner (Fig. 5.13(a) and Fig. 5.13(b)) shows a range of 740–760$K$ compared to 640–665$K$ for diesel simulation using EGRM, which is slightly higher. The lower profiles (corresponding to cross-sectional lines starting at $y = 0.2m$ above the burner bottom base and moving along the vertical axis with $0.05m$ increment) are shown in Fig. 5.13(c), also show a higher range close to the injector $T = 1605K$ compared to $T = 1000$ at the same location for the case of diesel (Fig. 5.1(c)) prediction using EGRM. Probably this is the main reason why high temperature range was witnessed at the exit of the burner in the case of diesel. It is also noticeable that the average temperature for the rest of the interior domain of the burner is of order $800K$ for the biodiesel simulation compared to $650K$ for the modelling of diesel combustion (Fig. 5.13(c)). This is also apparent from the temperature contours for a central (x,y)-plane displayed in Fig. 5.13(d) for the biodiesel computational predictions.

It might seem like an obvious discrepancy in modelling biodiesel at this point. However, one would not jump to this conclusion and much deeper understanding of the reasons that may be behind this phenomenon should be explained and argued. Prediction of higher temperature using EGRM was observed in modelling methanol earlier in Chapter 4, a fact that was stated by the developers of EXGAS even when only the kinetics of combustion were modelled with no turbulent flows having been taken into account. What is unique in this situation, however, is the fact that the same EXGAS used for biodiesel produced higher temperatures than diesel - there is no reduced reaction mechanism used for these two heavy hydrocarbons. There are two main issues the author of this thesis would raise in an attempt to explain the difference in the expected results for modelling biodiesel. The primary reason (with little effect) was that one may attribute this to the unsteady nature of the simulation where hot plumes eventually exit the burner and no matter how long the simulation is run, the steady solution may not be obtained exactly.

The second fundamental issue to be raised here to explain the difference in temperature range observed for biodiesel simulation is the nature of the reaction model developed using the EXGAS software. Although the software includes the class of such biofuels, in this regard, the EXGAS software seems to have deficiencies in dealing with oxygenated fuels. Developing an in-depth knowledge and analysis of the chemistry used in the EXGAS may not be the main target of this thesis, however, the author strongly believes that any further work in this area should focus on studying the chemical reactions used in EXGAS and how the intermediate products are developed under a turbulent flow environment for conventional and oxygenated fuels. Examining the reaction model (Appendix C), it is clear that more reactive intermediate products were produced for biodiesel than diesel. These are mainly influenced by the oxygen atoms and hence may have led to more reactions and heat liberation thus leading to higher temperature range that contradicts the fundamentals of combustion of conventional diesel compared to biodiesel. Therefore, the author of this thesis believes that more fundamental work related to developing adequate reaction mechanisms for oxygenated fuels need further investigation and that the EXGAS software needs more scrutiny when used for developing reaction mechanisms for turbulent combustion

in general and for oxygenated fuels in particular. Later in the thesis, experimental investigations for biodiesel indicate the existence of water, the percentage of which increases if the biodiesel is stored for longer period. Water may be one of the reasons leading to lower temperature (not energy content) when biodiesel replaces diesel. This will open a window to examine water content as a result from modelling the combustion of biodiesel and see whether a consolation of the results will be found there.

### 5.2.2 Turbulence Parameters

To examine the flow field for the simulation of biodiesel, Turbulence Reynolds number and turbulence intensity are presented in this section. Shown in Fig. 5.14(b) and Fig. 5.14(a) are respectively the Turbulence Reynolds number profiles for the vertical lines (Fig. 3.9) and the horizontal lines (Fig. 3.10) at the exit of the burner. In comparison with the simulation of diesel (Fig. 5.2(a) and Fig. 5.2(b)), it is clear that the range of this parameter is the same. Looking at the cross-sectional profiles of the turbulence Reynolds number close to the injector (starting at $y = 0.2m$ and moving $0.05m$ increment), are shown in Fig. 5.14(c). The maximum value reported at $y = 0.2m$ is of order 4500 compared to 5500 for the simulation of diesel. The difference is a result of slightly lower velocity in the case of biodiesel. Despite the small difference in inlet air velocity, the simulation of biodiesel produced more water vapour than diesel, which has slightly higher air velocity. This is an indication that biodiesel produces more water vapour both in computational modelling as well as in real experimental work as will be discussed later. Fig. 5.14(d) displays the contours for biodiesel simulation for a central (x,y)-plane. Both the low profiles (Fig. 5.14(c)) and the contours of Fig. 5.14(d) strongly support the nature of the fully turbulent flow, showing a symmetrical distribution around the center.

Turbulence intensity at the exit of the burner is shown for both the vertical (Fig. 3.9) and horizontal (Fig. 3.10) profiles in Fig. 5.15(a) and Fig. 5.15(b). Profile of turbulence intensity for cross-sectional profiles within the flame region (starting at $y = 0.2m$ progressing with an increment of $0.05m$ along the vertical axis) is shown in Fig. 5.15(c) while the contours for a central (x,y)-slice are

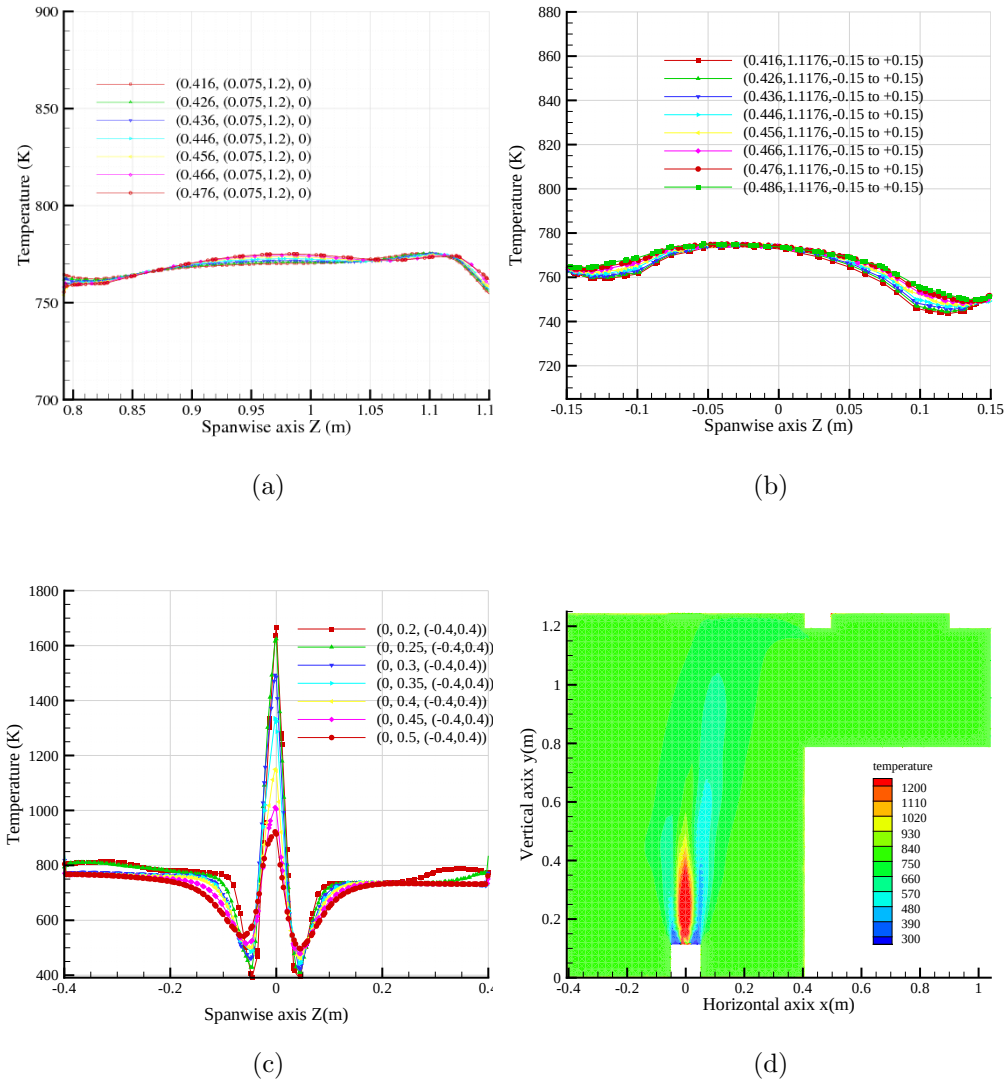


Figure 5.13: Biodiesel CFD simulation using EGRM: Temperature profiles corresponding to the (a) vertical lines shown in Fig. 3.9, (b) horizontal lines shown in Fig. 3.10, (c) cross-sectional profiles starting at $0.2m$ from the burner bottom wall at $0.05m$ increment along the vertical axis, and (d) contours for a central slice.

displayed in Fig. 5.15(d). The figures, especially the profiles both at the exit and within the flame region indicate a turbulent flow (turbulence intensity as high as 0.4) which is confirmed by the contours (Fig. 5.15(d)) which reflect quite

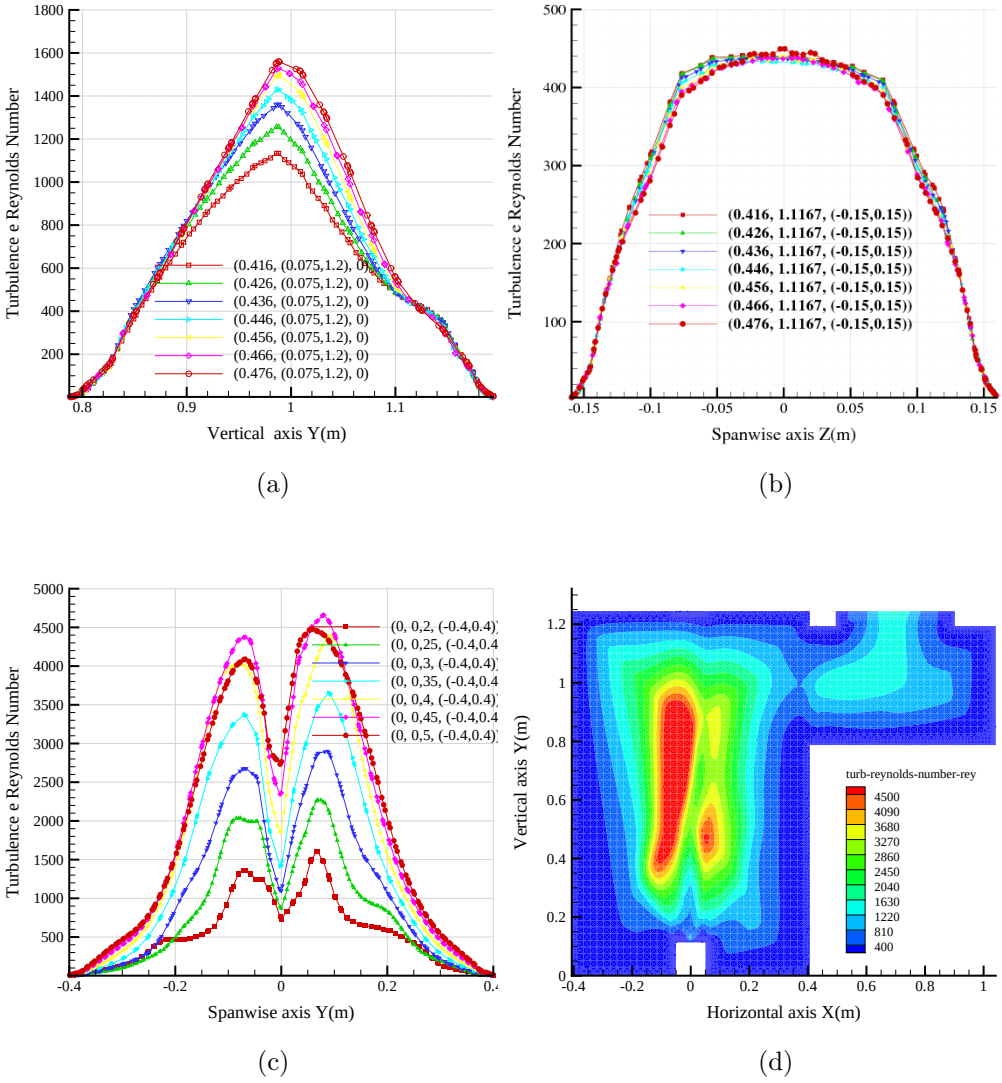


Figure 5.14: Biodiesel CFD simulation using EGRM: Turbulence e Reynolds number profiles corresponding to the (a) vertical lines shown in Fig. 3.9, (b) horizontal lines shown in Fig. 3.10, (c) cross-sectional profiles starting at $0.2m$ from the burner bottom wall at $0.05m$ increment along the vertical axis, and (d) contours for a central slice.

unsteady flow according to the distribution of turbulence intensity.

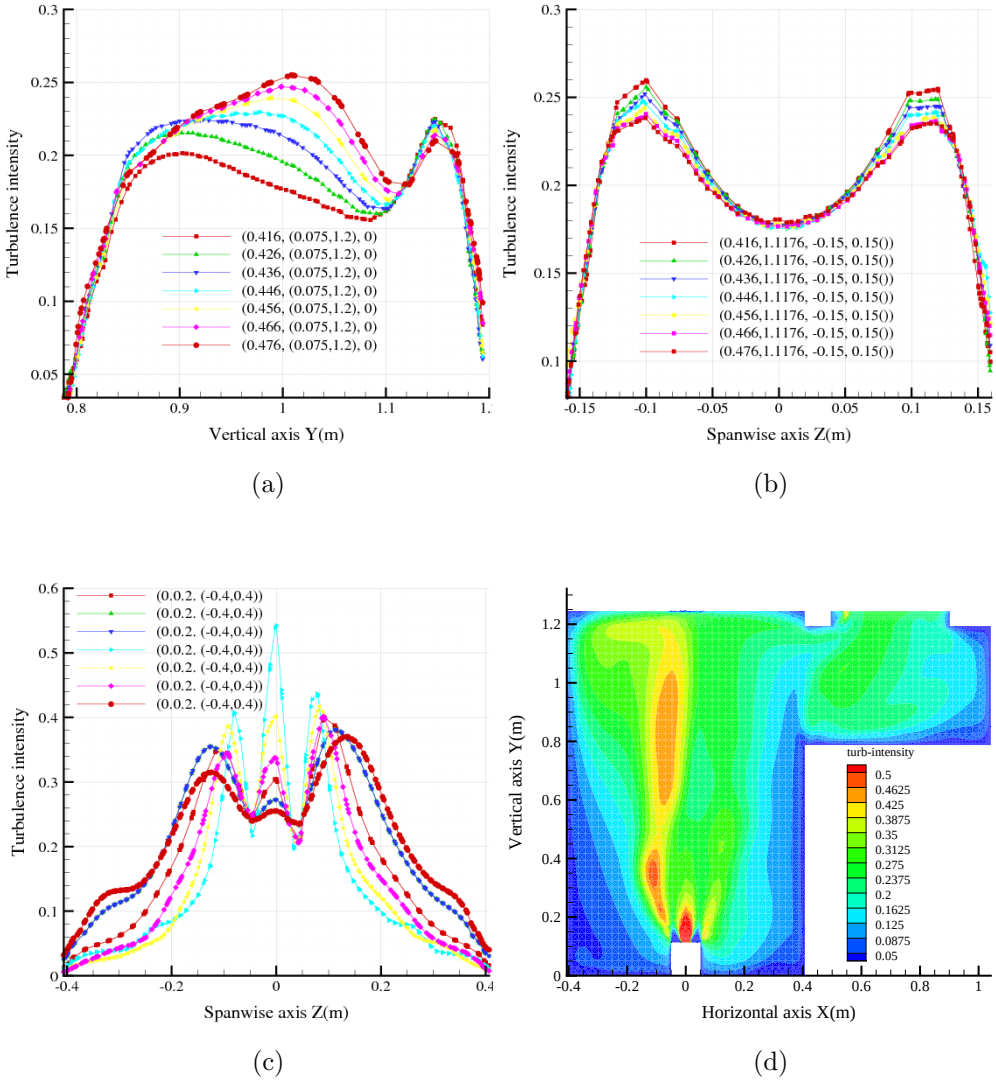


Figure 5.15: Biodiesel CFD simulation using EGRM: Turbulence intensity profiles corresponding to the (a) vertical lines in Fig. 3.9, (b) horizontal lines shown in Fig. 3.10, (c) cross-sectional profiles starting at $0.2m$ from the burner bottom wall at $0.05m$ increment along the vertical axis, and (d) contours for a central slice.

### 5.2.3 Emissions from Biodiesel Combustion Modelling

Having examined the temperature and flow field in Sections 5.2.1 and 5.2.2, it is worth to look at the emissions from modelling the biodiesel. The main component investigated for methanol and diesel would be the focus of this section with the intention to draw some comparison between these fuels.

#### 5.2.3.1 Carbon Dioxide ($CO_2$)

Carbon dioxide ($CO_2$) at the horizontal and vertical locations at the exit (Fig. 3.10 and Fig. 3.9) are respectively shown in Fig. 5.17(b) and Fig. 5.17(a). The approximate locations corresponding to Widmann and Presser [1] measurement stations for $CO_2$ are extracted and plotted against the values of other fuels (discussed previously) in Fig. 5.16. From these three figures, it is apparent that the EGRM model produced an elevated level for $CO_2$ for biodiesel. In terms of figures, and considering the maximum and minimum values for $CO_2$, for methanol (using SDRM), the predicted mole fraction for $CO_2$ values at the exit ranges between 0.0096–0.0149 with 0.045 near the injector. This is compared to 0.016–0.0185 at the exit locations for the diesel simulation (using EGRM) with 0.045 near the injector. For biodiesel, the mole faction of $CO_2$ at the exit locations ranges between 0.023–0.025 with a value slightly above 0.1 near the injector. These are slightly higher values compared to the other two fuels. However, these results are in line with the experimental results for a diesel engine to be discussed later and agree with the findings of many other studies cited in the literature (Table 7.2 in Chapter 7) although the combustion infrastructure (CIE) may differ from the current environment under consideration. Biodiesel indeed produces higher rates of both soot and $CO_2$, most likely due to two factors. The first is associated with the oxygenated nature of biodiesel which influences the combustion process of biodiesel favouring the formation of $CO_2$. However, this property may also impact the way EXGAS generates the necessary reaction mechanism for such classes of fuels, which means that close scrutiny to the reaction mechanism is necessary to identify sources, if any, responsible for it. The second reason is probably associated with the density and viscosity of biodiesel and this is mainly related to the experimental part. Overall, the prediction of EGRM for $CO_2$ in

the simulation of biodiesel considered here is at acceptable levels and agrees with the literature. The contours of this variables ($CO_2$) for a central (x,y)-plane are shown in Fig. 5.17(d) which shows the high concentration of $CO_2$ within the flame region.

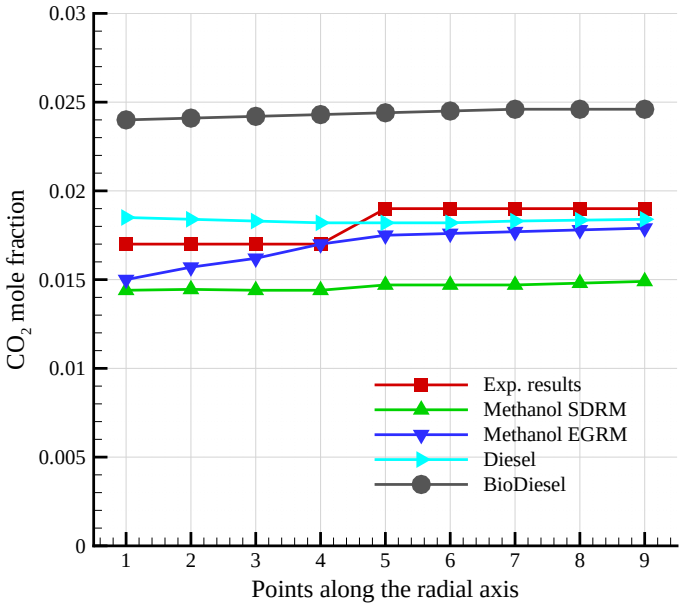


Figure 5.16: $CO_2$ comparison between the experimental, SDRM and EGRAM simulations for methanol, diesel and biodiesel

#### 5.2.3.2 Water Vapour ($H_2O$)

Shown in Fig. 5.18(a) and Fig. 5.18(b) are water vapour profiles for the biodiesel simulation at the exit of the burner (corresponding to the vertical and horizontal lines of Fig. 3.9 and Fig. 3.10). In comparison to diesel modelling case (Fig. 5.7(a) and Fig. 5.7(b)), it is apparent that biodiesel water vapour predictions are slightly higher than those for diesel (mole fraction is of order 0.025 for biodiesel and 0.02 for diesel). Similarly, closer to the injector and above, cross-sectional profiles for biodiesel (Fig. 5.18(c) shows that it produces more water vapour as the maximum mole fraction at $y = 0.2m$ is of order 0.065 compared to 0.0525 for the diesel

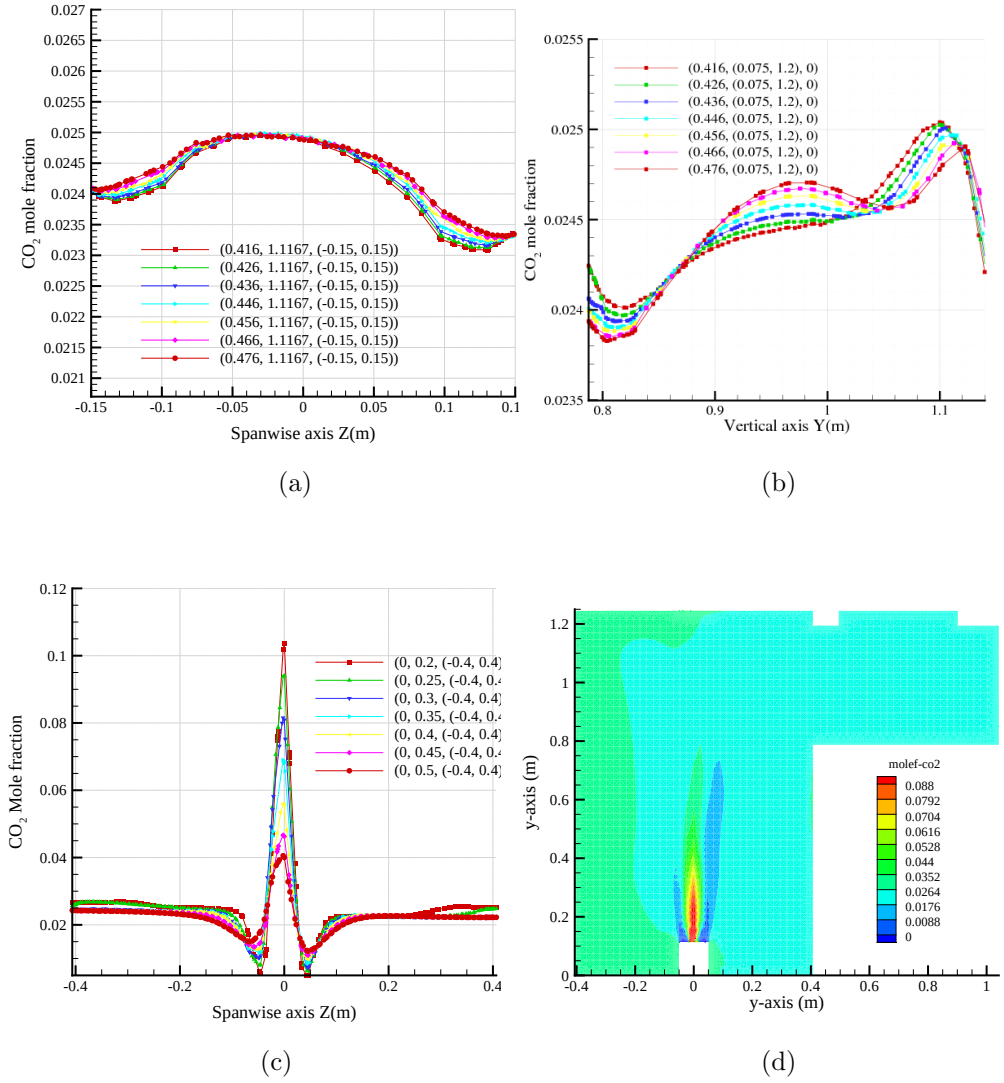


Figure 5.17: Biodiesel CFD simulation using EGRM: $CO_2$ profiles corresponding to the (a) vertical lines of Fig. 3.9, (b) horizontal lines shown in Fig. 3.10, (c) cross-sectional profiles starting at $0.2m$ from the burner bottom wall at $0.05m$ increment along the vertical axis, and (d) contours for a central slice.

simulation (Fig. 5.7(c)). The water vapour contours for a central (x,y)-plane for the biodiesel simulation shown in Fig. 5.18(d) shows water concentration within the flame region, with the mole fraction of water vapour decreasing with increase in the vertical distance.

It is evident from the results that the predicted water vapour values for biodiesel are higher than those for diesel. This is in line with the fundamental theory and the composition of the two hydrocarbons discussed here. However, whether at high temperature flows, water vapour is supposed to play a cooling effect or not, is not clear. The cooling effect of any water content (if any) in modelling biodiesel was not considered, however, that cannot be avoided in the experiment as will be discussed later in this thesis. This leaves the reaction model developed using EXGAS as the main component to observe in any further investigation. It also explains the increase in water content is mainly due to the existence of oxygen atoms in biodiesel. In this regard, the EXGAS-based developed reaction model has led to reasonable results, however, for the temperature range, the author strongly recommends more investigation and simulation under a range of boundary conditions in order to figure out what led to predicting higher temperatures for biodiesel compared to diesel.

#### 5.2.3.3 Nitrogen Oxides ($NO$ and $NO_x$)

Nitrogen oxide profile at the exit vertical and horizontal lines (Fig. 3.9 and Fig. 3.10) of the burners from the simulation of biodiesel are shown respectively in Fig. 5.19(a) and Fig. 5.19(b). The profiles show that the concentration (mole fraction) of $NO$ at the exit is of order 0.001. In comparison to the diesel simulation, the reported value is of 0.0015 to 0.00325. It is apparent that biodiesel has produced much higher rates of $NO$ compared to diesel and, as a matter of fact, much more than that of methanol (recorded as 0.0001 to 0.00014). Two points need to be noted here. The first is that, the range of $NO$ is very small and probably, predicting it accurately depends on many factors including the turbulence model used. The outcome here is in line with what is expected considering the many studies cited in the literature. With reference to Table 2.2, much of the literature indicates that burning biofuels in a CIE environment produces higher $NO_x$. Within the context of the combustion in a CIE, it is well established that $NO_x$ is promoted as a result of the high temperature and the lean nature of the mixture. However, what is reflected here seems to be associated with the chemical structure of biodiesel and the reaction mechanism developed for such a class

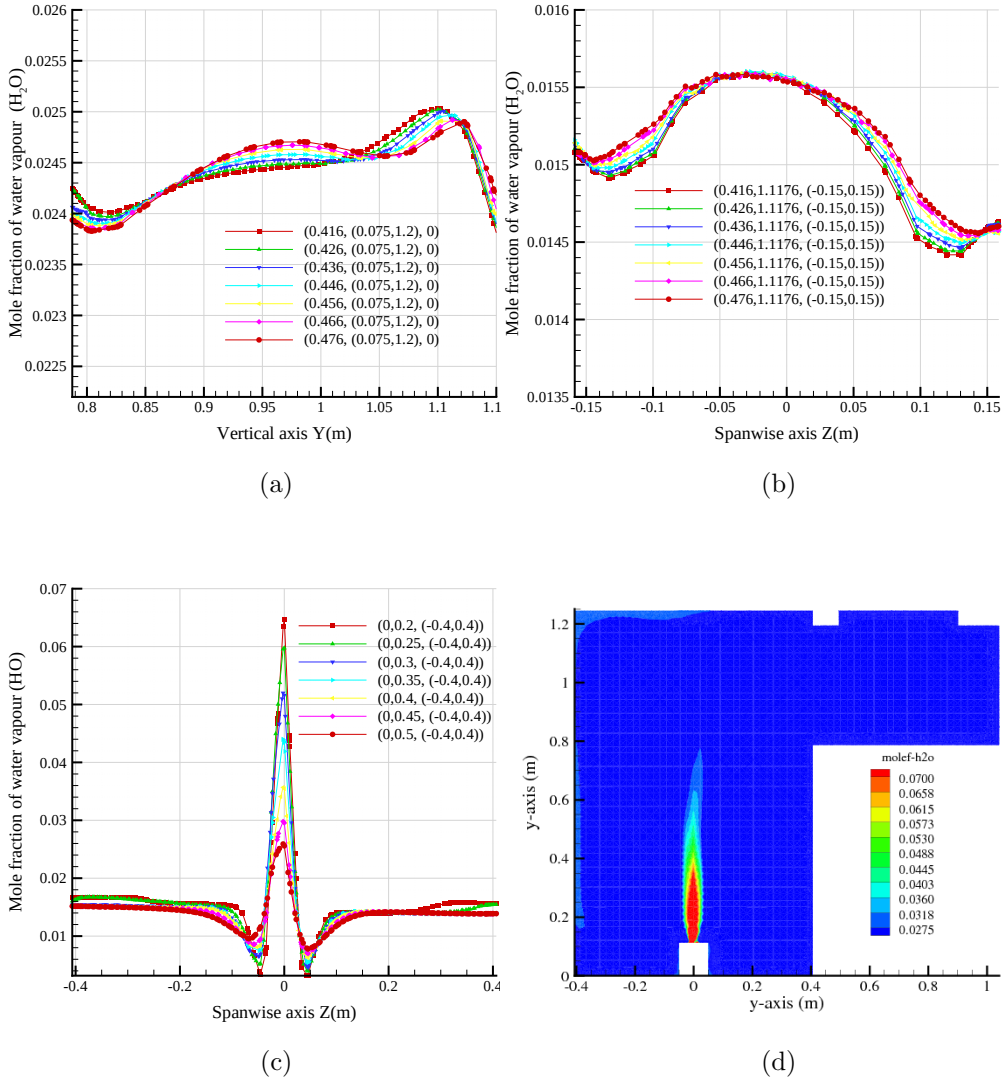


Figure 5.18: Biodiesel CFD simulation using EGRM: Water vapour ($H_2O$) profiles corresponding to the (a) vertical lines shown in Fig. 3.9, (b) horizontal lines shown in Fig. 3.10, (c) cross-sectional profiles starting at $y = 0.2m$ from the burner bottom wall at $0.05m$ increment along the vertical axis, and (d) contours for a central slice.

of fuels. It seems that these two factors play the role of a catalyst in encouraging higher formation of $NO_x$. A detailed investigation of this particular point should be the subject of future research.

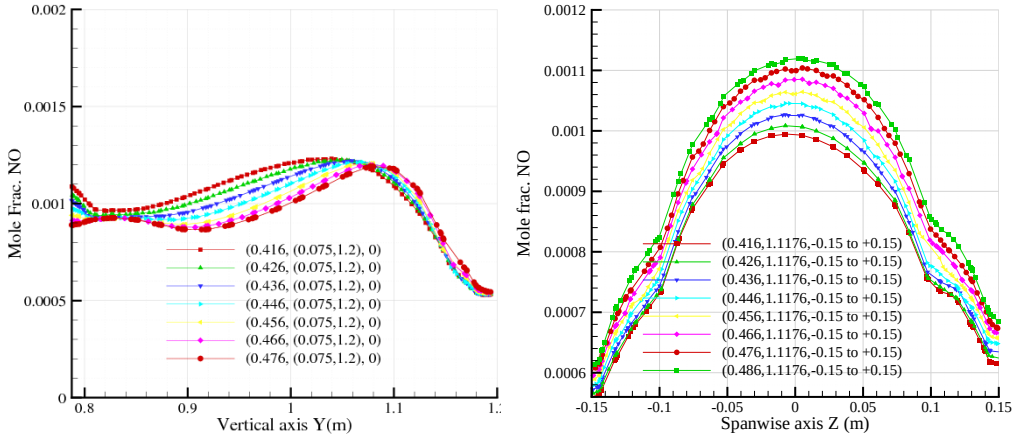


(a) (b)

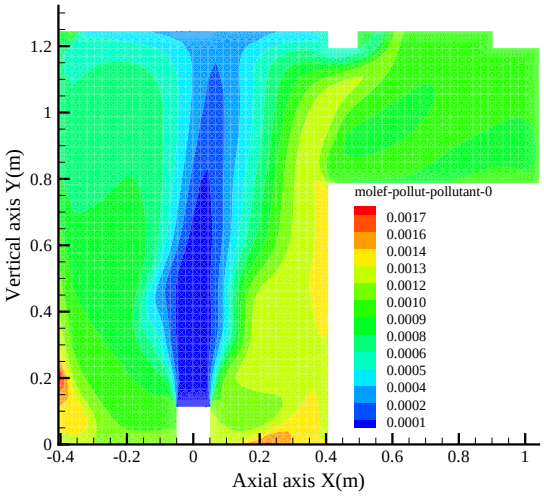


(c)

Figure 5.19: Biodiesel CFD simulation using EGRM-biodiesel: Nitrogen oxide ($NO$) mole fraction profiles corresponding to the (a) vertical lines shown in Fig. 3.9, (b) horizontal lines shown in Fig. 3.10, and (c) contours for a central (x,y)-plane.

#### 5.2.3.4 Concentration of Soot

The concentration of soot has not been discussed before for methanol and diesel simulations because the predicted values are of order zero. The predicted values for biodiesel simulation at the exit of the burner are shown in Fig. 5.20(a) and Fig. 5.20(b) (corresponding to the vertical lines of Fig. 3.9 and Fig. 3.10) and are also negligible. However, the contours of the central (x,y)-slice shown in Fig. 5.20(c) does show some significant levels of soot at the edge of the flame distinction and just above the flame region. This was not observed for the prediction for the other fuels discussed in previous chapters and indicates that combustion of biodiesel has the affinity of producing higher rates of soot compared to other fuels.

#### 5.2.3.5 Fuel $C_{11}H_{22}O_2$ and PDF Variables

This section will examine the PDF variables mean mixture fraction, mixture fraction variance and scalar dissipation together with the traces of the fuel (biodiesel) within the computational domain. From previous discussions, it is apparent that these variables are linked and hence discussing them as a unit is thought to shed light and produce related facts on the spray combustion of biodiesel.

Shown in Fig. 5.21(a) and Fig. 5.21(b) are respectively the mole fraction profiles for the fuel (biodiesel) at the exit of the burner (the vertical and horizontal lines respectively shown in Fig. 3.9 and Fig. 3.10) corresponding to the measuring locations in the simulations of the Widmann and Presser [1]. It is clear from these two figures that the unburned amount of the fuels is of order $10^{-7}$ which is negligible. Similar values were observed for the case of diesel, indicating that the fuels are burnt well before the exit. Close to the injector starting from $y = 0.2m$ the profiles for cross-sectional lines along the vertical axis (with increment of order $0.05m$) are shown in Fig. 5.21(c) with the contours for a central (x,y)-plane displayed in Fig. 5.21(d). The maximum mole fraction of biodiesel at $y = 0.2m$ is of order 0.015 reducing to an order of 0.002 at higher heights ($y = 0.4m$, $y = 0.45m$ and $y = 0.5m$). This is compared to a value of 0.002 at $y = 0.2m$ for the simulation of diesel (Fig. 5.8(b)) and 0.004 at $y = 0.4m$, $y = 0.45m$, and $y = 0.5m$. It is apparent that the rate of burning of biodiesel is slower than that

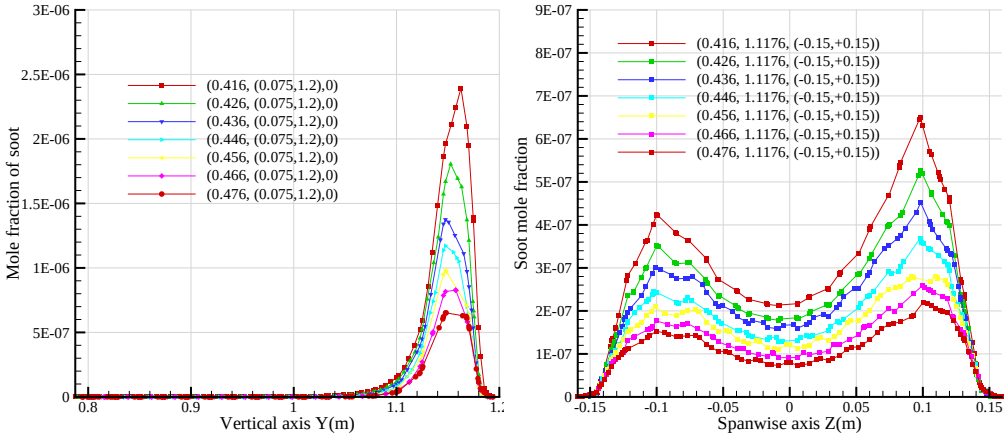


(a) (b)

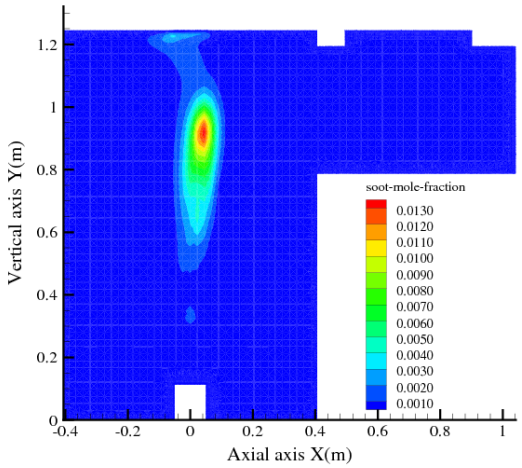


(c)

Figure 5.20: Biodiesel CFD simulation using EGRM-biodiesel: Soot mole fraction profiles corresponding to the (a) vertical lines shown in Fig. 3.9, (b) horizontal lines shown in Fig. 3.10, and (c) contours for a central (x,y)-plane.

of diesel. It gets more evident when examining the contours for the central slice Fig. 5.21(d). For the same range of resolution of the contours used for diesel (Fig. 5.8(c)), it is clear that unburned biodiesel can be detected up to a height of $0.85m$ with significant mole fraction compared to diesel simulation. This means

that the burning process continues up to this height leading to a longer flame and hence the elevated temperatures are observed in the combustion of biodiesel compared to diesel. It is an observation from the developers of EXGAS that the reaction models indeed lead to a better flame prediction, however, associated with this is the higher range of temperature which might be against the theory known so far. Hence, the author believes that more fundamental work is needed to understand the factors associated with developing advanced reaction mechanisms for oxygenated fuels. More work is needed in areas related to the structure of the flame under different environments and how the structure of the flame affects other parameters such as temperature and emissions is necessary to elucidate the physics of combustion of such fuels.

The above discussion shows that droplets of biodiesel have the chance to travel much deeper along the vertical axis and continue burning and releasing heat at those heights with slower burning rates predicted. This would explain why the simulation of biodiesel revealed an elevated temperature range compared to diesel. This behaviour can be questioned. Again, the author has no reason but to doubt the reaction mechanism developed using the EXGAS software which influences the combustion process of the fuel. It is apparent that the higher than diesel temperature observed in the case of biodiesel combustion modelling is mainly due to the slower combustion process in the case of biodiesel despite the same boundary conditions used in the two simulations. Therefore, much more is required to study the reaction mechanism of biofuels and specifically focus on the effect of oxygen atoms present in such fuels. As the heat released from burning any fuel is partly a function of the bonds that connect Hydrogen (and oxygen in the case of biodiesel) to carbon atoms, it is apparent that the accurate mechanism to produce good results for biofuels should take this important fact into consideration.

The slower rate of burning of biodiesel was supported by the PDF parameters, the mean mixture fraction and the scalar dissipation. Shown in Fig. 5.22(b) and Fig. 5.22(a) are the mean mixture fractions obtained from the EGRM simulation of biodiesel at the exit of the burner. These are the locations that cover the experimental data measuring stations of Widmann and Presser [1] and correspond to the vertical and horizontal lines appearing in Fig. 3.9 and Fig. 3.10. It is apparent

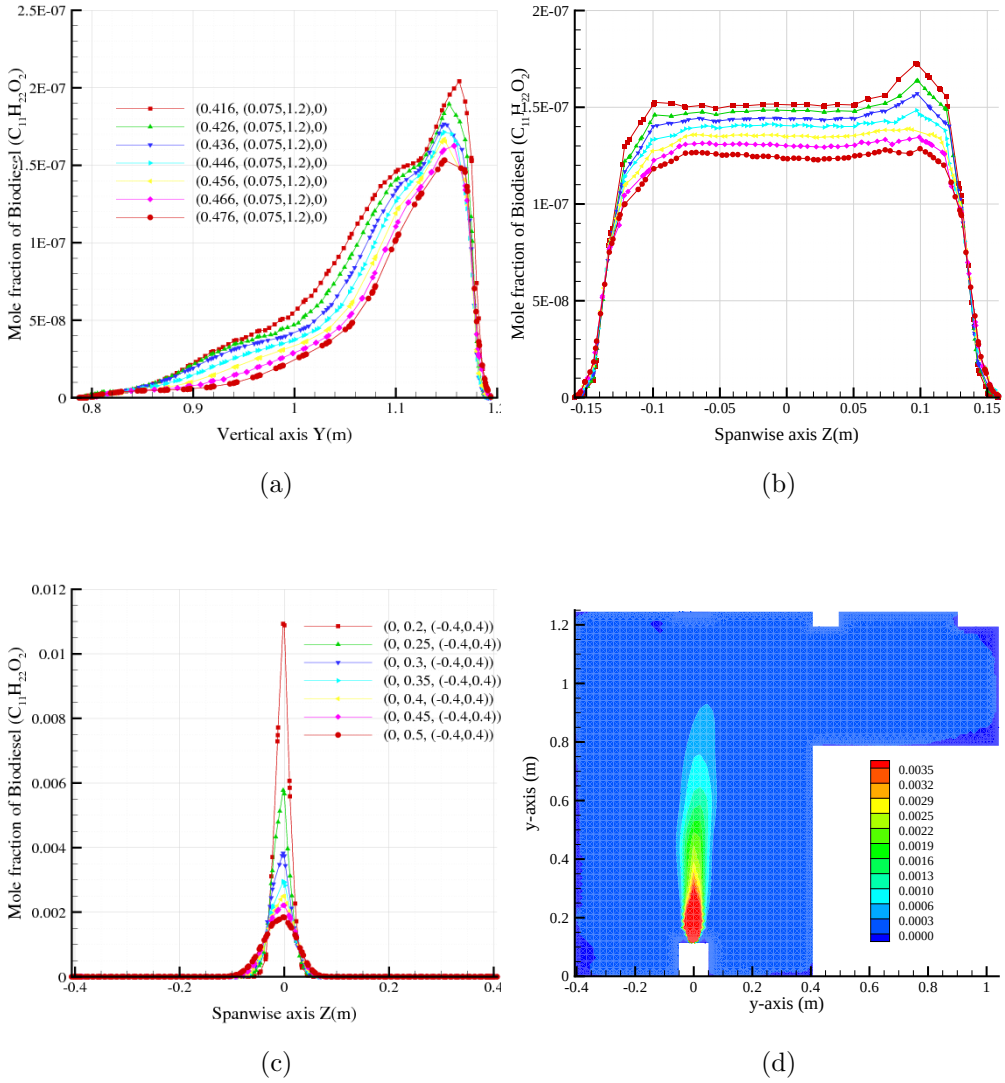


Figure 5.21: Biodiesel CFD simulation using EGRM-biodiesel: Mole fraction of biodiesel ($C_{11}H_{22}O_2$ profiles corresponding to the (a) vertical lines shown in Fig. 3.9, (b) horizontal lines shown in Fig. 3.10, (c) cross-sectional profiles starting at $0.2m$ from the burner bottom wall at $0.05m$ increment along the vertical axis., (d) contours for a central slice.

that at the exit of the burner, the mean mixture fraction for the EGRM simulation of biodiesel ranges between 0.014–0.0146. This is compared to a mean mixture fraction of order 0.008–0.009 at the same location from the EGRM simulation of diesel. Similarly the profiles of the mean mixture fraction for cross-sectional lines (starting to $y = 0.2m$) along the vertical axis shown in Fig. 5.22(c) together with the contours for the same variable for a central (x,y)-plane support the fact that the mixture fraction for the EGRM simulation for biodiesel is much higher than that for diesel. The maximum detected mean mixture fraction (at $y = 0.2m$) is of order 0.1375 compared to a value of 0.04 as appears in Fig. 5.9(c), whilst the minimum detected mean mixture fraction (at $y = 0.5m$) is of order 0.0275 compared to a value of 0.014 as appears in Fig. 5.9(c). It is apparent that within the flame region, the burning of biodiesel is much slower than diesel with the mixture fraction almost twice that of diesel within the height $0.5m$ above the injection point. All these results show that the burning of biodiesel is slower than that of diesel which allows more chances for the injected fuel to travel to upper heights above the injection point leading to a longer flame and higher rates of heat. This adds to the explanation why the predicted temperature is higher in the case of biodiesel than diesel. However, it is the point of view of the author that much deeper scrutiny, using both advanced and simple turbulence (LES/DNS) as well as simple and comprehensive reaction mechanisms, is necessary to confirm and possibly to adjust the outcome with concrete experimental data.

#### 5.2.3.6 Mixture Fraction Variance and Dissipation Rate

The mixture fraction variance at the burner exit (corresponding to the profiles of the vertical and horizontal lines of Fig. 3.10 and Fig. 3.9) are shown in Fig. 5.24(a) and Fig. 5.24(b). The dissipation rate at similar locations appear in Fig. 5.23(b) and Fig. 5.23(a). Both the parameters at the exit show small values (of order $10^{-5}$ for the mixture fraction variance and order $1-4\times10^{-5}$). This is expected as these locations are far from the flame region. What is noticeable between these two parameters (observed for almost all fuels discussed previously) was that the dissipation rate is higher than the mixture fraction variance, an indication to the fact that the simulation is highly dissipative. This could be associated with the

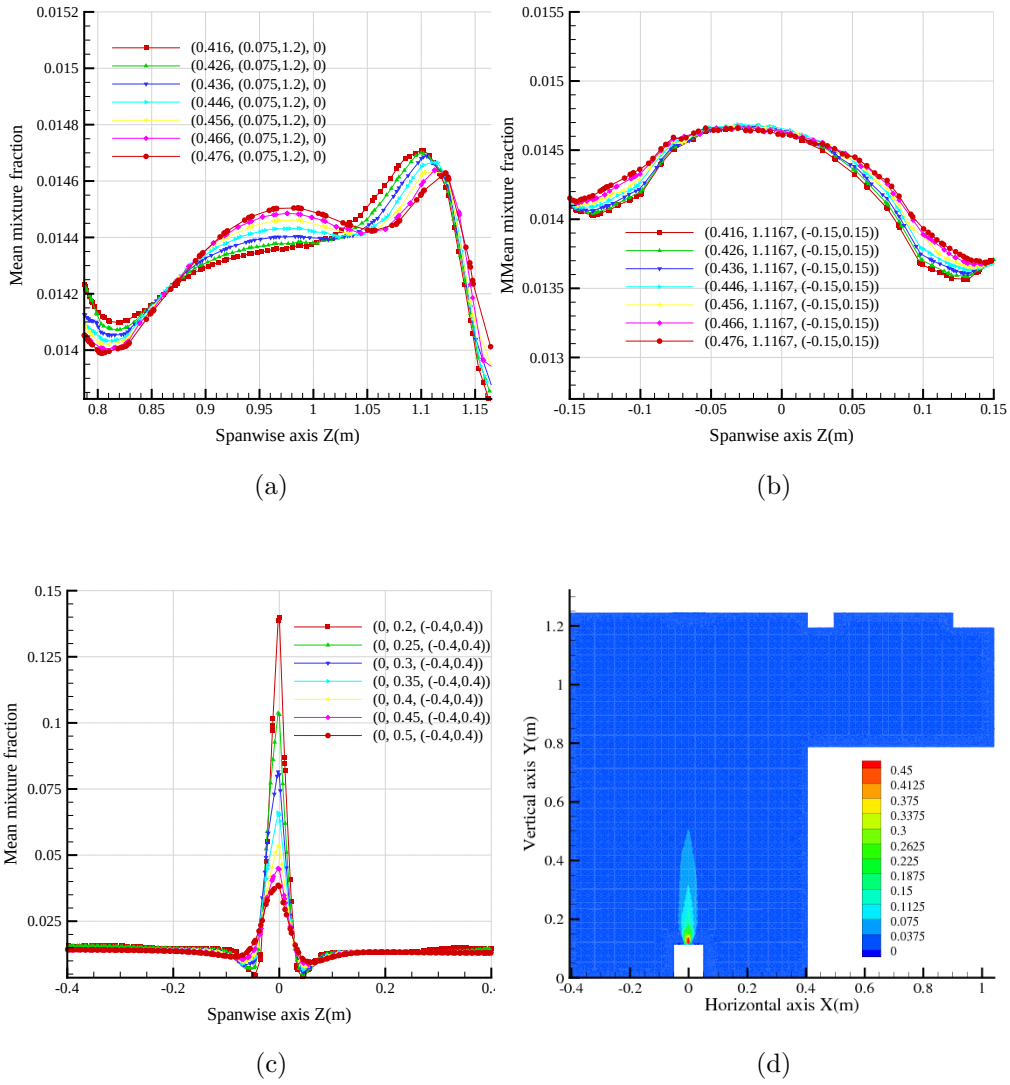


Figure 5.22: Biodiesel CFD simulation using EGRM-biodiesel: Mean mixture fraction profiles corresponding to the (a) vertical lines shown in Fig. 3.9, (b) horizontal lines shown in Fig. 3.10, (c) cross-sectional profiles starting at $0.2m$ from the burner bottom wall of $0.05m$ increment along the vertical axis, and (d) contours for a central slice.

turbulence model used and probably better models are necessary to adjust in such a situation.

The mixture fraction variance distribution for cross-sectional profiles close to

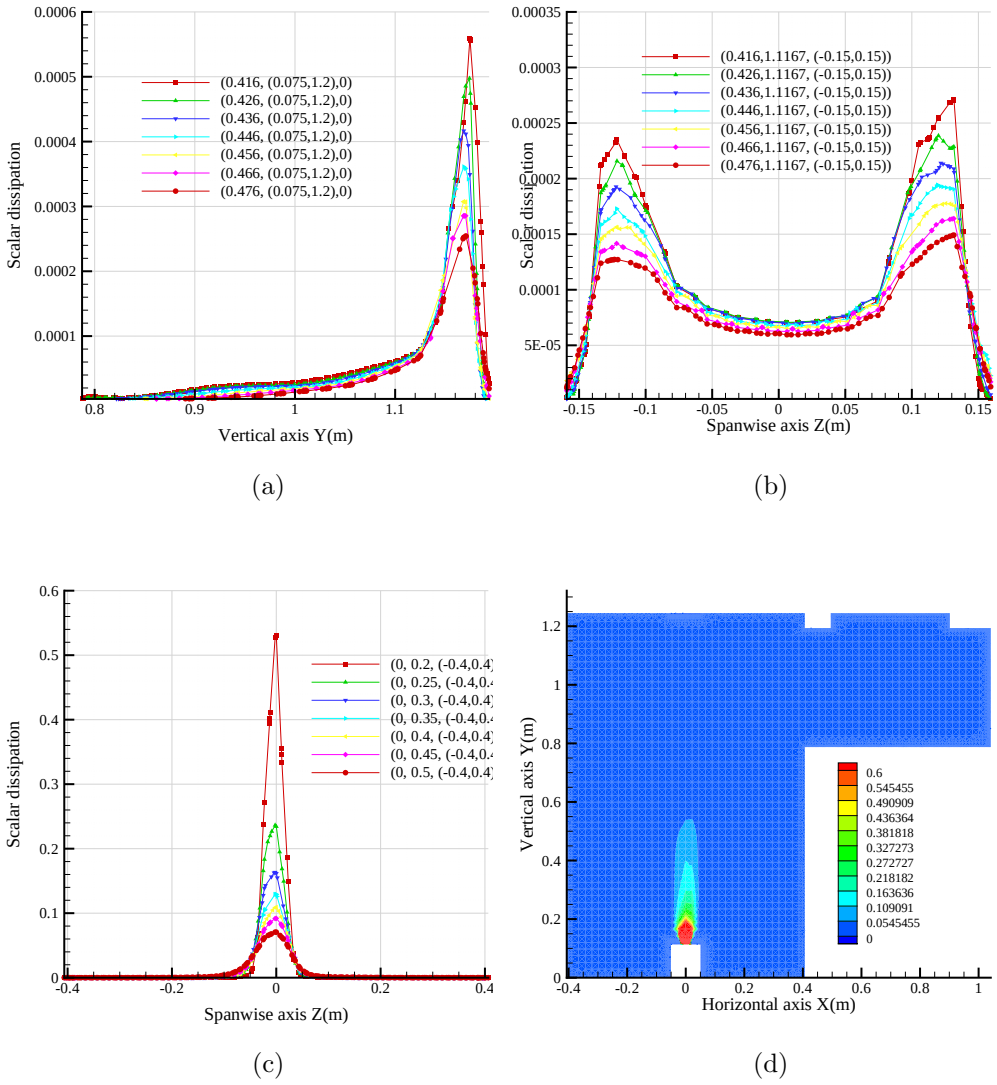


Figure 5.23: Biodiesel CFD simulation using EGRM-biodiesel: Dissipation rate corresponding to the (a) vertical lines shown in Fig. 3.9, (b) horizontal lines shown in Fig. 3.10, (c) cross-sectional profiles starting at $0.2m$ from the burner bottom wall of $0.05m$ increment along the vertical axis, and (d) contours for a central slice.

the injector and above is shown in Fig. 5.24(c), with the contours for a central (x,y)-slice shown in Fig. 5.24(d). Corresponding figures showing the dissipation rate at the same locations are shown in Fig. 5.23(c) and Fig. 5.23(d) respectively.

It is apparent that both of these parameters have considerable values within the flame region, although the variance is very small (of order 0.00575 at $y = 0.2m$). This is an indication to the laminar nature of the flame as this parameter (mixture fraction variance) is an indicator of the level of fluctuation and hence mixing within the flow field and the injected fuel. The dissipation rate, however, exhibits high values (of order 0.525 at $y = 0.2m$), an indication to a high dissipation rate of the method used in this simulation. To reiterate, it is essential to use a more accurate turbulence model to solve this problem.

## 5.3 Summary

Chapter 4 has provided a solid ground for setting up a CFD case using advanced reaction mechanism developed with the aid of EXGAS software. The results well agree with the experimental data in almost all available data. Based on that, Chapter 5 addressed modelling of larger hydrocarbon representing both conventional (decane ($C_{10}H_{22}$)) and biofuels (methyl decanoate ($C_{11}H_{22}O_2$)). Widman and Presser [1] experimental work was based on methanol ($CH_3OH$), a low hydrocarbon (alcohol). Setting up a CFD model for large hydrocarbons such as the two considered in this thesis did not prove easy. Using the same input air used for methanol as in previous section did not lead to combustion and more air was needed to adjust the stoichiometric conditions.

The results obtained are not expected to agree exactly with the experimental data of Widman and Presser [1] as the hydrocarbon dealt with here are from different microstructure compared to methanol. However, and in order to build more confidence on the obtained results, some of the CFD predictions for decane ($C_{10}H_{22}$) and methyl decanoate ($C_{11}H_{22}O_2$) were compared with the Methanol experimental and CFD prediction previously discussed (whenever data is available). The CFD results for modelling decane ($C_{10}H_{22}$) and methyl decanoate ($C_{11}H_{22}O_2$) have shown good acceptable value for temperature field, $CO_2$ at the burner exit. With reference to what is cited in the literature, the obtained CFD prediction for the two large hydrocarbons is inline with the findings. For the oxygenated fuel, methyl decanoate ($C_{11}H_{22}O_2$)), some of the obtained results indicate that the comprehensive reaction mechanism may need more scrutiny and

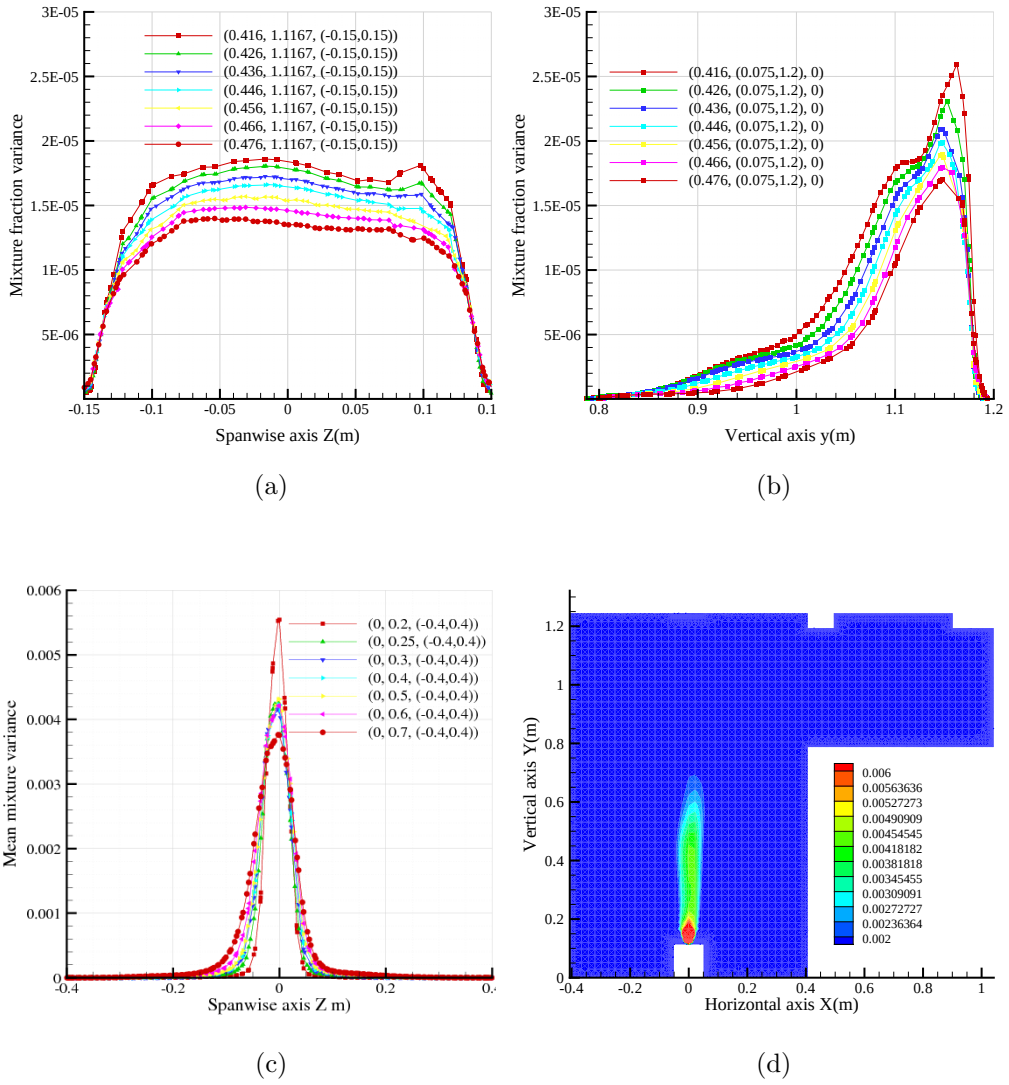


Figure 5.24: Biodiesel CFD simulation using EGRM-biodiesel: Mean mixture fraction variance profiles corresponding to the (a) vertical lines shown in Fig. 3.9, (b) horizontal lines shown in Fig. 3.10, (c) cross-sectional profiles starting at $0.2m$ from the burner bottom wall at $0.05m$ increment along the vertical axis, and (d) contours for a central slice.

development. Most likely that the existence of oxygen atoms has its influence on the mechanism generated and more investigation is recommended in this matter.

Within the burner interior, Widman and Presser [1] did not present any exper-

imental data. As mentioned previously, the only work that attempted to model was that of Collazo et al [65] and they did not present any relevant data which can help in presenting the data presented in this chapter. However, referring to the literature, the pattern observed in the results that have not been compared with the available experimental, especially the work of Sadasivuni [120] and other, strongly indicate that what was observed is in line with the literature and reasonably accepted. As the work has not be done before, this opens the door for more related simulation to use the current results and develop the subject further which can be put for recommendation for future work.

# Chapter 6

# Study of the Effect of Radiative Heat Transfer on the Outcome of the Combustion

The previous computational studies do not include the effect of radiation. Heat transfer by radiation is an important parameter in combustion and its effect should be included to provide a complete scenario of the combustion process. Having said this, the results without radiative heat transfer that have been modelled so far are quite representative as the discussion in the sections below reveals that radiation effect produced minimum and marginal differences on the overall results. One reason behind its exclusion in the previous and the later simulations is that including the $P-1$ model did not perform as expected. In this chapter, a simulation using SDRM with radiation modelled by the single-step model (discussed in Section 3.5) will be discussed to shed light on the effect of radiative heat transfer in such computational work which includes a detailed reaction mechanism. The same burner geometry of Widmann and Presser's [1] experimental benchmark is adopted to study the effect of including radiative heat transfer. The only difference between this CFD case study and the simulations discussed in Chapter 4 is the inclusion of the $P-1$ model that represents the radiative heat transfer. Thus, the $P-1$ radiation model (covered in Section 3.5) is used to model the effect of radiation and SDRM is used to model the spray combustion of

methanol ($CH_3OH$). The section below discusses and sheds light on the effect of radiation on the main parameters that represent the outcome of combustion and compare the results with the SDRM simulation without radiative heat transfer discussed in Chapter 4.

## 6.1 Temperature Field

The temperature field, one of the most important parameters to draw comparison against, has been examined in the radiation simulations at the same location as that of the previous ones. Shown in Fig. 6.1(a) and Fig. 6.1(b) are the temperature profiles for the vertical and horizontal lines (shown in Fig. 3.9 and Fig. 3.10) at the exit of the burner where Widmann and Presser [1] obtained their experimental measurements. The profile of temperature for cross-sectional lines starting at $y = 0.2m$ with an increment of $0.05m$ along the vertical axis is shown in Fig. 6.1(c) while Fig. 6.1(d) displays the temperature contours for a central (x,y)-plane. Fig.6.1(b) and Fig. 6.1(a) clearly indicate that the predicted temperature at the exit of the burner is of order 640–760$K$. In comparison with the SDRM simulation (without modelling the radiation (Fig. 4.3(b) and Fig. 4.3(a))), the temperature prediction at the same location is of order 500–512$K$. In the judgement of the author of this thesis, the $P-1$ radiation model over-estimated the prediction of temperature although the results are reasonably acceptable. The inclusion of radiation will definitely lead to an increment of temperature. However, with this significant difference, it is difficult to confirm as there is no guide and credible relevant benchmarks to refer to. It is worth including more advanced radiation models as well as the $P-1$ is the most crude radiation model that is implemented in Fluent. Rosseland Radiation Model, Discrete Transfer Radiation Model, Discrete Ordinates Radiation Model and Surface-to-Surface Radiation Model are all available to be examined. However, as the scope of this thesis to obtain results that shed light on the combustion of conventional and biofuels and to perform a comparative study of the combustion process and by-products in the context of reduced and comprehensive reaction mechanisms as the main point of focus, it is thought that exploring the radiation models is another huge topic that can be left for further investigation.

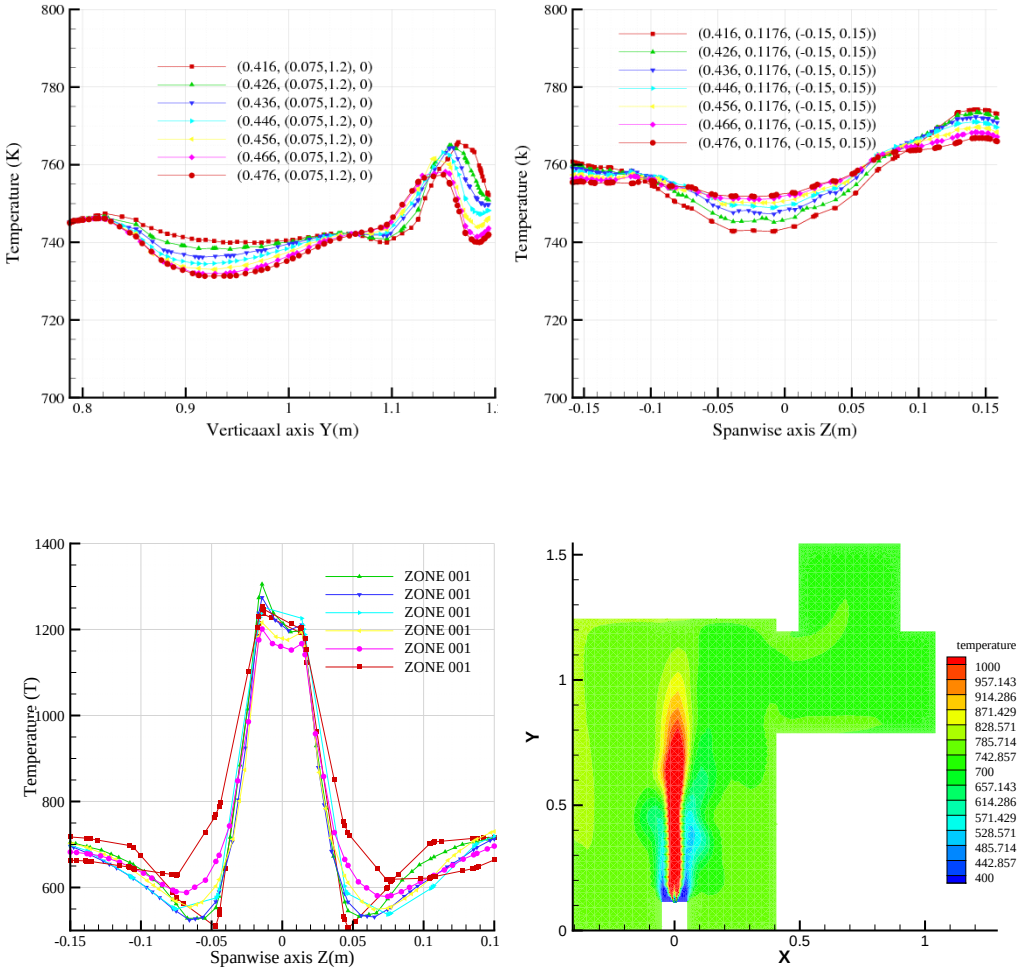


Figure 6.1: Temperature profiles corresponding to the (a) vertical lines shown in Fig. 3.9, (b) horizontal lines shown in Fig. 3.10, and (c) cross-sectional profiles close to the injector (starting at $y = 0.2m$), and (d) contours for a central (x,y)-plane.

Another observation related to the temperature field, and specifically to the cross-sectional temperature profiles of Fig. 6.1(c) is that of a much wider flame region compared to the result obtained without including the radiation model (Fig. 4.3(c)). This is confirmed by Fig. 6.1(d). The peak temperature at $y = 0.2m$ is of order 1200 which is similar to that predicted by the simulation without the

modelling of radiation (Fig. 4.3(c)). Hence, the larger flame width predicted by the simulation with radiation model is probably the main reason that explains the higher temperature predicted at the exit of the burner. In conclusion, the simulation with radiation modelled have predicted a flame having larger width in comparison to that in which the radiation is not taken into account. This leads to a relatively high temperature at the exit.

## 6.2 Turbulence Parameters

Having examined the temperature field in Section 6.1, to shed light on the flow field, turbulence Reynolds number is presented in this section. Fig. 6.2(a) and Fig. 6.2(b) show the values of Reynolds number at the exit, corresponding to the vertical and horizontal lines shown in Fig. 3.9 and Fig. 3.10. The value and distribution of Reynolds number is similar to the SDRM simulations discussed in Chapter 4. A similar picture is presented by the cross-sectional profiles of $Re_y$ shown in Fig. 6.2(c) and the contours for a central plane shown in Fig. 6.2(d). However, it is noticeable that the distribution of $Re$ is more symmetrical than that observed in the SDRM simulation without radiation modelling (Fig. 4.4). Hence, in this regard, the inclusion of the effect of radiation using the $P-1$ model did not have a significant effect on turbulence and relevant turbulent variables including turbulence intensity which is not shown here.

## 6.3 Effect of Radiation Model on Emissions

To examine the products of combustion taking radiation model into account, profile and contours of carbon dioxide and water vapour are presented. The profiles of $CO_2$ at the exit locations (vertical and horizontal lines of Fig. 3.9 and Fig. 3.10) are shown in Fig. 6.3(a) and Fig. 6.3(b) respectively. The figures show that at the exit (at positions matching the measurements of Widmann and Presser [1]) the mole fraction of $CO_2$ is of order 0.022–0.032 which is slightly higher than that predicted for methanol simulation with SDRM without radiation modelled radiation (Fig. 4.7(b) and Fig. 4.7(a)) which is of order 0.015–0.0175. However, cross-sectional profiles along the vertical axis (starting at $y = 0.2m$)

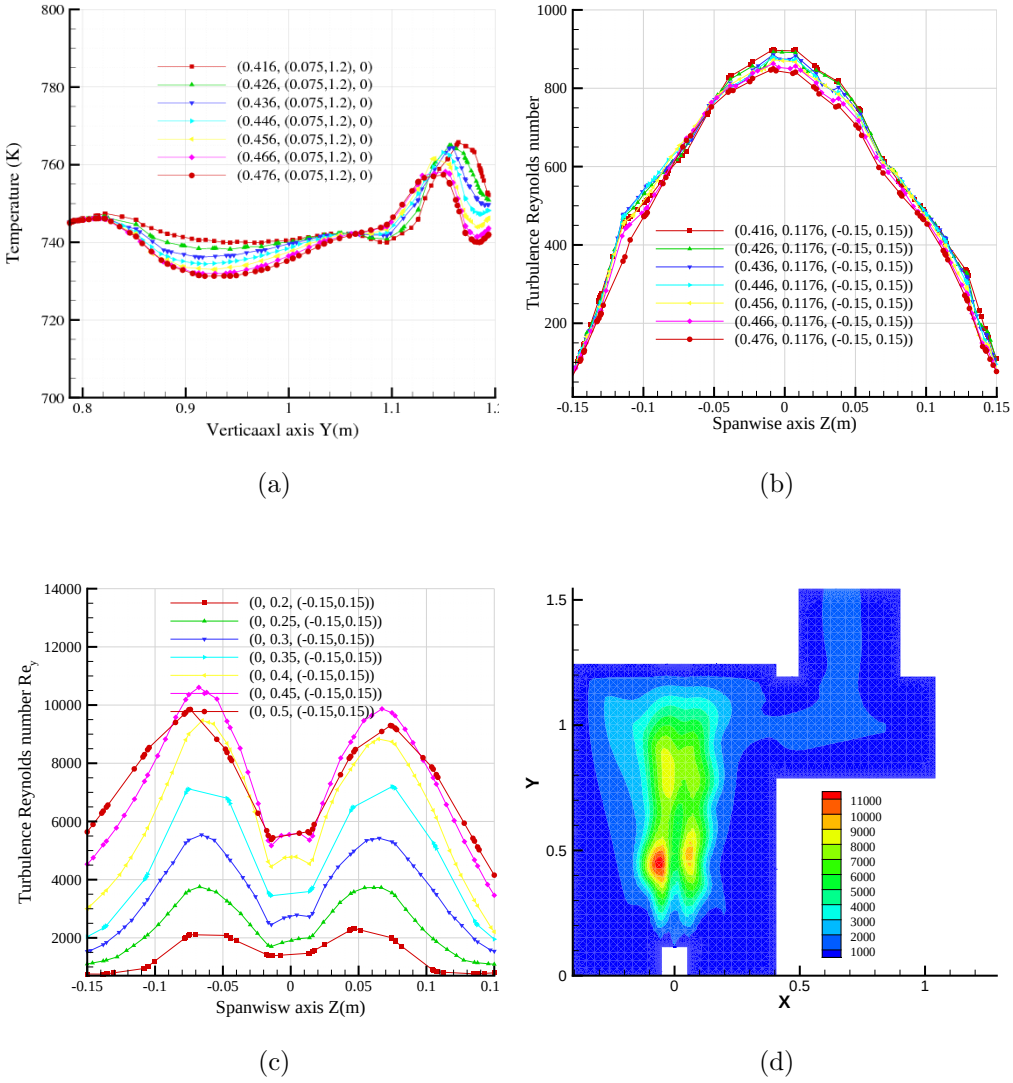


Figure 6.2: Turbulence Reynolds number profiles corresponding to the (a) vertical lines shown in Fig. 3.9, (b) horizontal lines shown in Fig. 3.10, (c) cross-sectional profiles close to the injector (starting at $y = 0.2m$), and (d) contours for a central (x,y)-plane.

shown in Fig. 6.3(c) and supported by the contours for a central (x,y)-plane (Fig. 6.3(d)) shows similar values to those predicted by SDRM without modelling radiation (Fig. 4.7(c) and Fig. 4.7(d)). Hence one would say that higher values observed at the exit in the case of radiation model could be due to the nature of

the flow field rather than due to the higher rates generated as a result of including the effect of radiation.

Water vapour has been examined both at the exit of the burner and close to the injection within the flame region. Fig. 6.4(a) and Fig. 6.4(b) show $H_2O$ distribution for the vertical and vertical profiles at the exit of the burner (corresponding to Fig. 3.9 and Fig. 3.10). Fig. 6.4(c) and Fig. 6.4(d) display the profile contours for cross-sectional profiles starting at $y = 0.2m$ from the burner bottom wall progressing with an increment of $0.05m$ along the vertical axis. The contours of a central (x,y)-plane appear in Fig. 6.4(d). Similar to the situation of $CO_2$, the range of $H_2O$ mole fraction at the exit of the burner (Fig. 6.4(a) and Fig. 6.4(b)) is of order 0.041–0.044 which is slightly higher than the predicted values for the SDRM simulation without modelling radiation. As can be seen from Fig. 4.13(a) and Fig. 4.13(b), the mole fraction of water vapour for the SDRM simulation without the inclusion of radiation effect is of order 0.019–0.021, thus the simulation with radiation included has twice the rate of water vapour at the exit. Within the flame region, the prediction including radiative heat transfer is shown in Fig. 6.4(c) and the contours for a central plane is shown in Fig. 6.4(d). It is apparent that the maximum value of the mole fraction of water vapour (at $y = 0.2m$) is of order 0.15 compared to 0.1 for the methanol simulation using the SDRM without the inclusion of radiation heat transfer (Fig. 4.13(d)). It is apparent that the inclusion of heat transfer by radiation has led to higher temperature range and hence slightly higher rates of water vapour. Whether the increase in temperature is the mechanism behind the increased rate of water vapour as it is most likely to be the case, or there is another relation between radiative heat transfer and water vapour formation, is an issue that remain in need of further investigation.

## 6.4 PDF Variables

Having addressed the temperature and emission for the methanol simulations with radiative heat transfer considered, it is worth to look at the rate of burning of the fuel under the new circumstances i.e., with the inclusion of radiative heat transfer. The case has shown that including radiation effect increases the temperature

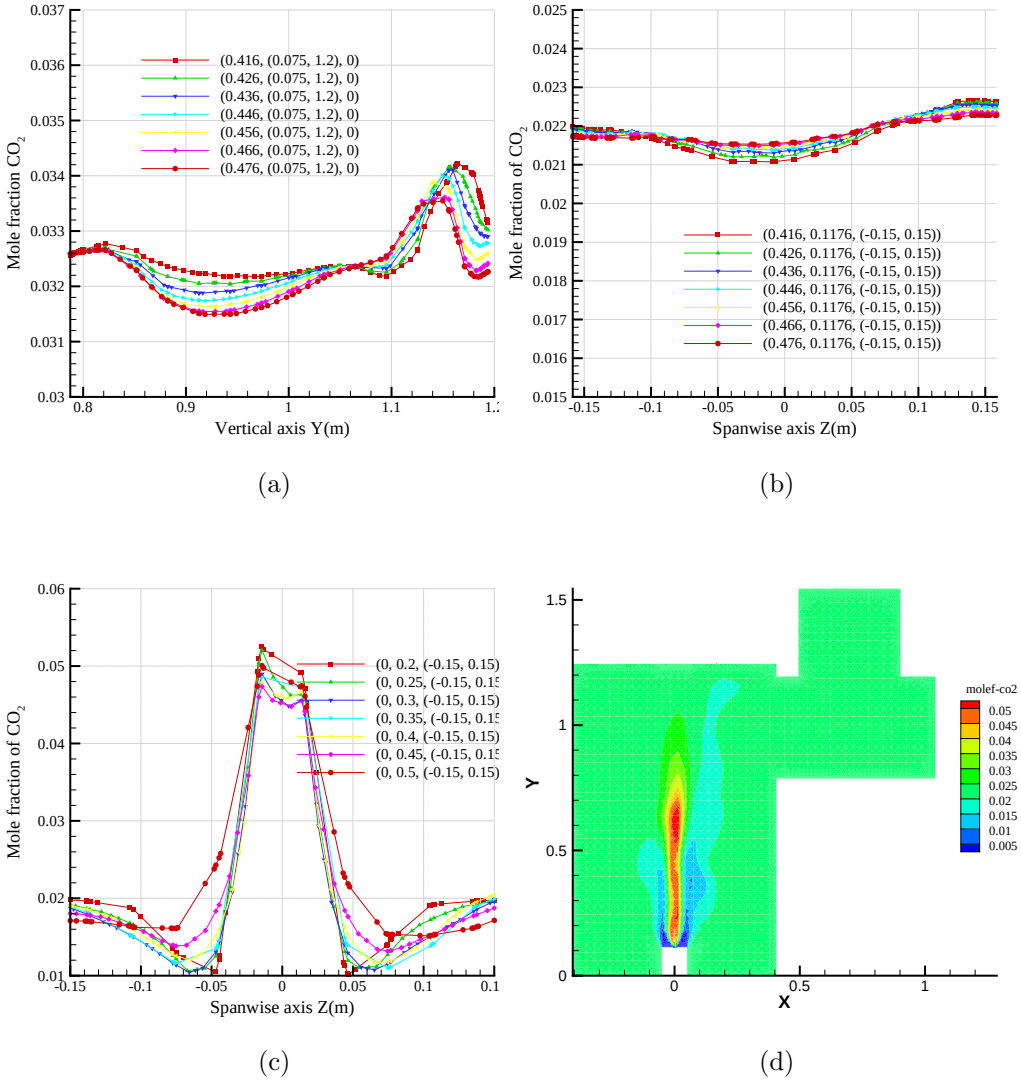


Figure 6.3: Carbon Dioxide ($CO_2$) profiles corresponding to the (a) vertical lines shown in Fig. 3.9, (b) horizontal lines shown in Fig. 3.10, (c) cross-sectional profiles close to the injector (starting at $y = 0.2m$), and (d) contours for a central (x,y)-plane.

range compared to the simulation without radiation. Hence, it would be worth examining the mixture fraction and other related PDF variables in order to study the combustion process under radiation heat transfer effects.

The mean mixture fraction at the exit locations (corresponding to the hori-

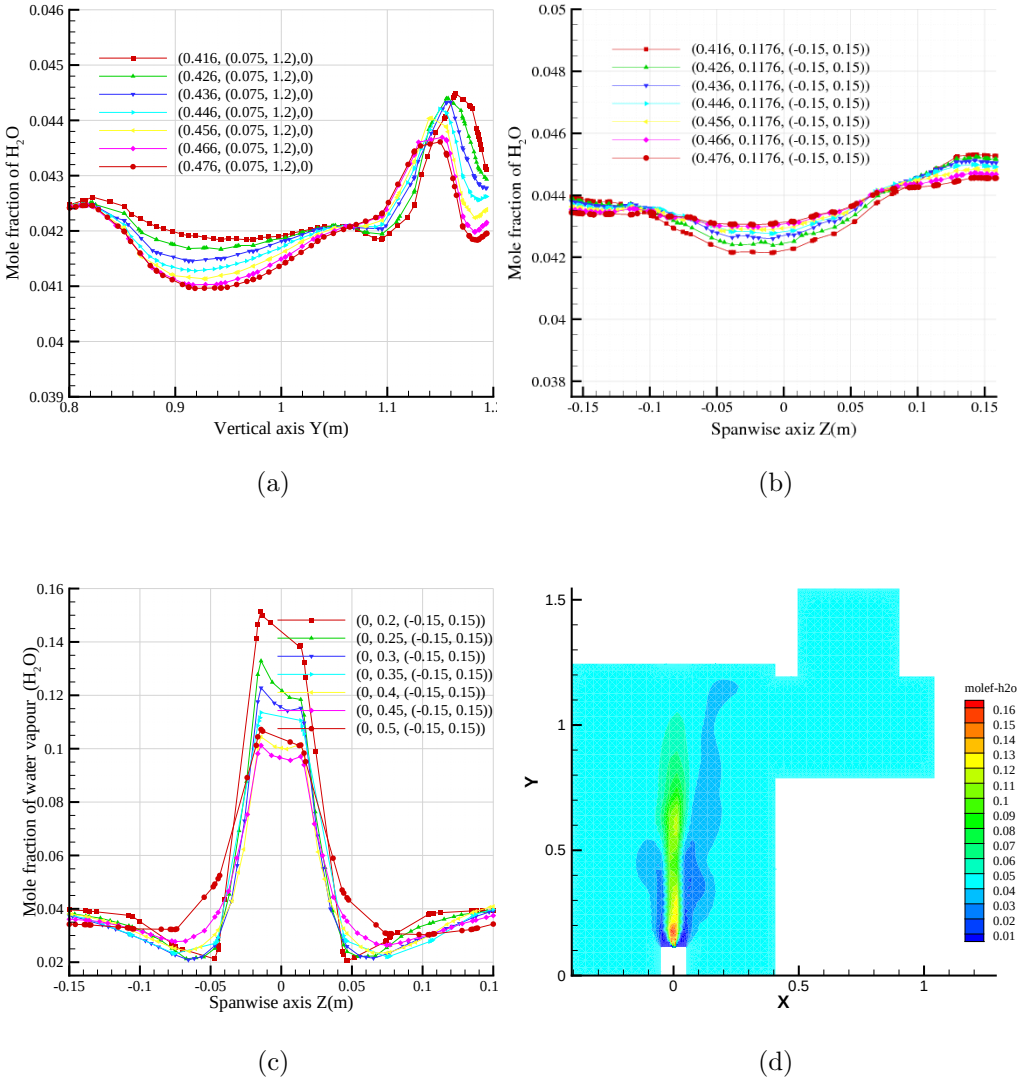


Figure 6.4: Water vapour ($H_2O$) profiles corresponding to the (a) vertical lines shown in Fig. 3.9, (b) horizontal lines shown in Fig. 3.10, (c) cross-sectional profiles close to the injector (starting at $y = 0.2m$), and (d) contours for a central (x,y)-plane.

zontal lines of Fig. 3.10) is shown in Fig. 6.5(a). Similarly values on the vertical lines (Fig. 3.9) were observed but not shown here. At the exit, the mean mixture fraction detected for the radiative heat transfer case is of order 0.024 compared to 0.01 in the case in which radiative heat transfer is not involved (Fig. 4.14(a)). This fact is supported by the profile of cross-sectional lines along the span-wise at a height close to the injection point shown in Fig. 6.5(b) and the contours of the same parameter at a central (x,y)-slice shown in Fig. 6.5(c). At $y = 0.2m$ above the burner bottom wall, the mixture fraction peak value is of order 0.25 and of order 0.06 at $y = 0.5m$ above the burner bottom wall. For the SDRM simulation without the radiation heat transfer included, the maximum mixture fraction at $y = 0.2m$ is of order 0.09 and of order 0.02 at $y = 0.5m$ above the burner bottom wall. Thus, it is apparent that the inclusion of radiative heat transfer has led to a slow burning rate of the fuels. This partly explains the fact that higher temperature was reported when radiation heat transfer was included.

The mixture fraction variance at the exit locations and for cross-sectional profiles along the vertical axis are shown in Fig. 6.6(b), Fig. 6.6(a) and Fig. 6.6(c) respectively, while a central slice showing the contours for this variable is displayed in Fig. 6.6(d). The figures clearly shows that the mixture fraction variance is very small at the exit as these positions are far from the flame region. Within the flame region (Fig. 6.6(c)), the peak value of the variance is of order 0.005 which is still small and indicates the laminar nature of the flame. Comparing Fig. 6.6(c) with its counterpart, Fig. 4.25(b), it is apparent that the predicted values for the mixture fraction variance are almost the same as that of the case in which radiative heat transfer is not included.

From this discussion, one can conclude that the effect of including radiation heat transfer would have minor effect. It was reflected in slightly slower burning rate leading to slightly higher temperature, else other variables remain comparable. Not only that, it is worth noting that in order to predict the effect of radiative heat transfer in the combustion process and its by-products, one needs to employ a more accurate model than the P-1 model used in this simulation.

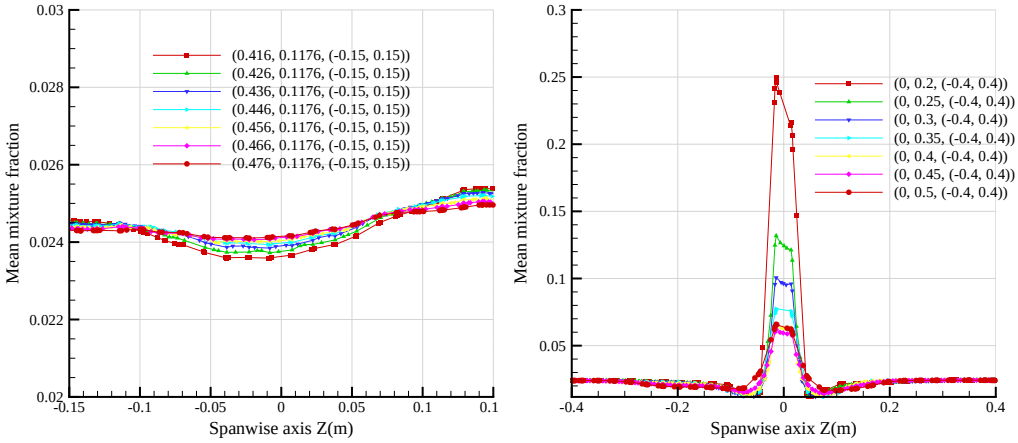


(a) (b)

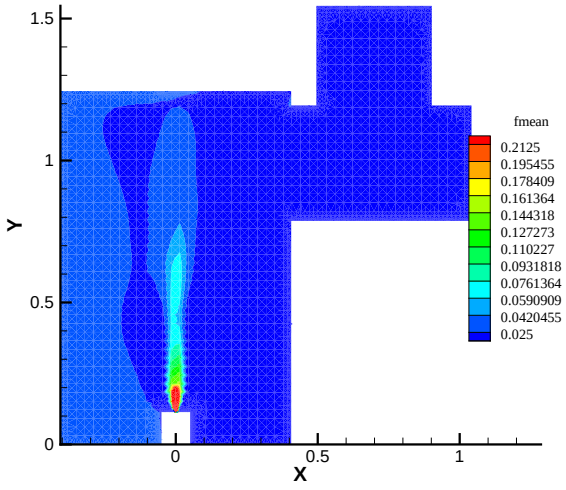


(c)

Figure 6.5: Mean mixture fraction profiles corresponding to the (a) horizontal lines shown in Fig. 3.10, (b) cross-sectional profiles close to the injector (starting at $y = 0.2m$), and (c) contours for a central (x,y)-plane.

## 6.5 Summary

Including the effect of radiation heat transfer in modelling the combustion process is an important factor and adds to the realistic picture of the combustion process.

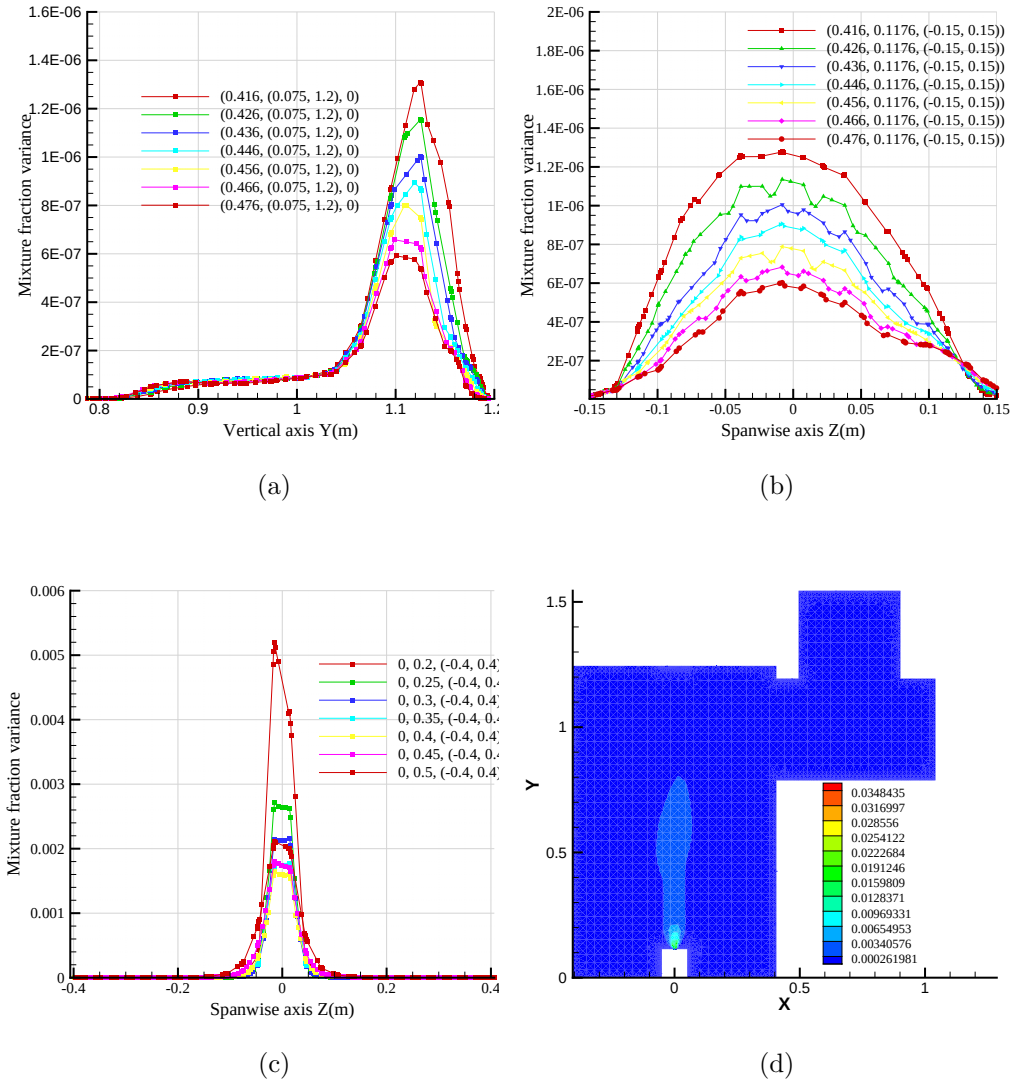


Figure 6.6: Mixture fraction variance profiles corresponding to the (a) vertical lines shown in Fig. 3.9, (b) horizontal lines shown in Fig. 3.10, (c) cross-sectional profile close to the injector (starting at $y = 0.2m$), and (d) contours for a central (x,y)-plane.

The outcome of this chapter can be summarised in few statements. The effect of including radiative heat transfer has increased the range of temperature at the exit and within the inner region of the burner. The emissions have also reported some increase possibly related to the increase of temperature that promote the

formation of some emission such as $NO_x$. In comparison to the experimental results, and the SDRM simulation of methanol including radiative heat transfer model has predicted reasonable agreement in terms of by-products of combustion especially water vapour. In terms of literature, there are no reported data that can be used to compare the current results with. As mentioned previously that the work of Widman and Presser [1] has not been used by any other study other than that of Collazo et al [65] only a small amount of data is presented. The current work represents a new benchmark for any future work in this field.

# Chapter 7

# Biodiesel Analysis

An extensive review of biofuels was presented in Chapter 5 which revealed that such fuels can have a range of values for any associated property such as density, depending on the source (vegetable sources or animal fat sources) and raw material from which it was manufactured. One point that was not covered in detail in the literature was the effect of storing biodiesel for some periods before using it. As this section deals with the use of biodiesel that has been purchased from a UK supplier, in a diesel engine, its basic properties and the effect of storage on these properties are investigated first. In this chapter, Section 7.1 examines the basic properties of the obtained biodiesel, diesel and nine surrogate fuels while Section 7.1.11 casts a deeper look into the spectral behaviour of these fuels at two different periods of times. The performance of a diesel engine using diesel, biodiesel, and four surrogate fuels will be the subject of Section 7.2. The whole chapter is meant to supplement the computational work done in previous chapters.

## 7.1 Physicochemical Properties of Biodiesel Fuels

For biodiesel to be adopted as an alternative to diesel fuel (in CIEs), it had to satisfy specific internationally recognised criteria and standards which is a function of its representative physicochemical properties. Its physical and chemical

properties had to match the international standards (ASTM 6571–3, EN 14214) [135]. When biodiesel (in its pure form or as a blend) is used as a fuel, it is subjected to the requirements set by these standards.

Similar to diesel, biodiesel fuels are differentiated by their CN, density, viscosity, CP, PP, FP, copper corrosion, ash content, distillation range, sulfur content, carbon residue, acid value, free glycerine content, total glycerine content and Higher Heating Value (HHV), etc. Although there is an abundance of research done already to establish these properties for bidiesel processed from different sources, of interest to this work are the biodiesel blends (mixture of diesel and biodiesel) rather than biodiesel itself. Hence, the question is how do these properties vary when a mixture of diesel and biodiesel is prepared.

The physicochemical properties of biodiesel such as density, viscosity, heat capacity and enthalpy may influence the combustion and exhaust emission. The sections below presents a comparative study of some of the basic properties of biodiesel mixtures (heat capacities, enthalpy, density, viscosity, and iodine value of nine biodiesel mixtures. The biodiesel used originate from vegetable sources. The rest of this section summarises the result of an extensive experimental campaign meant to establish the properties of biodiesl surrogate fuels.

### 7.1.1 Density

Density is considered as one of the most important properties of fuels, because it influences the performance of injection systems (pumps and injectors). In spray combustion in diesel compression engines, the injection system must deliver the exact amount of fuel precisely adjusted to provide complete and efficient combustion. In this sense, density plays an important part in the spray characteristics which are at the heart of effective combustion processes determining both the enregy released and emissions.

Table 7.1: Density of diesel fuel (DF), biodiesel (BD) and nine surrogate fuels.

| Fuel | DF | B10 | B20 | B30 | B40 | B50 | B60 | B70 | B80 | B90 | BD |
|---|---|---|---|---|---|---|---|---|---|---|---|
| Density | 847.5 | 850.8 | 854.9 | 858.5 | 862.4 | 866.0 | 870.0 | 873.8 | 877.7 | 881.6 | 885.3 |

Although the properties of diesel fuel are rather loosely regulated, the primary

diesel fuel properties are controlled by legislation associated with the country of use. The density of red diesel such as the one used in this study varies between 850-900 $\frac{kg}{m^3}$. This is in agreement with the measurement performed on the sample

Table 7.2: Viscosity, density and FP measurements of eight vegetable oil methyl esters [136]

| Methyl ester | Viscosity ($\frac{mm^2}{s}$ (at 313 K)) | Density (kg/m3 (at 288 K)) | FP (K) |
|---|---|---|---|
| Cottonseed oil | 3.69 | 880 | 437 |
| Hazelnut kernel oil | 3.59 | 860 | 401 |
| Mustard oil | 4.10 | 881 | 446 |
| Palm oil | 3.70 | 870 | 443 |
| Rapeseed oil | 4.63 | 885 | 428 |
| Safflower oil | 4.03 | 880 | 453 |
| Soybean oil | 4.08 | 885 | 447 |
| Sunflower oil | 4.22 | 880 | 443 |

Table 7.3: Viscosity, density and FP measurements of ten vegetable oils [37]

| Oil source | Viscosity ($\frac{mm^2}{s}$ (at 311 K)) | Density (kg/m3) | FP(K) |
|---|---|---|---|
| Corn | 34.9 | 909.5 | 550 |
| Cottonseed | 33.5 | 914.8 | 509 |
| Crambe | 53.6 | 904.4 | 447 |
| Linseed | 27.2 | 923.6 | 514 |
| Peanut | 39.6 | 902.6 | 544 |
| Rapeseed | 37.0 | 911.5 | 519 |
| Safflower | 31.3 | 914.4 | 533 |
| Sesame | 35.5 | 913.3 | 533 |
| Soybean | 32.6 | 913.8 | 527 |
| Sunflower | 33.9 | 916.1 | 447 |

There are many studies that focus on establishing the density of oils and their biodiesl product (e.g. the work of Sridharan and Mathai [136] and Goering et al. [37]). The densities of vegetable oils range between 902.6 and 923.6 $\frac{kg}{m^3}$ (Table 7.3). On the other hand, the densities of vegetable oil methyl esters range

between 860 and 885 $\frac{kg}{m^3}$ (Table 7.2). It is clear that the densities of the former decrease significantly because of the transesterification process that is used to produce biodiesel.

The international standard (EN 14214) requirements for biodiesel [135] shown in Table 7.3 indicate that the acceptable range of biodiesel density at 15$^o$C should be 860–900 $kg/m^3$. In this work, the density and viscosity were obtained with the help of Stabinger Viscometer SVM 3000 (Anton Paar) and were measured at 15$^o$C (278.15$K$) according to the ASTM D445. The density of diesel fuel, biodiesel and the nine surrogate fuels B10–B90 is shown in Table 7.1 (also shown graphically in Fig. 7.2(a)). The measured density of diesel fuel is 847.5 compared to 885.3 for biodiesel. Hence biodiesel is $\frac{885.3-847.5}{847.5} = 4.46\%$ heavier than diesel fuel.

Interestingly, the densities of the nine surrogate fuels display a perfectly linear behaviour with the density value increasing with increasing the percentage of biodiesel in the mixture. This is a strong indication of the fact that the resultant solution from diesel fuel and biodiesel mixtures is an ideal one and that other properties can be calculated by the linear combination of the properties of its components. Checking this fact based on B50, the density should be $\frac{847.5+885.3}{2} = 866.4\frac{kg}{m^3}$ and the experimental data shows that it is 866.0 $\frac{kg}{m^3}$, with a negligible marginal error of order ($\frac{0.4}{866.4} = 0.046\%$).

### 7.1.2 Viscosity

Engines can lose power because of injection pumps and injector leakages. That is why a minimum viscosity is necessary for some engines. Biodiesel (B100) does not have this issue. It is assigned a minimum value which is similar to that assigned for petroleum diesel. However, its maximum viscosity is restricted by the design of the injection systems for engine fuel. Highly viscous fuels can result in low fuel combustion which can lead to the formation of deposits. It can also result in higher in-cylinder penetration of the fuel spray, which can cause excessive dilution of engine oil with fuel. ASTM D975 specification for DF2 allows a viscosity of 4.1 $\frac{mm^2}{s}$ max. at 104F (40C) [42]. The allowable viscosity is relatively higher in D6751 specification. This is mainly due to fact that, commonly, viscosity of B100

lies there. The blends of biodiesel which are in the range of 20% or less, must have a viscosity value which is within the limits specified in the D975 specification. The study of Sharma et al. [137] has shown that the viscosity values of vegetable oils decrease sharply after transesterification reaction.

Viscosity is a key attribute of biodiesel fuels. The operations of fuel injection equipments are especially effected by it. This is particularly true at lower temperatures since, at such temperatures, an increase in viscosity affects the fluidity of the fuel [138]. It has been found in [139, 140] that higher viscosity results in poorer atomization of the fuel spray which affects the accuracy of the operation of fuel injectors. However, according to [138], the lesser viscous the biodiesel is, the easier will it be to pump, to atomize, and to achieve finer droplets.

Kinematic viscosity is an index which measures the adhesiveness of a fuel [138]. Optimum viscosity values hinder nebulization of fuel in the ignition chamber. On the other hand, while non-optimal viscosity values hamper the engine lubrication effects. For this reason, for biodiesel, it is necessary to keep the viscosity values within the stipulated range of international standard specification.

Fangrui et al. [141] studied the transesterification reactions. They reported that the reactions convert triglyceride into methyl or ethyl esters. They further concluded that the transesterification reactions minimize the molecular weight to a third of that of the triglyceride. Moreover, they tend to decrease the viscosity of vegetable oils by a ratio of about eight to one. The viscosity of biodiesel fuel depends on its source. For example biodiesel fuel from animal fats such as lard and tallow is more viscous than those from soybean and rapeseed. Virgin and waste vegetable oils are even more viscous. That is why, while they can be used as fuels in CIEs, but because of their exceptionally high viscosities compared to diesel fuel, they cannot be readily used in diesel engines before major modifications to the engine are made. According to Gunvachai et al. [142], when vegetable oil is burned in a diesel engine, it produces acrolein and organic acid. These are unwanted materials. Thus, it is not a clean fuel. These materials have undesirable effects on the performance and durability of longitudinal engines. On the other hand, it is possible to transform vegetable oils into their fatty acid methyl esters with the help of transesterification reaction and to use them as fuels in diesel engines without requiring any significant changes [135]. Table 7.10 adopted from

Hidek et al. [143] summarizes the physicochemical properties of major biodiesel fuels, in addition to Table 7.2 and Table 7.3 shown earlier in this chapter.

Of interest to this thesis work is the variations in Kinematic viscosity of surrogate fuels. Using Stabinger Viscometer SVM 3000 (Anton Paar), the viscosities of diesel fuel, biodiesel and the nine mixtures (B10–B90) were measured. The values are listed in Table 7.4 and graphically plotted in Fig. 7.1. Similar to density, the variation of viscosity exhibits linearity. The biodiesel under consideration has a higher viscosity (4.6221 $cSt$) compared to diesel fuel (2.9112 $cSt$). These values are in range within the scatter of data of viscosities of diesel fuel and biodiesel discussed in the paragraph above. However, it is apparent that biodiesel has considerably higher viscosity ($\frac{4.6221-2.9112}{2.9112} = 58.8\%$ higher) compared to diesel fuel. If such a biodiesel is adopted as an alternative fuel in a CIE, this could be a serious challenge to the pumping and atomising system designed for conventional diesel fuel. Even an equal mixture of diesel fuel and biodiesel(B50) may have a high viscosity value for the pumping/atomising system to cope with and a trade-off with biodiesel percentage or modification to CIE pumping/atomization systems may be necessary for biodiesel fuels in the future. However, this point would be discussed further when the experimental tests have been performed on a CIE.

Table 7.4: Viscosity of diesel fuel (DF), biodiesel (BD) and nine surrogate fuels (B10–B90)

| Fuel | DF | B10 | B20 | B30 | B40 | B50 | B60 | B70 | B80 | B90 | BD |
|---|---|---|---|---|---|---|---|---|---|---|---|
| $\mu$ (at 40°C) cSt | 2.9112 | 3.1113 | 3.2445 | 3.3855 | 3.5112 | 3.6745 | 3.8112 | 4.0434 | 4.2101 | 4.431 | 4.6221 |

#### 7.1.2.1 Density - Viscosity Correlation

The relationship of density and viscosity of diesel fuel, biodiesel and the nine mixtures is depicted in Fig. 7.3. The variation is linear and it is clear that increasing the percentage of biodiesel in the mixture increases the viscosity in almost a perfect linear fashion. The findings of these tests agree with what has been reported in the literature as shown in Table 7.5.

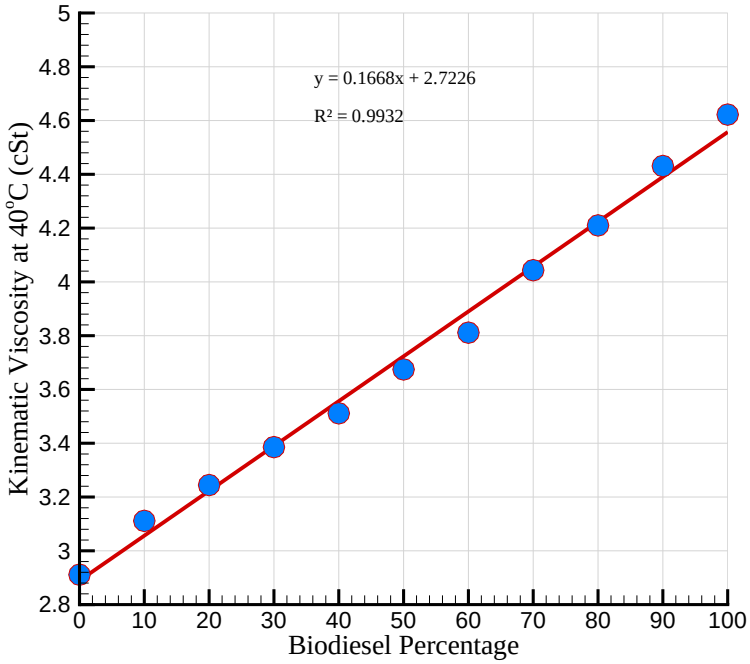


Figure 7.1: Viscosity variation

Table 7.5: Viscosity, density and FP measurements of oil methyl esters (Sridharan and Mathai [136])

| Methyl ester | Viscosity ($\frac{mm^2}{s}$ (at 313 K)) | Density (kg/m3 (at 288 K)) | FP (K) |
|---|---|---|---|
| Cottonseed oil | 3.69 | 880 | 437 |
| Hazelnut kernel oil | 3.59 | 860 | 401 |
| Mustard oil | 4.10 | 881 | 446 |
| Palm oil | 3.70 | 870 | 443 |
| Rapeseed oil | 4.63 | 885 | 428 |
| Safflower oil | 4.03 | 880 | 453 |
| Soybean oil | 4.08 | 885 | 447 |
| Sunflower oil | 4.22 | 880 | 443 |

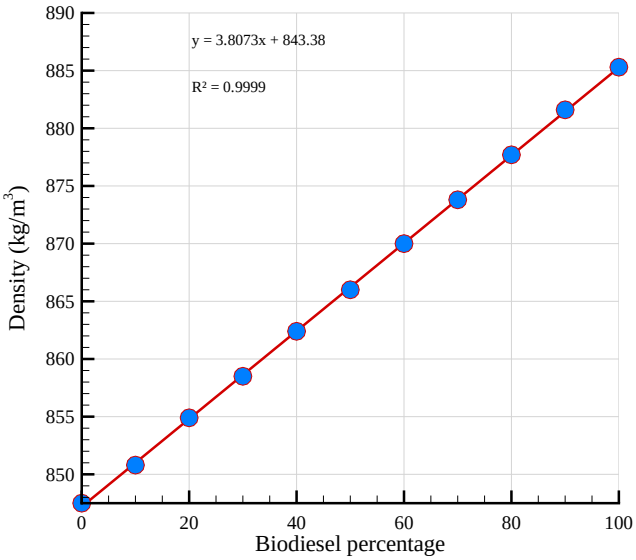


(a)

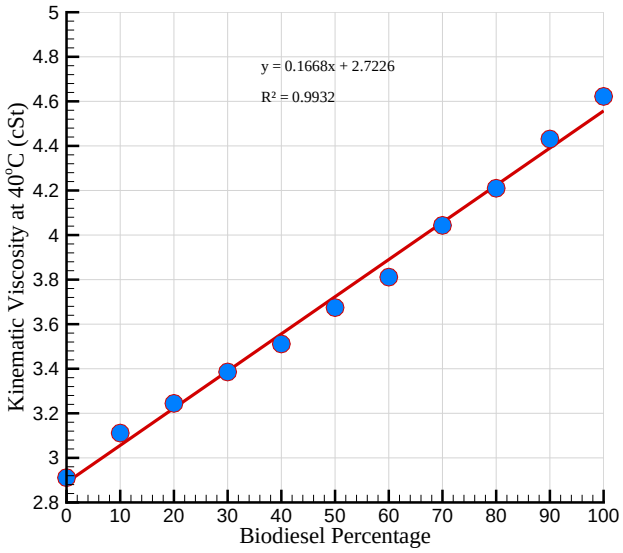


(b)

Figure 7.2: (a) Density relation. (b) Viscosity relation.

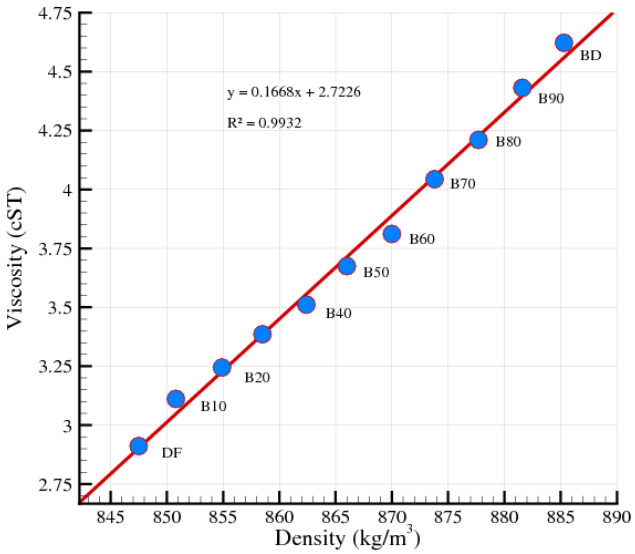


Figure 7.3: Relationship between density and viscosity of diesel-biodiesel mixture.

### 7.1.3 Cetane Number

Considering the use of fuels in internal combustion engines, gasoline is spark-ignited, while diesel fuel (after injection) is ignited by the heat of compression in a diesel engine. Based on this ignition principle, the diesel engine is termed a CIE. Since the ignition processes for gasoline and diesel fuels are different, they require fuels with significantly different physical and chemical properties. In a CIE, the time from fuel injection into the chamber to ignition is referred to as ignition delay. CN is a measure of the ignition delay. Fuels with lower ignition delay times, have higher CNs. CN thus represents a qualitative measure of the ignitability of a fuel.

Historically, the concept of CN was presented by Boerlage and Broeze [144], where they compared the ignition quality of different blends of two reference fuels: cetane ($C_{16}H_{34}$) and mesitylene ($C_9H_{12}$). Cetane is a paraffin that is prone to ignition, while mesitylene is an aromatic hydrocarbon that would not combust in the test engine. They measured the ignition delay of the different blends of cetane and mesitylene, and based on their experimental work, produced a chart

relating measured ignition delay to cetane concentration in the fuel blend.

The CN scale is important for understanding the molecular structure of the compounds that make up diesel fuel. The scale indicates that the CNs of saturated, unbranched hydrocarbons that have long chains (alkanes) are high and such hydrocarbons have favourable ignition characteristics while those of branched hydrocarbons are low with unfavourable ignition characteristics.

It is a common belief that higher CNs provide easier starting and quieter operation. On the other hand, extremely high or extremely low CNs can cause problems in the operation of a CIEs. Theoretically, in the case of extremely high CNs, combustion can take place before the fuel and air have completely mixed together which can render the combustion process incomplete and can result in the emission of smoke. On the other hand, too low CNs can cause other problems such as: it can lead to roughness in engines, it can cause misfiring, it can raise the temperature of the air, it can slow-down the warming up of engines and can render the combustion process incomplete.

Table 7.6: CN of diesel fuel (DF), biodiesel (BD) and nine surrogate fuels (B10–B90)

| Fuel | DF | B10 | B20 | B30 | B40 | B50 | B60 | B70 | B80 | B90 | BD |
|---|---|---|---|---|---|---|---|---|---|---|---|
| CN | 49 | 49.08 | 48.68 | 49.07 | 49.94 | 50.16 | 50.40 | 50.86 | 52.00 | 61.8 | 62.34 |

The ignition quality or CN of diesel fuel is regulated by ASTM. They designed the ASTM D613 [145] as a standard for measurement. To position various compounds on the cetane scale, hexadecane ($C_{16}H_{34}$), which has a very low ignition delay, has been given a CN of 100. At the other extreme is 2, 2, 4, 4, 6, 8, 8-heptamethylnonane (HMN), also $C_{16}H_{34}$, which has bad ignition characteristics. Its CN has been set to 15. It is important however to note that the cetane scale is arbitrary and that compounds with $CN > 100$ or $CN < 15$ have been identified. The ASTM specification for conventional diesel fuel (ASTM D975) requires a minimum CN of 40.

As the use of biodiesel has gained momentum as a feasible replacement for diesel, ASTM has also developed ASTM D6751 standard in an attempt to regulate

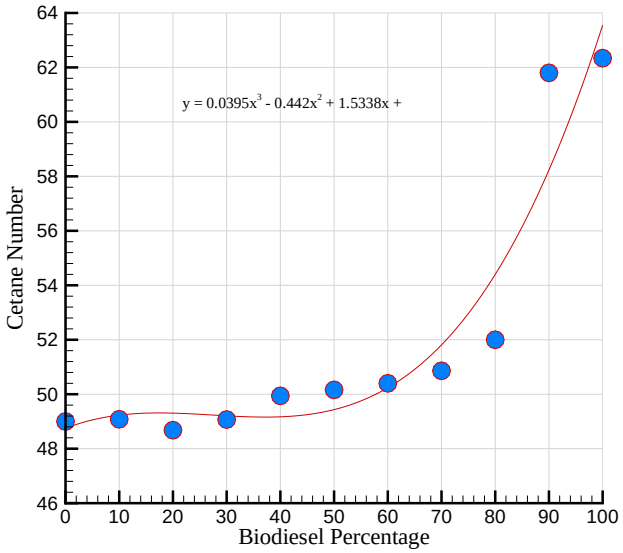


Figure 7.4: Cetane index variation

its standards. The ASTM D6751 specification has set a minimum CN of 47 for biodiesel compared to 40 for petroleum diesel fuel. When B100 is produced from highly saturated feedstocks, it can have a CN of over 60 [42]. Biodiesel produced from soy, sunflower, corn, and canola has CN of around 47. Table 7.6 compares the CNs of different varieties of biodiesel and diesels.

The CN scale has been very useful guide for engine manufacturers as it can help them to assign a CN limit for their engines. CN 40–50 is one such range.

The CN value is important for healthy engine performance. In the US, diesel fuel is required to have a CN value of 40 or more. Higher CNs values are desirable as they help to make sure that the cold start properties are good and that the formation of white smoke is kept minimal. For B100, the ASTM allows a CN of 47. It is important to mention that the National Conference of Weights and Measures has set this value for premium diesel fuel. Moreover, the lowest CN found in the biodiesel fuels in the US is also 47. It is noteworthy that, for biodiesel or its blends, the cetane index (ASTM D976) is not a good predictor of CN. A reason for this is that its calculation involves the use of specific gravity and distillation curves. Both of these do not remain the same for biodiesel and

petroleum diesel [42].

Of interest to the work of this thesis is the behaviour of the CN for surrogate fuels. It is clearly an expensive task to determine the CN of diesel fuel, biodiesel and nine surrogate fuels B10–B90. On the other hand, the cetane index is calculated using, ASTM D4737. The data is shown in Table 7.6 and graphically presented in Fig. 7.4. The general trend shown by the results indicate an increase in the CN by increasing the biodiesel percentage within the mixture. However, it is not a linear variation as in the case of density and viscosity and the reason could be associated with the accuracy adopted in measuring such a parameter for biodiesel or biodiesel mixtures. ASTM D4737 shares similar principles as of ASTM D976 and one can conclude that the results in Fig. 7.4 should be treated with caution. The output from the measurement is however logical in the sense that the CN increases with increasing biodiesel content and that the measured value for diesel fuel and biodiesel are in range with values mentioned in the literature. An important observation was that in up 80% biodiesel content, the mixture shows small increase from the value of diesel fuel and if this test is 100% correct, it can be assumed that the effect of biodiesel percentage in a mixture is of minimal effect to the CN or cetane index. However, one would again repeat that the cetane data obtained via ASTM D4737 method carries a marginal error.

### 7.1.4 Flash Point

In a study conducted by Demirbas [135], the FP values of fatty acid methyl esters were found to be much smaller than the FP values of vegetable oils. Demirbas also found the density values of vegetable oil methyl esters to be very different than their viscosity values. Moreover, the viscosity values of these methyl esters were found to be considerably regular with respect to their FP values. The easy storage, easy handling and ease of use of biodiesel come from the fact that biodiesel has a comparably higher FP values compared to diesel-petrol. The study conducted by Dube et al. [146], concludes that biodiesel is an excellent fuel, particularly, for use in delicate settings e.g., marine areas, national parks and forests, and heavily polluted cities for its comparably low emission profile.

Fire safety requires diesel fuel to have a minimum FP. The FP of B100 is

required to be not less than 93 °C (200 °F) to ensure a non-hazardous classification for it according to the National Fire Protection Association (NFPA) code. With reference to the handbook [42], for B6 to B20, the FP is 52 °C. The measurement of the FP for diesel, biodiesel and nine surrogate fuels is shown in Fig. 7.5(a) which shows that the temperature drops continuously by adding biodisel with diesel. For B20, the measured temperature is exactly 52 °C matching the value mentioned in the literature which strengthens the credibility of these results.

### 7.1.5 Low-Temperature Properties

CP and PP are important factors of a fuel, especially in low temperature applications. CP can be defined as the temperature point at which wax first becomes visible after the cooling down of a fuel. On the other hand, PP can be defined as the temperature point at which the amount of wax produced by the solution is enough to gel the fuel. In other words, the lowest temperature at which it is possible for the fuel to flow is called its PP. It has been shown in [77], that compared to convetional diesel, biodiesel has both higher CP and higher PP values.

The properties of biodiesel and normal petroleum diesel at low temperatures are of major significance. Both these fuels, unlike gasoline, can freeze or gel at very temperatures. That is why, in the winters, in areas with extremely cold weather, diesel fuel is usually available for sale in different formulations. Gelling of fuel is undesirable as it can block filters on dispensing equipment and, with time, can become so heavy that it is almost impossible to pump. In such cold weathers, B100 is usually stocked in heated above-ground tanks for blending. Some of the key metrics for evaluating the low-temperature performance of handling and blending of B100 are as follows:

#### 7.1.5.1 Cloud Point

CP can be defined as the temperature at which small solid crystals are no longer soluble and can be visually seen. This happens when the fuel is cooled down. Below CP, these crystals either block filters or drop down to the bottom of a storage tank. Although it is possible to pump fuels even below the CP, considering this issue with respect to the performance of atomisation system in CIEs, one

would expect a negative impact. The temperatures at which B100 freezes is, generally, higher than those at which other diesel fuels freeze. This fact should be considered when B100 is handled or used, especially in above-ground storage tanks or as a fuel in aviation (for aeroplane). Most B100 fuels start to cloud at 35 °F to 60 °F (2 °C to 15 °C ), so heated fuel lines and tanks may be needed, even in moderate climates, during winter [42]. As B100 begins to gel, the levels to which its viscosity rises are much higher than those to which most diesel fuels do. This can cause an increase in the pressure on pumps. The high CP value makes using B100 in colder climates, a challenging task.

CP is one of the most commonly used factors to determine the operation of a fuel at low temperatures. Generally, it is considered that a fuel will operate well above its CP. The CP of B100 fuel is normally higher than the CP of standard diesel fuel. It is necessary that the CP of a fuel is reported to indicate the effect of biodiesel on the CP of the final blend.

There is much scattered information about the range of CP of biodiesel and one would cite the work of Imahara et al. [147] who performed extensive measurements as well as developing some mathematical relation to predict the CP of biodiesel from different sources as shown in Table 7.7. It is clear that biodiesel could have a CP ranging from -6 to +13 $^o$C compared to a range of -3 and 15 mentioned in [42].

Of interest to this work is the CP temperature of a mixture of biodiesel and diesel. The measurement of the CPs for diesel, biodiesel and B10–B90 mixtures are listed in Table 7.8 and graphically shown in Fig. 7.5(b). The measurement shows that the CP range for surrogate fuels are all below 0$^o$C and range between -3 and -0.6 and that the distribution follows a linear variation with the CP moving up the scale as the biodiesel content increases in the mixture. These measurements are within the range of the data mentioned in the literature.

Table 7.7: Measured and calculated CP (in degrees Kelvin) of biodiesel fuel from various oils/fats feedstocks with their fatty acid composition [147]

| Source | Linseed | Safflower | Sunflower | Rapeseed | Soybean | Olive | Palm | Beef tallow |
|---|---|---|---|---|---|---|---|---|
| Measured | 268 | 267 | 274 | 267 | 272 | 268 | 283 | 286 |
| Calculated | 269 | 273 | 275 | 267 | 273 | 273 | 288 | 289 |

Table 7.8: CP for diesel (DF), biodiesel (BD) and surrogate fuels (B10–B90)

| Fuel | DF | B10 | B20 | B30 | B40 | B50 | B60 | B70 | B80 | B90 | BD |
|---|---|---|---|---|---|---|---|---|---|---|---|
| CP | -3.3 | -3.0 | -2.5 | -2.1 | -2 | -1.9 | -1.5 | -1.1 | -0.9 | -0.6 | 0.4 |

#### 7.1.5.2 Pour Point Temperature

PP temperature is the lowest temperature at which a fuel loses its flow characteristics as a result of the agglomerated crystals. It is used to indicate whether a fuel can be pumped. This is regardless of the fact that whether it will require any other steps such as heating [42].

The PP of B100 is, generally, slightly lower than its CP. So, as biodiesel starts freezing, gelling can happen fast if the temperature falls even slightly. Based on a piezoelectric quartz crystal and ASTM, Gomes et al. [148] has shown that the range of the pour of diesel fuel, biodiesel and some surrogate fuels range between 0 to -15$^o$C as seen in Table 7.9. It is clear that the range of pour temperatures for the surrogate fuels (B80–BD) is around -3$^o$C to -21$^o$C, which higher than the range shown by Gomes et al. [148], an indication of the fact that the current biodiesel used, has lower pour temperature than those examined by Gomes et al. [148]. The outcome of this analysis indicates that biodiesel is less favourable for use in cold flow properties compared to conventional diesel. Although the engine test was done at slightly cold temperature, the author used a mixing device to ensure that the tested surrogate fuels are in a liquid state taking these established temperatures as a guide.

Table 7.9: PP for biodiesel B2 and biodiesel fuels blends (four replicates) [148]

| | Piezoelectric method | | ASTM method | |
|---|---|---|---|---|
| Blend | Minimum | Maximum | Minimum | Maximum |
| B100 | 2.2 | 2.3 | 0 | 3 |
| B80 | -0.3 | -0.2 | -3 | 0 |
| B60 | -4.2 | -4.0 | -6 | -3 |
| B40 | -7.4 | -7.2 | -9 | -6 |
| B20 | -11.9 | -11.7 | -12 | -9 |
| B0 | -15.1 | -14.9 | -15 | -12 |

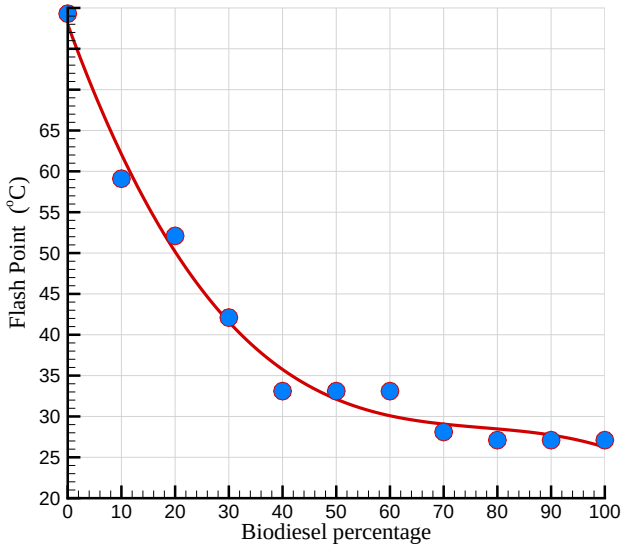


(a)

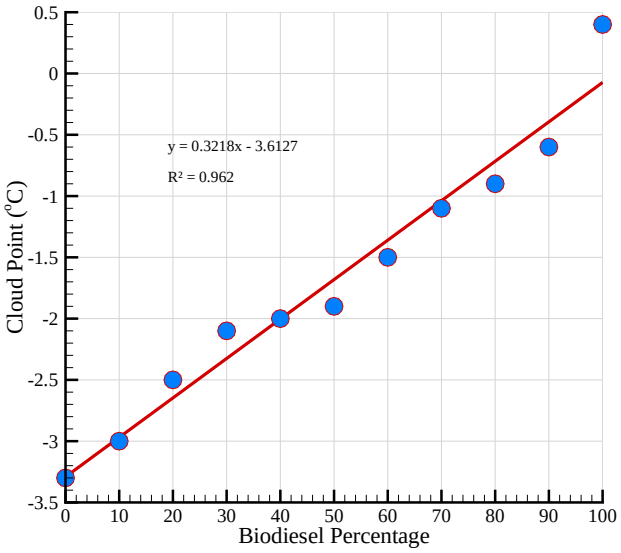


(b)

Figure 7.5: (a) FP variation. (b) CP variation

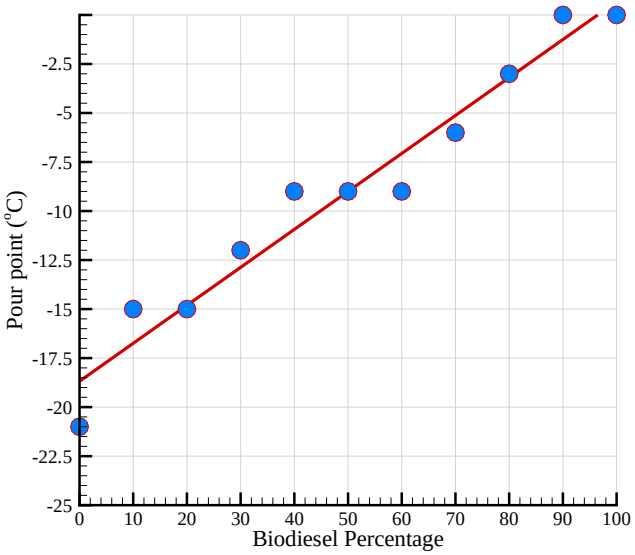


Figure 7.6: PP variation

Although no tests were done to establish the energy contents from the fuels used in this thesis, it is worth citing relevant information about the enthalpies and the heating values of such fuels. With reference to the work of Hideki et al. [143], for both the temperature's heating values and other physical properties, it is apparent that different kinds of vegetable oils have different lower heating values (ranging between 45-70$\frac{MJ}{l}$) which makes a difference when such fuels burn in a specific combustion structure.

### 7.1.6 Sulfer Content

The sulfer content of a fuel is relevant to acid pollutant emissions from the combustion process and it is always desirable to reduce the pollutant emission of sulfate and sulfuric acid. Moreover, it is desirable to save exhaust catalyst systems when they are employed in diesel engines. Also, it is important for the normal functioning of diesel particle filters that the sulfur content not over 15 ppm. The sulfur content of biodiesel is usually under 15 ppm. For accurate results, the test for low sulfur fuel (ASTM D5453) should be used in place of other

Table 7.10: Physicochemical properties of biodiesel fuels Hideki et al. [143]

| Vegetable Oil Methyl Ester | Kinematic Viscosity ($\frac{mm^2}{s}$) | CN | Lower Heating Value (MJ/l) | CP (8 C) | FP (8 C) | Density (g/l) | Sulfur (wt.%) |
|---|---|---|---|---|---|---|---|
| Peanut | 4.9 (37.8 8C) | 54 | 33.6 | 5 | 176 | 0.883 | - |
| Soybean | 4.5 (37.8 8C) | 45 | 33.5 | 1 | 178 | 0.885 | - |
| Soybean | 4.0 (40 8C) | 45.7-56 | 32.7 | - | - | 0.880 (15 8C) | - |
| Babassu | 3.6 (37.8 8C) | 63 | 31.8 | 4 | 127 | 0.879 | - |
| Palm | 5.7 (37.8 8C) | 62 | 33.5 | 13 | 164 | 0.880 | - |
| Palm | 4.3-4.5 (40 8C) | 64.3-70 | 32.4 | - | - | 0.872-0.877 (15 8C) | - |
| Sunflower | 4.6 (37.8 8C) | 49 | 33.5 | 1 | 183 | 0.860 | - |
| Tallow | - | - | - | 12 | 96 | - | - |
| Rapessed | 4.2 (40 8C) | 51-59.7 | 32.8 | - | - | 0.882 (15 8C) | - |
| Used rapeseed | 9.48 (30 8C) | 53 | 36.7 | - | 192 | 0.895 | 0.002 |
| Used corn oil | 6.23 (30 8C) | 63.9 | 42.3 | - | 166 | 0.884 | 0.0013 |
| Diesel oil | 12-3.5 (40 8C) | 51 | 35.5 | - | - | 0.830-0.840 (15 8C) | - |

standards (such as the D2622) as it might provide unexpectedly high results. Such results can be caused by the intereference of the test with the oxygen in the

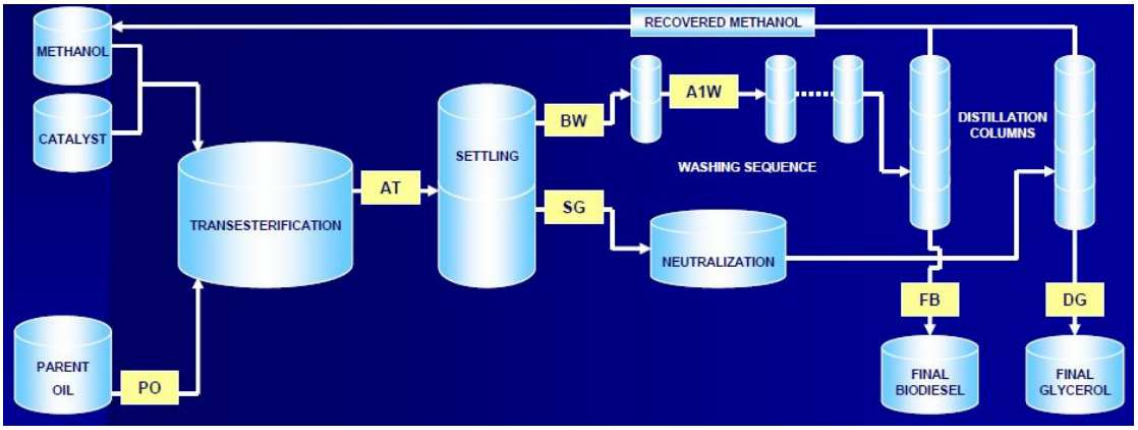


Figure 7.7: Transesterification process and biodiesel production

biodiesel.

Based on ASTM D5433, sulphur content for convention diesel can go up to 309.0 mg/kg (wt%). This method was adopted in this analysis and the results are listed in Table 7.11 and plotted in the graph of Fig. 7.8(a). It is important to mention that the ASTM has developed many other methods which express the sulfer content using different scales. For example, the ASTM D975 used for diesel fuel indicates the sulfur wt% 0.0015 max while the ASTM D6751 used for biodiesel indicates the sulfur, wt% range to be 0.00–0.0024 [42]. The fuel characterization data shows that while some of the properties of biodiesel and diesel are similar, there are some properties which are different [2]: the sulfur content of biodiesel is 20-50% less than that of diesel fuel [41].

The method used to estimate the sulfur content showed that red diesel considered in this study has 250mg/kg compared to 27 mg/kg for the biodiesel. This indicates that biodiesel has sulfur content almost one tenth that of diesel. This would autmatically mean that biodiesel would produces less of the harmful sulfur oxide gas. It is now well-established that green house gases such as carbon-dioxide, carbon monoxide, nitrogen oxide, and sulfur cause destruction of the climate and are a cause of droughts and other environmental disasters for both plant and animal lives.

The sulfur content decreases with the increase in biodiesel content in the mixture as shown in Fig. 7.8(a). However, it is not a linear trend as expected for

ideal solution as mentioned in the above sections. Rather, it follows a $3^{rd}$ order polynomial trend, which could be real or as a result of the accuracy followed. There is no tracks on the literature against which this analysis can be compared with. However, what the results show is that the emission of sulfur dioxide ($SO_2$) is expected to reduce when the two fuels are blended, as the level of sulfur in the blend reduces. It is reported that a 20% blend of biodiesel in heating oil reduces $SO_2$ by around 20% [42].

Table 7.11: Sulfur content for diesel fuel (DF), biodiesel (BD) and surrogate fuels (mg/kg)

| Fuel | DF | B10 | B20 | B30 | B40 | B50 | B60 | B70 | B80 | B90 | BD |
|---|---|---|---|---|---|---|---|---|---|---|---|
| Sulfur | 250 | 220 | 160 | 125 | 105 | 95 | 90 | 86 | 70 | 52 | 27 |

### 7.1.7 Water Content

Water content refers to free water droplets and sediment particles. The permissible range of water content for B100 is set at the same range that is permitted for conventional diesel fuel. But the water content of B100 can easily change if poor drying techniques are used during production or if it stays in close proximity with excessive water during transport or storage. This can lead the water content of B100 beyond its allowable range. Abudance of water can also result in corrosion and can provide a climate for micro organisms. The oxidation of fuel can also increase the levels of sediment, so water content test can be used in combination with acid number and viscosity tests to ascertain the level of oxidization of fuels during storage.

Water content is a parameter that must be controlled in the final biodiesel product and the European Standard EN 14214 [149] therefore imposes a maximum content of 0.05% (m/m) of water in fuels. Felizardo et al. [150] performed measurement of water content on biodiesel made from soybean, mixtures of soybean and palm, and from waste frying oils using the the Karl Fisher titration [151]. Their study has shown that the content of water in the samples ranged from 218 to 1859 $\frac{mg}{kg}$.

In this study, diesel fuel, biodiesel and their nine mixtures were tested to determine the water content variation. The measurements were shown in Table 7.12 and plotted in the graph of Fig. 7.8(b). The data clearly indicates that biodiesel contains much more water than diesel. This is expected and backed by the fact that the production process (Fig. 7.7) of biodiesel involves the addition of water and separating it at later stage depends on the manufacturer and the method followed. The final stage of the purification of biodiesel includes washing it thrice with water. This is done to wash away unwanted by-products that are soluble in water and to remove unreacted catalysts [152]. At the end of this process, the biodiesel may still contain 1800 ppm of water. Many methods including (heating and microgel particles) are used to minimize the water content in biodiesel [153].

The measurement also indicates that the water content increases with an increase in the proportion of biodiesel in the mixture and that the variation follows a perfect linear trend ($R^2 = 0.9954$). The magnitude of water in biodiesel influences the calorific value. Most importantly, it increases the shelf life of the fuel. The oxidation stability also depends on water content. For example, the oxidation stability of a biodiesel which has high water content, is low. Oxidation stability is an important factor as it determines the likelihood of the formation of oxidation products as a result of long-time storage. When the oxidation stability is small, the formation of oxidation products as a result of long-time storage, is highly likely. The engines can face problems because of the presence of deposits, especially in the injection system. That is why, the maximum water content is limited to 500 ppm by DIN EN 14214.

Table 7.12: Water content of diesel fuel (DF), biodiesel (BD) and surrogate fuels (B10–B90)(mg/kg)

| Fuel | DF | B10 | B20 | B30 | B40 | B50 | B60 | B70 | B80 | B90 | BD |
|---|---|---|---|---|---|---|---|---|---|---|---|
| Water | 0.004 | 0.0126 | 0.0232 | 0.0331 | 0.0470 | 0.052 | 0.065 | 0.075 | 0.092 | 0.103 | 0.111 |

### 7.1.8 Acid Number

In chemistry, the mass of potassium hydroxide, $KOH$, (in mgs.) that is needed for neutralizing a single gram of a chemical substance is known as the acid number. It is also referred to as the neutralization number, acid value or acidity. Moreover, it is an estimate of the amount of carboxylic acid groups in a chemical compound, such as a fatty acid, or in a mixture of compounds.

The acid number of a fuel (e.g., biodiesel) is used to specify the amount of acid present in it. It is the total amount of base (in mgs.) of potassium hydroxide, $KOH$, needed for neutralizing the acidic components in a single gram of a sample.

The acid number of biodiesel is mainly an indicator of free fatty acids (natural degradation products of fats and oils). If a fuel has not been prepared well or if it has suffered oxidative degradation, its acid number can be raised. Acid numbers that are above 0.50 have been associated with fuel system deposits and with the reduction of life of fuel pumps and filters.

The acid number can be found using standard methods. These are the ASTM D974 and DIN 51558 (for mineral oils, biodiesel), or the European standard EN 14104 and ASTM D664 (specifically for biodiesel). Both the standard methods for biodiesel are widely used internationally. Acid number (mg KOH/g oil) of biodiesel should be less than 0.50 mgKOH/g in both EN 14214 [149] and ASTM D6751 standard fuels. A reason for this is that high degree of acidity produced, can result in the corrosion of some parts of an automobile. By taking these limits into consideration, engines and fuel tanks of vehicles can be saved.

As oil-fats rancidify, triglycerides are converted into fatty acids and glycerol. This results in increasing the acid number. A similar behaviour is noted with biodiesel ageing through analogous oxidation processes and when subjected to high temperatures for a long time (ester thermolysis) or through exposure to acids or bases (acid/base ester hydrolysis).

In the following analysis, acid number for diesel fuel, biodiesel and nine mixtures, B10–B90 were measured using ASTM D664 [154]. The results are shown in Table 7.13 and plotted in Fig. 7.8(c). It is clear that the biodiesel used in the current experimental work has a low acid value (0.085 mgKOH/g) which is comparable to that of the diesel fuel used (0.065 mgKOH/g). The acid number

increases with increasing the biodiesel percentage in the mixture, best described by a polynomial of order 2. However, the outcome from this analysis is that the measured acid number is low enough not to cause the negative effects mentioned above.

Table 7.13: Water content for diesel fuel (DF), biodiesel (BD) and surrogate fuels (mg/kg)

| Fuel | DF | B10 | B20 | B30 | B40 | B50 | B60 | B70 | B80 | B90 | BD |
|---|---|---|---|---|---|---|---|---|---|---|---|
| Acid Nuber (mgKOH/g) | 0.065 | 0.066 | 0.067 | 0.068 | 0.068 | 0.069 | 0.071 | 0.071 | 0.08 | 0.083 | 0.085 |

### 7.1.9 Nitrogen Contents

D5762 method covers the determination of nitrogen in liquid hydrocarbons, including petroleum process streams and lubricating oils in the concentration range from 40 to 10000 $\frac{\mu g}{g}$ nitrogen. For light hydrocarbons containing less than 100 $\frac{\mu g}{g}$ nitrogen, the test method D4629 can be more appropriate. That is why it has been used to analyse diesel fuel, biodiesel and the nine mixtures (B10–B90) as part of the fuels. The measured values are presented in Table 7.14 and plotted in Fig. 7.8(d). It is clear that biodiesel (B100) contain quite low nitrogen (weight%) compared to diesel fuel. The nitrogen content in the mixture decreases with the increase in biodiesel percentage in the mixture with a trend best described by a polynomial of degree 2.

Table 7.14: Nitrogen content for diesel fuel (DF), biodiesel (BD) and surrogate fuels (B10–B90)(mg/kg)

| Fuel | DF | B10 | B20 | B30 | B40 | B50 | B60 | B70 | B80 | B90 | BD |
|---|---|---|---|---|---|---|---|---|---|---|---|
| Acid Nuber (mgKOH/g) | 73 | 65 | 60 | 56 | 52 | 49 | 46 | 40 | 37 | 36 | 35 |

Of interest to this research is the fact that biodiesel has been shown to increase the emissions of nitrogen oxide ($NO_x$) in many engines on engine stand tests [155] despite the very low content of nitrogen in biodiesel. Thus the increase in $NO_x$ is not associated to the nitrogen content of fuel. $NO_x$ is created in the engine as the

nitrogen in the intake air reacts with oxygen at the high in-cylinder combustion temperatures. A comprehensive review by Sun et al. [155], while, failed to identify a specific cause for changes in $NO$ emissions between biodiesel and petroleum diesel fuel, does collect all the important parameters that are likely to contribute to such changes and qualitatively summarizes them.

The literature has reported contradictory claims showing that $NO_x$ increase (but not always) observed for B20 is believed to occur mainly at low engine speeds but high load (or torque) conditions. It might be more useful to test complete vehicles to predict the real-world impact of emissions than to only perform engine stand tests. This is one of the objectives of this proposed work, to test more than one surrogate fuel in a diesel engine and identify the exact output of $NO_x$.

### 7.1.10 Boiling Point

The boiling range distribution of petroleum fractions is a good indicator and is commonly used to provide an insight into the make-up of feedstocks and products related to the refining processes of petroleum. The gas chromatographic simulation is a modern approach for measuring the BP for such fuels and has been continuously used to replace conventional distillation techniques for control of refining operations. This technique can be used for the testing of product specifications if the concerned parties agree to do so.

Biodiesel boiling range material is of particular interest because it has been shown to significantly reduce particulate emissions relative to petroleum diesel [156]. Fuel spray atomization and penetration affect air mixing and evaporation rate, are affected by a fuel's composition, viscosity, density, surface tension, bulk modulus, and BP [157, 158, 159].

Many techniques have been shown to minimize soot formation in biodiesel, including decreased BP [75] among others such as: increased fuel-bound oxygen, lower stoichiometric air-fuel ratio, reduced concentration of aromatics, advanced start of combustion, changed soot particle structure, decrease of fuel-bound sulfur, and different sooting characteristics of various biodiesel esters [160]. It has been shown in Ullman et al. [161], that the high oxygen content and low sulfur content of biodiesel fuel are two of the most important parameters showing comparatively

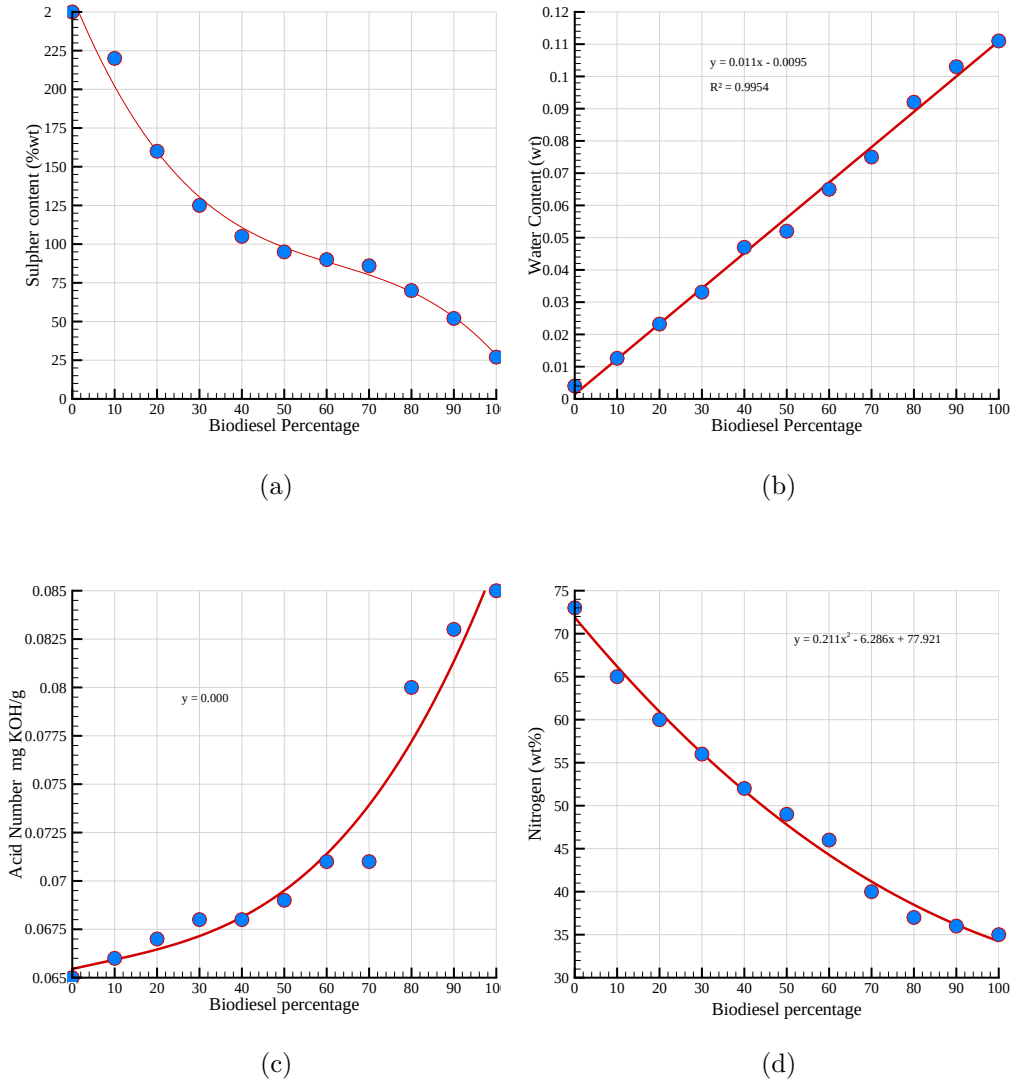


Figure 7.8: (a) Sulfur content variation, (b) Water content variation, (c) Acid number, and (d) Nitrogen content

low formation of particulate matter with respect to petroleum diesel. The general mechanism affected by increased oxygen is summarized by Nylund et al. [162]: the presence of fuel-bound oxygen suppresses soot nucleation early in the formation on the fuel side of the mixing-controlled flame. This nucleation suppression inhibits peak soot production, leads to more complete burning, and reduces the formation

of soot precursors (cracked hydrocarbons such as acetylene and ethylene).

The ASTM D2887 test method is used to ascertain the distribution of boiling range of different petroleum products. This technique is normally used for petroleum products and fractions that have a final BP of 538 °C (1000 °F) or lower at the atmospheric pressure that is calculated by this technique. This technique is limited to samples having a boiling range greater than 55.5 °C (100 °F), and having a vapour pressure low enough to allow sampling at ambient temperature. The method is used to measure the BP of diesel fuel, biodiesel and the nine surrogate fuels (B10–B90). The obtained data is plotted in Fig. 7.9. The figure clearly indicates that the BP of diesel fuel, biodiesel and their surrogates (B10–B90) is of order 350$^o$C. However, the difference comes from the fact that biodiesel reaches this range with almost no change in the mass % while the others reach this point at increased mass percentages.

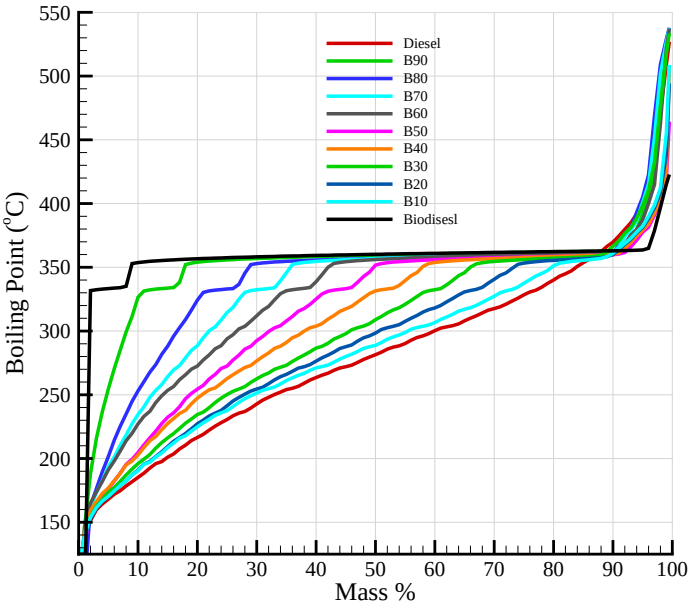


Figure 7.9: Boiling point

### 7.1.11 Oxygen Behavior and Stability

In the literature, some works emphasize that biodiesel is an oxygenated fuel. This implies that its oxygen content is important in making fatty compounds fit to be used as diesel fuel with the help of cleaner burning. However, this mainly depends on the hydrocarbon portion which is very similar to that of standard diesel fuel. Moreover, it is possible to remove the oxygen in fatty compounds from the combustion process with the help of decarboxylation process, which yields incombustible $CO_2$, as precombustion [163], pyrolysis and thermal decomposition studies discussed below, imply. Also, the CNs of pure unoxygenated hydrocarbons are higher than those of biodiesel. The oxygen content of fatty alcohols is smaller than that of the corresponding esters. Moreover, when their CN values are computed using ASTM D613, they are higher than those of their corresponding methyl esters as found using ASTM D613. For example, the CN of 1-tetradecanol is 80.8 [164]. The CNs of fatty alcohols also increase with an increase in chain length. 1-pentanol has a CN of 18.2 [164]. The CNs of 1-hexadecanol and 1-octadecanol have not been found in this work due to their high melting points [164]. Having said that, its ignition delay was measured with the help of Constant Volume Combustion Apparatus (CVCA) vessel. It is worth mentioning that when CVCA was employed, the CNs of some of the fatty alcohols were found to be lower. It has been shown that the CNs of Fatty ethers [165] are higher compared to the corresponding fatty esters and have been recommended as diesel fuel extenders. Compared to esters, their main drawback is their complex synthesis.

The stability of a fuel could mean two things: (i) the stability of the fuel with respect to long-term storage or ageing, or (ii) the stability of a fuel at high temperatures or pressures as the fuel is recirculated through the fuel system of an engine. For petroleum diesel, the former is commonly known as oxidative stability while the latter is commonly called thermal stability. For B100, oxidative stability is of prime importance. Thus, ASTM D6751 specifies oxidation stability as a necessary condition. The oxidation stability test, EN14112 (also referred to as the Oil Stability Index (OSI) or the Rancimat test) has the following stages: first a particular amount of B100 is heated to 230 °F (110 °C) while air is bubbled

through at a particular flow rate. The air is then passed through a water bath that gathers the turbulent acids formed during oxidation. The water is monitored with the help of a conductivity meter. In these conditions, a stable B100 can be used for a long time and it will not produce any turbulent oxidation products. This span of time, before the formation of oxidation products, is called the induction time/period. According to D6751, B100 is required to have an induction time of at least three hours. Since, at the time of blending, this requirement is used, B100 is usually made with an induction time of four to five hours. The oxidation and ageing of biodiesel fuel is undesirable. It can increase both the acid numbers and viscosity. Moreover, as a result, gums and sediments can form which can block filters. The increase in acid numbers and viscosity can degrade B100 significantly i.e., it may not meet the requirements for D6751, and thus, making it not fit for use. A biodiesel fuel which has a high oxidation stability takes more time to reach this undesirable state compared to one with low oxidation stability. The oxidization of B100 can be assessed by regular monitoring of its acid number and viscosity. Thus, on purchase, it can be useful to test the B100 to make sure that it meets the specification.

It is apparent that for pure diesel and biodiesel, establishing the stability of the fuels is easy and well-characterised. However, for surrogate fuels, many questions of interest pop up. Of interest to this work was to establish the most possible information about the surrogate fuels, both from composition point of view as well as stability issues. To facilitate this point, a Fourier Transform Infra-red spectrophotometer model FTIR-8300 was used to obtain a spectra that could help in elucidating the composition of the surrogate fuels. Table 7.15 and Table 7.16 show the characteristic infra-red absorption want-embers of some functional groups and pattern of Benzene rings - it is the only data-analysis that one can rely on to inspect the resultant mixture composition. Two spectra were obtained, ten days apart. This was done to inspect the impact of storing surrogate fuels and to investigate any changes in composition.

The initial spectra for diesel fuel, biodiesel, B10 and B20 are shown in Fig. 7.10. Fig. 7.11 displays the spectra for B30 and B40, B50, and B60, while Fig. 7.13 shows the spectra for B70 and B80, B90, and (diesel fuel, biodiesel, B20, B40, B60 and B80) in one graph for the sake of comparison. With reference to Table 7.15

Table 7.15: Characteristic infrared absorption wavenumbers of some functional groups

| **Group** | **Type of Compound** | **Wavenumber** ($cm^{-1}$) | **Intensity** |
|---|---|---|---|
| -O-H st | Alcohols, phenols | 3650–3590 | Variable, sharp |
| -O-H st | Hydrogen bonded alcohols & phenols | 3400–3200 | Strong, broad |
| -$NH_2$ & =NH st | Hydrogen bonded amines | 3400–3100 | Medium |
| -$NH_2$ st | Amines (primary) | 3500–3300 double peak | Medium |
| =NH st | Amines (secondary) | 3500–3300 single peak | Medium |
| -O-H st | Hydrogen bonded acid | 3200–2500 | Variable, broad |
| ≡C-H st | Alkynes | 3250 | Strong, sharp |
| =C-H st | Alkenes & arenas | 3100–3010 | Medium |
| -C-H st | Alkanes | 2960–2850 | Strong |
| -O=C-H st | Aldehydes | 2900–2700 | Weak |
| -C≡N st | Nitrites | 2300–2200 | Strong |
| -C≡C- st | Alkynes | 2260–2150 | Variable |
| -C=O st | Acid chlorides | 1815–1790 | Strong |
| -C=O st | Aldehydes | 1740–1720 | Strong |
| -C=O st | ketones | 1740–1705 | Strong |
| -C=O st | Acids & esters | 1750–1700 | Strong |
| -C=O st | Amides | 1650 | Strong |
| -C=C- st | Alkenes | 1660–1610 | Weak |
| -$NH_2$ def | Amines (primary) | 1620–1600 | Medium |
| -NH def | Amines (secondary) | 1600–1560 | Weak |
| -C=C- st | Arenas | 1600–1500 | Medium |
| -$NO_2$ st | Nitro-compounds | 1550–1350 | Strong |
| -$CH_2$ & -$CH_3$ def | Alkanes | 1460–1430 | Strong |
| -$CH_3$ def | Alkanes | 1390–1370 | Medium |
| -C-O- st | Alcohols, ethers, acids, and esters | 1300–1000 | Variable |
| -O-H def | Acids | 1000–940 | Medium, broad |
| =C-H def | Alkenes & arenes | 950–700 | Variable |

Table 7.16: Substitution patterns of the banzene ring

| Group | Band | Description |
|---|---|---|
| Five adjacent hydrogens | 770–730 strong | Mono-substitution |
| Four adjacent hydrogens | 770–735 strong | Ortho-substitution |
| Three adjacent hydrogens | 810–750 strong | Meta-substitution |
| Two adjacent hydrogens | 860–800 strong | Para-substitution |
| Isolated hydrogens | 900–800 weak | Meta-substitution |

and Table 7.16, there are few distinct features one can read and summarised as follows:

- Band 1: this is a band at wave numbers between 3900–3800 common to all surrogate fuels (B10–B90) and barely apparent for diesel fuel and biodiesel and at higher wave numbers. This band mainly corresponds to water content.
- Band 2: the second major band is centred at around a wave number of 2900 and with reference to Table 7.15, this band represents the presence of alkanes $(-C-H)$ and aldehydes $(O=C-H)$
- Band 3: this band is centred at a wave number of 1740 and with reference to Table 7.15, this band represents the presence of aldehydes $(-C=O)$ which are different in microstructure than those in the second band.
- Band 4: the third band is followed by a weak band concentrated in the wave number 1200 and with reference to Table 7.15, this band represents the presence of alcohols, ethers, acids and esters with the microstructure of the type $(-C-H)$.

It is apparent that the $O_2$ atoms that exist in the structure of biodiesel has led to a diverse structure in the surrogate fuels. With reference to Table 7.15, the bands described below vary in their strength. For example B90 shows quite strong Band 2 compared to B80 which probably means that the presence of aldehydes increases with an increase in biodiesel content in the surrogate. The comparison done between diesel fuel, biodiesel and B20, B40, B60 and B80 shown in Fig. 7.13 $(d)$ does show the variation of the band strength with respect to each fuel.

After storing the samples for ten days, another round of spectral analysis was performed using the same instrument. The purpose of this second analysis was to establish whether the surrogate fuels show any reactions leading to fundamental changes in their structures.

Fig. 7.14 displays the spectra for B10 and B20, B30, and B40, while Fig. 7.13 shows the spectra for B50 and B60, B70, and B80. Each figure shows the old (ten days old) and the newly established spectra. In comparison with the spectra taken ten days earlier, it is apparent that the water contents increased in the surrogate fuels with water band showing a band at higher wave numbers while the surrogate fuels are stored. There are also some variations of the other bands with the spectra taken ten days later showing stronger signals although not for all fuels. This strongly indicates that storing biodiesel and its surrogates may lead to reactions leading to different microstructure of the fuels. This strongly indicates that biodiesel should be used immediately after production or some sort of legislation should be established to limit the storage of biodiesel to a limited period of time.

## 7.2 Diesel Engine Anlysis

During the late nineties and early 2000s, many studies were conducted to investigate the impact of using various mixtures of oxygenated additives of fuel in gasoline and diesel engines. These studies also measured the performance, efficiency and emission characteristics of engines. A swirling turbulent jet diffusion flame was utilized in place of an ICE. This was done for two reasons: (i) to make measurements of emissions in a well-characterized, steady flame and (ii) not to be dependent on the operating parameters of the engine. The parameters that effect emissions (unburned hydrocarbon emissions ([11, 166, 167, 168, 32, 169]), and $NO/NO_x$ formation ([11, 166, 167, 168, 32, 169, 170]) are: speed, loading, fuel injection and ignition timing. However, the focus of most of these studies was on mixtures with fuel-bound oxygen mass fractions, denoted as $YO$, $FB$, of less than 10%. This is mainly the result of operational and practical limitations of the engines and the fuels used. The gist of the earlier studies is that the adding oxygenated additives of fuel can increase the efficiency of an engine

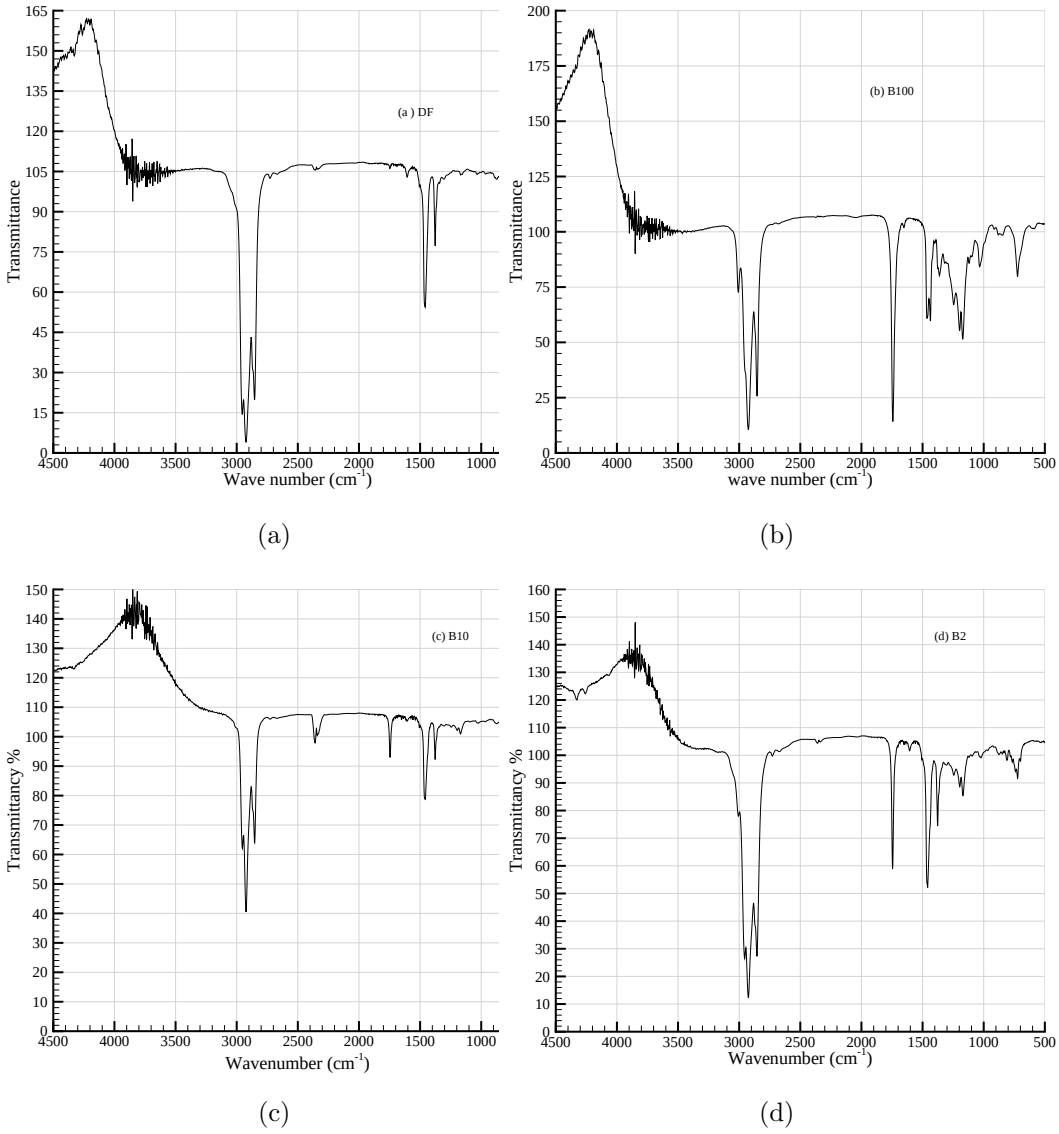


Figure 7.10: Transmittance wave number spectra for diesel, biodiesel, B10 and B20.

but it can also increase $NO_x$ formation ([11, 171, 168, 169, 172]). The work in [11, 171, 168, 32, 169] has shown, that increasing $YO$, $FB$ beyond a critical value can minimize the $NO_x$ emissions. The mechanism and its parameters have not been studied in detail, especially, the parameters that are responsible for the peak in the formation of $NO_x$ as a function of $YO$, $FB$. The combustion char-

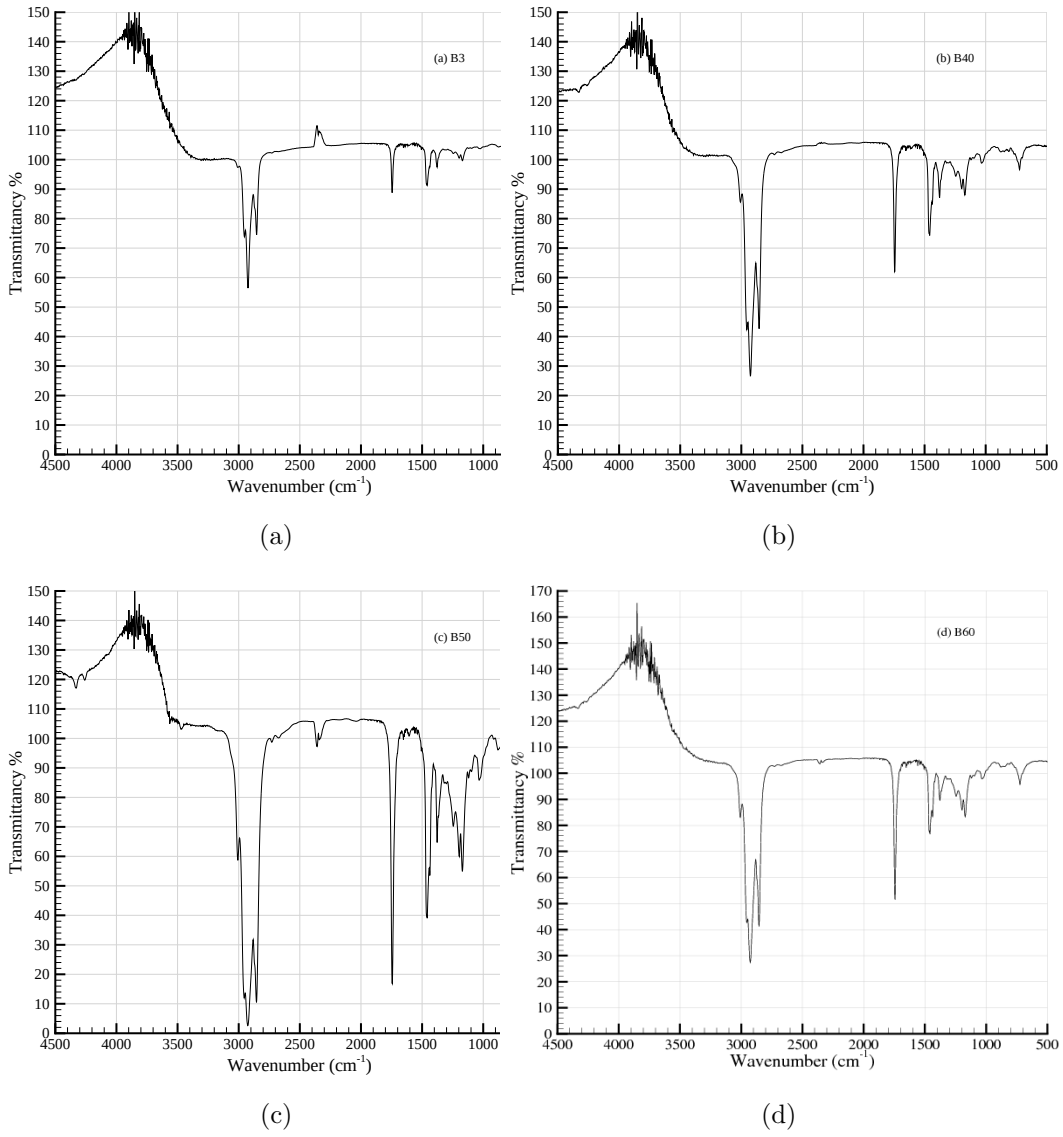


Figure 7.11: Transmittance wave number spectra for B30 and B40, B50 and B60.

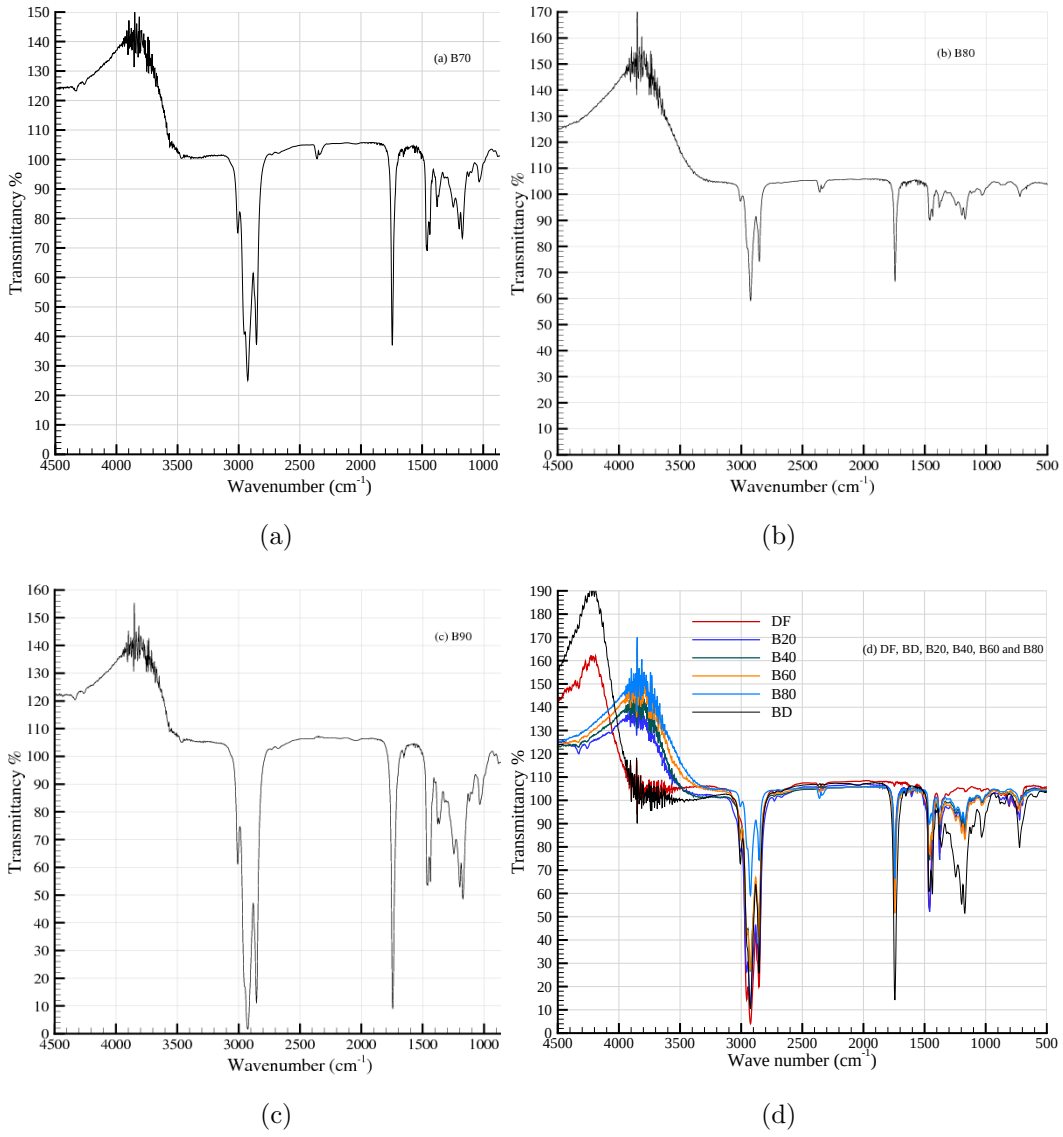


Figure 7.12: Transmittance wave number spectra for B70 and B80, B90 and (diesel fuel (DF), biodiesel (BD), B20, B40, B60 and B80) in one graph.

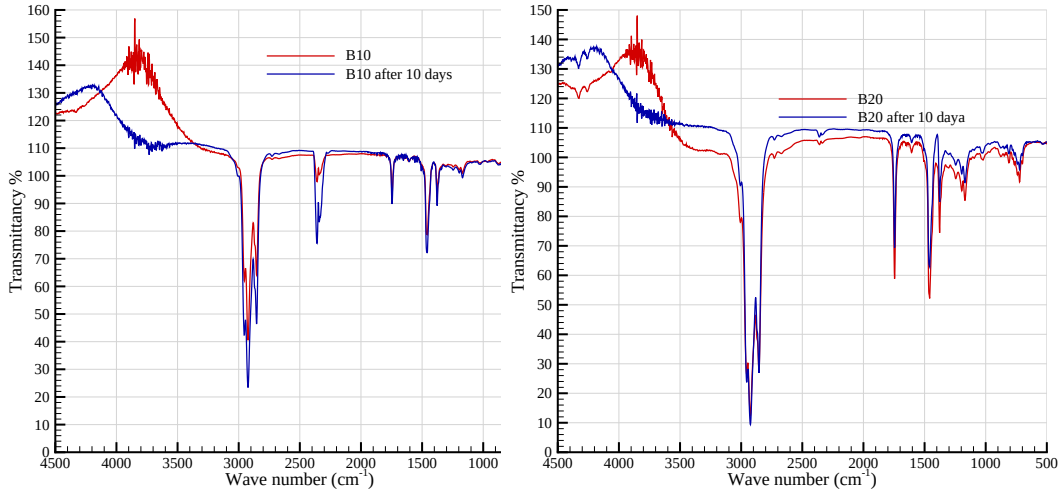


Figure 7.13: Transmittance wave number spectra for B10 and B20, B30 and B40 before and after ten days storage period.

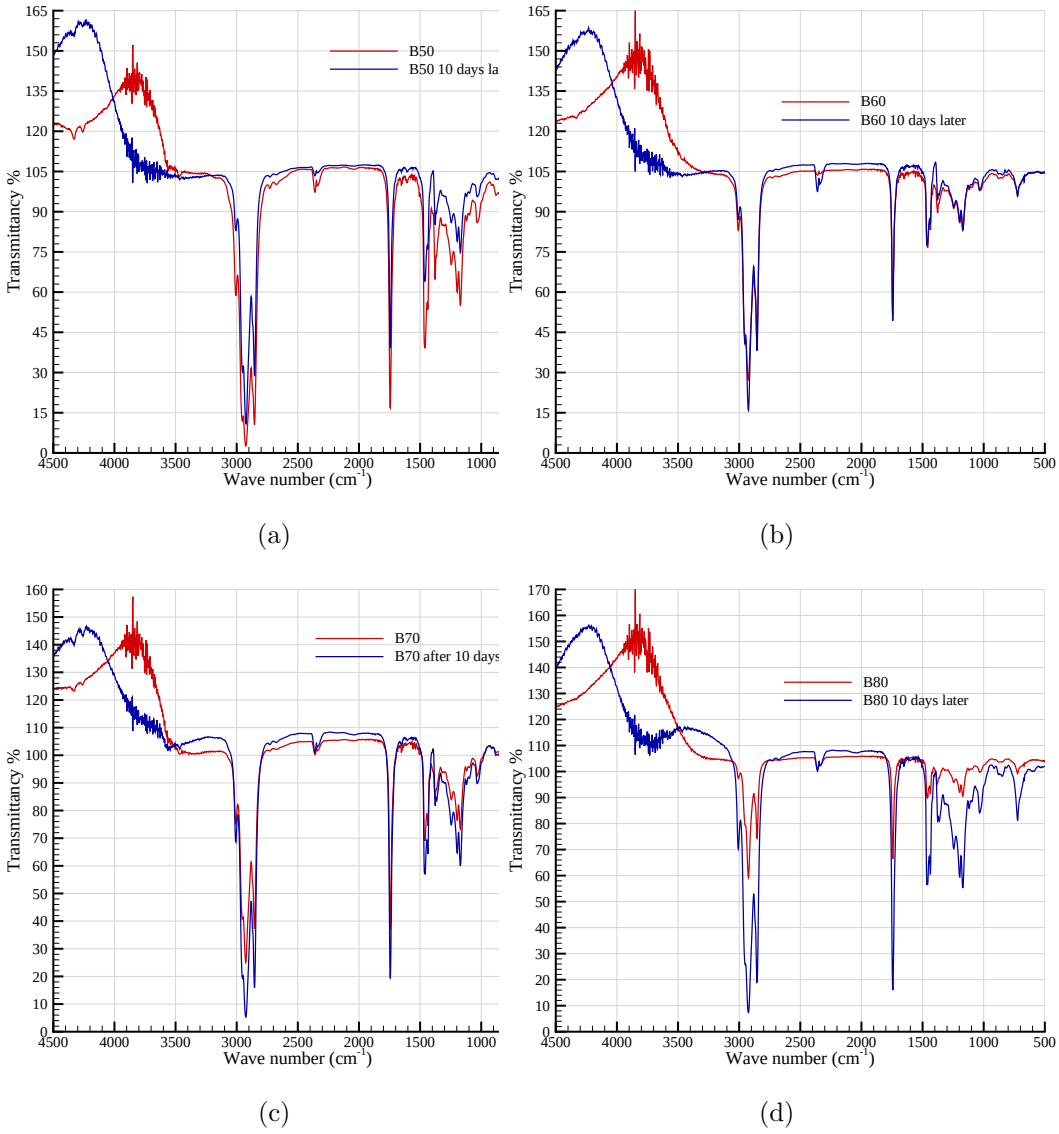


Figure 7.14: Transmittance wave number spectra for B50 and B60, B70 and B80 before and after ten days storage period.

acteristics of very high $YO$, $FB$ fuels has been studied in even lesser detail. To improve combustion emissions from more conventional fuels, using fuels with high $YO$, $FB$ can be useful since their combustion results in lower formation of $NO_x$. That is why, the main aim of this study was to investigate the $NO_x$ emissions from the combustion of glycerol, C3H5(OH)3, which is 52% oxygen by mass, in

a high-swirl turbulent jet diffusion flame at atmospheric pressure.

Glycerol was selected as a sample fuel because of its high $YO$, $FB$ and potential benefits of using this by-product of the transesterification process as a boiler fuel for on-site process heat in a biodiesel production facility ([173, 33]). For a comprehensive review of almost all the work on how biodiesel is used in CIEs, the reader is advised to consult a recent review in this matter presented by Sadeghinezhad et al. [134].

Following the general investigation of the main characteristics of diesel, biodiesel and surrogate fuels (B10–B90), a diesel engine was tested with give fuels including diesel, biodiesel, B25, B50 and B75 as representatives for conventional, biofuels and surrogate fuels. The engine's main specifications are shown in Table 7.17. Fig. 7.15 shows the main test rig components that are worth acknowledging. Figure 7.15 ($a$) shows the engine setup including the dynamometer. The fuel mixing tank is shown in Fig. 7.15 ($b$) where a pump seen below the tank is used to stir and provide a good mixture of the three surrogate fuels. Fuel was supplied to the engine from this tank passed by the fuel meter seen in Fig. 7.15 ($c$). Measuring the fuels is a rather crude procedure where the time for the engine to consume 10 ml of fuel is measured based on which fuel consumption is calculated taking fuel density as 842.4 $\frac{kg}{m^3}$

The engine was tested at one speed of 2000 rpm at five loads measured as a strain (units in volts) and the brake horse power is obtained using the relation:

$$BHP = \frac{WeightLoad(involts)}{4500} \times \frac{100}{0.6} \times N$$

All runs started with a reasonable time (one hour) warm-up period prior to data collection. A short period (of order ten minutes) is also allowed upon changing the load before collecting relevant data for the new load. Finally, a sample of the exhaust gas is passed through a gas analyser that is recently installed in the engine test cell, which measures emissions in tons of carbon oxides ($CO$ and $CO_2$), nitrogen oxides ($NO_x$) as well as the total unburned hydrocarbon. Bosch opacity and Bosch smoke number were also obtained via a specific device that processes traces of smoke collected on pressed paper discs exposed to the engine exhaust. Fig. 7.16 is a schematic diagram showing how the test rig has been connected.

The data obtained are processed and discussion here will be limited to some specific parameters to complement both the experimental and computational work that is performed on the fuels and their combustion processes.

All parameters under consideration here are plotted against the Brake Mean Effective Pressure (BMEP). BMEP is considered as measure or indicator of an engine's capacity to do work that is independent of engine displacement, which is a design parameter. In this way, it is thought that a comparison of the different thermal performance and emission characteristics of the engine using different fuels will be viewed independent of the geometrical and design parameters of the engine, rather comparison will take the physical operating conditions into account.

Figure 7.15: (top-left) Ford Transit 4-Stroke DI Diesel Engine & Dynamometer, (top-right) Fuel mixing tank and , (bottom-left) Fuel Meter, (bottom-right) Total Unburned Hydrocarbon (THC) and $NO_x$ Emission Analyser

Table 7.17: Diesel engine specifications

| | |
|---|---|
| Model | Ford Transit |
| Type | 4-cylinder in-line overhead valve |
| Injection method | 2 Direct injection |
| capacity | 2496cc |
| Bore | 93.67mm |
| Stroke | 90.54mm |
| Compression Ratio | 19:1 |
| Rated power | 68 BHP |

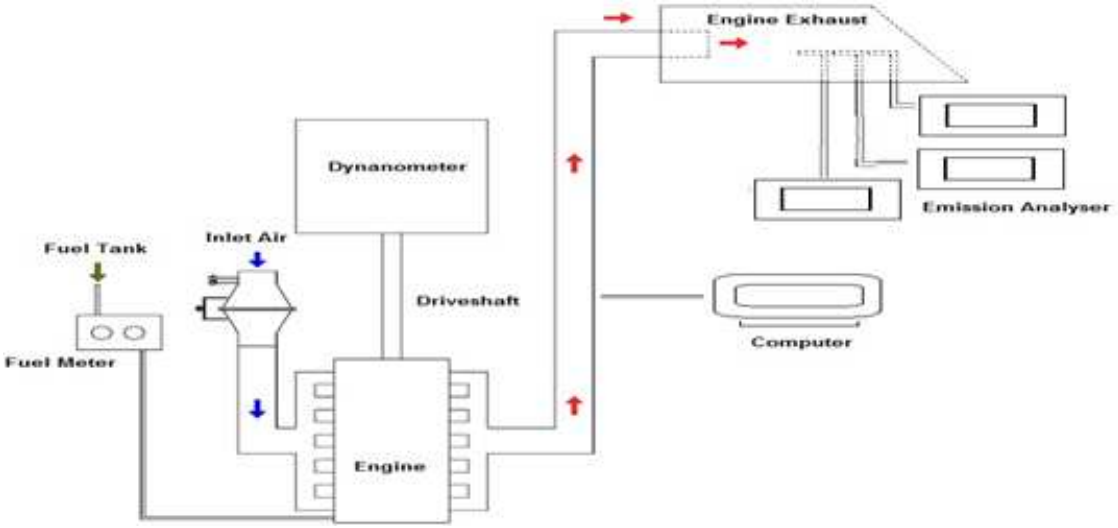


Figure 7.16: Schematic Diagram of Experimental Setup

### 7.2.1 Thermal Performance Analysis

Indicated power, rated on fuel consumption and relevant calorific value of fuels represent the energy released from burning the fuels. Theoretically, and based on the energy content (calorific value of diesel and biodiesel), one would expect diesel to produce the highest indicated power, followed by B25, then B50, then B75 followed by biodiesel. However, Fig. 7.17(a) agrees little with the theoretical expectation. Indicated power from diesel is the highest at all loads at a constant speed of 2000 rpm which is in line with most of the cited work in the paragraphs

above. B25 follows diesel, producing the next to diesel indicated power which still follows the logic that more diesel in the surrogate means more energy. However this trend is broken after B25 as biodiesel record the third highest energy after B25, followed by B50 then B75. B75 scoring less than B50, is according to the theoretical expectations. However, the question is why biodiesel, expected to produce the least indicated power, scored higher than its surrogates B50 and B75? To answer the question, one needs to remember that these tests are not performed on a calorimeter, rather, they are used in a CIE. At this point, one would go back to Section 5.2 where the CFD results from the combustion of biofuels indicate that it burns slower than diesel and hence this (longer delay period) allows a longer flame and hence a higher temperature within the burner computational domain. Although the issue of density is not apparent there, in the case of the experimental work, biodiesel density and purity may play a role in the gasification and burning processes. This may prolong the life of a droplet in comparison to diesel and could be one of the reasons why biodiesel scored higher indicated power than its surrogate B50. The longer combustion process with continuous heat released may lead to both higher temperatures and higher released energy. However, a similar feature was observed in the CFD modelling, which is the result of the performance of the advanced reaction model and the influence of the two-oxygen atoms associated with biodiesel. Physically, this would definitely play a vital role in the combustion of biodiesel in the compression ignition engine used in this experimental work. However, to quantify the significance of each effect (density and viscosity on one side and the existence of oxygen atoms on the other) is difficult and needs much more sophisticated equipments and engine runs under varying operation conditions.

The Air/Fuel (A/F) ratio for the five fuels is shown in Fig. 7.17(b) which suggests that the higher the load on the engine (low BMEP), the higher the A/F ratio. That is a typical behaviour, however, it is noticeable that biodiesel, followed by B25 has the lowest A/F ratio followed by diesel, while B50 and B75 have the higher A/F ratio. One needs to remember that the test was carried at the same speed and loading conditions. The fact that biodiesel has the lowest A/F ratio indicates that less air is required to burn biodiesel compared to diesel. This can be explained by the oxiginated nature of biodiesel, however, one needs

to be careful about the exact pace and reaction steps that occurs for the two fuels which could be very different and the outcome of the combustion would also vary both in terms of emissions and rated power. This point was reflected when discussing the CFD work on modelling diesel and biodiesel.

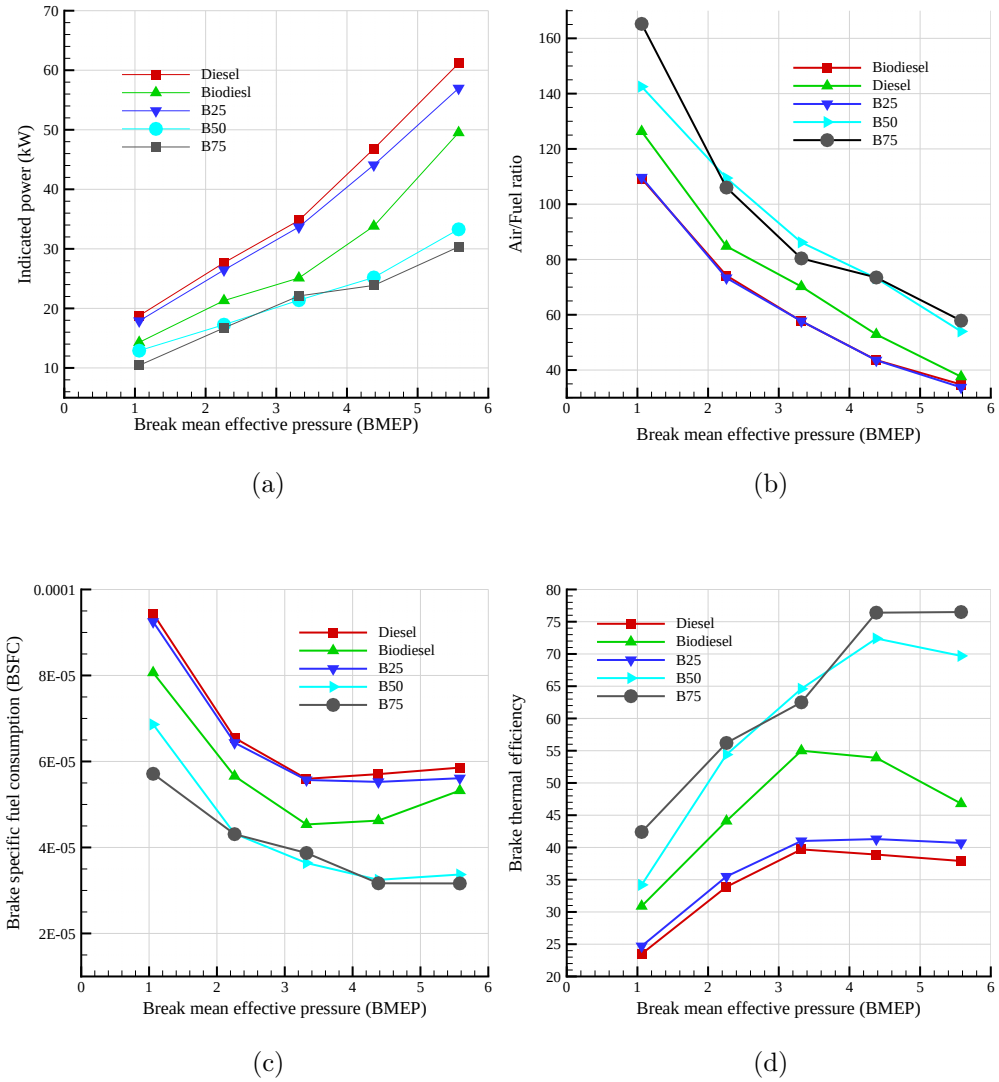


Figure 7.17: (a) Indicated power, (b) Air/Fuel (A/F) ratio, (c) Specific fuel consumption, and (d) Brake thermal efficiency

The Specific Fuel Consumption (SFC) for the five fuels under the same speed

(2000 rpm) and loading conditions is plotted in Fig. 7.17(c). It is clear that the fuel consumption of diesel is the highest followed by B25, then biodiesel with B50 and B75 lagging. One would mention first that both the consumption in kg/s and kg/kWh is very small and some of the results reflected in Fig. 7.17(c) could be due to experimental errors and measurement discrepancies. However, testing the engine more than once and comparing this data with previous work on the engine using the same biodiesel supplier showed similar results. As energy content of diesel is higher than biofuel (calorific value of diesel is taken as 45MJ/kg compared to 40MJ/kg for biodiesel), one would expect the fuel consumption would be less for the diesel compared to biodiesel under similar speed and loading conditions. The only way to explain what is seen in Fig. 7.17(c) would be based on the combustion process of the two fuels in the experimental setup. It is apparent that biodiesel burns more efficiently than diesel hence releasing most, if not all, of its energy in a good timing (longer delay period) hence satisfying the engine loading conditions. However, the author of this thesis believe that the engine used is slightly old and more sophisticated equipment may be required to draw a conclusion on this point. B50 and B75 are the most efficient fuels for the diesel engine under consideration. Again this can only be attributed to the nature of the mixture. With reference to the spectra of these two fuels, it is apparent that the oxygen signature is significant and that is most likely the reason behind the efficient combustion of such fuels leading to lower fuel consumption and higher thermal efficiency..

Following the sfc, the brake thermal efficiency is expected to display relevant behaviour as shown in Fig. 7.17(d) with diesel and B25 the least efficient fuels.

### 7.2.2 Emission Analysis

Having examined the thermal performance of the engine, this section will look at the emission from the diesel engine while operating at the same speed under the five loads. The gas analysers available can only detect carbon oxides ($CO$ and $CO_2$), Nitrogen oxides ($NO$ and $NO_x$) and total unburned hydrocarbons. The smoke measurements are obtained in terms of Bosch smoke number and Bosch smoke opacity.

The measured values for carbon monoxide ($CO$) from the five fuels under the five loads with the engine running at 2000 rpm are plotted in Fig. 7.18(a). It is apparent that biodiesel produces a high rate of $CO$ at both low and moderate loads although the level drops at high loads. Having said so, biodiesel produces high level of $CO$ at all loads compared with diesel. Out of the surrogate fuels, B25 produces a higher rate $CO$ compared to B50 and B75. $CO$ is an indication to incomplete combustion in general. Both the CFD computations and the thermal performance of the experiment in this chapter strongly indicates that under the same conditions, biodiesel droplets may have longer life compared to diesel, which explains the relatively higher rate of $CO$ in the case of biodiesel. What needs more explanation is the fact that B25 produces higher rates of $CO$ compared to B50 and B75. More micro-level investigation to such surrogate fuels is needed to explain why such mixtures behave in a way that defies the logical theory.

Carbon dioxide ($CO_2$) measurement from the engine is shown in Fig. 7.19(a) for the five fuels that have been experimented with. It is apparent that the rates are high for all the fuels with low loads and decrease gradually with increasing load. Again biodiesel produces higher rates of $CO_2$ compared to diesel at all loads with the exception of the second and last loads corresponding to bmef of order 2.25 and 5.5 respectively, which can be explained as due to experimental errors that might be associated with the measuring instruments. Hence, one can conclude that the current experiments agree with those studies listed in Table 2.2 which indicate that biodiesel produces higher rates of carbon oxides when it replaces diesel in CIEs.

It would have been of great benefit if the surrogate fuels were stored for ten days and were used in the engine to see whether the chain reaction that took place as a result of storing biodiesel and its surrogates and the increased rate of water production has any effect on the thermal performance and emission from the diesel engine. However, in these closing stages, one can only recommend this for further work in this topic.

Nitrogen oxides ($NO$ ans $NO_X$) for the five fuels under the five loads with the engine running at 2000 rpm are respectively shown in Fig. 7.18(b) and 7.19(b). A similar trend is reported for the $NO$ and $NO_x$ with biodiesel recording higher rate of $NO$ and $NO_x$, followed by the other three surrogate fuels which more or

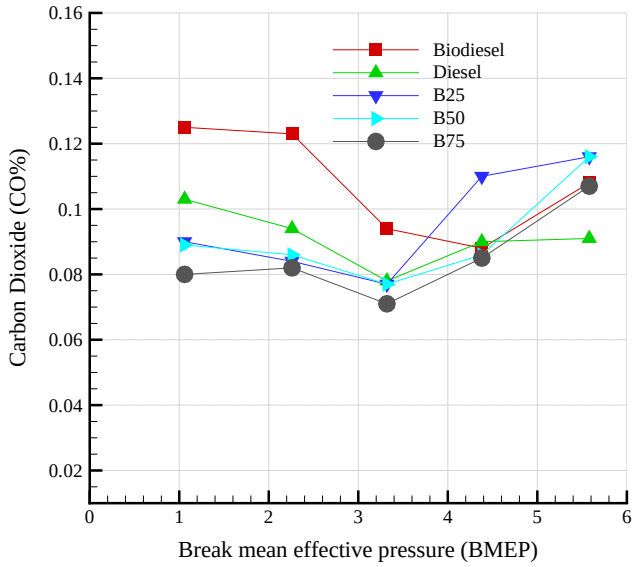


(a)

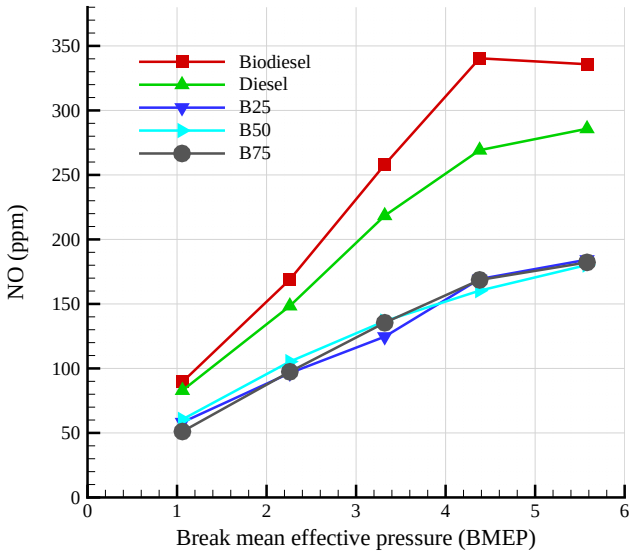


(b)

Figure 7.18: (a) Carbon monoxide ($CO$) and (b) Nitrogen oxide ($NO$).

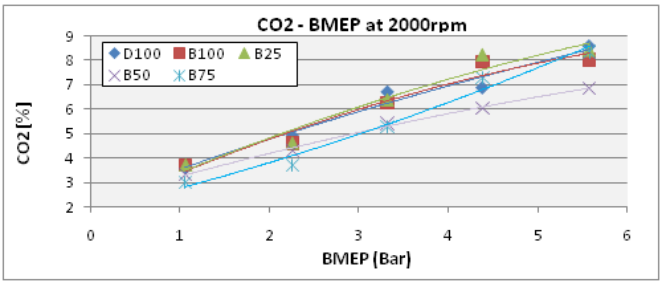


(a)

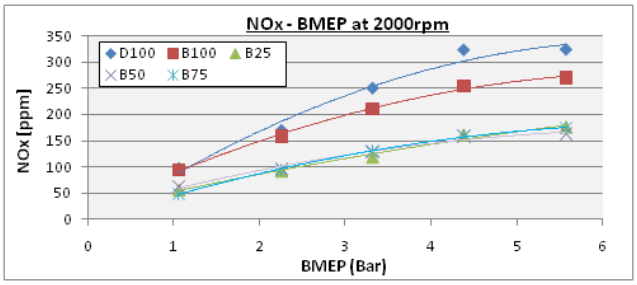


(b)

Figure 7.19: (a) Carbon dioxide ($CO_2$) and (b) Nitrogen oxide ($NO_x$)

less produces the same rates of $NO$ and $NO_x$. There seems any conflicting results here, clear that biodiesel produces both higher rates of $NO$ and $NO_x$ compared to conventional diesel, however, the surrogate fuels produces far less $NO$ and $NO_x$ than pure biodiesel and diesel, a strong indication to the fact that the way forward is not really using biodiesel as a replacment for diesel, rather a surgoate fuel that optimise both the themal and emissions from CIEs should be sought.

The smoke measurement in particle per million (ppm) has been assessed using two parameters, the Bosch Opacity and the Bosch Smoke Number shown respectively in Fig. 7.20(a) and Fig. 7.20(b). This is done using two types of instruments, an opacity meter, which evaluates smoke in the exhaust gas, and smoke number meter, which optically evaluates soot collected on white disc paper filters. The results clearly show that for low and moderate loads biodiesel produces the lowest level of smoke. However, at high loads, biodiesel produces incredibly high level of smoke in the form of particulate matters. In the opinion of the author, the results seem logical. As biodiesel is denser, more viscous with higher impurities compared to diesel, this makes it difficult to atomise as fine

as diesel. As a result, one would expect burning biodiesel would produce higher rates of smoke than diesel. However, on the other hand, the combustion process of biodiesel is totally different from that of diesel because it is chemically different with embedded oxygen atoms that may influence its combustion. One would expect that at low and moderate loads, biodiesel would burn in a fashion that produces less particulate matters.

Finally, the total unburned hydrocarbon measurements were shown in Fig. 7.20(c). It is apparent that biodiesel has a significant unburned hydrocarbon content followed by diesel with the three surrogate fuels lagging. The higher rates of unburned hydrocarbons in the case of biodiesel is expected as both computational results and experimental work support it. As discussed in Section 4.3, one of the reason the EGRM model predicted high temperature when modelling the combustion of methyl docanoate is due to the fact that the model predicted a long flame region which is attributed to droplet of the fuels travelling longer distance along the vertical axis. This fact was also supported by examining the rate of unburned methyl decanoate in Fig. 7.20(c). However, in the case of experimental work, the rate of unburned biodiesel may be aggravated further by the impurities and the difficulty of atomising using the same infrastructure designed to atomise diesel which is lighter (less density) and less viscous than biodiesel. The result will be larger diameter droplet for the atomised biodiesel compared to diesel which gives it a chance to travel further and most chances that part of it will not be completely burned. Having said so, this might be one reason only that is leading to the results seen in Fig. 7.20(c) as the kinetic of combustion could also affect the combustion of biodiesel. One would also observe in Fig. 7.20(c) that the surrogate fuels (B25, B50, and B75) produce the least unburned rate of unburned hydrocarbon. This indicates that surrogate fuels may be the best alternative for operating existing diesel engines.

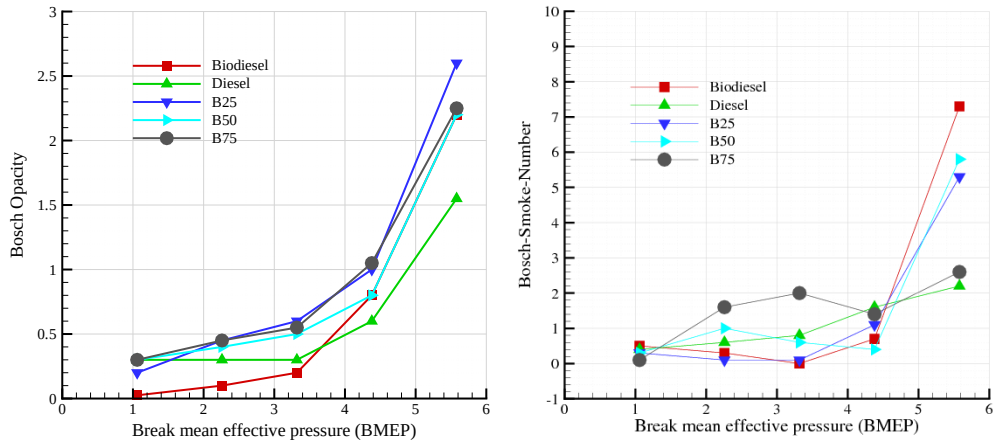


(a) (b)

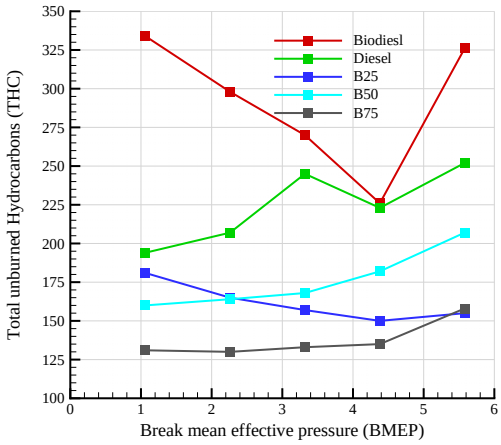


(c)

Figure 7.20: (a) Bosch opacity, (b) Bosch smoke number, and (c) Total unburned hydrocarbon.

# Chapter 8

# Conclusions and Recommendations for Further Work

The work in this thesis included extensive CFD computations and experimental work and was aimed to address the outcome of spray combustion of conventional, bio- and surrogate fuels in both a burner geometry and in a CIE. Both the computational results and the experimental work examined the thermal performance and the emission rates of a diverse range of fuels in the two combustion infrastructures. The work has yielded many important results, most of which are in line with the theory and agree with the literature, while few minor points may need further investigation to confirm their validity although nothing is controversial. The outcome from this thesis can be summarised in the following paragraphs.

The spray combustion of liquid methanol ($CH_3OH$), a low-carbon fuel, was modelled in a burner following experimental work of Widmann and Presser [1], using both San Diego reaction mechanism and another mechanism developed using the EXGAS software. These simulations were used as a validation route for the simulation setup as well as for testing the new mechanism developed using the EXGAS software. The outcome from these initial tests has shown a good agreement between the experimental data of Widmann and Presser [1] and the predicted results in both the temperature field and available data from

the by-products of combustion (particularly $CO$, $CO_2$ and $H_2O$). In fact, the developed comprehensive reaction model has shown better prediction for the by-products than the San Diego reaction mechanism which strongly supports the fact that including more reaction mechanisms and reaction steps is essential for accurately predicting the by-products of combustion. On the other hand, the comprehensive mechanism has shown relatively higher temperature range than the prediction of San Diego reaction mechanism and the experimental data. Also, there is evidence that it slows down the combustion kinetics. Whilst, the author is not inclined to criticise the output from both the reduced (San Diego) mechanism and the experimental data, it is worth to point out that Widmann and Presser [1] mentioned a level of inaccuracy in their measurement. Considering this last point, one would still conclude that the predicted results using the developed comprehensive mechanism are good.

The second phase of the simulation considered modelling large hydrocarbons, taking decane ($C_{10}H_{22}$) from conventional fuels and methyl decanoate ($C_{11}H_{22}O_2$) from biofuels family. The outcome from this study has shown many good results. The predicted temperature from burning diesel (decane) is quite acceptable when compared with the prediction of methanol considering the higher energy density in diesel. However, the simulation of biodiesel (methyl decanoate) has shown higher range of temperature than that for diesel. This should not be the case as it is well established that diesel has about 10-15% higher energy density compared to biodiesel. This discrepancy is most likely associated with the reaction mechanism generated for biodiesel, and in particular, the author strongly believes that the EXGAS software did not handle the existence of the oxygen atoms in biodiesel in an accurate way leading to these results. Having said so, the prediction of by-products from these two simulations still shows the superiority of the comprehensive mechanism. Including the effect of radiation in such simulation has been proved to lead to a slight increase in temperature, however, the right radiation model should be considered.

The experimental work focused on establishing some basic physical properties for diesel, a typical UK-based biodiesel and nine surrogate fuels (B10–B90) using the standard test methods (ASTM D) in qualified laboratory facilities. With biodiesel having higher density and viscosity, the results show that adding

biodiesel to diesel leads to linear increase in these two physical properties with the range of values agreeing with the data for diesel, biodiesel and their blends including that in the latest National Renewable Energy Lab (NREL) report [42]. The CN was also found to increase in the blends with an increase in the percentage of biodiesel in the mixture, however, the variation is not linear. Both the CP and the PP temperatures showed linear increase with an increase in the percentage of biodiesel in the blend while the flash point decreased with an increase in the percentage of biodiesel but the variation is not linear. All these findings agree with the available data. Other properties looked at include sulphur content, water content, acid number and nitrogen content. Both the sulphur and nitrogen content decreased with increasing biodiesel percentage in the blend while the acid number and water content increased with the water content showing a linear increase.

FTIR spectral analysis was performed for the nine blends as well as for diesel, and biodiesel. The spectra showed a range of peaks at different values of wave numbers which correspond to a range of constituents in the fuels including oxygen atoms connected with single and double bonds to oxygen. The results clearly indicate that the strength of the signal of the double bond connecting oxygen to carbon increases with increasing the percentage of biodiesel in the mixture.

The experimental work on establishing thermal, physical and chemical properties of diesel, biodiesel and the nine surrogates was followed by testing five fuels on a compression ignition (diesel) engine including diesel, biodiesel B25, B50 and B75. In terms of thermal performance, the engine indicates that it worked with the lowest Air to Fuel (A/F) rate for biodiesel and B25, an indication to the influence of the existence of oxygen in the fuels on the combustion process. Other results in terms of indicated power, brake thermal efficiency, specific fuel efficiency are consistent with the literature with differences explained. In terms of emission, the surrogate fuels (blends) were found to produce far lower $CO_x$ and $NO_x$ compared to diesel and biodiesel while less smoke was detected in the case of biodiesel compared to diesels and blends.

## 8.1 Recommendation for further work

The work presented in this thesis has some limitations and, in fact, many questions and scenarios have surfaced that need to be addressed. The points below summarize these points but by no means indicate any shortcomings from this thesis.

- The developed reaction model for all fuels (methanol, dodecane and methyl decanoate) considered high-temperature reactions only, which is not the most ideal consideration in the opinion of the author. It is highly recommended that a future work that takes into consideration, reactions associated with both low and high temperatures and related intermediate species. Some radicals which have been eliminated in the current work, should be considered in a future study, as they might be important in contribution to energy releases, especially at high temperatures. This is expected to lead to a complete picture of the combustion process and will provide a comprehensive data to analyse and to comment on.

- One of the findings of the CFD modelling of the combustion process was that, including a comprehensive reaction model leads to a delay in the burning process and this causes an increase in the temperature field. In order to elucidate this further, an unsteady turbulence model, such as LES, is necessary to investigate this point and reveal the transient evolution of the combustion and flame propagation both in simple geometry burners and in CIEs. This is expected to make up for some of the variation of the results obtained in this work.

- The developed reactions model using EXGAS has produced very good results for all fuels considered in this thesis. One of the predicted results is the faster burning rate of light fuels compared to heavy hydrocarbons. One of the points that needs further investigation is the detailed evolution of the combustion by-products when such fuels are modelled and how these intermediate products influence the path of combustion. This further means that an in-depth knowledge of the chemistry used to develop the EXGAS software and possible modification should be the focus of any further work

in this direction. Further, EXGAS produced quite interesting results when used to model biofuels (oxygenated types) compared to conventional fuels where no oxygen is embedded in their microstructure as in the case of biofuels. The difference appeared in the rate of by-products such as water vapour contents and an in-depth investigation on this issues may be essential both to understand the mechanisms through which such by-products form and how the developed reaction model influence their generation.

- The experimental testing of biodiesel and its surrogates has shown that the stability of the fuel and the composition may change with time with water forming at higher rates with time. While the experimental work using the freshly purchased biodiesel produced a set of results in agreement with the literature, it is of great interest to examine the performance of such fuels, after a specific period of time, on the CIE and establish both the thermal performance and emission from the engine. This is expected to provide some guidelines for biodiesel handling and its effect on the combustion process.

- Some technical aspects of the CFD work can be improved. This includes a structured mesh that resolves regions of interest with higher accuracy as well as using unsteady turbulence models. The effect of radiation should be modelled using more advanced radiation models.

- Finally, the author believes that the modelled flow is buoyant and the effect of buoyancy should be included in the vertical burner used in this study.

# References


[1] Widman, J. F. and Presser, C. A benchmark experimental database for multiphase combustion model input and validation, in Combustion and Flame. Vol. 129, no. 1, pp.47–86, 2002. xx, 17, 20, 21, 23, 45, 49, 50, 53, 57, 63, 64, 67, 69, 72, 78, 81, 83, 88, 93, 94, 97, 99, 100, 101, 102, 105, 109, 114, 117, 139, 145, 147, 152, 153, 155, 156, 158, 166, 214, 215

[2] Anonymous, International Energy Outlook 2010, International Information Administration (US), Government Printing Office, 2010. xi, 1

[3] http://www.worldenergyoutlook.org/media/weo2010.pdf. [Accessed: September 2012]. xi, 2, 3

[4] EPC. Directive 98/69/EC of the European Parliament and of the Council of 13 October 1998 relating to measures to be taken against air pollution by emissions from motor vehicles and amending council directive 70/220/EEC. Official Journal of the European Communities. L350. Luxembourg. pp. 1–56, 1998. 2

[5] EPC. Regulation (EC) No 715/2007 of the European Parliament and of the Council of 20 June 2007 on type approval of motor vehicles with respect to emissions from light passenger and commercial vehicles (Euro 5 and Euro 6) and on access to vehicle repair and maintenance information. Official Journal of the European Communities. 50, L171. Luxembourg. pp. 1–16, 2007. 2, 3

[6] Graboski, M. S. and McCormick, R. L. Combustion of fat and vegetable

oil derived fuels in diesel engines, in Progress in Energy and Combustion Science. Vol. 24, no. 2, pp. 125–164, 1998. xi, 4, 9

[7] Miyamoto, N., Ogawa, H., Nurun, N. M., Obata, K., and Arima, T. Low $NO_x$, high thermal efficiency, and low noise diesel combustion with oxygenated agents as main fuel, in Society of Automotive Engineers technical paper SAE-980506, 1998. 4

[8] Westbrook, C. K., Pitz, W. J., and Curran, H. J. Chemical kinetic modelling study of the effects of oxygenated hydrocarbons on soot emissions from diesel engines, in Journal of Physical Chemistry A. Vol. 110, no. 21, pp. 6912–6922, 2006. 4

[9] MacLeana H. L. and Laveb, L.B. Evaluating automobile fuel/propulsion system technologies, in Progress in Energy and Combustion Science. Vol. 29, no. 1, pp. 1–69, 2003. 4

[10] Nitske, W. R., Wilson, C. M. Rudolf Diesel, pioneer of the Age of Power. University of Oklahoma Press, 1965. 7

[11] Cvengro, J. and Povaz, A. F. Production and treatment of rapeseed oil methyl esters as alternative fuels for diesel engines, in Bioresource Technology. Vol. 55, no. 13, pp. 145–150, 1996. 8, 9, 197, 198

[12] Boro, J., Thakur, A. J., and Deka, D. Solid oxide derived from waste shells of Turbonilla striatula as a renewable catalyst for biodiesel production, in Fuel Processing Technology. Vol. 92, no. 10, pp. 2061–2067, 2011. 8

[13] Jham, G. N., Moser, B. R., Shah, S. N., Holser, R. A., Dhingra, O. D., and Vaughn, S. F. Wild Brazilian mustard (Brassica juncea L.) seed oil methyl esters as biodiesel fuel, in Journal of the American Oil Chemists' Society. Vol. 86, no. 9, pp. 917–926, 2009. 8

[14] Chapagain, B. P., Yehoshua, Y., and Wiesman, Z. Desert date (Balanites aegyptiaca) as an arid lands sustainable bioresource for biodiesel, in Bioresource Technology. Vol. 100, no. 3, pp. 1221–1226, 2009. 8

[15] Hayyan, A., Alam, M. Z., Mirghani, M. E. S., Kabbashi, N. A., Hakimi, N. I. N., Siran, Y. M., and Tahiruddin, S. Reduction of high content of free fatty acid in sludge palm oil via acid catalyst for biodiesel production, in Fuel Processing Technology. Vol. 92, no. 5, pp. 920–924, 2011. 8

[16] Mekhilefa, S., Sigaa, S., and Saidurb, R. A review on palm oil biodiesel as a source of renewable fuel, in Renewable and Sustainable Energy Reviews. Vol. 15, no. 4, pp. 1937–1949, 2011. 8

[17] Piyanuch, N. and Sasiwimol, W. High free fatty acid coconut oil as a potential feedstock for biodiesel production in Thailand, in Renewable Energy. Vol. 35, no. 8, pp. 1682–1687, 2010. 8

[18] Karmakar, A., Karmakar, S., and Mukherjee, S. Properties of various plants and animals feedstocks for biodiesel production, in Bioresource Technology. Vol. 101, no. 19, pp. 7201–7210, 2010. 8

[19] Varma, M. N., Deshpande, P. A., and Madras, G. Synthesis of biodiesel in supercritical alcohols and supercritical carbon dioxide, in Fuel. Vol 89, no. 7, pp. 1641–1646, 2010. 8

[20] Moser, B. R. and Vaughn, S. F. Coriander seed oil methyl esters as biodiesel fuel: Unique fatty acid composition and excellent oxidative stability, in Biomass and bioenergy. Vol. 34, no. 4, pp. 550–558, 2010. 8

[21] Ilkilic, C., Aydin, S., Behcet, R., and Aydin, H. Biodiesel from safflower oil and its application in a diesel engine, in Fuel Processing Technology. Vol. 92, no. 3, pp. 356–362, 2011. 8

[22] Duz, M. Z., Saydut, A., and Ozturk, G. Alkali catalyzed transesterification of safflower seed oil assisted by microwave irradiation, in Fuel Processing Technology. Vol. 92, no. 3, pp. 308–313, 2011. 8

[23] Montefrio, M. J., Xinwen, T., and Obbard, J. P. Recovery and pretreatment of fats, oil and grease from grease interceptors for biodiesel production, in Applied Energy. Vol. 87, no. 10, pp. 3155–3161, 2010. 8

[24] Demirbas, A. and Demirbas, M. F. Importance of algae oil as a source of biodiesel, in Energy Conversion and Management. Vol. 52, no. 1, pp. 163–170, 2011. 8

[25] Munson-McGee, S., Rhodes, I., Lammers, P., and Nirmalakhandan, N. Optimization of direct conversion of wet algae to biodiesel under supercritical methanol conditions, in Bioresource Technology. Vol. 102, no. 1, pp. 118–122, 2011. 8

[26] Vicentea, L. G., Bautistaa, Rosalia Rodrigueza, F., Gutierreza, F. J., Sadabaa, I., Ruiz-Vazquezb, R. M., Torres-Martinezb, S., and Garreb, V. Biodiesel production from biomass of an oleaginous fungus, in Biochemical Engineering Journal. Vol. 48, no. 1, pp. 22–27, 2009. 8

[27] Cheirsilp, B., Suwannarat, W., and Niyomdecha, R. Mixed culture of oleaginous yeast Rhodotorula glutinis and microalga Chlorella vulgaris for lipid production from industrial wastes and its use as biodiesel feedstock, in New Biotechnology. Vol. 28, no. 4, pp. 362–368, 2011. 8

[28] Dixit, S., kanakraj, S., and Rehmanb, A. Linseed oil as a potential resource for bio-diesel: A review, in Renewable and Sustainable Energy Reviews. Vol. 16, no. 7, pp. 4415–4421, 2012. 9

[29] Garcia-Perez, M., Shena, J., Wang, X. S., and Li, C. Z. Production and fuel properties of fast pyrolysis oil/bio-diesel blends, in Fuel Processing Technology. Vol. 91, no. 3, pp. 296–305, 2010. 9

[30] Avinasha, A., Subramaniamb, D., and Murugesanc, A. Bio-diesel - A global scenario, in Renewable and Sustainable Energy Reviews. Vol. 29, pp. 517–527, 2014. 9

[31] Ahn, E., Koncar, M., Mittelbach, M., and Marr, R. A low-waste process for the production of biodiesel, in Separation Science and Technology. Vol. 30, no. 7–9, pp. 2021–2033, 1995. 9

[32] Crabbe, E., Nolasco-Hipolito C., Kobayashi, G., Sonomoto, K., and Ishizaki, A. Biodiesel production from crude palm oil and evaluation of

butanol extraction and fuel properties, in Process Biochemistry. Vol. 37, no. 1, pp. 65–71, 2001. 10, 197, 198

[33] Zhang, Y., Dube, M. A., McLean D. D, and Kates, M. Biodiesel production from waste cooking oil: 1. Process design and technological assessment, in Bioresource Technology. Vol. 89, no. 1, 2003. 10, 203

[34] J. V. Gerpen. Biodiesel processing and production, in Fuel Processing Technology, Vol. 86, pp. 1097–1107, 2005. 10

[35] Karmee, S. K. and Chadha, A. Preparation of biodiesel from crude oil of pongamia pinnata, in Bioresource Technology. Vol. 96, no. 13, pp. 1425–1429, 2005. 10, 14

[36] Ranganathan, L. and Sampath, S. A review on biodiesel production, combustion, emissions and performance, in International journal of Advanced Scientific and Technical Research. Vol. 1, 2011. 10

[37] Goering, E., Schwab, W., Daugherty J., Pryde, H., and Heakin, J. Fuel properties of eleven vegetable oils, in Transactions of the American Society of Agricultural Engineers. Vol. 25, 1982. xx, 10, 169

[38] Pryor, R. W., Hanna, M. A., Schinstock J. L., and Bashford, L. L. Soybean oil fuel in a small diesel engine, in Transactions of the American Society of Agricultural Engineers, 1982. 10

[39] Knothe, G., Dunn, R. O., and Bagby, M. O. Biodiesel: The Use of Vegetable Oils and Their Derivatives as Alternative Diesel Fuels, in ACS symposium series. Vol. 666, pp. 172–208, 1997. 10

[40] Demirbas, A. Biodiesel production from vegetable oils via catalytic and non-catalytic supercritical methanol transesterification methods, in Progress in Energy and Combustion Science. Vol. 31, no. 5, pp. 466–487, 2005. 11

[41] Demirbas A. Biodiesel fuels from vegetable oils via catalytic and non-catalytic supercritical alcohol transesterifications and other methods: a survey, in Energy Conversion and Management. Vol. 44, no. 13, pp. 2093–2109, 2003. 11, 185

[42] National Renewable Energy Laboratory, Biodiesel Handling and Use Guide, NREL/TP-540-43672, 2009. Available online: http://www.nrel.gov/vehiclesandfuels/pdfs/43672.pdf. [Accessed: 15 July 2011]. xi, xx, 11, 12, 13, 170, 177, 178, 179, 180, 181, 185, 186, 216

[43] NAFS. North American Fuel Survey–Diesel Fuel. Alliance of Automobile Manufacturers. Washington D.C. 2003. 12

[44] Peckham, J. High Quality Diesel Fuel Could Boost, Hinder North American Light-Duty Prospects, in Diesel Fuel News. Vol. 7, no. 21, pp. 3–4, November 10, 2003. 12

[45] Vaitilingom, G., Perilhon, C., Liennard, A., and Gandon, M. Development of rape seed oil burners for drying and heating, in Industrial Crops and Products. Vol. 7, no. 2, pp. 273–279, 1998. 15

[46] Korus, R. A., Mousetis, T. L., and Lloyd, L. Polymerization of vegetable oils, in No. CONF-820860-. Univ. of Idaho, Moscow, 1982. 16

[47] Srivastava, A. and Prasad, R. Triglycerides-based diesel fuels, in Renewable and Sustainable Energy Reviews. Vol. 4, no. 2, pp. 111-133, 2000. 16

[48] Kalam, M. A. and Masjuki, H. H. Emissions and deposit characteristics of a small diesel engine when operated on preheated crude palm oil, in Biomass and Bioenergy. Vol. 27, no. 3, pp. 289–297, 2004 16

[49] Ramadhas, A. S., Jayaraj, S., and Muraleedharan, C. Characterization and effect of using rubber seed oil as fuel in the compression ignition engines, in Renewable Energy. Vol. 30, no. 5, pp. 795–803, 2005. 16

[50] Holt, G. A. and Hooker, J. D. Gaseous emissions from burning diesel, crude and prime bleachable summer yellow cottonseed oil in a burner for drying seed-cotton, in Bioresource Technology. Vol. 92, no. 3, pp. 261–267, 2004. 16

[51] Alonso, J. S. J., Sastre, J. A. L., vila, C. R., and Romero, E. J. L. Combustion of rapeseed oil and diesel oil mixtures for use in the production of heat energy, in Fuel Processing Technology. Vol. 87, no. 2, pp.97–102, 2006.

[52] Alonso, J. S. J., Sastre, J. A. L., vila, C. R., and Romero, E. J. L. A note on the combustion of blends of diesel and soya, sunflower and rapeseed vegetable oils in a light boiler, in Biomass and Bioenergy. Vol. 32, no. 9, pp. 880–886, 2008.

[53] Macor, A. and Pavanello, P. Performance and emissions of biodiesel in a boiler for residential heating, in Energy. Vol. 34, no. 12, pp. 2025–2032, 2009.

[54] Daho, T., Vaitilingom, G., and Sanogo, O. Optimization of the combustion of blends of domestic fuel oil and cottonseed oil in a non-modified domestic boiler, in Fuel. Vol. 88, no. 7, 2009.

[55] Jos, J. S., Al-Kassir, A., and Gan, J. Analysis of biodiesel combustion in a boiler with a pressure operated mechanical pulverisation burner, in Fuel Processing Technology. Vol. 92, no. 2, pp. 271–277, 2011.

[56] Bazooyar, B., Ghorbani, A., Shariati, A. Combustion performance and emissions of petrodiesel and biodiesels based on various vegetable oils in a semi industrial boiler, in Fuel. Vol. 90, no. 10, pp. 3078–3092, 2011. 16

[57] Dahoa, T., Vaitilingomb, G., Sanogoc, O., Ouimingaa, S. K., Zongoa, A. S., Pirioud, B., and Koulidiati, J. Combustion of vegetable oils under optimized conditions of atomization and granulometry in a modified fuel oil burner, in Fuel. Vol. 118, pp 329–334, 2014. 16

[58] Herbinet, O., Biet, J., Hakka, M. H., Warth, V., Glaude, P. A., Nicolle, A., Leclerc, F. B. Modelling study of the low-temperature oxidation of large methyl esters from C11 to C19, in Proceedings of the Combustion Institute. Vol. 33, no. 1, pp. 391–398, 2011. 16, 33

[59] Warth, V., Stef, N., Glaude, P. A., Battin-Leclerc, F., Scacchi, G., Cme, G. M. Computer aided derivation of gas-phase oxidation mechanisms: application to the modelling of the oxidation of n-butane, in Combustion and Flame. Vol. 114, no. 1–2, pp. 81–102, 1998. 16, 44, 85

[60] Thoo, W. J., Kevric, A., Ng, H. K., Ganc, S., and Shayler, P. Characterisation of ignition delay period for a compression ignition engine operating on blended mixtures of diesel and gasoline, in Applied Thermal Engineering. Vol. 66, pp 55–64, 2014. 16

[61] Sanjid, A., Masjuki, H. H., Kalam, M. A., Rahman, S. M. A., Abedin, S. M., and Palash, M. J. Impact of palm, mustard, waste cooking oil and Calophyllum inophyllum biofuels on performance and emission of CI engine, in Renewable and Sustainable Energy Reviews. Vol. 27, pp. 664–682, 2013. 16

[62] Hoekman, S. K. and Robbins, C. Review of the effects of biodiesel on NOx emissions, in Fuel Processing Technology, Vol. 96, pp. 237–249, April 2012. 16

[63] Song, H., Tompkins, B. T., Bittle, J. A., and Jacobs, T. J. Comparisons of NO emissions and soot concentrations from biodiesel-fuelled diesel engine, in Fuel. Vol. 96, pp. 446–453, June 2012. 16

[64] Han, D., Ickes, A. M., Bohac, S. V., Huang, Z., and Assanis, D. N. HC and CO emissions of premixed low-temperature combustion fueled by blends of diesel and gasoline, in Fuel. Vol. 99, pp. 13–19, September 2012. 16

[65] Collazo, J. Porteiro, J., Patio, D., Miguez, J. L., E. Granada, E., Moran, J. Simulation and experimental validation of a methanol burner, in Fuel. Vol. 88, pp. 326–334, 2009. 17, 21, 63, 69, 100, 154, 166

[66] Dinica, V. V. Renewable electricity production costs - A framework to assist policy-makers' decisions on price support, in Energy Policy. Vol. 39, no. 7, pp. 4153–4167, 2011.

[67] Krozer, Y. Cost and benefit of renewable energy in the European Union, in Renewable Energy. Vol. 50, pp. 68–73, 2013.

[68] Nigama, P. S., and Singh, A. Production of liquid Biofuels from renewable resources, in Progress in Energy and Combustion Science. Vol. 37, no. 1, pp. 52–68, 2011.

[69] Sheehan, J., Cambreco, V., Duffield, J., Garboski, M., Shapouri, H. An overview of biodiesel and petroleum diesel life cycles, in No. NREL/TP-580-24772. National Renewable Energy Lab., Golden, CO (US), 2000.

[70] Hill, J., Nelson, E., Tilman, D., Polasky, S., Tiffany, D. Environmental, economic and energetic costs and benefits of biodiesel and ethanol biofuels, in Proceedings of the National Academy of Sciences. Vol. 103, no. 30, pp. 11206–11210, 2006.

[71] Knothe, G. Biodiesel and renewable diesel: A comparison, in Progress in Energy and Combustion Science. Vol. 36, no. 3, pp. 364–373, 2010.

[72] Demirbas, A. Progress and recent trends in biofuels, in Progress in Energy and Combustion Science. Vol. 33, no. 1, pp. 1–18, 2007.

[73] Enweremadu, C. C., Rutto, H. L. Combustion, emission and engine performance characteristics of used cooking oil biodiesel, in Renewable and Sustainable Energy Reviews. Vol. 14, no. 9, pp. 2863–2873, 2010. 18

[74] Gumus, M. A comprehensive experimental investigation of combustion and heat release characteristics of a biodiesel (hazelnut kernel oil methyl ester) fuelled direct injection compression ignition engine Original Research Article, in Fuel, Vol. 89, no. 10, pp. 2802–2814, 2010. 18

[75] Lapuerta, M., Armas, O. O., Fernndez, J. R. Effect of biodiesel fuels on diesel engine emissions, in Progress in Energy and Combustion Science. Vol. 34, no. 2, pp. 198–223, 2008. 18, 190

[76] Agarwal, A. K. Biofuels (alcohols and biodiesel) applications as fuels for internal combustion engines, in Progress in Energy and Combustion Science. Vol. 33, no. 3, pp. 233–271, 2007. 18

[77] Jaichandar, S., Annamalai, K. Effects of open combustion chamber geometries on the performance of pongamia biodiesel in a DI diesel engine, in Fuel. Vol. 98, pp. 272–279, 2012. 18

[78] Ranzi, E., Frassoldati, A., Grana, R., Cuoci, A., Faravelli, T., Kelley, A. P., Lawb, C. K. Hierarchical and comparative kinetic modeling of laminar flame speeds of hydrocarbon and oxygenated fuels, in Progress in Energy and Combustion Science. Vol. 38, no. 4, pp. 468–501, 2012. 18

[79] Xue, J., Grift, T. E., Hansena, A. C. Effect of biodiesel on engine performances and emissions, in Renewable and Sustainable Energy Reviews. Vol. 15, pp. 1098–1116, 2011. xx, 18

[80] Cant, R. S. and Mastorrakos, E. An introduction to turbulent reacting flows. Imperial College Press, 2008. 21, 24, 36

[81] Fox, R. O. Computational models for turbulent reacting flows. Cambridge University Press, 2003. 21

[82] ANSYS Inc., ANSYS Fluent 12.1 Theory Guide, 2009. [Accessed: 15 January 2012]. 23, 24, 25, 39, 40, 58

[83] Peters, N. Laminar Diffusion Flamelet Models in Non-Premixed Turbulent Combustion, in Progress in Energy and Combustion Science. Vol. 10, pp 319–339, 1984. 24

[84] Peters, N. Laminar flamelet concepts in turbulent combustion, in 21st Symposium (International) on Combustion, The Combustion Institute, pp. 1231–1250, 1986. 24, 35, 36, 44

[85] Menter, F. R. Two-equation eddy-viscosity turbulence models for engineering applications, AIAA Journal. Vol. 32, no. 8, pp. 1598-1605, 1994. 24, 29

[86] Poinsot, T. and Veynante, D. Theoretical and numerical combustion. RT Edwards, Inc., 2005. 25, 36, 78

[87] Champion, M. and Libby, P. A. Turbulent premixed combustion in a boundary layer, in Combustion Science and Technology. Vol. 38, no. 5. pp. 267–291, 1984. 25, 36

[88] Williams, F. A. Combustion theory. Perseus Books, 1985. 25, 36

[89] Borghi, R. and Champion, M. Modélisation et théorie des flammes. Editions Technip. 2000. 25, 36

[90] Nomura, H., Takahashi, H., Suganuma, Y., Kikuchi, M. Droplet ignition behavior in the vicinity of the leading edge of a flame spreading along a fuel droplet array in fuel-vapor/air mixture, in Proceedings of the Combustion Institute, Vol. 34, no. 1, pp. 1593–1600, 2013. 30

[91] Fox, R. O. Computational Models for Turbulent Reacting Flows. Cambridge University Press. Cambridge, 2003. 32

[92] Pierre Alexandre Glaude, Olivier Herbinet, Sarah Bax, Joffrey Biet, Valrie Warth, Frdrique Battin-Leclerc. Modelling of the oxidation of methyl estersValidation for methyl hexanoate, methyl heptanoate, and methyl decanoate in a jet-stirred reactor, in Combustion and Flame. Vol. 157, no. 11, pp. 2035–2050, 2010. 33, 44

[93] Biet, J., Hakka, M. H., Warth, V., Glaude, P. A., Battin-Leclerc, F. Experimental and Modelling Study of the Low-Temperature Oxidation of Large Alkanes, in Energy & Fuels. Vol. 22, pp. 2258–2269, 2008.

[94] Olivier Herbinet, Benoit Husson, Zeynep Serinyel, Maximilien Cord, Valrie Warth, Ren Fournet, Pierre-Alexandre Glaude, Baptiste Sirjean, Frdrique Battin-Leclerc, Zhandong Wang, Mingfeng Xie, Zhanjun Cheng, Fei Qi. Experimental and modelling investigation of the low-temperature oxidation of n-heptane, in Combustion and Flame. Vol. 159, no. 12, pp. 3455–3471, 2012.

[95] Roda Bounaceur, Valrie Warth, Paul-Marie Marquaire, Grard Scacchi, Florent Domin, Daniel Dessort, Bernard Pradier, Olivier Brevart. Modelling of hydrocarbons pyrolysis at low temperature. Automatic generation of free radicals mechanisms, in Journal of Analytical and Applied Pyrolysis. Vol. 64, no. 1, pp. 103–122, 2002.

[96] Olivier Herbinet, Paul-Marie Marquaire, Frdrique Battin-Leclerc, Ren Fournet. Thermal decomposition of n-dodecane: Experiments and kinetic

modelling, in Journal of Analytical and Applied Pyrolysis. Vol. 78, no. 2, pp. 419–429, 2007.

[97] Luc Sy Tran, Baptiste Sirjean, Pierre-Alexandre Glaude, Ren Fournet, Frdrique Battin-Leclerc. Progress in detailed kinetic modelling of the combustion of oxygenated components of biofuels, in Energy. Vol. 43, no. 1, pp. 4–18, 2012.

[98] Haowei Wang, Steven J. Warner, Matthew A. Oehlschlaeger, Roda Bounaceur, Joffrey Biet, Pierre-Alexandre Glaude, Frdrique Battin-Leclerc. An experimental and kinetic modelling study of the autoignition of $\alpha$-methylnaphthalene/air and $\alpha$-methylnaphthalene/n-decane/air mixtures at elevated pressures, in Combustion and Flame. Vol. 157, no. 10, pp. 1976–1988, 2010.

[99] Benoit Husson, Maude Ferrari, Olivier Herbinet, Syed S. Ahmed, Pierre-Alexandre Glaude, Frdrique Battin-Leclerc. New experimental evidence and modelling study of the ethylbenzene oxidation, in Proceedings of the Combustion Institute. Vol. 34, no. 1, pp. 325–333, 2013. 33

[100] http://garfield.chem.elte.hu/Burcat/burcat.html. [Accessed: 1 August 2012]. 33, 83

[101] http://web.eng.ucsd.edu/mae/groups/combustion/mechanism.html. [Accessed: 1 September 2012]. 34, 35, 44

[102] Williams, F. A. Turbulent Mixing in Non-reactive and Reactive Flows (S. N. B. Murthy, Ed.). Plenum Press, 1975. 36

[103] Turns, S. R. An introduction to combustion: concepts and applications. McGraw-Hill, 2000. 36

[104] Schmidt, D. P., Corradini, M. L., Rutland, C. J. A two-dimensional, non-equilibrium model of flashing nozzle flow, in 3rd ASME/JSME Joint Fluids Engineering Conference. Vol. 208, p. 616. 1999. 40

[105] Han, Z., Perrish, S., Farrell, P. V., Reitz, R. D. Modelling atomization processes of pressure-swirl hollow-cone fuel sprays, in Atomization and Sprays. Vol. 7, no. 6, pp. 663–684, 1997. 40

[106] Squire, H. B. Investigation of the instability of a moving liquid film, in British journal of applied physics. Vol. 4, p.167, 1953. 41

[107] Li, X., and Tankin, R. S. On the temporal instability of a two-dimensional viscous liquid sheet, in Journal of Fluid Mechanics. Vol. 226, pp. 425–443, 1991. 41

[108] Hagerty, W. W. and Shea, J. F. A study of the stability of plane Fluid Sheets, in Journal of Applied Mechanics. Vol. 22, pp. 509, 1955. 41

[109] Senecal, P. K., Schmidt, D. P., Nouar, I., Rutland, C. J., Reitz, R. D. Modelling high speed viscous liquid sheet atomization, in Internatioanl Journal of Multiphase Flow. Vol. 25, pp. 1073–1097, 1999. 42

[110] Dombrowski, N, and Johns, W. R. The aerodynamic Instability and Disintegration of Viscous Liquid Sheets, in Chemical Engineering Science. Vol. 18, pp. 203–214, 1963. 42, 43

[111] Weber, C. Zum Zerfall eines Flssigkeitsstrahles. ZAMM-Journal of Applied Mathematics and Mechanics. Vol. 11, no. 2, pp. 136–154, 1931. 43

[112] Buda, F., Bounaceur, R., Warth, V., Glaude, P. A., Fournet, R., and Battin-Leclerc, F. Progress toward a unified detailed kinetic model for the autoignition of alkanes from C4 to C10 between 600 and 1200 K, in Combustion and flame. Vol. 142, no. 1, pp. 170–186, 2005. 44

[113] Biet, J., Delfau, J. L., Seydi, A., and Vovelle, C. Experimental and modelling study of lean premixed atmospheric-pressure propane/O2/N2 flames, in Combustion and flame. Vol. 142, no. 3, pp. 197–209, 2005. 44

[114] Touchard, S., Fournet, R., Glaude, P. A., Warth, V., Battin-Leclerc, F., Vanhove, G., Ribaucour, R., and Minetti, R. Modelling of the oxidation of large alkenes at low temperature, in Proceedings of the Combustion Institute. Vol. 30, no. 1, pp. 1073–1081, 2005. 44

[115] Modest, M. F., Radiative Heat Transfer. Academic Press, New York, 2003. 44

[116] Chemical-Kinetic Mechanisms for Combustion Applications, San Diego Mechanism web page, Mechanical and Aerospace Engineering (Combustion Research), University of California at San Diego (http://combustion.ucsd.edu). 52

[117] Wolfstein, M. The Velocity and Temperature Distribution of One-Dimensional Flow with Turbulence Augmentation and Pressure Gradient, in International Journal of Heat Mass Transfer. Vol. 12, pp 301–318, 1969. 59

[118] Magnussen, B. F. On the structure of turbulence and a generalized eddy dissipation concept for chemical reaction in turbulent flow, in 19th AIAA Meeting, 1981. 63

[119] Sadasivuni, S. K. LES modelling of non-premixed and partially premixed turbulent flames. A Doctoral Thesis. 2010. 78

[120] Sadasivuni, S. K., Malalasekera, W., Ibrahim, S. S. Unsteady flamelet/progress variable approach for non-premixed turbulent lifted flames. in Russian Journal of Physical Chemistry B. Vol. 4, no. 3, pp. 465–474, 2010. 78, 154

[121] Wallington, T. J., Kaiser, E. W., Farrellc, J. T. Automotive fuels and internal combustion engines: a chemical perspective, in Chemical Society Reviews. Vol. 35, no. 4, pp 335–347, 2005. 81, 82

[122] http://cds.dl.ac.uk/. [Accessed: 1 August 2012]. 83

[123] Valerie Warth, Frederique Battin-Leclerc, Rene Fournet, Pierre-Alexandre Glaude, Guy-Marie Com, and Gerard Scacchi. Computer based generation of reaction mechanisms for gas-phase oxidation, in Computers and Chemistry. Vol. 24, pp. 541–560, 2000. 84

[124] Guy-Marie Come. Gas-Phase Thermal Reactions, in Chemical Engineering Kinetics. Kluwer Academic Publishers, 2001. 84

[125] Glaude, P. A., Warth, V., Fournet, R., Battin-Leclerc, F., Cme, G. M., Scacchi, G. Modelling of n-heptane and iso-octane gas-phase oxidation at low temperature by using computer-aided designed mechanisms, in Bulletin des societes Chimiques Belges. Vol. 106, no. 6, pp. 343–348, 1997. 85

[126] Cme, G. M., Warth, V., Glaude, P. A., Battin-Leclerc, F., Scacchi, G. Computer aided design of gas-phase oxidation mechanisms–Application to the modelling of n-heptane and iso-octane oxidation, in Symposium on Combustion. Vol. 26, no. 1, pp. 755–762, 1996. 85

[127] Glaude, P. A., Warth, V., Fournet, R., Battin-Leclerc, F., Scacchi, G., Cme, G. M. Modelling of the oxidation of n-octane and n-decane using an automatic generation of mechanisms, in International Journal of Chemical Kinetics. Vol. 30, pp. 949–959, 1998. 85

[128] Battin-Leclerc, F., Fournet, R., Glaude, P. A., Judenherc, B., Warth, V., Cme, G. M., Scacchi, G. Modelling of the gas-phase oxidation of n-decane from 550 to 1600 K, in Proceedings of the Combustion Institute. Vol. 28, no. 2, pp. 1597–1605, 2000. 85

[129] Glaude, P. A., Warth, V., Fournet, R., Battin-Leclerc, R., Cme, G. M., Scacchi, G., Dagaut, P., Cathonnet, M. Modeling the oxidation of mixtures of primary reference automobile fuels, in Energy and Fuels. Vol. 16, pp. 1186–1195, 2002. 86

[130] Oehlschaeger, M. A., Davidson, D. F., Herbon, J. T., Hanson, R. K. International Journal of Chemical Kinetics. Vol. 36, 2003. 86

[131] Sarathy, S. M., Westbrook, C. K., Mehl, M., Pitz, W. J., Togbe, C., Dagaut, P., Wang, H., Oehlschlaeger, M. A., Niemann, U., Seshadri, K., Veloo, P. S., Ji, C., Egolfopoulos, F. N., Lu, T. Comprehensive chemical kinetic modelling of the oxidation of 2-methylalkanes from C7 to C20, in Combustion and Flame. Vol. 158, pp. 2338–2357, 2011. 86, 93

[132] Sadasivuni, S. K. LES modelling of non-premixed and partially premixed turbulent flames (Doctoral dissertation), 2009. 105

[133] Arbab, M. I., Masjuki, H. H., Varman, M., Kalam, M. A., Imtenan, S., Sajjad, H. Fuel properties, engine performance and emission characteristic of common biodiesels as a renewable and sustainable source of fuel, in Renewable and Sustainable Energy Reviews. Vol. 22, pp. 133–147, 2013. xx, 110

[134] Sadeghinezhad, E., Kazi S. N., Badarudina, A., Oona, C. S., Zubir, M. N. M., Mehrali, M. A comprehensive review of bio-diesel as alternative fuel for compression ignition engines, in Renewable and Sustainable Energy Reviews. Vol. 28, pp. 410–424, 2013. xx, 110, 203

[135] Demirbas, A. Progress and recent trends in biodiesel fuels, in Energy Conversion and Management. Vol. 50, no. 1, pp. 14–34, 2009. 168, 170, 171, 178

[136] Sridharan R., Mathai I. M. Transesterification reactions, in Journal of Scientific and Industrial Research. Vol. 33, no. 4, pp. 178–187, 1974. xx, 169, 173

[137] Sharma, Y. C., Singh, B., Upadhyay, S. N. Advancements in development and characterization of biodiesel: a review, in Fuel. Vol. 87, pp. 2355–2373, 2008. 171

[138] Islam, M. N., Islam, M. N., Beg, M. R. A. The fuel properties of pyrolysis liquid derived from urban solid wastes in Bangladesh, in Bioresource Technology. Vol. 92, no. 2, pp. 181–186, 2004. 171

[139] Park, S. H., Suh, H. K., Lee, C. S. Nozzle flow and atomization characteristics of ethanol blended biodiesel fuel, in Renewable Energy. Vol. 35, pp. 144–150, 2010. 171

[140] Park, S. H., Kim, H. J., Suh, H. K., Lee, C. S. Atomization and spray characteristics of bioethanol and bioethanol blended gasoline fuel injected through a direct injection gasoline injector, in International Journal of Heat and Fluid Flow. Vol. 30, no. 6, pp. 1183-1192, 2009. 171

[141] Fangrui, M., Clement, L. D., Hanna, M. A. Biodiesel fuel from animal fats. Ancillary studies on transesterification of beef tallow, in Industrial and Engineering Chemistry Research. Vol. 37, pp. 3768–3771, 1998. 171

[142] Gunvachai, K., Hassan, M. G., Shama, G., Hellgardt, C. A new solubility model to describe biodiesel formation kinetics, in Process Safety and Environmental Protection. Vol. 85, no. 5, pp. 383–389, 2007. 171

[143] Hideki F., Akihiko K., Hideo N. Biodiesel fuel production by transesterification of oils: review, in Journal of Bioscience and Bioengineering. Vol. 92, no. 5, pp. 405–416, 2001. xxi, 172, 183, 184

[144] Boerlage, G., and Broeze, J. Ignition Quality of Diesel Fuel as Expressed in Cetane Numbers, in S.A.E. Journal. Vol. 31, no. 1, pp. 283–295, 1932. 175

[145] Avialable online: http://www.astm.org/Standards/D613.htm 176

[146] M.A. Dube, A.Y. Tremblay, J. Liu Biodiesel production using a membrane reactor Bioresource Technology, 98 (2007), pp. 639647 178

[147] Imahara, H., Minami, E., Saka, S. Thermodynamic study on cloud point of biodiesel with its fatty acid composition, in Fuel. Vol. 85, pp. 1666–1670, 2006. xxi, 180

[148] Verissimo, M. I. S., Teresa, M., Gomes, S. R. Assessment on the use of biodiesel in cold weather: Pour point determination using a piezoelectric quartz crystal, in Fuel. Vol. 90, pp. 2315–2320, 2011. xxi, 181

[149] European Standard EN 14214, CEN European Committee for Standardization, Brussels, Belgium, 2003. 186, 188

[150] Felizardo, P., Baptista, P., Menezes, J. M., Correia, M. J. N. Multivariate near infrared spectroscopy models for predicting methanol and water content in biodiesel, in Analytica Chimica Acta. Vol. 595, no. 1, pp. 107–113, 2007. 186

[151] European Standard EN 12937, CEN European Committee for Standardization, Brussels, Belgium, 2000. 186

[152] Demirbas, A. Biodiesel from vegetable oils via transesterification in supercritical methanol, in Energy Conversion and Management. Vol. 43, no. 17, pp. 2349–2356, 2002. 187

[153] Nur, H., Snowden, M. J., Cornelius, V. J., Mitchell, J. C., Harvey, V, Bene, L. S. Colloidal microgel in removal of water from biodiesel, in Colloids and Surfaces A: Physicochemical and Engineering Aspects. Vol. 335, no 1, pp. 133–137, 2009. 187

[154] http://www.astm.org/Standards/D664.htm 188

[155] Sun, J., Caton, J. A., Jacobs, T. J. Oxides of nitrogen emissions from biodiesel-fuelled diesel engines, in Progress in Energy and Combustion Science. Vol. 36, pp. 677–695, 2010. 189, 190

[156] Giannelos, P. N., Zannikos, F., Stournas, S., Lois, E. Anastopoulos G. Tobacco seed oil as an alternative diesel fuel: physical and chemical properties, in Industrial Crops and Products. Vol. 6, no. 1, pp. 1–9., 2002. 190

[157] Pradeep, V., Sharma, R. Evaluation of performance, emission and combustion parameters of a CI engine fuelled with bio-diesel from rubber seed oil and its blends, in Training, 2005. 190

[158] Taylor, D. and Walsham, B. Combustion processes in a medium-speed diesel engine, in Proceedings of the Institution of Mechanical Engineers, Conference Proceedings. Vol. 184, no, 10, pp. 67–76, 1970. 190

[159] Burt, R. and Troth, K. Penetration and vaporization of diesel fuel sprays, in Proceedings of the Institution of Mechanical Engineers, Conference Proceedings. Vol. 184, no. 10, pp. 147–170, 1970. 190

[160] Capareda, S., Caton, J. A., Jacobs, T. J. Root Cause Analysis of Changes in NOx Emissions due to Biodiesel Combustion in Diesel Engines. Report No. HARC N-30. Work funded by the State of Texas through a grant from the Texas Environmental Research Consortium with funding provided by the Texas Commission on Environmental Quality, 2009. 190

[161] Ullman, T. L, Spreen, K. B, Mason, R. L. Effects of cetane number, cetane improver, aromatics, and oxygenates on 1994 heavy-duty diesel engine emissions, in SAE technical paper. No. 941020, 1994. 190

[162] Aakko, P., Nylund, N. O., Westerholm, M., Marjamaki, M., Moisio, M., Hillamo, R., Makela, T. Emissions from heavy-duty engine with and without aftertreatment using selected biofuels, in FISITA 2002 World Automotive Congress Proceedings, pp. 2–7, 2002. 191

[163] Knothe, G., Bagby, M. O., Ryan, T. W., Callahan, T. J., Wheeler, H. G. Soc. Automot. Eng., [Spec. Publ.] SP 1992, SP-900, pp. 37-63, 1992. 193

[164] Freedman, B., Bagby, M. O. Predicting cetane numbers of n-alcohols and methyl esters from their physical properties, in Journal of the American Oil Chemists' Society. Vol. 67, no. 9, pp. 565–571, 1990. 193

[165] Douros, T., Schindlbauer, H. Fettether als mglicher Dieselkraftstoffzusatz. Erdoel, Erdgas, Kohle. Vol. 103, no. 5, pp. 228–230, 1987. 193

[166] Masaru, K., Taichi, S., Takeshi, M., Kazuhiro, B., Akihiko, K., Yuji, S. Biodiesel fuel production from plant oil catalyzed by Rhizopus oryzae lipase in a water-containing system without an organic solvent, in Journal of Bioscience and Bioengineering. Vol. 88, no. 6, pp. 627–631, 1999. 197

[167] Fangrui, M., Hanna, M. A. Biodiesel production: a review, in Bioresource Technology. Vol. 70, no. 1, pp. 1–15, 1999. 197

[168] Ikwuagwu. O. E, Ononogbu I. C., Njoku, O. U. Production of biodiesel using rubber [Hevea brasiliensis (Kunth Muell.)] seed oil, in Industrial Crops and Products. Vol. 12, pp. 57–62, 2000. 197, 198

[169] Saka, S., Kusdiana, D. Biodiesel fuel from rapeseed oil as prepared in supercritical methanol, in Fuel. Vol. 80, pp. 225–231, 2001. 197, 198

[170] Yuji, S., Yomi, W., Akio, S., Yoshio, T. Enzymatic alcoholysis for biodiesel fuel production and application of the reaction to oil processing, in Journal of Molecular Catalysis B Enzymatic. Vol. 17, pp. 133–142, 2002. 197

[171] Uosukainen, E., Lamsa, M., Linko, Y., Linko, P., Leisola, M. Optimization of enzymatic transesterification of rapeseed oil ester using response surface and principal component methodology, in Enzyme and Microbial Technology. Vol. 25, pp. 236–243, 1999. 198

[172] Pizarro, L., Ana, V., Park, E. Y. Lipase-catalyzed production of biodiesel fuel from vegetable oils contained in waste activated bleaching earth, in Process Biochemistry. Vol. 38, pp. 1077–1082, 2003. 198

[173] Shieh, C. J, Liao, H. F., Lee, C. C. Optimization of lipase-catalyzed biodiesel by response surface methodology, in Bioresource Technology. Vol. 88, pp. 10–36, 2003. 203

# Appendix A: San Diego Mechanism - Methanol

```
ELEMENTS
N  AR HE H  O  C
END
SPECIES
N2                  AR                  HE                  H                   O2
OH                  O                   H2                  H2O                 HO2
H2O2                CO                  CO2                 HCO                 CH3
CH4                 CH2O                T-CH2               S-CH2               C2H4
CH3O                C2H5                C2H6                CH                  C2H2
C2H4OOH             OC2H3OOH            C2H3                CH2CHO              C2H4O
HCCO                CH2CO               C2H                 CH2OH               CH3OH
CH3CHO              CH3CO               C2H5OH              CH2CH2OH            CH3CHOH
CH3CH2O             C3H4                C3H3                C3H5                C3H6
C3H8                I-C3H7              N-C3H7              C3H6OOH             OC3H5OOH
END
REACTIONS
H+O2<=>OH+O                                 3.520e+16   -0.700   17069.79
H2+O<=>OH+H                                 5.060e+04    2.670    6290.63
H2+OH<=>H2O+H                               1.170e+09    1.300    3635.28
H2O+O<=>2 OH                                7.600e+00    3.840   12779.64
2 H+M<=>H2+M                                1.300e+18   -1.000       0.00
AR/0.50/ HE/0.50/ H2/2.50/ H2O/12.00/ CO/1.90/ CO2/3.80/
H+OH+M<=>H2O+M                              4.000e+22   -2.000       0.00
AR/0.38/ HE/0.38/ H2/2.50/ H2O/12.00/ CO/1.90/ CO2/3.80/
2 O+M<=>O2+M                                6.170e+15   -0.500       0.00
AR/0.20/ HE/0.20/ H2/2.50/ H2O/12.00/ CO/1.90/ CO2/3.80/
H+O+M<=>OH+M                                4.710e+18   -1.000       0.00
AR/0.75/ HE/0.75/ H2/2.50/ H2O/12.00/ CO/1.90/ CO2/3.80/
O+OH+M<=>HO2+M                              8.000e+15    0.000       0.00
AR/0.75/ HE/0.75/ H2/2.50/ H2O/12.00/ CO/1.90/ CO2/3.80/
H+O2(+M)<=>HO2(+M)                          4.650e+12    0.440       0.00
AR/0.70/ HE/0.70/ H2/2.50/ H2O/16.00/ CO/1.20/ CO2/2.40/ C2H6/1.50/
      LOW  /  5.750e+19   -1.400       0.00 /
      TROE/      0.5     1e-30      1e+30         /
HO2+H<=>2 OH                                7.080e+13    0.000     294.93
HO2+H<=>H2+O2                               1.660e+13    0.000     822.90
HO2+H<=>H2O+O                               3.100e+13    0.000    1720.84
HO2+O<=>OH+O2                               2.000e+13    0.000       0.00
HO2+OH<=>H2O+O2                             2.890e+13    0.000    -497.13
2 OH(+M)<=>H2O2(+M)                         7.400e+13   -0.370       0.00
AR/0.40/ HE/0.40/ H2/2.00/ H2O/6.00/ CO/1.50/ CO2/2.00/ CH4/2.00/ C2H6/3.00/
      LOW  /  2.300e+18   -0.900   -1701.72 /
      TROE/    0.735        94       1756       5182 /
2 HO2<=>H2O2+O2                             3.020e+12    0.000    1386.23
H2O2+H<=>HO2+H2                             2.300e+13    0.000    7950.05
H2O2+H<=>H2O+OH                             1.000e+13    0.000    3585.09
H2O2+OH<=>H2O+HO2                           7.080e+12    0.000    1434.03
```

```
H2O2+O<=>HO2+OH                                 9.630e+06    2.000    3991.40
CO+O(+M)<=>CO2(+M)                              1.800e+11    0.000    2384.08
AR/0.70/ HE/0.70/ H2/2.50/ H2O/12.00/ CO/2.00/ CO2/4.00/
      LOW   /   1.550e+24    -2.790    4190.97 /
CO+OH<=>CO2+H                                   4.400e+06    1.500    -740.92
CO+HO2<=>CO2+OH                                 2.000e+13    0.000   22944.55
CO+O2<=>CO2+O                                   1.000e+12    0.000   47700.05
HCO+M<=>CO+H+M                                  1.860e+17   -1.000   17000.48
H2/1.90/ H2O/12.00/ CO/2.50/ CO2/2.50/
HCO+H<=>CO+H2                                   5.000e+13    0.000       0.00
HCO+O<=>CO+OH                                   3.000e+13    0.000       0.00
HCO+O<=>CO2+H                                   3.000e+13    0.000       0.00
HCO+OH<=>CO+H2O                                 3.000e+13    0.000       0.00
HCO+O2<=>CO+HO2                                 7.580e+12    0.000     409.89
HCO+CH3<=>CO+CH4                                5.000e+13    0.000       0.00
H+HCO(+M)<=>CH2O(+M)                            1.090e+12    0.480    -260.04
AR/0.70/ H2/2.00/ H2O/6.00/ CO/1.50/ CO2/2.00/ CH4/2.00/ C2H6/3.00/
      LOW   /   1.350e+24    -2.570     424.95 /
      TROE/   0.7824       271       2755       6570 /
CH2O+H<=>HCO+H2                                 5.740e+07    1.900    2748.57
CH2O+O<=>HCO+OH                                 3.500e+13    0.000    3513.38
CH2O+OH<=>HCO+H2O                               3.900e+10    0.890     406.31
CH2O+O2<=>HCO+HO2                               6.000e+13    0.000   40674.00
CH2O+HO2<=>HCO+H2O2                             4.110e+04    2.500   10210.33
CH4+H<=>H2+CH3                                  1.300e+04    3.000    8037.76
CH4+OH<=>H2O+CH3                                1.600e+07    1.830    2782.03
CH4+O<=>CH3+OH                                  1.900e+09    1.440    8675.91
CH4+O2<=>CH3+HO2                                3.980e+13    0.000   56890.54
CH4+HO2<=>CH3+H2O2                              9.030e+12    0.000   24641.49
CH3+H<=>T-CH2+H2                                1.800e+14    0.000   15105.16
CH3+H<=>S-CH2+H2                                1.550e+14    0.000   13479.92
CH3+OH<=>S-CH2+H2O                              4.000e+13    0.000    2502.39
CH3+O<=>CH2O+H                                  8.430e+13    0.000       0.00
CH3+T-CH2<=>C2H4+H                              4.220e+13    0.000       0.00
CH3+HO2<=>CH3O+OH                               5.000e+12    0.000       0.00
CH3+O2<=>CH2O+OH                                3.300e+11    0.000    8941.20
CH3+O2<=>CH3O+O                                 1.100e+13    0.000   27820.03
2 CH3<=>C2H4+H2                                 1.000e+14    0.000   32002.87
2 CH3<=>C2H5+H                                  3.160e+13    0.000   14698.85
H+CH3(+M)<=>CH4(+M)                             1.270e+16   -0.630     382.89
AR/0.70/ H2/2.00/ H2O/6.00/ CO/1.50/ CO2/2.00/ CH4/2.00/
      LOW   /   2.470e+33    -4.760    2440.01 /
      TROE/    0.783        74       2941       6964 /
2 CH3(+M)<=>C2H6(+M)                            1.810e+13    0.000       0.00
AR/0.70/ H2/2.00/ H2O/6.00/ CO/1.50/ CO2/2.00/ CH4/2.00/ C2H6/3.00/
      LOW   /   1.270e+41    -7.000    2762.91 /
      TROE/     0.62        73    1.2e+03        /
S-CH2+OH<=>CH2O+H                               3.000e+13    0.000       0.00
S-CH2+O2<=>CO+OH+H                              3.130e+13    0.000       0.00
S-CH2+CO2<=>CO+CH2O                             3.000e+12    0.000       0.00
S-CH2+M<=>T-CH2+M                               6.000e+12    0.000       0.00
H2/2.40/ H2O/15.40/ CO/1.80/ CO2/3.60/
T-CH2+H<=>CH+H2                                 6.020e+12    0.000   -1787.76
T-CH2+OH<=>CH2O+H                               2.500e+13    0.000       0.00
T-CH2+OH<=>CH+H2O                               1.130e+07    2.000    2999.52
T-CH2+O<=>CO+2 H                                8.000e+13    0.000       0.00
T-CH2+O<=>CO+H2                                 4.000e+13    0.000       0.00
T-CH2+O2<=>CO2+H2                               2.630e+12    0.000    1491.40
T-CH2+O2<=>CO+OH+H                              6.580e+12    0.000    1491.40
2 T-CH2<=>C2H2+2 H                              1.000e+14    0.000       0.00
CH+O<=>CO+H                                     4.000e+13    0.000       0.00
CH+O2<=>HCO+O                                   1.770e+11    0.760    -478.01
CH+H2O<=>CH2O+H                                 1.170e+15   -0.750       0.00
CH+CO2<=>HCO+CO                                 4.800e+01    3.220   -3226.58
CH3O+H<=>CH2O+H2                                2.000e+13    0.000       0.00
CH3O+H<=>S-CH2+H2O                              1.600e+13    0.000       0.00
CH3O+OH<=>CH2O+H2O                              5.000e+12    0.000       0.00
```

```
CH3O+O<=>OH+CH2O                          1.000e+13    0.000       0.00
CH3O+O2<=>CH2O+HO2                        4.280e-13    7.600   -3537.28
CH3O+M<=>CH2O+H+M                         7.780e+13    0.000   13513.38
AR/0.70/ H2/2.00/ H2O/6.00/ CO/1.50/ CO2/2.00/ CH4/2.00/
C2H6+H<=>C2H5+H2                          5.400e+02    3.500    5210.33
C2H6+O<=>C2H5+OH                          1.400e+00    4.300    2772.47
C2H6+OH<=>C2H5+H2O                        2.200e+07    1.900    1123.33
C2H6+CH3<=>C2H5+CH4                       5.500e-01    4.000    8293.50
C2H6(+M)<=>C2H5+H(+M)                     8.850e+20   -1.230  102222.75
AR/0.70/ H2/2.00/ H2O/6.00/ CO/1.50/ CO2/2.00/ CH4/2.00/ C2H6/3.00/
      LOW  /  4.900e+42   -6.430  107169.93 /
      TROE/     0.84       125       2219       6882 /
C2H6+HO2<=>C2H5+H2O2                      1.320e+13    0.000   20469.89
C2H5+H<=>C2H4+H2                          3.000e+13    0.000       0.00
C2H5+O<=>C2H4+OH                          3.060e+13    0.000       0.00
C2H5+O<=>CH3+CH2O                         4.240e+13    0.000       0.00
C2H5+O2<=>C2H4+HO2                        7.500e+14   -1.000    4799.95
C2H5+O2<=>C2H4OOH                         2.000e+12    0.000       0.00
C2H4OOH<=>C2H4+HO2                        4.000e+34   -7.200   23000.00
C2H4OOH+O2<=>OC2H3OOH+OH                  7.500e+05    1.300   -5799.95
OC2H3OOH<=>CH2O+HCO+OH                    1.000e+15    0.000   43000.00
C2H5(+M)<=>C2H4+H(+M)                     1.110e+10    1.037   36768.64
AR/0.70/ H2/2.00/ H2O/6.00/ CO/1.50/ CO2/2.00/ CH4/2.00/
      LOW  /  3.990e+33   -4.990   40000.00 /
      TROE/    0.168   1.2e+03         0         /
C2H4+H<=>C2H3+H2                          4.490e+07    2.120   13360.42
C2H4+OH<=>C2H3+H2O                        5.530e+05    2.310    2963.67
C2H4+O<=>CH3+HCO                          2.250e+06    2.080       0.00
C2H4+O<=>CH2CHO+H                         1.210e+06    2.080       0.00
2 C2H4<=>C2H3+C2H5                        5.010e+14    0.000   64700.05
C2H4+O2<=>C2H3+HO2                        4.220e+13    0.000   57623.09
C2H4+HO2<=>C2H4O+OH                       2.230e+12    0.000   17189.29
C2H4O+HO2<=>CH3+CO+H2O2                   4.000e+12    0.000   17007.65
C2H4+M<=>C2H3+H+M                         2.600e+17    0.000   96568.12
AR/0.70/ H2/2.00/ H2O/6.00/ CO/1.50/ CO2/2.00/ CH4/2.00/
C2H4+M<=>C2H2+H2+M                        3.500e+16    0.000   71532.03
AR/0.70/ H2/2.00/ H2O/6.00/ CO/1.50/ CO2/2.00/ CH4/2.00/
C2H3+H<=>C2H2+H2                          4.000e+13    0.000       0.00
C2H3(+M)<=>C2H2+H(+M)                     6.380e+09    1.000   37626.67
AR/0.70/ H2/2.00/ H2O/6.00/ CO/1.50/ CO2/2.00/ CH4/2.00/
      LOW  /  1.510e+14    0.100   32685.95 /
      TROE/      0.3     1e+30     1e-30         /
C2H3+O2<=>CH2O+HCO                        1.700e+29   -5.312    6503.11
C2H3+O2<=>CH2CHO+O                        7.000e+14   -0.611    5262.43
C2H3+O2<=>C2H2+HO2                        5.190e+15   -1.260    3312.62
C2H2+O<=>HCCO+H                           4.000e+14    0.000   10659.66
C2H2+O<=>T-CH2+CO                         1.600e+14    0.000    9894.84
C2H2+O2<=>CH2O+CO                         4.600e+15   -0.540   44933.08
C2H2+OH<=>CH2CO+H                         1.900e+07    1.700     999.04
C2H2+OH<=>C2H+H2O                         3.370e+07    2.000   14000.96
CH2CO+H<=>CH3+CO                          1.500e+09    1.430    2688.81
CH2CO+O<=>T-CH2+CO2                       2.000e+13    0.000    2294.46
CH2CO+O<=>HCCO+OH                         1.000e+13    0.000    2000.48
CH2CO+CH3<=>C2H5+CO                       9.000e+10    0.000       0.00
HCCO+H<=>S-CH2+CO                         1.500e+14    0.000       0.00
HCCO+OH<=>HCO+CO+H                        2.000e+12    0.000       0.00
HCCO+O<=>2 CO+H                           9.640e+13    0.000       0.00
HCCO+O2<=>2 CO+OH                         2.880e+07    1.700    1001.43
HCCO+O2<=>CO2+CO+H                        1.400e+07    1.700    1001.43
C2H+OH<=>HCCO+H                           2.000e+13    0.000       0.00
C2H+O<=>CO+CH                             1.020e+13    0.000       0.00
C2H+O2<=>HCCO+O                           6.020e+11    0.000       0.00
C2H+O2<=>CH+CO2                           4.500e+15    0.000   25095.60
C2H+O2<=>HCO+CO                           2.410e+12    0.000       0.00
CH2OH+H<=>CH2O+H2                         3.000e+13    0.000       0.00
CH2OH+H<=>CH3+OH                          2.500e+17   -0.930    5126.91
CH2OH+OH<=>CH2O+H2O                       2.400e+13    0.000       0.00
```

```
CH2OH+O2<=>CH2O+HO2                          5.000e+12    0.000       0.00
CH2OH+M<=>CH2O+H+M                           5.000e+13    0.000   25119.50
AR/0.70/ H2/2.00/ H2O/6.00/ CO/1.50/ CO2/2.00/ CH4/2.00/
CH3O+M<=>CH2OH+M                             1.000e+14    0.000   19120.46
AR/0.70/ H2/2.00/ H2O/6.00/ CO/1.50/ CO2/2.00/ CH4/2.00/
CH2CO+OH<=>CH2OH+CO                          1.020e+13    0.000       0.00
CH3OH+OH<=>CH2OH+H2O                         1.440e+06    2.000    -838.91
CH3OH+OH<=>CH3O+H2O                          4.400e+06    2.000    1505.74
CH3OH+H<=>CH2OH+H2                           1.354e+03    3.200    3490.68
CH3OH+H<=>CH3O+H2                            6.830e+01    3.400    7239.96
CH3OH+O<=>CH2OH+OH                           1.000e+13    0.000    4684.51
CH3OH+HO2<=>CH2OH+H2O2                       8.000e+13    0.000   19383.37
CH3OH+O2<=>CH2OH+HO2                         2.000e+13    0.000   44933.08
CH3OH(+M)<=>CH3+OH(+M)                       1.900e+16    0.000   91729.92
AR/0.70/ H2/2.00/ H2O/6.00/ CO/1.50/ CO2/2.00/ CH4/2.00/
      LOW  /  2.950e+44   -7.350   95460.09 /
      TROE/    0.414   2.8e+02    5.5e+03        /
CH2CHO<=>CH2CO+H                             1.047e+37   -7.189   44340.34
CH2CHO+H<=>CH3+HCO                           5.000e+13    0.000       0.00
CH2CHO+H<=>CH2CO+H2                          2.000e+13    0.000       0.00
CH2CHO+O<=>CH2O+HCO                          1.000e+14    0.000       0.00
CH2CHO+OH<=>CH2CO+H2O                        3.000e+13    0.000       0.00
CH2CHO+O2<=>CH2O+CO+OH                       3.000e+10    0.000       0.00
CH2CHO+CH3<=>C2H5+CO+H                       4.900e+14   -0.500       0.00
CH2CHO+HO2<=>CH2O+HCO+OH                     7.000e+12    0.000       0.00
CH2CHO+HO2<=>CH3CHO+O2                       3.000e+12    0.000       0.00
CH2CHO<=>CH3+CO                              1.170e+43   -9.800   43799.95
CH3CHO<=>CH3+HCO                             7.000e+15    0.000   81700.05
CH3CO(+M)<=>CH3+CO(+M)                       3.000e+12    0.000   16700.05
AR/0.70/ H2/2.00/ H2O/6.00/ CO/1.50/ CO2/2.00/ CH4/2.00/
      LOW  /  1.200e+15    0.000   12500.00 /
CH3CHO+OH<=>CH3CO+H2O                        3.370e+12    0.000    -619.98
CH3CHO+OH<=>CH2CHO+H2O                       3.370e+11    0.000    -619.98
CH3CHO+O<=>CH3CO+OH                          1.770e+18   -1.900    2979.92
CH3CHO+O<=>CH2CHO+OH                         3.720e+13   -0.200    3559.99
CH3CHO+H<=>CH3CO+H2                          4.660e+13   -0.300    2989.96
CH3CHO+H<=>CH2CHO+H2                         1.850e+12    0.400    5359.94
CH3CHO+CH3<=>CH3CO+CH4                       3.900e-07    5.800    2200.05
CH3CHO+CH3<=>CH2CHO+CH4                      2.450e+01    3.100    5729.92
CH3CHO+HO2<=>CH3CO+H2O2                      3.600e+19   -2.200   14000.00
CH3CHO+HO2<=>CH2CHO+H2O2                     2.320e+11    0.400   14900.10
CH3CHO+O2<=>CH3CO+HO2                        1.000e+14    0.000   42200.05
C2H5OH(+M)<=>CH3+CH2OH(+M)                   5.000e+15    0.000   82000.00
AR/0.70/ H2/2.00/ H2O/6.00/ CO/1.50/ CO2/2.00/ CH4/2.00/
      LOW  /  3.000e+16    0.000   58000.00 /
      TROE/      0.5     1e-30     1e+30        /
C2H5OH(+M)<=>C2H4+H2O(+M)                    8.000e+13    0.000   65000.00
AR/0.70/ H2/2.00/ H2O/6.00/ CO/1.50/ CO2/2.00/ CH4/2.00/
      LOW  /  1.000e+17    0.000   54000.00 /
      TROE/      0.5     1e-30     1e+30        /
C2H5OH+OH<=>CH2CH2OH+H2O                     1.810e+11    0.400     717.02
C2H5OH+OH<=>CH3CHOH+H2O                      3.090e+10    0.500    -380.02
C2H5OH+OH<=>CH3CH2O+H2O                      1.050e+10    0.800     717.02
C2H5OH+H<=>CH2CH2OH+H2                       1.900e+07    1.800    5099.90
C2H5OH+H<=>CH3CHOH+H2                        2.580e+07    1.600    2830.07
C2H5OH+H<=>CH3CH2O+H2                        1.500e+07    1.600    3039.91
C2H5OH+O<=>CH2CH2OH+OH                       9.410e+07    1.700    5460.09
C2H5OH+O<=>CH3CHOH+OH                        1.880e+07    1.900    1820.03
C2H5OH+O<=>CH3CH2O+OH                        1.580e+07    2.000    4450.05
C2H5OH+CH3<=>CH2CH2OH+CH4                    2.190e+02    3.200    9619.98
C2H5OH+CH3<=>CH3CHOH+CH4                     7.280e+02    3.000    7950.05
C2H5OH+CH3<=>CH3CH2O+CH4                     1.450e+02    3.000    7650.10
C2H5OH+HO2<=>CH3CHOH+H2O2                    8.200e+03    2.500   10799.95
C2H5OH+HO2<=>CH2CH2OH+H2O2                   2.430e+04    2.500   15799.95
C2H5OH+HO2<=>CH3CH2O+H2O2                    3.800e+12    0.000   24000.00
C2H4+OH<=>CH2CH2OH                           2.410e+11    0.000   -2380.02
C2H5+HO2<=>CH3CH2O+OH                        4.000e+13    0.000       0.00
```

```
CH3CH2O+M<=>CH3CHO+H+M                    5.600e+34   -5.900   25299.95
AR/0.70/ H2/2.00/ H2O/6.00/ CO/1.50/ CO2/2.00/ CH4/2.00/
CH3CH2O+M<=>CH3+CH2O+M                    5.350e+37   -7.000   23799.95
AR/0.70/ H2/2.00/ H2O/6.00/ CO/1.50/ CO2/2.00/ CH4/2.00/
CH3CH2O+O2<=>CH3CHO+HO2                   4.000e+10    0.000    1099.90
CH3CH2O+CO<=>C2H5+CO2                     4.680e+02    3.200    5380.02
CH3CH2O+H<=>CH3+CH2OH                     3.000e+13    0.000       0.00
CH3CH2O+H<=>C2H4+H2O                      3.000e+13    0.000       0.00
CH3CH2O+OH<=>CH3CHO+H2O                   1.000e+13    0.000       0.00
CH3CHOH+O2<=>CH3CHO+HO2                   4.820e+13    0.000    5020.08
CH3CHOH+O<=>CH3CHO+OH                     1.000e+14    0.000       0.00
CH3CHOH+H<=>C2H4+H2O                      3.000e+13    0.000       0.00
CH3CHOH+H<=>CH3+CH2OH                     3.000e+13    0.000       0.00
CH3CHOH+HO2<=>CH3CHO+2 OH                 4.000e+13    0.000       0.00
CH3CHOH+OH<=>CH3CHO+H2O                   5.000e+12    0.000       0.00
CH3CHOH+M<=>CH3CHO+H+M                    1.000e+14    0.000   25000.00
AR/0.70/ H2/2.00/ H2O/6.00/ CO/1.50/ CO2/2.00/ CH4/2.00/
C3H4+O<=>C2H4+CO                          2.000e+07    1.800    1000.00
CH3+C2H2<=>C3H4+H                         2.560e+09    1.100   13643.88
C3H4+O<=>HCCO+CH3                         7.300e+12    0.000    2250.00
C3H3+H(+M)<=>C3H4(+M)                     3.000e+13    0.000       0.00

     LOW  /  9.000e+15    1.000       0.00 /
     TROE/      0.5     1e+30          0        /
C3H3+HO2<=>C3H4+O2                        2.500e+12    0.000       0.00
C3H4+OH<=>C3H3+H2O                        5.300e+06    2.000    2000.00
C3H3+O2<=>CH2CO+HCO                       3.000e+10    0.000    2868.07
C3H4+H(+M)<=>C3H5(+M)                     4.000e+13    0.000       0.00

     LOW  /  3.000e+24   -2.000       0.00 /
     TROE/      0.8     1e+30          0        /
C3H5+H<=>C3H4+H2                          1.800e+13    0.000       0.00
C3H5+O2<=>C3H4+HO2                        4.990e+15   -1.400   22428.06
C3H5+CH3<=>C3H4+CH4                       3.000e+12   -0.320    -130.98
C2H2+CH3(+M)<=>C3H5(+M)                   6.000e+08    0.000       0.00

     LOW  /  2.000e+09    1.000       0.00 /
     TROE/      0.5     1e+30          0        /
C3H5+OH<=>C3H4+H2O                        6.000e+12    0.000       0.00
C3H3+HCO<=>C3H4+CO                        2.500e+13    0.000       0.00
C3H3+HO2<=>OH+CO+C2H3                     8.000e+11    0.000       0.00
C3H4+O2<=>CH3+HCO+CO                      4.000e+14    0.000   41826.00
C3H6+O<=>C2H5+HCO                         3.500e+07    1.650    -972.75
C3H6+OH<=>C3H5+H2O                        3.100e+06    2.000    -298.28
C3H6+O<=>CH2CO+CH3+H                      1.200e+08    1.650     327.44
C3H6+H<=>C3H5+H2                          1.700e+05    2.500    2492.83
C3H5+H(+M)<=>C3H6(+M)                     2.000e+14    0.000       0.00
AR/0.70/ H2/2.00/ H2O/6.00/ CO/1.50/ CO2/2.00/ CH4/2.00/ C2H6/3.00/
     LOW  /  1.330e+60  -12.000    5967.97 /
     TROE/     0.02      1097       1097       6860 /
C3H5+HO2<=>C3H6+O2                        2.660e+12    0.000       0.00
C3H5+HO2<=>OH+C2H3+CH2O                   3.000e+12    0.000       0.00
C2H3+CH3(+M)<=>C3H6(+M)                   2.500e+13    0.000       0.00
AR/0.70/ H2/2.00/ H2O/6.00/ CO/1.50/ CO2/2.00/ CH4/2.00/ C2H6/3.00/
     LOW  /  4.270e+58  -11.940    9770.55 /
     TROE/    0.175      1341     6e+04 1.014e+04 /
C3H6+H<=>C2H4+CH3                         1.600e+22   -2.390   11185.47
CH3+C2H3<=>C3H5+H                         1.500e+24   -2.830   18618.55
C3H8(+M)<=>CH3+C2H5(+M)                   1.100e+17    0.000   84392.93

     LOW  /  7.830e+18    0.000   64978.01 /
     TROE/     0.76   1.9e+03         38        /
C3H8+O2<=>I-C3H7+HO2                      4.000e+13    0.000   47500.00
C3H8+O2<=>N-C3H7+HO2                      4.000e+13    0.000   50932.12
C3H8+H<=>I-C3H7+H2                        1.300e+06    2.400    4471.08
C3H8+H<=>N-C3H7+H2                        1.330e+06    2.540    6761.47
C3H8+O<=>I-C3H7+OH                        4.760e+04    2.710    2107.31
```

```
C3H8+O<=>N-C3H7+OH                                1.900e+05    2.680    3718.45
C3H8+OH<=>N-C3H7+H2O                              1.000e+10    1.000    1599.90
C3H8+OH<=>I-C3H7+H2O                              2.000e+07   -1.600     -99.90
C3H8+HO2<=>I-C3H7+H2O2                            9.640e+03    2.600   13917.30
C3H8+HO2<=>N-C3H7+H2O2                            4.760e+04    2.550   16491.40
I-C3H7+C3H8<=>N-C3H7+C3H8                         8.400e-03    4.200    8675.91
C3H6+H(+M)<=>I-C3H7(+M)                           1.330e+13    0.000    1560.71
AR/0.70/ H2/2.00/ H2O/6.00/ CO/1.50/ CO2/2.00/ CH4/2.00/ C2H6/3.00/
      LOW   /   8.700e+42   -7.500    4732.31 /
      TROE/        1      1000      645.4       6844 /
I-C3H7+O2<=>C3H6+HO2                              1.300e+11    0.000       0.00
N-C3H7(+M)<=>CH3+C2H4(+M)                         1.230e+13   -0.100   30210.33

      LOW   /   5.490e+49  -10.000   35778.92 /
      TROE/     -1.17       251      1e-15       1185 /
H+C3H6(+M)<=>N-C3H7(+M)                           1.330e+13    0.000    3260.04
AR/0.70/ H2/2.00/ H2O/6.00/ CO/1.50/ CO2/2.00/ CH4/2.00/ C2H6/3.00/
      LOW   /   6.260e+38   -6.660    7000.48 /
      TROE/        1      1000       1310   4.81e+04 /
N-C3H7+O2<=>C3H6+HO2                              3.500e+16   -1.600    3500.00
N-C3H7+O2<=>C3H6OOH                               2.000e+12    0.000       0.00
C3H6OOH<=>C3H6+HO2                                2.500e+35   -8.300   22000.00
C3H6OOH+O2<=>OC3H5OOH+OH                          1.500e+08    0.000   -7000.00
OC3H5OOH<=>CH2CHO+CH2O+OH                         1.000e+15    0.000   43000.00
END
```

# Appendix B: EXGAS Mechanism - Methanol

```
ELEMENTS
H O C N HE AR
END
SPECIES

! Biradicals :
B1O
B2CO
B3C
B4CH
B5CH2
B6CH2

! Primary molecules :
! Reactants:
H2
H2O
O2
H2O2
CH4
HCHO
CH3OH
CO2
CH3OOH
C2H2T
C2H4Z
C2H6
CH2COZ
CH3CHO
C2H5OH
C2H5OOH
CH3COOOH
C3H6Y
C3H8
C4H8Y
C4H10
C2H5CHO
C3H7OH
C2H6CO
C3H8CO
C4H6Z2
C2H3CHOZ

! Secondary molecules :

! Cyclic primary molecules :
C2H4O#3
```

```
! Cyclic secondary molecules :
C3H6O#3
C4H8O#3
C6H10Z#6

! Free radicals :
R1H
R2OH
R3OOH
R4CH3
R5CHO
R6CH2OH
R7CH3O
R8CH3OO
R9C2HT
R10C2H3V
R11C2H5
R12CHCOV
R13CH2CHO
R14CH3CO
R15C2H5O
R16C2H4OOH
R17C2H5OO
R18CH3COOO
R19C3H7
R20C4H9
 !Cyclic free radicals:

! lumped Free radicals :
! lumped Cyclic free radicals :

N2
HE
AR
END
!
!
REACTIONS

!     ------------------
!     PRIMARY REACTIONS
!     ------------------
!   molecular elimination :
! ene reaction :
!   retro-ene reaction :
!   unimolecular initiations :

!   bimolecular initiations :

!   additions :

!   additions with oxygen:

!   isomerisations :

!   Decomposition of OOQOOH into branching agents:

!   beta-scissions :
R19C3H7=>R4CH3+C2H4Z     2.0E+0013   0.000   31000.0   ! DE 1 CN
R19C3H7=>R1H+C3H6Y     3.0E+0013   0.000   38000.0   ! DE 2 CN
R20C4H9=>R11C2H5+C2H4Z     2.0E+0013   0.000   28700.0   ! DE 3 CW
R20C4H9=>R1H+C4H8Y     3.0E+0013   0.000   38000.0   ! DE 4 CN
! decomposition of R(.)CO free radicals

!   decomposition to o-rings :
```

```
!   oxidations :

!   oxidations of R(.)(OH) radicals:

!   metathesis :

!   combinations :

!   dismutations :

!    ____________________
!    SECONDARY MECHANISM
!    ____________________

! Hydroperoxide decomposition

! Dihydroperoxide decomposition

! Ketohydroperoxide decomposition

! Aldohydroperoxide decomposition

! Hydroperoxy ring decomposition

! Alcane reactions
C3H8+R1H=>H2+R4CH3+C2H4Z     2.7E+0007   2.000   5000.0   ! ALC 5
C3H8+R2OH=>H2O+R4CH3+C2H4Z     7.8E+0006   2.000   -765.0   ! ALC 6
C3H8+R3OOH=>H2O2+R4CH3+C2H4Z     1.2E+0012   0.000   15500.0   ! ALC 7
C3H8+R4CH3=>CH4+R4CH3+C2H4Z     6.0E+0011   0.000   9600.0   ! ALC 8
C3H8+R8CH3OO=>CH3OOH+R4CH3+C2H4Z     4.5E+0012   0.000   17500.0   ! ALC 9
C3H8+R11C2H5=>C2H6+R4CH3+C2H4Z     6.0E+0011   0.000   11000.0   ! ALC 10
C4H10+R1H=>H2+R11C2H5+C2H4Z     2.7E+0007   2.000   5000.0   ! ALC 11
C4H10+R2OH=>H2O+R11C2H5+C2H4Z     7.8E+0006   2.000   -765.0   ! ALC 12
C4H10+R3OOH=>H2O2+R11C2H5+C2H4Z     1.2E+0012   0.000   15500.0   ! ALC 13
C4H10+R4CH3=>CH4+R11C2H5+C2H4Z     6.0E+0011   0.000   9600.0   ! ALC 14
C4H10+R8CH3OO=>CH3OOH+R11C2H5+C2H4Z     4.5E+0012   0.000   17500.0   ! ALC 15
C4H10+R11C2H5=>C2H6+R11C2H5+C2H4Z     6.0E+0011   0.000   11000.0   ! ALC 16

! O-ring decomposition
C3H6O#3+R1H=>H2+CH2COZ+R4CH3     2.7E+0007   2.000   5000.0   ! DOR 17
C3H6O#3+R2OH=>H2O+CH2COZ+R4CH3     7.8E+0006   2.000   -765.0   ! DOR 18
C3H6O#3+R3OOH=>H2O2+CH2COZ+R4CH3     1.2E+0012   0.000   15500.0   ! DOR 19
C3H6O#3+R4CH3=>CH4+CH2COZ+R4CH3     6.0E+0011   0.000   9600.0   ! DOR 20
C3H6O#3+R8CH3OO=>CH3OOH+CH2COZ+R4CH3     6.0E+0011   0.000   9600.0   ! DOR 21
C3H6O#3+R11C2H5=>C2H6+CH2COZ+R4CH3     6.0E+0011   0.000   11000.0   ! DOR 22
C4H8O#3+R1H=>H2+CH2COZ+R11C2H5     2.7E+0007   2.000   5000.0   ! DOR 23
C4H8O#3+R2OH=>H2O+CH2COZ+R11C2H5     7.8E+0006   2.000   -765.0   ! DOR 24
C4H8O#3+R3OOH=>H2O2+CH2COZ+R11C2H5     1.2E+0012   0.000   15500.0   ! DOR 25
C4H8O#3+R4CH3=>CH4+CH2COZ+R11C2H5     6.0E+0011   0.000   9600.0   ! DOR 26
C4H8O#3+R8CH3OO=>CH3OOH+CH2COZ+R11C2H5     6.0E+0011   0.000   9600.0   ! DOR 27
C4H8O#3+R11C2H5=>C2H6+CH2COZ+R11C2H5     6.0E+0011   0.000   11000.0   ! DOR 28
C3H6O#3+B1O=>R2OH+R5CHO+C2H4Z     7.8E+0013   0.000   5200.0   ! DOR 29
C4H8O#3+B1O=>R2OH+R13CH2CHO+C2H4Z     7.8E+0013   0.000   5200.0   ! DOR 30


! Metatheses of oxiranes and furanes

! decompositions of cyclo-ether radicals

! Addition of oxygen on cyclo-ether radicals

! Isomerization of peroxy-radicals

!Addition of oxygen on cyclo-peroxy radicals

! Formation of cyclo-ether ketohydroperoxydes
```

```
! Decomposition of cyclo-ether ketohydroperoxydes

! Olefin reactions
!  addition of H and CH3 on olefins
C3H6Y+R1H=>C2H4Z+R4CH3     7.2E+0012  0.000  2900.0  ! ROL 31
C4H8Y+R1H=>C2H4Z+R11C2H5    7.2E+0012  0.000  2900.0  ! ROL 32

!  addition of OH on olefins
C3H6Y+R2OH=>R4CH3+CH3CHO     1.4E+0012  0.000  -900.0  ! ALD 33
C4H8Y+R2OH=>R4CH3+C2H5CHO     1.4E+0012  0.000  -900.0  ! ALD 34

C3H6Y+R2OH=>HCHO+R11C2H5     1.4E+0012  0.000  -900.0  ! FOH 35
C4H8Y+R2OH=>HCHO+R4CH3+C2H4Z     1.4E+0012  0.000  -900.0  ! FOH 36

!  addition of O on olefins
C3H6Y+B1O=>CH2COZ+R4CH3+R1H     3.4E+0007  1.830  550.0  ! AOZ 37
C4H8Y+B1O=>CH2COZ+R11C2H5+R1H     3.4E+0007  1.830  550.0  ! AOZ 37

!  addition of OOH on olefins
C3H6Y+R3OOH=>R2OH+C3H6O#3     1.0E+0012  0.000  14400.0  ! FCY 37
C4H8Y+R3OOH=>R2OH+C4H8O#3     1.0E+0012  0.000  14400.0  ! FCY 38

!   olefin to dienes

! Metathesis with YH

! Addition of .Y on YH

! Alkohol reactions

! Aldehydes metathesis

! Keto radicals to products of the base and :CO


! keto radicals addition to O2

! Peracide radical decomposition

! Ketones reactions



! Alkohol ene to dienes

! Diels Alder
C4H6Z2+C2H4Z=>C6H10Z#6     3.0E+0010  0.000  27500.0  ! DA 39

! .Y termination


! Pascal C0 C2 lumped data base ********************************************
! VERSION X.X 01/2002       ************************************************

!REACTIONS DE LA MATRICE O(0)C(y)H(z)!

!REACTIONS DE H2!
R1H+R1H+M=H2+M                1.87E18        -1.00      0.0    !(1,-1)<BAULCH94>!
       O2/0.4/ B2CO/0.75/ CO2/1.5/ H2O/6.5/ CH4/3.0/ H2/0.0/
       C2H6/3.0/ AR/0.35/ N2/0.4/ HE/0.35/

!REACTIONS DE B4CH!
B4CH+R1H=B3C+H2                7.8E13          0.        0.     !(2,-2)<PEETERS97>!

!REACTIONS DE B6CH2!
B6CH2+M=B5CH2+M                1.51E13         0.0       0.0    !(3,-3)<BAULCH94>!
       N2/.4/ O2/.4/ B2CO/.75/ CO2/1.5/ H2O/6.5/ CH4/.48/
```

```
      HE/0.35/ C2H4Z/1.6/ AR/.24/
B6CH2+R1H=B4CH+H2                3.0E13          0.        0.      !(4,-4)<TSANG86>!

!REACTIONS DE B5CH2!
B5CH2+R1H=B4CH+H2                 6.0E12         0.       -1.8E3 !(5,-5)<BAULCH94>!
B5CH2+B3C=R9C2HT+R1H              5.0E13         0.        0.     !(6,-6)<RANZI94>!
B5CH2+B5CH2=>C2H2T+R1H+R1H        1.2E14         0.        0.8E3 !(7)<BAULCH94>!

!REACTIONS DE R4CH3!
R4CH3+M=B5CH2+R1H+M               2.91E16       0.0       90.7E3 !(8,-8)<BAULCH94>!
      O2/0.4/ B2CO/0.75/ CO2/1.5/ H2O/6.5/ CH4/3.0/ C2H6/3.0/ AR/0.35/
      N2/0.4/ HE/0.35/
R4CH3+R1H=B6CH2+H2                6.0E13         0.        15.0E3 !(9,-9)<BAULCH94>!
R4CH3+B4CH=R10C2H3V+R1H           3.0E13         0.          0.   !(10,-10)<DAGAUT91>
R4CH3+B6CH2=C2H4Z+R1H             1.8E13         0.          0.   !(11,-11)<TSANG86>!
R4CH3+B5CH2=C2H4Z+R1H             4.2E13         0.          0.   !(12,-12)<BAULCH94>!
R4CH3+B3C=C2H2T+R1H               5.0E13         0.          0.   !(13,-13)<RANZI94>!
R4CH3+R4CH3(+M)=>C2H6(+M)         3.61E13        0.          0.   !(14)<BAULCH94>!
      O2/0.4/ B2CO/0.75/ CO2/1.5/ H2O/6.5/ CH4/3.0/ C2H6/3.0/ AR/0.35/
      N2/0.4/ HE/0.35/
      LOW / 3.63E41   -7.0    2.76E3 /
      TROE /  0.62   73   1180 /
C2H6(+M)=>R4CH3+R4CH3(+M)         1.8E21       -1.24      90.9E3 !(-14)<BAULCH94>!
      O2/0.4/ B2CO/0.75/ CO2/1.5/ H2O/6.5/ CH4/3.0/ C2H6/3.0/ AR/0.35/
      N2/0.4/ HE/0.35/
      LOW / 1.89E49    -8.24    93.7E3/
      TROE /  0.62   73   1180 /
R4CH3+R4CH3=R11C2H5+R1H           3.0E13         0.        13.5E3 !(15,-15)<BAULCH94>!
R4CH3+R4CH3=C2H4Z+H2              2.1E14         0.        19.3E3 !(16,-16)<FRANK86NIST>!

!REACTIONS DE CH4!
R1H+R4CH3(+M)=>CH4(+M)            1.67E14        0.          0. !(17)<BAULCH94>!
      O2/0.4/ B2CO/0.75/ CO2/1.5/ H2O/6.5/ CH4/3.0/ C2H6/3.0/ AR/0.35/
      N2/0.4/ HE/0.35/
      LOW /  1.408E24   -1.8    0.0 /
      TROE / 0.37 3315 61 /
CH4(+M)=>R4CH3+R1H(+M)            2.4E16         0.      105.0E3 !(-17)<BAULCH94>!
      O2/0.4/ B2CO/0.75/ CO2/1.5/ H2O/6.5/ CH4/0.0/ C2H6/3.0/ AR/0.35/
      N2/0.4/ HE/0.35/
      LOW / 1.29E18     0.00   90.9E3 /
      TROE / 0   1350   1   7830 /
CH4(+CH4)=>R4CH3+R1H(+CH4)        2.4E16         0.      105.0E3 !(-17')<BAULCH94>!
      LOW / 8.43E17     0.00   90.9E3 /
      TROE / 0.69   90   2210 /
CH4+R1H=R4CH3+H2                  1.3E04         3.        8.0E3 !(18,-18)<BAULCH94>!
CH4+B4CH=C2H4Z+R1H                3.0E13         0.       -0.4E3 !(19,-19)<DAGAUT91BAULCH94>!
CH4+B6CH2=R4CH3+R4CH3             4.2E13         0.          0. !(20,-20)<TSANG86>!

!REACTIONS DE R9C2HT!
R9C2HT+B6CH2=C2H2T+B4CH           1.8E13         0.          0. !(21,-21)<TSANG86>!
R9C2HT+B5CH2=C2H2T+B4CH           1.8E13         0.          0. !(22,-22)<TSANG86>!
R9C2HT+CH4=C2H2T+R4CH3            1.2E12         0.          0. !(23,-23)<BAULCH94>!

!REACTIONS DE C2H2T!
C2H2T+M=R9C2HT+R1H+M              1.14E17        0.      107.0E3 !(24,-24)<BAULCH94>!
      O2/0.4/ B2CO/0.75/ CO2/1.5/ H2O/6.5/ CH4/3.0/ C2H6/3.0/ AR/0.35/
      N2/0.4/ HE/0.35/
C2H2T+R1H=R9C2HT+H2               6.6E13         0.        27.7E3 !(25,-25)<BAULCH94>!

!REACTIONS DE R10C2H3V!
R10C2H3V(+M)=C2H2T+R1H(+M)        2.0E14         0.        39.8E3 !(26,-26)<BAULCH94>!
      O2/0.4/ B2CO/0.75/ CO2/1.5/ H2O/6.5/ CH4/3.0/ AR/0.35/
      N2/0.4/ HE/0.35/
      LOW / 1.19E42   -7.50   45.55E3 /
      TROE     /0.35    1.0        1.E8/
R10C2H3V+R1H=C2H2T+H2             1.2E13         0.          0. !(27,-27)<BAULCH94>!
R10C2H3V+B6CH2=C2H2T+R4CH3        1.8E13         0.          0. !(28,-28)<TSANG86>!
```

```
R10C2H3V+B5CH2=C2H2T+R4CH3       1.8E13       0.          0. !(29,-29)<TSANG86>!
R10C2H3V+R4CH3=CH4+C2H2T         3.9E11       0.          0. !(30,-30)<TSANG86>!
R10C2H3V+R9C2HT=2C2H2T            9.6E11       0.          0. !(31,-31)<TSANG86>!
R10C2H3V+R10C2H3V=C2H4Z+C2H2T    9.6E11       0.          0. !(32,-32)<TSANG86>!

!REACTIONS DE C2H4Z!
C2H4Z+M=C2H2T+H2+M               9.97E16      0.       71.6E3 !(33,-33)<BAULCH94>!
      O2/0.4/ B2CO/0.75/ CO2/1.5/ H2O/6.5/ CH4/3.0/ C2H6/3.0/ AR/0.35/
      N2/0.4/ HE/0.35/
C2H4Z+M=R10C2H3V+R1H+M           7.40E17      0.       96.7E3 !(34,-34)<BAULCH94>!
      O2/0.4/ B2CO/0.75/ CO2/1.5/ H2O/6.5/ CH4/3.0/ C2H6/3.0/ AR/0.35/
      N2/0.4/ HE/0.35/
C2H4Z+R1H=R10C2H3V+H2            5.0E7      1.93       13.0E3 !(35,-35)SLAGLE96!
C2H4Z+R4CH3=CH4+R10C2H3V         6.3E11       0.       16.0E3 !(36,-36)BACK89!

!REACTIONS DE R11C2H5!
R11C2H5(+M)=C2H4Z+R1H(+M)        8.2E13       0.     40.0E3  !(37,-37) BAULCH94!
      O2/0.4/ B2CO/0.75/ CO2/1.5/ H2O/6.5/ CH4/3.0/ C2H6/3.0/ AR/0.35/
      N2/0.4/ HE/0.35/
      LOW / 3.40E17    0.00    33.4E3 /
      TROE / 0.75   97   1379/
R11C2H5+R1H=C2H4Z+H2             1.8E12       0.          0. !(38,-38)<TSANG86>!
R11C2H5+R1H=C2H6                 3.6E13       0.          0. !(39,-39><TSANG86>!
R11C2H5+B6CH2=C2H4Z+R4CH3        9.0E12       0.          0. !(40,-40)<TSANG86>!
R11C2H5+B5CH2=C2H4Z+R4CH3        1.8E13       0.          0. !(41,-41)<TSANG86>!
R11C2H5+R4CH3=C2H4Z+CH4          1.1E12       0.          0. !(42,-42)<BAULCH94>!
R11C2H5+R9C2HT=C2H2T+C2H4Z       1.8E12       0           0. !(43,-43)<TSANG86>!
R11C2H5+R10C2H3V=2C2H4Z          4.8E11       0.          0. !(44,-44)<TSANG86>!
R11C2H5+R10C2H3V=C2H2T+C2H6      4.8E11       0.          0. !(45,-45)<TSANG86>!
R11C2H5+R11C2H5=C2H4Z+C2H6       1.4E12       0.          0. !(46,-46)<BAULCH94>!

!REACTIONS DE C2H6!
C2H6+M=C2H4Z+H2+M                2.3E17       0.       67.4E3 !(47,-47)<SCHULTZ85NIST>!
C2H6+R1H=R11C2H5+H2              1.4E9        1.5       7.4E3 !(48,-48)<BAULCH94>!
C2H6+B6CH2=R4CH3+R11C2H5         1.1E14       0.           0. !(49,-49)<TSANG86>!
C2H6+R4CH3=R11C2H5+CH4           1.5E-7       6.0       5.8E3 !(50,-50)<BAULCH94>!
C2H6+R9C2HT=C2H2T+R11C2H5        3.6E12       0.           0. !(51,-51)<TSANG86>!
C2H6+R10C2H3V=R11C2H5+C2H4Z      6.0E2        3.3      10.5E3 !(52,-52)<TSANG86>!


!************************************************************************!

!************************************************************************!


!REACTIONS DE LA MATRICE O(x)C(y)H(z)  x>0 !


!REACTIONS DE B1O!
B1O+H2=R2OH+R1H                  5.1E4        2.67      6.2E3 !(53,-53)<BAULCH94>!
B1O+B4CH=B2CO+R1H                3.9E13       0.           0. !(54,-54)<BAULCH94>!
B1O+B4CH=B3C+R2OH                1.5E13       0.        4.7E3  !(55,-55)<MUR86NIS>!
B1O+B6CH2=>B2CO+2R1H             1.5E13       0.           0. !(56)       <TSANG86>!
B1O+B6CH2=B2CO+H2                1.5E13       0.           0. !(57,-57) <TSANG86>!
B1O+B5CH2=>B2CO+2R1H             7.2E13       0.           0. !(58)     <BAULCH94>!
B1O+B5CH2=B2CO+H2                4.8E13       0.           0. !(59,-59)<BAULCH94>!
B1O+R4CH3=HCHO+R1H               8.4E13       0.           0. !(60,-60)<BAULCH94>!
B1O+R4CH3=R7CH3O                 8.0E15      -2.12       0.6E3 !(61,-61)<DEAN87NIS>!
B1O+CH4=R4CH3+R2OH               7.2E8        1.56      8.4E3 !(62,-62)<BAULCH94>!
B1O+R9C2HT=B4CH+B2CO             1.0E13       0.           0. !(63,-63)<DAGAUT91>!
B1O+C2H2T=B5CH2+B2CO             2.17E06      2.1       1.6E3 !(64,-64)<BAULCH LEEDS>!
B1O+C2H2T=R12CHCOV+R1H           5.06E06      2.1       1.6E3 !(65,-65)<BAULCH LEEDS>!
B1O+R10C2H3V=R4CH3+B2CO          3.0E13       0.           0. !(66,-66)<DAGAUT91>!
B1O+R10C2H3V=CH2COZ+R1H          9.6E13       0.           0. !(67,-67)<TSANG86>!
B1O+C2H4Z=R4CH3+R5CHO            8.1E6        1.88      0.2E3 !(68,-68)<BAULCH94>!
B1O+C2H4Z=HCHO+B5CH2             4.00E5       1.88      0.2E3 !(69,-69)<BAULCH94>!
B1O+C2H4Z=CH2COZ+H2              6.6E5        1.88      0.2E3 !(70,-70)<BAULCH94>!
```

```
B1O+C2H4Z=R13CH2CHO+R1H          4.7E6        1.88      0.2E3 !(71,-71)<BAULCH94>!
B1O+C2H4Z=R2OH+R10C2H3V          1.5E7        1.91      3.7E3 !(72,-72)<MAHMUD87NIST>!
B1O+R11C2H5=HCHO+R4CH3           1.1E13       0.           0. !(73,-73)<BAULCH94>!
B1O+R11C2H5=CH3CHO+R1H           5.5e13       0.           0. !(74,-74)<BAULCH94>!
B1O+R11C2H5=C2H4Z+R2OH           3.0E13       0.           0. !(75,-75)<DAGAUT91>!
B1O+C2H6=R11C2H5+R2OH            1.0E9        1.5       5.8E3 !(76,-76)<BAULCH94>!

!REACTIONS DE R2OH!
R1H+B1O+M=R2OH+M                 1.18E19     -1.0         0.0  !(77,-77)<BAULCH94>!
        O2/0.4/ B2CO/0.75/ CO2/1.5/ H2O/6.5/ CH4/3.0/ C2H6/3.0/ AR/0.35/
        N2/0.4/ HE/0.35/
R1H+R2OH+M=H2O+M                  5.53E+22    -2.0         0.0  !(78,-78)<BAULCH94>!
        O2/0.4/ B2CO/0.75/ CO2/1.5/ H2O/2.55/ CH4/3.0/ C2H6/3.0/ AR/0.15/
        N2/0.4/ HE/0.35/
R2OH+H2=R1H+H2O                  1.0E8        1.6       3.3E3 !(79,-79)<BAULCH94>!
R2OH+B3C=B2CO+R1H                5.0E13       0.           0. !(80,-80)<RANZI94>!
R2OH+B4CH=R5CHO+R1H              3.0E13       0.           0. !(81,-81)<DAGAUT91>!
R2OH+B6CH2=HCHO+R1H              3.0E13       0.           0. !(82,-82)<TSANG86>!
R2OH+B5CH2=HCHO+R1H              1.8E13       0.           0. !(83,-83)<TSANG86>!
R2OH+R4CH3=B6CH2+H2O             7.2E13       0.        2.7E3 !(84,-84)<BAULCH94>!
R2OH+R4CH3(+M)=CH3OH(+M)         6.0E13       0.           0. !(85,-85)<BAULCH94>!
        LOW      /1.4E44      -8.2          0./
        TROE     /0.82        200.       1438./
R2OH+R4CH3=HCHO+H2               3.2E12      -0.53     10.8E3 !(86,-86)<DAGAUT91>!
R2OH+R4CH3=R7CH3O+R1H            5.7E12      -0.23     13.9E3 !(87,-87)<DAGAUT91>!
R2OH+CH4=R4CH3+H2O               1.6E7        1.83      2.7E3 !(88,-88)<BAULCH94>!
R2OH+R9C2HT=C2H2T+B1O            1.8E13       0.           0. !(89,-89)<TSANG86>!
R2OH+R9C2HT=B5CH2+B2CO           1.8E13       0.           0. !(90,-90)<TSANG86>!
R2OH+R9C2HT=R12CHCOV+R1H         2.0E13       0.           0. !(91,-91)<DAGAUT91>!
R2OH+C2H2T=R9C2HT+H2O            1.4E4        2.68     12.0E3 !(92,-92)<TSANG86>!
R2OH+C2H2T=CH2COZ+R1H            2.2E-4       4.5      -1.0E3 !(93,-93)<DAGAUT91>!
R2OH+C2H2T=R4CH3+B2CO            4.8E-4       4.       -2.0E3 !(94,-94)<DAGAUT91>!
R2OH+R10C2H3V=C2H2T+H2O          3.0E13       0.           0. !(95,-95)<TSANG86>!
R2OH+R10C2H3V=CH3CHO             3.0E13       0.           0. !(96,-96)<TSANG86>!
R2OH+C2H4Z=R10C2H3V+H2O          2.0E13       0.        5.9E3 !(97,-97)<BAULCH94>!
R2OH+C2H4Z=R4CH3+HCHO            2.0E12       0.        0.9E3 !(98,-98)<GLARBORG86>!
R2OH+R11C2H5=C2H4Z+H2O           2.4E13       0.           0. !(99,-99)<TSANG86>!
R2OH+R11C2H5=>R4CH3+R1H+HCHO     2.4E13       0.           0. !(100)    <TSANG86>!
R2OH+C2H6=R11C2H5+H2O            7.2E6        2.        0.9E3 !(101,-101)<BAULCH94>!
R2OH+R2OH=H2O+B1O                1.5E9        1.14      0.1E3 !(102,-102)<BAULCH94>!

!REACTIONS DE H2O!
H2O+B4CH=R6CH2OH                 5.7E12       0.       -0.8E3 !(103,-103)<BAULCH94>!
H2O+B6CH2=CH3OH                  1.8E13       0.           0. !(104,-104)<TSANG86>!

!REACTIONS DE B2CO!
B2CO+R4CH3(+M)=R14CH3CO(+M)      5.0E11       0.        6.9E3 !(105,-105)<BAULCH94>!
        LOW      /1.1E14      0.         3.8E3/
        TROE     /0.5         1.0        1.0E8/
B2CO+B1O+M=CO2+M                 1.54E15      0.0       3.0E3 !(106,-106)<TSANG86>!
        O2/0.4/ B2CO/0.75/ CO2/1.5/ H2O/6.5/ CH4/3.0/ C2H6/3.0/ AR/0.35/
        N2/0.4/ HE/0.35/
B2CO+R2OH=CO2+R1H                6.3E6        1.5      -0.5E3 !(107,-107)<BAULCH94>!

!REACTIONS DE R5CHO!
R5CHO+M=R1H+B2CO+M               1.9E17      -1.       17.0E3 !(108,-108)<WANG97>!
        H2/2.0/ B2CO/1.5/ CO2/2.0/ H2O/6.0/
R5CHO+R1H=H2+B2CO                9.0E13       0.           0. !(109,-109)<BAULCH94>!
R5CHO+R1H=B1O+B5CH2              4.0E13       0.      102.5E3 !(110,-110)<TSUBOI81NIST>!
R5CHO+B6CH2=R4CH3+B2CO           1.8E13       0.           0. !(111,-111)<TSANG86>!
R5CHO+B5CH2=R4CH3+B2CO           1.8E13       0.           0. !(112,-112)<TSANG86>!
R5CHO+R4CH3=CH4+B2CO             1.2E14       0.           0. !(113,-113)<TSANG86>!
R5CHO+R4CH3=CH3CHO               1.8E13       0.           0. !(114,-114)<TSANG86>!
R4CH3+HCHO=R5CHO+CH4             7.7E-8       6.1      1.97E3 !(115,-115)<BAULCH94>!
R5CHO+R9C2HT=C2H2T+B2CO            6.0E13       0.           0. !(116,-116)<TSANG86>!
R5CHO+R10C2H3V=C2H4Z+B2CO        9.0E13       0.           0. !(117,-117)<TSANG86>!
R10C2H3V+HCHO=R5CHO+C2H4Z        5.4E3        2.81      5.9E3 !(118,-118)<TSANG86>!
```

```
R5CHO+R11C2H5=C2H6+B2CO          1.2E14      0.          0. !(119,-119)<TSANG86>!
R11C2H5+HCHO=R5CHO+C2H6          5.57E3      2.81    5.86E3 !(120,-120)<TSANG86>!
R5CHO+B1O=R1H+CO2                3.0E13      0.          0. !(121,-121)<BAULCH94>!
R5CHO+B1O=R2OH+B2CO              3.0E13      0.          0. !(122,-122)<BAULCH94>!
R5CHO+R2OH=H2O+B2CO              1.1E14      0.          0. !(123,-123)<BAULCH94>!
R5CHO+R5CHO=HCHO+B2CO            3.0E13      0.          0. !(124,-124)<BAULCH94>!

!REACTIONS DE HCHO!
HCHO+M=R5CHO+R1H+M               1.40E36    -5.54    96.8E3 !(125,-125)<BAULCH94>!
        O2/0.4/ B2CO/0.75/ CO2/1.5/ H2O/6.5/ CH4/3.0/ C2H6/3.0/ AR/0.35/
        N2/0.4/ HE/0.35/
HCHO+M=H2+B2CO+M                 3.26E36    -5.54    96.8E3 !(126,-126)<BAULCH94>!
        O2/0.4/ B2CO/0.75/ CO2/1.5/ H2O/6.5/ CH4/3.0/ C2H6/3.0/ AR/0.35/
        N2/0.4/ HE/0.35/
HCHO+R1H=R5CHO+H2                1.3E8       1.62     2.1E3 !(127,-127)<BAULCH94>!
HCHO+B4CH=R13CH2CHO              9.6E13      0.      -0.5E3 !(128,-128)<BAULCH94average>!
HCHO+B6CH2=R4CH3+R5CHO           1.2E12      0.          0. !(129,-129)<TSANG86>!
HCHO+B1O=R5CHO+R2OH              4.1E11      0.57     2.7E3 !(130,-130)<BAULCH94>!
HCHO+R2OH=R5CHO+H2O              3.4E9       1.18    -0.4E3 !(131,-131)<BAULCH94>!

!REACTIONS DE R7CH3O!
R7CH3O+M=HCHO+R1H+M              1.55E14     0.00    13.5E3 !(132,-132)<BAULCH94>!
       O2/0.4/ B2CO/0.75/ CO2/1.5/ H2O/6.5/ CH4/3.0/ C2H6/3.0/ AR/0.35/
       N2/0.4/ HE/0.35/
R7CH3O+R1H=HCHO+H2               1.8E13      0.          0. !(133,-133)<BAULCH94>!
R7CH3O+B6CH2=R4CH3+HCHO          1.8E13      0.          0. !(134,-134)<TSANG86>!
R7CH3O+B5CH2=R4CH3+HCHO          1.8E13      0.          0. !(135,-135)<TSANG86>!
R7CH3O+R4CH3=HCHO+CH4            2.4E13      0.          0. !(136,-136)<TSANG86>!
R7CH3O+CH4=R4CH3+CH3OH           1.6E11      0.       8.8E3 !(137,-137)<TSANG86>!
R7CH3O+R9C2HT=HCHO+C2H2T         2.4E13      0.          0. !(138,-138)<TSANG86>!
R7CH3O+R10C2H3V=HCHO+C2H4Z       2.4E13      0.          0. !(139,-139)<TSANG86>!
R7CH3O+C2H4Z=HCHO+R11C2H5        1.2E11      0.       6.7E3 !(140,-140)<TSANG86>!
R7CH3O+R11C2H5=HCHO+C2H6         2.4E13      0.          0. !(141,-141)<TSANG86>!
R7CH3O+C2H6=R11C2H5+CH3OH        2.4E11      0.       7.0E3 !(142,-142)<TSANG86>!
R7CH3O+B1O=HCHO+R2OH             1.8E12      0.          0. !(143,-143)<BAULCH94>!
R7CH3O+R2OH=HCHO+H2O             1.8E13      0.          0. !(144,-144)<TSANG86>!
R7CH3O+B2CO=R4CH3+CO2            1.6E13      0.      11.7E3 !(145,-145)<TSANG86>!
R7CH3O+R5CHO=CH3OH+B2CO          9.1E13      0.          0. !(146,-146)<TSANG86>!
R7CH3O+HCHO=CH3OH+R5CHO          1.0E11      0.       3.0E3 !(147,-147)<TSANG86>!
R7CH3O+R7CH3O=CH3OH+HCHO         6.0E13      0.          0. !(148,-148)<TSANG86>!

!REACTIONS DE R6CH2OH!
R6CH2OH+M=HCHO+R1H+M             1.26E16     0.00    30.0E3 !(149,-149)<BAULCH>!
       O2/0.4/ B2CO/0.75/ CO2/1.5/ H2O/6.5/ CH4/3.0/ C2H6/3.0/ AR/0.35/
       N2/0.4/ HE/0.35/
R6CH2OH+R1H=R4CH3+R2OH           9.6E13      0.          0. !(150,-150)<TSANG87>!
R6CH2OH+R1H=HCHO+H2              6.0E12      0.          0. !(151,-151)<TSANG87>!
R6CH2OH+H2=CH3OH+R1H             6.7E5       2.      13.4E3 !(152,-152)<TSANG87>!
R6CH2OH+B6CH2=CH3CHO+R1H         1.8E13      0.          0. !(153,-153)<TSANG87>!
R6CH2OH+B5CH2=C2H4Z+R2OH         2.4E13      0.          0. !(154,-154)<TSANG87>!
R6CH2OH+B5CH2=R4CH3+HCHO         1.2E12      0.          0. !(155,-155)<TSANG87>!
R6CH2OH+R4CH3=C2H5OH             1.2E13      0.          0. !(156,-156)<TSANG87>!
R6CH2OH+R4CH3=CH4+HCHO           2.4E12      0.          0. !(157,-157)<TSANG87>!
R6CH2OH+CH4=CH3OH+R4CH3          21.7        3.1     16.2E3 !(158,-158)<TSANG87>!
R6CH2OH+R9C2HT=C2H2T+HCHO        4.8E13      0.          0. !(159,-159)<TSANG87>!
!la constante de vitesse du processus 159 est globalisee!
!R6CH2OH+R9C2HT=C3H3+R2OH          1.2E13      0.          0. !(159a,-159a)<TSANG87>!
!R6CH2OH+R9C2HT=C2H2T+HCHO         3.6E13      0.          0. !(159b,-159b)<TSANG87>!
R6CH2OH+C2H2T=R10C2H3V+HCHO      7.2E11      0.       9.0E3 !(160,-160)<TSANG87>!
R6CH2OH+R10C2H3V=C2H4Z+HCHO      4.2E13      0.          0. !(161,-161)<TSANG87>!
!La constante de vitesse du processus 161 est globalisee!
R6CH2OH+R11C2H5=C2H4Z+CH3OH      2.4E12      0.          0. !(162,-162)<TSANG87>!
R6CH2OH+R11C2H5=C2H6+HCHO        2.4E12      0.          0. !(163,-163)<TSANG87>!
R6CH2OH+C2H6=CH3OH+R11C2H5       199.        3.      14.0E3 !(164,-164)<TSANG87>!
R6CH2OH+B1O=HCHO+R2OH            4.2E13      0.          0. !(165,-165)<TSANG87>!
R6CH2OH+R2OH=H2O+HCHO            2.4E13      0.          0. !(166,-166)<TSANG87>!
R6CH2OH+R5CHO=CH3OH+B2CO         1.2E14      0.          0. !(168,-168)<TSANG87>!
```

```
R6CH2OH+R5CHO=HCHO+HCHO          1.8E14      0.          0. !(169,-169)<TSANG87>!
R6CH2OH+HCHO=CH3OH+R5CHO         5.5E3       2.8      5.9E3 !(170,-170)<TSANG87>!
R6CH2OH+R7CH3O=CH3OH+HCHO        2.4E13      0.          0. !(171,-171)<TSANG87>!
R6CH2OH+R6CH2OH=CH3OH+HCHO       1.4E13      0.          0. !(172,-172)<TSANG87>!
!la constante de vitesse du processus 172 est globalisee!
!R6CH2OH+R6CH2OH=CH3OH+HCHO      4.8E12      0.          0. !(172a,-172a)<TSANG87>!
!R6CH2OH+R6CH2OH=HOCH2CH2OH      9.6E12      0.          0. !(172b,-172b)<TSANG87>!

!REACTIONS DE CH3OH!
CH3OH+R1H=R4CH3+H2O              2.0E14      0.       5.3E3 !(173,-173)<HIDAKA89NIST>!
CH3OH+R1H=R7CH3O+H2              4.2E6       2.1      4.9E3 !(174,-174)<TSANG87>!
CH3OH+B6CH2=R6CH2OH+R4CH3        1.5E12      0.          0. !(175,-175)<TSANG87>!
CH3OH+B5CH2=R4CH3+R6CH2OH        31.9        3.2      7.2E3 !(176,-176)<TSANG87>!
CH3OH+B5CH2=R4CH3+R7CH3O         14.4        3.1      6.9E3 !(177,-177)<TSANG87>!
CH3OH+R9C2HT=C2H2T+R6CH2OH       6.0E12      0.          0. !(178,-178)<TSANG87>!
CH3OH+R9C2HT=C2H2T+R7CH3O        1.2E12      0.          0. !(179,-179)<TSANG87>!
CH3OH+R10C2H3V=C2H4Z+R6CH2OH     31.9        3.2      7.2E3 !(180,-180)<TSANG87>!
CH3OH+R10C2H3V=C2H4Z+R7CH3O      14.4        3.1      6.9E3 !(181,-181)<TSANG87>!
CH3OH+B1O=R6CH2OH+R2OH           3.4E13      0.       5.5E3 !(182,-182)<GROTHEER81NIST>!
CH3OH+B1O=R7CH3O+R2OH            1.0E13      0.       4.7E3 !(183,-183)<WARNATZ84>!
CH3OH+R2OH=R6CH2OH+H2O           3.1E06      2.      -3.4E2 !(184a,-184a)<Atkinson86>85%!
CH3OH+R2OH=R7CH3O+H2O            5.4E05      2.      -3.4E2 !(184b,-184b)<Atkinson86>15%!
CH3OH+R7CH3O=CH3OH+R6CH2OH       3.0E11      0.       4.1E3 !(185,-185)<TSANG87>!

!REACTIONS DE R12CHCOVD!
R12CHCOV+M=B4CH+B2CO+M           6.0E15      0.      58.8E3 !(186,-186)<DAGAUT91>!
R12CHCOV+R1H=B5CH2+B2CO          1.5E14      0.          0. !(187a,-187a)<BAULCH94>!
R12CHCOV+R1H=B6CH2+B2CO          1.3E14      0.          0. !(187b,-187b)<PEETERS97>!
R12CHCOV+B5CH2=R9C2HT+HCHO       1.0E13      0.       2.0E3 !(188,-188)<DAGAUT91>!
R12CHCOV+B5CH2=R10C2H3V+B2CO     3.0E13      0.          0. !(189,-189)<DAGAUT91>!
R12CHCOV+B1O=>B2CO+B2CO+R1H      9.6E13      0.          0. !(190)<BAULCH94>!
R12CHCOV+R2OH=>R5CHO+B2CO+R1H    1.0E13      0.          0. !(191)<DAGAUT91>!


!REACTIONS DE CH2COZD!
CH2COZ+M=B6CH2+B2CO+M            6.57E15     0.0     57.6E3 !(192,-192)<FRANK86NIST>!
        O2/0.4/ B2CO/0.75/ CO2/1.5/ H2O/6.5/ CH4/3.0/ C2H6/3.0/ AR/0.35/
        N2/0.4/ HE/0.35/
CH2COZ+M=R12CHCOV+R1H+M          2.7E17      0.      87.0E3 !(193,-193)<FRANK86NIST>!
        O2/0.4/ B2CO/0.75/ CO2/1.5/ H2O/6.5/ CH4/3.0/ C2H6/3.0/ AR/0.35/
        N2/0.4/ HE/0.35/
CH2COZ+R1H=R4CH3+B2CO            1.8E13      0.       3.4E3 !(194,-194)<BAULCH94>!
CH2COZ+R1H=R12CHCOV+H2           5.0E13      0.       8.0E3 !(195,-195)<DAGAUT91>!
CH2COZ+B5CH2=C2H4Z+B2CO          1.3E14      0.          0. !(196,-196)<CANOSA-MAS84NIST>!
CH2COZ+B1O=B5CH2+CO2             1.8E12      0.       1.3E3 !(197,-197)<DAGAUT91>!
CH2COZ+B1O=R12CHCOV+R2OH         1.0E13      0.       8.0E3 !(198,-198)<DAGAUT91>!
CH2COZ+R2OH=R12CHCOV+H2O         7.5E12      0.       2.0E3 !(199,-199)<DAGAUT91>!
CH2COZ+R2OH=R4CH3+CO2            2.52E12     0.          0. !(200a,-200a)<BAULCH LEEDS>!
CH2COZ+R2OH=R6CH2OH+B2CO         4.68E12     0.          0. !(200b,-200b)<BAULCH LEEDS>!


!REACTIONS DE R14CH3CO!
R14CH3CO+R1H=R4CH3+R5CHO          9.6E13     0.          0. !(201,-201)<TSANG86>!
R14CH3CO+B6CH2=R4CH3+CH2COZ       1.8E13     0.          0. !(202,-202)<TSANG86>!
R14CH3CO+B5CH2=R4CH3+CH2COZ       1.8E13     0.          0. !(203,-203)<TSANG86>!
R14CH3CO+B1O=R4CH3+CO2            9.6E12     0.          0. !(204,-204)<TSANG86>!
R14CH3CO+R2OH=CH2COZ+H2O          1.2E13     0.          0. !(205,-205)<TSANG86>!
R14CH3CO+R2OH=>R4CH3+B2CO+R2OH    3.0E13     0.          0. !(206)<TSANG86>!
R14CH3CO+R5CHO=CH3CHO+B2CO        9.0E12     0.          0. !(207,-207)<TSANG86>!
R14CH3CO+HCHO=CH3CHO+R5CHO        1.8E11     0.       12.9E3!(208,-208)<TSANG86>!
R14CH3CO+R7CH3O=CH3OH+CH2COZ      6.0E12     0.          0. !(209,-209)<TSANG86>!
R14CH3CO+R7CH3O=HCHO+CH3CHO       6.0E12     0.          0. !(210,-210)<TSANG86>!
R14CH3CO+CH3OH=CH3CHO+R6CH2OH     4.85E3     3.       12.3E3!(211,-211)<TSANG87>!
R14CH3CO+R14CH3CO=CH2COZ+CH3CHO   1.2E13     0.          0. !(212,-212)<TSANG86>!

!REACTIONS DE R13CH2CHO!
R13CH2CHO=R14CH3CO                1.0E13     0.       47.0E3!(213,-213)<COLKET75NIST>!
```

```
R13CH2CHO=R1H+CH2COZ                    1.6E13      0.       35.0E3!(214,-214)<COLKET75NIST>!

!REACTIONS DE CH3CHO!
CH3CHO+R1H=H2+R14CH3CO                  4.0E13      0.        4.2E3 !(215,-215)<WARNATZ84>!
CH3CHO+R4CH3=R14CH3CO+CH4               2.0E-6      5.6       2.5E3 !(216,-216)<BAULCH94>!
CH3CHO+R10C2H3V=C2H4Z+R14CH3CO          8.1E10      0.        3.7E3 !(217,-217)<SCHERZER87>!
CH3CHO+R11C2H5=C2H6+R14CH3CO            1.3E12      0.        8.5E3 !(218,-218)<HOHLEIN70>!
CH3CHO+B1O=R14CH3CO+R2OH                1.4E13      0.        2.3E3 !(219,-219)<CAVANAGH90>!
CH3CHO+R2OH=R14CH3CO+H2O                4.2E12      0.        0.5E3 !(220,-220)<CAVANAGH90>!
CH3CHO+R7CH3O=R14CH3CO+CH3OH            2.4E11      0.        1.8E3 !(221,-221)<CAVANAGH90>!
CH3CHO+R13CH2CHO=CH3CHO+R14CH3CO        2.5E7       0.          0.  !(222,-222)<SCHUCHMANN70NIST>!

!REACTIONS DE C2H4O#!
C2H4O#3=CH4+B2CO                          1.2E13      0.       57.2E3 !(223,-223)<LIFSHITZ83NIST>!
C2H4O#3=CH3CHO                            7.3E13      0.       57.2E3 !(224,-224)<LIFSHITZ83NIST>!
C2H4O#3=R4CH3+R5CHO                       3.6E13      0.       57.2E3 !(225,-225)<LIFSHITZ83NIST>!
C2H4O#3+R1H=H2+R13CH2CHO                  2.0E13      0.        8.3E3 !(226,-226)<LIFSHITZ83NIST*>!
C2H4O#3+R1H=H2O+R10C2H3V                  5.0E9       0.        5.0E3 !(227,-227)<LIFSHITZ83NIST>!
C2H4O#3+R1H=C2H4Z+R2OH                    9.5E10      0.        5.0E3 !(228,-228)<LIFSHITZ83NIST>!
C2H4O#3+R4CH3=CH4+R13CH2CHO               1.1E12      0.       11.8E3 !(229,-229)<BALDWIN84NIST*>!
C2H4O#3+R4CH3=R11C2H5+HCHO                1.4E11      0.        7.6E3 !(230,-230)<RANZI94>!
C2H4O#3+R4CH3=C2H4Z+R7CH3O                1.5E10      0.        7.6E3 !(231,-231)<RANZI94>!
C2H4O#3+R9C2HT=C2H2T+R13CH2CHO            1.2E12      0.        9.8E3 !(232,-232)<RANZI94>!
C2H4O#3+R10C2H3V=C2H4Z+R13CH2CHO          2.0E12      0.        9.3E3 !(233,-233)<RANZI94>!
C2H4O#3+R11C2H5=C2H6+R13CH2CHO            6.8E11      0.       11.4E3 !(234,-234)<RANZI94>!
C2H4O#3+B1O=R2OH+R13CH2CHO                1.9E12      0.        5.2E3 !(235,-235)<BOGAN78NIST>!
C2H4O#3+R2OH=H2O+R13CH2CHO                1.8E13      0.        3.6E3 !(236,-236)<BALDWIN84NIST*>!
C2H4O#3+R5CHO=HCHO+R13CH2CHO              3.7E12      0.       15.8E3 !(237,-237)<RANZI94>!
C2H4O#3+R7CH3O=CH3OH+R13CH2CHO            1.3E12      0.        5.8E3 !(238,-238)<RANZI94>!
C2H4O#3+R6CH2OH=CH3OH+R13CH2CHO           8.4E11      0.       13.4E3 !(239,-239)<RANZI94>!
C2H4O#3+R14CH3CO=CH3CHO+R13CH2CHO         4.0E12      0.       17.5E3 !(240,-240)<RANZI94>!
C2H4O#3+R13CH2CHO=CH3CHO+R13CH2CHO        6.8E11      0.       15.4E3 !(241,-241)<RANZI94>!
!* assuming that C2H3O decompose rapidly to R13CH2CHO!

!REACTIONS DE R15C2H5O!
R15C2H5O=HCHO+R4CH3                       8.0E13      0.       21.5E3 !(242,-242)<BAULCH94>!
R15C2H5O=CH3CHO+R1H                       2.0E14      0.       23.3E3 !(243,-243)<HEICKLEN88NIST>!

!REACTIONS DE C2H5OH!
!Sous-mecanisme repris de Marinov, IJCK 1999
C2H5OH(+M)=R11C2H5+R2OH(+M)               1.2E+23    -1.54     96.0E3  !<MARINOV99!
                                LOW      /3.2E85     -18.81    114.9E3/
                                TROE     /0.5          300.0       9.0E2       5.0E3/
        CO2/3.0/ H2O/5.0/ B2CO/2.0/ H2/2.0/
C2H5OH(+M)=C2H4Z+H2O(+M)                  2.8E+13     0.09     66.1E3 !<MARINOV99!
                                LOW      /2.6E83     -18.85    86.5E3/
                                TROE     /0.7          350.0       8.0E2       3.8E3/
        H2O/5.0/
C2H5OH(+M)=CH3CHO+H2(+M)                  7.2E+11     0.095    91.0E3  !<MARINOV99!
                                LOW      /4.5E87     -19.42    115.6E3/
                                TROE     /0.9          900.0       1.1E3       3.5E3/
        H2O/5.0/
C2H5OH+R1H=H2+R15C2H5O                    1.5E+07     1.6     3.04E+3 !<MARINOV99>!
C2H5OH+B1O=R2OH+R15C2H5O                  1.6E+07     2.0     4.45E+3 !<MARINOV99>!
C2H5OH+R2OH=H2O+R15C2H5O                  7.5E+11     0.3      1.6E+3 !<MARINOV99>!
C2H5OH+R3OOH=H2O2+R15C2H5O                2.5E+12     0.      24.0E+3 !<MARINOV99>!
C2H5OH+R4CH3=CH4+R15C2H5O                 1.4E+02     2.99    7.65E+3 !<MARINOV99>!
C2H5OH+R1H=H2+R2OH+C2H4Z                  1.2E+07     1.8      5.1E+3 !<MARINOV99>!
C2H5OH+B1O=R2OH+R2OH+C2H4Z                9.4E+07     1.7     5.46E+3 !<MARINOV99>!
C2H5OH+R2OH=H2O+R2OH+C2H4Z                1.7E+11     0.27     0.6E+3 !<MARINOV99>!
C2H5OH+R3OOH=H2O2+R2OH+C2H4Z              1.2E+04     2.55    15.7E+3 !<MARINOV99>!
C2H5OH+R4CH3=CH4+R2OH+C2H4Z               2.2E+02     3.18     9.6E+3 !<MARINOV99>!
C2H5OH+R1H=H2+CH3CHO+R1H                  2.6E+07     1.65     2.8E+3 !<MARINOV99>!
C2H5OH+B1O=R2OH+CH3CHO+R1H                1.9E+07     1.85    1.82E+3 !<MARINOV99>!
C2H5OH+R2OH=H2O+CH3CHO+R1H                4.6E+11     0.15        0. !<MARINOV99>!
C2H5OH+R3OOH=H2O2+CH3CHO+R1H              8.2E+03     2.55    10.7E+3 !<MARINOV99>!
C2H5OH+R4CH3=CH4+CH3CHO+R1H               7.3E+02     2.99     7.9E+3 !<MARINOV99>!
```

```
!REACTIONS DE O2!
B1O+B1O+M=O2+M                          5.40E13     0.      -1.79E3  !(244,-244)<BAULCH94>!
        O2/0.4/ B2CO/0.75/ CO2/1.5/ H2O/6.5/ CH4/3.0/ C2H6/3.0/ AR/0.35/
        N2/0.4/ HE/0.35/
O2+R1H=R2OH+B1O                  9.8E13      0.      14.8E3   !(245,-245)<BAULCH94>!
O2+R1H(+M)=R3OOH(+M)             4.52E13     0.       0.      !(246,-246)<COBOS85>!
                  LOW    /1.8E18     -0.8      0.00/     !k0 BAULCH94!
                  TROE   /0.5         1.0       1.0E8/
        O2/0.4/ B2CO/0.75/ CO2/1.5/ H2O/0.0/ CH4/3.0/ C2H6/3.0/ AR/0.29/
        HE/0.35/ N2/0.67/
O2+R1H(+H2O)=R3OOH(+H2O)         4.52E13     0.       0. !(246b,-246b)<BAULCH94>!
                  LOW    /6.9E15     0.0      -2080/
                  TROE   /0.45        1.0      1.0E8/
O2+B3C=B2CO+B1O                  1.2E14      0.       0. !(247,-247)<RANZI94>!
O2+B4CH=R5CHO+B1O                3.3E13      0.       0. !(248,-248)<DAGAUT91>!
O2+B4CH=B2CO+R2OH                3.2E13      0.       0. !(249,-249)<PEETERS97>!
O2+B6CH2=>B2CO+R2OH+R1H          3.1E12      0.       0. !(250)<BAULCH94>!
O2+B5CH2=R5CHO+R2OH              4.3E10      0.     -0.5E3 !(251,-251)<DAGAUT91>!
O2+B5CH2=CO2+H2                  6.9E11      0.      0.5E3 !(252,-252)<DAGAUT91>!
O2+B5CH2=>CO2+R1H+R1H            1.6E12      0.      1.0E3 !(253)<DAGAUT91>!
O2+B5CH2=B2CO+H2O                1.9E10      0.     -1.0E3 !(254,-254)<DAGAUT91>!
O2+B5CH2=>B2CO+R2OH+R1H          8.6E10      0.     -0.5E3 !(255)<DAGAUT91>!
O2+B5CH2=HCHO+B1O                1.0E14      0.      4.5E3 !(256,-256)<DAGAUT91>!
O2+R4CH3(+M)=R8CH3OO(+M)         7.8E8       1.2       0. !(257,-257)<BAULCH94>!
                        LOW    /5.6E25     -3.3       0./
                        TROE   /0.36        1.0      1.0E8/
O2+R4CH3=R7CH3O+B1O              1.3E14      0.      31.3E3 !(258,-258)<BAULCH94>!
O2+R4CH3=HCHO+R2OH               3.0E30     -4.69    36.6E3 !(259,-259)<DAGAUT91>!
O2+CH4=R4CH3+R3OOH               4.0E13      0.      56.7E3 !(260,-260)<BAULCH94>!
O2+R9C2HT=B2CO+R5CHO             3.8E13     -0.16       0. !(261,-261)<TIESEMANN97/TSANG86>!
O2+R9C2HT=R12CHCOV+B1O           9.0E12     -0.16       0. !(262,-262)<TIESEMANN97/TSANG86>!
O2+C2H2T=R9C2HT+R3OOH            1.2E13      0.      74.5E3 !(263,-263)<TSANG86>!
O2+C2H2T=R5CHO+R5CHO             7.0E7       1.8     30.6E3 !(264,-264)<BENSON95>!
O2+R10C2H3V=C2H2T+R3OOH          1.34E6      1.61    -0.4E3 !(265,-265)<MEBEL NIST>!
O2+R10C2H3V=HCHO+R5CHO           4.5E16     -1.39     1.0E3 !(266a,-266a)<MEBEL NIST>!
O2+R10C2H3V=B1O+R13CH2CHO        3.3E11     -0.29       10. !(266b,-266b)<MEBEL NIST>!
O2+C2H4Z=R10C2H3V+R3OOH          4.2E13      0.      57.4E3 !(267,-267)<TSANG86>!
O2+R11C2H5=R17C2H5OO             2.2E10      0.77    -0.6E3 !(268,-268)<WAGNER90>!
O2+R11C2H5=C2H4Z+R3OOH           8.4E11      0.       3.9E3 !(269,-269)<TSANG86>!
O2+R11C2H5=R15C2H5O+B1O          1.2E13     -0.2     27.9E3 !(270,-270)<BOZZELLI90NIST>!
O2+R11C2H5=CH3CHO+R2OH           6.0E10      0.       6.9E3 !(271,-271)<TSANG86>!
O2+C2H6=R11C2H5+R3OOH            6.0E13      0.      51.7E3 !(272,-272)<BAULCH94>!
O2+R2OH=R3OOH+B1O                2.2E13      0.      52.5E3 !(273,-273)<TSANG86>!
O2+B2CO=CO2+B1O                  2.5E12      0.      47.7E3 !(274,-274)<TSANG86>!
O2+R5CHO=B2CO+R3OOH              7.6E12      0.      0.41E3 !(275,-275)<TIMONEN88>!
O2+HCHO=R5CHO+R3OOH              2.0E13      0.      38.8E3 !(276,-276)<TSANG86)!
O2+R7CH3O=HCHO+R3OOH             2.2E10      0.       1.7E3 !(277,-277)<BAULCH94>!
O2+R6CH2OH=HCHO+R3OOH            1.2E12      0.         0. !(278,-278)<TSANG87>!
O2+CH3OH=R6CH2OH+R3OOH           2.0E13      0.      44.9E3 !(279,-279)<TSANG87>!
O2+R12CHCOV=>B2CO+B2CO+R2OH      1.5E12      0.       2.5E3 !(280)      <DAGAUT91>!
O2+R14CH3CO=R18CH3COOO           2.4E12      0.         0. !(282,-282)<COX90>!
O2+R13CH2CHO=>HCHO+R2OH+B2CO     5.9E9       0.      -1.4E3 !(283)      <COX90>!
O2+R13CH2CHO=CH2COZ+R3OOH        1.0E10      0.      -1.4E3 !(284,-284)<COX90>!
O2+CH3CHO=R14CH3CO+R3OOH         5.0E13      0.      36.4E3 !(285,-285)<COX90>!
O2+CH3CHO=R13CH2CHO+R3OOH        1.0E13      0.5     46.0E3 !(285',-285)<Ranzi94>!
O2+C2H4O#3=R3OOH+R13CH2CHO       5.0E13      0.      48.0E3 !(286,-286)<RANZI94>!
O2+R15C2H5O=CH3CHO+R3OOH         6.0E10      0.       1.7E3 !(287,-287)<BAULCH94>!

!REACTIONS DE R3OOH!
R3OOH+R1H=H2+O2                  4.3E13      0.       1.4E3 !(288,-288)<BAULCH94>!
R3OOH+R1H=2R2OH                  1.7E14      0.       0.9E3 !(289,-289)<BAULCH94>!
R3OOH+R1H=H2O+B1O                3.0E13      0.       1.7E3 !(290,-290)<BAULCH94>!
R3OOH+B6CH2=HCHO+R2OH            3.0E13      0.         0. !(291,-291)<TSANG86>!
R3OOH+B5CH2=HCHO+R2OH            1.8E13      0.         0. !(292,-292)<TSANG86>!
R3OOH+R4CH3=R7CH3O+R2OH          1.8E13      0.         0. !(293,-293)<BAULCH94>!
!R3OOH+R4CH3=R7CH3O+R2OH          4.0E13      0.       5.0E3 !(293,-293)<DAGAUT>
```

```
R3OOH+CH4=R4CH3+H2O2                9.0E12      0.      24.6E3 !(294,-294)<BAULCH94>!
R3OOH+R9C2HT=R12CHCOV+R2OH           1.8E13      0.        0. !(295,-295)<TSANG86>!
R3OOH+C2H2T=CH2COZ+R2OH              6.0E9       0.       8.0E3 !(296,-296)<TSANG86>!
!incertitude au moins un facteur 10
R3OOH+R10C2H3V=>R2OH+R4CH3+B2CO     3.0E13      0.        0. !(297)      <TSANG86>!
R3OOH+C2H4Z=CH3CHO+R2OH             6.0E9       0.       7.9E3 !(298,-298)<TSANG86>!
R3OOH+C2H4Z=C2H4O#3+R2OH            2.2E12      0.      17.2E3 !(299,-299)<BAULCH94>!
R3OOH+R11C2H5=>R4CH3+HCHO+R2OH      2.4E13      0.        0. !(300)      <TSANG86>!
R3OOH+R11C2H5=C2H4Z+H2O2            3.0E11      0.        0. !(301,-301)<TSANG86>!
R3OOH+C2H6=R11C2H5+H2O2             1.3E13      0.      20.4E3 !(302,-302)<BAULCH94>!
R3OOH+R2OH=H2O+O2                   2.9E13      0.      -0.5E3 !(303,-303)<BAULCH94>!
R3OOH+B2CO=CO2+R2OH                 1.5E14      0.      23.6E3 !(304,-304)<TSANG86>!
R3OOH+R5CHO=>R2OH+R1H+CO2           3.0E13      0.        0. !(305)      <TSANG86>!
R3OOH+HCHO=R5CHO+H2O2               3.0E12      0.      13.0E3 !(306,-306)<BAULCH94>!
R3OOH+R7CH3O=HCHO+H2O2              3.0E11      0.        0. !(307,-307)<TSANG86>!
R3OOH+R6CH2OH=HCHO+H2O2             1.2E13      0.        0. !(308,-308)<TSANG87>!
R3OOH+CH3OH=R6CH2OH+H2O2            9.6E10      0.      12.6E3 !(309,-309)<TSANG87>!
R3OOH+R14CH3CO=>R4CH3+CO2+R2OH      3.0E13      0.        0. !(310)<TSANG86>!
R3OOH+CH3CHO=R14CH3CO+H2O2          1.0E12      0.      10.0E3 !(311,-311)<CAVANAGH90>!
R3OOH+C2H4O#3=H2O2+R13CH2CHO        1.6E12      0.      15.0E3 !(312,-312)<RANZI94>
R3OOH+R3OOH=H2O2+O2                 1.3E11      0.     -1.63E3 !(313,-313)<BAULCH 94>!
      DUPLICATE
R3OOH+R3OOH=H2O2+O2                 4.2E14      0.     11.98E3 !(313,-313)<BAULCH 94>!
      DUPLICATE

!REACTIONS DE H2O2!
R2OH+R2OH(+ M)=>H2O2 (+ M)        7.23E13     -0.37     0.00   !(314)<BAULCH94>!
         O2/0.4/ B2CO/0.75/ CO2/1.5/ H2O/6.5/ CH4/3.0/ C2H6/3.0/ AR/0.35/
         N2/0.4/ HE/0.35/
         LOW   /5.53E19   -0.76      0.00 /
         TROE /0.5 1 1.E8/
H2O2(+M)=>R2OH+R2OH(+M)           3.00E14      0.00     48.5E3 !(-314)<BAULCH94>!
         O2/0.4/ B2CO/0.75/ CO2/1.5/ H2O/6.5/ CH4/3.0/ C2H6/3.0/ AR/0.35/
         N2/0.4/ HE/0.35/
         LOW   /3.0E17    0.0       45.5E3/
         TROE /0.5 1. 1.E8/
H2O2+R1H=H2+R3OOH                   1.7E12      0.       3.7E3 !(315,-315)<BAULCH94>!
H2O2+R1H=H2O+R2OH                   1.0E13      0.       3.6E3 !(316,-316)<BAULCH94>!
H2O2+B6CH2=R7CH3O+R2OH              3.0E13      0.         0. !(317,-317)<TSANG86>!
H2O2+R10C2H3V=C2H4Z+R3OOH           1.2E10      0.      -0.6E3 !(318,-318)<TSANG86>!
H2O2+B1O=R2OH+R3OOH                 6.6E11      0.       4.0E3 !(319,-319)<BAULCH94>!
H2O2+R2OH=H2O+R3OOH                 7.8E12      0.       1.3E3 !(320,-320)<BAULCH94>!

!REACTIONS DE CO2!
CO2+B5CH2=HCHO+B2CO                 2.3E10      0.         0. !(321,-321)<TSANG86>!

!REACTIONS DE R8CH3OO!
R8CH3OO=HCHO+R2OH                    1.5E13      0.      47.0E3 !(322,-322)<RANZI94>!
R8CH3OO+R1H=R7CH3O+R2OH              9.6E13      0.        0. !(323,-323)<TSANG86>!
R8CH3OO+H2=CH3OOH+R1H                3.0E13      0.      26.0E3 !(324,-324)<TSANG86>!
R8CH3OO+B6CH2=HCHO+R7CH3O            1.8E13      0.        0. !(325,-325)<TSANG86>!
R8CH3OO+B5CH2=HCHO+R7CH3O            1.8E13      0.        0. !(326,-326)<TSANG86>!
R8CH3OO+R4CH3=R7CH3O+R7CH3O          5.0E12      0.      -1.4E3 !(327,-327)<CAVANAGH90>!
R8CH3OO+CH4=CH3OOH+R4CH3             1.8E11      0.      18.5E3 !(328,-328)<TSANG86>!
R8CH3OO+R9C2HT=R7CH3O+R12CHCOV       2.4E13      0.        0. !(329,-329)<TSANG86>!
R8CH3OO+C2H2T=CH3OOH+R9C2HT          5.6E11      0.      24.5E3 !(330,-330)<RANZI94>!
R8CH3OO+R10C2H3V=R7CH3O+R13CH2CHO   2.4E13      0.        0. !(331,-331)<TSANG86*>!
!* assuming that C2H3O decompose rapidly to R13CH2CHO!
R8CH3OO+C2H4Z=R7CH3O+C2H4O#3         1.1E15      0.      20.0E3 !(332,-332)<NIKISHA81/MOSHKINA80NIST>!
R8CH3OO+C2H4Z=CH3OOH+R10C2H3V        3.9E12      0.      24.5E3 !(333,-333)<RANZI94>!
R8CH3OO+R11C2H5=R7CH3O+R15C2H5O      2.4E13      0.        0. !(334,-334)<TSANG86>!
R8CH3OO+C2H6=CH3OOH+R11C2H5          2.9E11      0.      14.9E3 !(335,-335)<TSANG86>!
R8CH3OO+B1O=R7CH3O+O2                3.6E13      0.        0. !(336,-336)<TSANG86>!
R8CH3OO+R2OH=CH3OH+O2                6.0E13      0.        0. !(337,-337)<TSANG86>!
R8CH3OO+R2OH=R7CH3O+R3OOH            3.0E12      0.        0. !(338,-338)<RANZI94>!
R8CH3OO+B2CO=R7CH3O+CO2              1.0E14      0.      24.0E3 !(339,-339)<RANZI94>!
R8CH3OO+R5CHO=>R7CH3O+R1H+CO2        3.0E13      0.        0. !(340)      <TSANG86>!
```

```
R8CH3OO+HCHO=CH3OOH+R5CHO                1.0E12    0.     12.1E3 !(341,-341)<CAVANAGH90>!
R8CH3OO+R7CH3O=HCHO+CH3OOH               3.0E11    0.      0. !(342,-342)<TSANG86>!
R8CH3OO+R6CH2OH=>R7CH3O+R2OH+HCHO        1.2E13    0.      0. !(343)<TSANG87>!
R8CH3OO+CH3OH=CH3OOH+R6CH2OH             1.8E12    0.     13.7E3 !(344,-344)<TSANG87>!
R8CH3OO+CH3OH=CH3OOH+R7CH3O              2.8E11    0.     18.8E3 !(345,-345)<RANZI94>!
R8CH3OO+CH2COZ=CH3OOH+R12CHCOV           1.7E12    0.     27.0E3 !(346,-346)<RANZI94>!
R8CH3OO+R14CH3CO=R4CH3+CO2+R7CH3O        2.4E13    0.      0. !(347,-347)<TSANG86>!
R8CH3OO+CH3CHO=CH3OOH+R14CH3CO           1.0E12    0.     12.1E3 !(348,-348)<CAVANAGH90>!
R8CH3OO+CH3CHO=CH3OOH+R13CH2CHO          1.7E12    0.     19.2E3 !(349,-349)<RANZI94>!
R8CH3OO+C2H4O#3=CH3OOH+R13CH2CHO         2.2E12    0.     16.0E3 !(350,-350)<RANZI94>!
R8CH3OO+R3OOH=CH3OOH+O2                  2.5E11    0.     -1.6E3 !(351,-351)<BAULCH94>!
R8CH3OO+R3OOH=>O2+HCHO+H2O               5.0E10    0.      0. !(352)<RANZI94>!
R8CH3OO+H2O2=CH3OOH+R3OOH                2.4E12    0.      9.9E3 !(353,-353)<TSANG86>!
R8CH3OO+R8CH3OO=CH3OH+HCHO+O2            2.5E10    0.     -0.8E3 !(354,-354)<BAULCH94>!
R8CH3OO+R8CH3OO=R7CH3O+R7CH3O+O2         2.5E10    0.     -0.8E3 !(355,-355)<BAULCH94>!

!REACTIONS DE CH3OOH!
CH3OOH=R7CH3O+R2OH                       6.0E14    0.     42.3E3 !(356,-356)<BAULCH94>!
CH3OOH+B1O=R8CH3OO+R2OH                  2.0E13    0.      4.8E3 !(357,-357)<BAULCH94average>!
CH3OOH+R2OH=H2O+R8CH3OO                  1.8E12    0.    -0.37E3 !(358,-358)<BAULCH94average>!
CH3OOH+R7CH3O=>CH3OH+R2OH+HCHO           1.5E11    0.      6.5E3 !(359)<RANZI94>!

!REACTIONS DE R17C2H5OO!
R17C2H5OO=R16C2H4OOH                     4.2E12    0.     36.9E3 !(360,-360)<HUGHES93>!
R17C2H5OO+H2=C2H5OOH+R1H                 7.9E12    0.     21.0E3 !(361,-361)<RANZI94>!
R17C2H5OO+R4CH3=R15C2H5O+R7CH3O          2.0E12    0.     -1.2E3 !(362,-362)<RANZI94>!
R17C2H5OO+CH4=C2H5OOH+R4CH3              3.9E12    0.     24.0E3 !(363,-363)<RANZI94>!
R17C2H5OO+C2H2T=C2H5OOH+R9C2HT           5.6E11    0.     24.4E3 !(364,-364)<RANZI94>!
R17C2H5OO+C2H4Z=C2H5OOH+R10C2H3V         3.9E12    0.     24.4E3 !(365,-365)<RANZI94>!
R17C2H5OO+C2H4Z=R15C2H5O+C2H4O#3         2.3E16    0.     21.9E3 !(366,-366)<MOSHKINA80NIST>!
R17C2H5OO+C2H6=C2H5OOH+R11C2H5           5.1E12    0.     19.5E3 !(367,-367)<RANZI94>!
R17C2H5OO+H2O=C2H5OOH+R2OH               5.6E12    0.     30.6E3 !(368,-368)<RANZI94>!
R17C2H5OO+B2CO=CO2+R15C2H5O              1.0E14    0.     24.0E3 !(369,-369)<RANZI94>!
R17C2H5OO+HCHO=C2H5OOH+R5CHO             4.5E12    0.     14.4E3 !(370,-370)<RANZI94>!
R17C2H5OO+CH3OH=C2H5OOH+R7CH3O           2.8E11    0.     18.4E3 !(371,-371)<RANZI94>!
R17C2H5OO+CH3OH=C2H5OOH+R6CH2OH          2.8E12    0.     19.5E3 !(372,-372)<RANZI94>!
R17C2H5OO+CH2COZ=C2H5OOH+R12CHCOV        1.7E12    0.     24.4E3 !(373,-373)<RANZI94>!
R17C2H5OO+CH3CHO=C2H5OOH+R14CH3CO        3.9E12    0.     14.4E3 !(374,-374)<RANZI94>!
R17C2H5OO+CH3CHO=C2H5OOH+R13CH2CHO       1.7E12    0.     19.5E3 !(375,-375)<RANZI94>!
R17C2H5OO+C2H4O#3=C2H5OOH+R13CH2CHO      2.2E12    0.     16.3E3 !(376,-376)<RANZI94>!
R17C2H5OO+R3OOH=O2+C2H5OOH               3.9E11    0.     -1.3E3 !(377,-377)<BAULCH89>!
!Rate constant measured between 240 and 380K!
R17C2H5OO+H2O2=C2H5OOH+R3OOH             4.5E11    0.     10.8E3 !(378,-378)<RANZI94>!
R17C2H5OO+R8CH3OO=>R15C2H5O+R7CH3O+O2    2.0E11    0.      0. !(379)<RANZI94>!
R17C2H5OO+CH3OOH=C2H5OOH+R8CH3OO         1.1E12    0.     16.3E3 !(380,-380)<RANZI94>!
R17C2H5OO+R17C2H5OO=2R15C2H5O+O2         4.1E10    0.      0.2E3 !(381,-381)<LIGHTFOOT92>!
R17C2H5OO+R17C2H5OO=C2H5OH+CH3CHO+O2     1.8E10    0.      0.2E3 !(382,-382)<LIGHTFOOT92>!

!REACTIONS DE R16C2H4OOH!
R16C2H4OOH=C2H4O#3+R2OH                  1.5E11    0.     20.0E3 !(383,-383)<RANZI94>!
R16C2H4OOH=R6CH2OH+HCHO                  2.5E13    0.     27.5E3 !(384,-384)<RANZI94>!
R16C2H4OOH=C2H4Z+R3OOH                   2.0E13    0.     23.5E3 !(385,-385)<RANZI94>!

!REACTIONS DE C2H5OOH
C2H5OOH=R15C2H5O+R2OH                    4.0E15    0.     42.9E3 !(386,-386)<BAULCH94>!
C2H5OOH+R1H=>CH3CHO+R2OH+H2              3.2E13    0.      7.7E3 !(387)<RANZI94>!
C2H5OOH+R4CH3=>CH3CHO+R2OH+CH4           5.7E11    0.      8.7E3 !(388)<RANZI94>!
C2H5OOH+R9C2HT=>CH3CHO+R2OH+C2H2T        6.0E11    0.      9.2E3 !(389)<RANZI94>!
C2H5OOH+R10C2H3V=>CH3CHO+R2OH+C2H4Z      1.0E12    0.      8.7E3 !(390)<RANZI94>!
C2H5OOH+R11C2H5=>CH3CHO+R2OH+C2H6        3.4E11    0.     11.4E3 !(391)<RANZI94>!
C2H5OOH+R2OH=>CH3CHO+R2OH+H2O            5.9E12    0.      0.9E3 !(392)<RANZI94>!
C2H5OOH+R5CHO=>CH3CHO+R2OH+HCHO          1.8E12    0.     16.7E3 !(393)<RANZI94>!
C2H5OOH+R7CH3O=>CH3CHO+R2OH+CH3OH        6.3E11    0.      5.5E3 !(394)<RANZI94>!
C2H5OOH+R6CH2OH=>CH3CHO+R2OH+CH3OH       4.2E11    0.     13.6E3 !(395)<RANZI94>!
C2H5OOH+R14CH3CO=>2CH3CHO+R2OH           2.0E12    0.     18.5E3 !(396)<RANZI94>!
C2H5OOH+R13CH2CHO=>2CH3CHO+R2OH          3.4E11    0.     15.7E3 !(397)<RANZI94>!
C2H5OOH+R3OOH=>CH3CHO+R2OH+H2O2          8.0E11    0.     16.2E3 !(398)<RANZI94>!
```

```
C2H5OOH+R8CH3OO=>CH3CHO+R2OH+CH3OOH  1.1E12    0.     16.7E3 !(399)<RANZI94>!
C2H5OOH+R17C2H5OO=>CH3CHO+R2OH+C2H5OOH  1.1E12    0.     16.7E3 !(400)<RANZI94>!

!REACTIONS DE R18CH3COOO!
R18CH3COOO+C2H4O#3=CH3COOOH+R13CH2CHO    1.0E12    0.     9.3E3 !(401,-402)<RANZI94>!
R18CH3COOO+R3OOH=CH3COOOH+O2             5.5E10    0.    -2.6E3 !(402,-402)<COX90>!
R18CH3COOO+C2H5OOH=CH3COOOH+R17C2H5OO    5.0E11    0.     9.2E3 !(403,-403)<RANZI94>!
R18CH3COOO+C2H5OOH=>CH3CHO+R2OH+CH3COOOH 5.0E11    0.     9.2E3 !(404)<RANZI94>!
R18CH3COOO+R18CH3COOO=>2R4CH3+O2+2CO2    1.7E12    0.    -1.0E3 !(405)<CAVANAGH90>!

!REACTIONS DE CH3COOOH!
CH3COOOH=>R4CH3+CO2+R2OH                 1.0E16    0.    40.0E3 !(406)<CAVANAGH90>!

!*******************************************************

!REACTIONS PRODUISANT DES C2+ RADICALAIRES
C2H4Z+R4CH3=>R19C3H7                     2.1E11    0.     7.35E3  !(407)<BAULCH94>!
R11C2H5+C2H4Z=>R20C4H9                   1.1E11    0.     7.3E3   !(408)<BAULCH94>!

!REACTIONS PRODUISANT DES C2+ MOLECULAIRES
!REACTIONS DE R9C2HT!
!R9C2HT+R9C2HT=>C4H2                     1.8E13    0.      0. !(24,-24)<TSANG86>!

!REACTIONS DE C2H2T!
!C2H2T+B6CH2=>C3H4                       1.7E14    0.      0. !(27,-27)<BAULCH94>!
!C2H2T+B5CH2=>C3H4                       3.5E12    0.      0. !(28,-28)<TSANG86>!
!C2H2T+R4CH3=>C3H4+R1H                   6.7E19   -2.08   31.6E3 !(29,-29)<DEAN87>!
!C2H2T+R9C2HT=>C4H2+R1H                  9.0E13    0.      0. !(30,-30)<BAULCH94>!
!C2H2T+C2H2T=>C4H4                       5.5E12    0.     37.0E3 !(31,-31)<DURAN89>!

!REACTIONS DE C2H3!
!R10C2H3V+R4CH3=>C3H6Y                   2.5E13    0.      0. !(37,-37)<TSANG86>!
!R10C2H3V+R9C2HT=>C4H4                   1.8E13    0.      0. !(38,-38)<TSANG86>!
!R10C2H3V+C2H2T=>C4H4+R1H                2.0E12    0.     5.0E3 !(40,-40)<FAHR89>!
!R10C2H3V+R10C2H3V=>C4H6YZ               9.6E12    0.      0. !(41,-41)<TSANG86>!

!REACTIONS DE C2H4!
!C2H4Z+B4CH=>C3H4+R1H                    1.3E14    0.    -0.3E3 !(46,-46)<BAULCH94>!
!C2H4Z+B6CH2=>C3H6Y                      9.6E13    0.      0. !(47,-47)<BAULCH94>!
!C2H4Z+B5CH2=>C3H6Y                      3.2E12    0.     5.1E3 !(48,-48)<BAULCH94>!
!C2H4Z+R9C2HT=>C4H4+R1H                  1.2E13    0.      0. !(50,-50)<TSANG86>!
!C2H4Z+R4CH3=>C3H6Y+R1H                  6.6E11    0.     15.9E3  !<TSANG86>!
!C2H4Z+R10C2H3V=>C4H6YZ+R1H              5.0E11    0.     7.3E3 !(51,-51)<TSANG86>!

!REACTIONS DE C2H5!
R11C2H5+R10C2H3V=>C4H8Y                  1.5E13    0.      0. !(61,-61)<TSANG86>!
R11C2H5+R11C2H5=>C4H10                   1.1E13    0.      0. !(65,-65)<BAULCH94>!

!REACTIONS DE HCO!
R5CHO+R10C2H3V=>C2H3CHOZ                 1.8E13    0.      0. !(138,-138)<TSANG86>!
R5CHO+R11C2H5=>C2H5CHO                   1.8E13    0.      0. !(141,-141)<TSANG86>!

!REACTIONS DE CH3O!
!R7CH3O+R4CH3=CH3OCH3                    1.2E13    0.      0. !(159,-159)<TSANG86>!
!R7CH3O+R7CH3O=>CH3OOCH3                 1.8E12    0.      0. !(172,-172)<TSANG86>!

!REACTIONS DE CH2OH!
R6CH2OH+R11C2H5=C3H7OH                   1.2E13    0.      0. !(189,-189)<TSANG87>!

!REACTIONS DE CH3CO!
R14CH3CO+R4CH3=>C2H6CO                   4.0E15   -0.8     0. !(231,-231)<TSANG86>!
R14CH3CO+R11C2H5=>C3H8CO                 3.1E14   -0.5     0. !(232,-232)<TSANG86>!
!R14CH3CO+R5CHO=>CH3COCHO                1.8E13    0.      0. !(237,-237)<TSANG86>!
!R14CH3CO+R6CH2OH=>CH3COCH2OH            1.2E13    0.      0. !(241,-241)<TSANG87>!
!R14CH3CO+R14CH3CO=>CH3COCOCH3           1.2E13    0.    12.3E3 !(243,-243)<TSANG86>!
```

!REACTIONS RAJOUTEES POUR TENIR COMPTE DE L ACROLEINE

| | | | | |
|---|---|---|---|---|
| !C3H6Y+B1O=CH3CHCO+2R1H | 5.0E7 | 1.76 | −1.22E3 | !<TSANG91>! |
| !CH3CHCO+R2OH=B2CO+R10C2H3V+H2O | 4.0E6 | 2.0 | 0.0 | !<MARINOV>! |
| !CH3CHCO+B1O=B2CO+R10C2H3V+R2OH | 7.2E12 | 0.0 | 2.0E3 | !<MARINOV>! |
| !CH3CHCO+R1H=B2CO+R10C2H3V+H2 | 2.0E5 | 2.5 | 2.5E3 | !<MARINOV>! |
| !CH3CHCO+R1H=R11C2H5+B2CO | 2.0E13 | 0.0 | 2.0E3 | !<MARINOV>! |
| !CH3CHCO+B1O=R4CH3+R5CHO+B2CO | 3.0E7 | 2.0 | 0.0 | !<MARINOV>! |
| !tC3H5+O2=CH3CHCO+R1H+B1O | 1.6E15 | −0.78 | 3.1E3 | !<MARINOV>! |
| !tC3H5+B1O=CH3CHCO+R1H | 1.0E14 | 0.0 | 0.0E3 | !<MARINOV>! |
| !aC4H5+O2=CH3CHCO+R5CHO | 4.2E10 | 0.0 | 2.5E3 | !<SLAGLE92>! |
| C2H3CHOZ+R2OH=B2CO+R10C2H3V+H2O | 1.0E13 | 0.0 | 0.0 | !<MARINOV>! |
| C2H3CHOZ+B1O=B2CO+R10C2H3V+R2OH | 7.2E12 | 0.0 | 2.0E3 | !<MARINOV>! |
| C2H3CHOZ+B1O=CH2COZ+R5CHO+R1H | 5.0E7 | 1.76 | 0.08E3 | !<MARINOV>! |
| C2H3CHOZ+R1H=B2CO+R10C2H3V+H2 | 4.0E13 | 0.0 | 4.2E3 | !<MARINOV>! |
| C2H3CHOZ+R1H=C2H4Z+R5CHO | 2.0E13 | 0.0 | 3.5E3 | !<MARINOV>! |
| C2H3CHOZ+O2=B2CO+R10C2H3V+R3OOH | 3.0E13 | 0.0 | 36.0E3 | !<MARINOV>! |
| !.C3H5Y+R3OOH=C2H3CHOZ+R1H+R2OH | 7.0E18 | −2.0 | 0.0 | !<TSANG91>! |
| !.C3H5Y+O2=C2H3CHOZ+R2OH | 1.8E13 | −0.41 | 22.9E3 | !<BOZELLI93>! |
| !.C3H5Y+B1O=C2H3CHOZ+R1H | 1.8E14 | 0.0 | 0.0 | !<SLAGLE92>! |

END

# Appendix C: EXGAS Mechanism - Decane (Diesel)

```
ELEMENTS
H O C N HE AR
END
SPECIES
! 150 especes

! Biradicals :
B1O
B2CO
B3C
B4CH
B5CH2
B6CH2

! Primary molecules :
! Reactants:
C8H18-1
C12H26-1
H2
H2O
O2
H2O2
CH4
HCHO
CH3OH
CO2
CH3OOH
C2H2T
C2H4Z
C2H6
CH2COZ
CH3CHO
C2H5OH
C2H5OOH
CH3COOOH
C3H6Y
C3H8
C4H8Y
C4H10
C2H5CHO
C3H7OH
C2H6CO
C3H8CO
C4H6Z2
C2H3CHOZ
C8H16Z
```

```
C7H14Z
C5H10Z
C6H12Z
C12H24Z
C11H22Z
C10H20Z
C9H18Z
C5H10Y

! Secondary molecules :
C7H14OA
C6H12OA
C4H8OA
C5H10OA
C11H22OA
C10H20OA
C9H18OA
C8H16OA
C4H8OLY
C4H8O2PY
C5H8OAY
C5H10OLY
C8H14Y2
C9H16Y2
C5H10O2PY
C6H10OAY
C6H12OLY
C10H18Y2
C4H6OKZ
C6H10OKZ
C5H8OKZ

! Cyclic primary molecules :
!C2H4OE#3

! Cyclic secondary molecules :
!C4H8OE#3
!C8H16OE#3
!C7H14OE#3
!C5H10OE#3
!C6H12OE#3
!C12H24OE#3
!C11H22OE#3
!C10H20OE#3
!C9H18OE#3

! Benzenic primary molecules :

! Free radicals :
R1H    !    .h
R2OH    !    .oh
R3OOH    !    .o/oh
R4CH3    !    .ch3
R5CHO    !    .ch//o
R6CH2OH    !    .ch2/oh
R7CH3O    !    .o/ch3
R8CH3OO    !    .o/o/ch3
R9C2HT    !    .c///ch
R10C2H3V    !    .ch//ch2
R11C2H5    !    .ch2/ch3
R12CHCOV    !    .ch//c//o
R13CH2CHO    !    .ch2/ch//o
R14CH3CO    !    .c(//o)/ch3
R15C2H5O    !    .o/ch2/ch3
R16C2H4OOH    !    .ch2/ch2/o/oh
R17C2H5OO    !    .o/o/ch2/ch3
R18CH3COOO    !    .o/o/c(//o)/ch3
```

```
R19C3H7    !    .ch2/ch2/ch3
R20C4H9    !    .ch2/ch2/ch2/ch3
R21CH3OCO    !    .c(//o)/o/ch3
R22CO2H    !    .c(//o)/oh
R23C2H3O2B    !    .ch2/c(//o)/oh
R24C2H4OH    !    .ch2/ch2/oh
R25C2H4OH    !    .ch(/oh)/ch3
R26C8H17    !    .ch2/ch2/ch2/ch2/ch2/ch2/ch2/ch3
R27C8H17    !    .ch(/ch3)/ch2/ch2/ch2/ch2/ch2/ch3
R28C8H17    !    .ch(/ch2/ch3)/ch2/ch2/ch2/ch2/ch3
R29C8H17    !    .ch(/ch2/ch2/ch3)/ch2/ch2/ch2/ch3
R30C12H25    !    .ch2/ch2/ch2/ch2/ch2/ch2/ch2/ch2/ch2/ch2/ch2/ch3
R31C12H25    !    .ch(/ch3)/ch2/ch2/ch2/ch2/ch2/ch2/ch2/ch2/ch2/ch3
R32C12H25    !    .ch(/ch2/ch3)/ch2/ch2/ch2/ch2/ch2/ch2/ch2/ch2/ch3
R33C12H25    !    .ch(/ch2/ch2/ch3)/ch2/ch2/ch2/ch2/ch2/ch2/ch2/ch3
R34C12H25    !    .ch(/ch2/ch2/ch2/ch3)/ch2/ch2/ch2/ch2/ch2/ch2/ch3
R35C12H25    !    .ch(/ch2/ch2/ch2/ch2/ch3)/ch2/ch2/ch2/ch2/ch2/ch3
R36C4H9    !    .ch(/ch3)/ch2/ch3
R37C6H13    !    .ch2/ch2/ch2/ch2/ch2/ch3
R38C5H11    !    .ch2/ch2/ch2/ch2/ch3
R39C10H21    !    .ch2/ch2/ch2/ch2/ch2/ch2/ch2/ch2/ch2/ch3
R40C9H19    !    .ch2/ch2/ch2/ch2/ch2/ch2/ch2/ch2/ch3
R41C7H15    !    .ch2/ch2/ch2/ch2/ch2/ch2/ch3
R42C6H13    !    .ch(/ch2/ch3)/ch2/ch2/ch3
R43C6H13    !    .ch(/ch3)/ch2/ch2/ch2/ch3
R44C5H11    !    .ch(/ch2/ch3)2
R45C5H11    !    .ch(/ch3)/ch2/ch2/ch3
R46C10H21    !    .ch(/ch2/ch3)/ch2/ch2/ch2/ch2/ch2/ch2/ch3
R47C10H21    !    .ch(/ch2/ch2/ch3)/ch2/ch2/ch2/ch2/ch2/ch3
R48C10H21    !    .ch(/ch2/ch2/ch2/ch3)/ch2/ch2/ch2/ch2/ch3
R49C9H19    !    .ch(/ch2/ch3)/ch2/ch2/ch2/ch2/ch2/ch3
R50C9H19    !    .ch(/ch2/ch2/ch3)/ch2/ch2/ch2/ch2/ch3
R51C9H19    !    .ch(/ch2/ch2/ch2/ch3)2
R52C7H15    !    .ch(/ch2/ch3)/ch2/ch2/ch2/ch3
R53C7H15    !    .ch(/ch2/ch2/ch3)2
R54C7H15    !    .ch(/ch3)/ch2/ch2/ch2/ch2/ch3
R55C10H21    !    .ch(/ch3)/ch2/ch2/ch2/ch2/ch2/ch2/ch2/ch3
R56C9H19    !    .ch(/ch3)/ch2/ch2/ch2/ch2/ch2/ch2/ch3
R57C11H23    !    .ch2/ch2/ch2/ch2/ch2/ch2/ch2/ch2/ch2/ch2/ch3
 !Cyclic free radicals:
 !Benzenic free radicals:

! lumped Free radicals :
RC4H7Y
RC5H9Y
RC7H13O
RC6H11O
RC4H7O
RC5H9O
RC11H21O
RC10H19O
RC9H17O
RC8H15O
RC7H13O3
RC6H11O3
RC4H7O3
RC5H9O3
RC11H21O3
RC10H19O3
RC9H17O3
RC8H15O3
RC3H5Y
! lumped Cyclic free radicals :

N2
HE
AR
```

```
END
REACTIONS
! 402 reactions

!     ____________________
!     PRIMARY REACTIONS
!     ____________________
!   molecular elimination :
! ene reaction :
!   retro-ene reaction :
!   Unimolecular decomposition of ethylesters:
!   unimolecular initiations :
C8H18-1=>R20C4H9+R20C4H9     1.1E+0017  0.000   85408.9   ! UI 1 KB
C8H18-1=>R19C3H7+R38C5H11     1.9E+0017  0.000   85837.2   ! UI 2 KB
C8H18-1=>R11C2H5+R37C6H13     1.7E+0017  0.000   85796.2   ! UI 3 KB
C8H18-1=>R4CH3+R41C7H15     3.5E+0017  0.000   87674.5   ! UI 4 KB
C12H26-1=>R37C6H13+R37C6H13     1.1E+0017  0.000   86963.4   ! UI 5 KB
C12H26-1=>R38C5H11+R41C7H15     2.4E+0017  0.000   87002.4   ! UI 6 KB
C12H26-1=>R20C4H9+R26C8H17     2.5E+0017  0.000   86915.7   ! UI 7 KB
C12H26-1=>R19C3H7+R40C9H19     1.9E+0017  0.000   87301.2   ! UI 8 KB
C12H26-1=>R11C2H5+R39C10H21     1.7E+0017  0.000   86541.8   ! UI 9 KB
C12H26-1=>R4CH3+R57C11H23     3.3E+0017  0.000   87662.9   ! UI 10 KB

!   bimolecular initiations :
C8H18-1+O2=>R3OOH+R26C8H17     4.2E+0013  0.000   53033.3   ! BI 11 CN
C8H18-1+O2=>R3OOH+R27C8H17     2.8E+0013  0.000   50588.3   ! BI 12 CN
C8H18-1+O2=>R3OOH+R28C8H17     2.8E+0013  0.000   50652.8   ! BI 13 CN
C8H18-1+O2=>R3OOH+R29C8H17     2.8E+0013  0.000   50652.8   ! BI 14 CN
C12H26-1+O2=>R3OOH+R30C12H25     4.2E+0013  0.000   53033.1   ! BI 15 CN
C12H26-1+O2=>R3OOH+R31C12H25     2.8E+0013  0.000   50588.2   ! BI 16 CN
C12H26-1+O2=>R3OOH+R32C12H25     2.8E+0013  0.000   50652.6   ! BI 17 CN
C12H26-1+O2=>R3OOH+R33C12H25     2.8E+0013  0.000   50652.6   ! BI 18 CN
C12H26-1+O2=>R3OOH+R34C12H25     2.8E+0013  0.000   50652.6   ! BI 19 CN
C12H26-1+O2=>R3OOH+R35C12H25     2.8E+0013  0.000   50652.6   ! BI 20 CN

!   additions :

!   additions with oxygen:

!   isomerisations :
R20C4H9=R36C4H9     3.3E+0009  1.000   37000.0   ! IS 21 KB
R26C8H17=R28C8H17     1.7E+0007  1.000   37000.0   ! IS 22 KB
R26C8H17=R29C8H17     9.9E+0007  1.000   17300.0   ! IS 23 KB
R26C8H17=R27C8H17     2.9E+0006  1.000   20900.0   ! IS 24 KB
R27C8H17=R29C8H17     5.7E+0008  1.000   37000.0   ! IS 25 KB
R27C8H17=R28C8H17     9.9E+0007  1.000   12000.0   ! IS 26 KB
R28C8H17=R29C8H17     3.3E+0009  1.000   37000.0   ! IS 27 KB
R30C12H25=R32C12H25     3.3E+0009  1.000   37000.0   ! IS 28 KB
R30C12H25=R33C12H25     5.7E+0008  1.000   17300.0   ! IS 29 KB
R30C12H25=R34C12H25     9.9E+0007  1.000   12000.0   ! IS 30 KB
R30C12H25=R35C12H25     1.7E+0007  1.000   17400.0   ! IS 31 KB
R31C12H25=R33C12H25     5.0E+0005  1.000   37000.0   ! IS 32 KB
R31C12H25=R34C12H25     5.7E+0008  1.000   17300.0   ! IS 33 KB
R31C12H25=R35C12H25     9.9E+0007  1.000   12000.0   ! IS 34 KB
R32C12H25=R34C12H25     1.7E+0007  1.000   37000.0   ! IS 35 KB
R32C12H25=R35C12H25     9.9E+0007  1.000   17300.0   ! IS 36 KB
R32C12H25=R33C12H25     2.9E+0006  1.000   20900.0   ! IS 37 KB
R33C12H25=R35C12H25     5.7E+0008  1.000   37000.0   ! IS 38 KB
R33C12H25=R34C12H25     9.9E+0007  1.000   12000.0   ! IS 39 KB
R34C12H25=R35C12H25     3.3E+0009  1.000   37000.0   ! IS 40 KB
R37C6H13=R42C6H13     5.7E+0008  1.000   37000.0   ! IS 41 KB
R37C6H13=R43C6H13     9.9E+0007  1.000   12000.0   ! IS 42 KB
R38C5H11=R44C5H11     3.3E+0009  1.000   37000.0   ! IS 43 KB
R38C5H11=R45C5H11     5.7E+0008  1.000   17300.0   ! IS 44 KB
R39C10H21=R46C10H21     5.0E+0005  1.000   37000.0   ! IS 45 KB
R39C10H21=R47C10H21     5.7E+0008  1.000   17300.0   ! IS 46 KB
R39C10H21=R48C10H21     9.9E+0007  1.000   12000.0   ! IS 47 KB
```

```
R40C9H19=R49C9H19      2.9E+0006   1.000   37000.0   ! IS 48 KB
R40C9H19=R50C9H19      5.7E+0008   1.000   17300.0   ! IS 49 KB
R40C9H19=R51C9H19      9.9E+0007   1.000   12000.0   ! IS 50 KB
R41C7H15=R52C7H15      9.9E+0007   1.000   37000.0   ! IS 51 KB
R41C7H15=R53C7H15      5.7E+0008   1.000   17300.0   ! IS 52 KB
R41C7H15=R54C7H15      1.7E+0007   1.000   17400.0   ! IS 53 KB
R42C6H13=R43C6H13      3.3E+0009   1.000   37000.0   ! IS 54 KB
R46C10H21=R48C10H21      5.7E+0008   1.000   37000.0   ! IS 55 KB
R46C10H21=R47C10H21      9.9E+0007   1.000   12000.0   ! IS 56 KB
R46C10H21=R55C10H21      2.9E+0006   1.000   20900.0   ! IS 57 KB
R47C10H21=R55C10H21      1.7E+0007   1.000   37000.0   ! IS 58 KB
R47C10H21=R48C10H21      3.3E+0009   1.000   37000.0   ! IS 59 KB
R48C10H21=R55C10H21      9.9E+0007   1.000   17300.0   ! IS 60 KB
R49C9H19=R51C9H19      3.3E+0009   1.000   37000.0   ! IS 61 KB
R49C9H19=R50C9H19      5.7E+0008   1.000   17300.0   ! IS 62 KB
R49C9H19=R56C9H19      1.7E+0007   1.000   17400.0   ! IS 63 KB
R50C9H19=R56C9H19      9.9E+0007   1.000   37000.0   ! IS 64 KB
R51C9H19=R56C9H19      1.1E+0009   1.000   17300.0   ! IS 65 KB
R52C7H15=R54C7H15      5.7E+0008   1.000   17300.0   ! IS 66 KB
R53C7H15=R54C7H15      6.7E+0009   1.000   37000.0   ! IS 67 KB

!   Decomposition of OOQOOH into branching agents:

!   beta-scissions :
R19C3H7=>R4CH3+C2H4Z      2.0E+0013   0.000   31000.0   ! DE 68 CN
R19C3H7=>R1H+C3H6Y      3.0E+0013   0.000   38000.0   ! DE 69 CN
R20C4H9=>R11C2H5+C2H4Z      2.0E+0013   0.000   28700.0   ! DE 70 CW
R20C4H9=>R1H+C4H8Y      3.0E+0013   0.000   38000.0   ! DE 71 CN
R26C8H17=>R37C6H13+C2H4Z      2.0E+0013   0.000   28700.0   ! DE 72 CW
R26C8H17=>R1H+C8H16Z      3.0E+0013   0.000   38000.0   ! DE 73 CN
R27C8H17=>R38C5H11+C3H6Y      2.0E+0013   0.000   28700.0   ! DE 74 CW
R27C8H17=>R1H+C8H16Z      3.0E+0013   0.000   38000.0   ! DE 75 CN
      DUPLICATE
R27C8H17=>R1H+C8H16Z      3.0E+0013   0.000   39000.0   ! DE 76 CN
      DUPLICATE
R28C8H17=>R20C4H9+C4H8Y      2.0E+0013   0.000   28700.0   ! DE 77 CW
R28C8H17=>R1H+C8H16Z      3.0E+0013   0.000   38000.0   ! DE 78 CN
      DUPLICATE
R28C8H17=>R1H+C8H16Z      3.0E+0013   0.000   38000.0   ! DE 79 CN
      DUPLICATE
R28C8H17=>R4CH3+C7H14Z      2.0E+0013   0.000   31000.0   ! DE 80 CN
R29C8H17=>R1H+C8H16Z      3.0E+0013   0.000   38000.0   ! DE 81 CN
      DUPLICATE
R29C8H17=>R1H+C8H16Z      3.0E+0013   0.000   38000.0   ! DE 82 CN
      DUPLICATE
R29C8H17=>R19C3H7+C5H10Z      2.0E+0013   0.000   28700.0   ! DE 83 CW
R29C8H17=>R11C2H5+C6H12Z      2.0E+0013   0.000   28700.0   ! DE 84 CW
R30C12H25=>R39C10H21+C2H4Z      2.0E+0013   0.000   28700.0   ! DE 85 CW
R30C12H25=>R1H+C12H24Z      3.0E+0013   0.000   38000.0   ! DE 86 CN
R31C12H25=>R40C9H19+C3H6Y      2.0E+0013   0.000   28700.0   ! DE 87 CW
R31C12H25=>R1H+C12H24Z      3.0E+0013   0.000   38000.0   ! DE 88 CN
      DUPLICATE
R31C12H25=>R1H+C12H24Z      3.0E+0013   0.000   39000.0   ! DE 89 CN
      DUPLICATE
R32C12H25=>R26C8H17+C4H8Y      2.0E+0013   0.000   28700.0   ! DE 90 CW
R32C12H25=>R1H+C12H24Z      3.0E+0013   0.000   38000.0   ! DE 91 CN
      DUPLICATE
R32C12H25=>R1H+C12H24Z      3.0E+0013   0.000   38000.0   ! DE 92 CN
      DUPLICATE
R32C12H25=>R4CH3+C11H22Z      2.0E+0013   0.000   31000.0   ! DE 93 CN
R33C12H25=>R41C7H15+C5H10Z      2.0E+0013   0.000   28700.0   ! DE 94 CW
R33C12H25=>R1H+C12H24Z      3.0E+0013   0.000   38000.0   ! DE 95 CN
      DUPLICATE
R33C12H25=>R1H+C12H24Z      3.0E+0013   0.000   38000.0   ! DE 96 CN
      DUPLICATE
R33C12H25=>R11C2H5+C10H20Z      2.0E+0013   0.000   28700.0   ! DE 97 CW
R34C12H25=>R37C6H13+C6H12Z      2.0E+0013   0.000   28700.0   ! DE 98 CW
```

```
R34C12H25=>R1H+C12H24Z      3.0E+0013   0.000   38000.0   ! DE 99 CN
      DUPLICATE
R34C12H25=>R1H+C12H24Z      3.0E+0013   0.000   38000.0   ! DE 100 CN
      DUPLICATE
R34C12H25=>R19C3H7+C9H18Z     2.0E+0013   0.000   28700.0   ! DE 101 CW
R35C12H25=>R20C4H9+C8H16Z     2.0E+0013   0.000   28700.0   ! DE 102 CW
R35C12H25=>R38C5H11+C7H14Z     2.0E+0013   0.000   28700.0   ! DE 103 CW
R35C12H25=>R1H+C12H24Z      3.0E+0013   0.000   38000.0   ! DE 104 CN
      DUPLICATE
R35C12H25=>R1H+C12H24Z      3.0E+0013   0.000   38000.0   ! DE 105 CN
      DUPLICATE
R36C4H9=>R4CH3+C3H6Y      2.0E+0013   0.000   31000.0   ! DE 106 CN
R36C4H9=>R1H+C4H8Y      3.0E+0013   0.000   38000.0   ! DE 107 CN
      DUPLICATE
R36C4H9=>R1H+C4H8Y      3.0E+0013   0.000   39000.0   ! DE 108 CN
      DUPLICATE
R37C6H13=>R20C4H9+C2H4Z     2.0E+0013   0.000   28700.0   ! DE 109 CW
R37C6H13=>R1H+C6H12Z      3.0E+0013   0.000   38000.0   ! DE 110 CN
R38C5H11=>R19C3H7+C2H4Z     2.0E+0013   0.000   28700.0   ! DE 111 CW
R38C5H11=>R1H+C5H10Z      3.0E+0013   0.000   38000.0   ! DE 112 CN
R39C10H21=>R26C8H17+C2H4Z     2.0E+0013   0.000   28700.0   ! DE 113 CW
R39C10H21=>R1H+C10H20Z      3.0E+0013   0.000   38000.0   ! DE 114 CN
R40C9H19=>R41C7H15+C2H4Z     2.0E+0013   0.000   28700.0   ! DE 115 CW
R40C9H19=>R1H+C9H18Z      3.0E+0013   0.000   38000.0   ! DE 116 CN
R41C7H15=>R38C5H11+C2H4Z     2.0E+0013   0.000   28700.0   ! DE 117 CW
R41C7H15=>R1H+C7H14Z      3.0E+0013   0.000   38000.0   ! DE 118 CN
R42C6H13=>R11C2H5+C4H8Y     2.0E+0013   0.000   28700.0   ! DE 119 CW
R42C6H13=>R4CH3+C5H10Z      2.0E+0013   0.000   31000.0   ! DE 120 CN
R42C6H13=>R1H+C6H12Z      3.0E+0013   0.000   38000.0   ! DE 121 CN
      DUPLICATE
R42C6H13=>R1H+C6H12Z      3.0E+0013   0.000   38000.0   ! DE 122 CN
      DUPLICATE
R43C6H13=>R19C3H7+C3H6Y     2.0E+0013   0.000   28700.0   ! DE 123 CW
R43C6H13=>R1H+C6H12Z      3.0E+0013   0.000   38000.0   ! DE 124 CN
      DUPLICATE
R43C6H13=>R1H+C6H12Z      3.0E+0013   0.000   39000.0   ! DE 125 CN
      DUPLICATE
R44C5H11=>R4CH3+C4H8Y      4.0E+0013   0.000   31000.0   ! DE 126 CN
R44C5H11=>R1H+C5H10Y      6.0E+0013   0.000   38000.0   ! DE 127 CN
R45C5H11=>R11C2H5+C3H6Y     2.0E+0013   0.000   28700.0   ! DE 128 CW
R45C5H11=>R1H+C5H10Z      3.0E+0013   0.000   39000.0   ! DE 129 CN
R45C5H11=>R1H+C5H10Y      3.0E+0013   0.000   38000.0   ! DE 130 CN
R46C10H21=>R37C6H13+C4H8Y     2.0E+0013   0.000   28700.0   ! DE 131 CW
R46C10H21=>R1H+C10H20Z      3.0E+0013   0.000   38000.0   ! DE 132 CN
      DUPLICATE
R46C10H21=>R1H+C10H20Z      3.0E+0013   0.000   38000.0   ! DE 133 CN
      DUPLICATE
R46C10H21=>R4CH3+C9H18Z     2.0E+0013   0.000   31000.0   ! DE 134 CN
R47C10H21=>R11C2H5+C8H16Z     2.0E+0013   0.000   28700.0   ! DE 135 CW
R47C10H21=>R38C5H11+C5H10Z     2.0E+0013   0.000   28700.0   ! DE 136 CW
R47C10H21=>R1H+C10H20Z      3.0E+0013   0.000   38000.0   ! DE 137 CN
      DUPLICATE
R47C10H21=>R1H+C10H20Z      3.0E+0013   0.000   38000.0   ! DE 138 CN
      DUPLICATE
R48C10H21=>R19C3H7+C7H14Z     2.0E+0013   0.000   28700.0   ! DE 139 CW
R48C10H21=>R20C4H9+C6H12Z     2.0E+0013   0.000   28700.0   ! DE 140 CW
R48C10H21=>R1H+C10H20Z      3.0E+0013   0.000   38000.0   ! DE 141 CN
      DUPLICATE
R48C10H21=>R1H+C10H20Z      3.0E+0013   0.000   38000.0   ! DE 142 CN
      DUPLICATE
R49C9H19=>R38C5H11+C4H8Y     2.0E+0013   0.000   28700.0   ! DE 143 CW
R49C9H19=>R4CH3+C8H16Z      2.0E+0013   0.000   31000.0   ! DE 144 CN
R49C9H19=>R1H+C9H18Z      3.0E+0013   0.000   38000.0   ! DE 145 CN
      DUPLICATE
R49C9H19=>R1H+C9H18Z      3.0E+0013   0.000   38000.0   ! DE 146 CN
      DUPLICATE
R50C9H19=>R11C2H5+C7H14Z     2.0E+0013   0.000   28700.0   ! DE 147 CW
```

```
R50C9H19=>R20C4H9+C5H10Z      2.0E+0013   0.000   28700.0   ! DE 148 CW
R50C9H19=>R1H+C9H18Z      3.0E+0013   0.000   38000.0   ! DE 149 CN
      DUPLICATE
R50C9H19=>R1H+C9H18Z      3.0E+0013   0.000   38000.0   ! DE 150 CN
      DUPLICATE
R51C9H19=>R19C3H7+C6H12Z      4.0E+0013   0.000   28700.0   ! DE 151 CW
R51C9H19=>R1H+C9H18Z      6.0E+0013   0.000   38000.0   ! DE 152 CN
R52C7H15=>R19C3H7+C4H8Y      2.0E+0013   0.000   28700.0   ! DE 153 CW
R52C7H15=>R1H+C7H14Z      3.0E+0013   0.000   38000.0   ! DE 154 CN
      DUPLICATE
R52C7H15=>R1H+C7H14Z      3.0E+0013   0.000   38000.0   ! DE 155 CN
      DUPLICATE
R52C7H15=>R4CH3+C6H12Z      2.0E+0013   0.000   31000.0   ! DE 156 CN
R53C7H15=>R1H+C7H14Z      6.0E+0013   0.000   38000.0   ! DE 157 CN
R53C7H15=>R11C2H5+C5H10Z      4.0E+0013   0.000   28700.0   ! DE 158 CW
R54C7H15=>R20C4H9+C3H6Y      2.0E+0013   0.000   28700.0   ! DE 159 CW
R54C7H15=>R1H+C7H14Z      3.0E+0013   0.000   38000.0   ! DE 160 CN
      DUPLICATE
R54C7H15=>R1H+C7H14Z      3.0E+0013   0.000   39000.0   ! DE 161 CN
      DUPLICATE
R55C10H21=>R41C7H15+C3H6Y      2.0E+0013   0.000   28700.0   ! DE 162 CW
R55C10H21=>R1H+C10H20Z      3.0E+0013   0.000   38000.0   ! DE 163 CN
      DUPLICATE
R55C10H21=>R1H+C10H20Z      3.0E+0013   0.000   39000.0   ! DE 164 CN
      DUPLICATE
R56C9H19=>R37C6H13+C3H6Y      2.0E+0013   0.000   28700.0   ! DE 165 CW
R56C9H19=>R1H+C9H18Z      3.0E+0013   0.000   38000.0   ! DE 166 CN
      DUPLICATE
R56C9H19=>R1H+C9H18Z      3.0E+0013   0.000   39000.0   ! DE 167 CN
      DUPLICATE
R57C11H23=>R40C9H19+C2H4Z      2.0E+0013   0.000   28700.0   ! DE 168 CW
R57C11H23=>R1H+C11H22Z      3.0E+0013   0.000   38000.0   ! DE 169 CN
! decomposition of R(.)CO free radicals

!   decomposition to o-rings :

!   oxidations :
R26C8H17+O2=>C8H16Z+R3OOH      1.9E+0012   0.000   5000.0   ! OX 170 CN
R27C8H17+O2=>C8H16Z+R3OOH      1.9E+0012   0.000   5000.0   ! OX 171 CN
      DUPLICATE
R27C8H17+O2=>C8H16Z+R3OOH      8.1E+0011   0.000   5000.0   ! OX 172 CN
      DUPLICATE
R28C8H17+O2=>C8H16Z+R3OOH      1.9E+0012   0.000   5000.0   ! OX 173 CN
      DUPLICATE
R28C8H17+O2=>C8H16Z+R3OOH      1.9E+0012   0.000   5000.0   ! OX 174 CN
      DUPLICATE
R29C8H17+O2=>C8H16Z+R3OOH      1.9E+0012   0.000   5000.0   ! OX 175 CN
      DUPLICATE
R29C8H17+O2=>C8H16Z+R3OOH      1.9E+0012   0.000   5000.0   ! OX 176 CN
      DUPLICATE
R30C12H25+O2=>C12H24Z+R3OOH      1.9E+0012   0.000   5000.0   ! OX 177 CN
R31C12H25+O2=>C12H24Z+R3OOH      1.9E+0012   0.000   5000.0   ! OX 178 CN
      DUPLICATE
R31C12H25+O2=>C12H24Z+R3OOH      8.1E+0011   0.000   5000.0   ! OX 179 CN
      DUPLICATE
R32C12H25+O2=>C12H24Z+R3OOH      1.9E+0012   0.000   5000.0   ! OX 180 CN
      DUPLICATE
R32C12H25+O2=>C12H24Z+R3OOH      1.9E+0012   0.000   5000.0   ! OX 181 CN
      DUPLICATE
R33C12H25+O2=>C12H24Z+R3OOH      1.9E+0012   0.000   5000.0   ! OX 182 CN
      DUPLICATE
R33C12H25+O2=>C12H24Z+R3OOH      1.9E+0012   0.000   5000.0   ! OX 183 CN
      DUPLICATE
R34C12H25+O2=>C12H24Z+R3OOH      1.9E+0012   0.000   5000.0   ! OX 184 CN
      DUPLICATE
R34C12H25+O2=>C12H24Z+R3OOH      1.9E+0012   0.000   5000.0   ! OX 185 CN
      DUPLICATE
```

```
R35C12H25+O2=>C12H24Z+R3OOH      1.9E+0012   0.000   5000.0   ! OX 186 CN
      DUPLICATE
R35C12H25+O2=>C12H24Z+R3OOH      1.9E+0012   0.000   5000.0   ! OX 187 CN
      DUPLICATE

!   oxidations of R(.)(OH) radicals:

!   metathesis :
B1O+C8H18-1=>R2OH+R26C8H17     1.0E+0014   0.000   7850.0   ! ME 188 CW
B1O+C8H18-1=>R2OH+R27C8H17     5.2E+0013   0.000   5200.0   ! ME 189 CW
B1O+C8H18-1=>R2OH+R28C8H17     5.2E+0013   0.000   5200.0   ! ME 190 CW
B1O+C8H18-1=>R2OH+R29C8H17     5.2E+0013   0.000   5200.0   ! ME 191 CW
B1O+C12H26-1=>R2OH+R30C12H25     1.0E+0014   0.000   7850.0   ! ME 192 CW
B1O+C12H26-1=>R2OH+R31C12H25     5.2E+0013   0.000   5200.0   ! ME 193 CW
B1O+C12H26-1=>R2OH+R32C12H25     5.2E+0013   0.000   5200.0   ! ME 194 CW
B1O+C12H26-1=>R2OH+R33C12H25     5.2E+0013   0.000   5200.0   ! ME 195 CW
B1O+C12H26-1=>R2OH+R34C12H25     5.2E+0013   0.000   5200.0   ! ME 196 CW
B1O+C12H26-1=>R2OH+R35C12H25     5.2E+0013   0.000   5200.0   ! ME 197 CW
C8H18-1+R1H=>H2+R26C8H17     5.7E+0007   2.000   7700.0   ! ME 198 CW
C8H18-1+R1H=>H2+R27C8H17     1.8E+0007   2.000   5000.0   ! ME 199 CW
C8H18-1+R1H=>H2+R28C8H17     1.8E+0007   2.000   5000.0   ! ME 200 CW
C8H18-1+R1H=>H2+R29C8H17     1.8E+0007   2.000   5000.0   ! ME 201 CW
C12H26-1+R1H=>H2+R30C12H25     5.7E+0007   2.000   7700.0   ! ME 202 CW
C12H26-1+R1H=>H2+R31C12H25     1.8E+0007   2.000   5000.0   ! ME 203 CW
C12H26-1+R1H=>H2+R32C12H25     1.8E+0007   2.000   5000.0   ! ME 204 CW
C12H26-1+R1H=>H2+R33C12H25     1.8E+0007   2.000   5000.0   ! ME 205 CW
C12H26-1+R1H=>H2+R34C12H25     1.8E+0007   2.000   5000.0   ! ME 206 CW
C12H26-1+R1H=>H2+R35C12H25     1.8E+0007   2.000   5000.0   ! ME 207 CW
C8H18-1+R2OH=>H2O+R26C8H17     5.4E+0006   2.000   450.0   ! ME 208 CW
C8H18-1+R2OH=>H2O+R27C8H17     5.2E+0006   2.000   -765.0   ! ME 209 CW
C8H18-1+R2OH=>H2O+R28C8H17     5.2E+0006   2.000   -765.0   ! ME 210 CW
C8H18-1+R2OH=>H2O+R29C8H17     5.2E+0006   2.000   -765.0   ! ME 211 CW
C12H26-1+R2OH=>H2O+R30C12H25     5.4E+0006   2.000   450.0   ! ME 212 CW
C12H26-1+R2OH=>H2O+R31C12H25     5.2E+0006   2.000   -765.0   ! ME 213 CW
C12H26-1+R2OH=>H2O+R32C12H25     5.2E+0006   2.000   -765.0   ! ME 214 CW
C12H26-1+R2OH=>H2O+R33C12H25     5.2E+0006   2.000   -765.0   ! ME 215 CW
C12H26-1+R2OH=>H2O+R34C12H25     5.2E+0006   2.000   -765.0   ! ME 216 CW
C12H26-1+R2OH=>H2O+R35C12H25     5.2E+0006   2.000   -765.0   ! ME 217 CW
C8H18-1+R3OOH=>H2O2+R26C8H17     1.2E+0012   0.000   17000.0   ! ME 218 CN
C8H18-1+R3OOH=>H2O2+R27C8H17     8.0E+0011   0.000   15500.0   ! ME 219 CN
C8H18-1+R3OOH=>H2O2+R28C8H17     8.0E+0011   0.000   15500.0   ! ME 220 CN
C8H18-1+R3OOH=>H2O2+R29C8H17     8.0E+0011   0.000   15500.0   ! ME 221 CN
C12H26-1+R3OOH=>H2O2+R30C12H25     1.2E+0012   0.000   17000.0   ! ME 222 CN
C12H26-1+R3OOH=>H2O2+R31C12H25     8.0E+0011   0.000   15500.0   ! ME 223 CN
C12H26-1+R3OOH=>H2O2+R32C12H25     8.0E+0011   0.000   15500.0   ! ME 224 CN
C12H26-1+R3OOH=>H2O2+R33C12H25     8.0E+0011   0.000   15500.0   ! ME 225 CN
C12H26-1+R3OOH=>H2O2+R34C12H25     8.0E+0011   0.000   15500.0   ! ME 226 CN
C12H26-1+R3OOH=>H2O2+R35C12H25     8.0E+0011   0.000   15500.0   ! ME 227 CN
C8H18-1+R4CH3=>CH4+R26C8H17     6.0E-0001   4.000   8200.0   ! ME 228 CN
C8H18-1+R4CH3=>CH4+R27C8H17     4.0E+0011   0.000   9600.0   ! ME 229 CN
C8H18-1+R4CH3=>CH4+R28C8H17     4.0E+0011   0.000   9600.0   ! ME 230 CN
C8H18-1+R4CH3=>CH4+R29C8H17     4.0E+0011   0.000   9600.0   ! ME 231 CN
C12H26-1+R4CH3=>CH4+R30C12H25     6.0E-0001   4.000   8200.0   ! ME 232 CN
C12H26-1+R4CH3=>CH4+R31C12H25     4.0E+0011   0.000   9600.0   ! ME 233 CN
C12H26-1+R4CH3=>CH4+R32C12H25     4.0E+0011   0.000   9600.0   ! ME 234 CN
C12H26-1+R4CH3=>CH4+R33C12H25     4.0E+0011   0.000   9600.0   ! ME 235 CN
C12H26-1+R4CH3=>CH4+R34C12H25     4.0E+0011   0.000   9600.0   ! ME 236 CN
C12H26-1+R4CH3=>CH4+R35C12H25     4.0E+0011   0.000   9600.0   ! ME 237 CN
C8H18-1+R5CHO=>HCHO+R26C8H17     2.0E+0005   2.500   18500.0   ! ME 238 CN
C8H18-1+R5CHO=>HCHO+R27C8H17     2.2E+0007   1.900   17000.0   ! ME 239 CN
C8H18-1+R5CHO=>HCHO+R28C8H17     2.2E+0007   1.900   17000.0   ! ME 240 CN
C8H18-1+R5CHO=>HCHO+R29C8H17     2.2E+0007   1.900   17000.0   ! ME 241 CN
C12H26-1+R5CHO=>HCHO+R30C12H25     2.0E+0005   2.500   18500.0   ! ME 242 CN
C12H26-1+R5CHO=>HCHO+R31C12H25     2.2E+0007   1.900   17000.0   ! ME 243 CN
C12H26-1+R5CHO=>HCHO+R32C12H25     2.2E+0007   1.900   17000.0   ! ME 244 CN
C12H26-1+R5CHO=>HCHO+R33C12H25     2.2E+0007   1.900   17000.0   ! ME 245 CN
C12H26-1+R5CHO=>HCHO+R34C12H25     2.2E+0007   1.900   17000.0   ! ME 246 CN
```

```
C12H26-1+R5CHO=>HCHO+R35C12H25      2.2E+0007   1.900   17000.0   ! ME 247 CN
C8H18-1+R6CH2OH=>CH3OH+R26C8H17      2.0E+0002   2.950   14000.0   ! ME 248 CN
C8H18-1+R6CH2OH=>CH3OH+R27C8H17      1.2E+0002   2.950   12000.0   ! ME 249 CN
C8H18-1+R6CH2OH=>CH3OH+R28C8H17      1.2E+0002   2.950   12000.0   ! ME 250 CN
C8H18-1+R6CH2OH=>CH3OH+R29C8H17      1.2E+0002   2.950   12000.0   ! ME 251 CN
C12H26-1+R6CH2OH=>CH3OH+R30C12H25      2.0E+0002   2.950   14000.0   ! ME 252 CN
C12H26-1+R6CH2OH=>CH3OH+R31C12H25      1.2E+0002   2.950   12000.0   ! ME 253 CN
C12H26-1+R6CH2OH=>CH3OH+R32C12H25      1.2E+0002   2.950   12000.0   ! ME 254 CN
C12H26-1+R6CH2OH=>CH3OH+R33C12H25      1.2E+0002   2.950   12000.0   ! ME 255 CN
C12H26-1+R6CH2OH=>CH3OH+R34C12H25      1.2E+0002   2.950   12000.0   ! ME 256 CN
C12H26-1+R6CH2OH=>CH3OH+R35C12H25      1.2E+0002   2.950   12000.0   ! ME 257 CN
C8H18-1+R7CH3O=>CH3OH+R26C8H17      3.2E+0011   0.000   7300.0   ! ME 258 CN
C8H18-1+R7CH3O=>CH3OH+R27C8H17      2.9E+0011   0.000   4500.0   ! ME 259 CN
C8H18-1+R7CH3O=>CH3OH+R28C8H17      2.9E+0011   0.000   4500.0   ! ME 260 CN
C8H18-1+R7CH3O=>CH3OH+R29C8H17      2.9E+0011   0.000   4500.0   ! ME 261 CN
C12H26-1+R7CH3O=>CH3OH+R30C12H25      3.2E+0011   0.000   7300.0   ! ME 262 CN
C12H26-1+R7CH3O=>CH3OH+R31C12H25      2.9E+0011   0.000   4500.0   ! ME 263 CN
C12H26-1+R7CH3O=>CH3OH+R32C12H25      2.9E+0011   0.000   4500.0   ! ME 264 CN
C12H26-1+R7CH3O=>CH3OH+R33C12H25      2.9E+0011   0.000   4500.0   ! ME 265 CN
C12H26-1+R7CH3O=>CH3OH+R34C12H25      2.9E+0011   0.000   4500.0   ! ME 266 CN
C12H26-1+R7CH3O=>CH3OH+R35C12H25      2.9E+0011   0.000   4500.0   ! ME 267 CN
C8H18-1+R8CH3OO=>CH3OOH+R26C8H17      1.2E+0013   0.000   20000.0   ! ME 268 CN
C8H18-1+R8CH3OO=>CH3OOH+R27C8H17      6.0E+0012   0.000   17500.0   ! ME 269 CN
C8H18-1+R8CH3OO=>CH3OOH+R28C8H17      6.0E+0012   0.000   17500.0   ! ME 270 CN
C8H18-1+R8CH3OO=>CH3OOH+R29C8H17      6.0E+0012   0.000   17500.0   ! ME 271 CN
C12H26-1+R8CH3OO=>CH3OOH+R30C12H25      1.2E+0013   0.000   20000.0   ! ME 272 CN
C12H26-1+R8CH3OO=>CH3OOH+R31C12H25      6.0E+0012   0.000   17500.0   ! ME 273 CN
C12H26-1+R8CH3OO=>CH3OOH+R32C12H25      6.0E+0012   0.000   17500.0   ! ME 274 CN
C12H26-1+R8CH3OO=>CH3OOH+R33C12H25      6.0E+0012   0.000   17500.0   ! ME 275 CN
C12H26-1+R8CH3OO=>CH3OOH+R34C12H25      6.0E+0012   0.000   17500.0   ! ME 276 CN
C12H26-1+R8CH3OO=>CH3OOH+R35C12H25      6.0E+0012   0.000   17500.0   ! ME 277 CN
C8H18-1+R11C2H5=>C2H6+R26C8H17      6.0E+0011   0.000   13500.0   ! ME 278 CR
C8H18-1+R11C2H5=>C2H6+R27C8H17      4.0E+0011   0.000   11000.0   ! ME 279 CN
C8H18-1+R11C2H5=>C2H6+R28C8H17      4.0E+0011   0.000   11000.0   ! ME 280 CN
C8H18-1+R11C2H5=>C2H6+R29C8H17      4.0E+0011   0.000   11000.0   ! ME 281 CN
C12H26-1+R11C2H5=>C2H6+R30C12H25      6.0E+0011   0.000   13500.0   ! ME 282 CR
C12H26-1+R11C2H5=>C2H6+R31C12H25      4.0E+0011   0.000   11000.0   ! ME 283 CN
C12H26-1+R11C2H5=>C2H6+R32C12H25      4.0E+0011   0.000   11000.0   ! ME 284 CN
C12H26-1+R11C2H5=>C2H6+R33C12H25      4.0E+0011   0.000   11000.0   ! ME 285 CN
C12H26-1+R11C2H5=>C2H6+R34C12H25      4.0E+0011   0.000   11000.0   ! ME 286 CN
C12H26-1+R11C2H5=>C2H6+R35C12H25      4.0E+0011   0.000   11000.0   ! ME 287 CN

!    combinations :

!    dismutations :

!     ---------------------
!     SECONDARY MECHANISM
!     ---------------------

!         Peroxide decomposition

! Hydroperoxide decomposition
C4H8O2PY=>R2OH+R4CH3+C2H3CHOZ      1.5E+0016   0.000   43000.0   ! DHP 288
C5H10O2PY=>R2OH+R11C2H5+C2H3CHOZ      1.5E+0016   0.000   43000.0   ! DHP 289

! Alcoholhydroperoxide decomposition

! Dihydroperoxide decomposition

! Ketohydroperoxide decomposition

! Aldohydroperoxide decomposition

! Peroxy-ester decomposition

! Hydroperoxy ring decomposition
```

```
! Alkane reactions

! O-ring decomposition


! Metatheses of oxetanes, furanes and pyranes

! decompositions of cyclo-ether radicals

! Addition of oxygen on cyclo-ether radicals
!       O2 elimination
!       Isomerization
!       Cylo-ether keto-hydroperoxide ester formation
!       Decomposition of cylo-ether keto-hydroperoxide ester

! Isomerization of peroxy-radicals

!Addition of oxygen on cyclo-peroxy radicals

! Formation of cyclo-ether ketohydroperoxydes

! Decomposition of cyclo-ether ketohydroperoxydes

! Olefin reactions
!  addition of H and CH3 on olefins
C4H8Y+R1H=>R20C4H9     1.3E+0013  0.000  1560.0  ! ADZ 398
      DUPLICATE
C4H8Y+R1H=>R20C4H9     1.3E+0013  0.000  3260.0  ! ADZ 399
      DUPLICATE
C4H8Y+R4CH3=>C3H6Y+R11C2H5     9.6E+0010  0.000  8000.0  ! ADZ 400
C8H16Z+R1H=>R26C8H17     1.3E+0013  0.000  1560.0  ! ADZ 401
      DUPLICATE
C8H16Z+R1H=>R26C8H17     1.3E+0013  0.000  3260.0  ! ADZ 402
      DUPLICATE
C8H16Z+R4CH3=>C4H8Y+R38C5H11     1.7E+0011  0.000  7400.0  ! ADZ 403
C8H16Z+R4CH3=>C3H6Y+R37C6H13     9.6E+0010  0.000  8000.0  ! ADZ 404
C7H14Z+R1H=>R41C7H15     1.3E+0013  0.000  1560.0  ! ADZ 405
      DUPLICATE
C7H14Z+R1H=>R41C7H15     1.3E+0013  0.000  3260.0  ! ADZ 406
      DUPLICATE
C7H14Z+R4CH3=>C4H8Y+R20C4H9     1.7E+0011  0.000  7400.0  ! ADZ 407
C7H14Z+R4CH3=>C3H6Y+R38C5H11     9.6E+0010  0.000  8000.0  ! ADZ 408
C5H10Z+R1H=>R38C5H11     1.3E+0013  0.000  1560.0  ! ADZ 409
      DUPLICATE
C5H10Z+R1H=>R38C5H11     1.3E+0013  0.000  3260.0  ! ADZ 410
      DUPLICATE
C5H10Z+R4CH3=>C4H8Y+R11C2H5     1.7E+0011  0.000  7400.0  ! ADZ 411
C5H10Z+R4CH3=>C3H6Y+R19C3H7     9.6E+0010  0.000  8000.0  ! ADZ 412
C6H12Z+R1H=>R37C6H13     1.3E+0013  0.000  1560.0  ! ADZ 413
      DUPLICATE
C6H12Z+R1H=>R37C6H13     1.3E+0013  0.000  3260.0  ! ADZ 414
      DUPLICATE
C6H12Z+R4CH3=>C4H8Y+R19C3H7     1.7E+0011  0.000  7400.0  ! ADZ 415
C6H12Z+R4CH3=>C3H6Y+R20C4H9     9.6E+0010  0.000  8000.0  ! ADZ 416
C12H24Z+R1H=>R30C12H25     1.3E+0013  0.000  1560.0  ! ADZ 417
      DUPLICATE
C12H24Z+R1H=>R30C12H25     1.3E+0013  0.000  3260.0  ! ADZ 418
      DUPLICATE
C12H24Z+R4CH3=>C4H8Y+R40C9H19     1.7E+0011  0.000  7400.0  ! ADZ 419
C12H24Z+R4CH3=>C3H6Y+R39C10H21     9.6E+0010  0.000  8000.0  ! ADZ 420
C11H22Z+R1H=>R57C11H23     1.3E+0013  0.000  1560.0  ! ADZ 421
      DUPLICATE
C11H22Z+R1H=>R57C11H23     1.3E+0013  0.000  3260.0  ! ADZ 422
      DUPLICATE
C11H22Z+R4CH3=>C4H8Y+R26C8H17     1.7E+0011  0.000  7400.0  ! ADZ 423
C11H22Z+R4CH3=>C3H6Y+R40C9H19     9.6E+0010  0.000  8000.0  ! ADZ 424
```

```
C10H20Z+R1H=>R39C10H21      1.3E+0013   0.000   1560.0   ! ADZ 425
      DUPLICATE
C10H20Z+R1H=>R39C10H21      1.3E+0013   0.000   3260.0   ! ADZ 426
      DUPLICATE
C10H20Z+R4CH3=>C4H8Y+R41C7H15      1.7E+0011   0.000   7400.0   ! ADZ 427
C10H20Z+R4CH3=>C3H6Y+R26C8H17      9.6E+0010   0.000   8000.0   ! ADZ 428
C9H18Z+R1H=>R40C9H19      1.3E+0013   0.000   1560.0   ! ADZ 429
      DUPLICATE
C9H18Z+R1H=>R40C9H19      1.3E+0013   0.000   3260.0   ! ADZ 430
      DUPLICATE
C9H18Z+R4CH3=>C4H8Y+R37C6H13      1.7E+0011   0.000   7400.0   ! ADZ 431
C9H18Z+R4CH3=>C3H6Y+R41C7H15      9.6E+0010   0.000   8000.0   ! ADZ 432
C5H10Y+R1H=>R38C5H11      1.3E+0013   0.000   1560.0   ! ADZ 433
      DUPLICATE
C5H10Y+R1H=>R38C5H11      1.3E+0013   0.000   3260.0   ! ADZ 434
      DUPLICATE
C5H10Y+R4CH3=>C4H8Y+R11C2H5      1.7E+0011   0.000   7400.0   ! ADZ 435
C5H10Y+R4CH3=>C3H6Y+R19C3H7      9.6E+0010   0.000   8000.0   ! ADZ 436

!  addition of OH on olefins
C4H8Y+R2OH=>R4CH3+C2H5CHO      1.4E+0012   0.000   -1040.0   ! ADZ 437
C4H8Y+R2OH=>R19C3H7+HCHO      1.4E+0012   0.000   -1040.0   ! ADZ 438
C8H16Z+R2OH=>R4CH3+C7H14OA      1.4E+0012   0.000   -1040.0   ! ADZ 439
C8H16Z+R2OH=>R41C7H15+HCHO      1.4E+0012   0.000   -1040.0   ! ADZ 440
C7H14Z+R2OH=>R4CH3+C6H12OA      1.4E+0012   0.000   -1040.0   ! ADZ 441
C7H14Z+R2OH=>R37C6H13+HCHO      1.4E+0012   0.000   -1040.0   ! ADZ 442
C5H10Z+R2OH=>R4CH3+C4H8OA      1.4E+0012   0.000   -1040.0   ! ADZ 443
C5H10Z+R2OH=>R20C4H9+HCHO      1.4E+0012   0.000   -1040.0   ! ADZ 444
C6H12Z+R2OH=>R4CH3+C5H10OA      1.4E+0012   0.000   -1040.0   ! ADZ 445
C6H12Z+R2OH=>R38C5H11+HCHO      1.4E+0012   0.000   -1040.0   ! ADZ 446
C12H24Z+R2OH=>R4CH3+C11H22OA      1.4E+0012   0.000   -1040.0   ! ADZ 447
C12H24Z+R2OH=>R57C11H23+HCHO      1.4E+0012   0.000   -1040.0   ! ADZ 448
C11H22Z+R2OH=>R4CH3+C10H20OA      1.4E+0012   0.000   -1040.0   ! ADZ 449
C11H22Z+R2OH=>R39C10H21+HCHO      1.4E+0012   0.000   -1040.0   ! ADZ 450
C10H20Z+R2OH=>R4CH3+C9H18OA      1.4E+0012   0.000   -1040.0   ! ADZ 451
C10H20Z+R2OH=>R40C9H19+HCHO      1.4E+0012   0.000   -1040.0   ! ADZ 452
C9H18Z+R2OH=>R4CH3+C8H16OA      1.4E+0012   0.000   -1040.0   ! ADZ 453
C9H18Z+R2OH=>R26C8H17+HCHO      1.4E+0012   0.000   -1040.0   ! ADZ 454
C5H10Y+R2OH=>R4CH3+C4H8OA      1.4E+0012   0.000   -1040.0   ! ADZ 455
C5H10Y+R2OH=>R20C4H9+HCHO      1.4E+0012   0.000   -1040.0   ! ADZ 456


!  addition of O on olefins
C4H8Y+B1O=>CH2COZ+R1H+R11C2H5      1.2E+0005   2.560   -1130.0   ! AOZ 457
C8H16Z+B1O=>CH2COZ+R1H+R37C6H13      1.2E+0005   2.560   -1130.0   ! AOZ 457
C7H14Z+B1O=>CH2COZ+R1H+R38C5H11      1.2E+0005   2.560   -1130.0   ! AOZ 457
C5H10Z+B1O=>CH2COZ+R1H+R19C3H7      1.2E+0005   2.560   -1130.0   ! AOZ 457
C6H12Z+B1O=>CH2COZ+R1H+R20C4H9      1.2E+0005   2.560   -1130.0   ! AOZ 457
C12H24Z+B1O=>CH2COZ+R1H+R39C10H21      1.2E+0005   2.560   -1130.0   ! AOZ 457
C11H22Z+B1O=>CH2COZ+R1H+R40C9H19      1.2E+0005   2.560   -1130.0   ! AOZ 457
C10H20Z+B1O=>CH2COZ+R1H+R26C8H17      1.2E+0005   2.560   -1130.0   ! AOZ 457
C9H18Z+B1O=>CH2COZ+R1H+R41C7H15      1.2E+0005   2.560   -1130.0   ! AOZ 457
C5H10Y+B1O=>CH2COZ+R1H+R19C3H7      1.2E+0005   2.560   -1130.0   ! AOZ 457

! retroene reactions
C8H16Z=>C3H6Y+C5H10Z      8.0E+0012   0.000   56500.0   ! RTZ 457
C7H14Z=>C3H6Y+C4H8Y      8.0E+0012   0.000   56500.0   ! RTZ 458
C5H10Z=>C3H6Y+C2H4Z      8.0E+0012   0.000   56500.0   ! RTZ 459
C6H12Z=>C3H6Y+C3H6Y      8.0E+0012   0.000   56500.0   ! RTZ 460
C12H24Z=>C3H6Y+C9H18Z      8.0E+0012   0.000   56500.0   ! RTZ 461
C11H22Z=>C3H6Y+C8H16Z      8.0E+0012   0.000   56500.0   ! RTZ 462
C10H20Z=>C3H6Y+C7H14Z      8.0E+0012   0.000   56500.0   ! RTZ 463
C9H18Z=>C3H6Y+C6H12Z      8.0E+0012   0.000   56500.0   ! RTZ 464
C5H10Y=>C3H6Y+C2H4Z      8.0E+0012   0.000   56500.0   ! RTZ 465

!  addition of OOH on olefins
```

```
!   olefin to dienes
C8H16Z+R1H=>H2+C4H6Z2+R20C4H9      5.4E+0004   2.500   -1900.0   ! MZ 476
      DUPLICATE
C8H16Z+R1H=>H2+C4H6Z2+R20C4H9      2.9E+0007   2.000   7700.0   ! MZ 477
      DUPLICATE
C8H16Z+R1H=>H2+C4H6Z2+R20C4H9      3.6E+0007   2.000   5000.0   ! MZ 478
      DUPLICATE
C8H16Z+R2OH=>H2O+C4H6Z2+R20C4H9      3.0E+0006   2.000   -1520.0   ! MZ 479
      DUPLICATE
C8H16Z+R2OH=>H2O+C4H6Z2+R20C4H9      2.7E+0006   2.000   450.0   ! MZ 480
      DUPLICATE
C8H16Z+R2OH=>H2O+C4H6Z2+R20C4H9      1.0E+0007   2.000   -765.0   ! MZ 481
      DUPLICATE
C8H16Z+R3OOH=>H2O2+C4H6Z2+R20C4H9      6.4E+0003   2.600   12400.0   ! MZ 482
      DUPLICATE
C8H16Z+R3OOH=>H2O2+C4H6Z2+R20C4H9      6.0E+0011   0.000   17000.0   ! MZ 483
      DUPLICATE
C8H16Z+R3OOH=>H2O2+C4H6Z2+R20C4H9      1.6E+0012   0.000   15500.0   ! MZ 484
      DUPLICATE
C8H16Z+R4CH3=>CH4+C4H6Z2+R20C4H9      1.0E+0011   0.000   7300.0   ! MZ 485
      DUPLICATE
C8H16Z+R4CH3=>CH4+C4H6Z2+R20C4H9      3.0E-0001   4.000   8200.0   ! MZ 486
      DUPLICATE
C8H16Z+R4CH3=>CH4+C4H6Z2+R20C4H9      8.0E+0011   0.000   9600.0   ! MZ 487
      DUPLICATE
C8H16Z+R8CH3OO=>CH3OOH+C4H6Z2+R20C4H9      1.0E+0012   0.000   14550.0   ! MZ 488
      DUPLICATE
C8H16Z+R8CH3OO=>CH3OOH+C4H6Z2+R20C4H9      6.0E+0012   0.000   20000.0   ! MZ 489
      DUPLICATE
C8H16Z+R8CH3OO=>CH3OOH+C4H6Z2+R20C4H9      1.2E+0013   0.000   17500.0   ! MZ 490
      DUPLICATE
C8H16Z+R11C2H5=>C2H6+C4H6Z2+R20C4H9      1.5E+0000   3.500   4140.0   ! MZ 491
      DUPLICATE
C8H16Z+R11C2H5=>C2H6+C4H6Z2+R20C4H9      3.0E+0011   0.000   13500.0   ! MZ 492
      DUPLICATE
C8H16Z+R11C2H5=>C2H6+C4H6Z2+R20C4H9      8.0E+0011   0.000   11000.0   ! MZ 493
      DUPLICATE
C7H14Z+R1H=>H2+C4H6Z2+R19C3H7      5.4E+0004   2.500   -1900.0   ! MZ 494
      DUPLICATE
C7H14Z+R1H=>H2+C4H6Z2+R19C3H7      2.9E+0007   2.000   7700.0   ! MZ 495
      DUPLICATE
C7H14Z+R1H=>H2+C4H6Z2+R19C3H7      2.7E+0007   2.000   5000.0   ! MZ 496
      DUPLICATE
C7H14Z+R2OH=>H2O+C4H6Z2+R19C3H7      3.0E+0006   2.000   -1520.0   ! MZ 497
      DUPLICATE
C7H14Z+R2OH=>H2O+C4H6Z2+R19C3H7      2.7E+0006   2.000   450.0   ! MZ 498
      DUPLICATE
C7H14Z+R2OH=>H2O+C4H6Z2+R19C3H7      7.8E+0006   2.000   -765.0   ! MZ 499
      DUPLICATE
C7H14Z+R3OOH=>H2O2+C4H6Z2+R19C3H7      6.4E+0003   2.600   12400.0   ! MZ 500
      DUPLICATE
C7H14Z+R3OOH=>H2O2+C4H6Z2+R19C3H7      6.0E+0011   0.000   17000.0   ! MZ 501
      DUPLICATE
C7H14Z+R3OOH=>H2O2+C4H6Z2+R19C3H7      1.2E+0012   0.000   15500.0   ! MZ 502
      DUPLICATE
C7H14Z+R4CH3=>CH4+C4H6Z2+R19C3H7      1.0E+0011   0.000   7300.0   ! MZ 503
      DUPLICATE
C7H14Z+R4CH3=>CH4+C4H6Z2+R19C3H7      3.0E-0001   4.000   8200.0   ! MZ 504
      DUPLICATE
C7H14Z+R4CH3=>CH4+C4H6Z2+R19C3H7      6.0E+0011   0.000   9600.0   ! MZ 505
      DUPLICATE
C7H14Z+R8CH3OO=>CH3OOH+C4H6Z2+R19C3H7      1.0E+0012   0.000   14550.0   ! MZ 506
      DUPLICATE
C7H14Z+R8CH3OO=>CH3OOH+C4H6Z2+R19C3H7      6.0E+0012   0.000   20000.0   ! MZ 507
      DUPLICATE
C7H14Z+R8CH3OO=>CH3OOH+C4H6Z2+R19C3H7      9.0E+0012   0.000   17500.0   ! MZ 508
```

```
      DUPLICATE
C7H14Z+R11C2H5=>C2H6+C4H6Z2+R19C3H7      1.5E+0000   3.500   4140.0   ! MZ 509
      DUPLICATE
C7H14Z+R11C2H5=>C2H6+C4H6Z2+R19C3H7      3.0E+0011   0.000   13500.0   ! MZ 510
      DUPLICATE
C7H14Z+R11C2H5=>C2H6+C4H6Z2+R19C3H7      6.0E+0011   0.000   11000.0   ! MZ 511
      DUPLICATE
C5H10Z+R1H=>H2+C4H6Z2+R4CH3      5.4E+0004   2.500   -1900.0   ! MZ 512
      DUPLICATE
C5H10Z+R1H=>H2+C4H6Z2+R4CH3      2.9E+0007   2.000   7700.0   ! MZ 513
      DUPLICATE
C5H10Z+R1H=>H2+C4H6Z2+R4CH3      9.0E+0006   2.000   5000.0   ! MZ 514
      DUPLICATE
C5H10Z+R2OH=>H2O+C4H6Z2+R4CH3      3.0E+0006   2.000   -1520.0   ! MZ 515
      DUPLICATE
C5H10Z+R2OH=>H2O+C4H6Z2+R4CH3      2.7E+0006   2.000   450.0   ! MZ 516
      DUPLICATE
C5H10Z+R2OH=>H2O+C4H6Z2+R4CH3      2.6E+0006   2.000   -765.0   ! MZ 517
      DUPLICATE
C5H10Z+R3OOH=>H2O2+C4H6Z2+R4CH3      6.4E+0003   2.600   12400.0   ! MZ 518
      DUPLICATE
C5H10Z+R3OOH=>H2O2+C4H6Z2+R4CH3      6.0E+0011   0.000   17000.0   ! MZ 519
      DUPLICATE
C5H10Z+R3OOH=>H2O2+C4H6Z2+R4CH3      4.0E+0011   0.000   15500.0   ! MZ 520
      DUPLICATE
C5H10Z+R4CH3=>CH4+C4H6Z2+R4CH3      1.0E+0011   0.000   7300.0   ! MZ 521
      DUPLICATE
C5H10Z+R4CH3=>CH4+C4H6Z2+R4CH3      3.0E-0001   4.000   8200.0   ! MZ 522
      DUPLICATE
C5H10Z+R4CH3=>CH4+C4H6Z2+R4CH3      2.0E+0011   0.000   9600.0   ! MZ 523
      DUPLICATE
C5H10Z+R8CH3OO=>CH3OOH+C4H6Z2+R4CH3      1.0E+0012   0.000   14550.0   ! MZ 524
      DUPLICATE
C5H10Z+R8CH3OO=>CH3OOH+C4H6Z2+R4CH3      6.0E+0012   0.000   20000.0   ! MZ 525
      DUPLICATE
C5H10Z+R8CH3OO=>CH3OOH+C4H6Z2+R4CH3      3.0E+0012   0.000   17500.0   ! MZ 526
      DUPLICATE
C5H10Z+R11C2H5=>C2H6+C4H6Z2+R4CH3      1.5E+0000   3.500   4140.0   ! MZ 527
      DUPLICATE
C5H10Z+R11C2H5=>C2H6+C4H6Z2+R4CH3      3.0E+0011   0.000   13500.0   ! MZ 528
      DUPLICATE
C5H10Z+R11C2H5=>C2H6+C4H6Z2+R4CH3      2.0E+0011   0.000   11000.0   ! MZ 529
      DUPLICATE
C6H12Z+R1H=>H2+C4H6Z2+R11C2H5      5.4E+0004   2.500   -1900.0   ! MZ 530
      DUPLICATE
C6H12Z+R1H=>H2+C4H6Z2+R11C2H5      2.9E+0007   2.000   7700.0   ! MZ 531
      DUPLICATE
C6H12Z+R1H=>H2+C4H6Z2+R11C2H5      1.8E+0007   2.000   5000.0   ! MZ 532
      DUPLICATE
C6H12Z+R2OH=>H2O+C4H6Z2+R11C2H5      3.0E+0006   2.000   -1520.0   ! MZ 533
      DUPLICATE
C6H12Z+R2OH=>H2O+C4H6Z2+R11C2H5      2.7E+0006   2.000   450.0   ! MZ 534
      DUPLICATE
C6H12Z+R2OH=>H2O+C4H6Z2+R11C2H5      5.2E+0006   2.000   -765.0   ! MZ 535
      DUPLICATE
C6H12Z+R3OOH=>H2O2+C4H6Z2+R11C2H5      6.4E+0003   2.600   12400.0   ! MZ 536
      DUPLICATE
C6H12Z+R3OOH=>H2O2+C4H6Z2+R11C2H5      6.0E+0011   0.000   17000.0   ! MZ 537
      DUPLICATE
C6H12Z+R3OOH=>H2O2+C4H6Z2+R11C2H5      8.0E+0011   0.000   15500.0   ! MZ 538
      DUPLICATE
C6H12Z+R4CH3=>CH4+C4H6Z2+R11C2H5      1.0E+0011   0.000   7300.0   ! MZ 539
      DUPLICATE
C6H12Z+R4CH3=>CH4+C4H6Z2+R11C2H5      3.0E-0001   4.000   8200.0   ! MZ 540
      DUPLICATE
C6H12Z+R4CH3=>CH4+C4H6Z2+R11C2H5      4.0E+0011   0.000   9600.0   ! MZ 541
      DUPLICATE
```

```
C6H12Z+R8CH3OO=>CH3OOH+C4H6Z2+R11C2H5      1.0E+0012   0.000   14550.0   ! MZ 542
      DUPLICATE
C6H12Z+R8CH3OO=>CH3OOH+C4H6Z2+R11C2H5      6.0E+0012   0.000   20000.0   ! MZ 543
      DUPLICATE
C6H12Z+R8CH3OO=>CH3OOH+C4H6Z2+R11C2H5      6.0E+0012   0.000   17500.0   ! MZ 544
      DUPLICATE
C6H12Z+R11C2H5=>C2H6+C4H6Z2+R11C2H5      1.5E+0000   3.500   4140.0   ! MZ 545
      DUPLICATE
C6H12Z+R11C2H5=>C2H6+C4H6Z2+R11C2H5      3.0E+0011   0.000   13500.0   ! MZ 546
      DUPLICATE
C6H12Z+R11C2H5=>C2H6+C4H6Z2+R11C2H5      4.0E+0011   0.000   11000.0   ! MZ 547
      DUPLICATE
C12H24Z+R1H=>H2+C4H6Z2+R26C8H17      5.4E+0004   2.500   -1900.0   ! MZ 548
      DUPLICATE
C12H24Z+R1H=>H2+C4H6Z2+R26C8H17      2.9E+0007   2.000   7700.0   ! MZ 549
      DUPLICATE
C12H24Z+R1H=>H2+C4H6Z2+R26C8H17      7.2E+0007   2.000   5000.0   ! MZ 550
      DUPLICATE
C12H24Z+R2OH=>H2O+C4H6Z2+R26C8H17      3.0E+0006   2.000   -1520.0   ! MZ 551
      DUPLICATE
C12H24Z+R2OH=>H2O+C4H6Z2+R26C8H17      2.7E+0006   2.000   450.0   ! MZ 552
      DUPLICATE
C12H24Z+R2OH=>H2O+C4H6Z2+R26C8H17      2.1E+0007   2.000   -765.0   ! MZ 553
      DUPLICATE
C12H24Z+R3OOH=>H2O2+C4H6Z2+R26C8H17      6.4E+0003   2.600   12400.0   ! MZ 554
      DUPLICATE
C12H24Z+R3OOH=>H2O2+C4H6Z2+R26C8H17      6.0E+0011   0.000   17000.0   ! MZ 555
      DUPLICATE
C12H24Z+R3OOH=>H2O2+C4H6Z2+R26C8H17      3.2E+0012   0.000   15500.0   ! MZ 556
      DUPLICATE
C12H24Z+R4CH3=>CH4+C4H6Z2+R26C8H17      1.0E+0011   0.000   7300.0   ! MZ 557
      DUPLICATE
C12H24Z+R4CH3=>CH4+C4H6Z2+R26C8H17      3.0E-0001   4.000   8200.0   ! MZ 558
      DUPLICATE
C12H24Z+R4CH3=>CH4+C4H6Z2+R26C8H17      1.6E+0012   0.000   9600.0   ! MZ 559
      DUPLICATE
C12H24Z+R8CH3OO=>CH3OOH+C4H6Z2+R26C8H17      1.0E+0012   0.000   14550.0   ! MZ 560
      DUPLICATE
C12H24Z+R8CH3OO=>CH3OOH+C4H6Z2+R26C8H17      6.0E+0012   0.000   20000.0   ! MZ 561
      DUPLICATE
C12H24Z+R8CH3OO=>CH3OOH+C4H6Z2+R26C8H17      2.4E+0013   0.000   17500.0   ! MZ 562
      DUPLICATE
C12H24Z+R11C2H5=>C2H6+C4H6Z2+R26C8H17      1.5E+0000   3.500   4140.0   ! MZ 563
      DUPLICATE
C12H24Z+R11C2H5=>C2H6+C4H6Z2+R26C8H17      3.0E+0011   0.000   13500.0   ! MZ 564
      DUPLICATE
C12H24Z+R11C2H5=>C2H6+C4H6Z2+R26C8H17      1.6E+0012   0.000   11000.0   ! MZ 565
      DUPLICATE
C11H22Z+R1H=>H2+C4H6Z2+R41C7H15      5.4E+0004   2.500   -1900.0   ! MZ 566
      DUPLICATE
C11H22Z+R1H=>H2+C4H6Z2+R41C7H15      2.9E+0007   2.000   7700.0   ! MZ 567
      DUPLICATE
C11H22Z+R1H=>H2+C4H6Z2+R41C7H15      6.3E+0007   2.000   5000.0   ! MZ 568
      DUPLICATE
C11H22Z+R2OH=>H2O+C4H6Z2+R41C7H15      3.0E+0006   2.000   -1520.0   ! MZ 569
      DUPLICATE
C11H22Z+R2OH=>H2O+C4H6Z2+R41C7H15      2.7E+0006   2.000   450.0   ! MZ 570
      DUPLICATE
C11H22Z+R2OH=>H2O+C4H6Z2+R41C7H15      1.8E+0007   2.000   -765.0   ! MZ 571
      DUPLICATE
C11H22Z+R3OOH=>H2O2+C4H6Z2+R41C7H15      6.4E+0003   2.600   12400.0   ! MZ 572
      DUPLICATE
C11H22Z+R3OOH=>H2O2+C4H6Z2+R41C7H15      6.0E+0011   0.000   17000.0   ! MZ 573
      DUPLICATE
C11H22Z+R3OOH=>H2O2+C4H6Z2+R41C7H15      2.8E+0012   0.000   15500.0   ! MZ 574
      DUPLICATE
C11H22Z+R4CH3=>CH4+C4H6Z2+R41C7H15      1.0E+0011   0.000   7300.0   ! MZ 575
```

```
      DUPLICATE
C11H22Z+R4CH3=>CH4+C4H6Z2+R41C7H15      3.0E-0001   4.000   8200.0   ! MZ 576
      DUPLICATE
C11H22Z+R4CH3=>CH4+C4H6Z2+R41C7H15      1.4E+0012   0.000   9600.0   ! MZ 577
      DUPLICATE
C11H22Z+R8CH3OO=>CH3OOH+C4H6Z2+R41C7H15      1.0E+0012   0.000   14550.0   ! MZ 578
      DUPLICATE
C11H22Z+R8CH3OO=>CH3OOH+C4H6Z2+R41C7H15      6.0E+0012   0.000   20000.0   ! MZ 579
      DUPLICATE
C11H22Z+R8CH3OO=>CH3OOH+C4H6Z2+R41C7H15      2.1E+0013   0.000   17500.0   ! MZ 580
      DUPLICATE
C11H22Z+R11C2H5=>C2H6+C4H6Z2+R41C7H15      1.5E+0000   3.500   4140.0   ! MZ 581
      DUPLICATE
C11H22Z+R11C2H5=>C2H6+C4H6Z2+R41C7H15      3.0E+0011   0.000   13500.0   ! MZ 582
      DUPLICATE
C11H22Z+R11C2H5=>C2H6+C4H6Z2+R41C7H15      1.4E+0012   0.000   11000.0   ! MZ 583
      DUPLICATE
C10H20Z+R1H=>H2+C4H6Z2+R37C6H13      5.4E+0004   2.500   -1900.0   ! MZ 584
      DUPLICATE
C10H20Z+R1H=>H2+C4H6Z2+R37C6H13      2.9E+0007   2.000   7700.0   ! MZ 585
      DUPLICATE
C10H20Z+R1H=>H2+C4H6Z2+R37C6H13      5.4E+0007   2.000   5000.0   ! MZ 586
      DUPLICATE
C10H20Z+R2OH=>H2O+C4H6Z2+R37C6H13      3.0E+0006   2.000   -1520.0   ! MZ 587
      DUPLICATE
C10H20Z+R2OH=>H2O+C4H6Z2+R37C6H13      2.7E+0006   2.000   450.0   ! MZ 588
      DUPLICATE
C10H20Z+R2OH=>H2O+C4H6Z2+R37C6H13      1.5E+0007   2.000   -765.0   ! MZ 589
      DUPLICATE
C10H20Z+R3OOH=>H2O2+C4H6Z2+R37C6H13      6.4E+0003   2.600   12400.0   ! MZ 590
      DUPLICATE
C10H20Z+R3OOH=>H2O2+C4H6Z2+R37C6H13      6.0E+0011   0.000   17000.0   ! MZ 591
      DUPLICATE
C10H20Z+R3OOH=>H2O2+C4H6Z2+R37C6H13      2.4E+0012   0.000   15500.0   ! MZ 592
      DUPLICATE
C10H20Z+R4CH3=>CH4+C4H6Z2+R37C6H13      1.0E+0011   0.000   7300.0   ! MZ 593
      DUPLICATE
C10H20Z+R4CH3=>CH4+C4H6Z2+R37C6H13      3.0E-0001   4.000   8200.0   ! MZ 594
      DUPLICATE
C10H20Z+R4CH3=>CH4+C4H6Z2+R37C6H13      1.2E+0012   0.000   9600.0   ! MZ 595
      DUPLICATE
C10H20Z+R8CH3OO=>CH3OOH+C4H6Z2+R37C6H13      1.0E+0012   0.000   14550.0   ! MZ 596
      DUPLICATE
C10H20Z+R8CH3OO=>CH3OOH+C4H6Z2+R37C6H13      6.0E+0012   0.000   20000.0   ! MZ 597
      DUPLICATE
C10H20Z+R8CH3OO=>CH3OOH+C4H6Z2+R37C6H13      1.8E+0013   0.000   17500.0   ! MZ 598
      DUPLICATE
C10H20Z+R11C2H5=>C2H6+C4H6Z2+R37C6H13      1.5E+0000   3.500   4140.0   ! MZ 599
      DUPLICATE
C10H20Z+R11C2H5=>C2H6+C4H6Z2+R37C6H13      3.0E+0011   0.000   13500.0   ! MZ 600
      DUPLICATE
C10H20Z+R11C2H5=>C2H6+C4H6Z2+R37C6H13      1.2E+0012   0.000   11000.0   ! MZ 601
      DUPLICATE
C9H18Z+R1H=>H2+C4H6Z2+R38C5H11      5.4E+0004   2.500   -1900.0   ! MZ 602
      DUPLICATE
C9H18Z+R1H=>H2+C4H6Z2+R38C5H11      2.9E+0007   2.000   7700.0   ! MZ 603
      DUPLICATE
C9H18Z+R1H=>H2+C4H6Z2+R38C5H11      4.5E+0007   2.000   5000.0   ! MZ 604
      DUPLICATE
C9H18Z+R2OH=>H2O+C4H6Z2+R38C5H11      3.0E+0006   2.000   -1520.0   ! MZ 605
      DUPLICATE
C9H18Z+R2OH=>H2O+C4H6Z2+R38C5H11      2.7E+0006   2.000   450.0   ! MZ 606
      DUPLICATE
C9H18Z+R2OH=>H2O+C4H6Z2+R38C5H11      1.3E+0007   2.000   -765.0   ! MZ 607
      DUPLICATE
C9H18Z+R3OOH=>H2O2+C4H6Z2+R38C5H11      6.4E+0003   2.600   12400.0   ! MZ 608
      DUPLICATE
```

```
C9H18Z+R3OOH=>H2O2+C4H6Z2+R38C5H11      6.0E+0011   0.000   17000.0   ! MZ 609
      DUPLICATE
C9H18Z+R3OOH=>H2O2+C4H6Z2+R38C5H11      2.0E+0012   0.000   15500.0   ! MZ 610
      DUPLICATE
C9H18Z+R4CH3=>CH4+C4H6Z2+R38C5H11       1.0E+0011   0.000   7300.0   ! MZ 611
      DUPLICATE
C9H18Z+R4CH3=>CH4+C4H6Z2+R38C5H11       3.0E-0001   4.000   8200.0   ! MZ 612
      DUPLICATE
C9H18Z+R4CH3=>CH4+C4H6Z2+R38C5H11       1.0E+0012   0.000   9600.0   ! MZ 613
      DUPLICATE
C9H18Z+R8CH3OO=>CH3OOH+C4H6Z2+R38C5H11      1.0E+0012   0.000   14550.0   ! MZ 614
      DUPLICATE
C9H18Z+R8CH3OO=>CH3OOH+C4H6Z2+R38C5H11      6.0E+0012   0.000   20000.0   ! MZ 615
      DUPLICATE
C9H18Z+R8CH3OO=>CH3OOH+C4H6Z2+R38C5H11      1.5E+0013   0.000   17500.0   ! MZ 616
      DUPLICATE
C9H18Z+R11C2H5=>C2H6+C4H6Z2+R38C5H11      1.5E+0000   3.500   4140.0   ! MZ 617
      DUPLICATE
C9H18Z+R11C2H5=>C2H6+C4H6Z2+R38C5H11      3.0E+0011   0.000   13500.0   ! MZ 618
      DUPLICATE
C9H18Z+R11C2H5=>C2H6+C4H6Z2+R38C5H11      1.0E+0012   0.000   11000.0   ! MZ 619
      DUPLICATE
C8H16Z+B1O=>R2OH+C4H6Z2+R20C4H9      8.8E+0010   0.700   3250.0   ! MZ 620
      DUPLICATE
C8H16Z+B1O=>R2OH+C4H6Z2+R20C4H9      5.1E+0013   0.000   7850.0   ! MZ 621
      DUPLICATE
C8H16Z+B1O=>R2OH+C4H6Z2+R20C4H9      1.0E+0014   0.000   5200.0   ! MZ 622
      DUPLICATE
C7H14Z+B1O=>R2OH+C4H6Z2+R19C3H7      8.8E+0010   0.700   3250.0   ! MZ 623
      DUPLICATE
C7H14Z+B1O=>R2OH+C4H6Z2+R19C3H7      5.1E+0013   0.000   7850.0   ! MZ 624
      DUPLICATE
C7H14Z+B1O=>R2OH+C4H6Z2+R19C3H7      7.8E+0013   0.000   5200.0   ! MZ 625
      DUPLICATE
C5H10Z+B1O=>R2OH+C4H6Z2+R4CH3      8.8E+0010   0.700   3250.0   ! MZ 626
      DUPLICATE
C5H10Z+B1O=>R2OH+C4H6Z2+R4CH3      5.1E+0013   0.000   7850.0   ! MZ 627
      DUPLICATE
C5H10Z+B1O=>R2OH+C4H6Z2+R4CH3      2.6E+0013   0.000   5200.0   ! MZ 628
      DUPLICATE
C6H12Z+B1O=>R2OH+C4H6Z2+R11C2H5      8.8E+0010   0.700   3250.0   ! MZ 629
      DUPLICATE
C6H12Z+B1O=>R2OH+C4H6Z2+R11C2H5      5.1E+0013   0.000   7850.0   ! MZ 630
      DUPLICATE
C6H12Z+B1O=>R2OH+C4H6Z2+R11C2H5      5.2E+0013   0.000   5200.0   ! MZ 631
      DUPLICATE
C12H24Z+B1O=>R2OH+C4H6Z2+R26C8H17      8.8E+0010   0.700   3250.0   ! MZ 632
      DUPLICATE
C12H24Z+B1O=>R2OH+C4H6Z2+R26C8H17      5.1E+0013   0.000   7850.0   ! MZ 633
      DUPLICATE
C12H24Z+B1O=>R2OH+C4H6Z2+R26C8H17      2.1E+0014   0.000   5200.0   ! MZ 634
      DUPLICATE
C11H22Z+B1O=>R2OH+C4H6Z2+R41C7H15      8.8E+0010   0.700   3250.0   ! MZ 635
      DUPLICATE
C11H22Z+B1O=>R2OH+C4H6Z2+R41C7H15      5.1E+0013   0.000   7850.0   ! MZ 636
      DUPLICATE
C11H22Z+B1O=>R2OH+C4H6Z2+R41C7H15      1.8E+0014   0.000   5200.0   ! MZ 637
      DUPLICATE
C10H20Z+B1O=>R2OH+C4H6Z2+R37C6H13      8.8E+0010   0.700   3250.0   ! MZ 638
      DUPLICATE
C10H20Z+B1O=>R2OH+C4H6Z2+R37C6H13      5.1E+0013   0.000   7850.0   ! MZ 639
      DUPLICATE
C10H20Z+B1O=>R2OH+C4H6Z2+R37C6H13      1.6E+0014   0.000   5200.0   ! MZ 640
      DUPLICATE
C9H18Z+B1O=>R2OH+C4H6Z2+R38C5H11      8.8E+0010   0.700   3250.0   ! MZ 641
      DUPLICATE
C9H18Z+B1O=>R2OH+C4H6Z2+R38C5H11      5.1E+0013   0.000   7850.0   ! MZ 642
```

```
      DUPLICATE
C9H18Z+B1O=>R2OH+C4H6Z2+R38C5H11      1.3E+0014   0.000   5200.0   ! MZ 643
      DUPLICATE

! Metathesis with YH
C4H8Y+R1H=>RC4H7Y+H2      5.4E+0004   2.500   -1900.0   ! MES 644
      DUPLICATE
C4H8Y+R1H=>RC4H7Y+H2      2.9E+0007   2.000   7700.0   ! MES 645
      DUPLICATE
C4H8Y+R2OH=>RC4H7Y+H2O      3.0E+0006   2.000   -1520.0   ! MES 646
      DUPLICATE
C4H8Y+R2OH=>RC4H7Y+H2O      2.7E+0006   2.000   450.0   ! MES 647
      DUPLICATE
C4H8Y+R3OOH=>RC4H7Y+H2O2      6.4E+0003   2.600   12400.0   ! MES 648
      DUPLICATE
C4H8Y+R3OOH=>RC4H7Y+H2O2      6.0E+0011   0.000   17000.0   ! MES 649
      DUPLICATE
C4H8Y+R4CH3=>RC4H7Y+CH4      1.0E+0011   0.000   7300.0   ! MES 650
      DUPLICATE
C4H8Y+R4CH3=>RC4H7Y+CH4      3.0E-0001   4.000   8200.0   ! MES 651
      DUPLICATE
C4H8Y+R8CH3OO=>RC4H7Y+CH3OOH      1.0E+0012   0.000   14550.0   ! MES 652
      DUPLICATE
C4H8Y+R8CH3OO=>RC4H7Y+CH3OOH      6.0E+0012   0.000   20000.0   ! MES 653
      DUPLICATE
C4H8Y+R11C2H5=>RC4H7Y+C2H6      1.5E+0000   3.500   4140.0   ! MES 654
      DUPLICATE
C4H8Y+R11C2H5=>RC4H7Y+C2H6      3.0E+0011   0.000   13500.0   ! MES 655
      DUPLICATE
C5H10Y+R1H=>RC5H9Y+H2      5.4E+0004   2.500   -1900.0   ! MES 656
      DUPLICATE
C5H10Y+R1H=>RC5H9Y+H2      2.9E+0007   2.000   7700.0   ! MES 657
      DUPLICATE
C5H10Y+R1H=>RC5H9Y+H2      9.0E+0006   2.000   5000.0   ! MES 658
      DUPLICATE
C5H10Y+R2OH=>RC5H9Y+H2O      3.0E+0006   2.000   -1520.0   ! MES 659
      DUPLICATE
C5H10Y+R2OH=>RC5H9Y+H2O      2.7E+0006   2.000   450.0   ! MES 660
      DUPLICATE
C5H10Y+R2OH=>RC5H9Y+H2O      2.6E+0006   2.000   -765.0   ! MES 661
      DUPLICATE
C5H10Y+R3OOH=>RC5H9Y+H2O2      6.4E+0003   2.600   12400.0   ! MES 662
      DUPLICATE
C5H10Y+R3OOH=>RC5H9Y+H2O2      6.0E+0011   0.000   17000.0   ! MES 663
      DUPLICATE
C5H10Y+R3OOH=>RC5H9Y+H2O2      4.0E+0011   0.000   15500.0   ! MES 664
      DUPLICATE
C5H10Y+R4CH3=>RC5H9Y+CH4      1.0E+0011   0.000   7300.0   ! MES 665
      DUPLICATE
C5H10Y+R4CH3=>RC5H9Y+CH4      3.0E-0001   4.000   8200.0   ! MES 666
      DUPLICATE
C5H10Y+R4CH3=>RC5H9Y+CH4      2.0E+0011   0.000   9600.0   ! MES 667
      DUPLICATE
C5H10Y+R8CH3OO=>RC5H9Y+CH3OOH      1.0E+0012   0.000   14550.0   ! MES 668
      DUPLICATE
C5H10Y+R8CH3OO=>RC5H9Y+CH3OOH      6.0E+0012   0.000   20000.0   ! MES 669
      DUPLICATE
C5H10Y+R8CH3OO=>RC5H9Y+CH3OOH      3.0E+0012   0.000   17500.0   ! MES 670
      DUPLICATE
C5H10Y+R11C2H5=>RC5H9Y+C2H6      1.5E+0000   3.500   4140.0   ! MES 671
      DUPLICATE
C5H10Y+R11C2H5=>RC5H9Y+C2H6      3.0E+0011   0.000   13500.0   ! MES 672
      DUPLICATE
C5H10Y+R11C2H5=>RC5H9Y+C2H6      2.0E+0011   0.000   11000.0   ! MES 673
      DUPLICATE
C4H8Y+B1O=>RC4H7Y+R2OH      8.8E+0010   0.700   3250.0   ! MES 674
      DUPLICATE
```

```
C4H8Y+B1O=>RC4H7Y+R2OH      5.1E+0013   0.000   7850.0   ! MES 675
      DUPLICATE
C5H10Y+B1O=>RC5H9Y+R2OH     8.8E+0010   0.700   3250.0   ! MES 676
      DUPLICATE
C5H10Y+B1O=>RC5H9Y+R2OH     5.1E+0013   0.000   7850.0   ! MES 677
      DUPLICATE
C5H10Y+B1O=>RC5H9Y+R2OH     2.6E+0013   0.000   5200.0   ! MES 678
      DUPLICATE

! Addition of .Y on YH
RC4H7Y+C5H10Y=>R10C2H3V+C7H14Z     6.0E+0009   0.000   11400.0   ! ADY 679
RC4H7Y+C4H8Y=>R10C2H3V+C6H12Z      6.0E+0009   0.000   11400.0   ! ADY 680
RC5H9Y+C5H10Y=>R10C2H3V+C8H16Z     6.0E+0009   0.000   11400.0   ! ADY 681
RC5H9Y+C4H8Y=>R10C2H3V+C7H14Z      6.0E+0009   0.000   11400.0   ! ADY 682

! Alkohol reactions

! Aldehydes metathesis
C7H14OA+R1H=>H2+RC7H13O     4.0E+0013   0.000   4200.0   ! ADZ 683
C7H14OA+R2OH=>H2O+RC7H13O      4.2E+0012   0.000   500.0   ! ADZ 684
C7H14OA+R3OOH=>H2O2+RC7H13O     1.0E+0012   0.000   10000.0   ! ADZ 685
C7H14OA+R4CH3=>CH4+RC7H13O     2.0E-0006   5.600   2500.0   ! ADZ 686
C7H14OA+R11C2H5=>C2H6+RC7H13O     1.3E+0012   0.000   8500.0   ! ADZ 687
C6H12OA+R1H=>H2+RC6H11O     4.0E+0013   0.000   4200.0   ! ADZ 688
C6H12OA+R2OH=>H2O+RC6H11O      4.2E+0012   0.000   500.0   ! ADZ 689
C6H12OA+R3OOH=>H2O2+RC6H11O     1.0E+0012   0.000   10000.0   ! ADZ 690
C6H12OA+R4CH3=>CH4+RC6H11O     2.0E-0006   5.600   2500.0   ! ADZ 691
C6H12OA+R11C2H5=>C2H6+RC6H11O     1.3E+0012   0.000   8500.0   ! ADZ 692
C4H8OA+R1H=>H2+RC4H7O      4.0E+0013   0.000   4200.0   ! ADZ 693
C4H8OA+R2OH=>H2O+RC4H7O     4.2E+0012   0.000   500.0   ! ADZ 694
C4H8OA+R3OOH=>H2O2+RC4H7O      1.0E+0012   0.000   10000.0   ! ADZ 695
C4H8OA+R4CH3=>CH4+RC4H7O     2.0E-0006   5.600   2500.0   ! ADZ 696
C4H8OA+R11C2H5=>C2H6+RC4H7O     1.3E+0012   0.000   8500.0   ! ADZ 697
C5H10OA+R1H=>H2+RC5H9O      4.0E+0013   0.000   4200.0   ! ADZ 698
C5H10OA+R2OH=>H2O+RC5H9O     4.2E+0012   0.000   500.0   ! ADZ 699
C5H10OA+R3OOH=>H2O2+RC5H9O     1.0E+0012   0.000   10000.0   ! ADZ 700
C5H10OA+R4CH3=>CH4+RC5H9O     2.0E-0006   5.600   2500.0   ! ADZ 701
C5H10OA+R11C2H5=>C2H6+RC5H9O     1.3E+0012   0.000   8500.0   ! ADZ 702
C11H22OA+R1H=>H2+RC11H21O     4.0E+0013   0.000   4200.0   ! ADZ 703
C11H22OA+R2OH=>H2O+RC11H21O     4.2E+0012   0.000   500.0   ! ADZ 704
C11H22OA+R3OOH=>H2O2+RC11H21O     1.0E+0012   0.000   10000.0   ! ADZ 705
C11H22OA+R4CH3=>CH4+RC11H21O     2.0E-0006   5.600   2500.0   ! ADZ 706
C11H22OA+R11C2H5=>C2H6+RC11H21O     1.3E+0012   0.000   8500.0   ! ADZ 707
C10H20OA+R1H=>H2+RC10H19O     4.0E+0013   0.000   4200.0   ! ADZ 708
C10H20OA+R2OH=>H2O+RC10H19O     4.2E+0012   0.000   500.0   ! ADZ 709
C10H20OA+R3OOH=>H2O2+RC10H19O     1.0E+0012   0.000   10000.0   ! ADZ 710
C10H20OA+R4CH3=>CH4+RC10H19O     2.0E-0006   5.600   2500.0   ! ADZ 711
C10H20OA+R11C2H5=>C2H6+RC10H19O     1.3E+0012   0.000   8500.0   ! ADZ 712
C9H18OA+R1H=>H2+RC9H17O     4.0E+0013   0.000   4200.0   ! ADZ 713
C9H18OA+R2OH=>H2O+RC9H17O     4.2E+0012   0.000   500.0   ! ADZ 714
C9H18OA+R3OOH=>H2O2+RC9H17O     1.0E+0012   0.000   10000.0   ! ADZ 715
C9H18OA+R4CH3=>CH4+RC9H17O     2.0E-0006   5.600   2500.0   ! ADZ 716
C9H18OA+R11C2H5=>C2H6+RC9H17O     1.3E+0012   0.000   8500.0   ! ADZ 717
C8H16OA+R1H=>H2+RC8H15O     4.0E+0013   0.000   4200.0   ! ADZ 718
C8H16OA+R2OH=>H2O+RC8H15O     4.2E+0012   0.000   500.0   ! ADZ 719
C8H16OA+R3OOH=>H2O2+RC8H15O     1.0E+0012   0.000   10000.0   ! ADZ 720
C8H16OA+R4CH3=>CH4+RC8H15O     2.0E-0006   5.600   2500.0   ! ADZ 721
C8H16OA+R11C2H5=>C2H6+RC8H15O     1.3E+0012   0.000   8500.0   ! ADZ 722

C5H8OAY+R1H=>H2+RC3H5Y+CH2COZ     4.0E+0013   0.000   4200.0   ! ADZ 723
C5H8OAY+R2OH=>H2O+RC3H5Y+CH2COZ     4.0E+0012   0.000   500.0   ! ADZ 724
C5H8OAY+R3OOH=>H2O2+RC3H5Y+CH2COZ     1.0E+0012   0.000   10000.0   ! ADZ 725
C5H8OAY+R4CH3=>CH4+RC3H5Y+CH2COZ     2.0E-0006   0.000   2500.0   ! ADZ 726
C5H8OAY+R11C2H5=>C2H6+RC3H5Y+CH2COZ     1.3E+0012   0.000   8500.0   ! ADZ 727
C6H10OAY+R1H=>H2+R10C2H3V+CH2COZ+C2H4Z     4.0E+0013   0.000   4200.0   ! ADZ 728
C6H10OAY+R2OH=>H2O+R10C2H3V+CH2COZ+C2H4Z     4.0E+0012   0.000   500.0   ! ADZ 729
C6H10OAY+R3OOH=>H2O2+R10C2H3V+CH2COZ+C2H4Z     1.0E+0012   0.000   10000.0   ! ADZ 730
```

```
C6H10OAY+R4CH3=>CH4+R10C2H3V+CH2COZ+C2H4Z      2.0E-0006  0.000   2500.0   ! ADZ 731
C6H10OAY+R11C2H5=>C2H6+R10C2H3V+CH2COZ+C2H4Z     1.3E+0012  0.000   8500.0   ! ADZ 732

! Keto radicals decomposition
RC7H13O=>B2CO+R37C6H13      1.8E+0014  0.000   15600.0   ! COR 733
RC6H11O=>B2CO+R38C5H11      1.8E+0014  0.000   15600.0   ! COR 734
RC4H7O=>B2CO+R19C3H7      1.8E+0014  0.000   15600.0   ! COR 735
RC5H9O=>B2CO+R20C4H9      1.8E+0014  0.000   15600.0   ! COR 736
RC11H21O=>B2CO+R39C10H21      1.8E+0014  0.000   15600.0   ! COR 737
RC10H19O=>B2CO+R40C9H19      1.8E+0014  0.000   15600.0   ! COR 738
RC9H17O=>B2CO+R26C8H17      1.8E+0014  0.000   15600.0   ! COR 739
RC8H15O=>B2CO+R41C7H15      1.8E+0014  0.000   15600.0   ! COR 740


! keto radicals addition to O2
RC7H13O+O2=>RC7H13O3      3.0E+0019  -2.500   0.0   ! COR 741
RC6H11O+O2=>RC6H11O3      3.0E+0019  -2.500   0.0   ! COR 742
RC4H7O+O2=>RC4H7O3      3.0E+0019  -2.500   0.0   ! COR 743
RC5H9O+O2=>RC5H9O3      3.0E+0019  -2.500   0.0   ! COR 744
RC11H21O+O2=>RC11H21O3      3.0E+0019  -2.500   0.0   ! COR 745
RC10H19O+O2=>RC10H19O3      3.0E+0019  -2.500   0.0   ! COR 746
RC9H17O+O2=>RC9H17O3      3.0E+0019  -2.500   0.0   ! COR 747
RC8H15O+O2=>RC8H15O3      3.0E+0019  -2.500   0.0   ! COR 748

! Peracide radical decomposition
RC7H13O3=>C6H12Z+R2OH+CO2      4.5E+0011  0.000   25000.0   ! PER 749
RC6H11O3=>C5H10Y+R2OH+CO2      4.5E+0011  0.000   25000.0   ! PER 750
RC4H7O3=>C3H6Y+R2OH+CO2      4.5E+0011  0.000   25000.0   ! PER 751
RC5H9O3=>C4H8Y+R2OH+CO2      4.5E+0011  0.000   25000.0   ! PER 752
RC11H21O3=>C10H20Z+R2OH+CO2      4.5E+0011  0.000   25000.0   ! PER 753
RC10H19O3=>C9H18Z+R2OH+CO2      4.5E+0011  0.000   25000.0   ! PER 754
RC9H17O3=>C8H16Z+R2OH+CO2      4.5E+0011  0.000   25000.0   ! PER 755
RC8H15O3=>C7H14Z+R2OH+CO2      4.5E+0011  0.000   25000.0   ! PER 756

! Ketones reactions



! Unsaturated ester reactions
! Esters metatesis

! Ester with aldehyde function metathesis

! Ester with ceton function metathesis
! Addition on unsaturated esters

! Carboxylic acid reactions
! Carboxylic acid metathesis

! Carboxylic acid decomposition

! Alkohol ene to dienes
C4H8OLY+R1H=>H2+HCHO+RC3H5Y      5.4E+0004  2.500   -1900.0   ! ROH 757
C4H8OLY+R2OH=>H2O+HCHO+RC3H5Y      3.0E+0006  2.000   -1520.0   ! ROH 758
C4H8OLY+R3OOH=>H2O2+HCHO+RC3H5Y      6.4E+0003  2.600   12400.0   ! ROH 759
C4H8OLY+R4CH3=>CH4+HCHO+RC3H5Y      1.0E+0011  0.000   7300.0   ! ROH 760
C4H8OLY+R8CH3OO=>CH3OOH+HCHO+RC3H5Y      1.0E+0012  0.000   14550.0   ! ROH 761
C4H8OLY+R11C2H5=>C2H6+HCHO+RC3H5Y      1.5E+0000  3.500   4140.0   ! ROH 762
C5H10OLY+R1H=>H2+HCHO+RC4H7Y      5.4E+0004  2.500   -1900.0   ! ROH 763
C5H10OLY+R2OH=>H2O+HCHO+RC4H7Y      3.0E+0006  2.000   -1520.0   ! ROH 764
C5H10OLY+R3OOH=>H2O2+HCHO+RC4H7Y      6.4E+0003  2.600   12400.0   ! ROH 765
C5H10OLY+R4CH3=>CH4+HCHO+RC4H7Y      1.0E+0011  0.000   7300.0   ! ROH 766
C5H10OLY+R8CH3OO=>CH3OOH+HCHO+RC4H7Y      1.0E+0012  0.000   14550.0   ! ROH 767
C5H10OLY+R11C2H5=>C2H6+HCHO+RC4H7Y      1.5E+0000  3.500   4140.0   ! ROH 768
C6H12OLY+R1H=>H2+HCHO+RC5H9Y      5.4E+0004  2.500   -1900.0   ! ROH 769
C6H12OLY+R2OH=>H2O+HCHO+RC5H9Y      3.0E+0006  2.000   -1520.0   ! ROH 770
C6H12OLY+R3OOH=>H2O2+HCHO+RC5H9Y      6.4E+0003  2.600   12400.0   ! ROH 771
```

```
C6H12OLY+R4CH3=>CH4+HCHO+RC5H9Y      1.0E+0011   0.000   7300.0   ! ROH 772
C6H12OLY+R8CH3OO=>CH3OOH+HCHO+RC5H9Y      1.0E+0012   0.000   14550.0   ! ROH 773
C6H12OLY+R11C2H5=>C2H6+HCHO+RC5H9Y      1.5E+0000   3.500   4140.0   ! ROH 774

! Additions on dienes
C8H14Y2+R1H=>H2+C4H6Z2+R10C2H3V+C2H4Z      1.0E+0005   2.500   -1900.0   ! AD 775
C8H14Y2+R2OH=>H2O+C4H6Z2+R10C2H3V+C2H4Z      6.0E+0006   2.000   -1520.0   ! AD 776
C8H14Y2+R3OOH=>H2O2+C4H6Z2+R10C2H3V+C2H4Z      1.2E+0004   2.600   12400.0   ! AD 777
C8H14Y2+R4CH3=>CH4+C4H6Z2+R10C2H3V+C2H4Z      2.0E+0011   0.000   7300.0   ! AD 778
C8H14Y2+R8CH3OO=>CH3OOH+C4H6Z2+R10C2H3V+C2H4Z      2.0E+0011   0.000   7300.0   ! AD 779
C8H14Y2+R11C2H5=>C2H6+C4H6Z2+R10C2H3V+C2H4Z      3.0E+0000   3.500   4140.0   ! AD 780
C9H16Y2+R1H=>H2+C4H6Z2+RC3H5Y+C2H4Z      1.0E+0005   2.500   -1900.0   ! AD 781
C9H16Y2+R2OH=>H2O+C4H6Z2+RC3H5Y+C2H4Z      6.0E+0006   2.000   -1520.0   ! AD 782
C9H16Y2+R3OOH=>H2O2+C4H6Z2+RC3H5Y+C2H4Z      1.2E+0004   2.600   12400.0   ! AD 783
C9H16Y2+R4CH3=>CH4+C4H6Z2+RC3H5Y+C2H4Z      2.0E+0011   0.000   7300.0   ! AD 784
C9H16Y2+R8CH3OO=>CH3OOH+C4H6Z2+RC3H5Y+C2H4Z      2.0E+0011   0.000   7300.0   ! AD 785
C9H16Y2+R11C2H5=>C2H6+C4H6Z2+RC3H5Y+C2H4Z      3.0E+0000   3.500   4140.0   ! AD 786
C10H18Y2+R1H=>H2+C4H6Z2+R10C2H3V+2C2H4Z      1.0E+0005   2.500   -1900.0   ! AD 787
C10H18Y2+R2OH=>H2O+C4H6Z2+R10C2H3V+2C2H4Z      6.0E+0006   2.000   -1520.0   ! AD 788
C10H18Y2+R3OOH=>H2O2+C4H6Z2+R10C2H3V+2C2H4Z      1.2E+0004   2.600   12400.0   ! AD 789
C10H18Y2+R4CH3=>CH4+C4H6Z2+R10C2H3V+2C2H4Z      2.0E+0011   0.000   7300.0   ! AD 790
C10H18Y2+R8CH3OO=>CH3OOH+C4H6Z2+R10C2H3V+2C2H4Z      2.0E+0011   0.000   7300.0   ! AD 791
C10H18Y2+R11C2H5=>C2H6+C4H6Z2+R10C2H3V+2C2H4Z      3.0E+0000   3.500   4140.0   ! AD 792

! Diels Alder

! .Y termination
RC4H7Y+R1H=>C4H8Y      1.0E+0013   0.000   0.0   ! TER 793
RC4H7Y+R2OH=>C4H8OLY      1.0E+0013   0.000   0.0   ! TER 794
RC4H7Y+R3OOH=>C4H8O2PY      5.0E+0012   0.000   0.0   ! TER 795
RC4H7Y+R4CH3=>C5H10Y      1.0E+0013   0.000   0.0   ! TER 796
RC4H7Y+R5CHO=>C5H8OAY      1.0E+0013   0.000   0.0   ! TER 797
RC4H7Y+R6CH2OH=>C5H10OLY      1.0E+0013   0.000   0.0   ! TER 798
RC4H7Y+R8CH3OO=>HCHO+R7CH3O+RC3H5Y      1.0E+0013   0.000   0.0   ! TER 799
RC4H7Y+R11C2H5=>C6H12Z      1.0E+0013   0.000   0.0   ! TER 800
RC5H9Y+R1H=>C5H10Y      1.0E+0013   0.000   0.0   ! TER 801
RC5H9Y+R2OH=>C5H10OLY      1.0E+0013   0.000   0.0   ! TER 802
RC5H9Y+R3OOH=>C5H10O2PY      5.0E+0012   0.000   0.0   ! TER 803
RC5H9Y+R4CH3=>C6H12Z      1.0E+0013   0.000   0.0   ! TER 804
RC5H9Y+R5CHO=>C6H10OAY      1.0E+0013   0.000   0.0   ! TER 805
RC5H9Y+R6CH2OH=>C6H12OLY      1.0E+0013   0.000   0.0   ! TER 806
RC5H9Y+R8CH3OO=>HCHO+R7CH3O+RC4H7Y      1.0E+0013   0.000   0.0   ! TER 807
RC5H9Y+R11C2H5=>C7H14Z      1.0E+0013   0.000   0.0   ! TER 808
RC4H7Y+RC4H7Y=>C8H14Y2      1.0E+0013   0.000   0.0   ! TER 809
RC4H7Y+RC5H9Y=>C9H16Y2      1.0E+0013   0.000   0.0   ! TER 810
RC5H9Y+RC5H9Y=>C10H18Y2      1.0E+0013   0.000   0.0   ! TER 811
RC5H9Y+RC3H5Y=>C8H14Y2      1.0E+0013   0.000   0.0   ! TER 812


! Pascal C0 C2 lumped data base ********************************************
! VERSION X.X 01/2002       ************************************************

!REACTIONS DE LA MATRICE O(0)C(y)H(z)!

!REACTIONS DE H2!
R1H+R1H+M=H2+M                  1.87E18          -1.00      0.0    !(1,-1)<BAULCH94>!
       O2/0.4/ B2CO/0.75/ CO2/1.5/ H2O/6.5/ CH4/3.0/ H2/0.0/
       C2H6/3.0/ AR/0.35/ N2/0.4/ HE/0.35/

!REACTIONS DE B4CH!
B4CH+R1H=B3C+H2                 7.8E13           0.         0.      !(2,-2)<PEETERS97>!

!REACTIONS DE B6CH2!
B6CH2+M=B5CH2+M                 1.51E13          0.0        0.0     !(3,-3)<BAULCH94>!
       N2/.4/ O2/.4/ B2CO/.75/ CO2/1.5/ H2O/6.5/ CH4/.48/
       HE/0.35/ C2H4Z/1.6/ AR/.24/
B6CH2+R1H=B4CH+H2               3.0E13           0.         0.      !(4,-4)<TSANG86>!
```

```
!REACTIONS DE B5CH2!
B5CH2+R1H=B4CH+H2                 6.0E12        0.        -1.8E3 !(5,-5)<BAULCH94>!
B5CH2+B3C=R9C2HT+R1H              5.0E13        0.         0.    !(6,-6)<RANZI94>!
B5CH2+B5CH2=>C2H2T+R1H+R1H        1.2E14        0.         0.8E3 !(7)<BAULCH94>!

!REACTIONS DE R4CH3!
R4CH3+M=B5CH2+R1H+M               2.91E16      0.0       90.7E3 !(8,-8)<BAULCH94>!
       O2/0.4/ B2CO/0.75/ CO2/1.5/ H2O/6.5/ CH4/3.0/ C2H6/3.0/ AR/0.35/
       N2/0.4/ HE/0.35/
R4CH3+R1H=B6CH2+H2                6.0E13        0.        15.0E3 !(9,-9)<BAULCH94>!
R4CH3+B4CH=R10C2H3V+R1H           3.0E13        0.         0.    !(10,-10)<DAGAUT91>
R4CH3+B6CH2=C2H4Z+R1H             1.8E13        0.         0.    !(11,-11)<TSANG86>!
R4CH3+B5CH2=C2H4Z+R1H             4.2E13        0.         0.    !(12,-12)<BAULCH94>!
R4CH3+B3C=C2H2T+R1H               5.0E13        0.         0.    !(13,-13)<RANZI94>!
R4CH3+R4CH3(+M)=>C2H6(+M)         3.61E13       0.         0.    !(14)<BAULCH94>!
       O2/0.4/ B2CO/0.75/ CO2/1.5/ H2O/6.5/ CH4/3.0/ C2H6/3.0/ AR/0.35/
       N2/0.4/ HE/0.35/
       LOW / 3.63E41   -7.0    2.76E3 /
       TROE /  0.62   73   1180 /
C2H6(+M)=>R4CH3+R4CH3(+M)         1.8E21       -1.24      90.9E3 !(-14)<BAULCH94>!
       O2/0.4/ B2CO/0.75/ CO2/1.5/ H2O/6.5/ CH4/3.0/ C2H6/3.0/ AR/0.35/
       N2/0.4/ HE/0.35/
       LOW / 1.89E49    -8.24    93.7E3/
       TROE /  0.62   73   1180 /
R4CH3+R4CH3=R11C2H5+R1H           3.0E13        0.        13.5E3 !(15,-15)<BAULCH94>!
R4CH3+R4CH3=C2H4Z+H2              2.1E14        0.        19.3E3 !(16,-16)<FRANK86NIST>!

!REACTIONS DE CH4!
R1H+R4CH3(+M)=>CH4(+M)            1.67E14       0.         0.    !(17)<BAULCH94>!
       O2/0.4/ B2CO/0.75/ CO2/1.5/ H2O/6.5/ CH4/3.0/ C2H6/3.0/ AR/0.35/
       N2/0.4/ HE/0.35/
       LOW /  1.408E24   -1.8    0.0 /
       TROE / 0.37  3315  61 /
CH4(+M)=>R4CH3+R1H(+M)            2.4E16        0.       105.0E3 !(-17)<BAULCH94>!
       O2/0.4/ B2CO/0.75/ CO2/1.5/ H2O/6.5/ CH4/0.0/ C2H6/3.0/ AR/0.35/
       N2/0.4/ HE/0.35/
       LOW / 1.29E18     0.00   90.9E3 /
       TROE / 0   1350   1   7830 /
CH4(+CH4)=>R4CH3+R1H(+CH4)        2.4E16        0.       105.0E3 !(-17')<BAULCH94>!
       LOW / 8.43E17     0.00   90.9E3 /
       TROE / 0.69   90   2210 /
CH4+R1H=R4CH3+H2                  1.3E04        3.         8.0E3 !(18,-18)<BAULCH94>!
CH4+B4CH=C2H4Z+R1H                3.0E13        0.        -0.4E3 !(19,-19)<DAGAUT91BAULCH94>!
CH4+B6CH2=R4CH3+R4CH3             4.2E13        0.         0.    !(20,-20)<TSANG86>!

!REACTIONS DE R9C2HT!
R9C2HT+B6CH2=C2H2T+B4CH           1.8E13        0.         0.    !(21,-21)<TSANG86>!
R9C2HT+B5CH2=C2H2T+B4CH           1.8E13        0.         0.    !(22,-22)<TSANG86>!
R9C2HT+CH4=C2H2T+R4CH3            1.2E12        0.         0.    !(23,-23)<BAULCH94>!

!REACTIONS DE C2H2T!
C2H2T+M=R9C2HT+R1H+M              1.14E17       0.       107.0E3 !(24,-24)<BAULCH94>!
       O2/0.4/ B2CO/0.75/ CO2/1.5/ H2O/6.5/ CH4/3.0/ C2H6/3.0/ AR/0.35/
       N2/0.4/ HE/0.35/
C2H2T+R1H=R9C2HT+H2               6.6E13        0.        27.7E3 !(25,-25)<BAULCH94>!

!REACTIONS DE R10C2H3V!
R10C2H3V(+M)=C2H2T+R1H(+M)        2.0E14        0.        39.8E3 !(26,-26)<BAULCH94>!
       O2/0.4/ B2CO/0.75/ CO2/1.5/ H2O/6.5/ CH4/3.0/ AR/0.35/
       N2/0.4/ HE/0.35/
       LOW / 1.19E42   -7.50   45.55E3 /
       TROE     /0.35    1.0        1.E8/
R10C2H3V+R1H=C2H2T+H2             1.2E13        0.         0.    !(27,-27)<BAULCH94>!
R10C2H3V+B6CH2=C2H2T+R4CH3        1.8E13        0.         0.    !(28,-28)<TSANG86>!
R10C2H3V+B5CH2=C2H2T+R4CH3        1.8E13        0.         0.    !(29,-29)<TSANG86>!
R10C2H3V+R4CH3=CH4+C2H2T          3.9E11        0.         0.    !(30,-30)<TSANG86>!
```

```
R10C2H3V+R9C2HT=2C2H2T              9.6E11      0.          0. !(31,-31)<TSANG86>!
R10C2H3V+R10C2H3V=C2H4Z+C2H2T   9.6E11      0.          0. !(32,-32)<TSANG86>!

!REACTIONS DE C2H4Z!
C2H4Z+M=C2H2T+H2+M                  9.97E16     0.      71.6E3 !(33,-33)<BAULCH94>!
      O2/0.4/ B2CO/0.75/ CO2/1.5/ H2O/6.5/ CH4/3.0/ C2H6/3.0/ AR/0.35/
      N2/0.4/ HE/0.35/
C2H4Z+M=R10C2H3V+R1H+M          7.40E17     0.      96.7E3 !(34,-34)<BAULCH94>!
      O2/0.4/ B2CO/0.75/ CO2/1.5/ H2O/6.5/ CH4/3.0/ C2H6/3.0/ AR/0.35/
      N2/0.4/ HE/0.35/
C2H4Z+R1H=R10C2H3V+H2           5.0E7     1.93      13.0E3 !(35,-35)SLAGLE96!
C2H4Z+R4CH3=CH4+R10C2H3V        6.3E11      0.      16.0E3 !(36,-36)BACK89!

!REACTIONS DE R11C2H5!
R11C2H5(+M)=C2H4Z+R1H(+M)       8.2E13      0.      40.0E3  !(37,-37) BAULCH94!
      O2/0.4/ B2CO/0.75/ CO2/1.5/ H2O/6.5/ CH4/3.0/ C2H6/3.0/ AR/0.35/
      N2/0.4/ HE/0.35/
      LOW / 3.40E17    0.00    33.4E3 /
      TROE / 0.75   97   1379/
R11C2H5+R1H=C2H4Z+H2            1.8E12      0.          0. !(38,-38)<TSANG86>!
R11C2H5+R1H=C2H6                3.6E13      0.          0. !(39,-39><TSANG86>!
R11C2H5+B6CH2=C2H4Z+R4CH3       9.0E12      0.          0. !(40,-40)<TSANG86>!
R11C2H5+B5CH2=C2H4Z+R4CH3       1.8E13      0.          0. !(41,-41)<TSANG86>!
R11C2H5+R4CH3=C2H4Z+CH4         1.1E12      0.          0. !(42,-42)<BAULCH94>!
R11C2H5+R9C2HT=C2H2T+C2H4Z      1.8E12      0           0. !(43,-43)<TSANG86>!
R11C2H5+R10C2H3V=2C2H4Z         4.8E11      0.          0. !(44,-44)<TSANG86>!
R11C2H5+R10C2H3V=C2H2T+C2H6     4.8E11      0.          0. !(45,-45)<TSANG86>!
R11C2H5+R11C2H5=C2H4Z+C2H6      1.4E12      0.          0. !(46,-46)<BAULCH94>!

!REACTIONS DE C2H6!
C2H6+M=C2H4Z+H2+M               2.3E17      0.      67.4E3 !(47,-47)<SCHULTZ85NIST>!
C2H6+R1H=R11C2H5+H2             1.4E9       1.5      7.4E3 !(48,-48)<BAULCH94>!
C2H6+B6CH2=R4CH3+R11C2H5        1.1E14      0.          0. !(49,-49)<TSANG86>!
C2H6+R4CH3=R11C2H5+CH4          1.5E-7      6.0      5.8E3 !(50,-50)<BAULCH94>!
C2H6+R9C2HT=C2H2T+R11C2H5       3.6E12      0.          0. !(51,-51)<TSANG86>!
C2H6+R10C2H3V=R11C2H5+C2H4Z     6.0E2       3.3     10.5E3 !(52,-52)<TSANG86>!


!************************************************************************!

!************************************************************************!


!REACTIONS DE LA MATRICE O(x)C(y)H(z)  x>0 !


!REACTIONS DE B1O!
B1O+H2=R2OH+R1H                 5.1E4       2.67     6.2E3 !(53,-53)<BAULCH94>!
B1O+B4CH=B2CO+R1H               3.9E13      0.          0. !(54,-54)<BAULCH94>!
B1O+B4CH=B3C+R2OH               1.5E13      0.       4.7E3  !(55,-55)<MUR86NIS>!
B1O+B6CH2=>B2CO+2R1H            1.5E13      0.          0. !(56)       <TSANG86>!
B1O+B6CH2=B2CO+H2               1.5E13      0.          0. !(57,-57) <TSANG86>!
B1O+B5CH2=>B2CO+2R1H            7.2E13      0.          0. !(58)     <BAULCH94>!
B1O+B5CH2=B2CO+H2               4.8E13      0.          0. !(59,-59)<BAULCH94>!
B1O+R4CH3=HCHO+R1H              8.4E13      0.          0. !(60,-60)<BAULCH94>!
B1O+R4CH3=R7CH3O                8.0E15     -2.12     0.6E3 !(61,-61)<DEAN87NIS>!
B1O+CH4=R4CH3+R2OH              7.2E8       1.56     8.4E3 !(62,-62)<BAULCH94>!
B1O+R9C2HT=B4CH+B2CO            1.0E13      0.          0. !(63,-63)<DAGAUT91>!
B1O+C2H2T=B5CH2+B2CO            2.17E06     2.1      1.6E3 !(64,-64)<BAULCH LEEDS>!
B1O+C2H2T=R12CHCOV+R1H          5.06E06     2.1      1.6E3 !(65,-65)<BAULCH LEEDS>!
B1O+R10C2H3V=R4CH3+B2CO         3.0E13      0.          0. !(66,-66)<DAGAUT91>!
B1O+R10C2H3V=CH2COZ+R1H         9.6E13      0.          0. !(67,-67)<TSANG86>!
B1O+C2H4Z=R4CH3+R5CHO           8.1E6       1.88     0.2E3 !(68,-68)<BAULCH94>!
B1O+C2H4Z=HCHO+B5CH2            4.00E5      1.88     0.2E3 !(69,-69)<BAULCH94>!
B1O+C2H4Z=CH2COZ+H2             6.6E5       1.88     0.2E3 !(70,-70)<BAULCH94>!
B1O+C2H4Z=R13CH2CHO+R1H         4.7E6       1.88     0.2E3 !(71,-71)<BAULCH94>!
B1O+C2H4Z=R2OH+R10C2H3V         1.5E7       1.91     3.7E3 !(72,-72)<MAHMUD87NIST>!
```

```
B1O+R11C2H5=HCHO+R4CH3              1.1E13      0.          0. !(73,-73)<BAULCH94>!
B1O+R11C2H5=CH3CHO+R1H              5.5e13      0.          0. !(74,-74)<BAULCH94>!
B1O+R11C2H5=C2H4Z+R2OH              3.0E13      0.          0. !(75,-75)<DAGAUT91>!
B1O+C2H6=R11C2H5+R2OH               1.0E9       1.5      5.8E3 !(76,-76)<BAULCH94>!

!REACTIONS DE R2OH!
R1H+B1O+M=R2OH+M                    1.18E19     -1.0       0.0  !(77,-77)<BAULCH94>!
        O2/0.4/ B2CO/0.75/ CO2/1.5/ H2O/6.5/ CH4/3.0/ C2H6/3.0/ AR/0.35/
        N2/0.4/ HE/0.35/
R1H+R2OH+M=H2O+M                     5.53E+22    -2.0       0.0  !(78,-78)<BAULCH94>!
        O2/0.4/ B2CO/0.75/ CO2/1.5/ H2O/2.55/ CH4/3.0/ C2H6/3.0/ AR/0.15/
        N2/0.4/ HE/0.35/
R2OH+H2=R1H+H2O                     1.0E8       1.6      3.3E3 !(79,-79)<BAULCH94>!
R2OH+B3C=B2CO+R1H                   5.0E13      0.          0. !(80,-80)<RANZI94>!
R2OH+B4CH=R5CHO+R1H                 3.0E13      0.          0. !(81,-81)<DAGAUT91>!
R2OH+B6CH2=HCHO+R1H                 3.0E13      0.          0. !(82,-82)<TSANG86>!
R2OH+B5CH2=HCHO+R1H                 1.8E13      0.          0. !(83,-83)<TSANG86>!
R2OH+R4CH3=B6CH2+H2O                7.2E13      0.       2.7E3 !(84,-84)<BAULCH94>!
R2OH+R4CH3(+M)=CH3OH(+M)            6.0E13      0.          0. !(85,-85)<BAULCH94>!
        LOW       /1.4E44      -8.2          0./
        TROE      /0.82        200.       1438./
R2OH+R4CH3=HCHO+H2                  3.2E12      -0.53    10.8E3 !(86,-86)<DAGAUT91>!
R2OH+R4CH3=R7CH3O+R1H               5.7E12      -0.23    13.9E3 !(87,-87)<DAGAUT91>!
R2OH+CH4=R4CH3+H2O                  1.6E7        1.83     2.7E3 !(88,-88)<BAULCH94>!
R2OH+R9C2HT=C2H2T+B1O               1.8E13      0.          0. !(89,-89)<TSANG86>!
R2OH+R9C2HT=B5CH2+B2CO              1.8E13      0.          0. !(90,-90)<TSANG86>!
R2OH+R9C2HT=R12CHCOV+R1H            2.0E13      0.          0. !(91,-91)<DAGAUT91>!
R2OH+C2H2T=R9C2HT+H2O               1.4E4       2.68     12.0E3 !(92,-92)<TSANG86>!
R2OH+C2H2T=CH2COZ+R1H               2.2E-4      4.5      -1.0E3 !(93,-93)<DAGAUT91>!
R2OH+C2H2T=R4CH3+B2CO               4.8E-4      4.       -2.0E3 !(94,-94)<DAGAUT91>!
R2OH+R10C2H3V=C2H2T+H2O             3.0E13      0.          0. !(95,-95)<TSANG86>!
R2OH+R10C2H3V=CH3CHO                3.0E13      0.          0. !(96,-96)<TSANG86>!
R2OH+C2H4Z=R10C2H3V+H2O             2.0E13      0.       5.9E3 !(97,-97)<BAULCH94>!
R2OH+C2H4Z=R4CH3+HCHO               2.0E12      0.       0.9E3 !(98,-98)<GLARBORG86>!
R2OH+R11C2H5=C2H4Z+H2O              2.4E13      0.          0. !(99,-99)<TSANG86>!
R2OH+R11C2H5=>R4CH3+R1H+HCHO        2.4E13      0.          0. !(100)    <TSANG86>!
R2OH+C2H6=R11C2H5+H2O               7.2E6       2.       0.9E3 !(101,-101)<BAULCH94>!
R2OH+R2OH=H2O+B1O                   1.5E9       1.14     0.1E3 !(102,-102)<BAULCH94>!

!REACTIONS DE H2O!
H2O+B4CH=R6CH2OH                    5.7E12      0.       -0.8E3 !(103,-103)<BAULCH94>!
H2O+B6CH2=CH3OH                     1.8E13      0.          0. !(104,-104)<TSANG86>!

!REACTIONS DE B2CO!
B2CO+R4CH3(+M)=R14CH3CO(+M)         5.0E11      0.       6.9E3 !(105,-105)<BAULCH94>!
        LOW       /1.1E14      0.        3.8E3/
        TROE      /0.5         1.0       1.0E8/
B2CO+B1O+M=CO2+M                    1.54E15     0.0      3.0E3 !(106,-106)<TSANG86>!
        O2/0.4/ B2CO/0.75/ CO2/1.5/ H2O/6.5/ CH4/3.0/ C2H6/3.0/ AR/0.35/
        N2/0.4/ HE/0.35/
B2CO+R2OH=CO2+R1H                   6.3E6       1.5      -0.5E3 !(107,-107)<BAULCH94>!

!REACTIONS DE R5CHO!
R5CHO+M=R1H+B2CO+M                  1.9E17      -1.      17.0E3 !(108,-108)<WANG97>!
        H2/2.0/ B2CO/1.5/ CO2/2.0/ H2O/6.0/
R5CHO+R1H=H2+B2CO                   9.0E13      0.          0. !(109,-109)<BAULCH94>!
R5CHO+R1H=B1O+B5CH2                 4.0E13      0.     102.5E3 !(110,-110)<TSUBOI81NIST>!
R5CHO+B6CH2=R4CH3+B2CO              1.8E13      0.          0. !(111,-111)<TSANG86>!
R5CHO+B5CH2=R4CH3+B2CO              1.8E13      0.          0. !(112,-112)<TSANG86>!
R5CHO+R4CH3=CH4+B2CO                1.2E14      0.          0. !(113,-113)<TSANG86>!
R5CHO+R4CH3=CH3CHO                  1.8E13      0.          0. !(114,-114)<TSANG86>!
R4CH3+HCHO=R5CHO+CH4                7.7E-8      6.1      1.97E3 !(115,-115)<BAULCH94>!
R5CHO+R9C2HT=C2H2T+B2CO              6.0E13      0.          0. !(116,-116)<TSANG86>!
R5CHO+R10C2H3V=C2H4Z+B2CO           9.0E13      0.          0. !(117,-117)<TSANG86>!
R10C2H3V+HCHO=R5CHO+C2H4Z           5.4E3       2.81     5.9E3 !(118,-118)<TSANG86>!
R5CHO+R11C2H5=C2H6+B2CO             1.2E14      0.          0. !(119,-119)<TSANG86>!
R11C2H5+HCHO=R5CHO+C2H6             5.57E3      2.81     5.86E3 !(120,-120)<TSANG86>!
```

```
R5CHO+B1O=R1H+CO2                3.0E13      0.          0. !(121,-121)<BAULCH94>!
R5CHO+B1O=R2OH+B2CO              3.0E13      0.          0. !(122,-122)<BAULCH94>!
R5CHO+R2OH=H2O+B2CO              1.1E14      0.          0. !(123,-123)<BAULCH94>!
R5CHO+R5CHO=HCHO+B2CO            3.0E13      0.          0. !(124,-124)<BAULCH94>!

!REACTIONS DE HCHO!
HCHO+M=R5CHO+R1H+M               1.40E36    -5.54    96.8E3 !(125,-125)<BAULCH94>!
        O2/0.4/ B2CO/0.75/ CO2/1.5/ H2O/6.5/ CH4/3.0/ C2H6/3.0/ AR/0.35/
        N2/0.4/ HE/0.35/
HCHO+M=H2+B2CO+M                 3.26E36    -5.54    96.8E3 !(126,-126)<BAULCH94>!
        O2/0.4/ B2CO/0.75/ CO2/1.5/ H2O/6.5/ CH4/3.0/ C2H6/3.0/ AR/0.35/
        N2/0.4/ HE/0.35/
HCHO+R1H=R5CHO+H2                1.3E8       1.62     2.1E3 !(127,-127)<BAULCH94>!
HCHO+B4CH=R13CH2CHO              9.6E13      0.      -0.5E3 !(128,-128)<BAULCH94average>!
HCHO+B6CH2=R4CH3+R5CHO           1.2E12      0.          0. !(129,-129)<TSANG86>!
HCHO+B1O=R5CHO+R2OH              4.1E11      0.57     2.7E3 !(130,-130)<BAULCH94>!
HCHO+R2OH=R5CHO+H2O              3.4E9       1.18    -0.4E3 !(131,-131)<BAULCH94>!

!REACTIONS DE R7CH3O!
R7CH3O+M=HCHO+R1H+M              1.55E14     0.00    13.5E3 !(132,-132)<BAULCH94>!
        O2/0.4/ B2CO/0.75/ CO2/1.5/ H2O/6.5/ CH4/3.0/ C2H6/3.0/ AR/0.35/
        N2/0.4/ HE/0.35/
R7CH3O+R1H=HCHO+H2               1.8E13      0.          0. !(133,-133)<BAULCH94>!
R7CH3O+B6CH2=R4CH3+HCHO          1.8E13      0.          0. !(134,-134)<TSANG86>!
R7CH3O+B5CH2=R4CH3+HCHO          1.8E13      0.          0. !(135,-135)<TSANG86>!
R7CH3O+R4CH3=HCHO+CH4            2.4E13      0.          0. !(136,-136)<TSANG86>!
R7CH3O+CH4=R4CH3+CH3OH           1.6E11      0.       8.8E3 !(137,-137)<TSANG86>!
R7CH3O+R9C2HT=HCHO+C2H2T         2.4E13      0.          0. !(138,-138)<TSANG86>!
R7CH3O+R10C2H3V=HCHO+C2H4Z       2.4E13      0.          0. !(139,-139)<TSANG86>!
R7CH3O+C2H4Z=HCHO+R11C2H5        1.2E11      0.       6.7E3 !(140,-140)<TSANG86>!
R7CH3O+R11C2H5=HCHO+C2H6         2.4E13      0.          0. !(141,-141)<TSANG86>!
R7CH3O+C2H6=R11C2H5+CH3OH        2.4E11      0.       7.0E3 !(142,-142)<TSANG86>!
R7CH3O+B1O=HCHO+R2OH             1.8E12      0.          0. !(143,-143)<BAULCH94>!
R7CH3O+R2OH=HCHO+H2O             1.8E13      0.          0. !(144,-144)<TSANG86>!
R7CH3O+B2CO=R4CH3+CO2            1.6E13      0.      11.7E3 !(145,-145)<TSANG86>!
R7CH3O+R5CHO=CH3OH+B2CO          9.1E13      0.          0. !(146,-146)<TSANG86>!
R7CH3O+HCHO=CH3OH+R5CHO          1.0E11      0.       3.0E3 !(147,-147)<TSANG86>!
R7CH3O+R7CH3O=CH3OH+HCHO         6.0E13      0.          0. !(148,-148)<TSANG86>!

!REACTIONS DE R6CH2OH!
R6CH2OH+M=HCHO+R1H+M             1.26E16     0.00    30.0E3 !(149,-149)<BAULCH>!
        O2/0.4/ B2CO/0.75/ CO2/1.5/ H2O/6.5/ CH4/3.0/ C2H6/3.0/ AR/0.35/
        N2/0.4/ HE/0.35/
R6CH2OH+R1H=R4CH3+R2OH           9.6E13      0.          0. !(150,-150)<TSANG87>!
R6CH2OH+R1H=HCHO+H2              6.0E12      0.          0. !(151,-151)<TSANG87>!
R6CH2OH+H2=CH3OH+R1H             6.7E5       2.      13.4E3 !(152,-152)<TSANG87>!
R6CH2OH+B6CH2=CH3CHO+R1H         1.8E13      0.          0. !(153,-153)<TSANG87>!
R6CH2OH+B5CH2=C2H4Z+R2OH         2.4E13      0.          0. !(154,-154)<TSANG87>!
R6CH2OH+B5CH2=R4CH3+HCHO         1.2E12      0.          0. !(155,-155)<TSANG87>!
R6CH2OH+R4CH3=C2H5OH             1.2E13      0.          0. !(156,-156)<TSANG87>!
R6CH2OH+R4CH3=CH4+HCHO           2.4E12      0.          0. !(157,-157)<TSANG87>!
R6CH2OH+CH4=CH3OH+R4CH3          21.7        3.1     16.2E3 !(158,-158)<TSANG87>!
R6CH2OH+R9C2HT=C2H2T+HCHO        4.8E13      0.          0. !(159,-159)<TSANG87>!
!la constante de vitesse du processus 159 est globalisee!
!R6CH2OH+R9C2HT=C3H3+R2OH          1.2E13      0.          0. !(159a,-159a)<TSANG87>!
!R6CH2OH+R9C2HT=C2H2T+HCHO         3.6E13      0.          0. !(159b,-159b)<TSANG87>!
R6CH2OH+C2H2T=R10C2H3V+HCHO      7.2E11      0.       9.0E3 !(160,-160)<TSANG87>!
R6CH2OH+R10C2H3V=C2H4Z+HCHO      4.2E13      0.          0. !(161,-161)<TSANG87>!
!La constante de vitesse  du processus 161 est globalisee!
R6CH2OH+R11C2H5=C2H4Z+CH3OH      2.4E12      0.          0. !(162,-162)<TSANG87>!
R6CH2OH+R11C2H5=C2H6+HCHO        2.4E12      0.          0. !(163,-163)<TSANG87>!
R6CH2OH+C2H6=CH3OH+R11C2H5       199.        3.      14.0E3 !(164,-164)<TSANG87>!
R6CH2OH+B1O=HCHO+R2OH            4.2E13      0.          0. !(165,-165)<TSANG87>!
R6CH2OH+R2OH=H2O+HCHO            2.4E13      0.          0. !(166,-166)<TSANG87>!
R6CH2OH+R5CHO=CH3OH+B2CO         1.2E14      0.          0. !(168,-168)<TSANG87>!
R6CH2OH+R5CHO=HCHO+HCHO          1.8E14      0.          0. !(169,-169)<TSANG87>!
R6CH2OH+HCHO=CH3OH+R5CHO         5.5E3       2.8      5.9E3 !(170,-170)<TSANG87>!
```

```
R6CH2OH+R7CH3O=CH3OH+HCHO        2.4E13      0.          0. !(171,-171)<TSANG87>!
R6CH2OH+R6CH2OH=CH3OH+HCHO       1.4E13      0.          0. !(172,-172)<TSANG87>!
!la constante de vitesse du processus 172 est globalisee!
!R6CH2OH+R6CH2OH=CH3OH+HCHO      4.8E12      0.          0. !(172a,-172a)<TSANG87>!
!R6CH2OH+R6CH2OH=HOCH2CH2OH      9.6E12      0.          0. !(172b,-172b)<TSANG87>!

!REACTIONS DE CH3OH!
CH3OH+R1H=R4CH3+H2O              2.0E14      0.       5.3E3 !(173,-173)<HIDAKA89NIST>!
CH3OH+R1H=R7CH3O+H2              4.2E6       2.1      4.9E3 !(174,-174)<TSANG87>!
CH3OH+B6CH2=R6CH2OH+R4CH3        1.5E12      0.          0. !(175,-175)<TSANG87>!
CH3OH+B5CH2=R4CH3+R6CH2OH        31.9        3.2      7.2E3 !(176,-176)<TSANG87>!
CH3OH+B5CH2=R4CH3+R7CH3O         14.4        3.1      6.9E3 !(177,-177)<TSANG87>!
CH3OH+R9C2HT=C2H2T+R6CH2OH       6.0E12      0.          0. !(178,-178)<TSANG87>!
CH3OH+R9C2HT=C2H2T+R7CH3O        1.2E12      0.          0. !(179,-179)<TSANG87>!
CH3OH+R10C2H3V=C2H4Z+R6CH2OH     31.9        3.2      7.2E3 !(180,-180)<TSANG87>!
CH3OH+R10C2H3V=C2H4Z+R7CH3O      14.4        3.1      6.9E3 !(181,-181)<TSANG87>!
CH3OH+B1O=R6CH2OH+R2OH           3.4E13      0.       5.5E3 !(182,-182)<GROTHEER81NIST>!
CH3OH+B1O=R7CH3O+R2OH            1.0E13      0.       4.7E3 !(183,-183)<WARNATZ84>!
CH3OH+R2OH=R6CH2OH+H2O           3.1E06      2.      -3.4E2 !(184a,-184a)<Atkinson86>85%!
CH3OH+R2OH=R7CH3O+H2O            5.4E05      2.      -3.4E2 !(184b,-184b)<Atkinson86>15%!
CH3OH+R7CH3O=CH3OH+R6CH2OH       3.0E11      0.       4.1E3 !(185,-185)<TSANG87>!

!REACTIONS DE R12CHCOVD!
R12CHCOV+M=B4CH+B2CO+M           6.0E15      0.      58.8E3 !(186,-186)<DAGAUT91>!
R12CHCOV+R1H=B5CH2+B2CO          1.5E14      0.          0. !(187a,-187a)<BAULCH94>!
R12CHCOV+R1H=B6CH2+B2CO          1.3E14      0.          0. !(187b,-187b)<PEETERS97>!
R12CHCOV+B5CH2=R9C2HT+HCHO       1.0E13      0.       2.0E3 !(188,-188)<DAGAUT91>!
R12CHCOV+B5CH2=R10C2H3V+B2CO     3.0E13      0.          0. !(189,-189)<DAGAUT91>!
R12CHCOV+B1O=>B2CO+B2CO+R1H      9.6E13      0.          0. !(190)<BAULCH94>!
R12CHCOV+R2OH=>R5CHO+B2CO+R1H    1.0E13      0.          0. !(191)<DAGAUT91>!


!REACTIONS DE CH2COZD!
CH2COZ+M=B6CH2+B2CO+M            6.57E15     0.0     57.6E3 !(192,-192)<FRANK86NIST>!
        O2/0.4/ B2CO/0.75/ CO2/1.5/ H2O/6.5/ CH4/3.0/ C2H6/3.0/ AR/0.35/
        N2/0.4/ HE/0.35/
CH2COZ+M=R12CHCOV+R1H+M          2.7E17      0.      87.0E3 !(193,-193)<FRANK86NIST>!
        O2/0.4/ B2CO/0.75/ CO2/1.5/ H2O/6.5/ CH4/3.0/ C2H6/3.0/ AR/0.35/
        N2/0.4/ HE/0.35/
CH2COZ+R1H=R4CH3+B2CO            1.8E13      0.       3.4E3 !(194,-194)<BAULCH94>!
CH2COZ+R1H=R12CHCOV+H2           5.0E13      0.       8.0E3 !(195,-195)<DAGAUT91>!
CH2COZ+B5CH2=C2H4Z+B2CO          1.3E14      0.          0. !(196,-196)<CANOSA-MAS84NIST>!
CH2COZ+B1O=B5CH2+CO2             1.8E12      0.       1.3E3 !(197,-197)<DAGAUT91>!
CH2COZ+B1O=R12CHCOV+R2OH         1.0E13      0.       8.0E3 !(198,-198)<DAGAUT91>!
CH2COZ+R2OH=R12CHCOV+H2O         7.5E12      0.       2.0E3 !(199,-199)<DAGAUT91>!
CH2COZ+R2OH=R4CH3+CO2            2.52E12     0.          0. !(200a,-200a)<BAULCH LEEDS>!
CH2COZ+R2OH=R6CH2OH+B2CO         4.68E12     0.          0. !(200b,-200b)<BAULCH LEEDS>!


!REACTIONS DE R14CH3CO!
R14CH3CO+R1H=R4CH3+R5CHO          9.6E13     0.          0. !(201,-201)<TSANG86>!
R14CH3CO+B6CH2=R4CH3+CH2COZ       1.8E13     0.          0. !(202,-202)<TSANG86>!
R14CH3CO+B5CH2=R4CH3+CH2COZ       1.8E13     0.          0. !(203,-203)<TSANG86>!
R14CH3CO+B1O=R4CH3+CO2            9.6E12     0.          0. !(204,-204)<TSANG86>!
R14CH3CO+R2OH=CH2COZ+H2O          1.2E13     0.          0. !(205,-205)<TSANG86>!
R14CH3CO+R2OH=>R4CH3+B2CO+R2OH    3.0E13     0.          0. !(206)<TSANG86>!
R14CH3CO+R5CHO=CH3CHO+B2CO        9.0E12     0.          0. !(207,-207)<TSANG86>!
R14CH3CO+HCHO=CH3CHO+R5CHO        1.8E11     0.       12.9E3!(208,-208)<TSANG86>!
R14CH3CO+R7CH3O=CH3OH+CH2COZ      6.0E12     0.          0. !(209,-209)<TSANG86>!
R14CH3CO+R7CH3O=HCHO+CH3CHO       6.0E12     0.          0. !(210,-210)<TSANG86>!
R14CH3CO+CH3OH=CH3CHO+R6CH2OH     4.85E3     3.       12.3E3!(211,-211)<TSANG87>!
R14CH3CO+R14CH3CO=CH2COZ+CH3CHO   1.2E13     0.          0. !(212,-212)<TSANG86>!

!REACTIONS DE R13CH2CHO!
R13CH2CHO=R14CH3CO                1.0E13     0.       47.0E3!(213,-213)<COLKET75NIST>!
R13CH2CHO=R1H+CH2COZ              1.6E13     0.       35.0E3!(214,-214)<COLKET75NIST>!
```

```
!REACTIONS DE CH3CHO!
CH3CHO+R1H=H2+R14CH3CO                4.0E13    0.      4.2E3 !(215,-215)<WARNATZ84>!
CH3CHO+R4CH3=R14CH3CO+CH4             2.0E-6    5.6     2.5E3 !(216,-216)<BAULCH94>!
CH3CHO+R10C2H3V=C2H4Z+R14CH3CO        8.1E10    0.      3.7E3 !(217,-217)<SCHERZER87>!
CH3CHO+R11C2H5=C2H6+R14CH3CO          1.3E12    0.      8.5E3 !(218,-218)<HOHLEIN70>!
CH3CHO+B1O=R14CH3CO+R2OH              1.4E13    0.      2.3E3 !(219,-219)<CAVANAGH90>!
CH3CHO+R2OH=R14CH3CO+H2O              4.2E12    0.      0.5E3 !(220,-220)<CAVANAGH90>!
CH3CHO+R7CH3O=R14CH3CO+CH3OH          2.4E11    0.      1.8E3 !(221,-221)<CAVANAGH90>!
CH3CHO+R13CH2CHO=CH3CHO+R14CH3CO      2.5E7     0.      0.    !(222,-222)<SCHUCHMANN70NIST>!

!REACTIONS DE C2H4O#!
!
!* assuming that C2H3O decompose rapidly to R13CH2CHO!

!REACTIONS DE R15C2H5O!
R15C2H5O=HCHO+R4CH3                   8.0E13    0.      21.5E3 !(242,-242)<BAULCH94>!
R15C2H5O=CH3CHO+R1H                   2.0E14    0.      23.3E3 !(243,-243)<HEICKLEN88NIST>!


!Ractions de la base alcool

! bta-scissions:
C2H4Z+R2OH(+M)=R24C2H4OH(+M)                5.420E+12    0.0          0.0
      LOW / 1.19E27   -3.1    0.0 /
R24C2H4OH=R1H+CH3CHO                        3.000E+13    0.0      34800.0
R25C2H4OH=CH3CHO+R1H                        3.000E+13    0.0      38000.0  ! 3H primaire
R25C2H4OH+M=CH3CHO+R1H+M                    5.000E+13    0.0      21860.0  ! Konnov


! isomrisation :
R24C2H4OH=R25C2H4OH                         1.000E+11    0.0      27000.0  ! Konnov

!oxydations :
R24C2H4OH+O2=CH3CHO+R3OOH                   1.600E+12    0.0       5000.0
R25C2H4OH+O2=CH3CHO+R3OOH                   8.400E+15   -1.20         0.0  ! Konnov
         DUPLICATE
R25C2H4OH+O2=CH3CHO+R3OOH                   4.800E+14    0.0       5000.0  ! Konnov
         DUPLICATE


R25C2H4OH+R1H=CH3CHO+H2                     2.000E+13    0.0          0.0
R25C2H4OH+R2OH=CH3CHO+H2O                   1.500E+13    0.0          0.0
R25C2H4OH+B1O=CH3CHO+R2OH                   9.040E+13    0.0          0.0

!!!!!! Ractions de l'thanol (  substituer aux ractions de l'thanol dans la base C0-C2)

!Amorage bimolculaire de l'thanol
C2H5OH+O2=R24C2H4OH+R3OOH                   4.000E+13    0.0      50900.0
C2H5OH+O2=R25C2H4OH+R3OOH                   4.000E+13    0.0      51200.0

!Mtathse de l'thanol C2H5OH
C2H5OH+R2OH=R24C2H4OH+H2O                   2.563E+06    2.06       860.0
C2H5OH+R2OH=R25C2H4OH+H2O                   3.000E+13    0.0       5960.0
C2H5OH+B1O=R25C2H4OH+R2OH                   6.000E+05    2.46      1850.0
C2H5OH+B1O=R24C2H4OH+R2OH                   5.000E+12    0.0       4411.0
C2H5OH+R1H=R25C2H4OH+H2                     4.400E+12    0.0       4570.0
C2H5OH+R3OOH=R25C2H4OH+H2O2                 2.000E+13    0.0      17000.0
C2H5OH+R4CH3=R25C2H4OH+CH4                  4.000E+11    0.0       9700.0
C2H5OH+R4CH3=R24C2H4OH+CH4                  3.000E+00    4.0      10480.0
C2H5OH+R1H=R24C2H4OH+H2                     2.000E+12    0.0       9500.0
C2H5OH+R11C2H5=R24C2H4OH+C2H6               1.500E+12    0.0      11700.0
C2H5OH+R11C2H5=R25C2H4OH+C2H6               4.000E+13    0.0      10000.0
C2H5OH+R6CH2OH=R25C2H4OH+CH3OH              4.000E+11    0.0       9700.0
C2H5OH+R7CH3O=R25C2H4OH+CH3OH               2.000E+11    0.0       7000.0

C2H5OH+R15C2H5O=C2H5OH+R25C2H4OH            2.000E+11    0.0       7000.0
```

```
!REACTIONS DE O2!
B1O+B1O+M=O2+M                          5.40E13     0.      -1.79E3  !(244,-244)<BAULCH94>!
        O2/0.4/ B2CO/0.75/ CO2/1.5/ H2O/6.5/ CH4/3.0/ C2H6/3.0/ AR/0.35/
        N2/0.4/ HE/0.35/
O2+R1H=R2OH+B1O                     9.8E13      0.      14.8E3   !(245,-245)<BAULCH94>!
O2+R1H(+M)=R3OOH(+M)                4.52E13     0.        0.     !(246,-246)<COBOS85>!
                    LOW    /1.8E18     -0.8      0.00/     !k0 BAULCH94!
                    TROE   /0.5          1.0     1.0E8/
        O2/0.4/ B2CO/0.75/ CO2/1.5/ H2O/0.0/ CH4/3.0/ C2H6/3.0/ AR/0.29/
        HE/0.35/ N2/0.67/
O2+R1H(+H2O)=R3OOH(+H2O)            4.52E13     0.        0. !(246b,-246b)<BAULCH94>!
                    LOW    /6.9E15     0.0     -2080/
                    TROE   /0.45        1.0     1.0E8/
O2+B3C=B2CO+B1O                     1.2E14      0.        0. !(247,-247)<RANZI94>!
O2+B4CH=R5CHO+B1O                   3.3E13      0.        0. !(248,-248)<DAGAUT91>!
O2+B4CH=B2CO+R2OH                   3.2E13      0.        0. !(249,-249)<PEETERS97>!
O2+B6CH2=>B2CO+R2OH+R1H             3.1E12      0.        0. !(250)<BAULCH94>!
O2+B5CH2=R5CHO+R2OH                 4.3E10      0.     -0.5E3 !(251,-251)<DAGAUT91>!
O2+B5CH2=CO2+H2                     6.9E11      0.      0.5E3 !(252,-252)<DAGAUT91>!
O2+B5CH2=>CO2+R1H+R1H               1.6E12      0.      1.0E3 !(253)<DAGAUT91>!
O2+B5CH2=B2CO+H2O                   1.9E10      0.     -1.0E3 !(254,-254)<DAGAUT91>!
O2+B5CH2=>B2CO+R2OH+R1H             8.6E10      0.     -0.5E3 !(255)<DAGAUT91>!
O2+B5CH2=HCHO+B1O                   1.0E14      0.      4.5E3 !(256,-256)<DAGAUT91>!
O2+R4CH3(+M)=R8CH3OO(+M)            7.8E8       1.2       0. !(257,-257)<BAULCH94>!
                          LOW    /5.6E25     -3.3       0./
                          TROE   /0.36        1.0     1.0E8/
O2+R4CH3=R7CH3O+B1O                 1.3E14      0.     31.3E3 !(258,-258)<BAULCH94>!
O2+R4CH3=HCHO+R2OH                  3.0E30     -4.69   36.6E3 !(259,-259)<DAGAUT91>!
O2+CH4=R4CH3+R3OOH                  4.0E13      0.     56.7E3 !(260,-260)<BAULCH94>!
O2+R9C2HT=B2CO+R5CHO                3.8E13     -0.16     0. !(261,-261)<TIESEMANN97/TSANG86>!
O2+R9C2HT=R12CHCOV+B1O              9.0E12     -0.16     0. !(262,-262)<TIESEMANN97/TSANG86>!
O2+C2H2T=R9C2HT+R3OOH               1.2E13      0.     74.5E3 !(263,-263)<TSANG86>!
O2+C2H2T=R5CHO+R5CHO                7.0E7       1.8    30.6E3 !(264,-264)<BENSON95>!
O2+R10C2H3V=C2H2T+R3OOH             1.34E6      1.61   -0.4E3 !(265,-265)<MEBEL NIST>!
O2+R10C2H3V=HCHO+R5CHO              4.5E16     -1.39    1.0E3 !(266a,-266a)<MEBEL NIST>!
O2+R10C2H3V=B1O+R13CH2CHO           3.3E11     -0.29      10. !(266b,-266b)<MEBEL NIST>!
O2+C2H4Z=R10C2H3V+R3OOH             4.2E13      0.     57.4E3 !(267,-267)<TSANG86>!
O2+R11C2H5=R17C2H5OO                2.2E10      0.77   -0.6E3 !(268,-268)<WAGNER90>!
O2+R11C2H5=C2H4Z+R3OOH              8.4E11      0.      3.9E3 !(269,-269)<TSANG86>!
O2+R11C2H5=R15C2H5O+B1O             1.2E13     -0.2    27.9E3 !(270,-270)<BOZZELLI90NIST>!
O2+R11C2H5=CH3CHO+R2OH              6.0E10      0.      6.9E3 !(271,-271)<TSANG86>!
O2+C2H6=R11C2H5+R3OOH               6.0E13      0.     51.7E3 !(272,-272)<BAULCH94>!
O2+R2OH=R3OOH+B1O                   2.2E13      0.     52.5E3 !(273,-273)<TSANG86>!
O2+B2CO=CO2+B1O                     2.5E12      0.     47.7E3 !(274,-274)<TSANG86>!
O2+R5CHO=B2CO+R3OOH                 7.6E12      0.     0.41E3 !(275,-275)<TIMONEN88>!
O2+HCHO=R5CHO+R3OOH                 2.0E13      0.     38.8E3 !(276,-276)<TSANG86)!
O2+R7CH3O=HCHO+R3OOH                2.2E10      0.      1.7E3 !(277,-277)<BAULCH94>!
O2+R6CH2OH=HCHO+R3OOH               1.2E12      0.        0. !(278,-278)<TSANG87>!
O2+CH3OH=R6CH2OH+R3OOH              2.0E13      0.     44.9E3 !(279,-279)<TSANG87>!
O2+R12CHCOV=>B2CO+B2CO+R2OH         1.5E12      0.      2.5E3 !(280)      <DAGAUT91>!
O2+R14CH3CO=R18CH3COOO              2.4E12      0.        0. !(282,-282)<COX90>!
O2+R13CH2CHO=>HCHO+R2OH+B2CO        5.9E9       0.     -1.4E3 !(283)      <COX90>!
O2+R13CH2CHO=CH2COZ+R3OOH           1.0E10      0.     -1.4E3 !(284,-284)<COX90>!
O2+CH3CHO=R14CH3CO+R3OOH            5.0E13      0.     36.4E3 !(285,-285)<COX90>!
O2+CH3CHO=R13CH2CHO+R3OOH           1.0E13      0.5    46.0E3 !(285',-285)<Ranzi94>!
!O2+C2H4OE#3=R3OOH+R13CH2CHO        5.0E13      0.     48.0E3 !(286,-286)<RANZI94>!
O2+R15C2H5O=CH3CHO+R3OOH            6.0E10      0.      1.7E3 !(287,-287)<BAULCH94>!

!REACTIONS DE R3OOH!
R3OOH+R1H=H2+O2                     4.3E13      0.      1.4E3 !(288,-288)<BAULCH94>!
R3OOH+R1H=2R2OH                     1.7E14      0.      0.9E3 !(289,-289)<BAULCH94>!
R3OOH+R1H=H2O+B1O                   3.0E13      0.      1.7E3 !(290,-290)<BAULCH94>!
R3OOH+B6CH2=HCHO+R2OH               3.0E13      0.        0. !(291,-291)<TSANG86>!
R3OOH+B5CH2=HCHO+R2OH               1.8E13      0.        0. !(292,-292)<TSANG86>!
R3OOH+R4CH3=R7CH3O+R2OH             1.8E13      0.        0. !(293,-293)<BAULCH94>!
!R3OOH+R4CH3=R7CH3O+R2OH            4.0E13      0.      5.0E3 !(293,-293)<DAGAUT>
```

```
R3OOH+CH4=R4CH3+H2O2                9.0E12      0.      24.6E3 !(294,-294)<BAULCH94>!
R3OOH+R9C2HT=R12CHCOV+R2OH           1.8E13      0.        0. !(295,-295)<TSANG86>!
R3OOH+C2H2T=CH2COZ+R2OH              6.0E9       0.       8.0E3 !(296,-296)<TSANG86>!
!incertitude au moins un facteur 10
R3OOH+R10C2H3V=>R2OH+R4CH3+B2CO     3.0E13      0.        0. !(297)      <TSANG86>!
R3OOH+C2H4Z=CH3CHO+R2OH             6.0E9       0.       7.9E3 !(298,-298)<TSANG86>!
!R3OOH+C2H4Z=C2H4OE#3+R2OH           2.2E12      0.      17.2E3 !(299,-299)<BAULCH94>!
R3OOH+R11C2H5=>R4CH3+HCHO+R2OH      2.4E13      0.        0. !(300)      <TSANG86>!
R3OOH+R11C2H5=C2H4Z+H2O2            3.0E11      0.        0. !(301,-301)<TSANG86>!
R3OOH+C2H6=R11C2H5+H2O2             1.3E13      0.      20.4E3 !(302,-302)<BAULCH94>!
R3OOH+R2OH=H2O+O2                   2.9E13      0.      -0.5E3 !(303,-303)<BAULCH94>!
R3OOH+B2CO=CO2+R2OH                 1.5E14      0.      23.6E3 !(304,-304)<TSANG86>!
R3OOH+R5CHO=>R2OH+R1H+CO2           3.0E13      0.        0. !(305)      <TSANG86>!
R3OOH+HCHO=R5CHO+H2O2               3.0E12      0.      13.0E3 !(306,-306)<BAULCH94>!
R3OOH+R7CH3O=HCHO+H2O2              3.0E11      0.        0. !(307,-307)<TSANG86>!
R3OOH+R6CH2OH=HCHO+H2O2             1.2E13      0.        0. !(308,-308)<TSANG87>!
R3OOH+CH3OH=R6CH2OH+H2O2            9.6E10      0.      12.6E3 !(309,-309)<TSANG87>!
R3OOH+R14CH3CO=>R4CH3+CO2+R2OH      3.0E13      0.        0. !(310)<TSANG86>!
R3OOH+CH3CHO=R14CH3CO+H2O2          1.0E12      0.      10.0E3 !(311,-311)<CAVANAGH90>!
!R3OOH+C2H4OE#3=H2O2+R13CH2CHO      1.6E12      0.      15.0E3 !(312,-312)<RANZI94>
R3OOH+R3OOH=H2O2+O2                 1.3E11      0.     -1.63E3 !(313,-313)<BAULCH 94>!
      DUPLICATE
R3OOH+R3OOH=H2O2+O2                 4.2E14      0.     11.98E3 !(313,-313)<BAULCH 94>!
      DUPLICATE

!REACTIONS DE H2O2!
R2OH+R2OH(+ M)=>H2O2 (+ M)        7.23E13     -0.37     0.00   !(314)<BAULCH94>!
         O2/0.4/ B2CO/0.75/ CO2/1.5/ H2O/6.5/ CH4/3.0/ C2H6/3.0/ AR/0.35/
         N2/0.4/ HE/0.35/
         LOW   /5.53E19   -0.76      0.00 /
         TROE /0.5 1 1.E8/
H2O2(+M)=>R2OH+R2OH(+M)           3.00E14      0.00     48.5E3 !(-314)<BAULCH94>!
         O2/0.4/ B2CO/0.75/ CO2/1.5/ H2O/6.5/ CH4/3.0/ C2H6/3.0/ AR/0.35/
         N2/0.4/ HE/0.35/
         LOW   /3.0E17    0.0      45.5E3/
         TROE /0.5 1. 1.E8/
H2O2+R1H=H2+R3OOH                   1.7E12      0.       3.7E3 !(315,-315)<BAULCH94>!
H2O2+R1H=H2O+R2OH                   1.0E13      0.       3.6E3 !(316,-316)<BAULCH94>!
H2O2+B6CH2=R7CH3O+R2OH              3.0E13      0.         0. !(317,-317)<TSANG86>!
H2O2+R10C2H3V=C2H4Z+R3OOH           1.2E10      0.      -0.6E3 !(318,-318)<TSANG86>!
H2O2+B1O=R2OH+R3OOH                 6.6E11      0.       4.0E3 !(319,-319)<BAULCH94>!
H2O2+R2OH=H2O+R3OOH                 7.8E12      0.       1.3E3 !(320,-320)<BAULCH94>!

!REACTIONS DE CO2!
CO2+B5CH2=HCHO+B2CO                 2.3E10      0.         0. !(321,-321)<TSANG86>!

!REACTIONS DE R8CH3OO!
R8CH3OO=HCHO+R2OH                    1.5E13      0.      47.0E3 !(322,-322)<RANZI94>!
R8CH3OO+R1H=R7CH3O+R2OH              9.6E13      0.        0. !(323,-323)<TSANG86>!
R8CH3OO+H2=CH3OOH+R1H                3.0E13      0.      26.0E3 !(324,-324)<TSANG86>!
R8CH3OO+B6CH2=HCHO+R7CH3O            1.8E13      0.        0. !(325,-325)<TSANG86>!
R8CH3OO+B5CH2=HCHO+R7CH3O            1.8E13      0.        0. !(326,-326)<TSANG86>!
R8CH3OO+R4CH3=R7CH3O+R7CH3O          5.0E12      0.      -1.4E3 !(327,-327)<CAVANAGH90>!
R8CH3OO+CH4=CH3OOH+R4CH3             1.8E11      0.      18.5E3 !(328,-328)<TSANG86>!
R8CH3OO+R9C2HT=R7CH3O+R12CHCOV       2.4E13      0.        0. !(329,-329)<TSANG86>!
R8CH3OO+C2H2T=CH3OOH+R9C2HT          5.6E11      0.      24.5E3 !(330,-330)<RANZI94>!
R8CH3OO+R10C2H3V=R7CH3O+R13CH2CHO   2.4E13      0.        0. !(331,-331)<TSANG86*>!
!* assuming that C2H3O decompose rapidly to R13CH2CHO!
!R8CH3OO+C2H4Z=R7CH3O+C2H4OE#3       1.1E15      0.      20.0E3 !(332,-332)<NIKISHA81/MOSHKINA80NIST>!
R8CH3OO+C2H4Z=CH3OOH+R10C2H3V        3.9E12      0.      24.5E3 !(333,-333)<RANZI94>!
R8CH3OO+R11C2H5=R7CH3O+R15C2H5O      2.4E13      0.        0. !(334,-334)<TSANG86>!
R8CH3OO+C2H6=CH3OOH+R11C2H5          2.9E11      0.      14.9E3 !(335,-335)<TSANG86>!
R8CH3OO+B1O=R7CH3O+O2                3.6E13      0.        0. !(336,-336)<TSANG86>!
R8CH3OO+R2OH=CH3OH+O2                6.0E13      0.        0. !(337,-337)<TSANG86>!
R8CH3OO+R2OH=R7CH3O+R3OOH            3.0E12      0.        0. !(338,-338)<RANZI94>!
R8CH3OO+B2CO=R7CH3O+CO2              1.0E14      0.      24.0E3 !(339,-339)<RANZI94>!
R8CH3OO+R5CHO=>R7CH3O+R1H+CO2        3.0E13      0.        0. !(340)      <TSANG86>!
```

```
R8CH3OO+HCHO=CH3OOH+R5CHO                1.0E12    0.     12.1E3 !(341,-341)<CAVANAGH90>!
R8CH3OO+R7CH3O=HCHO+CH3OOH               3.0E11    0.      0. !(342,-342)<TSANG86>!
R8CH3OO+R6CH2OH=>R7CH3O+R2OH+HCHO        1.2E13    0.      0. !(343)<TSANG87>!
R8CH3OO+CH3OH=CH3OOH+R6CH2OH             1.8E12    0.     13.7E3 !(344,-344)<TSANG87>!
R8CH3OO+CH3OH=CH3OOH+R7CH3O              2.8E11    0.     18.8E3 !(345,-345)<RANZI94>!
R8CH3OO+CH2COZ=CH3OOH+R12CHCOV           1.7E12    0.     27.0E3 !(346,-346)<RANZI94>!
R8CH3OO+R14CH3CO=R4CH3+CO2+R7CH3O        2.4E13    0.      0. !(347,-347)<TSANG86>!
R8CH3OO+CH3CHO=CH3OOH+R14CH3CO           1.0E12    0.     12.1E3 !(348,-348)<CAVANAGH90>!
R8CH3OO+CH3CHO=CH3OOH+R13CH2CHO          1.7E12    0.     19.2E3 !(349,-349)<RANZI94>!
!R8CH3OO+C2H4OE#3=CH3OOH+R13CH2CHO       2.2E12    0.     16.0E3 !(350,-350)<RANZI94>!
R8CH3OO+R3OOH=CH3OOH+O2                  2.5E11    0.     -1.6E3 !(351,-351)<BAULCH94>!
R8CH3OO+R3OOH=>O2+HCHO+H2O               5.0E10    0.      0. !(352)<RANZI94>!
R8CH3OO+H2O2=CH3OOH+R3OOH                2.4E12    0.      9.9E3 !(353,-353)<TSANG86>!
R8CH3OO+R8CH3OO=CH3OH+HCHO+O2            2.5E10    0.     -0.8E3 !(354,-354)<BAULCH94>!
R8CH3OO+R8CH3OO=R7CH3O+R7CH3O+O2         2.5E10    0.     -0.8E3 !(355,-355)<BAULCH94>!

!REACTIONS DE CH3OOH!
CH3OOH=R7CH3O+R2OH                       6.0E14    0.     42.3E3 !(356,-356)<BAULCH94>!
CH3OOH+B1O=R8CH3OO+R2OH                  2.0E13    0.      4.8E3 !(357,-357)<BAULCH94average>!
CH3OOH+R2OH=H2O+R8CH3OO                  1.8E12    0.     -0.37E3 !(358,-358)<BAULCH94average>!
CH3OOH+R7CH3O=>CH3OH+R2OH+HCHO           1.5E11    0.      6.5E3 !(359)<RANZI94>!

!REACTIONS DE R17C2H5OO!
R17C2H5OO=R16C2H4OOH                     4.2E12    0.     36.9E3 !(360,-360)<HUGHES93>!
R17C2H5OO+H2=C2H5OOH+R1H                 7.9E12    0.     21.0E3 !(361,-361)<RANZI94>!
R17C2H5OO+R4CH3=R15C2H5O+R7CH3O          2.0E12    0.     -1.2E3 !(362,-362)<RANZI94>!
R17C2H5OO+CH4=C2H5OOH+R4CH3              3.9E12    0.     24.0E3 !(363,-363)<RANZI94>!
R17C2H5OO+C2H2T=C2H5OOH+R9C2HT           5.6E11    0.     24.4E3 !(364,-364)<RANZI94>!
R17C2H5OO+C2H4Z=C2H5OOH+R10C2H3V         3.9E12    0.     24.4E3 !(365,-365)<RANZI94>!
!R17C2H5OO+C2H4Z=R15C2H5O+C2H4OE#3       2.3E16    0.     21.9E3 !(366,-366)<MOSHKINA80NIST>!
R17C2H5OO+C2H6=C2H5OOH+R11C2H5           5.1E12    0.     19.5E3 !(367,-367)<RANZI94>!
R17C2H5OO+H2O=C2H5OOH+R2OH               5.6E12    0.     30.6E3 !(368,-368)<RANZI94>!
R17C2H5OO+B2CO=CO2+R15C2H5O              1.0E14    0.     24.0E3 !(369,-369)<RANZI94>!
R17C2H5OO+HCHO=C2H5OOH+R5CHO             4.5E12    0.     14.4E3 !(370,-370)<RANZI94>!
R17C2H5OO+CH3OH=C2H5OOH+R7CH3O           2.8E11    0.     18.4E3 !(371,-371)<RANZI94>!
R17C2H5OO+CH3OH=C2H5OOH+R6CH2OH          2.8E12    0.     19.5E3 !(372,-372)<RANZI94>!
R17C2H5OO+CH2COZ=C2H5OOH+R12CHCOV        1.7E12    0.     24.4E3 !(373,-373)<RANZI94>!
R17C2H5OO+CH3CHO=C2H5OOH+R14CH3CO        3.9E12    0.     14.4E3 !(374,-374)<RANZI94>!
R17C2H5OO+CH3CHO=C2H5OOH+R13CH2CHO       1.7E12    0.     19.5E3 !(375,-375)<RANZI94>!
!R17C2H5OO+C2H4OE#3=C2H5OOH+R13CH2CHO    2.2E12    0.     16.3E3 !(376,-376)<RANZI94>!
R17C2H5OO+R3OOH=O2+C2H5OOH               3.9E11    0.     -1.3E3 !(377,-377)<BAULCH89>!
!Rate constant measured between 240 and 380K!
R17C2H5OO+H2O2=C2H5OOH+R3OOH             4.5E11    0.     10.8E3 !(378,-378)<RANZI94>!
R17C2H5OO+R8CH3OO=>R15C2H5O+R7CH3O+O2    2.0E11    0.      0. !(379)<RANZI94>!
R17C2H5OO+CH3OOH=C2H5OOH+R8CH3OO         1.1E12    0.     16.3E3 !(380,-380)<RANZI94>!
R17C2H5OO+R17C2H5OO=2R15C2H5O+O2         4.1E10    0.      0.2E3 !(381,-381)<LIGHTFOOT92>!
R17C2H5OO+R17C2H5OO=C2H5OH+CH3CHO+O2     1.8E10    0.      0.2E3 !(382,-382)<LIGHTFOOT92>!

!REACTIONS DE R16C2H4OOH!

R16C2H4OOH=C2H4Z+R3OOH                   2.0E13    0.     23.5E3 !(385,-385)<RANZI94>!

!REACTIONS DE C2H5OOH
C2H5OOH=R15C2H5O+R2OH                    4.0E15    0.     42.9E3 !(386,-386)<BAULCH94>!
C2H5OOH+R1H=>CH3CHO+R2OH+H2              3.2E13    0.      7.7E3 !(387)<RANZI94>!
C2H5OOH+R4CH3=>CH3CHO+R2OH+CH4           5.7E11    0.      8.7E3 !(388)<RANZI94>!
C2H5OOH+R9C2HT=>CH3CHO+R2OH+C2H2T        6.0E11    0.      9.2E3 !(389)<RANZI94>!
C2H5OOH+R10C2H3V=>CH3CHO+R2OH+C2H4Z      1.0E12    0.      8.7E3 !(390)<RANZI94>!
C2H5OOH+R11C2H5=>CH3CHO+R2OH+C2H6        3.4E11    0.     11.4E3 !(391)<RANZI94>!
C2H5OOH+R2OH=>CH3CHO+R2OH+H2O            5.9E12    0.      0.9E3 !(392)<RANZI94>!
C2H5OOH+R5CHO=>CH3CHO+R2OH+HCHO          1.8E12    0.     16.7E3 !(393)<RANZI94>!
C2H5OOH+R7CH3O=>CH3CHO+R2OH+CH3OH        6.3E11    0.      5.5E3 !(394)<RANZI94>!
C2H5OOH+R6CH2OH=>CH3CHO+R2OH+CH3OH       4.2E11    0.     13.6E3 !(395)<RANZI94>!
C2H5OOH+R14CH3CO=>2CH3CHO+R2OH           2.0E12    0.     18.5E3 !(396)<RANZI94>!
C2H5OOH+R13CH2CHO=>2CH3CHO+R2OH          3.4E11    0.     15.7E3 !(397)<RANZI94>!
C2H5OOH+R3OOH=>CH3CHO+R2OH+H2O2          8.0E11    0.     16.2E3 !(398)<RANZI94>!
C2H5OOH+R8CH3OO=>CH3CHO+R2OH+CH3OOH      1.1E12    0.     16.7E3 !(399)<RANZI94>!
```

```
C2H5OOH+R17C2H5OO=>CH3CHO+R2OH+C2H5OOH    1.1E12        0.       16.7E3 !(400)<RANZI94>!

!REACTIONS DE R18CH3COOO!
R18CH3COOO+R3OOH=CH3COOOH+O2                5.5E10        0.       -2.6E3 !(402,-402)<COX90>!
R18CH3COOO+C2H5OOH=CH3COOOH+R17C2H5OO       5.0E11        0.        9.2E3 !(403,-403)<RANZI94>!
R18CH3COOO+C2H5OOH=>CH3CHO+R2OH+CH3COOOH    5.0E11        0.        9.2E3 !(404)<RANZI94>!
R18CH3COOO+R18CH3COOO=>2R4CH3+O2+2CO2       1.7E12        0.       -1.0E3 !(405)<CAVANAGH90>!

!REACTIONS DE CH3COOOH!
CH3COOOH=>R4CH3+CO2+R2OH                    1.0E16        0.       40.0E3 !(406)<CAVANAGH90>!

!REACTIONS DE R21CH3OCO = CH3-O-C(.)=O
R4CH3+CO2=R21CH3OCO                         4.76E7        1.54      3.47E4 ! <GLAUDE05>!
R7CH3O+B2CO=R21CH3OCO                       1.55E6        2.02      5.73E3 ! <GLAUDE05>!

! REACTIONS DE R22CO2H = O=C(.)-OH
R22CO2H(+M)=B2CO+R2OH(+M)      5.9E+12   0.53   33980 ! Larson
             LOW / 2.20E23   -1.83   35260.0 /
R22CO2H(+M)=CO2+R1H(+M)        1.7E+12   0.31   32920 ! Larson
             LOW / 2.9E26   -3.02   35070.0 /
! REACTION DE R23C2H3O2B
R23C2H3O2B=>CO2+R4CH3     1.70E9   1.0       38640

!*****************************************************

!REACTIONS PRODUISANT DES C2+ RADICALAIRES
C2H4Z+R4CH3=>R19C3H7                        2.1E11      0.       7.35E3   !(407)<BAULCH94>!
R11C2H5+C2H4Z=>R20C4H9                      1.1E11      0.       7.3E3    !(408)<BAULCH94>!

!REACTIONS PRODUISANT DES C2+ MOLECULAIRES
!REACTIONS DE R9C2HT!
!R9C2HT+R9C2HT=>C4H2                         1.8E13        0.           0. !(24,-24)<TSANG86>!

!REACTIONS DE C2H2T!
!C2H2T+B6CH2=>C3H4                           1.7E14        0.           0. !(27,-27)<BAULCH94>!
!C2H2T+B5CH2=>C3H4                           3.5E12        0.           0. !(28,-28)<TSANG86>!
!C2H2T+R4CH3=>C3H4+R1H                       6.7E19       -2.08    31.6E3 !(29,-29)<DEAN87>!
!C2H2T+R9C2HT=>C4H2+R1H                      9.0E13        0.           0. !(30,-30)<BAULCH94>!
!C2H2T+C2H2T=>C4H4                           5.5E12        0.       37.0E3 !(31,-31)<DURAN89>!

!REACTIONS DE C2H3!
!R10C2H3V+R4CH3=>C3H6Y                       2.5E13        0.           0. !(37,-37)<TSANG86>!
!R10C2H3V+R9C2HT=>C4H4                       1.8E13        0.           0. !(38,-38)<TSANG86>!
!R10C2H3V+C2H2T=>C4H4+R1H                    2.0E12        0.       5.0E3 !(40,-40)<FAHR89>!
!R10C2H3V+R10C2H3V=>C4H6YZ                   9.6E12        0.           0. !(41,-41)<TSANG86>!

!REACTIONS DE C2H4!
!C2H4Z+B4CH=>C3H4+R1H                        1.3E14        0.       -0.3E3 !(46,-46)<BAULCH94>!
!C2H4Z+B6CH2=>C3H6Y                          9.6E13        0.           0. !(47,-47)<BAULCH94>!
!C2H4Z+B5CH2=>C3H6Y                          3.2E12        0.        5.1E3 !(48,-48)<BAULCH94>!
!C2H4Z+R9C2HT=>C4H4+R1H                      1.2E13        0.           0. !(50,-50)<TSANG86>!
!C2H4Z+R4CH3=>C3H6Y+R1H                      6.6E11        0.          15.9E3  !<TSANG86>!
!C2H4Z+R10C2H3V=>C4H6YZ+R1H                  5.0E11        0.        7.3E3 !(51,-51)<TSANG86>!

!REACTIONS DE C2H5!
R11C2H5+R10C2H3V=>C4H8Y                     1.5E13        0.           0. !(61,-61)<TSANG86>!
R11C2H5+R11C2H5=>C4H10                      1.1E13        0.           0. !(65,-65)<BAULCH94>!

!REACTIONS DE HCO!
R5CHO+R10C2H3V=>C2H3CHOZ                    1.8E13        0.           0. !(138,-138)<TSANG86>!
R5CHO+R11C2H5=>C2H5CHO                      1.8E13        0.           0. !(141,-141)<TSANG86>!

!REACTIONS DE CH3O!
!R7CH3O+R4CH3=CH3OCH3                        1.2E13        0.           0. !(159,-159)<TSANG86>!
!R7CH3O+R7CH3O=>CH3OOCH3                     1.8E12        0.           0. !(172,-172)<TSANG86>!

!REACTIONS DE CH2OH!
```

```
R6CH2OH+R11C2H5=C3H7OH                    1.2E13      0.          0. !(189,-189)<TSANG87>!

!REACTIONS DE CH3CO!
R14CH3CO+R4CH3=>C2H6CO                    4.0E15     -0.8         0. !(231,-231)<TSANG86>!
R14CH3CO+R11C2H5=>C3H8CO                  3.1E14     -0.5         0. !(232,-232)<TSANG86>!
!R14CH3CO+R5CHO=>CH3COCHO                  1.8E13      0.          0. !(237,-237)<TSANG86>!
!R14CH3CO+R6CH2OH=>CH3COCH2OH              1.2E13      0.          0. !(241,-241)<TSANG87>!
!R14CH3CO+R14CH3CO=>CH3COCOCH3             1.2E13      0.       12.3E3 !(243,-243)<TSANG86>!


!REACTIONS RAJOUTEES POUR TENIR COMPTE DE L ACROLEINE

!C3H6Y+B1O=CH3CHCO+2R1H                    5.0E7       1.76   -1.22E3 !<TSANG91>!
!CH3CHCO+R2OH=B2CO+R10C2H3V+H2O                4.0E6       2.0      0.0     !<MARINOV>!
!CH3CHCO+B1O=B2CO+R10C2H3V+R2OH                7.2E12      0.0      2.0E3   !<MARINOV>!
!CH3CHCO+R1H=B2CO+R10C2H3V+H2                  2.0E5       2.5      2.5E3   !<MARINOV>!
!CH3CHCO+R1H=R11C2H5+B2CO                  2.0E13      0.0      2.0E3   !<MARINOV>!
!CH3CHCO+B1O=R4CH3+R5CHO+B2CO              3.0E7       2.0      0.0     !<MARINOV>!
!tC3H5+O2=CH3CHCO+R1H+B1O                  1.6E15     -0.78     3.1E3 !<MARINOV>!
!tC3H5+B1O=CH3CHCO+R1H                     1.0E14      0.0      0.0E3 !<MARINOV>!
!aC4H5+O2=CH3CHCO+R5CHO                    4.2E10      0.0      2.5E3 !<SLAGLE92>!
C2H3CHOZ+R2OH=B2CO+R10C2H3V+H2O                1.0E13      0.0      0.0     !<MARINOV>!
C2H3CHOZ+B1O=B2CO+R10C2H3V+R2OH                7.2E12      0.0      2.0E3   !<MARINOV>!
C2H3CHOZ+B1O=CH2COZ+R5CHO+R1H              5.0E7       1.76     0.08E3 !<MARINOV>!
C2H3CHOZ+R1H=B2CO+R10C2H3V+H2                  4.0E13      0.0      4.2E3   !<MARINOV>!
C2H3CHOZ+R1H=C2H4Z+R5CHO                   2.0E13      0.0      3.5E3   !<MARINOV>!
C2H3CHOZ+O2=B2CO+R10C2H3V+R3OOH                3.0E13      0.0     36.0E3   !<MARINOV>!
!.C3H5Y+R3OOH=C2H3CHOZ+R1H+R2OH            7.0E18     -2.0      0.0     !<TSANG91>!
!.C3H5Y+O2=C2H3CHOZ+R2OH                   1.8E13     -0.41    22.9E3 !<BOZELLI93>!
!.C3H5Y+B1O=C2H3CHOZ+R1H                   1.8E14      0.0      0.0     !<SLAGLE92>!

END
```